UNIVERSITY OF SHEFFIELD

DOCTORAL THESIS

Intelligent Construction using Irregular, Untooled Rock

Author:
Alan G. HOODLESS

Supervisor:
Prof. Colin C. SMITH

A thesis submitted in fulfillment of the requirements for the degree of Doctor of Philosophy

in the

Geotechnical Engineering Group
Department of Civil and Structural Engineering
Faculty of Engineering

May 29, 2024

Declaration of Authorship

I, Alan G. HOODLESS, declare that this thesis titled, "Intelligent Construction using Irregular, Untooled Rock" and the work presented in it are my own. I confirm that:

- This work was done wholly or mainly while in candidature for a research degree at this University.
- Where any part of this thesis has previously been submitted for a degree or any other qualification at this University or any other institution, this has been clearly stated.
- Where I have consulted the published work of others, this is always clearly attributed.
- Where I have quoted from the work of others, the source is always given. With the exception of such quotations, this thesis is entirely my own work.
- I have acknowledged all main sources of help.
- Where the thesis is based on work done by myself jointly with others, I have made clear exactly what was done by others and what I have contributed myself.

Signed: Alan George Hoodless

Date: 29/05/2024

Abstract

Alan G. HOODLESS

Intelligent Construction using Irregular, Untooled Rock

Current methods in the construction industry leave much to be desired in terms of efficient material use and a result of this is high consumption of resources with high greenhouse gas emissions. Traditional methods tend to involve the use of concrete or steel. The increased awareness of the limited amount of resources has sparked a desire to move away from these materials. It is suggested that earthen materials are a suitable replacement as they have low energy requirements and are available globally. Furthermore, waste materials such as construction demolition waste or mining rock that would otherwise go unused is suitable for geotechnical structures such as drystone retaining walls or embankments. With the increased computational power available there lies potential for improving techniques of construction using a high intelligence, low resource method. Autonomous construction performed by robot is an area gaining interest that utilises such capabilities. Previous work sees construction of drystone walls made from large boulders and construction demolition waste. However, placement of the material is based on suitability for fitting a designed shape and stability of the particle. Improvements can be found by determining position to optimise the shear strength of the structure.

The purpose of this thesis is to produce a packing technique that selects placement on criteria derived from the shear strength of soil structures. Parameters are derived from literature and based on commonly seen features in these systems. Low void ratio, high contact area of a particle with other particles and coordination number are all selected for the basis of an objective function to score placement. Additionally, the centroid of the particle is considered as it is shown to be a sign of stability when particles are located further down in a system indicating less potential energy.

The packing algorithm is designed to pack all particle shapes that can be defined by a closed-loop coordinate system in clockwise order for both convex and concave shapes. Two scenarios are tested to ensure this is the case, one based on the packing of irregular, untooled rock particles to replicate the autonomous construction method. This is based in two-dimensions to keep the problem simplied and to reduce computational times. The other replicates the Tetris videogame. Tetris is seen as a scenario where a clear objective to minimise void ratio is present for simplified, orthogonal shapes. As a result, it is adopted as a verification that the algorithm works as intended. Results for particle placement in the Tetris scenario using an objective function based on the features of high shear strength soil structures is shown to be an efficient method of packing. Minimal gaps between particles are observed and when compared to the deepest-bottom-left method for bin packing it was found to outperform this heuristic. As such, it is suggested that this could be adapted to be a novel approach for the bin packing optimisation problem with the further comparison to other bin packing solutions.

The packing of rock particles is also achieved and it is shown that structures can be produced by the algorithm. Void ratio is thought to be a good indication of mechanical strength for systems of soil however it should not be taken as an individual measure for this. Therefore the number of disrupted running joints was adopted as an indication of shear strength of the structure. However, packing in the soil particle scenario found that there is no correlation between disruption of running joints and void ratio of the packing and therefore it was difficult to conclude on the efficiency of the algorithm in terms of optimising shear strength. Results of the algorithm using rock particles presents well packed structures in a domain. From this visual inspection it is determined that the algorithm could be adopted as a novel approach for specimen generation for fields such as DEM modelling. Verification of strength through rotating drum to measure angle of repose is suggested with structures of high shear strength exhibiting higher angles of repose.

Keywords: Particle packing; untooled rock; precision structures; bin packing; Tetris

Acknowledgements

I would like to express my deepest appreciation towards my supervisor, Professor Colin Smith, for his help and guidance during the project. Throughout I have faced many barriers and struggles and I thank you for being so understanding and for supporting me. I would also like to thank the members of the Geotechncial Engineering Group in Sheffield, both old and new, who I have been able to discuss ideas with as well as enjoy the company of when work is not at the forefront of our minds. Special mention goes to Gabriella, Jared, and Rowena for being ever-present during lunch as eating alone is never an enjoyable experience, and as well to all those that have formed to create such a great crowd of people to spend my lunchtime with. Further appreciation is expressed towards all of the technical and support staff in the Department at the University of Sheffield. Without such a brilliant team the functioning of the department would grind to a halt. Special thanks goes to Holly for her invaluable advice when it was most needed.

My greatest thanks goes to my parents, without whom I would never have been able to complete such an enormous task. I appreciate everything you have done for me so that I can reach my full potential both academically and personally. I would also like to thank my family for their support and asking just the right amount of questions about my work when visiting.

I express my gratitude to every friend that I have made during my time studying at the University of Sheffield. I feel so delighted to have such a wonderful, inspirational, and kind circle of people to surround myself with and who I am fortunate enough to be blessed by their company. There are so many names that I want to put here that I would not know where to start and it feels unfair to those that do not appear. From those that I spent my undergraduate with, to the "Chem Crew" who I have been fortunate enough to frequent with, and for the Boys who Brunch. I hope to actually get to enjoy a brunch with you all one day. But although I am reluctant to give specific names, I could not go on without thanking those who I have lived with during the completion of my doctorate. Joe, Lili, James, Adam, Dan, Jozias, Acushla, and Jen. Thank you for being such marvellous people. Every minute that we spent together I have cherished. It is rare that someone can say they went through a time when the UK was in lockdown and have no regrets about their choice of housemates.

And finally, Amelia. Thank you for all you have done and for always believing in me. You have been there when I am at my best and you have been there when I am at my worst and throughout you have never faltered. I honestly do not think I could have produced what I have without you. Every day that we spend together you inspire me to be the best person that I can be. You are motivated, thoughtful, loving, and passionate about what you do. You make me laugh and, best of all, you even laugh at my jokes. Thank you for being who you are and for your constant supporting and love.

Contents

List of Figures

List of Tables

List of Abbreviations

ASTM	**A**merican **S**ociety for **T**esting and **M**aterials
AAF	**A**lmost **A**ny **F**it
AD	**A**lternate **D**irections
AF	**A**ny **F**it
AWF	**A**lmost-**W**orst **F**it
B	**B**ar Tetromino
BF	**B**est-**F**it
BFD	**B**est-**F**it **D**ecreasing
BFDH	**B**est-**F**it **D**ecreasing **H**eight
BL	**B**ottom **L**eft
BLI	**B**ottom **L**eft for **I**rregular Shapes
BLR	**B**ottom **L**eft with **R**otation
BLP	**B**est **L**ocal **P**osition
BLLT	Improved-**B**ottom **Left** (Least **T**ravelled)
BLP	**B**est **L**ocal **P**osition
BSI	**B**ritish **S**tandards **I**nstitution
CA	**C**onstructive **A**pproach
CB	**C**rushed **B**rick
CDW	**C**onstruction **D**emolition **W**aste
CI	**C**onfidence **I**nterval
CPT	**C**one **P**enetration **T**est
DBL	**D**eepest **B**ottom **L**eft Fill
DEM	**D**iscrete **E**lement **M**ethod
DMTS	**D**BLF and **M**TA **T**abu **S**earch
DSRW	**D**ry **S**tone **R**etaining **W**all
EP	**E**xtreme **P**oints
FBL	**F**inite **B**ottom-**L**eft
FBS	**F**inite **B**est-**S**trip
FC	**F**loor-**C**eiling
FEM	**F**inite **E**lement **M**odelling
FF	**F**irst-**F**it
FFD	**F**irst-**F**it **D**ecreasing
FFF	**F**inite **F**irst-**F**it
FFDH	**F**irst-**F**it **D**ecreasing **H**eight
FNF	**F**inite **N**ext-**F**it
FRG	**F**ine **R**ecycled **G**lass
GA	**G**enetic **A**lgorithm
HEAP	**H**ydraulic **E**xcavator for an **A**utonomous **P**urpose
HFF	**H**ybrid **F**irst-**F**it
HNF	**H**ybrid **N**ext-**F**it
LE	**L**eft **Elbow** Tetromino
LiDAR	**Li**ght **D**etection **A**nd **R**anging

LK	**L**eft **K**ink Tetromino
MRG	**M**edium **R**ecycled **G**lass
MRJ	**M**ean Number of **R**unning **J**oints Distrubted in the Structure
MSW	**M**unicipal **S**olid **W**aste
MTA	**M**aximum **T**ouching **A**rea
MVR	**M**ean **V**oid **R**atio
MW	**M**ining **W**aste
NBL	**N**ext **B**ottom-**L**eft
NF	**N**ext-**F**it
NFDH	**N**ext-**F**it **D**ecreasing **H**eight
NP	**N**ondeterministic **P**olynomial Time
NZS	**N**ew **Z**ealand **S**tandards
PSD	**P**article **S**ize **D**istribution
RAP	**R**eclaimed **A**sphalt **P**avement
RCA	**R**ecylced **C**oncrete **A**ggregate
RE	**R**ight **E**lbow Tetromino
RGB-D	**R**ed **G**reen **B**lue-**D**epth
RK	**R**ight **K**ink Tetromino
RMS	**R**oot **Me**ean **S**quare
SA	**S**imulated **A**nnealing
SEC	**S**traight **E**dge **C**orner
SMB	**S**tabilised **M**ud **B**rick
SMT	**S**ynchrotron **M**icro-Computed **T**omography
SPT	**S**tandard **P**enetration **T**est
SQ	**SQ**uare Tetromino
SRE	**S**tabilised **R**ammed **E**arth
T	**T**ee Tetromino
TP	**T**ouching **P**erimeter
TSF	**T**otal **S**olid **F**raction
UCS	**U**nconfined **C**ompressive **S**trength
URE	**U**nstabilised **R**ammed **E**arth
VA	**V**irgin **A**ggregate
WF	**W**orst **F**it
WR	**W**aste **R**ock
2BP	**2** Dimensional **B**in **P**acking

List of Symbols

a	Distance of separation	$[m]$
c	Cohesion	$[kN/m^2]$
c_f	Two dimensional conversion factor	[-]
c_p	Perimeter of a circle with same area as particle	$[m]$
c'	Effective cohesion intercept	$[rad]$
d	Width of a particle	$[m]$
d_{large}	Diameter of the larger sphere in a two sphere system	$[m]$
d_{small}	Diameter of the smaller sphere in a two sphere system	$[m]$
e	Void ratio	[-]
e_t	Void ratio of the domain including void above the placement surface	[-]
e_o	Initial void ratio	[-]
e_{max}	Maximum void ratio	[-]
e_{min}	Minimum void ratio	[-]
g	Gravitational Acceleration	$[ms^{-2}]$
h	Height of a particle	$[m]$
k	Strength coefficient of granular material	[-]
p_{atm}	Atmospheric pressure	$[kPa]$
p_{hull}	Perimeter of the convex hull	$[m]$
p'_o	Mean effective stress	$[kPa]$
$p_{particle}$	Perimeter of the particle	$[m]$
m	Mass	$[kg]$
n	Sample size	[-]
n_b	Number of coordinates in the bottom line	[-]
n_T	Number of contact points in bottom line	[-]
s	Shear strength	$[kPa]$
s_p	Surface area of a sphere with same volume as particle	$[m^2]$
t	Time	$[s]$
x_{ij}	i^{th} Abscissa for particle j	[-]
x_{pl}	Left-most abscissa of the particle	[-]
x_{pr}	Right-most abscissa of the particle	[-]
x_r	Abscissa of running joint	[-]
y_{ij}	i^{th} Ordinate for particle j	[-]
z	Confidence level	[-]
A	angularity	[-]
A_m	Median area	$[m^2]$
A_p	Area of particle	$[m^2]$
A_S	Area of solids	$[m^2]$
A_{SLE}	Area of solids in the localised area	$[m^2]$
A_T	Area underneath the placement surface	$[m^2]$
A_V	Area of voids	$[m^2]$
A_{VLE}	Area of voids created by the placement of a particle in the localised area	$[m^2]$

A_{VP}	Area of voids created below the particle	$[m^2]$
A_{2D}	Degree of angularity for two-dimensional outline	[-]
A_{3D}	Degree of angularity for three-dimensional shape	[-]
AR	Aspect ratio	[-]
C	Convexity	[-]
C_p	Perimeter of particle	$[m]$
C_{CN}	Weighting coefficient for coordination number criteria	[-]
C_D	Weighting coefficient for potential energy criteria	[-]
C_J	Weighting coefficient for running joint criteria	[-]
C_T	Weighting coefficient for contact area criteria	[-]
C_u	Coefficient of uniformity	[-]
C_V	Weighting coefficient for void ratio criteria	[-]
CI	Confidence interval	[-]
CN	Coordination number	[-]
D	Scoring criteria for potential energy	[-]
D_c	Smallest circumscribed circle diameter	$[m]$
D_{domain}	Height of the domain	$[m]$
D^F	Feret diameter	$[m]$
D_i	Largest inscribed circle diameter	$[m]$
D_m	Scoring criteria for depth using mean depth of the placement surface	[-]
D_{ms}	Mean depth of the placement surface	$[m]$
D_n	Diameter of curvature at corner n	$[m]$
$D_{particle}$	Depth of the particle	$[m]$
D_R	Relative density	[-]
$D_{surface}$	Depth of deepest placement surface coordinate	$[m]$
D_v	Scoring criteria for depth using deepest part of the placement surface	[-]
D_2	Fourier descriptor for elongation	[-]
D_3	Fourier descriptor for irregularity	[-]
D_8	Fourier descriptor for roughness	[-]
F_s	form	[-]
F	Force	$[N]$
F_r	Frictional force	$[N]$
H	Height	$[m]$
I	Breadth/intermediate dimension	$[m]$
I_F	Flatness index	[-]
I_R	Degree of roundness	[-]
I_{2D}	Irregularity index for two-dimensional shape	[-]
I_{3D}	Irregularity index for three-dimensional shape	[-]
J	Scoring criteria for number of running joints disrupted	[-]
L	Length/longest dimension	$[m]$
L_o	Lower bound solution	[-]
N	Number	[-]
OR	Overall regularity	[-]
P	Probability	[-]
$P_{j,max}$	Maximum height of particle j	$[m]$
Q_{25}	25^{th} Quantile value	[-]
Q_{75}	75^{th} Quantile value	[-]
Q_{90}	90^{th} Quantile value	[-]
R	Radius	$[m]$
R_q	Root-mean-square texture	$[m]$
R^2	Coefficient of determination	[-]

S_p	Surface area of particle	$[m^2]$
S	Thickness/shortest dimension	$[m]$
T	Scoring criteria for contact area	[-]
V	Scoring criteria for void ratio	[-]
V_{AB}	Scoring criteria for void ratio below the particle	[-]
V_{LE}	Scoring criteria for void ratio using localised area	[-]
W	Width	$[m]$
W_{ij}	Weighted score for i^{th} position and j^{th}	[-]
(X, Y)	Coordinate of placement surface	[-]
Z	Ordinate value of line for determining top and bottom line	[-]
α	Platiness	[-]
ϵ	Contact distance error	[-]
ζ	Elongation	[-]
θ	Angle of the slope	$[^o]$
μ	Coefficient of friction	[-]
ρ	Particle density	$[kgm^{-3}]$
σ'	Effective normal stress on failure plane	$[kPa]$
σ_p	Standard deviation	[-]
σ_{square}	Standard deviation as square of void in the Tetris Scenario	[-]
$\sigma_{\%}$	Standard deviation as a percentage	[-]
ϕ	Angle of shearing resistance	$[^o]$
ϕ_{cs}	Critical state friction angle	$[^o]$
ϕ'	Effective stress angle of shearing resistance	$[^o]$
ϕ_{cv}	Constant volume critical state friction angle	$[^o]$
ϕ_p	Peak state friction angle	$[^o]$
ϕ_μ	Interparticle friction angle (based on coefficient of friction)	$[^o]$
ϕ_{max}	Maximum angle of shearing resistance	$[^o]$
ψ	Angle of dilatancy	$[^o]$
Λ	Degree of circularity	[-]
Λ_I	Inscribed circle sphericity	[-]
Λ_P	Projection sphericity	[-]
Ψ	Degree of sphericity	[-]

Note that this list contains only the symbols that are likely to be of use to the reader throughout this thesis. Symbols that are locally defined and used have been omitted.

Chapter 1

Introduction and Objectives

1.1 Background

In order to tackle the looming climate crisis, the need for a reduction in material use and increase of low carbon construction techniques has become more prominent. The construction industry accounts for nearly 30% of raw material use and 33% of related greenhouse gas emissions (Chau et al., 2015). As material resources and CO_2 emissions become increasingly expensive both economically and in terms of environmental impact, modern developments in technology have led to high levels of computing power available at low costs. Taking account of these factors, an opportunity for a high intelligence, low resource construction method arises.

Current methods for reinforcement of soil tend to involve the use of concrete or steel, for example, where soil masses may be held back by a concrete retaining wall. However, a transition away from these conventional materials is required for tackling issues of climate impact. The production of cement contributes to roughly 8% of the world's CO_2 emissions (Lehne and Preston, 2018). Additionally, developing countries have an ever increasing demand for construction materials due to their need to build and improve infrastructure. Concrete is the predominant use of riverbed sands, however such sands are also required for glass manufacturing and asphalt roads (Cousins, 2019) and sand and gravel are the most extracted materials globally (Torres et al., 2017). Due to the demand of materials that are created with sand, illegal dredging along riverbeds and coastlines have occurred as a result of this shortage causing the change in the shape of riverbeds and floodplains, affecting wildlife habitats, as well as causing alterations to groundwater reserves and water quality (Cousins, 2019; Koehnken and Rintoul, 2018). The irregular shape of riverbed sand is what makes it desirable for concrete materials as grains from deserts are too rounded and do not bind well in concrete mixes (Cousins, 2019). Because of these reasons, a look away from current building techniques that use a high volume of concrete is required.

Geosynthetics have arisen as a suitable solution for soil reinforcement. These can take the form of geotextiles, geogrids or geonets (Patil et al., 2016). Geosynthetic products have gained popularity due to their flexibility during processing, high specific stiffness and low cost (Pujari et al., 2017). Materials used for geosynthetics range from low-modulus polymeric materials to high tensile strength metallic sheets (Bordoloi et al., 2017a; Bordoloi et al., 2017b). The synthetic materials made from polymers are derived from petroleum which is widely known to be a non-renewable resource and considered detrimental to the environment, whilst metallic materials are also non-renewable, can have a high energy cost to produce and can corrode which can be toxic to the surrounding environment (Gaw and Zamora-Palacios, 2010). The use of natural fibres as a geosynthetic has emerged as an option (Gowthaman et al., 2018). However, these materials readily degrade leading to shorter lifespans than traditional materials (Balan, 1995; Nguyen and Indraratna, 2023).

It is accepted that materials sourced locally are perceived to have a lower embodied environmental impact, since most of these materials have low-tech processing and therefore require less energy to be prepared for use (Fernandes et al., 2019). Several studies carried out by Fernandes et al. (2013), Melià et al. (2014), and Zabalza Bribián et al. (2011) have quantitatively compared vernacular or natural materials to conventional materials like concrete, steel and glass and confirmed that it is true that vernacular materials have a lower impact on the environment. Additionally, locally sourced materials reduce the environmental cost in terms of transportation if they can be processed on or close to site or if they do not need to be processed to begin with. Furthermore, Morel et al. (2001) and Ramesh (2012) concluded that using local materials also has socioeconomic benefits such as reducing construction cost and employing local labour forces.

Rock is a resource that is abundant. Historic constructions can be found worldwide of rock being formed to create major structures which have stood the test of time. Examples of these are the Incan retaining walls and cities in Peru, castles constructed in Japan in the 16th and 17th century, drystone walls which are found all across Europe, and the carved stone blocks utilised in the Pyramids of Giza which are found in Egypt. Such structures make use of the surrounding materials in the environment and have stood for long periods of time. The precedent set by these constructions should inspire modern research and, in combination with developing technologies, a method for using irregular rock particles as a construction material is entirely possible.

Rock material tends to have high compressive strengths when compared to concrete although tensile strengths tend to be small (in the order of 0.1 times the compressive strength, Vutukuri et al., 1974). Furthermore, constructions made of stone require little maintenance despite possessing long lifespans. As well as having favourable characteristics, the extraction of unprocessed rock from quarries is approximately 10% of the greenhouse gas emissions when compared to concrete or brick (Hammond and Jones, 2006 as cited by Lambert and Kennedy, 2012) making it a very sustainable alternative. However, the irregular shape of the material makes it difficult to construct with and requires specialised knowledge in how materials should be placed which is reliant on the analysis of the shape of individual particles. This differs when compared to regular shaped materials like brick where the construction pattern can always be predetermined. The necessity for expert knowledge of construction with these irregular shapes requires skilled workers which in turn increases cost.

In addition to rock, the use of waste materials such as construction demolition waste (CDW) is another possibility for a low-carbon alternative. The construction industry produced around 600 million tons of demolition waste in 2018 within the US alone, mostly consisting of concrete materials (EPA, 2020). Taking advantage of these otherwise waste materials can help recapture the embodied carbon within the material. Clifford et al. (2018) champions the reuse of waste material from demolition and produced a full-scale prototype of a wall constructed in a similar method as the Incan walls in Peru. Discarded rubble debris and stone offcuts were carved by a robotic arm to create flush fittings with minimal void ratio between stones. 73% of the selected starting material is utilised in this process. Whilst tooling of the rock can be beneficial for building of the structure, using the untooled material will lead to better capture of the embodied carbon and minimal waste. Slight tooling of the stone can be taken advantage of to make assembling these irregular shapes easier. However, the scope of this research does not look at this additional variable.

Using materials that can be located on or near site opens up numerous possibilities for in-situ construction. This can be seen by the research for in-situ building studied by NASA for extraterrestrial environments (Lim et al., 2017). Launching materials into space is very costly so therefore an entirely in-situ construction technique is desirable. Robotic construction prevents the need to transport human workers along with the required supplies and shelter to a given destination. Furthermore, structures such as embankments, erosion barriers, and walls where overall function does not rely on exact shape can be built through a similar process with just in-situ or minimal transported materials (Meer et al., 2005). Modern solutions to this problem have emerged harnessing the ever increasing computational power available. As a result, autonomous construction through robots has arisen as a solution.

Lambert and Kennedy (2012) produced a computer aided masonry design, analysis and construction (CAMDAC) software application called Rocksolver. The study was completed in two-dimensionals using a Simulated Annealing (SA) algorithm technique and heuristics based on traditional methods for building a drystone wall. Simulated Annealing is an optimisation technique which applies random changes to parameters being optimised with these changes being larger at the start of the simulation whilst decreasing as the algorithm runs. More detail is given on SA in Section 2.4.2. Unprocessed rocks are digitised and constructed virtually within a physics simulator. SA is performed on the stone being placed in the structure to locate its optimised position and this is repeated for each stone. Results of the final structure then outputs a build-sequence for the user. Lambert and Kennedy (2012) describe the work completed as the first proof-of-concept for CAMDAC software to fit irregular rocks into a wall structure. However, no physical construction of the rocks was completed, but testing of the wall to failure was completed within the physics simulator.

Furrer et al. (2017) were one of the first to stack irregular stones using a robotic arm on a desktop scale. Furrer et al. (2017) produced an algorithm that could stack a subset of irregular objects from a population set. To do this, the best position and orientation - defined as the "pose" in Furrer et al. (2017) - for the best object needs to be found. This is done in Furrer et al. (2017) by placing each object on top of the existing stack in a physics simulator. A valid pose is one which passes a stability check completed by the pose-search algorithm. For this, the centre of mass of the stone being placed must lie between where the below stones have contacts with lower stones in the stack or the surface on which the tower is being constructed i.e. if stacking is taking place on a table this would be the table surface. Additionally, within the physics engine, the kinetic energy caused by the placement of the particle onto the already placed particles is analysed and kept below a threshold value to cause minimal motion in the existing stack. Multiple orientations are attempted with a fixed initial position and a “goodness of fit” is determined which maximises the contact area for which the object is supported on the previous stone as well as other criteria described in Section 2.2.4. Goodness of fit is defined by a cost function based on the placement criteria set out in Furrer et al. (2017). The position with the highest "goodness of fit" is deemed to have the best pose and is taken as the object to be placed. 6 natural lime stones were used in Furrer et al. (2017) for testing experimentally. Towers were created from the stones using a robot arm with three-finger grasping end-effector for gripping and moving the stones. RGB-D (Red Green Blue - Depth) images were taken of the object by a mounted camera on the robot arm to create a 3D scan of the stones. RGB-D images provide information on colour as well as the depth of an object from the camera using a depth map. Images are taken for all stones to detect their features as well as location in the environment. From this, point cloud data is obtained and stored with key features from the stones obtained for tracking of the objects. Next, a pose location is determined for the next particle to be placed. After this, the robot arm grasps the stone and moves it into the desired position before detecting the stack and validating that the placement was successful. Tests were conducted using sets of four stones to create eleven towers. For two of the runs, all four stones were stacked successfully. Three stones were stacked in six instances but failed on the fourth stone and in three cases the third stone was not stacked successfully.

Liu et al. (2021) also proposed an algorithm for autonomous construction for irregular shaped objects. A greedy heuristic approach is taken to find the next best pose from a set of feasible poses rather than the best pose as in Furrer et al. (2017). The next best pose is tested to see if this will lead to better positions later on in the construction of the stones. These poses are generated and tested in a physics simulator to ensure that the position of the object is stable. If a wall structure is desired, the algorithm aims to construct objects in a layer by layer system. Multiple RGB-D images are used to create a point cloud dataset of an object from all angles which are fed into the program and physics simulator. Experiments were conducted in Liu et al. (2021) using a robot manipulator with two-finger grasping end effector to move and place irregular objects from a selection of twenty-three shale stones to create towers and walls. Each tower that was constructed within the physics simulator was aimed to be at least six stones high and nine random towers were selected for construction. All nine towers were constructed to be a minimum of three stones high. Of these nine, three towers did not make it past the fifth stone. Three towers failed on the seventh stone placement and one tower did not have a stone fall, although this was one of the towers that was constructed to be six stones tall. For the stone walls, seven of the thirteen walls were constructed successfully without collapse. Results showed that errors in placement increased as the layer of wall increased with poor placement of the stones increasing, whilst structural collapse of the wall (when more than one stone falls down) does increase after the first layer where no structural collapse is seen, but not significantly between subsequent layers.

Previously discussed literature has shown pilot studies with quite a limited number of particles being tested. Recently, Johns et al. (2023) has shown that automated construction on site with the use of irregular stones is very much a reality. The work in Johns et al. (2023) carries on from that conducted within Johns et al. (2020). Large-scale stone walls and landscapes were constructed by a twelve ton robotic excavation platform using natural and reclaimed materials. The fabrication of the walls was conducted by an autonomous hydraulic excavator. This is described in Johns et al. (2020) as a highly customised Menzi Muck M545 walking excavator and is named HEAP (Hydraulic Excavator for an Autonomous Purpose). In Johns et al. (2023), the drystone walls are built from boulders and CDW by method of detecting stones in-situ, grasping, scanning and reorienting stones to then be placed in an optimised position as determined by an algorithm similar to Furrer et al. (2017) and Liu et al. (2021). Two full-scale walls were constructed from more than 1000 stones. The first was a freestanding wall constructed on a flat concrete surface inside a facility so as not to be influenced by outside disturbances. Therefore a human operator was not used apart from a supervisor to ensure no unexpected failures occur. The other wall was a retaining wall built on an active construction site. For this wall, a human operator was placed inside the robot to ensure no accidents occurred due to needed access to the site by workers. Picking, placing and scanning of the stones was all autonomous and the human operator was there for driving the machinery between tasks. LiDAR mapping was utilised to understand the environment for which construction is being completed. This was mapped and segmented to discover stones in the location and point clouds were created of these objects. Stones were each individually picked up by the robot grasper and scanned to get a whole 3D image of the object before being returned to the ground. 20 to 40 stones were scanned to build a subset of defined objects so that the planning of stone placement could begin. Objects as well as the constructed wall are continuously digitised during the construction process to allow for settling and ensuring robustness if a building element becomes damaged or unavailable for use. The process repeats once all of the scanned stones are placed or no feasible placement can be obtained. The freestanding wall was constructed of 109 unique elements of waste concrete and gneiss boulders and was 10m in length and 4m in height with mean width of 1.7m. No smaller particles were used as fill which is traditionally seen in the construction of drystone walls.

As stated previously, the algorithm to detect potential poses and plan the geometry of the wall is similar to that suggested by Furrer et al. (2017) and Liu et al. (2021). However, when locating candidate positions an extra consideration is taken into account of placing stones above joints between two underlying stones. This comes from traditional masonry techniques and is done to improve bonding and stability (Vivian, 1976 and Environmental Action Foundation, 2019 as cited by Johns et al., 2023). Additionally, a heuristic is introduced so that construction is performed inwards from the wall corners as suggested by Cramb (1992) (as cited by Johns et al., 2023).

The precedent of the work completed by Johns et al. (2020) and Johns et al. (2023) is an example that autonomous construction of irregular, untooled rock is an upcoming possibility in the construction industry. These pieces of work are impressive and the research lays out highly promising methods for which the process of building with these sorts of materials can be achieved. Robots are beneficial to the construction industry as they fulfil requirement of labour meaning the need for labour can be increased whilst not causing increased levels of fatigue and decreased levels of safety to workers on site for what is already a dangerous and physical workplace (Kohler et al., 2014). As demonstrated by Johns et al. (2023) , the use of autonomous robotic construction provides solution to labour costs within the construction industry as well as providing potential for creating structures using the irregular stones and CDW that will lead to a decrease in CO_2 emissions when compared to current popular techniques of using concrete or brick. The need for skilled workers when using irregular objects is overcome by intelligent algorithms adopted by the robot to help determine particle placement. However, positioning of materials in Johns et al. (2023) is judged with a focus on ensuring stability rather than providing functionality. Whilst this is an important starting point, there is possibility of improving these constructions through a differing approach to identifying the best position for a stone to be positioned.

In this thesis a new system for assessing the placement of irregular, untooled rock within a construction is introduced. By use of a different heuristic, emphasis can be placed on the requirement of the structure leading to more possibilities of what could be constructed robotically. A focus on structures requiring high shear strength is placed upon the analysis. However it is thought that for this designed algorithm that if a different purpose for the structure is desired then the criteria for scoring within the heuristic algorithm can also be adapted to produce an alternative build sequence for the structure. Factors are determined by studying what is anticipated to determine high shear strength within a geotechnical soil structure and adopting these as ways to classify scoring placement of particles in a system through the use of an objective function. The following work takes place on a two-dimensional scale for simplicity of simulation but it is considered that this work could be extended into three dimensions like that seen in Furrer et al. (2017), Liu et al. (2021), and Johns et al. (2023). This construction could be carried out manually, but it is envisioned that the process would be autonomously completed via robot making use of modern day technologies and advancements.

1.2 Aims and Objectives

The primary aim presented in this thesis is to develop a new system for optimising the placement of irregular, untooled rock within a construction with the emphasis on producing structures with mechanical strength. The work in Johns et al. (2023) sets an important precedent, yet the improvement on placement of particles is a key aspect for development in this field of research. As such, the following objectives were formulated.

1. Examine existing structures made from drystone and earthen materials as well as factors that affect soil strength and optimal packing solutions to determine considerations for particle positioning in a system that exhibits high shear strengths.

2. Create an algorithm for packing of two-dimensional particles that represent outlines of irregular, untooled rock.

    (a) Describe an objective function that can score the placement of particles by an algorithm that can assess the strength of the system without further knowledge of sequential particle positions.

    (b) Ensure that this algorithm works for other shapes represented in two dimensions. This is an outlined objective as it is envisioned that this method could be taken into further areas of research outside of construction with granular materials. To achieve this, shapes from the videogame Tetris are used to verify the code with an objective for minimising void ratio.

    (c) Verify the strengths of the structure to provide evidence that the algorithm developed is achieving the objective set out by the user of possessing high shear strength. This is accomplished through the development of a laboratory testing method for the build sequence outputted by the algorithm.

    (d) Investigate the effect of placement error as it is rare for a particle to be placed in its exact desired location especially if being placed by robot.

3. Improve or suggest improvements to increase the speed of the algorithm as computational time is seen as a limiting factor for this method.

1.3 Etymology

For better understanding to the reader, it is important to define the origin of the words used throughout this thesis. In this section, words that are commonly found throughout the methodology and results are described with their meaning in the context of this research.

- **Packing**

The packing of a structure or the packing of soil particles is the arrangement of the objects and how they are placed with respect to each other. If two structures made up of the same particles are said to have different packings, then this means that the particles are arranged in different positions when compared to one another. This term could also be referred to as the fabric of the soil as commonly used when discussing DEM. The origin of this use comes from bin packing, the topic of which is explored in Section 2.4.3.

- **Particle**

It is expected that in a thesis around the topic of soil or rock that the term particle will be used frequently. In addition to the normal use of the term - to describe an individual grain in a soil system or an individual sphere to circle in a DEM simulation - “particle” is used within this thesis to describe the items that are in a system of packed particles. For example, in Section 2.2.1 where drystone retaining walls are discussed, the term "particle" refers to a stone within the system that creates the wall. This may seem contrary to intuition as usually particle describes objects on the microscale. Another term that could have been adopted here is "element".

For the work conducted in this thesis, the term particle describes an item being packed in the creation of two-dimensional structures by the algorithm described in Chapter 3. Specifically in Chapters 3-6, the use of “particle” directly correlates to two different types of item. The first are tetrominoes which are those from the videogame Tetris. These are made up of four squares in different arrangements to create seven different shapes. The second type of item described as particles are two-dimensional outlines that represent the outline of untooled rock. These outlines are generated using the method described in Section 2.5.3. Packing of these outlines are used rather than three-dimensional particles to directly relate to the example of tetrominoes being packed as well as to reduce computational time of the algorithm for packing.

- **Candidate Poses**

For the use of “candidate pose”, it is important to first describe the meaning of pose. A pose can be considered the position of a particle in the structure or the way in which it is sat on surface it is placed - whether this be the flat surface of a domain or upon other already placed particles. The use of the term “pose” is frequently used in the literature described in Section 1.1 and Section 2.2.4.

The addition of the term “candidate” describes that pose as one that can be considered for placement of the particle. In this way, a candidate pose meets all criteria required for the particle to be positioned in the described location. For example, a condition that particles must be stable in their final positioning may be added meaning that all poses that result in an unstable position cannot be described as a candidate pose. Again, this term arises due to its use in the literature mentioned in Section 1.1 and Section 2.2.4.

1.4 Layout

This thesis is separated into the following chapters. The layout of the chapters as well as a description of each chapter is presented. All chapters are introduced with the contents of that chapter stated so that the reader can easily navigate their way through the material. At the end of each, the material is again summarised with key details for each topic covered given. The chapters within this work are as follows:

Chapter 1: Introduction

This chapter provides the background and motivations for this thesis. The importance of developing the construction industry to take advantage of modern day advances is highlighted and the area of autonomous construction via robot is explored. The aim and objectives of the project are laid out followed by defining words commonly used within the project that may cause confusion to the reader.

Chapter 2: Literature Review

Here, a wide variety of topics are reviewed with the intention of deriving the criteria required for the autonomous construction of granular structures with an aim to optimise shear strength. This begins by looking at earthen materials, before moving to the finer detail of the structure of soils. Areas of optimisation with the purpose of minimising void space is also explored for inspiration. The final section of this chapter discusses methods of quantifying particle shape and the method of generating particle shapes from Fourier descriptors.

Chapter 3: Methodology for Particle Packing

An algorithm for packing particles that a robot designed for autonomous construction would follow is presented in this chapter. The algorithm was first developed in a simplified scenario representing the Tetris videogame where orthogonal-sided tetrominoes are packed with the objective to minimise void space. Once this is achieved, the algorithm is further developed to take into consideration the requirements for packing irregular, untooled rock particles. Placement of particles is determined by an objective function that uses scoring criteria derived from Chapter 2 to pick the most optimal location. Weighting coefficients are given to each of these criteria. The algorithm is summarised using a workflow chart and input parameters are stated with indication to whether this is a fixed or varied value.

Chapter 4: Determining Sample Size and Weighting Coefficients

Confirmation of the required sample size for representing the whole population of possible results is carried out here. Possible void ratios outputted by the algorithm are analysed and a minimum sample size for collecting results is specified. Furthermore, the method of determining the weighting coefficients for the most optimal solution is defined with the process of investigation stated.

Chapter 5: Results of the Tetris Scenario

Results of the simplified instance of the Tetris Scenario are presented in this chapter. The procedure defined in Chapter 4 is followed to determine the combination of weighting coefficients that produce the optimal solution for packing tetrominoes. These results are compared to other combinations of weighting coefficients as well as control samples of packings produced by the deepest-bottom-left heuristic used for solving bin packing as well as randomly placed tetrominoes.

Chapter 6: Results of the Soil Particle Scenario

In this chapter, results of particle outlines that represent irregular, untooled rock are packed using the placement method. Different coefficients of weighting are trialled as well as the optimal solutions determined in the Tetris Scenario. Again, control scenarios are adopted by packing particles randomly whilst the deepest-bottom-left heuristic is also tested against.

Chapter 7: Verification of Strength

The development of a method for verifying the strength of the structures packed using the algorithm is introduced in this section. Experimental setup as well as the procedure for testing are presented along with the expected results. This comprises of measuring the angle of repose of the produced packings by use of a rotating drum designed for testing two dimensional particles. A particle identification process is also defined and an procedure for the investigation into the tolerance of errors is given.

Chapter 8: Discussion

Chapter 9 discusses the many topics covered within this thesis. Results for the Tetris Scenario and Soil Particle Scenario are discussed. After this, suggested methods that could be adopted for improving shear strength of the packed systems are given based on further techniques that were reviewed in Chapter 2. Enhancement of the objective function utilised for scoring placement as well as how characterisation of particle shape could be implemented are also discussed. Techniques for increasing computational speed are introduced as it is recognised that the main limiting factor of the method developed in Chapter 3 in the runtime of irregular particles defined by many coordinates. Other areas of discussion include running joints as an additional objective function criteria, the use of the algorithm as a bin packing solution or a specimen generation approach, alternative areas of improvement of the autonomous construction method and the work required for the current two-dimensional system to be extended into three-dimensions.

Chapter 9: Conclusions and Future Work

This chapter summarises the key findings of the project. The aim and objectives produced in Section 1.2 are reviewed with work towards these objectives given. Findings from the work carried out in this thesis are then stated. Finally, the required future work for the advancement of this project is discussed.

Chapter 2

Literature review

2.1 Introduction

A wide body of literature exists that is relevant to the task of determining the key packing characteristics that can create high strength structures from irregular rock. Thus in this chapter a large variety of research is explored, from current work investigating the use of soil as a construction material to topics that are far from traditional geotechnical engineering. As far as the author is aware, no heuristic approach that scores particle placement through a criteria based on prioritising shear strength exists within the literature.

Firstly, current examples of geomaterials in construction are reviewed in Section 2.2 to provide insight into historical and conventional building methods and to distil any information concerning how particles are arranged for optimal performance. This section includes discussion of drystone retaining walls typically made up of large gravel, cobbles and boulders, Incan retaining walls found in South America that are made up of huge tooled rock pieces, and 16th and 17th century castles located in Japan. Furthermore, Section 2.2.4 examines the existing literature around the topic of autonomous construction using rock materials. These projects are already introduced in Section 1.1 and are expanded on to give detail of how the algorithms produced determine suitable placements of particles.

Section 2.3 then goes on to review parameters known to affect soil strength to give a full understanding of which aspects should be focused on when designing a method for intelligent construction with the aim to produce a structure with high angle of shearing resistance. Firstly, Section 2.3.1 defines what soil strength is when discussing granular material. Examples of expected values for different soil strengths are given. The parameters explored in the subsequent parts of Section 2.3 include particle shape and roughness, particle size, coordination number i.e. the average number of other particles that a given particle is touching, gradation as well as the density of the soil, friction between particles, and void ratio. Section 2.3.8 summarises each feature explored and concludes on which of these characteristics will be considered in the continuation of the project. From this review, a better understanding of the mechanisms that occur between soil particles is gained and will provide guidance for which factors that should be considered to determine particle placement.

Low void ratio is often associated with a high peak strength structure. Therefore in Section 2.4, optimisation of object placement to achieve low voids is investigated. First, packing structures found to minimise void ratio in a set of particles are investigated in Section 2.4.1. Secondly, deterministic and heuristic approaches to solving optimisation problems are described in Section 2.4.2 as well as the concept of non-deterministic polynomial time complexity to explain why heuristic approaches are normally adopted in optimisation for problems explored in Sections 2.4.3-2.4.5. The concepts of simulated annealing and genetic algorithms are also described. Following this, optimisation of the bin packing problem is considered as a method to pack an empty space with minimal void left between items. Next, techniques for solving jigsaws in the literature are reviewed as this is a traditional case of items being fitted together to have no void present in the system. Finally, the classic videogame Tetris is considered and relevant literature on optimising the space in the game and "beating" the computer to get the highest score possible are explored. These areas shed light on the methods that could be developed to minimise the space between particles. Furthermore, placement heuristics and packing strategies are outlined that can provide inspiration or be adopted within this project in Section 2.4.6.

Section 2.5 discusses different ways of classifying and quantifying particle shape. Section 2.5.1 is present to define terms that are discussed further in Section 8.6 where the possibility of selecting particles based on their characteristics is explored. The terms defined in Section 2.5.1 are form, sphericity, roundness and irregularity and are all used as morphological terms. Section 2.5.2 discusses how Fourier descriptors can be achieved through Fourier transforms of the particle outline to express two-dimensional particle shape in an alternative method with a discussion of what each descriptor indicates. Section 2.5.3 takes the work discussed in Section 2.5.2 and uses it to generate particle outlines from Fourier descriptors, specifically D_2, D_3 and D_8. This approach is adopted for generating particle outlines that represent irregular, untooled rock particles in Section 3.6.1 using software provided in Mollon (2023). Section 2.5.4 summarises Section 2.5 and highlights which terms of classification could be used in this project for defining two-dimensional particle outlines for purpose of selection of particles for packing which is then later discussed in Section 8.6.

In the final section of this chapter, important findings in the literature review are highlighted. Section 2.6 discusses these findings and links the parameters outlined in Section 2.3 with the methods described in Section 2.4 and information gained from both the literature and visually in Section 2.2. The key parameters from Section 2.3 which will be adopted for weighted criterion in scoring using an objective function in this project are then stated. Other key features which present potential useability are highlighted from throughout the literature review and outlined in how they can be presented in the produced algorithm for packing soil particles within a structure to produce high angle of friction.

2.2 Examples of Geomaterials in Construction

2.2.1 Drystone Retaining Walls

Dry stone walls provide an example of a structure formed from geomaterials. A drystone wall is made up of natural pieces of stone and are positioned in such a way to form a free standing wall structure, traditionally built in horizontal layers. Vivian (1976) states that the best wall stones for building drystone retaining walls (DSRW) are hard shales and schists that have large flat sides due to cleavage during metamorphosis whereas the hardest are those which are rounded. Stones of uniform thickness in a layer give a stronger and more aesthetically appealing structure (Mundell et al., 2009), as seen in Figure 2.1. An extensive library of images giving examples of drystone walls can be found in Snow (2001) and it can be interpreted that flatter stones are normally used in the horizontal layers and usually a low void ratio is present in the structure with minimal gaps between wall pieces. Heights of drystone retaining walls typically range between 2-4 meters, however are known to be strong enough to be 10 meters or higher (Alejano et al., 2012). The use of mortar is excluded in construction instead relying on friction and interlocking between particles for stability (Oetomo et al., 2016). A similar approach could be taken for this research to try and avoid the use of mortar or a binding agent where possible. It is thought that the materials are normally sourced locally, either from when the nearby fields were first cleared or from local quarries (Thompson, 2007).

FIGURE 2.1: Example of a drystone walling © Christine Johnstone. Photos used under the Creative Commons Attribution-Share Alike 2.0 license conditions (Creative Commons, 2011).

Vivian (1976) gives details on the construction of a stone wall by hand. Stones should rest on at least two other stones to reduce the number of “runs” in the wall. A build up of these runs is also known as a running joint (Adcock, 2012). Runs are stated to decrease stability in the wall. Small stones are used within the interior to fill gaps between the larger stones. Furthermore, Vivian (1976) states that the sides of a wall should be vertical except for large walls which should have a slight inward slope. For the corners of the wall, it is necessary to tie stones together. This is not with an additional material like a rope but, as Vivian (1976) describes, is to alternate layers like that seen at the corners of the walls of 15th-16th century castles found in Japan later described in Section 2.2.3 and presented in Figures 2.9 and 2.10. Vivian (1976) recommends to not align the edge of rocks being placed with the edge of any rock in the course below apart from at the outer and inner faces.

Adcock (2012) states that a running joint can be classed as disrupted if a "significant amount" of the placed stone covers the below run. Adcock (2012) explains that in drystone walls, diagonal joints may appear for irregular stones (Figure 2.2a) as well as "phantom" diagonal joints. A phantom diagonal joint is one which appears to be running diagonally through the wall. However, the stone above is resting with this "significant amount" over the running joint. Adcock (2012) does not state what proportion of overlap is required for this. Additionally, Adcock (2012) describes "zipped joints" which are those where a running joint may not be obvious in the

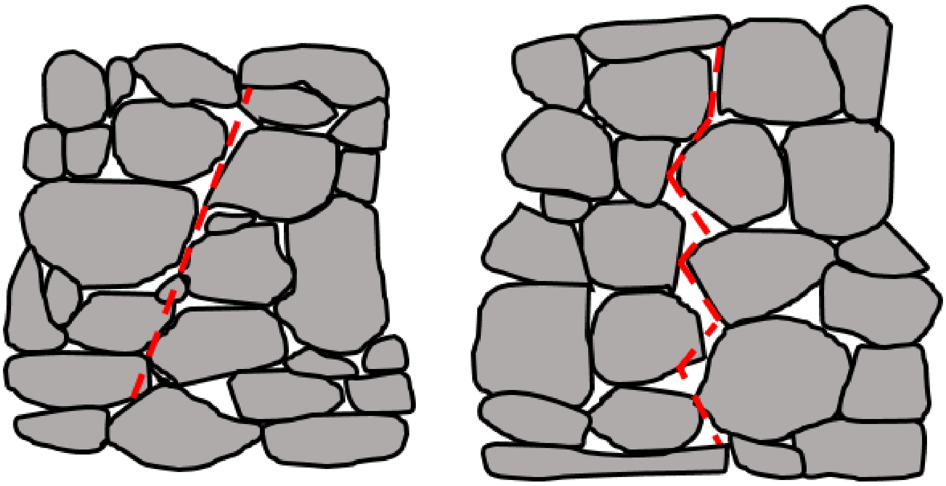

(A) (B)

FIGURE 2.2: Examples of (a) diagonal joints and (b) zipped joints that can occur in a drystone retaining wall system.

system but are present due to not enough material overlapping the below run. An example of a zipping joint is presented in Figure 2.2b.

Research conducted on dry stone walls typically takes form as a retaining wall analysis. The first recorded experiments were presented in Burgoyne (1853) in which 6m high walls of granite were tested under the loading of a backfill of uncompacted soil. The work examined the influence on the cross section of the wall. Burgoyne (1853) has been highly valued in the research of dry stone walls and has been used to validate studies in other work (Harkness et al., 2000), however the experiments conducted can be classed as qualitative and lack essential data such as angle of friction of the backfill or contact friction between the blocks of the wall. Additionally, the construction method and failure modes of the walls are not stated. Nevertheless, the work is considered a good first step.

Mundell et al. (2010) tested four full-scale drystone retaining walls under loading from a granular backfill to analyse bulging deformations from horizontal forces. Each wall was constructed using different techniques. For example, test wall 1 was constructed to replicate a well finished and tightly-packed DSRW whereas test wall 3 was designed to encourage bulging while limiting toppling. This was achieved by including a tapering to the wall but using rougher build quality and utilising comparatively smaller particles. The tests were conducted on walls with a height of 2.5m and a length of 12m and a platform to try and simulate the foundation of the wall. As with Burgoyne (1853), Mundell et al. (2010) applied a horizontal load to the wall. This was done in two ways. Firstly through the tilting of the platform on which the wall stood so the face of the wall is lowered to simulate differential settlement. Secondly, the application of a surcharge was applied to the backfill behind the centre of the wall by a suspended hydraulic jack. The walls failed due to bulging, as would be expected from the centralised loading case caused by the force from the hydraulic jack, and each showed horizontal displacements between 100mm to 200mm. Although all walls were tested in the same way, each had a different failure mechanism. Mundell et al. (2010) states that this means general material properties are not enough to predict failures of drystone retaining walls and that an understanding of the internal configuration is needed.

Villemus et al. (2007) completed experiments to assess dry stone walls as a retaining structure. Wall materials used were limestone from the local quarry and schist from St. Germain de Calberte. Theoretical approaches are outlined, but Villemus et al. (2007) goes on to state that a method based on experimental observations is preferred. The paper is made up of three parts. The first presents the work conducted in laboratory experiments completed on the material that makes up the wall. The purpose of these experiments was to analyse the mechanical behaviour. Direct shear box tests were conducted between two individual stones and between two beds of stone at sizes of $6x6cm^2$, $30x30cm^2$ and $100x100cm^2$. All produced a similar shearing resistance leading to only the $6x6cm^2$ shear box test being performed on the St. Germain de Calberte limestone due to the conclusions of the previous tests. For completeness, this test could have been carried out using different shear box sizes to ensure similar friction angles are produced. The next part describes the theoretical model proposed by Villemus et al. (2007). The model takes the wall as a homogeneous structure on a rigid foundation and differs from Burgoyne (1853) and Mundell et al. (2010) as it considers the characteristics of the material. The third part of the paper describes full-scale experiments used to validate this model. In-situ loading was completed on three drystone walls of 2m height and two of 4m height. Villemus et al. (2007) states that each was constructed by skilled masons using current and traditional approaches. Therefore it can be assumed that there is minimal error in construction when it comes to thinking about defects that could lead to areas of low strength in the wall. Unfortunately, Villemus et al. (2007) does not describe the difference between current and traditional methods, or go into detail over the construction of the different test walls.

From the reported five retaining walls that were tested, only one example is reviewed in full in Villemus et al. (2007) with details from before and after experimental testing. This wall is presented in Figure 2.3. Loading was completed using a PVC-lined bag that was filled with water to apply a hydrostatic pressure behind the wall. The use of water meant a more predicable loading case than the use of granular backfill. Hence more focus could be placed on internal shear strength of the drystone wall. Sensors attached to the wall were used to measure displacement. Given the time in which it would take to construct each wall, the limited number of tests completed is a fair amount to validate the model. However, as stated in Mundell et al. (2009), the use of short, free-standing test sections may have caused an issue with the behaviour of the walls due to the end effects of the structure. The analysis in Villemus et al. (2007) describes the internal mode of failure by shear and explains that this occurs by rotation of the stone particles to create a failure slope in the wall at which slip failure occurs. Of the measured walls, the theoretical failure slope and stone rotations were similar, with the maximum difference being 2^o and the theoretical value always being less than the value measured in the experiment.

It can be understood that drystone walls are going to be strong in compression and weak in shear. This is why the majority of research conducted on drystone walls focus on shear strength along the horizontal plane of the wall. Shear strength out of the horizontal plane has been tested using a tilting table method. Santa-Cruz et al. (2021) tested drystone walls with a height of 1.5m, length of 6m and a trapezoidal cross-section using a tilting platform. The aim of the research was to try and imitate the typical drystone wall structures found in Latin America. Nine scale specimens

FIGURE 2.3: An example of a constructed drystone wall from Villemus et al. (2007) before loading (left) and then after (central and right). Reprinted from Villemus et al. (2007) with permission from Elsevier.

were built with regular cobblestone blocks and irregular stone blocks. Examples of the specimens produced in Santa-Cruz et al. (2021) are presented in Figure 2.4. Rope was used in tension at the ends of some stone block specimens to anchor the wall and to replicate boundary restrictions when testing. Walls were loaded by gradually increasing the angle of the tilting platform from the horizontal by increments of 0.5^{o}. Coordinates at the left, centre and right of the wall were recorded and the test was continued until the wall collapsed. The regular cobblestone blocks collapsed at angles at around 19^{o} and, of the three tests, two of them presented a uniform 2D behaviour and all failed by toppling. The irregular stone blocks collapsed at an angle ranging from 13.5 - 15^{o} and failed by bending, starting in one location before extending along the wall. Tests undertaken with restricted ends had greater angles of failure, ranging from 18 - 21.5^{o}, and failed due to rotation of the blocks which led to a bending-like behaviour. As stated by Santa-Cruz et al. (2021), this behaviour is caused by contact forces and the lateral restrictions.

Other literature has covered testing a retaining wall using a tilting plate. Restrepo Vélez et al. (2014) used a tilting table on scaled drystone masonry walls made of marble. The research conducted found that the experimental mechanisms of failure are much more complex than the theoretical ones predicted. Restrepo Vélez et al. (2014) notes that for many cases explored, sliding and rotation of different sections of the wall occur not only along clear, sharp single lines as implied by underlying models, but also in a more distributed way. This is for both overturning facades and in return walls. The testing of a return wall is presented in Figure 2.5. Additionally, most of the failure mechanisms in Restrepo Vélez et al. (2014) are forms of hybrid mechanisms rather than a single, distinct mechanism. This is due to the fact that dry masonry walls have more internal kinematic degrees of freedom than what is assumed in most theoretical models. Grillanda et al. (2021) used a tilting table on essentially 2D problems using scale models of dry joint clay bricks. The tilting table was used to test them under shear. It was found that imperfections on the bricks (bricks with shapes not perfectly rectangular) resulted in less shear resistance due to the contact areas being variable.

(A)

(B)

(C)

FIGURE 2.4: Different specimens experimentally tested by tilting table in Santa-Cruz et al. (2021). (a) Cobblestone block specimen with unrestricted ends (b) Stone block specimen with unrestricted ends (c) Stone block specimen with restricted ends. Reprinted from Santa-Cruz et al. (2021) with permission from Elsevier.

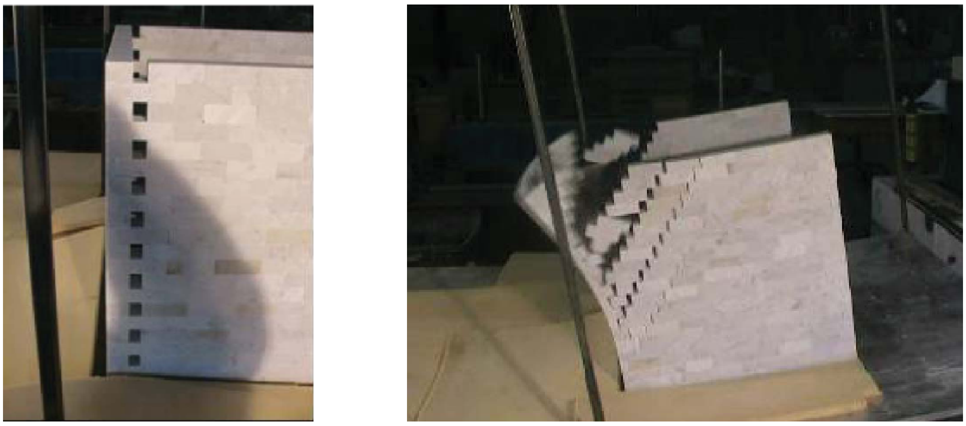

(A) (B)

FIGURE 2.5: Testing of a return wall as presented in Restrepo Vélez et al. (2014) (a) before testing (b) during testing at failure © Taylor & Francis with permission granted.

The typical cause of failure in a retaining wall comes from the lateral pressures imposed on the wall by the supported soil, any surcharge loads at the top of the structure, and hydrostatic pressures (Fontanese, 2007). One of the benefits that comes with drystone walling is the ability for water to flow through the structure thanks to the lack of mortar between stones preventing the build up of hydrostatic pressure. As described by Warren et al. (2013), it is common to grout drystone walls either to prevent movement of the wall or to protect the base from salt spray. Doing so blocks the drainage paths meaning water cannot easily pass through the system creating great loads on the back of the wall. Additionally, Warren et al. (2013) states that grouting of a wall will also reduce its flexibility. From this, the wall cannot redistribute load concentrations due to the reduced ductility of the structure. Hydrostatic pressure buildup can lead to catastrophic failures of retaining walls. Typically for retaining walls that are not drystone, paths made of a free-draining backfill material are utilised directly behind the wall for water to be directed through a weep-hole (Fontanese, 2007).

2.2.2 Retaining Walls of the Incas

Examples of geotechnical structures made from granular material are commonly found in the structures built by the Incas in South America. Areas like Machu Picchu in Peru are well known for their sprawling retaining wall systems which are constructed using tooled stone blocks. The age of these walls are more than 500 years old and many are still in good condition despite a lack of maintenance (Castro et al., 2017). The most impressive of these structures is the fortress of Sacsayhuaman which lies on the northern edge of Cuzco. The wall can be seen in Figure 2.6a. It is thought that this was constructed during the reign of Pachacuti between 1438-1471 (Cartwright, 2016). The walls of Sacsayhuaman are made up of massive pieces of stone shaped to fit together perfectly. The exact strength of these walls is not known, but the longevity of the walls and the fact that they are still standing suggests a high strength. The structure is created with minimal gaps between stones, suggesting that a lower void ratio may lead to an increased shear strength. This is shown in Figure 2.6b.

(A) (B)

FIGURE 2.6: Retaining wall structures located at Sacsayhuaman (A) © Diego Delso (B) © Alison Ruth Hughes. Photos used under the Creative Commons Attribution-Share Alike 4.0 license conditions (Creative Commons, 2013c).

Fontanese (2007) describes the walls built by the Incas to be constructed with backfilled layers of soil that increased in coarseness with depth. The increase of coarseness is stated to prevent topsoil from washing away as the material acts as a filter. The walls studied in Fontanese (2007) are drystacked walls that do not perfectly interlock. However, Fontanese (2007) describes that those which do perfectly interlock, such as the wall structures seen at Sacsayhuaman, were provided with weepholes to allow for drainage of water and to prevent the build up of hydrostatic pressures. The walls studied by Fontanese (2007) at the Incan site of Machu Picchu are described to have several layers of soil as a backfill. These were made of a base of gravel beneath a layer of fine sand and gravel. This is then capped with a topsoil for the growing of crops. The stacked stones used to make up the wall stucture continue below grade to act as a foundation system (Fontanese, 2007).

Vallejo and Fontanese (2014) analyses the stability of retaining walls built by the Incas in the area of Moray by looking at sliding and overturning failures as these are the two most common faults in retaining walls near the citadel of Machu Picchu (Wright and Zegarra, 2000). Each wall ranged from a height of 1.5m to 7m and are described by Vallejo and Fontanese (2014) to be made up of "prismatic stones measuring each between 70cm to 1m in length, 30cm to 1m in height and 1m in depth". Vallejo and Fontanese (2014) does not make it clear if this means all particles are 1m in depth into the wall or if the depth ranges from 30cm to 1m. The latter is assumed. The backfill consisted of crushed stones and sand. Vallejo and Fontanese (2014) states that a large part of the stability from the retaining walls constructed by the Incas is most likely due to the ability for water to flow with ease through the granular backfill and between the stones in the wall due to their rough interfaces between pieces. It should be noted that the walls assessed in Vallejo and Fontanese (2014) are not tooled to fit together like those for Sacsayhuaman but are similar to Fontanese (2007) where stones do not perfectly interlock. Another main reason for stability is due to the large sizes of the stones and the weight of these helping prevent against sliding and overturning.

Castro et al. (2017) analyses 10 Incan retaining walls through a DEM study. The work was also repeated in Castro et al. (2019). The walls were located in the Lower Agricultural Sector of Machu Picchu, Peru. Google Street View and Google Earth Pro images were used to identify the composition of the stone blocks. It is not possible to test the materials used to make up the wall as they are protected structures.

Therefore estimated values were adopted (taken from West, 2010 as cited by Castro et al., 2017). The DEM approach was used to analyse sliding and overturning failure mechanisms for one of the walls located at Machu Picchu. Figure 2.7 shows images presented in Castro et al. (2017) of the wall tested and the DEM simulation. Due to the large range in block sizes, the factors of safety calculated in Castro et al. (2017) resemble those that are found in geotechnical design standards.

Obviously, there are questions about the accuracy of these results due to inability to test the materials. However the outcome of this research demonstrates that the arrangement of blocks in structures such as the walls found in Machu Picchu and Sacsayhuaman have high strength values. Castro et al. (2017) suggests that the retaining walls are not only functional but also highly optimised because of the calculated factor of safety being close to 1.5. As referenced by Castro et al. (2017), this is the value recommended for factor of safety in modern geotechnical design standards in North America. This is most likely from a trial and error design procedure. From this case study it can be concluded that reducing the amount of void space between particles could potentially lead to a higher strength in a packing arrangement and may be a favourable type of system to target.

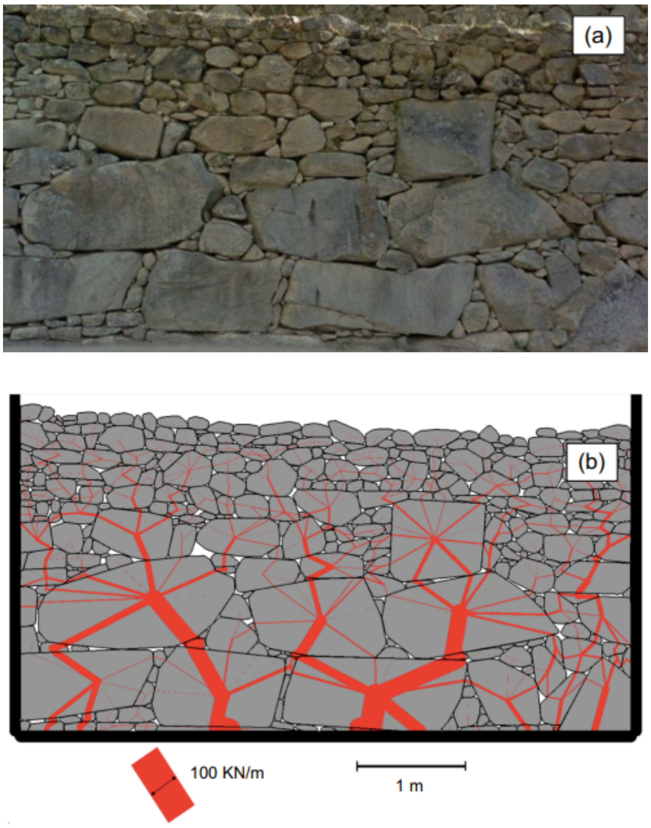

FIGURE 2.7: (a) Incan retaining wall in an agricultural terrace and (b) the DEM simulation of the wall. Red lines indicate the force paths through the wall with the width of the line indicating the magnitude as presented in Castro et al. (2017). Used under the Creative Commons Attribution 4.0 license conditions (Creative Commons, 2013c).

As mentioned in Section 1.1, Clifford et al. (2018) investigates tooling construction demolition waste (CDW) by robot to be constructed into a wall based on the techniques found in the historic structures within Peru such as Sacsayhuaman. The aim of Clifford et al. (2018) was to reuse the waste material, or to "cannibalise" it back into another architectural structure. Clifford et al. (2018) describes features of the Incan structures. The first of these are bed joints. Clifford et al. (2018) explains these to be horizontal joints carved into the rock underneath where a rock is to be placed. The bottom of the yet to be placed rock is also carved to be horizontal so that when it is put into position both rocks sit perfectly together with no gaps inbetween. Another of these features described in Clifford et al. (2018) are draft angles. These are located when a stone is of trapezoidal shape and the outline of the sides tends away from a vertically straight line. These can be located in a wall and are seen as starting points for building of a layer. Clifford et al. (2018) states that these rocks not only help describe the sequence of the wall but also the magnitude of the angle can determine how the stone was placed. These features were taken into account to create a prototype from scanned and digitally processed CDW. Rocks are placed within a virtual simulator manually by a designer with the ability to change location and orientation of the CDW. The virtual simulator creates polygons out of the stones and can determine where carvings are required to cut the stone so that each piece fits to create the wall. A stability check is performed as a final step. The prototype within Clifford et al. (2018) is cut by a six-axis robotic arm upon a rotary table and the pieces were assembled by a team of workers following the construction order produced by the virtual simulator. No structural assessment was performed on the wall but the prototype was able to support itself. As stated in Section 1.1, 73% of the stock material was retained for construction (Clifford et al., 2018).

2.2.3 Japanese Castle Walls and Foundations

Walls and foundations of Japanese castles are good examples of other structures that have used stone and rock pieces in a system with minimal void. These range from being built in the 16th and 17th centuary and it is not uncommon for several of these structures to have experienced earthquakes and still appear to be structurally sound. Nishida et al. (2005) describes the walls of Japanese castles to be made up of stones piled without any mortar or plaster. The size of the stones used ranges from small to extremely large. For example, the wall near Cherry Blossom Gate at Osaka Castle consists of a stone so large that it is not known how it was moved into position (Fujioka, 1969). It is stated by Fujioka (1969) that the size of this stone provides no real practical purpose. It could be that a stone this large was just used for aesthetic reasons or ostentatious display.

Stones of the wall in the castles found in Japan tend to be inclined so that the major principal axis is orthogonal to the local tangent of the curved profile to maximise shear strength (Utili and Nova, 2007). Hikone castle is an Edo-period construction located in Japan. It was built in the early 1600s and is said to have taken 20 years to construct (Hikone Sightseeing Association, 2017). The castle sits on a raised foundation made up of gravel and cobble pieces of various size. The placement of these are an example of that described in Nishida et al. (2005) and particles are positioned so that a minimum void ratio is achieved in the structure. As far as the author is aware, there is no current literature discussing the foundations of Hikone castle. Images of the castle and its foundations are presented in Figure 2.8. It is not known what is behind the surface of the particles - whether this be a continuation of the pattern of minimal void, some sort of backfill, or if this is a facade for a different structure or a pre-existing rock foundation on which the castle was built. However, the foundations have stood for 400 years and if it is assumed that this is due to the minimum amount of voids in the structure, it can be seen as similar to the structures discussed in Section 2.2.2 such as Sacsayhuaman. The castles in Japan with their walls made up of stone pieces are so renowned for their structural integrity that stone is used in Japanese as a synonym for "strength" or "firmness" (Fujioka, 1969).

(A) (B)

FIGURE 2.8: (A) Hikone Castle and its foundations and (B) a closer view of the foundations. (A) Photo by Philbert Ono. (B) Photo from Japan Experta website Murselovic and Godefroid (2019). Both photos used under the Creative Commons Attribution-Share Alike 3.0 license condition (Creative Commons, 2014).

Nishida et al. (2005) specifically looks at Osaka castle as it has the tallest wall among castles in Japan, standing at 32m tall at the maximum and 12km in length (Amano et al., 2000 as cited by Nishida et al., 2005). The outside wall consists of a similar makeup to the foundations of Hikone Castle with stones and rock creating a system with minimal voids inbetween. Nishida et al. (2005) describes the structure to be made from wall stones and cobbles with a backfill behind the wall and then the original ground. This description is very similar to those given to the Incan retaining walls in Vallejo and Fontanese (2014). It is to be assumed that this is the same for the foundation walls of Hikone Castle. For Osaka Castle, the wall stones and cobbles are made up of granite and the layout of the wall stones is described as "sangi-zumi" at the corners. Nishida et al. (2005) explains that this is when the wall stones are layered one above another in an alternative fashion. Figure 2.9 shows an example of the sangi-zumi pattern using rectangular blocks and Figure 2.10 is an image of Marugame Castle where this layout of stones is used at the corner of the castle walls. This "sangi-zumi" effect is commonly seen in many UK masony structures as well as in drystone walls as described by Vivian (1976) as discussed in Section 2.2.1.

The layering of stones above each other in the manner exhibited in Figure 2.9 and Figure 2.10 creates a more stable structure that exhibits stability in three dimensions. The overlaying pattern will mean more chance of particles interacting and interlocking with each other rather than blocks flush against each other on the same layer. An FEM analysis model was created to test the wall and it was found that the wall surface was mainly subject to compression forces both in the vertical and horizontal directions. Nishida et al. (2005) also presented work of field measurements on one of these castle walls. This was possible due to the reconstruction of Margame Castle wall that was rebuilt from its existing 15m to be 20m tall. Measurements were taken during the construction period at heights of 6.5m and 15m from the base. The strain readings from this study confirmed that the forces experienced in the wall were all compressive and act in the longitudinal direction.

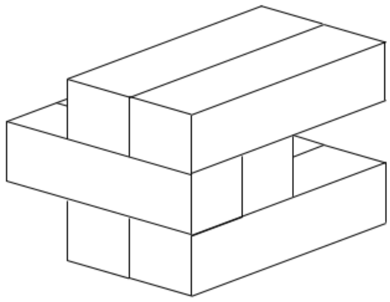

FIGURE 2.9: Example of rectangular blocks in the sangi-zumi pattern found at the corners of walls in Japanese Castles as described by Nishida et al. (2005).

FIGURE 2.10: Example of castle walls meeting at a corner at Marugame Castle. © Motokoka Photo used under the Creative Commons Attribution-Share Alike 4.0 license condition (Creative Commons, 2013c).

Utili and Nova (2007) use the cross-sectional profile of Osaka castle wall from the work produced by Nishida et al. (2005) and show that the shape of the wall mimics that of a log-spiral profile which was found to be more stable than a plane slope. However, it is thought that this matching of shape was more likely due to intuition, experience and aesthetic purposes rather than a fundamental knowledge of the problem (Utili and Nova, 2007). It should be noted that not all walls of Japanese castles analysed in the work were found to fit the spiral profile.

As well, Utili and Nova (2007) state that as the stability of the walls rely on shear resistance then these can be characterised by a Mohr-Coulomb failure. In addition, it claims the masonry must also be characterised by an overall cohesion-effect which results in a larger overall wall strength than would be expected in a purely frictional-based structure. It is theorised that this is due to the finite size and prismatic shape of the stones used and the dispersed nature in which these different sizes are found. As with Utili and Nova (2007), Fujioka (1969) agrees that the knowledge of construction for these impressive structures do not come from a technical knowledge but from experience. The layout of the stones in the wall appear random and haphazard, but the consistency of this construction method suggests that was purposefully intended.

Fujioka (1969) describes Kumamoto Castle as an example of the engineering skill at work in these constructions. It is stated that the main tower of Kumamoto Castle has very gently curving slopes extending to their wide bases. However, the watching tower of Kumamoto Castle has steeper walls and is less curved. The difference in these constructions are due to the fact the weight of the watching tower is much less than the main tower of the castle which the builders have taken into consideration. In addition, the main tower normally stands at the highest point and is therefore further from the substratum compared to structures like a watching tower. Therefore, the bases tend to be wider to help support the structure. Fujioka (1969) goes on to conclude that the manner of construction of the stone walls can be used to determine the firmness of the substratum below the castle.

2.2.4 Autonomous Construction of Irregular, Untooled Rock

Autonomous construction of irregular shaped particles is an area of research that has already been mentioned in Section 1.1. Focus of this research has been on stacks of stones or wall structures and particles used are all of similar size. As seen in Johns et al. (2023) and discussed in Section 1.1, autonomous construction is becoming a viable method for creating structures like drystone walls out of rock and gravel. Furrer et al. (2017), Johns et al. (2020), Johns et al. (2023), and Liu et al. (2021) focus on placement determined by identification of poses - stable positions detected on the surface of already placed particles or starting surface - with the best position being determined as that which has the highest “goodness of fit”. Placements are first calculated in a physics simulator to ensure stability before moving to an experiment replicating the patterns developed by the algorithms presented. For example, Furrer et al. (2017) produces a cost function evaluating “goodness” of each pose based on four criteria for the construction of stacks of single particles. These are

1. Contact area of the stone upon the surface it is being placed [C_i^{-1}]
2. Kinetic energy of the particle. While this is not specifically described in Furrer et al. (2017) it is thought that this relates to the measured kinetic energy from the movement of already placed particles caused by the placement of the current particle [$E_{kin}\ (P_i)$]

(A)

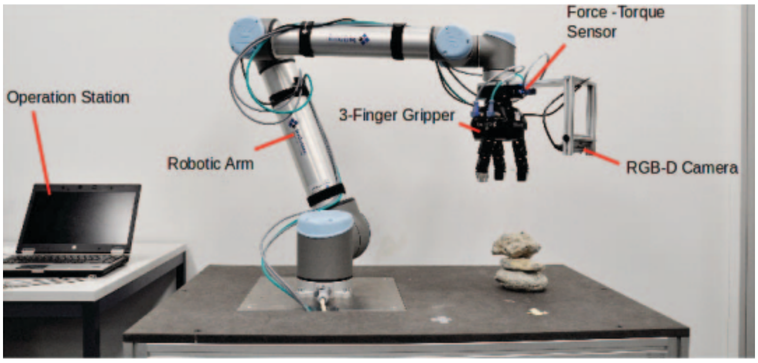

(B)

FIGURE 2.11: Images of (a) irregular lime stones stacked by (b) the robotic arm with three-fingered gripped from Furrer et al. (2017) © 2017 IEEE.

3. Length between newly placed object pose and the previous object placed as a centroidal distance $[\left\|\mathrm{r}_{P_jP_i}\right\|]$
4. The deviation of the normal to the surface compared to the thrust line, which is in the direction of gravity as self weight is the only force acting upon particles $[\|\mathrm{n}_i \cdot \mathrm{v}_i\|]$

and are represented as the cost function by the equation

$$f\left(P_i\right) = w_1 C_i^{-1} + w_2 E_{kin}\left(P_i\right) + w_3 \left\|\mathrm{r}_{P_jP_i}\right\| + w_4 \left\|\mathrm{n}_i \cdot \mathrm{v}_i\right\| \tag{2.1}$$

Each criteria is given a weight, which in Furrer et al. (2017) are manually selected. As described in Section 1.1, Furrer et al. (2017) stacked stones using robotic arm at a desktop scale. The six stones used are presented in Figure 2.11a and the robotic arm that experiments were conducted with is presented in Figure 2.11b. As stated previously in Section 1.1, tests were conducted using sets of four stones to create eleven towers. For two of the runs, all four stones were stacked successfully. Three stones were stacked in six instances but failed on the fourth stone and in three cases the third stone was not stacked successfully.

Liu et al. (2021) takes the same system for scoring placement as Furrer et al. (2017) with the use of a cost function. However, weightings were determined using a Bayesian optimisation. Additionally, as stated by Liu et al. (2021), the deviation of the normal to the surface compared to the thrust line decreases the cost function as it increases. Therefore this criteria is edited to be represented by $\|\mathrm{n}_i \cdot \mathrm{v}_i\|^{-1}$. Furthermore, Liu et al. (2021) also simulated and then produced wall structures of the stones. The heuristics of this are different to that of a tower of single stones which will only require stability along the central axis. Instead, Liu et al. (2021) creates a "hierarchical filtering approach" which applies conditions to each pose position for which the pose must meet to be deemed a suitable pose. These conditions are as follows and applied as filters to the potential pose locations in the order that they are presented.

1. The slope of the top surface must be inward so that the widest part of the wall is at the base
2. The deviation of the normal to the surface compared to the thrust line must be above the mean from the results of all possible poses
3. The contact area of the particle with the surface must be above the mean of all stable poses.
4. Unless the object being placed is a corner stone, the centroid height must be lower than the average of the centroid heights of the corner stones and already placed objects for the current layer being created. This is to ensure a layer by layer construction.
5. The number of interlocking objects for the pose must be higher than the mean number of interlocking for the other poses.

Liu et al. (2021) states that the use of a hierarchical filter heuristic rather than a scalar cost function eliminates the need for relative weights. The assessment of each requirement for the object being placed in isolation is less sensitive to the change of the physical properties of the object.

In Johns et al. (2023), as discussed in the Section 1.1, drystone walls were constructed autonomously by a HEAP platform robot with two-finger gripper. The work in Johns et al. (2023) carries on from Johns et al. (2020) which built small sections of drystone walls. Both Johns et al. (2020) and Johns et al. (2023) use the same technique and methods for construction and both use a HEAP robot. Similar to Furrer et al. (2017) and Liu et al. (2021), Johns et al. (2020) and Johns et al. (2023) both rely on detecting possible poses for placement of stones via LiDAR scanning of construction material as well as the landscape and already positioned objects. Like Liu et al. (2021), Johns et al. (2020) states that the work conducted in the research uses heuristics from conventional stone masonry techniques. The scoring of placements is ranked by minimising space between already placed stones and the outlined exposed stone face and geometry of the wall to be constructed. Therefore the suggested heuristic of avoiding the creation of runs from Vivian (1976) is excluded.

Candidate positions for placement of stones are found by searching the top-most geometry of already placed stones and starting surface, referred to as the upper surface in Johns et al. (2020). This upper surface is modelled as a single continuous surface across the wall. Fits are counted as locations where the volumetric space for the position is large enough for the stone to fit. These are attempted at different orientations of the stone. These fits are taken forward and a simple stability heuristic

(A)

(B)

FIGURE 2.12: Construction of wall in progress from Johns et al. (2020) for (a) 2 stones placed and (b) 20 stones placed out of the 40 in the experiment. Images used under Creative Commons Attribution 4.0 International License (Creative Commons, 2013c).

FIGURE 2.13: Construction of the wall in Johns et al. (2020) with placed stones with overlay of potential extension of structure. Image used under Creative Commons Attribution 4.0 International License (Creative Commons, 2013c).

is completed. If stones are placed on their narrowest dimension, these are deemed likely to be unstable. Therefore, this stability check consists of ensuring the horizontal dimension (d) and vertical dimension (h) are in a ratio greater than 0.5 ($d/h > 0.5$). After these checks, the actual position of the stone is located rather than a rough estimate through RANSAC-based 3D plane fitting. A stability check is conducted in the Bullet physics engine and solutions that cannot reach equilibrium are classed as unstable and not carried forward. Finally, each position is scored using a combination of reducing volume below the stone between itself and the upper surface and reducing the volume between the stone and the outline of the desired wall geometry. The best match is that with the highest score and is sent to the HEAP robot for physical placement. In Johns et al. (2020), a 3m by 5m test wall was constructed using 40 gneiss stones. Figure 2.12 shows the construction of the wall by the HEAP robot in process. Figure 2.13 presents the wall being constructed at a later stage, with an overlay to demonstrate where further extension of the wall construction could take place. As described in Section 1.1, the freestanding wall was 10m in length and 4m in height and constructed using 109 gneiss boulders and CDW stones and the retaining wall constructed was 65.5m long, consisting of 938 irregular stones and CDW stones. Work in Johns et al. (2020) and Johns et al. (2023) prioritises minimising void space between particles rather than any heuristic to try and quantify the benefits a placement will lead to in terms of additional strength to the structure.

The robots that are adopted in the literature reviewed in Section 2.2.4 are all completed using a top-down approach by an anthropomorhpic arm. Particles are grasped by a two or three finger gripper and are lowered to be placed in the desired location. For this project, it is assumed that a top-down approach will also be adopted. This assumption is highlighted here as this means there is no lateral movement of the particle when being placed by the algorithm.

2.2.5 Summary of Section 2.2

This section gives an overview of the various examples of structures and construction processes using granular materials. Section 2.2.1 gives examples of a structures constructed using gravel and larger stone pieces in the form of drystone walls. As described, drystone retaining walls are very strong in compaction but have a much lower strength in the shear plane. However, the structures give an idea of how a system could be created out of particles such as the stones and cobbles that make up a DSRW and the sort of packing that could be utilised. Typical DSRW construction techniques position particles in flat layers, building vertical with little interlocking between these layers. A crossing-over pattern is exhibited at the corner of these systems which was also found in Japanese castles and described as "sangi-zumi" as described by Nishida et al. (2005).

Sections 2.2.2 and 2.2.3 further highlight this with examples of retaining structures located in South America constructed by Incas and various historic castles found in Japan. These structures have been present for hundreds of years and are still standing, proving the quality of their construction methods. Incan retaining walls are tooled so that pieces fit together with essentially no void between particles and the walls present in Japanese castle constructions have soil particles placed so that minimal void is present. Both of these would suggest that a beneficial technique would be to minimise void ratio between particles in the construction of a structure if the desired outcome is one of high strength.

Section 2.2.4 explores current work into the area of autonomous construction using irregular particles by robot. The focus in these research projects has been using a heuristic approach focused on optimising how well a stone fits into the upper surface of the already placed particles. In addition to this, heuristics for the energy required to move the placed particle, lengths between newly placed objects and previously placed object and deviation of the normal to the particle contact from the thrust line are considered as seen in Furrer et al. (2017). Further criteria were set out in Liu et al. (2021) as filters for poses when designing for placement in a wall system as described in Section 2.2.4. Johns et al. (2020) introduced a stability check that consisted of ensuring the horizontal and vertical dimensions of a stone are in a ratio greater than 0.5 when considering a pose with any poses not meeting this criteria being discarded to save on computational time. The work in Johns et al. (2023) provides evidence that the autonomous construction of irregular rock particles by robot is indeed possible and that the production of an algoirthm for scoring placement in order to optimise shear strength is indeed a feasible solution to potentially improving these structures.

2.3 Parameters Affecting Soil Strength

2.3.1 Soil Strength

Shear strength of a soil is described as the ability of the soil to resist shear due to the interparticle friction and interlocking grains in the material (Terzaghi and Peck, 1967). In a granular material that lacks cohesion, the shear strength can be characterised by

$$s = \sigma' tan(\phi') \tag{2.2}$$

where s is the shear strength, σ' is the effective normal stress on the failure plane, and ϕ' is the effective stress angle of internal friction (Duncan et al., 2014). This is in accordance with Coulomb. Values for angle of internal friction can have a large range depending on the material and many other factors that are going to be explored in this section. Duncan et al. (2014) reviewed existing literature and collated results from experiments conducted. Ranges of 34-48^o, 41-58^o and 51-55^o for ϕ were presented for sands, gravels and rockfill respectively. The purpose of this table was to show reasonable values that would be expected from testing, and it is for this reason that the data has been presented here. Terzaghi and Peck (1967) gave representative values of ϕ and these are presented in Table 2.1.

Material	Loose (^{o})	Dense (^{o})
Sand, round grains, uniform	27.5	34
Sand, angular grains, well graded	33	45
Sandy gravels	35	50
Silty Sands	27-33	30-34
Inorganic silt	27-30	30-35

TABLE 2.1: Representative values of ϕ for sands and silts (Terzaghi and Peck, 1967).

2.3.2 Particle Shape and Roughness

It is known that the particle shape has an effect on the shear strength of soil. For example, Vallerga et al. (1957) states that shear strength appears to increase considerably with angularity of the particles. However, it is stated part of the increase may be due to a larger amount of surface roughness as the angularity was increased by crushing of particles. Koerner (1970) also shows that granular materials containing particles with an angular nature tend to have higher shear strength. Selig and Roner (1987) and Li et al. (2013) found that an increase of flaky and angular particles increases the shear resistance of a soil. Xiao et al. (2019) investigated the response of sand mixtures of round and angular shapes using triaxial testing. It was reported that an increase in overall regularity resulted in a reduction of both the peak-state and critical-state friction angles, indicating shear strength increases if the particles are more irregular.

Cho et al. (2006) used a large database of sand to look at the influence of particle morphology on stiffness and strength. Particles were characterised using 2D images of the sand. It was concluded that as particle irregularity increases, the critical state angle of friction also increases. Alshibli and Cil (2018) expands on the work by Cho et al. (2006), investigating glass beads and three types of silica sands and characterising these in 3D using high-resolution SMT images. Form, roundness and roughness were investigated. As the particle gets more irregular (so form and roundness decrease and roughness increases), the critical state angle of friction increases, agreeing with Cho et al. (2006). Models were formed using the results of Alshibli and Cil (2018) and predictors to analyse critical state friction angle (ϕ_{cs}), peak state friction angle (ϕ_p) and dilatancy angle (ψ) were given as

$$\phi_{cs} = 23 - 134.06F_s + 142.04I_R - 21.02R_q - 0.861(\frac{p'_o}{p_{atm}}) + 0.043D_R \tag{2.3}$$

$$\phi_p = 23 - 62.90F_s + 67.00I_R - 9.02R_q - 0.932(\frac{p'_o}{p_{atm}}) + 0.160D_R \tag{2.4}$$

$$\psi = 77.72F_s - 76.35I_R + 12.77R_q - 0.486(\frac{p'_o}{p_{atm}}) + 0.196D_R \tag{2.5}$$

where F_s, I_R, R_q and D_R represent form, roundness, surface texture (specifically the root-mean-square of the surface texture found using an optical interferometry technique) and relative density respectively. $(\frac{p'_o}{p_{atm}})$ represents mean effective stress normalised by atmospheric pressure. These models give very good predictions when compared to the experimental measurements presented in Alshibli and Cil (2018) with the coefficients of determination being 0.93, 0.86 and 0.95 for ϕ_{cs}, ϕ_p and ψ respectively.

Huu et al. (2017) conducted direct shear tests on silica sand and calcareous sand to compare the two. Calcareous sands are described by Huu et al. (2017) to be very angular and can exist at a higher void ratio than silica sands. Calcareous sands tend to exhibit a higher shear strength (Brandes, 2011; Cabalar et al., 2013; Hassanlourad et al., 2014) and show dilative behaviours at much lower relative densities than the smoother silica sands (Safinus et al., 2013). Huu et al. (2017) describes this behaviour to be due to the interlocking between aggregates created by their angular particle shape. The restriction on rotation and movement on the particles lead to an increase in shear strength which is a result of the increase in interparticle contacts (Brandes, 2011; Potticary et al., 2016).

At initial relative densities of both 40% and 80%, silica sand had lower shear strengths and friction angles at the peak and residual states than calcareous sand which was produced to have the same particle size distribution as the silica sands. Furthermore, even though calcareous sands showed higher shear strengths, the silica sand tested reached higher stresses at a small shear strain at the early stages of testing. Huu et al. (2017) suggests that this is because the shearing is what causes the particles to interlock with neighbouring particles which then initialises an increase in the shear strength, especially during the dilation process of the sand. This does not really explain the described phenomena and Huu et al. (2017) does not go into any more detail for the explanation beside what has already been stated. However, it is thought that perhaps the particles in the more angular systems have more spacing between them to move and rotate initially before becoming securely interlocked with each other. Direct shear tests were also completed on samples of calcareous sand with different values of sphericity. The results show that the residual shear strength and friction angle decrease as sphericity increases. According to Rowe (1962), interparticle friction, particle rearrangement and dilation - as well as crushing - all have major contributions to shear resistance of granular soils. It can be envisioned that angular particles at a higher density would have more interlocking between particles, which would require more particle rearrangement and therefore more dilation of the assembly.

Santamarina and Cho (2004) supports Huu et al. (2017) in terms of interlocking of particles as they hypothesised that increased angularity will make it more difficult for the particle to rotate. Additionally, roughness of the surface will prevent slipping between grains. Both of these features would create a greater need for dilation and contribute towards shear strength. Experimental evidence was presented in Santamarina and Cho (2004) showing that the critical angle of internal friction, ϕ_{cv}, decreases as roundness increases. Similarly, Yang and Luo (2015) conducted tests on fujian sand and fujian sand mixed with either round glass beads or angular crushed glass beads. Shapes of the grains were analysed and ϕ_{cv} decreased as roundness increased. Yang and Luo (2015) states that this is consistent with Cho et al. (2006) and Rousé et al. (2008). Chan and Page (1997) also provides evidence for this as they showed copper powders with a higher fractal dimensions had an increased angle of internal friction.

Guo and Su (2007) conducted triaxial tests on Ottawa sands and crushed angular limestone. Both samples were uniformly graded. Guo and Su (2007) concludes that shear strength is increased by the interlocking of particles which is more likely to occur in angular shaped soils. However, it should be noted that the particle sizes of the samples were massively different with D_{50} values of 0.376mm and 1.640mm for the Ottawa sand and the crushed limestone respectively.

Xiao et al. (2019) found that maximum dilatancy angle increased as overall regularity increased, which contradicts the idea that more angular particles will interlock and be harder to move. However, as stated in Xiao et al. (2019), these greater dilations are experienced at smaller strains whereas assemblies with more spherical particles dilate less overall at critical state compared with angular particles. Therefore these spherical particles are more readily available to move and do not contribute as much to the shear strength of the system. This is a similar explanation to the one suggested for the phenomenon described by Huu et al. (2017).

Roughness of a particle refers to the small asperities of the surface and is thought to have a major effect on interparticle friction. As stated in Rowe (1962), interparticle friction is thought to have a large effect on shear strength of granular soils. Santamarina and Cascante (1998) conducted triaxial tests on ball bearings with varying surface roughness and suggests that constant volume critical state friction angle, ϕ_{cv}, increases with roughness. This agrees with Bishop (1954) who derived a relationship for ϕ_{cv} and interparticle friction angle ϕ_μ,

$$\sin(\phi_{cv}) = 15\tan(\phi_\mu)/(10 + 3\tan(\phi_\mu)) \tag{2.6}$$

This leads to having an effect on the shear strength, as

$$\phi_{max} = \phi_{cv} + 0.8\psi_{max} \tag{2.7}$$

as presented in Bolton (1986), where ϕ_{max} is maximum angle of shearing resistance and ψ_{max} is maximum dilatancy angle.

Li (2013) tested 200 materials using a triaxial compression test. Grain shapes were characterised using two-dimensional angularity (A_{2D}) as proposed by Lees (1964) The materials were the same as those used in Miura et al. (1997b) which concluded that an increase in angularity led to an increase in void ratio extent (e_{max} - e_{min}) which represents the degree of possible change in the soil structure, as well as an increase in crushability index and angle of repose. Miura et al. (1998) showed that angle of internal friction at failure as well as ϕ_{cv} increased as A_{2D} increased.

Additional, the information presented in Table 2.1 listing typical values of internal friction angle for various sands and gravels shows that more angular materials (the angular sand grains and sandy gravels) tend to express a higher ϕ value. Li (2013) demonstrated that increasing elongation increases the constant volume friction angle and increasing convexity decreases this value. It was also found in Li (2013) that samples with a high proportion of coarse fraction experienced dilation due to particle interlocking while samples with a high proportion of fine fraction experienced volumetric contraction due to particle alignment and densification.

With the aim of producing a low cost solution in terms to the environment, it is intended that this project will focus on using locally sourced material. Although it is clear that angular particles tend to exhibit higher shear strength values than more spherical particles, it will not be guaranteed that these particles can be sourced locally. Therefore, selection of the particle by shape will not be considered for this project. Rather, by measuring other factors than can be classed a result of particle shape - which are discussed in the following parts of Section 2.3 - particle shape will not need to be considered as an additional parameter of this study. It is possible that particles could be characterised before selection so that only angular particles are stockpiled for construction. This possibility is discussed further in Section 8.6.1.

2.3.3 Particle Size

There are many sources indicating that particle size has a direct influence on shear strength. Wang et al. (2013) shows that angle of shearing resistance generally increases as median particle diameter increases. Holtz and Gibbs (1956) tested different mixtures of gravel and sand and concluded that shear strength increases with gravel content greater than 50-60% by weight. Simoni and Houlsby (2006) found that strength of sands mixed with gravel have higher strengths than pure sand, even with low gravel fractions of 10-20%. Pakbaz and Moqaddam (2012) performed direct shear tests on sands mixed with clay and Alias et al. (2014) carried out direct shear tests on granular material described as a well graded gravel with sand. Both presented that shear strength increases with particle size.

Contrary to the references stated, Winterkorn (1967) states that the influence of particle size on shear strength is negligible. Rather, the change in particle size results in a change in surface characteristics and shape of the particle which in turn has an effect on angle of internal friction. Winterkorn (1967) uses Herbst and Winterkorn (1964) and Idel (1960) to support their argument. Additionally, Vallerga et al. (1957) conducted tests on subrounded and angular gravel under a vacuum triaxial test. It was found that uniformly graded materials did not appear to be affected by particle size. Selig and Roner (1987) and Latha and Sitharam (2008) also report that changing particle size gives no significant difference in shear strength. It should be noted that Winterkorn (1967) is considering an idealised soil consisting of particles of uniform size and shape. This is an unrealistic case, but does show that particle size does not have a direct effect on angle of friction. This is assuming that the testing apparatus is also scaled, as maximum particle size can have an effect on the results of the test (Erlingsson and Magnusdottir, 2002) which can sometimes be an explanation for the observed increase in shear strength with particle size.

As stated by Winterkorn (1967), a change in particle size can lead to a change in shape of the particles. For silica sands, it is seen that larger particles are mostly spherical whilst smaller particles have an increased angularity (Pettijohn and Lundahl, 1943; Pollack, 1961). As discussed in Section 2.3.2, an increase in angularity leads to an increase in soil strength. Results for different materials have shown no unique relationship between grain size and grain shape (Barrett, 1980; Cho et al., 2006; Das and Ashmawy, 2007).

Another possible explanation for the effect on shear strength can be found in Santamarina and Cho (2004). Santamarina and Cho (2004) states that larger particles have a higher probability of imperfections and brittle fracturing. Therefore, smaller particles are stronger due to their lack of imperfections. However, this would suggest the opposite of increasing ϕ values with particle size. Alternatively, a smaller particle has a smaller mechanical momentum so it is less likely to induce surface features when colliding with other particles. This same reasoning would mean that larger particles tend to be rougher. Section 2.3.2 introduced Equation 2.6 from Bishop (1954) and the work conducted in Santamarina and Cascante (1998) to show that an increase in surface roughness leads to higher ϕ values.

Linero Molina et al. (2019) conducted discrete element simulations to investigate the effect of scaling PSD for testing materials with particles too large to be tested in traditional testing equipment. When particles were scaled down and kept their original shape, the effect on shear strength was marginal. In comparison, a study was conducted to simulate the change in particle shape that could occur when scaling the PSD of a material. More elongated and thinner particles were used than the spheres that replicated the same-shaped systems. It was found in the systems where shape was altered, scaling of the PSD affects the shear strength of the system. It is clear from this study that this is not an influence caused by the size of the particles but rather the shape, supporting the theory stated in Winterkorn (1967). Linero Molina et al. (2019) assumes that all other parameters stay the same including material strength and interparticle friction which may not be true in a physical study.

Ueda et al. (2011) shows a trend that angle of shearing resistance increases as the number of larger particles increases. However, the simulations and experiments were completed on binary mixtures of large and small particles. The increase in strength is due to the increase in mean coordination number caused by the larger particles being surrounded by the smaller particles (Oda, 1977). It should be noted that even with lower fractions of smaller particles a dip in shear strength was detected due to the prevention of the larger particles from touching leading each other. As will be discussed in Section 2.3.4, a soil sample with high mean coordination number will have a higher shear strength when compared to other soils with lower mean coordination number.

2.3.4 Coordination Number

Oda (1977) states that mean coordination number of a system can be a good indication of the strength of the soil with a higher coordination number indicating a higher internal angle of friction. Coordination number assists in transferring the forces exhibited onto a particle to neighbouring particles and is important for the development of force chains (Muir Wood, 2008). Particles with higher coordination numbers are more likely to be involved in force chains (Fonseca et al., 2016) meaning the force can be better distributed within the soil. This can take place through the main networks of the force chain (called the strong networks) as well as through a subset smaller networks (known as the weak networks) in the system. Additionally, a lower coordination number can lead to a particle being unstable in the system. As presented in Oda (1977), this will lead to a lower internal angle of friction. Oda (1977) uses Ishigami et al. (1973) and Bjerrum et al. (1961) to highlight this. Coordination number is also important when it comes to crushing of the particles with a higher coordination number meaning a higher survival probability (McDowell and Bolton, 1998; Tong et al., 2019; Todisco et al., 2017)

Thakur and Penumadu (2021) used X-ray computed tomography (CT) images of the assembly of sand in a triaxial test set up and FEM analysis to investigate the interparticle friction and coupled effect of shape and size on triaxial shearing of poorly graded sands. The sands used were rounded Ottawa sand and angular Q-Rok and both are poorly graded samples. The 3D samples of the scanned sand were transformed into a finite-element mesh and the sand grains were discretised into finite elements using small strain triangular shell elements. The results of the tests found that while the angular Q-Rok sand exhibited a higher peak friction angle, the mean coordination number for the angular sand was lower than the mean coordination number for the rounded Ottawa sands. This contradicts the idea that mean coordination number is a good indication of strength of a soil from Oda (1977). However, the Q-Rok sand samples had a significantly higher number of grains with a coordination number less than 2. These are referred to as "rattlers" in Thakur and Penumadu (2021) as these are unstable particles that are not contributing to the shear strength of the system. During shearing, 20-30% of the sand grains were rattlers for Q-Rok while Ottawa sand had less than 5%, with an initial peak of 12% at the start of testing. The mean coordination numbers of the Q-Rok system is being arbitrarily lowered by inclusion of the coordination number of the rattler particles.

Looking at the rotation of the particles in Figure 2.14a, the Q-Rok grains tend to have more rotation for the smaller particles. These are the rattlers in the sample moving. Observing rotations for particles above a diameter of 0.6mm (where most particles in the Q-Rok have a coordination number of 2 or more), the total rotation dramatically drops and is much lower than that of the Ottawa sand. Therefore, it can be determined that the particles that are interacting with the force chains in the sample for Q-Rok are not moving as much, explaining why the sample is experiencing a higher shear strength. The rattlers in the sample contribute only by lowering the mean coordination number giving the impression that the sample with the lower coordination number is stronger.

As seen in Figure 2.14b the PSD for Ottawa sand shows that there were fewer particles with a diameter less than 0.6mm with over 95% being between 0.7mm and 0.9mm in diameter, whereas only 20% of Q-Rok lay between these values. This explains why there are less rattlers in the Ottawa sand sample compared to the Q-Rok as there are less smaller sized particles to inhabit the spaces between the larger grains. The angularity of the soil particles in Q-Rok is what governs its higher shear strength when compared to Ottawa sands as the particles can interlock which stops the grains from moving freely as discussed in Section 2.3.2.

Alexander (1998) states that for a system of rigid spherical particles to be in equilibrium a minimum average coordination number is required, CN_{min}. For frictionless spheres CN_{min}=6 (Alexander, 1998), whereas for frictional spheres which undergo no slip between particles CN_{min}=4 (Edwards, 1998). This is because the minimum coordination number is directly related to internal degrees of freedom of the particle structure. Higher values of contact friction lead to an increase in constraints on the particle. At infinite interparticle friction with no rotation of the particles, both interparticle sliding and rolling are fully constrained and therefore the particles act as a rigid block expressing infinite shear strength and shear stiffness (Suiker and Fleck, 2004). Hence, the minimum coordination number tends to zero as only a small number of contacting particles make up the force network. Therefore, for this project, the minimum coordination number required for stability will depend on the determined interparticle friction between soil grains.

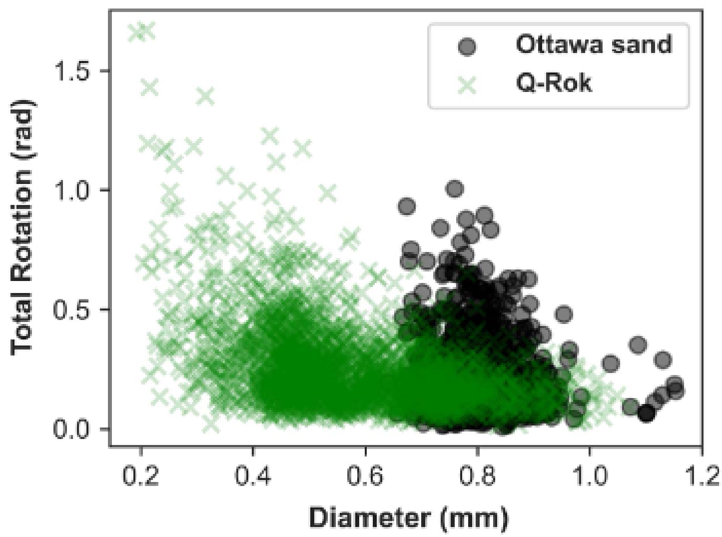

(A)

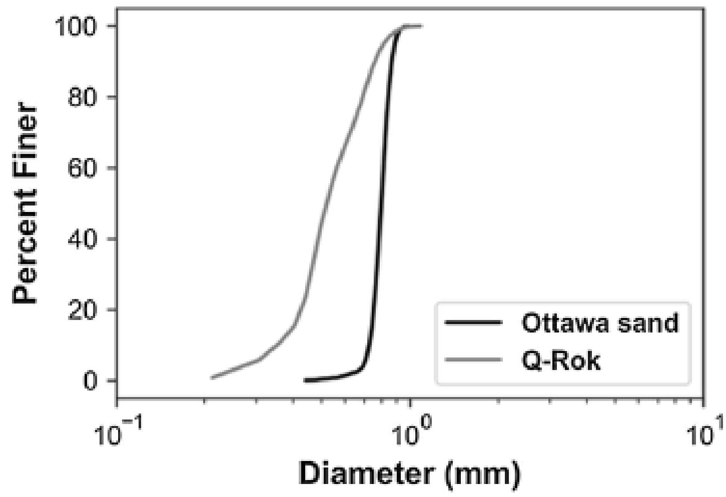

(B)

FIGURE 2.14: Figures from Thakur and Penumadu (2021) for (a) Variation in the rotation of individual grains with the size of grains for rounded Ottawa sand and angular Q-Rok at 15% axial strain (b) Particle size distribution of Ottawa sand and Q-Rok. Permission of use granted by American Society of Civil Engineers.

2.3.5 Grading and Density

Winterkorn (1967) investigates grading as another parameter concerning the shear strength of soils. Assuming minimum percentage of voids in the packing, the angle of internal friction were essentially the same for systems consisting of different sized components. Leslie (1969) shows that an increase of coefficient of uniformity, C_u, caused peak shear strength to increase significantly. Bayat and Bayat (2013) agrees with this and found that increasing C_u increased the shear resistance of pure sand samples. Bayat and Bayat (2013) conducted tests on sand grains and Leslie (1969) conducted tests on alluvial gravels which tend to be rounded.

Wang et al. (2013) completed triaxial tests on accumulation soil and yielded a range of angles of internal friction between 37.2^o and 50.7^o and found that angle of internal friction decreased as C_u increased. Accumulation soil is described to have characteristics as somewhere between soil and rock. Therefore it is most likely that these are more angular than the materials used in Bayat and Bayat (2013) and Leslie (1969), although no detail of the material is given even though it is stated that the grains of the soil were categorised using methods from Lees (1964). It could be that it is not the grading of the sample that determines a higher shear strength of the soil, as suggested by Winterkorn (1967), but rather other factors.

The angular particles may have a higher void ratio and less contacts with neighbouring particles than the rounded particles tested due to the irregular shapes of the grains. This is backed up by Chan and Page (1997) which conducted experiments and found that copper powders with high fractal dimensions have a lower packing density. This lower density will mean a lower coordination number and area of contact with neighbouring particles. In addition, Rousé et al. (2008) compiled data from six different references and highlights a trend that e_{max} and e_{min} are higher for angular particles than more rounded ones.

Azéma et al. (2017a) studied the effect of changing the size span and the shape of PSD. The study was completed using DEM to find the shear strength of granular materials composed of unbreakable discs. The PSDs were modelled using a normalised beta function and recreated expected soil PSDs with good results. It was shown that shear strength is independent of size span and the shape of the distribution. Instead, it is suggested that the change in shear strength when modifying the PSD of a real soil is due to the change of particle characteristics such as shape, strength and interaction laws. This is also the conclusion of Linero Molina et al. (2019) as discussed in Section 2.3.3. Azéma et al. (2017b) expands on the work produced in Azéma et al. (2017a), agreeing with the findings in Azéma et al. (2017a) and discussing the effect of the curvature of the PSD. A low curvature PSD, meaning one which has a much higher proportion of larger particles, show much denser packings than PSDs with a higher curvature. This creates large coordination numbers within the system, making the contact network more isotropic. These larger particles tend to "capture" force chains due to their increased coordination number, increasing branch lengths along the principal stress direction. It is stated in Azéma et al. (2017b) that shear strength is independent of the system’s connectivity. This mainly occurs due to packings being made up of weakly connected networks composed of larger proportions of particles and well-connected networks composed of low proportions of particles. This results in the shear strength being roughly the same value for the scenarios investigated in Azéma et al. (2017b).

Material	Gradation	Shape	ϕ	ϵ_{1f}	$\epsilon_v f$	σ_3	R***
Oroville Dredger tailings	well graded	Rounded	43	6.5	1.5	120	[1]
Sand and gravel (dry)	well graded	Rounded	39	8	4.7	60	[2]
Basalt	well graded	angular	39	15	6	60	[3]
Basalt	well graded	angular	38	**	**	**	[2]
Basalt	poorly graded	angular	37	20	6.5	40	[1]
Conglomerate (dry)	well-graded	angular	37	13	4.5	20	[2]
Silicified conglomerate	poorly-graded	angular	36.5	14	5.5	30	[4]
Argillite	poorly-graded	angular	36.5	20	5.5	25	[1]
Diorite (dry)	poorly-graded	angular	35	15	10	25	[2]
Shale*	well-graded	angular	35	>14	>10	10	[2]
Shale*	poorly-graded	angular	33	>14	>10	5	[2]
Granite gneiss*	well-graded	angular	32	>14	6	20	[3]
Granite gneiss*	poorly-graded	angular	25	>14	>10	5	[3]

TABLE 2.2: Strength and deformation characteristics of large rockfill specimens from Marachi (1969), summarising their own work and work from Marsal (1965), Marsal (1967b), and Marsal (1967a). All tests done at 350psi confining pressure. ϵ_{1f} is principal strain at failure and ϵ_{vf} is volumetric strain at failure.
*test not carried out until failure
** data not presented
***Reference: [1] Marachi (1969), [2] Marsal (1967b), [3] Marsal (1967a), [4] Marsal (1965)

An increase in relative density is thought to increase shear strength (Duncan et al., 2014). Lee and Seed (1967) conducted triaxial compression tests on uniformly graded Sacremento River sand at different relative densities. A value of ϕ_o of 35.2^o and 45^o were reported for relative densities of 38% and 100% respectively. Huu et al. (2017) found in their direct shear experiments that an increase in initial relative density (tested at 40% and 80% relative density) led to an increase in peak shear stress for both silica sands and calcareous sands. Higher densities are commonly considered to be possible in samples that are well-graded and it is not unusual for void ratio to be used to analyse gradation (Selig and Roner, 1987). Yan and Dong (2011) concluded that the influence of grain size distribution on the shear strengths of soils shows that well-graded sand gives a higher shear strength than uniformly graded sand. As Duncan et al. (2014) states, the smaller particles in a well-graded soil should fill the gaps between larger particles, hence it is possible to form denser packings which should offer greater resistance to shear. However, as with grading, it can be determined that the increase in shear strength found in higher density samples relates to the mean coordination number increasing.

Marachi (1969) conducted tests on sands, gravels and rockfill materials. Results of modeling the grain size distribution on the strength of rockfill materials are presented and discussed in the fourth chapter of the work. From the results, it is concluded that a soil is stronger if it is denser and well-graded as all the materials show a decrease of internal angle of friction as initial void ratio is increased. A comparison with other literature was also completed in Marachi (1969), which is repeated here in Table 2.2, and it was seen that well-graded materials tended to have higher strength properties than poorly-graded materials.

Packing type	Relative Density, D_R (%)	SPT blow count, N	ϕ' (°)
Very loose	<20	<4	<30
Loose	20-40	4-10	30-35
Compact	40-60	10-30	35-40
Dense	60-80	30-50	40-45
Very dense	>80	>50	>45

TABLE 2.3: Relationship between relative density, SPT blow count, and angle of internal friction for clean sands from research completed by Meyerhof (1956) (Duncan et al., 2014).

Packing type	Relative Density, D_R (%)	Cone resistance, q_c	ϕ' (°)
Very loose	<20	<20	<32
Loose	20-40	20-50	32-35
Compact	40-60	50-150	35-38
Dense	60-80	150-250	38-41
Very dense	>80	250-400	41-45

TABLE 2.4: Relationship between relative density, CPT cone resistance, and angle of internal friction for clean sands from research completed by Meyerhof (1976) (Duncan et al., 2014).

Meyerhof (1956) and Meyerhof (1976) demonstrated the relationship between relative density and angle of internal friction with tests using SPT and CPT on sands respectively. These results are found in Table 2.3 and Table 2.4. It can be seen from the data that internal angle of friction increases as density of a sample increases as a general trend.

The density of a packing relates to the voids in the structure, with a higher density meaning less void spaces. A high value of C_u is typically a good indication of shear strength but, as with Wang et al. (2013), this is not always true. It is understood that a well-graded soil will be able to achieve higher densities as the smaller particles are able to fill void spaces that would not be filled in a uniformly graded soil. However, the soil strength should not be directly linked to density but rather to another factor. It can be imagined that if a sample is very dense then that means that more particles will be contact with neighbouring particles. As discussed in Section 2.3.4, the number of contacting particles is coordination number and a higher mean coordination number typically leads to higher soil strengths.

2.3.6 Friction Between Particles

Thornton (2000) utilised a three-dimensional DEM program to prove that a larger area of particle in contact with other particles reduce the pressure on that particle and help distribute the force. Thornton (2000) also looked at the effect of interparticle friction. It is stated that it is difficult to distinguish between effects of contact friction and particle shape in a real experiment, so the use of a numerical simulation is favourable. The simulations conducted in Thornton (2000) show that increasing the interparticle friction produces an increase in the dissipation of energy and decrease in the sliding of contacts between particles showing that friction acts as a kinematic constraint. Simulations of axisymmetric compression were also presented in Thornton and Sun (1993) using two different values of coefficients of interparticle friction, μ=0.3 and μ=0.6 for both dense and loose soils. As interparticle friction increased, the shear strength for both systems increased and the ratio of sliding contacts decreased under equivalent forces. Also, the increased friction at contacts increases the stability of the system and reduces the number of contacts with other particles required to achieve a stable configuration. This was also found in Thornton (2000).

Skinner (1969) completed experimental tests on glass ballotini and suggests that the value of critical state angle of internal friction, ϕ_{cv}, and interparticle friction are independent, which is contradicted by the work in Thornton (2000). Thornton (2000) states that their work is more reliable as random assemblies of frictionless spheres are unstable at contacts making it difficult to develop any stable force transmission through the system. The results of Skinner (1969) also contradict multiple theoretical approaches (Bishop, 1954 and Caquot, 1934 as referenced by Skinner, 1969, Horne, 1965), although it does state that rolling occurs in the experiments in Skinner (1969) and, as Thornton (2000) states, these models tend to ignore the possibility of particle rotation. Skinner (1969) washed the glass balotini using water to increase the frictional coefficient by 10 times before washing. Santamarina and Cascante (1998) states that washing has no effect on the coefficient of friction on chemically clean quartz surfaces. However, the presence of water causes coefficient of friction to increase if the surfaces are not clean as surface chemicals which are acting as lubricants between particles can be absorbed. As Santamarina and Cascante (1998) states, there is no description of the surface condition in Skinner (1969). Therefore the change of surface chemicals on the particles may be the reasoning for an observed increase rather than the roughness of the material.

Suiker and Fleck (2004) performed DEM analysis on granular assemblies of spherical particles to analyse the impact of friction on the system. Interparticle friction angles of 4^o, 14^o, 24^o and 34^o were investigated for particles that could rotate and particles that were constrained in rotation. Suiker and Fleck (2004) shows that sliding between contacts decrease as contact friction angle increases, with both the particles that can rotate and constrained particles approaching a state where no sliding occurs as friction angle approaches infinity. Results from the DEM simulations as well as experimental triaxial tests on aggregate of steel spheres show an increase in macroscopic angle of friction for the assembly, with values from the DEM results asymptoting to 24^o as contact friction increases to infinity. Frictionless particles collapse under self-weight and hence have a macroscopic shear strength of zero. It is clear from this work that friction has an effect on the shear strength of the system, which is expected as a system with higher friction between particles would be stronger at resisting shear than that with less friction. It should be noted that a larger area of particle in contact with other particles, like those in Thornton (2000), will have more opportunity to create friction resistance as friction can only be created if the particle is touching another object.

2.3.7 Evidence for Lower Void Ratios Resulting in Higher Shear Strengths

From the previous sections, it can be seen that coordination number and internal frictional forces are two contributors to shear strength of a soil. Ueda et al. (2011) completed DEM modelling of disks and spheres in binary mixtures and showed a high mean coordination number leads to a lower void ratio. Additionally, lower void ratios will lead to more particles in contact with other particles, allowing for more frictional forces between soil grains. Therefore it can be concluded that a low void ratio can be take as an indication of high strength, although this will not always be true as there may be scenarios where strong bridges in the soil structure form over voids. As stated in Mogami (1965), void ratio cannot be used on its own to describe the properties of granular material and the distribution of void is also needed to be known.

Mogami (1965) shows that angle of internal friction should be given as a function of void ratio, e

$$sin\phi = \frac{k}{1+e}$$

where k is the strength coefficient relating to the granular material being tested. This relationship suggests that angle of internal friction is a measure of the crowdedness of the grains in the material. Mogami (1965) states that k is a measure of the avoidance of a change in void ratio due to shearing deformation which suggests that a stronger material would be more tightly packed as then more particles will interlock and prevent the movement of grains. It can be noted that this is not always true. For example, a system of frictionless rectangles laid out in a brick wall style pattern will have no voids present. However, the shearing resistance of the wall will be minimal as one layer may just slide over the other if pushed horizontally. Therefore, in this case, void ratio is not enough to determine shear strength of a material - hence the need for k, which is determined by the structure of the grains in the material. k is determined experimentally as stated by Moroto (1982) from shear tests and the initial void ratio using

$$k = sin\phi(1 + e_o)$$

and averaging the values for multiple tests on that soil. Expected values determined from experimental data are given in Moroto (1982) for k and are presented here in Table 2.5. These agree with expected values of 0.6-1.5 suggested by Mogami (1965) for no specific granular material type. These ranges show that k is varied meaning it is not necessarily determined by material type alone, reinforcing that it is linked to the structure of the particles and their packing arrangement.

Soil Type	Sand	Gravel	Volcanic Ash Sand
k Value Range	0.9 - 1.1	0.7 - 1.3	1.0 - 2.0

TABLE 2.5: Values of k from experimental analysis in Moroto (1982).

Moroto (1982) went on to show that a material with a smaller initial void ratio has a greater shearing strength at high confining pressure levels. Therefore, a sample that is well packed has better shear resistance when movement of particles are restricted. Moroto (1982) suggests that granular soils which are well graded and well rounded have higher strengths than those which are uniformly graded and angular as they can be more densely compacted. This contradicts the findings in Section 2.3.2 where it was concluded that angular particles tend to lead to higher shear strength due to interlocking between particles.

The tests analysed in Moroto (1982) are performed under high confining pressures. As stated by Huu et al. (2017), a sample with greater particle angularity can provide an interaction between particles so that particle movement is restrained when under a low normal stress even if the void ratio of the sample is relatively high. Under a higher confining pressure, particle movement increases due to the higher void ratio in the sample and particle polishing. For similar grain size distributions, samples of angular particles will tend to have void ratios higher than their minimum void ratio compared to rounded samples with the absence of compaction or vibration. This again is shown in Huu et al. (2017) where samples of angular calcareous sands compressed more easily compared to more rounded silica sand samples. Both samples had been designed to have matching grain size distribution. Therefore, in the experiments analysed by Moroto (1982), there was more space for particles to move into and the high confining pressures in the experiments assisted in creating movement of the particles. However, it is true that if rounded soil particles are tightly packed and well graded then they are more likely to have a higher mean coordination number which has already been shown to be strongly linked to soil strength.

2.3.8 Summary of Section 2.3

Presented here is a summary of key findings from Section 2.3. As presented in Section 2.3.2, particle shape is found to have an impact on the shear strength of a soil. Particles of an angular nature tend to have a higher shear strength when compared to more spherical particles due to the interlocking of grains limiting their ability to rotate resulting in an increase in dilatancy. Roughness also has an effect on shear strength. Rougher particle surfaces create higher amounts of friction through the increased number of contacts, making it harder for slipping between grains to occur as more energy is required to move particles. Additionally, in Section 2.3.3 it is determined that particle size has no effect on the shear strength of a granular material so long as the there is no difference in properties, defects, shape or surface characteristics of the material as size changes. It also assumes that testing equipment is scaled as maximum particle size can have an effect on the results of the test (Erlingsson and Magnusdottir, 2002).

The review of literature within Section 2.3.4 found that the more particles in contact with a given particle is usually an indication of higher shear strength. Systems with higher mean coordination numbers typically exhibit higher shear strengths than those with lower mean coordination numbers although an exception is seen if rattler particles exist in the packing as seen in Thakur and Penumadu (2021). The points of contact between particles helps assist with the transferring of forces and prevent particles from being unstable in their position leading to them having no contribution to the force chains in the material and no contribution towards strength. Furthermore from Section 2.3.6, an increase in interparticle friction leads to a higher resistance to shear. This can be concluded to be similar to an increase in roughness of a particle - the increased amounts of friction between particles makes it harder for slipping between grains to occur as more energy is required to move particles. As stated, particles with larger areas of their surface making contact with other particles will have more opportunity to create friction to prevent slipping. This may be more prevalent in systems that have higher mean coordination numbers.

From the review in Section 2.3.5, it can be determined that grading and density of a sample does have an effect on shear strength of the material but any observed change can be attributed to other factors. Mainly, this difference is down to the coordination number. If a sample is well graded then higher densities can be achieved as the smaller particles are able to fill the void spaces that would not be filled in a uniformly graded soil. This in turn can lead to higher coordination numbers for the larger particles in the system helping to spread force chains through the structure.

Additionally, more particles in contact with each other can lead to more internal frictional forces.

The use of void ratio as a sign of high shear strength was discussed in Section 2.3.7 Although void ratio alone cannot be used as an indication of a high strength soil structure, it can give signs that there is a high mean coordination number which is linked to a higher shear strength.

From this summary, the factors that will be considered for creating structures that have a high shear strength will be coordination number as well as the area of the particle that is in contact with other particles and the boundary of the system. Particle shape will not be considered. As the method envisioned to create structures is intended to use waste material, shapes of particles will not be specifically chosen due to the variability that could come with the available particles from local or waste sources. Void ratio will also be taken into account, but as a secondary sign of shear strength rather than a guaranteed indication that the sample produced is strong as void ratio is a good indication of shear strength but cannot be used on its own to describe the properties of granular material.

2.4 Optimising of Placement

2.4.1 Spherical and Non-Spherical Particle Packing Structures

For a method where building of a structure is done autonomously by careful placement of particles, it is required to consider how this can be optimised to get the best packing arrangement. As shown in Section 2.3, a low void ratio in a system can be a good indication of high shear strengths. Hence the discussion of efficient packing structures is presented here.

The first study of particle packing was introduced by Graton and Fraser (1935) who established four basic sphere packings: cubic, orthorhombic, tetragonal-sphenoidal and rhombohedral. Graton and Fraser (1935) take layers of spheres in a square, "simple" rhombic and special rhombic layer system to create unit cells which are the smallest portion of the packing that can give a complete representation of the system. Square layers have 90^o angles between centres of circles, whereas simple rhombic have 60^o. Special rhombic layers describe all packings between the 60^o and 90^o angles. These three types of layers are presented in Figure 2.15. Only the square and rhombic layers were considered in Graton and Fraser (1935) when determining packings due to them "being adequate to represent the limiting types of systematic packing actually encountered". It is stated that there are three geometrically simple ways of stacking either the square layers or simple rhombic layers upon one another. This would lead to six different packings which are presented in Figure 2.16. These are described as Cases 1-6 and are summarised as

- Case 1 and 4 - spheres in the second layer positioned vertically above those in first layer
- Cases 2 and 5 - spheres in the second layer horizontally offset with respect to those of the first layer, by a distance R along the direction of one of the sets of rows
- Cases 3 and 6 - spheres in the second layer horizontally offset with respect to those of the first layer, in a direction bisecting the angle between two sets of rows and by a distance of $R\sqrt{2}$ in Case 3 and $R\sqrt{1/3}$ in Case 6

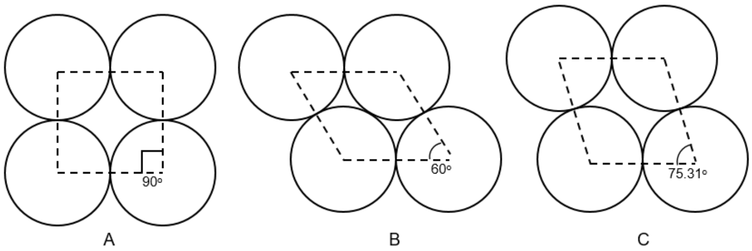

FIGURE 2.15: Types of layers that can be created from packing of spheres determined in Graton and Fraser (1935). A, square layers; B, "simple rhombic" layers; C, special rhombic layers.

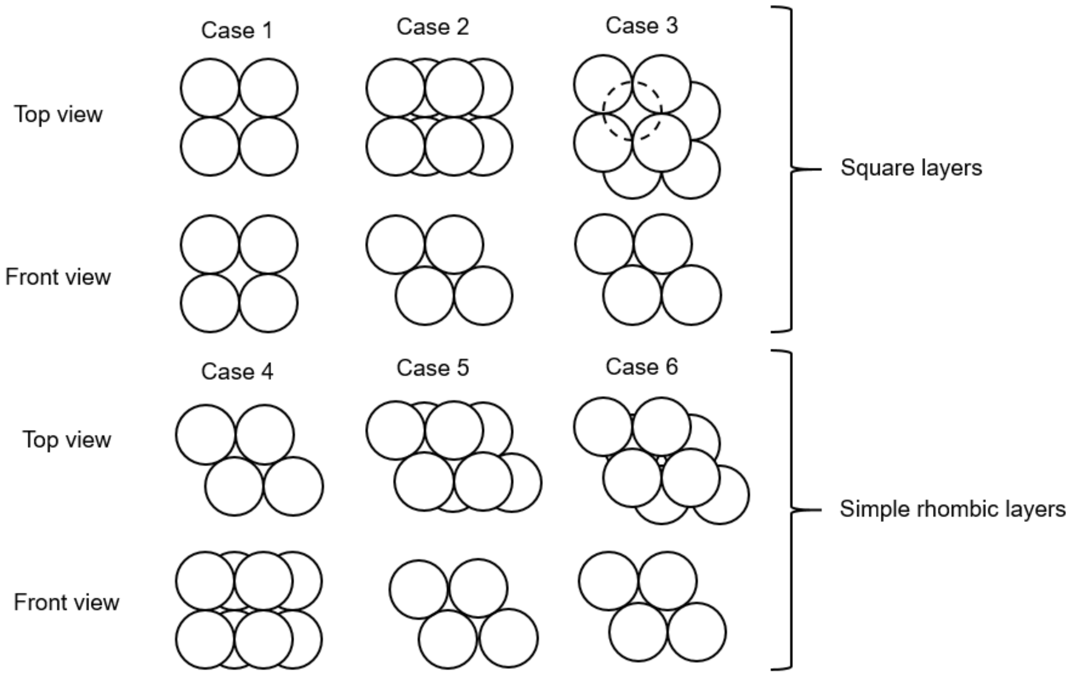

FIGURE 2.16: Six cases of stacking simple layers Graton and Fraser (1935)

where R is the radius of the sphere. It should be noted that Graton and Fraser (1935) is looking at simple systematic packing arrangements of either the square layer or simple rhombic layer and that there are other arrangements that would give intermediate packing structures with different values of void ratio present. These will not give the maximum or minimum values of porosity and permeability that is being investigated in Graton and Fraser (1935) and this is why they were not considered. Instead, just the loosest and tightest packing structures are.

Graton and Fraser (1935) state two of the ways of stacking the square layers are identical to the ways of stacking the rhombic layers if orientation in space is ignored. Therefore, there are only four different simple packings: cubic (Case 1), orthorhombic (Case 2 and Case 4), rhombohedral (Case 3 and Case 6) and tetragonal-sphenoidal (Case 5). However, it is later stated that the orientation of the packing is important as a structure that has spheres higher up in the system will possess a higher potential energy in these particles. Table 2.6 gives the calculated volume of void and total volume of a unit cell, with a unit cell being the minimum amount of particles required to describe the whole structure.

Packing Structure	Cubic	Orthorhombic	Rhombohedral	Tetragonal-Sphenoidal
Case	Case 1	Case 2, Case 4	Case 3, Case 6	Case 5
Volume of unit cell	$8.00R^3$	$6.93R^3$	$5.66R^3$	$6.00R^3$
Volume of unit void	$3.81R^3$	$2.74R^3$	$1.47R^3$	$1.81R^3$
Porosity	47.64%	39.54%	25.95%	30.19%
Void ratio	0.91	0.65	0.35	0.43

TABLE 2.6: Table of volumes in a unit cell and porosity from Graton and Fraser (1935) with void ratio calculated for each packing system.

Graton and Fraser (1935) discuss the stability of the packings. It can be appreciated that a system where spheres sit directly on top of each other - cubic as with Case 1 - will be less stable. Therefore a sphere could move in any direction. The sphere would then find itself in a laterally stable position with four points of contact. Meanwhile, a system like the orthorhombic packing is also positioned on a pinnacle and could topple in any direction. However, the sphere has less distance to fall before finding a stable position and the final position is more laterally stable as it would have six points of contact.

Additionally, a packing with a lower degree of stability will have a tendency to translate into a packing with a higher degree of stability when subject to an external force. As stated by Graton and Fraser (1935), a more stable packing will usually lead to the system having a lower center of gravity and this is achieved by the falling of particles to decrease the height of the system. This also leads to lateral spreading of the system. Graton and Fraser (1935) suggests that indications of the relative stability of the packings described are

- Lower porosity in the system
- The number of neighbouring spheres each sphere touches is larger, otherwise known as the coordination number
- The number of tangent neighbours in the underlying layer is larger.
- A lower centre of gravity that the body of the packing has i.e. the vertical spacing in the layers are less
- A system where spheres occupy a position where they have lower potential energy so are less likely to move.

White and Walton (1937) outlined that there are five simple ways for spheres of equal diameter to be packed. These packings were exact to those outlined in Graton and Fraser (1935). The five packings in White and Walton (1937) are named here and paired with their corresponding packing in Graton and Fraser (1935). Figure 2.17 presents these packings. In the figure is also the packing of ellipsoids-cubical, which is a packing system using ellipsoids rather than circles which White and Walton (1937) also included within the figure in their work. The five packings are

- Cubical, which Graton and Fraser (1935) defined as Case 1 and Cubic.
- Single-staggered or cubic-tetrahedral, which Graton and Fraser (1935) defined as Case 2 and Case 4 and orthorhombic.
- Double staggered, which Graton and Fraser (1935) defined as Case 5 and tetragonal-sphenoidal.

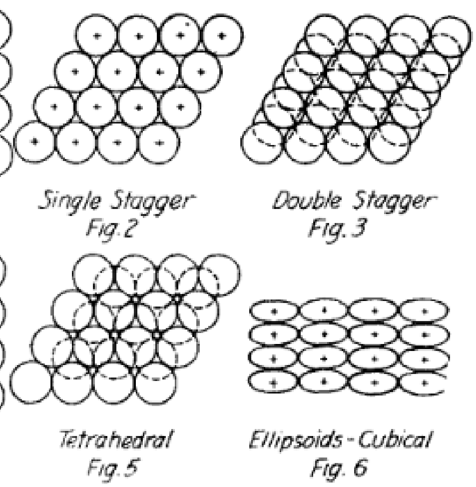

FIGURE 2.17: Packing structures of spheres (White and Walton, 1937) © Wiley. Image used with permission under the Creative Commons Attribution 3.0 license (Creative Commons, 2014)

- Pyramidal, which Graton and Fraser (1935) defined as Case 3 and rhombohedral.
- Tetrahedral, which Graton and Fraser (1935) defined as Case 6 and rhombohedral.

White and Walton (1937) also calculated the void ratio for each packing. These corresponded to the same values from Table 2.6 as presented in Graton and Fraser (1935). Notice the difference between the number of packings, with White and Walton (1937) outlining five different packings and Graton and Fraser (1935) outlining six before narrowing these down to four different types by ignoring orientation in space. As outlined, the height of the sphere in the system contributes to stability. Therefore it is important to take the orientation in space into account. White and Walton (1937) groups Case 2 and Case 4 together like Graton and Fraser (1935). This ignores the spacing between layers being different with Case 2 and Case 4 having spaces of $R\sqrt{3}$ $R\sqrt{4}$ between layers respectively, which again does not account for the potential energy of the spheres higher up in the system.

Whilst Graton and Fraser (1935) groups Case 3 and 6 together, it is clear that these systems do differ from examining Figure 2.16. Although both systems have the same volume of unit cell and unit volume, the spacing of layers differs with values of $R\sqrt{2}$ and $2R\sqrt{2/3}$ for Case 3 and Case 6 respectively. Again, this will not take into account potential energy of the spheres and the stability of the system. As Graton and Fraser (1935) and White and Walton (1937) are not concerned with the stability of the system but rather the minimisation of void, it is reasonable that they would group cases together by ignoring the orientation of the packing system.

White and Walton (1937) go on to discuss how the minimum void ratio of 0.26 can be further reduced by the inclusion of smaller spheres so long as these spheres are small enough so they do not displace the existing primary spheres in the structure. These spheres are referred to as the secondary spheres in the structure. The void ratio can then be further reduced using tertiary spheres that fit between the primary and secondary. This process can continue, although a point will be reached where the reduction in void is negligible. Sohn and Moreland (1968) agreed with this statement

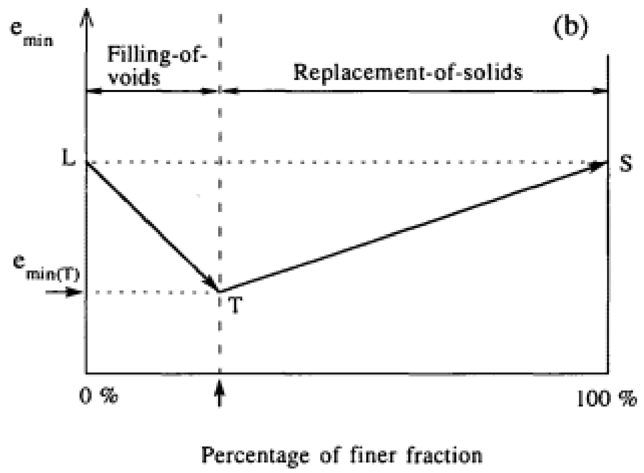

FIGURE 2.18: Effects of fines on binary packing of spherical particles (Cubrinovski and Ishihara, 2002). L denounces the most dense packing of the spherical particles without any fines. Figure used with permission from author.

and found that an extended particle size distribution in a multiparticle system will lead to an increase in density of the sample.

Smalley (1971) built on the work of Graton and Fraser (1935) and devised that there were nine different simple packing structures for ideal spheres, a subset of which are the four defined by Graton and Fraser (1935). Smalley (1971) defines the packings using the Voronoi polyhedron method that can be drawn between the centre of each sphere. Whilst the work completed by Graton and Fraser (1935), White and Walton (1937) and Smalley (1971) is helpful to understand the features that can be used to assess stability in a packing, the simple packing structures used are based on ideal spheres. These sorts of shapes are not adopted in this research. As stated by Smalley (1971), it is not possible to establish a real relationship with ideal models and real materials which are more likely to have a random packing structure.

Cubrinovski and Ishihara (2002) investigated the packing of ideal spheres further and looked at using a binary mixture. It was shown that the addition of finer material would fill the voids of the structure, reducing the value of e_{min}. This decrease stops at a percentage fine fraction where the finer material starts to replace the already present solids which is shown on Figure 2.18 at point T. At Here e_{min} begins to increases again. Cubrinovski and Ishihara (2002) outlines that the smaller spheres will only fill the gaps between particles if they are at least 6.5 times smaller than the larger spheres. This was originally proved in Lade et al. (1998) which illustrated the change in void ratio of a system of two spherical particles with varying ratio of $\frac{d_{large}}{d_{small}}$, where d_{large} is the diameter of the larger sphere and d_{small} is the diameter of the sphere making up the fines. As seen in Figure 2.19, void ratio decreases sharply from $\frac{d_{large}}{d_{small}}$=1 until approximately $\frac{d_{large}}{d_{small}}$=7, before starting to trend towards the theoretical minimum. The work in Cubrinovski and Ishihara (2002) and Lade et al. (1998) agrees with White and Walton (1937) and Sohn and Moreland (1968) that a well graded sample will lead to a lower void ratio, as the smaller particles can fill the gaps which larger ones may not be able to.

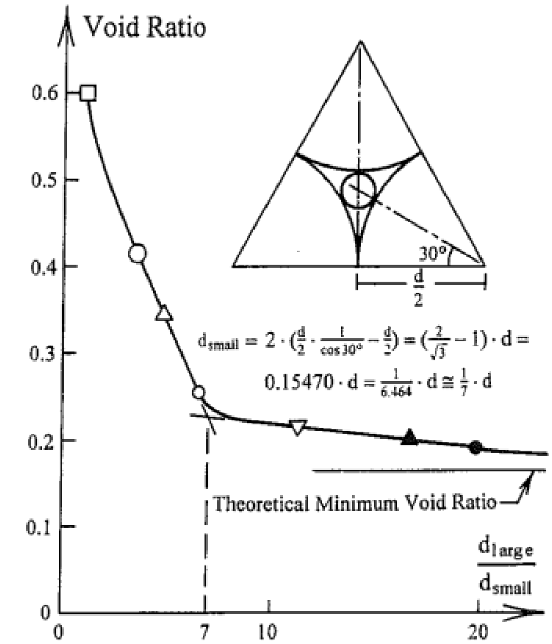

FIGURE 2.19: Minimum void ratios obtained for binary mixtures of steel shot plotted versus ratio of large to small diameters as presented by Lade et al. (1998) © ASTM.

Additionally, Cubrinovski and Ishihara (2002) reviewed existing experimental data in the literature to investigate the effect of fines content in gap-graded soil mixtures on e_{max} and e_{min}. Data for over 300 naturally sandy soils were analysed. It was observed that both e_{max} and e_{min} initially decrease as fines content increases from 0% to about 20% and at this stage it can be said that the fines are filling the voids in the structure. Between 20% and 40% a transitional stage is seen. From 40% and upwards, the fines start to replace the larger particles and an increase in e_{max} and e_{min} is exhibited. The minimum value for e_{max} and e_{max} are obtained in the transitional zone somewhere between 20% and 40%. Alternatively, the effect of fines content was investigated on natural sands with a range of fines from 0% to 70%. The relationship between e_{max} and the fines content is almost proportional whereas the relationship between e_{min} and the fines content shows only a slight increase. It is clear that the relationship between fines content and minimum void ratio is different in naturally occurring sands and gap-graded mixtures. This is most likely due to the gaps in which the fines would fill not being as present in the structure for naturally occurring sands. Cubrinovski and Ishihara (2002) shows that values for e_{max} and e_{min} of sands are typically around 0.98 and 0.61 respectively.

Shergold (1953) outlines three important factors affecting the void ratio in an aggregate. These are stated to be grading, compaction and particle shape which are also outlined to affect void ratio in White and Walton (1937). The work in Shergold (1953) was completed by measuring the void ratio for samples of very rounded beached gravel and slightly rounded river gravel. The results presented showed that the beached gravel had a lower percentage void compared to the river gravel. Additionally, samples which were compacted more had a lower percentage void. Lees (1964) disagrees with the findings in Shergold (1953) and states that nowhere in their work do they prove that angularity is the only (or even main) property of an aggregate controlling the porosity in a compacted condition. Lees (1964) argues that only a small number of samples were tested in Shergold (1953) . Furthermore, to add agreement with Lees (1964), only samples using rounded particles and slightly less rounded particles were trialled when angular gravel or fragmented particles could have been tested.

Wakeman (1975) investigates the density of samples where fluidisation using air was utilised to created looser packings. The research conducted in Wakeman (1975) suggests denser packings can be achieved with angular particles compared to spherical, as particles can tightly fit together into available void spaces given their range of shapes. This contrasts the work done by Shergold (1953), further suggesting that the study conducted was for two samples which can both be considered rounded and that samples of angular or very angular particles should have been tested. Shergold (1953) is mainly showing that rounded particles produce a better packing than less-rounded particles, which could be due to their shapes not fitting together and leaving more gaps compared to ideal spheres but does not necessarily mean this is the case with very angular particles. Physically it makes sense that angular particles would be able to fit together better, however, it relies on the condition that the angular particles are the correct shape to be able to slot between spaces.

From a study into particle size and shape, Cubrinovski and Ishihara (2002) found that there is an increase in e_{max} with increase in mean grain size and that this is more pronounced in systems with fine grains. From the relationship between e_{max} and e_{min}, it can be concluded that e_{min} must increase as mean grain size increases. Additionally, an increase in void ratio was experienced with an increase in angularity. White and Walton (1937) agrees with this as it was found that water rounded sand grains have 2-5% less voids than corresponding sharp grains because they form a better packing. Therefore, the void ratio in an aggregate depends on the size of the particle, the shape and the packing arrangement. However, it can be understood that the samples tested were poured or tampered to get the particles into a state of minimum void. It is more difficult for angular particles to rotate and find themselves in a position where they can reduce the void in a structure. If the particles possess shapes so that they can be fitted together so that each lie in the gaps between others, then potentially a lower minimum void ratio can be obtained by individual placement of particles like the approach seen in Johns et al. (2023). Therefore it is more important how the particles are fitted together rather than the actual shape of the grains.

2.4.2 Optimisation Approaches

Before exploring the optimisation of bin packing which is discussed in Section 2.4.3, it is important to discuss different types of optimisation. Two types of optimisation approach are explored: deterministic and heuristic. Both of these have been used to provide solutions for the bin packing problem.

Deterministic optimisation algorithms reject solutions which do not meet convergence conditions in different iteration steps (Yan et al., 2021). In this way, if a deterministic algorithm receives the same input then it will give the same output without need for communication required between other results (Ren et al., 2014). Deterministic approaches have less constraints upon them and are used to find an optimal solution that is replicable. The disadvantage of deterministic algorithms is that they can become trapped in a locally optimal solution (Yan et al., 2021). Additionally, there is no processing flexibility to reduce computational time due to the need for a strong guarantee on results (Ren et al., 2014).

Yan et al. (2021) states that heuristic optimisation approaches have a given possibility to accept all solutions including those that do not meet convergence conditions, enhancing the ability of the algorithm to escape from a locally optimal solution. In other words, a deterministic approach is usually adopted to find an exact solution whilst a heuristic approach is usually adopted to find an approximate solution but at a faster computational time. Heuristic solutions have no guarantee on produced an answer that is optimal but give a good estimation as to what an optimal solution could be.

It has been shown that the the bin packing problem is NP-hard (Garey and Johnson, 1979; Zehmakan, 2015). NP (nondeterministic polynomial time) is a complexity class used to classify decision problems. If a problem is NP-hard, then it can be said that no algorithm that can solve the problem in polynomial time is known (Bellare and Rogaway, 1995; Mann, 2017 as cited by Chen et al., 2021) and that the time to reach a solution is undetermined. Therefore, this makes these problems difficult to solve in a reasonable amount of time. Heuristic, meta-heuristics and hyper-heuristics are often used for solving NP-hard problems (Chen et al., 2021). Many heuristic approaches are explored in this literature review such as those in Section 2.2.4 as well as the ones in Sections 2.4.3-2.4.5. Two heuristic optimisation techniques are defined here to aid discussions that take place in Sections 2.4.3-2.4.5. These are simulated annealing and genetic algorithms.

Simulated Annealing

Simulated annealing (SA) optimisation was introduced by Kirkpatrick et al. (1983). Within it, an initial case is presented. Then a step is taken to apply a new state. The new state is evaluated and if this new state improves the system in terms of towards an aim or target then it is accepted and becomes the new design state. This can lead to the chance of finding a local minima and taking that as a false minimum solution. Therefore, if the step does not improve the system in relation to the objective function, it may still be accepted with a probability that is linked with an analogy of annealing metals. The probability is calculated by

$$P = e^{-\dfrac{\Delta C}{T}} \tag{2.8}$$

where ΔC is the change in objective function due to the step and T is the current temperature. This temperature decreases as time increases, simulating the cooling that occurs in the annealing of metals. Hence the name for this optimisation method. This leads to a broader exploration of the objective function to begin with.

Genetic Algorithms

Genetic Algorithms (GA) are an optimisation technique based on Charles Darwin's theory of evolution and natural selection. GA was first introduced by Holland (1975). The idea behind GA is that a starting population is modified, or "evolved", and over successive generations an optimal solution is formed. GA is generally composed of two processes. The first is a selection of individuals from the population

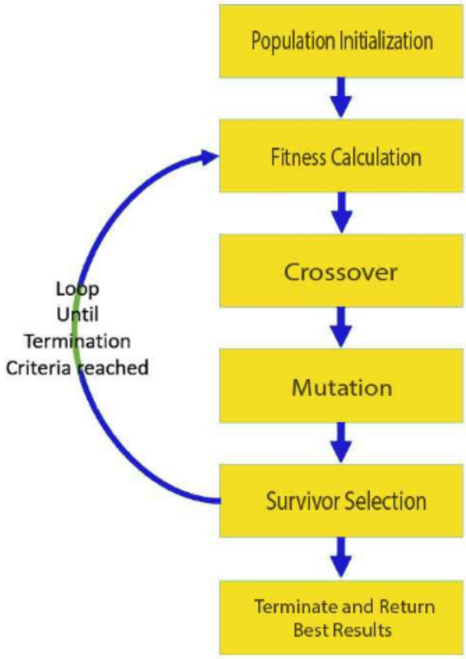

FIGURE 2.20: Flow chart of a GA system (Haldurai et al., 2016) © 2016, IJCSE used under Creative Commons Attribution License (Creative Commons, 2013b).

for the production of the next generation. The second is manipulation of the selection in order to produce the next generation. There are two techniques in which these are manipulated - crossover and mutation (Razali and Geraghty, 2011). A flow chart of the different processes in GA is presented in Figure 2.20. Note, GA is a form of evolutionary algorithm. GA focuses on representing the problem as forms of bit strings whereas evolutionary algorithms can represent the problem using vectors of real-valued numbers. Both work in a similar fashion.

As stated in Haldurai et al. (2016), the selection mechanism determines which individuals are chosen for reproduction as well as how many "offspring" each selected individual produce. Individuals have a higher chance of being selected for reproduction if they are of a higher quality result, although there is still chance a lower quality individual is chosen for reproduction. This process is in order to not lose features which might actually lead to more optimal solution, and it is this feature which stops the algorithm arriving at local minima. A good search technique must find a balance between exploration (adopting poor solutions in order to explore the search space) and exploitation (adopting food solutions for the next generation to improve results) within the mechanism of selection (Beasley et al., 1993). Each individual is given a "fitness score" dependent on how well the individual meets the objective criteria (Haldurai et al., 2016). The higher the fitness score, the higher the chance that this individual will be chosen to produce offspring. For further detail on different selection methods, see Haldurai et al. (2016).

The form of manipulation described as crossover is when two individuals "mate" with each other to produce offspring. Two parents are taken and different operators can be performed to produce offspring with a mixture of characteristics from both individuals. An example of single point crossover is given in Figure 2.21 for two individuals where characteristics are described in binary form. A point is made after

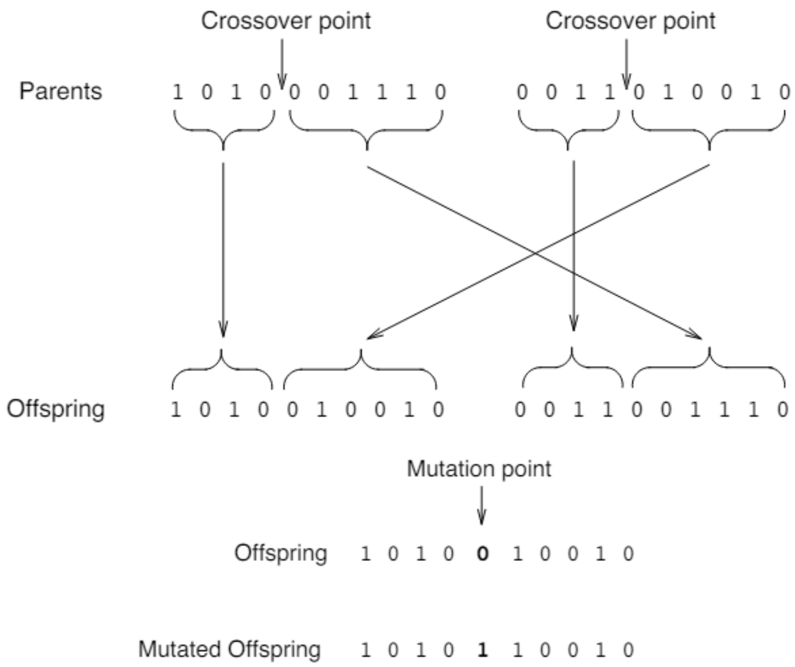

FIGURE 2.21: Crossover of two individuals to create offspring, with a mutation occurring in one of the offspring (Beasley et al., 1993) © ORCA (2021).

the 4th term and two offspring are produced - one with the first four terms from the first parent and six terms from the second parent and the other with four terms from the second parent and six terms from the first parent. Other methods exist such as two point crossover, uniform crossover and any other method specified by the user (Haldurai et al., 2016).

The second form of manipulation is mutation of an individual to produce a new set of characteristics. An example of this is also seen in Figure 2.21 where one of the produced offspring mutates by the change of one of its binary terms. This can be performed on offspring of individuals in a new generation or on parents without performing crossover. However, the process is normally formed after crossover (Haldurai et al., 2016). Mutation allows for a small amount of random search and prevents areas of the search space having zero probability of being investigated (Beasley et al., 1993).

Once the next generation is produced, survivor selection takes place. It is decided by the user if individuals are taken from the current generation or if individuals from older generations are taken forward additionally. The probability of survival is also described by the user and if this is determined by fitness score or another method. Once this is complete, individuals are again selected for producing the next generation and this process continues until termination of the program.

By selecting the best individuals from a current generation and mating them, a new generation is formed that contains a higher proportion of the characteristics possessed by individuals that score higher in the fitness score. In this way, "good" characteristics can be spread through the population and are mixed with other "good" characteristics. Favouring the mating of higher scoring individuals means that the search space is explored in the more promising areas. If the GA has been designed well the population will converge to an optimal solution to the problem (Beasley et al., 1993). GAs do not guarantee a global optimal solution to a problem but generally will provide an acceptably optimal solution to problems at an acceptable computational speed (Beasley et al., 1993).

2.4.3 Bin Packing and Stock Cutting

Examples of an optimisation problem where packing of shapes to create minimal void in an area are cutting and packing problems. Specifically, bin packing is the process of filling containers or "bins" with a number of objects and cutting refers to creating a number of items from "stock" materials. The general concept of these problems is to find a solution that minimises the amount of wasted space, which is normally taken to correlate to the minimisation of cost. This leads to the minimum number of bins or the least amount of stock used. These problems are linked to many industrial applications, such as the cutting of wood, glass or other materials from larger sheets to smaller sections or the packing of transportation vehicles and warehouses. Although bin packing and stock cutting are defined in different ways using real life scenarios, the problem can be described as having the same basic definition (Delorme et al., 2016). The user is required to cut/pack a given number of items from/into the minimum number of stock/bins, fitting the shapes into the dimensions of the bins. Further restraints can be added to the problem such as the weight of the combined items cannot be over a given limit or only certain types of cuts can be made. The bin packing problem is known to be NP-hard (Garey and Johnson, 1979). Therefore, research has concentrated on approximation algorithms.

Eisemann (1957) was one of the first papers to look at solving the cutting stock problem. Eisemann (1957) investigated the cutting of smaller rolls of a material from a large roll of the same width. This replicates the manufacturing of rolls of paper, textiles or metallic foil. The aim for the solution is to be able to cut the required rolls of material using the minimum number of larger rolls, therefore reducing the leftover trimmings to a minimum. Figure 2.22 shows an example of a stock with the placement of cuts along the length to produce a subset of items and the trim left over from the cutting. The problem can be considered one-dimensional as the diameter of the stock (the large roll) is the same as the diameter of the subset of items (the smaller rolls) so only the placement of cuts along the length of the roll is considered. Eisemann (1957) defines the constraints to the problem such as the number of cuts must equal the number of items created. This is demonstrated in Figure 2.22 as four cuts are utilised to produce four items, with trim being left over. As well, in Eisemann (1957) the use of two machines is considered with the restraint that one must not finish more than 2 hours after the other. The solution is calculated using linear programming as the problem is set out by linear constraints and Eisemann (1957) describes that this was produced in 5 minutes by computer. The paper was written in 1955, so it is sensible to assume that this would be completed at a much faster rate as computational powers have drastically improved since then. Gilmore and Gomory (1961) and Gilmore and Gomory (1963) expanded on the cutting problem and determined that it was necessary to use dynamic programming to derive a solution. A column generation approach was utilised to solve the problem, which generated such an immense number of columns that dynamically generating the columns was needed, hence the requirement for dynamic programming.

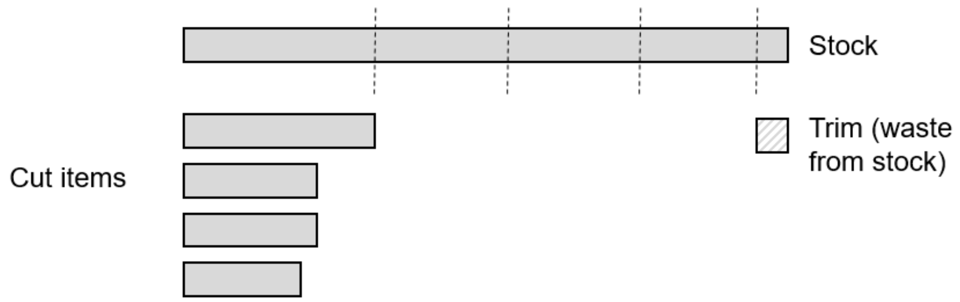

FIGURE 2.22: Example of one-dimensional cutting stock problem.

Gilmore and Gomory (1965) suggested the first model to attempt to solve two dimensional packing problems by looking at cutting rectangles from larger rectangular sheets. This built upon the column approach for one-dimensional problems in Gilmore and Gomory (1961) and Gilmore and Gomory (1963) which provides an enumeration of all the patterns of the items that are to be fit into the container. Gilmore and Gomory (1965) states that if a column generation technique is used for a two-dimensional problem then no economical method is known. Therefore, the concept of "guillotine cuts" to apply more constraints to the problem is introduced. A guillotine cut can be described as one which cuts all the way across the material and must end at an edge - either the border of the material or where a slice has already been made. An example of stock being cut using guillotine cuts is displayed in Figure 2.23. Restricting the number of cuts allows for a lower number of patterns that can be produced reducing the complexity of the problem. This is a fair assumption to make as methods in industry do use these styles of guillotines cuts but not all problems can be simplified by introducing constraints, for example if the solution required did not use guillotine cuts, so therefore a column generation technique is not an optimal solution for two or three dimensional problems.

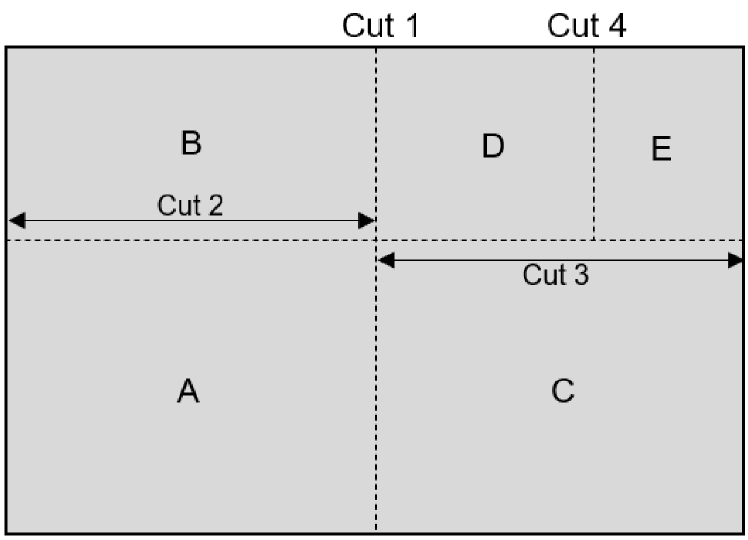

FIGURE 2.23: Example of two-dimensional cutting stock problem with guillotine cuts.

Herz (1972) took the problem outlined by Gilmore and Gomory (1965) and the use of guillotine cuts and produced a solution using a recursive tree search procedure. The algorithm involves trying every possible first dissection line and retaining the one which gives the maximal total value for the two partial dissections. The number of cuts is reduced by discretising the position of where cuts can occur by the abscissa and ordinate of the rectangle being cut. Additionally, the item being cut from the stock is forced to the left and bottom to minimise the number of positions a cut can be made, as a cut cannot be made within the size of the item. Herz (1972) states that recursive solutions are 20% quicker in computational time compared to iterative techniques like Gilmore and Gomory (1965) but that iterative techniques give optimal dissections to produce every subrectangle which the recursive method does not lead to. Therefore, it is possible that a true optimal solution could be missed by not testing all possible packing scenarios.

Beasley (1985) considered this cutting stock problem without guillotine cuts and chose a binary depth-first tree search procedure to solve the problem. Two dimensions were considered by using discrete coordinates at which items could be allocated. Integer linear programming was used so that

$$x_{ipq} = \begin{cases} 1 & \text{if item } i \text{ is placed with its bottom left hand corner at } (p, q) \\ 0 & \text{otherwise} \end{cases} \tag{2.9}$$

where i represents the item and p and q represent the coordinates at which an item can be placed. The problem is trying to cut rectangular objects from a larger rectangular stock and the orientation is fixed. Beasley (1985) states that this assumption can be removed by extending the problem formulation and solution algorithm to cope with non-square pieces that can be oriented in either direction. However, as rectangles are being created it is best to assume an orthogonal cutting pattern. Beasley (1985) shows that a Lagrangian-based tree search is capable of solving non-guillotine cutting problems with orthogonal cuts. However, as stated in De Cani (1978), orthogonal cuts restricts the size that can be cut from stock items and therefore non-orthogonal cutting should be considered.

In can be understood that bin packing and cutting stock problems are very similar, with both focusing on fitting smaller shapes into a larger shape. Focusing on bin packing problems, there is a wide range of literature on this subject. Bin packing algorithms can be described as "off-line" or "on-line". Off-line assumes the algorithm has full knowledge of the whole input (Lodi et al., 2002) whereas on-line algorithms pack every item using the information of that item and items already placed and assumes no knowledge of subsequent items (Csirik and Woeginger, 1998). In on-line packing, placed items cannot be repacked and their placed location is deemed their final positioning in the system.

A common method for bin packing problems is to fill these bins from left to right forming rows. These are called "levels". The height of these levels are determined by the tallest item packed on the level below, and therefore items are placed in decreasing height order. Lodi et al. (2002) gives a review for off-line bin packing problems. In the work, it describes that there are three classical strategies for level packing.

- Next-Fit Decreasing Height (NFDH) - the item is packed to the left of the bin on the current level starting on the first level. If it does not fit, a new level is created and the item is then packed onto this new level.
- First-Fit Decreasing Height (FFDH) - the item is packed to the left of the bin on the first level of which it will fit. If it cannot fit on a level, a new level is created.

- Best-Fit Decreasing Height (BFDH) - the item is packed onto a level in which it will fit. The placement which leaves the minimum horizontal space is prioritised. If it cannot fit on a level, a new level is created. For example, in Figure 2.24, item D could be placed on the first or second level. The placement of D on the second level leaves the minimum distance between the item and the right-hand side of the box, so this level is chosen. This provides a greater width on the first level. As width is not decreasing, there is a likelihood that this greater width is required.

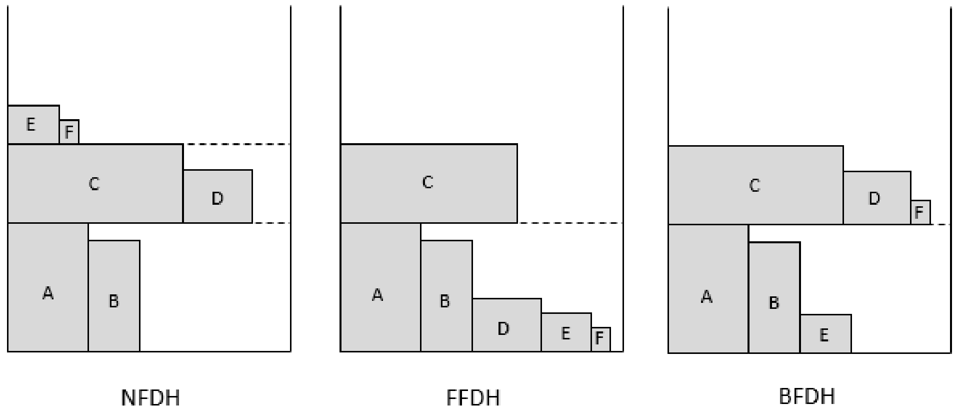

FIGURE 2.24: Bin packing strategies of NFDH, FFDH and BFDH suggested by Lodi et al. (2002) using a set of 6 items which are identical for each case of packing strategy.

These methods are commonly used in strip packing, where the bin's height has no constraint other than it should be the minimum value possible. An example of where these are used can be found in Coffman et al. (1980) where NFDH and FFDH algorithms are analysed. It can be understood that these approaches would need some sort of pre-processing step to sort the items into height order, therefore requiring an off-line assumption.

Chung et al. (1982) introduced a two-phase algorithm for finite bin packing. Firstly, a strip is packed using the FFDH method to give levels of items. These levels are then packing into bins of finite size using another First-Fit Decreasing algorithm. This algorithm was named Hybrid First-Fit (HFF). Berkey and Wang (1987) proposed a similar algorithm called Finite Best-Strip (FBS) that worked in a similar fashion, but used a BFDH strategy to create levels before packing these into bins using a Best-Fit Decreasing algorithm. It can be envisioned that a variation of these methods based on NFDH and then a Next-Fit Decreasing algorithm would be possible. As Lodi et al. (2002) describes, this is essentially a one-phase algorithm as the bins have a fixed height and choosing the next bin for the the levels in the order they are created is equivalent to creating a new bin and packing the level there. Frenk and Galambos (1987) tested this Hybrid Next-Fit (HNF) algorithm. The use of more bins can be expected as there is no possibility to return to a previous bin or level once a new bin or level is started.

Lodi et al. (1999a) and Lodi et al. (1999b) presented a two-phase algorithm solution called the Floor-Ceiling (FC) approach. Rather than just using the floor of each level to place items, the "ceiling" of the level was used which was the top of that current level (or the base of the next level). Items packed on the floor were packed left to

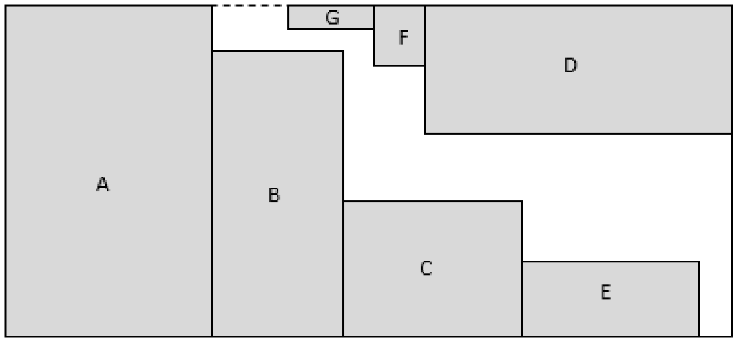

FIGURE 2.25: Results of an FC approach for bin packing.

right as with previous algorithms discussed. Items packed on the ceiling of each level were packed from right to left. These levels were then packed into bins using either a Best-Fit Decreasing algorithm or an exact algorithm for one-dimensional bin packing problems.

Berkey and Wang (1987) presented several heuristic algorithms and compared these with various test problems using rectangular bins and packing sets of randomly generated rectangles. The aim of the tests was to produce the minimum required number of bins. The algorithms developed are described in detail within Berkey and Wang (1987) but a summary is given here. A HFF algorithm was also tested for comparison. It should be noted that these are not two-phase algorithms as the items are being directly packed into finite bins. All rectangular items were pre-sorted into height order apart from the Finite Bottom-Left heuristic which was pre-sorted into decreasing width. The algorithms developed were as follows.

- Finite Next-Fit (FNF)
  For FNF packing, only one bin is available for packing at one time. Items are packed using the NFDH level-oriented packing method. Once this bin is filled, the next bin is created and this is packed. In this way, it is exactly the same as the HNF method described by Frenk and Galambos (1987).
- Finite First-Fit (FFF)
  FFF uses the FFDH method to pack bins using levels. However, whereas FNF only packs one bin at a time, all bins that are created are retained and available for packing. The packing is completed by checking the first bin at all levels. If no space is available, the next bin is checked. If no space is available for all bins, a new bin is created.
- Finite Best-Strip (FBS)
  The FBS algorithm packs items into an infinitely long strip using the Best-Fit packing approach to select the level for packing, like in Figure 2.24. These levels are then turned into blocks with a height equivalent to the tallest item in the level, which are then fitted to the bins using a best-fit algorithm. A binary search tree structure is utilised for packing the blocks created from the first phase which led to longer runtimes for small packings but showed increased efficiency as the number of items to be packed increased.
- Finite Bottom-Left (FBL)
  FBL algorithm searches each bin for the lowest and left-most location for which the item can be placed. If no bin exists which the item can be placed in then

a new bin is created. Each bin is represented as a linked list of vertices which define the boundaries. In this method, an area which becomes closed off by placed items is called a subhole and is described in Chazelle (1983). Possible packing locations must be searched for all subholes of all bins. As shown by Chazelle (1983), the searching for every subhole takes up computer processing time, and it was found in Berkey and Wang (1987) that the memory space to maintain the boundary of each subhole created was excessive leading to less items being packed compared to the other methods. To overcome this problem, a next bottom-left (NBL) heuristic was created which also packed bins using a bottom-left algorithm. However once a new bin was created, subholes of the previous bin were removed meaning essentially only one bin was active at a time (like in the FNF method).

From the results in Berkey and Wang (1987), it was observed that FFF, FBS and HFF led to the least number of bins suggesting the most efficient packing methods. The FBL algorithm resulted in less efficient packing and the Next-Fit heuristics led to the least efficient packing. In terms of computational time, FNF ran the fastest of all the tests which is to be expected as only one bin is ever available at one time. FFF and HFF were slow for large numbers of packed items whereas FBS was slower for small numbers of items but quicker as the number of items to be packed became larger. FBL and NBL took the most time out of all the packing methods.

Lodi et al. (1999a) proposed a new heuristic method that focused on creating patterns not requiring guillotine cuts by packing items from left to right, then from right to left in the lowest possible position and called it the Alternate Directions (AD) algorithm. A lower bound, L_o, is found for the most optimal solution for packing and the number of bins that this requires are initiated. A subset of items are packed using a BFDH method into these L_0 bins. The remaining items are then packed using a BFDH method so that the item touches the edge of the previously placed item (or the edge of the bin if the first item placed in that level) at the lowest location possible. When an item cannot be placed moving from left to right, placement moving from right to left is attempted. If the item can still not be placed, a new bin is initialised and selected for placement. An example of this is in Figure 2.26. The 12 items for the problem are displayed in height order and the lower bound value is found to be 2. Therefore, two bins are initiated and the subset of items is packed (Item 1, 2, 3, 5, 6 and 7). The rest are then placed in the BFDH method moving from right to left. For the 12th item, there is no vertical room for the item and this initialises a new bin for placement.

Lodi et al. (1999a) also proposed a third method of the Touching Perimeter (TP) algorithm. Items are first sorted into decreasing area of the item rather than decreasing height and are configured to be horizontally orientated. Like AD, the lower bound optimal solution is found and the number of bins required for this is initialised. The first item in a bin is always packed to the bottom left of the bin. After this, packing position is determined so that each item has its bottom edge touching the bottom of the bin or the top edge of another item and its left-most edge touching the left edge of the bin or the right edge of an item. Lodi et al. (1999a) states that each position is given a score defined by the percentage of the item's perimeter that touches the edge of the bin or already packed items and this is stated to favour patterns that do not trap small areas of space. The packing positions are analysed twice for two item orientations and the position chosen is that which has the highest score. An example of TP packing is repeated in Figure 2.27 with the 12 shapes used in the example of

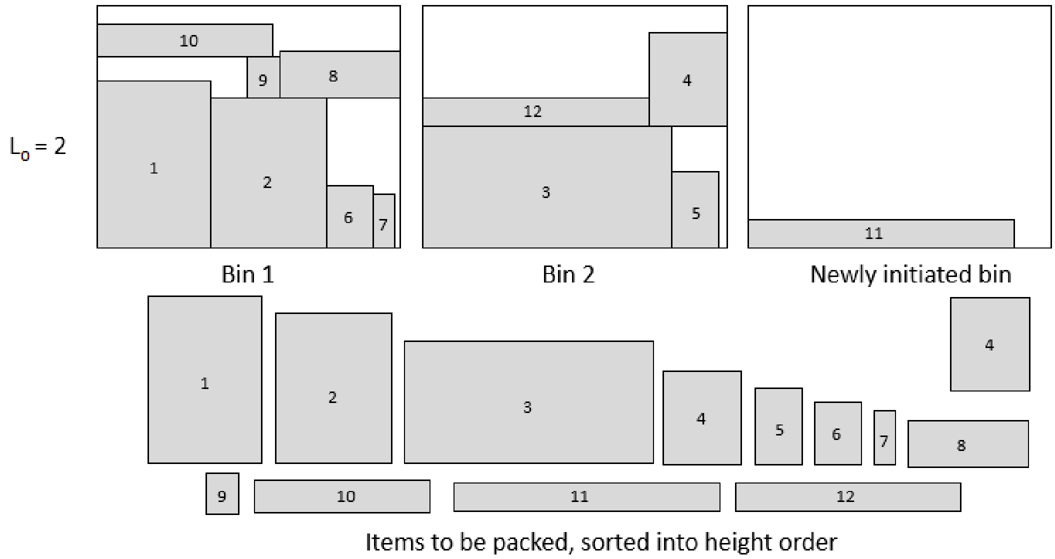

FIGURE 2.26: Example of AD bin packing approach.

AD packing in Figure 2.26. As the shapes are ordered into decreasing area, the new packing order becomes {3, 1, 2, 4, 11, 12, 10, 8, 5, 6, 9, 7} rather than 1 through to 12.

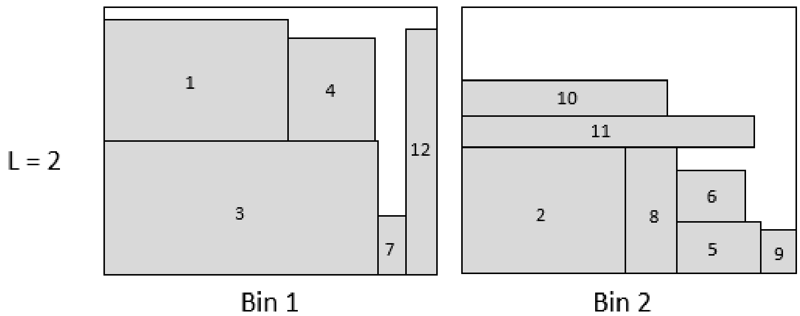

FIGURE 2.27: Example of TP bin packing approach using the same rectangles as Figure 2.26.

There are multiple techniques for calculating the lower bound of the solution for a bin packing problem. The first and simplest for two-dimensional bin packing (2BP) is the continuous lower bound solution (Lodi et al., 2002) which is used to solve a lower bound value for rectangular items being packing into a rectangular bin size. This is given as

$$L_o = \frac{\sum_{j=1}^{n} h_j w_j}{HW}$$

where L_o is the lower bound solution, h_j and w_j are the dimensions for each item being packed and HW is the area of the bin. The use of a lower bound solution will not be used in this project. The lower bound is used to calculate the minimum number of bins required for a certain number of items. In this scenario, there will only ever be one bin and the optimisation of placement is being examined. Although a lower bound could be calculated to find the maximum number of items that could fit into a bin giving an answer to the minimum void ratio possible, this will not necessarily lead to a maximum strength nor will it necessarily be an achievable void ratio. This formula is shown as an example to help understand the process of AD and TP. More information on lower bound solutions can be found in Martello and Vigo (1998).

The methods that have been covered so far are off-line packing methods which have full information on the whole problem. To consider an additive construction method that uses cobbles/boulders as its material, it can be imagined that this would consist of some sort of anthropomorphic arm placing particles whilst these are delivered by a device such as a conveyor belt. The system would not have full knowledge of every particle available for packing if the possibility of more particles arriving exists. Therefore it is necessary to look at on-line algorithms for bin packing to find more suitable solutions which would pack objects by an item by item basis. Csirik and Woeginger (1998) gives a review on on-line packing algorithms.

On-line algorithms have similar methods based on the classical methods described for off-line algorithms. These include Next-Fit (NF), First-Fit (FF) and Best-Fit (BF) which follow the same method as NFDH, FFDH and BFDH but without the pre-processing step of ordering the items as it is assumed that full information of the problem is unknown. Johnson (1974) also introduces and describes the FF and BF algorithms to be suitable for an "any fit" (AF) constraint, meaning that if a bin is empty then an item will not be placed in this bin unless it cannot be placed in any other bin. In addition, Johnson (1974) describes the "almost-any fit" (AAF) constraint which follows that an item cannot be placed into the bin at the level with the most space available unless the item does not fit into any other level. Johnson (1974) goes on to describe two more algorithms, the worst fit (WF) that follows an AF constraint and the almost-worst fit (AWF) that follows an AAF constraint. WF algorithms prioritise packing an item into a non-empty bin with the largest gap, and creating a new bin if the item does not fit into any bin. AWF does a similar process but chooses the second-largest gap for the item to be packed. If the item does not fit into this gap, it is placed into the largest gap providing it will fit and if this is not possible a new bin will be initialised. Csirik and Woeginger (1998) also discusses the idea of limiting the number of active bins that items can be placed and suggesting that once a bin is "closed" it cannot be returned to for more packing of items.

In addition, scenarios which can be classified as semi on-line bin packing problems can occur. These problems arose in dynamic bin packing problems, where it is thought that once a bin can no longer have an item placed within it, it is full and closed permanently. This is to emulate scenarios such as a lorry being filled with boxes that moves on once full to make space for the next lorry. Galambos and Woeginger (1993) introduced a scenario where repacking of items in the currently active bin is allowed. This repacking system means that the packer is allowed to take all items out of the currently active bin and reassign them before packing the next item. It can be envisioned that as the number of items in the bin increases then the increase in computational time will be exponential. As stated by Csirik and Woeginger (1998), the use of completely unlimited repacking leads to an off-line problem. As the last item is packed, the whole system can be repacked. This is the same as off-line bin problems for that bin as all items and their corresponding information that are to be packed are known. Instead, Gambosi et al. (1990) suggested for every new item that a small selection of repacking moves could be made. In this method, a single or multiple items are removed from the current bin and packed into the next bin. Gambosi et al. (1990) suggested two algorithms for this method, the first repacking three items per new item and the second repacking seven items per new item. Both these cases were found to improve on the results of the classic model that does not allow for any repacking of items (Csirik and Woeginger, 1998).

Research is not just limited to the packing of two-dimensional items, but also bin packing of three-dimensional problems has also been explored. The three-dimensional problem looks at packing items characterised by width w_j, height h_j, and depth d_j into bins characterised by width W, height H, and depth D. The three-dimensional case is harder to tackle than the two-dimensional case, and the approaches for 2BP problem cannot be extended for the three-dimensional case and still arrive at an optimal solution (Crainic et al., 2008). Like with two-dimensional problems where shelves of items are packed into an infinite strip and then later sorted into finite bins, for example in Chung et al. (1982), three-dimensional problems can be solved in a similar fashion by using a 2D algoirthm which can then be rearranged into three-dimensional containers. George and Robinson (1980) introduced this approach for the three-dimensional bin packing problem. The container is filled by a number of layers across the depth of the container. This approach leads to the under-utilisation of space in the containers as gaps are formed between layers.

Martello et al. (2000) introduced a new algorithm for 3D bin packing problems. This was completed by separating items according to their depth into a subset $J_o, \ldots, J_{q-1}$ where $q = [log_2 D_{domain}]$. Item j is assigned to set J_i if

$$\frac{D_{domain}}{2^{i+2}} < d_j \leq \frac{D_{domain}}{2^i} \tag{2.10}$$

These items are then packed for each slice into the depth of the domain, D_{domain}, with the corresponding items in the subset that represents that depth. All bin slices will have a width, W, and height, H. Thus, the slices can be combined to fill up the bins from one end to the other. This was used by Martello et al. (2000) to find the continuous lower bound solution.

Martello et al. (2000) goes on to develop a new algorithm which it named 3D-Corners. In this, corner points are found to be where the shape of the envelope of the surface of the packed items changes from vertical to horizontal. These are found in the 2D slices as described before and an example of an envelope with corner points highlighted is found in Figure 2.28. These are determined for each slice and used as possible locations for subsequent items to be placed. To prevent duplication of corner points upon items, corner points were removed if another lay "behind" it on the same plane. A branch and bound strategy is then used to determine the optimal placement of the items within the bin and whether a given set of items can be packed into the bin or not. Boef et al. (2005) states that the algorithm in Martello et al. (2000) only allows for "robot" packing and will therefore not be able to come up with a truly optimal solution. A robot packing is described to be one which cannot place an item in a location if there is another item in front of, right of or above the desired placement. The term comes from the use of robot manipulators used for packing and their limitations on placing of items. Thus, an extension of the algorithm was developed in Martello et al. (2007) which allowed for items to be located to the right of the object being placed. Crainic et al. (2008) states that even with this extension,

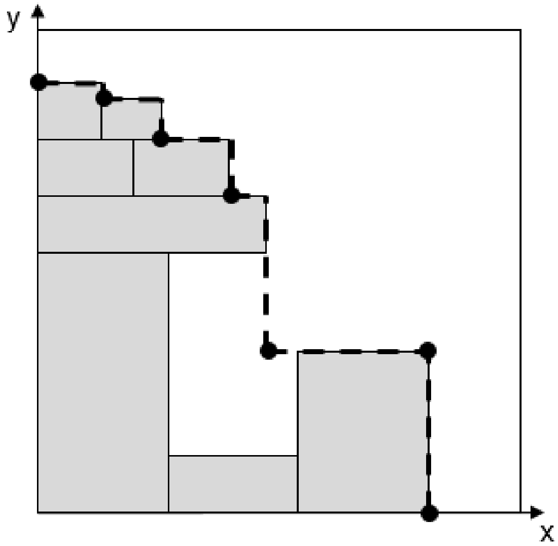

FIGURE 2.28: Envelope of a 2D slice with corner points indicated by black dots as would be determined by the method described in Martello et al. (2000).

the algorithm still leads to a loss of space and the method relies on the sequence of items as they are packed into the container.

Crainic et al. (2008) built on the idea of Corner Points in Martello et al. (2000) and introduced the concept of Extreme Points (EP) in order to tackle the problem of under-utilisation of space. If an item, k, with sizes w_k, d_k, and h_k is packed into a bin with its left-back corner in position (x_k,y_k,z_k), then Extreme Points are generated where additional items can be packed. These are generated at $(x_k + w_k, y_k, z_k)$, $(x_k, y_k + d_k, z_k)$, and $(x_k, y_k, z_k + h_k)$. If the item is the first to be placed these EP are generated as the first three EPs. If the item is not the first to be placed in the bin, these points are taken and projected through the other two axis (for example, at point $(x_k + w_k, y_k, z_k)$, a projection would be done in the Y and Z axis) to get two EPs, resulting in a maximum of six EPs in total. Each point is projected on all items lying between item k and the walls of the container in the respective direction, with the nearest one in that direction of projection being chosen. See Figure 2.29 for an example of the development of EPs by the placement of an item.

The use of EP and then a First-Fit Decreasing (FFD) or Best-Fit Decreasing (BFD) approach to packing was combined to fill bins with rectangular items. The order in which items are sorted to be decreasing can be determined by the user, whilst six different approaches were tested. One example of these would be Volume-Height, where the items are sorted into decreasing volume, with decreasing height being used when two items have the same volume. These methods are very similar to FFDH and BFDH methods used in the two-dimensional cases. However, it should be noted that the scoring system for the BFD method was tested against several different merit functions. These were

- Minimise the free volume left in the bin. In this way, it is the most similar to the BFDH where the minimum amount of area on the shelf is prioritised
- Minimise the maximum packing size on the X and Y axes

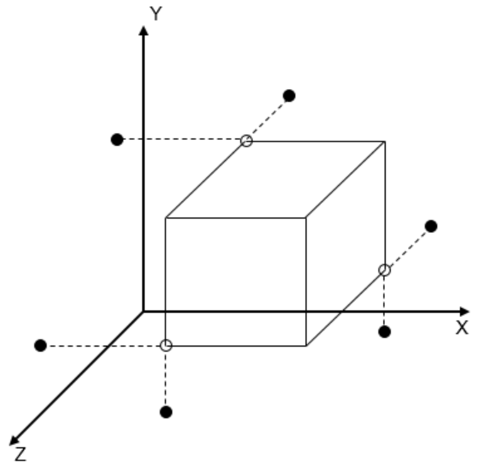

FIGURE 2.29: Example of the development of Extreme Points as suggested by Crainic et al. (2008). Clear circles represent intial EPs and black circles represent projected EPs.

- Level the packing on X and Y axes. This is a modified version of the previous. If the packing size is increased by the placement of the item, the position that minimises this increase is chosen like before. Otherwise, the position that minimises the distance between the side of the box envelope of the packing and the side of the accommodated item is chosen.
- Maximise the utilisation of the EPs residual space. The residual space is the distance from an EP, along each axis, from the bin edge or the nearest item.

A comparison between the use of EPs and Corner Points was conducted in Crainic et al. (2008) and it was determined that the use of EPs give better results for negligible computational effort. Indeed, from the comparison, it appears that the EP approach either matched or outperformed the Corner Point approach for each test when using an FFD heuristic. No comparison between the two was done for the BFD heuristics introduced.

It should be noted that the packings looked at so far have all been packings of regular, rectangular items into a regular, rectangular bin. When it comes to soil particles, these will not have rectangular shapes so it is required to consider packing with irregular shape profiles. Irregular shape packing problems hold lots of challenges due to the complex geometry which can massively increase computational time when compared to rectangle bin packing (Abeysooriya et al., 2018). As a result, exact solutions cannot be found in a reasonable amount of time and rather a heuristic approach should be taken forward (Terashima-Marín et al., 2010).

Jakobs (1996) introduced the Bottom-Left (BL) placement heuristic designed for packing polygons of any shape. The item starts at the top-right corner of the bin. It then slides vertically downwards until it hits another item or the bin's edge. The item then slides horizontally to the left as far as possible. This movement of down then left repeats until the item can no longer be moved, as demonstrated in Figure 2.30(a). Liu and Teng (1999) modified this to create the Improved-Bottom Left (BLLT) heuristic. This worked it the same way as the BL-algorithm. However, from the vertical movement downward, the item would then follow the contour of the already placed items. Therefore, it moves in each direction for less distance horizontally and vertically. Both of these methods were considered for rectangles in Jakobs (1996) and

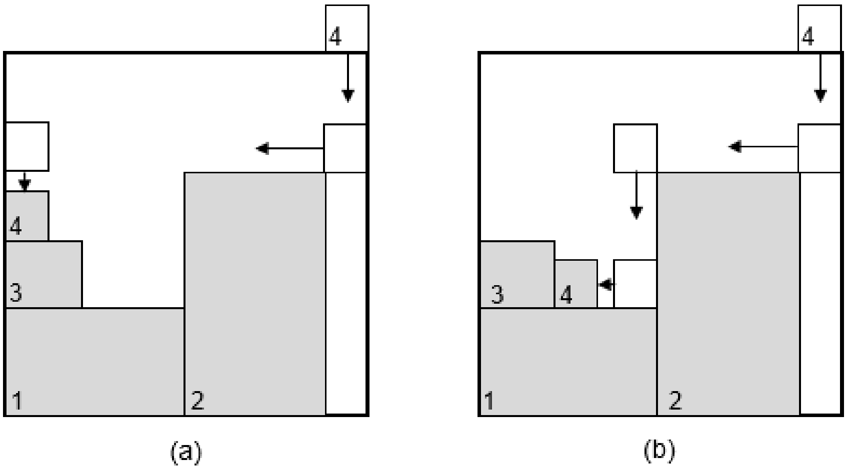

FIGURE 2.30: Example of (a) BL and (b) BLLT heuristics for the packing of 4 items in the order [1,2,3,4].

Liu and Teng (1999), but these methods can be used for irregular particles (BLI and BLLTI) and can be extended to the BLR and BLLTR heuristics which take into account rotation of the item as well. The advantages of the BL and BLLT are their speed and simplicity. However, the performance of this heuristic depends on the initial ordering of the pieces (Terashima-Marín et al., 2010).

Hifi and M'Hallah (2002) introduced the Best Local Position (BLP) Method. This method is used to place irregular polygons in a 2D bin. The first item is packed to the bottom left of the bin. This then produces five possible locations where subsequent items can be packed: (x_{max}, 0), (0, y_{max}) (x_{max}, y_{max}), (x_{min}, y_{max}) and (x_{max}, y_{min}) where x and y represent the horizontal and vertical coordinates of the item placed. This repeats as items are placed, with generated coordinates of the piece to be positioned that do no cause overlap with an already placed item retained as valid candidate positions. The item is then translated to be in contact with an already placed piece. Hifi and M'Hallah (2002) states the BLP method may be expensive in terms of run time for concave shapes. Out of all the final positions, the best location is chosen as the one that places the piece deepest in the system, to the bottom and to the left. This is overruled in the special case that the item fills a hole that has been formed. Terashima-Marín et al. (2010) built on the BLP heuristic by including the four corners of the bin as candidate positions and called this the Constructive Approach (CA) while also rating placement for two other methods based on the minimum area created when all shapes are fitted by a rectangular envelope and that with the largest adjacency to other particles rather than the bottom-left-most placement.

Dowsland et al. (1998) introduced a new method that also tried different points in the system of the bin. Rather than be created by already placed items, the bin is split into coordinates by unit intervals. Each location is tested and deemed if it is a feasible location for the item being placed. Once found, the item can be translated to be in its left most position from that coordinate. The coordinate system can be changed and an increased density of coordinates for positioning will lead to an increase in run time. The advantage of using a system like the one proposed in Dowsland et al. (1998) is that it can mean the utilisation of gaps created by concave particles which other methods may not be able to detect.

Wang et al. (2010) describes the concepts of Deepest-Bottom-Left Fit (DBLF) and

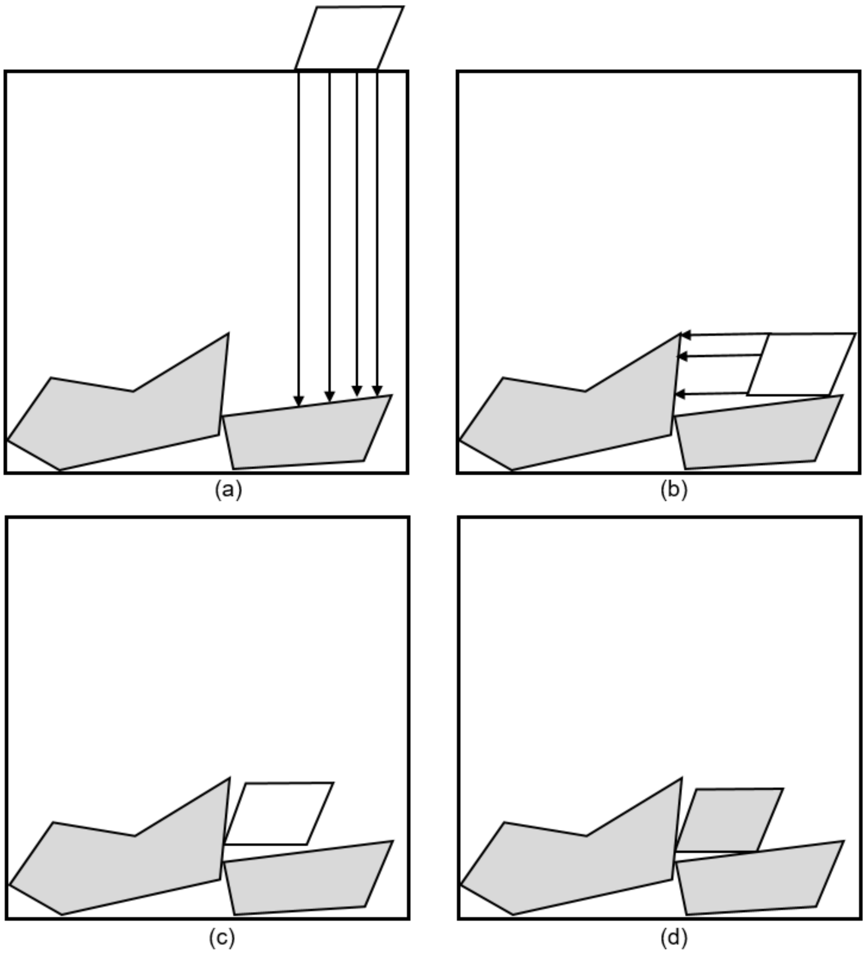

FIGURE 2.31: BLI packing of an item into a box with two items already placed, starting in the top-right location above the box.

Maximum Touching Area (MTA) as a heuristic for packing of 3D items. The DBLF is an adaption of the BL two-dimensional heuristic. Using this method, a face of the item must touch another face of the already placed items or the edge of the bin. The MTA heuristic places items into a bin so that the position maximises the total contact area of the face with faces of other items or the edge of the bin. This is similar to the Touching Perimeter method for two-dimensional cases. Wang et al. (2010) states that both these methods mimic the method that vehicles are loaded which was the problem proposed and investigated by Wang et al. (2010). Wang et al. (2010) goes on to combine these methods and names this as the DMTS (DBLF+MTA Tabu Search) algorithm which prioritises the MTA heuristic for each possible placement location and then chooses the best location based on the DBLF heuristic.

Wang et al. (2010) used a tabu search algorithm for plotting the route taken by the vehicle to minimise distance. The results were compared to a tabu search method not using the DMTS heurisitcs, as found in Gendreau et al. (2006), as well as an ant-colony optimisation method found in Fuellerer et al. (2010) which is another method for minimising distance for the vehicle routing problem. The method suggest by Wang et al. (2010) outperformed the other two methods for 22 out of 27 tests with an average improvement of about 1.31% and was found to be significantly faster in terms of run time for cases with more items. However, it appears the method for plotting routes may differ between Wang et al. (2010) and Gendreau et al. (2006). Wang et al. (2010) uses a method proposed by Clarke and Wright (1964). Gendreau et al. (2006) also uses this method but adapts it for their work. Therefore, it is hard to know if the difference in results is due to a change of heuristic for packing or change of algorithm for routing the vehicle. Yet, the use of two heuristics to distinguish between multiple final positions could be of potential use if packing soil particles and trying to rank their placement based on factors that do not just rely on the minimisation of space.

Wang and Hauser (2019) looked at the offline packing of 3D irregular shapes into a single container using a robot manipulator with consideration of stability and feasibility of placement by the robot gripper. A box is filled with 3-5 items from what might be considered a standard online shopping order. Placement of the items is calculated and the items are packed by a robot gripper into the determined positions. For the tests completed in Wang and Hauser (2019), 100% of the 3-5 object combinations were successfully packed into a small packing box. For stress testing of large item orders, 80% were successfully packed, although this was completed in a physics simulator rather than by the robot gripper. This improves on the standard packing solver that was tested by Wang and Hauser (2019) under the same conditions which had a success rate of 17%. No information is given about this standard packing solver but it is thought that this relies on a minimum of two constraints which were stated by Wang and Hauser (2019) to be each objective is placed without collision of the domain or already positioned objects and all items are placed within the container.

Stability was modeled using point contacts and a Coulomb friction model. Coefficient of static friction and the mass of the items as well as center of mass were known, so contact forces were required for stability to be calculated. Feasibility of the placement by robot manipulator was checked by considering the shape of the item and its initial position to ensure it was graspable so that it can be placed in its desired pose. Additionally, collision with environmental objects was also taken into consideration. A top-down placement trajectory was used to ensure no collision with already placed items from a horizontal direction. The procedure for the packing followed 4 steps:

1. Placement Sequence
2. Generate ranked transforms
3. Stability check
4. Manipulation feasibility check

Wang and Hauser (2019) stated that placement sequence can be user-specified or generated by non-increasing volume of the item. The generated sequence can also be adjusted if a solution is not found with the current order. The generating of ranked transforms first searches the space in the bin to find likely positions the item can be placed assuming the item cannot be manipulated by movement of the robotic grasper. If no feasible solution can be found, then the search is repeated whilst allowing for movement of the grasper so the item can be positioned using roll and pitch movements. Once all possible positions are found, another search is complete taking into account yaw movements of the item for an exact placement. Then, all collision-free positions are scored using a heuristic. For example, the Deepest-Bottom-Left-Fill (DBL) heuristic would score a placement based on

$$Z + c.(X + Y) \tag{2.11}$$

where X,Y,Z are the position of the item in the X,Y and Z coordinates, and c is a small constant. The placement with the "best" or highest score is chosen. The stability and manipulation feasibility check are then completed to ensure the item can be placed in this location. Wang and Hauser (2019) makes use of 2D height maps of the terrain and the item being placed, with a top-down heat map of the bin and a bottom-up heat map of the item being utilised. These are transposed onto each other to determine possible locations of placement by building the pixels of the heat maps upon one another.

Cagan et al. (1998) approached the packing of three-dimensional items using a simulated annealing algorithm for optimisation. Whilst not specifically looking at the packing of items to utilise space, the work in this research is relevant. Cagan et al. (1998) looks at many different objective functions. The two which are relevant to this project are the maximisation of packing density (or the minimisation of gaps) and the minimisation of the center of gravity. Additionally, Cagan et al. (1998) utilised a multi-resolution method when modelling particles. Due to high computational time in evaluating volume intersection of items in the bin, the items were decomposed to have a smaller resolution. This leads to quicker runtimes at the expense of accuracy of the result. But, with the use of the annealing optimisation process, the resolution of items can be increased as T increases. This is an interesting technique that could be taken forward in this project. A lower resolution soil particle (perhaps just represented by a rectangle or simple polygon) could be used to find initial placements, before moving to a higher resolution particle being tested in those locations.

Liu et al. (2015) also used SA optimisation in their approach for the three-dimensional bin packing problem called HAPE3D. In Liu et al. (2015), placement is ranked by minimum total potential energy, which is achieved by decreasing the centre height of the item. Items are sorted into decreasing volume and a discrete set of points are used for placement, like in Dowsland et al. (1998). As these points are discrete, the item is then moved using an advance-or-retreat method both horizontally and vertically. This is performed by moving the item by a designated distance, s. If the item does not overlap with another item or the bin edge, it is moved by the distance s again. If the particle does come into contact, the item moves back to its previous location. The s value is then reset to be half of the current s value. The process is then repeated until the value of s becomes less than the assigned error for the problem. This helps achieve contact with other items without having to compute overlapping volume between polygons. However, the large number of points tested and the iteration process of finding locations with touching edges of items leads to much higher runtime for the algorithm. Results from Liu et al. (2015) are presented in Figure 2.32 and Figure 2.33 for the packing of irregular shapes. Figure 2.32 shows the packing of the same 36 particles which could rotated to make 8 different orientations for packing. Figure 2.32(a) is the results without the use of SA and Figure 2.32(b) is the results with the use of SA. As can be seen, the packing in Figure 2.32(b) is much tighter and as a result the maximum height, h, is reduced compared to Figure 2.32(a). However, the time taken for the algorithm to run, t, is much greater for the case with SA.

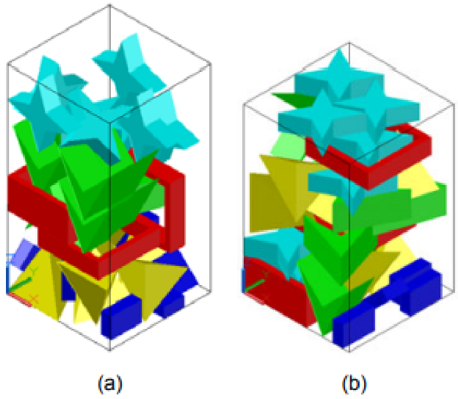

FIGURE 2.32: Layout generated using HAPE3D where 8 orientations of particles are trialled (RN=8) (a) HAPE3D (h=39.0 mm, t=16.1 s) (b) HAPE3D with SA (500 iterations, h=31.2 mm, t=9637.5 s) (Liu et al., 2015). Reproduced with permission from Springer Nature.

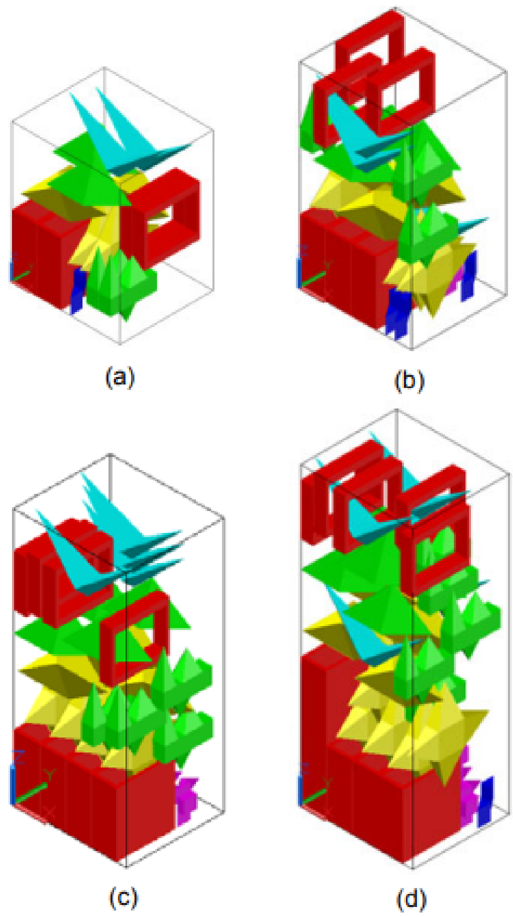

FIGURE 2.33: Layout generated using HAPE3D when rotation is forbidden (RN=1) where n is the number of polyhedrons packed (a) n=20, h=44.7 mm (b) n=30, h=62 mm; (c) n=40, h=79.9 mm; (d) n=50, h=92.0 mm (Liu et al., 2015). Reproduced with permission from Springer Nature.

2.4.4 Jigsaw Solving

The idea of fitting particles of soil together to form a structure in a two-dimensional sense can be related to the act of forming a jigsaw from the puzzle's pieces. A range of studies have been conducted in automatically solving jigsaw puzzles. It should be noted that for this study, colours and visual patterns on the jigsaw surface influencing the solving process are ignored as these are irrelevant when using particles of soil. Hence, apictorial jigsaw puzzles are focused on for this section of the literature review as these do not require an additional condition to satisfy image as well as shape. Furthermore, it should be noted that random soil particles will potentially never fit together perfectly unlike two jigsaw pieces which are designed to leave no space between matching pieces.

Freeman and Garder (1964) presented the first algorithm to solve an apictorial jigsaw which consisted of a 9-piece puzzle. This was completed using visual information only. The process of solving the puzzle was based on the mating between pieces, finding the two which would fit together with no voids. This is the luxury of solving a jigsaw puzzle as it is known that no voids will be present once the end solution is reached so this can be used as a condition of the solving algorithm. Solutions used to solve jigsaw puzzles may not be relevant to this research, however the identification process and moving and placing of pieces are ideas that can provide influence. A chain-encoding scheme was adopted in Freeman and Garder (1964). The outline of each piece was sketched upon a square grid and curve points are assigned at the closest grid node closest to each intersection. Curve points are then connected by straight lines, which can be one of eight directions (horizontal in two directions, vertical in two directions or diagonal in four directions). This is called a "chain" and is a straight-line approximation of the curve. These straight-line approximations are broken down into "chainlets" for matching pieces together. A backtracking approach is adopted as invalid matching can occur. Kong and Kimia (2001) stated that there are not enough constraints used in Freeman and Garder (1964) to gain good partial matches and therefore backtracking occurs often and the algorithm is not efficient.

Radack and Badler (1982) showed that it is possible to solve jigsaws using boundary fitting methods for two-dimensional objects. Curve maxima and minima for a puzzle piece are identified for each shape and these points are rated for their matching with other puzzle pieces. An example of two objects being matched together is presented in Figure 2.34. A pattern is created by measuring a sequence of distances from a point on the boundary being matched to other boundaries of that piece. This is completed along certain standard directions, usually multiples of a small angle. If there is a fit between the two matching regions, identical pattern subsequences will be obtained when plotting from the maxima/minima to points along the particle boundary. The method is stated to be able to solve jigsaw puzzles, but is not used for any puzzles above a maximum of four pieces in Radack and Badler (1982).

Woflson et al. (1988) developed an algorithm for assembling large jigsaw puzzles and then solved a 104 -piece puzzles. The technique uses the Schwartz-Sharir curve matching algorithm (Schwarz and Sharir, 1985) as well as an optimisation method to match pieces and solve the order in which they should be positioned. As with Freeman and Garder (1964), apictoral puzzles were used so the colour of the jigsaw pattern was ignored. A commercial puzzle was used for the experiment and turned upside down so the back of the puzzle (with no pattern on) was upwards facing and a black and white camera photographed each image separately. Due to this, there is expected noise from the imaging. As recommended by Schwarz and Sharir

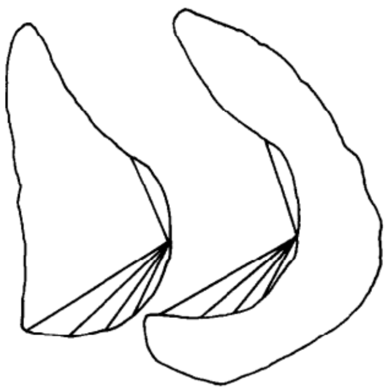

FIGURE 2.34: Pairing of two objects located at the maxima for the left piece and minima for the right piece if curves are observed as particle outlines. If there is a fit between the two matching regions, identical pattern subsequences will be obtained. Reprinted from Radack and Badler (1982) with permission from Elsevier.

(1985), a polygonal approximation of the shape is taken to reduce noise and smooth the boundaries. The Schwartz-Sharir algorithm is used initially for local matching of jigsaw pieces and this works by matching the curves of the sides of the jigsaw by transforming each piece closer to each other until a minimal area between the pieces is found. Curves were created between sharp corners of the pieces to created four sides to each item. The best fit between the sides of two pieces will give the least area.

Like a human might do when completing a jigsaw, Woflson et al. (1988) solves the frame of the jigsaw first before solving the entire puzzle. The placement of pieces are determined by an iterative, heuristic approach that is described in Fencl (1973) as it is time efficient. Woflson et al. (1988) states that it should take a very small number of iterations to arrive at the correct solution. Next, the interior of the jigsaw is completed. All pieces which were not edge pieces are located at the corner using all possible rotations and assigned a local matching score. A number of solutions, *K*, are assigned as possible solutions and taken to the next stage. *K* is taken as 200 in Woflson et al. (1988) but it is stated that it may be possible to use a value of 10 as the final solution usually lay among the 10 best solutions. The second corner is then taken and this procedure is repeated for all partial solutions from the previous stage, and *K* overall solutions are taken to the next stage. This is repeated iteratively for all corners. No analysis of the solutions to the jigsaws are given, but it can be seen in the paper that the algorithm can efficiently solve the 104 piece jigsaws presented.

Freeman and Garder (1964), Radack and Badler (1982) and Woflson et al. (1988) all rely on extracting critical points from local border information. As described by Webster et al. (1991), the problem with this method is the number of match segments can become many times the puzzle pieces which can lead to matching algorithm having an excessive computation time. Webster et al. (1991) suggests the use of isthmus critical points to prevent this. An isthmus point is found on each side where a jigsaw piece can be connected to the other and is described as the midpoint of the local minimum for each possible connection point. These connection points are later called tabs in Goldberg et al. (2002) and will be called this from here on. The endpoints of the line that stretches across the local minimum of the tab are the

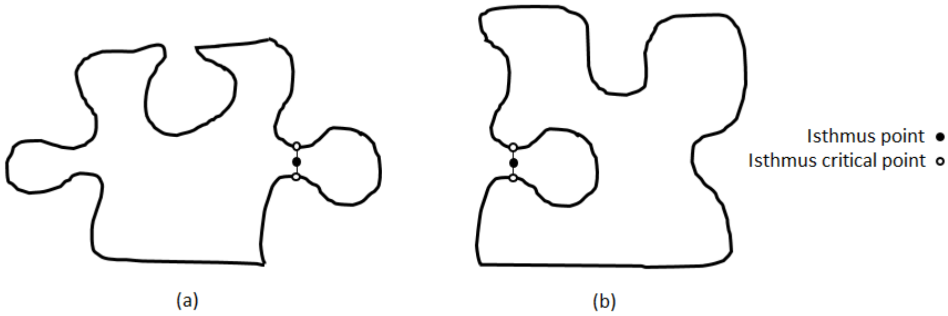

FIGURE 2.35: Example of (a) a positive isthmus critical point and (b) a negative isthmus critical point, both of which match together.

isthmus critical points. This method relies on the shapes taking the shape of conventional jigsaw pieces which soil particles do not tend to exhibit shapes of. A heuristic algorithm is then used for matching. First, bad candidate matches are removed by applying the condition that, for a possible placement, pieces must have a negative isthmus distance larger than the positive isthmus distance as well as the condition that the difference in size of each of the matched tabs cannot be greater than 50% of the height/depth of the longer segment. In this way, for a 24-piece jigsaw puzzle, a possible 2377 possible matches was reduced to 126 possible matches, greatly reducing the computational time taken for the heuristic check. The placement is then ranked based on the gap between the two pieces when matched. As stated before, it is unlikely that isthmus points could be described upon the outline of a soil particle and it is extremely unlikely that two soil particles will fit together perfectly to leave no gap. However, the use of conditions to limit possible matches could be of use when trying to limit the run time of any developed algorithm.

Goldberg et al. (2002) produced a method that did not rely on the condition that jigsaw pieces could be broken down into four sides which are clearly defined by sharp corners as a feature of the piece. Goldberg et al. (2002) follows the same principal as Woflson et al. (1988) by solving the border and then moving to filling the interior. However, the algorithm presented in Goldberg et al. (2002) differs in that it makes use of the global geometry. The border is first constructed by scoring placements of pieces next to each other using parallel lines between the two pieces. Parallel lines can be used as the edge of the jigsaw gives reference to the direction in which the piece must lie. For two jigsaw pieces to fit together, the distance between the two pieces must be equal from the right edge of the left-most piece to the left edge of the right-most piece when orientated in the correct plane for fitting, which is determined easily for the edge pieces by the straight edge. An example of this process is presented in Figure 2.36. Allowing for error in the visualisation of particles for the computer, if these pieces fit perfectly then the distribution of lengths should cluster tightly around a median value and the score is determined as an average difference to the median between lengths.

For the interior of the jigsaw, fiducial marker points were set up on the jigsaw piece at indents (where pieces would slot in to fit next to the jigsaw piece) and outdents (where the jigsaw piece would fit into an indent of another piece). The location of these points were chosen by fitting an ellipse to each tab. The ellipse is fit from the inflection and tangent points on the tab, indicated in Figure 2.37. Then, to align two neighbouring pieces, a least-square fit was used to match curves together.

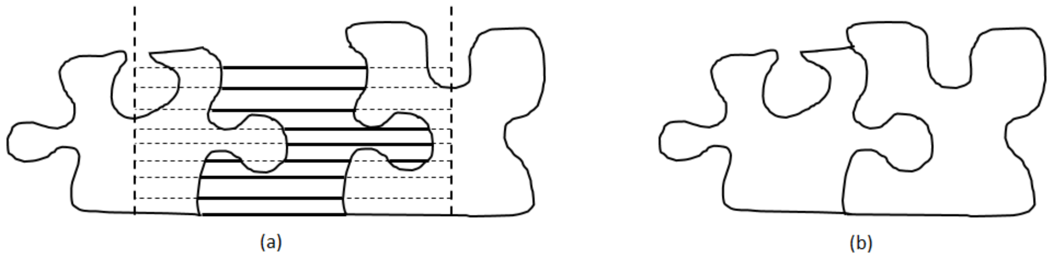

FIGURE 2.36: Two edge pieces of jigsaw being matched together. (a) Parallel lines between two pieces. Empty space between edges (bold parts of line) add up to be of equal length. (b) Pieces put together. As can be seen, they match and there are no gaps present.

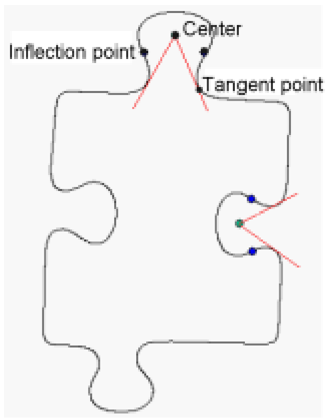

FIGURE 2.37: Example of the three feature points on a tab (inflection points, ellipse centers, and tangent points) used for matching. Figure used with permission of ACM (Association for Computing Machinery), taken from Goldberg et al. (2002). Permission conveyed through Copyright Clearance Center, Inc.

Solving interior pieces leads to a more difficult matter as there is no straight line present to aligning pieces. Therefore, a greedy algorithm, without backtracking or branch-and-bound, is utilised. Eligible pockets - positions where jigsaw pieces can be placed that have at least two existing pieces bordering it - are tested and the piece is scored by how well it fits into that space based on the least-square fit between the ellipses that make up the edge. Pieces with highest confidence are placed first. For the larger 204-piece jigsaw, a one step lookahead method was used. If piece P is placed, this creates some new eligible pockets around P. For each pocket, a new piece is fitted. The score for P is then calculated with these pieces placed, meaning that more information of the border is used to find a score for P. It is not specifically stated, but it is believed that this was done to avoid multiple pieces that may have an exact match with the adjacent sides to the eligible pocket but then would lead to weaker matches for sequential placement.

Kong and Kimia (2001) uses curve matching to solve puzzles in both two and three dimensions. For 2D puzzles, a matching algorithm based on Sebastian et al. (2000) in which two curves are averaged and the deviation from this average for both curves are found to see how well they match. The process was sped up by first using a more coarse description of the curves to remove obvious non-matches before then using a finer description. Matching is based on torsion and curvature functions as these are the same if the curves are the same. Kong and Kimia (2001) applies this principle when moving on three-dimensions whilst including torsion in the cost function. A best-first search with backtracking algorithm is adopted, so that the best fit for a match is done first and then continued. If this leads to an unfeasible solution, backtracking is completed. The algorithm was tested on puzzles of 18 and 25 pieces and was successfully able to piece these back together - although these represented two-dimensional problems. Three-dimensional fragments of a broken ceramic pot were scanned and matched together with seven pieces being used. All matches except one were picked out by this method, although three were chosen that were not correct matches. Hence the need for backtracking.

Hoff and Olver (2014) also used a curve matching approach to solve apictorial jigsaw puzzles. This matching process was based on the work in Hoff and Olver (2013). Curves are decomposed into a finite number of bivertex arcs (which are arcs which start and end at points of no curvature), circular arcs and straight line segments. Bivertex arcs are then compared to determine if a fit is possible between the two sides. The benefit of this method is that no assumptions are required for the shape of the puzzle or the individual puzzle pieces. The algorithm is used to solve two complicated commercial puzzles with non-traditional jigsaw shapes and final completed puzzle shapes that are non-rectangular. It is stated in Hoff and Olver (2014) that the starting piece is not important, but a piece with many well-defined features will maximise the chance of finding successful fits early on.

2.4.5 Tetris Optimisation

An example of a scenario where shapes are packed into an area with the objective to obtain the least amount of void ratio as possible is the classic videogame Tetris. Tetris was first programmed by Alexey Pajitnov in 1985 (Fahey, 2012) and involves filling a domain or “cup” with puzzle pieces made up of four squares known as tetrominoes. There has been some research in the area of strategies whilst playing the Tetris videogame. In Tetris, the user plays within a 2D domain of width and height equal to 10 squares and 20 squares respectively. Tetrominoes are placed separately, filling the area four squares at a time. Each tetromino can be shifted laterally by a squares width across the width of the domain and rotated by 90^o. However, the tetromino being placed falls one block for a given time frame, adding a limit to how long the user has to adjust the particle. This time frame decreases as the game goes on so the blocks fall faster which increases the difficulty. If a row is completed, to say that every square in that row is filled with squares of the placed tetrominoes, then this row is deleted from the domain and all other rows above it shift downwards whilst the top row will now be only empty squares.

Tetrominoes are delivered in a random order to the user. A "Tetris bag" with a "pull from bag" method is utilised in versions of the game, although it is unknown when this was first introduced. For this method, the seven different tetromino shapes are listed. The first tetromino is selected at random and placed by the user, leaving the remaining six. This process is repeated until there are no tetrominoes in the selection bag after which the bag is restored with one of each tetromino ready to randomly deliver the next particle. The aim of the game is to "delete" as many rows as possible without filling the domain past the 20^{th} row gaining a score for each row deleted. Particles placed outside of the domain will result in the game ending.

The first research to appear in this area was conducted in Brzustowski (1988). Brzustowski (1988) adopted what has now become known as "Standard Tetris". This adopts the traditional rules of the videogame, but assumes the player has unlimited time for determining rotation and horizontal positioning before the shape falls into place, removing the time limit that can be found in the videogame. The game still ends when a cell above row 20 of the domain is filled. The seven tetrominoes that are used within the Standard Tetris can be found in Figure 2.38. These are named by Brzustowski (1988) as

1. Left elbow (LE)
2. Right elbow (RE)
3. Square (SQ)
4. Right kink (RK)
5. Left kink (LK)
6. Tee (T)
7. Bar (B)

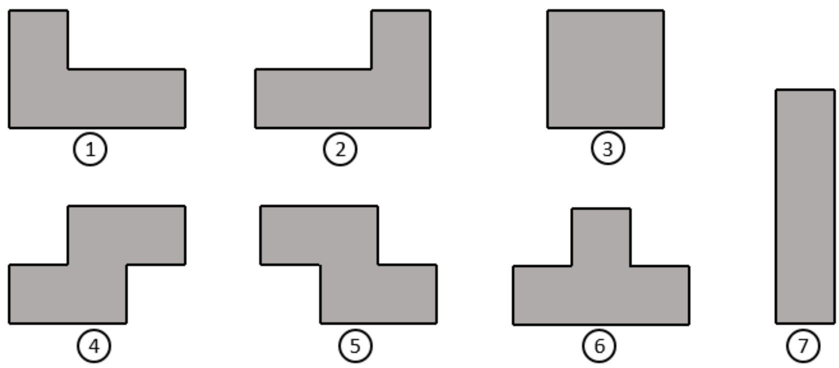

FIGURE 2.38: Different tetrominoes which occur in the Standard Tetris videogame.

Brzustowski (1988) shows that there are methods to play the game continuously by filing the domain in order to remove rows so that the domain is never filled above the 20^{th} row. However, the paper focus on permutations of shapes that only involve one or two of the tetrominoes and does not limit itself to the boundaries of the seven shaped game by using non-traditional shapes such as a 3x3 square. This is unrealistic in terms of playing the actual game, especially if the "pull from bag" method is deployed for the particle selection. Additionally, it is unlikely that in a real world situation using random particle shapes that the same particles will be produced in a specific order to maximise packing and it could be said that this tends towards masonry construction using bricks. Brzustowski (1988) concludes that there are certain permutations of shapes that the machine can give making the game impossible to win. Therefore, if the computer is aware of your moves and able to react then Tetris is impossible to win. Burgiel (1997) agrees with Brzustowski (1988) and shows that an alternating sequence of LK and RK will eventually cause a loss for any gameboard with a width of $2n$. Both these papers focus on just using one or two of the possible shapes in Tetris and look at failing at Tetris rather than trying to optimise the placement.

Breukelaar et al. (2004) looks at an offline approach in the scenario of Tetris, with the sequence of pieces to be dropped given in advance. Breukelaar et al. (2004) showed that the problem of solving Tetris is NP-complete, meaning that for problems of a larger size, an algorithm is unlikely to find a desired solution in a practical amount of time. This includes the offline scenario when the order of particles that will be produced is known. Like with Brzustowski (1988) and Burgiel (1997), Breukelaar et al. (2004) looks at solutions using no more than five different shapes as well as complicated initial gameboards that do not reflect the Tetris videogame scenario.

Kostreva and Hartman (2004) introduced a heuristic approach for determining placement of Tetris shapes in the domain based on an objective solution. The objectives of the solution are as follows

1. Minimise the number of empty cells created between the piece placed and the contour associated with placement. This is based on observing human players who are regarded at being “good” at the game.
2. Maximise the number of contacting cell walls resulting from placement.
3. Minimise the additional height added to the contour by the placed particle.
4. Maximise the number of rows cleared from the board as a result of the placement.

Each objective is evaluated for all rotations and placement locations of the particle. The four objectives are combined to give a single score for each possible placement with the optimal placing being that with the highest score. The objectives are given a weighted factor as each are not measured using the same scale. For the second and fourth objective, positive weighting factors are given as it is desired to maximise these factors, whereas negative weighting factors are given to the first and third objectives in order to minimise these factors. If a tie in the maximum score is found, the best placement is chosen arbitrarily by the user. The work conducted in Kostreva and Hartman (2004) is interesting and highlights the potential of using a weighted criterion when placing soil particles if the criteria are based on factors that control soil strength, given that a high soil strength is the objective of the system being created. Kostreva and Hartman (2004) uses fixed values for the weightings throughout the process, but suggests that these values could be dynamic as the placement of particles is performed.

Another example of where a heuristic approach is adopted based on objectives outlined by the user is in Böhm et al. (2005). Böhm et al. (2005) uses a rating function, $R(b)$, to get results within a reasonable amount of time rather than using a backtracking algorithm, as the computation of finding the perfect move is NP-complete as was demonstrated in Breukelaar et al. (2004). $R(b)$ is based on the objectives outline in Böhm et al. (2005). These are reproduced here for completeness.

1. Pile height: the row of the highest occupied cell in the board
2. Holes: The number of unoccupied cells that have at least one occupied above them.
3. Connected holes: same as holes above, however vertically connected unoccupied cells only count as one hole

4. Removed lines: the number of lines that were cleared in the last step to get to the current board
5. Altitude difference: the difference between the highest occupied and lowest free cell that are directly reachable from the top
6. Maximum well depth: the depth of the deepest well (with a width of one) on the board
7. Sum of all wells (CF): Sum of all wells on the board
8. Landing Height (PD): The height at which the last tetromino has been placed
9. Blocks (CF): Number of occupied cells on the board
10. Weighted Blocks (CF): Same as blocks above, but blocks in row n count n-times as much as blocks in row 1 (counting from bottom to top)
11. Row transitions (PD): Sum of all horizontal occupied/unoccupied-transitions on the board. The outside to the left and right counts as occupied.
12. Column transitions (PD): As row transitions but count vertical transitions. The outside below the game-board is considered occupied.

Objectives 1-6 were produced in Böhm et al. (2005) whereas 7-12 were from "Standard Tetris Application" originating from Colin Fahey and Pierre Dellacherie (Fahey, 2012), indicated as CF and PD respectively in the above list. Initial runs in a domain of 10x20 were conducted using objectives 1-6 and then runs including all of the objectives were conducted in a domain of 6x12. This decrease of domain was to decrease the computational time for the game to reach failure, as the domain would be filled up quicker as there is less area to be packed.

An evolutionary algorithm was used to solve the value for the different weights for each objective. It was found that the most important objectives (those with the highest weighting score) were Pile Height (1), Holes (2), Connected Holes (3) and Maximum Well Depth (6) for the runs completed using Objectives 1-6 only. In addition, some weighting values become or approached zero meaning that these objectives were not important in finding the best position for the tetrominoes, although the paper does not state which objectives were assigned a zero value and it is stated that this was not always the same in all evolutions of weighting values. For the runs utilising all 12 objectives, Connected Holes (3) and Maximum Well Depth (6) were the highest weighted criteria. However, it is thought that the evolutionary algorithm settled in local maxima which it could not escape from. Böhm et al. (2005) states that the performance of the evolved Tetris game-board rating function produced in the research compares nicely with other reported results. A question lies in the changing of the domain, as reducing the size of the width would give less positions for tetrominoes to be placed. No study was conducted on the change in domain size when using all 12 objectives and if this changes the weighting for each objective, although it is fair that the domain size was reduced as computational time was drastically reduced. Additionally, the program was rerun on the 6x12 domain size for Objectives 1-6 for fair comparison for when Objectives 7-12 were also included.

Kostreva and Hartman (2004) and Böhm et al. (2005) are both rule-based Tetris controllers, in that they are given a set of rules which they apply when determining the placement of the tetrominoes. These rules are given different weightings using an evolutionary process as the program learns more about their effect from different runs of playing the Tetris video game. An alternative approach for solving Tetris with a computer is to use a Reinforcement Learning technique. This technique learns how to place tetrominoes by playing games and giving each run a value function. From this, the program learns which policies it has previously used lead to the best solution, derived from the value function, and employs these policies moving forward. Bdolah and Livnat (2000), Driessens (2004), and Melax (2014) are all examples where Reinforced Learning has been used for finding an optimal Tetris solving method.

Melax (2014), which was first published in 1990, played a simplified version of Tetris in a width of six domain with infinite height using reduced tetrominoes. Although the height was infinite, two levels were only ever active at one time. If the placement of the reduced tetromino increased the height above two blocks, the lower levels were discarded and a score was kept of how many levels were discarded. The best performance was judged to have the lowest score. The reduced domain size and random order of particles increases the likelihood of voids being formed as tetrominoes are more likely to leave gaps due to there being less possible positions to be placed. The introduction of discarding levels means that these gaps can never be returned back to so filling at a later date is not possible. As described by Carr (2005), the agent in Melax (2014) is effectively trying to reduce the height after every placement of a tetromino rather than trying to reduce the height of the overall structure. This could lead to policies never being discovered and a biased is placed on the policy to reduce height for every step rather than for the final structure.

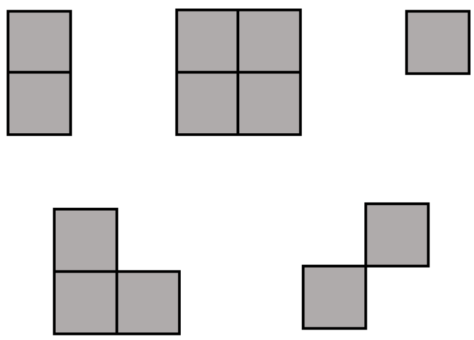

FIGURE 2.39: Reduced tetrominoes used in Melax (2014).

Bdolah and Livnat (2000) adopted the approach taken in Melax (2014) and extended to introduce state space optimisations. This included only using the top contour of the surface, so all information of gaps below are removed, rather than only using the top two lines as possible placement locations. As well, the use of mirror symmetry to reduce the state space was adopted to speed up the learning process as essentially one scenario could now represent what would have been two separate scenarios in Melax (2014). From the results in Bdolah and Livnat (2000), the policy produced led to superior results than in Melax (2014) and at a faster rate of learning. This is most likely due to the retention of more information of the surface leading to more possible locations of placement and the use of mirror symmetry halving the number of states required to describe the Tetris well.

Driessens (2004) applied relational reinforced learning to the full Tetris problem, referred to as Standard Tetris earlier. As described by Carr (2005), relational reinforcement learning means that the relationship between elements in the environment is utilised in developing a reduced state space rather than storing every possible state in a table to refer back to. These relationships are then stored in a decision tree structure. Carr (2005) goes on to state that Driessens (2004) actually led to poor results compared to other algorithms and actually were quite poor when compared to human standards. The reason is described to be due to the use of Q-learning, which relies on good estimates of future rewards to function properly. The stochastic nature of Tetris limits the accuracy of these estimates. However, Driessens (2004) did use a range of criteria when developing their instance based leaner. These included

- The height of individual columns
- The maximum, average and minimum height of the wall and the differences between the extremes and average
- The height difference between adjacent columns
- The number of holes and canyons of width 1
- The average depth of holes

These are all features which could be considered when developing a heuristic for the packing of tetrominoes, and this can be formed further into considering a policy for a heuristic when packing soil particles as this will help lead to reducing void ratio.

Phon-Amnuaisuk (2015) differs from previous research using weighted criterion by employing a GA and data mining process to automatically discover strategies to play Tetris. This was completed through an evolutionary algorithm based on 145 different tetromino sequences of a size of 50, uniformly distributed from the seven classic tetromino shapes. Each of the sequences were evolved using within 500 generations, taking the top 10% of results. The results of the program improved from around 80 unfilled tiles to 20 unfilled tiles after the 500^th generation. 44 concepts were created to help with placing of shapes and Phon-Amnuaisuk (2015) states that a human playing the same sequence of particles could not better the evolved strategy produced by the algorithm. The objective function of the GA was to reduce the presence of unfilled tiles, therefore reducing gaps. It is interesting that a simple function is used rather than an extensive heuristic function like in Böhm et al. (2005).

2.4.6 Summary of Section 2.4

The information gained from the literature presented in Section 2.4 provides great insight to factors that can lead to the reduction of void ratio and increase in stability for a soil packing structure. As discussed in Section 2.4.1, lower porosity or void ratio, coordination number, a lower center of gravity as well as a lower potential energy are suggest to increase stability in a packing system by Graton and Fraser (1935). Liu et al. (2015) (Section 2.4.3) also recognises lower potential energy as a measure of stability as it uses this as a heuristic for their packing procedure. If it is desired to reduce gaps in the system, the inclusion of a range of particle size should lead to a decrease in void ratio so long as the inclusion of smaller particles do not displace the existing particles (White and Walton, 1937; Sohn and Moreland, 1968; Lade et al., 1998; Cubrinovski and Ishihara, 2002). Void ratio is also affected by grading, compaction and particle shape (White and Walton, 1937; Shergold, 1953). While it is suggested that angular particles lead to more voids, this is due to it being hard for them to lie into a position where the particles fit together snugly in traditional compaction methods. Fitting of the particle shapes together using individual placement could potentially lead to overcoming this problem.

Section 2.4.2 describes the difference between deterministic and heuristic approaches for optimisation. The main difference between the two is that deterministic approaches provide an optimal solution that is replicable if the same input is given whilst heuristic approaches provide an estimated optimal answer but at a faster computational time. It is described that problems such as bin packing are NP-hard and therefore it is typical for heuristic, meta-heuristic, hyper-heuristic approaches are often adopted. Two heuristic approaches are then described in Section 2.4.2 - simulated annealing (SA) and genetic algorithms (GA) - as these terms are used in later sections of the thesis.

The approach of off-line or on-line bin packing introduced in Section 2.4.3 is one that is intriguing. Whilst it is clear off-line approaches will likely lead to better packing structures, this will require multiple attempts at positioning the particles and could lead to large computational times. The system taken forth by Galambos and Woeginger (1993) could be a good one to follow, only repacking a small number of items. This replicates the backtracking that is found in a tree-search algoirthm. Goldberg et al. (2002) scored jigsaw edge matching based on fit and then uses a one step lookahead as seen in Section 2.4.4. This reduces the total number of permutations by only looking one step ahead rather than having information of the whole problem.

The use of a heuristic is present within a vast amount of the work in the bin packing topic as well as for Jigsaw solving and Tetris optimisation. A large range of the literature reviewed feature some sort of depth criteria and tend to be placed in the bottom left of the domain. Within Section 2.4.3, Jakobs (1996) and Liu and Teng (1999) positioned items by lowering them and sliding them to the left using BL and BLLT approaches. Hifi and M'Hallah (2002) determined the best placement to be the bottom left unless a hole can be filled by the item and Wang et al. (2010) also prioritised the bottom-most position in their DBLF algorithm.

Another scoring method is based on the area of an item in contact with another item. Lodi et al. (1999a) introduced the TP algorithm based on the item's perimeter in contact with other items. Terashima-Marín et al. (2010) scored the placement based on the smallest envelope created around the placed particles which automatically looks to place particles tightly together. Wang et al. (2010) looked at the touching area as a heuristic for three-dimensional items. In the problem of solving jigsaws, placements are scored by their fits to each other i.e. the minimum amount of gap between edges. Many different variants of judging this match are done such as the straight-line approximation of the curve in Freeman and Garder (1964), using curve maxima and minima in Radack and Badler (1982) or isthmus critical points as suggested by Webster et al. (1991) as discussed in Section 2.4.4. Both Kong and Kimia (2001) and Hoff and Olver (2014) use curve marching to solve apictorial jigsaw puzzles which minimise space between the matching edges.

Within these problems, taking multiple best solutions before moving to the next step is common, like in Woflson et al. (1988) who took the 200 best solutions through to the next step where then the next 200 best solutions were selected. Additionally, a use of discarding obviously bad placements can be used like in Webster et al. (1991) who discarded bad matches who had specified criteria for possible matches. This would reduce runtime of the program.

For optimisation of Tetris (Section 2.4.5), objective functions are defined with many scoring criteria and usually a weighted function is utilised. Kostreva and Hartman (2004) and Böhm et al. (2005) are two examples of the use of a weighted function to score possible placements of tetrominoes in the Tetris problem. Of these criteria, minimising gaps below the placed block, maximising the number of contacting cell walls and minimising the height of the total structure stand out as those relevant to the other areas of research covered in Section 2.4.5. Every possible location and rotation are scored for placement and the best solution is selected. Driessens (2004) also prioritised minimising height as well as the number and depth of holes created. Phon-Amnuaisuk (2015) based their Genetic Algorithm on a criteria that reduced the presence of unfilled titles.

A top-down approach is present in many papers, such as Jakobs (1996) and Liu and Teng (1999). Tetris is inherently a top-down problem so most research based on Standard Tetris use this approach. Wang and Hauser (2019) uses top down to avoid collisions when placing items within the bin and even uses a feasibility check to avoid knocking into other items and displacing them. The stability check used in Wang and Hauser (2019) is also a process that should be taken note of as it would be beneficial to make use of this in this project. The stability was modelled using contact points and a Coulomb frictional model based on friction coefficient. This can be easily adapted into this work.

The splitting of the domain into coordinates considered within Section 2.4.3 as adopted by Dowsland et al. (1998) and Liu et al. (2015) is useful as it would help avoid gaps in the system. However, if we are using an on-line method, then it will not be possible to go back to place items in gaps that are missed. The shifting used in Liu et al. (2015) may also be used to ensure the touching of particles and to minimise gaps. Both of these processes could lead to a much larger computational time. To overcome this, the domain and items could be split into a smaller resolution for scoring before being scored at a higher resolution, like in Cagan et al. (1998).

From Section 2.4.5, The use of a top contour of the surface for possible placements in Bdolah and Livnat (2000) can be taken forward in this project. Unlike with Tetris, rows of filled space will not disappear. If a top-down method is adopted as is suggested in Section 2.2.4, then this will mean that any gaps below the surface will not be able to be filled without the use of backtracking or an off-line approach. Therefore, a surface contour for possible placements may lead to a reduction in computational time in a developed program for soil particle packing.

2.5 Characterisation of Particle Shape

2.5.1 Classifications of Particle Shape

The term morphology of a particle can be used to describe the overall external expression and can be split into two expressions, shape and surface texture (Blott and Pye, 2008). These describe the larger/medium scale and the small-scale features of the particle respectively. To quantify the shape of a particle, this term has been further split down into four aspects that contribute: form, sphericity, roundness, and irregularity. In some literature, form and sphericity are grouped together with sphericity being classed as a measure of form (Barrett, 1980). Here, they will be split into two separate groups in this section.

Three-dimensional shapes can be converted into two-dimensional shapes that represent the outline from a certain view of the particle. This can be achieved using numerous methods. For example, Pettijohn (1949) (as cited by Yudhbir and Abedinzadeh, 1991) used silhouettes of the grains for the grouping of particles into classes. Other methods involve taking images of the particles either by camera or microscope and producing two-dimensional outlines from these pictures (Huu et al., 2017). The outlines can be used to measure form, roundness, irregularity and sphericity without taking into consideration of the third dimension. Obviously this has the disadvantage of ignoring the third plane. If the third dimension is desired using these methods, the thickness of the particle is estimated by the shadow projection of the particle (Huu et al., 2017). Following this, form, roundness, irregularity and sphericity are described and methods of classifying particles or quantifying these measures are discussed for both two-dimensional and three-dimensional shapes. Note, sphericity for a two-dimensional shape is not possible but the term circularity can be adopted for a similar description.

Form

Sneed and Folk (1958) explained that form describes a particle by its length (L), breadth (I) and thickness (S). These are all measured orthogonally to each other. It is standard practice to assign L as the longest dimension of the particle, I as the longest dimension perpendicular to L, and S as the dimension perpendicular to L and S (Krumbein, 1941). For a two-dimensional shape, it is assumed that S acts into the plane and is of negligible size.

These three orthogonal dimensions can be plotted on charts to help define the particles. The first to do so was Zingg (1935) (as cited by Blott and Pye, 2008) which plots breadth to length (I/L) and thickness to breadth (S/L) in a two-axis plot. Four terms were used to describe the particles: flat, spherical, flat and columnar, and columnar. These have also been referred to as disc-shaped, spherical, bladed and rod-like (Krumbein, 1941). An example of the original form diagram proposed by Zingg (1935) (as cited by Blott and Pye, 2008) is represented in Figure 2.40. Sneed and Folk (1958) produced a triangular plot for describing particle shape, stating that a bivariate diagram like that in Figure 2.40 is not sufficient to plot a feature determined by three variables. The plot is presented in Figure 2.41. Sneed and Folk (1958) divided the plot into ten fields, each with a different descriptive term. These are indicated in the key in Figure 2.41.

Two parameters adopted to describe the form of a particle are platiness, α, and elongation, ζ. Potticary et al. (2016) described these using Equation 2.12 and Equation 2.13

$$\alpha = \frac{2(I - S)}{L + I + S} \tag{2.12}$$

$$\zeta = \frac{L - I}{L + I + S} \tag{2.13}$$

Figure 2.42 presents the α-ζ plane as plotted in Potticary et al. (2015). Potticary et al. (2015) states that the edges and corners of the triangle correspond to cases where some of the dimensions are equal and/or zero. A sphere resembles the shape where

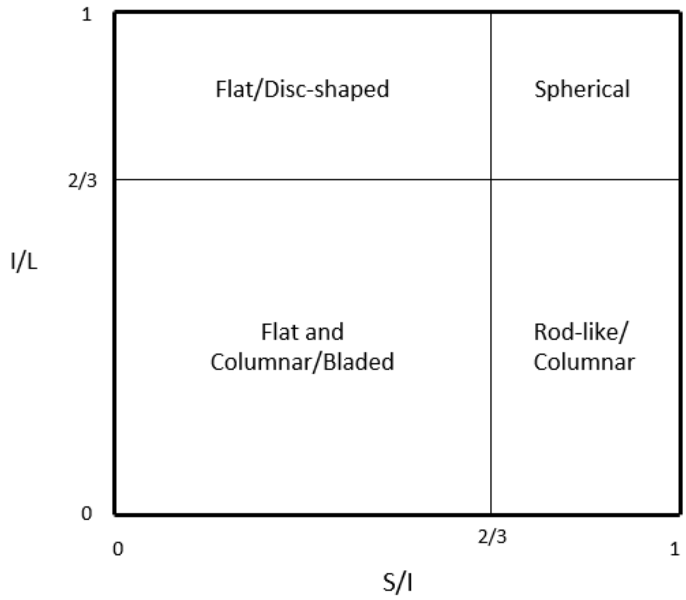

FIGURE 2.40: Zingg Diagram adapted from Zingg (1935) (as cited by Blott and Pye, 2008).

all values are equal, a circular disk resembles the shape where L and I are equal and S is zero, whilst a needle resembles the shape where L is the only non-zero value.

Li et al. (2013) states that elongation measures the symmetry of the particle shape and is calculated using Equation 2.14. Blott and Pye (2008) also suggests that elongation is calculated in this manner. The absence of S for measuring elongation means that this can be used to describe two-dimensional outlines with no consideration of the dimension into the plane the shape is cast.

$$\zeta = \frac{I}{L} \tag{2.14}$$

Wentworth (1923) attempted to quantify particle form defined as the flatness index, I_F, calculated using

$$I_F = \frac{L + I}{2S} \tag{2.15}$$

This is sometimes referred to as the Callieux Flatness Index as it was adopted by Cailleux (1945). I_F is very clearly a three-dimensional factor as it requires thickness to be a non-zero value. Several authors have used the ratio of thickness to length (S/L) to measure flatness (Ballantyne, 1982; Barrett, 1980; Howard, 1992). However, particles with an S/L ratio of 0.2 can range from square, flat forms to highly elongated forms. Illenberger (1992) considered S/L to be a measure of equancy and recognises the parameter

$$\frac{I - S}{L} \tag{2.16}$$

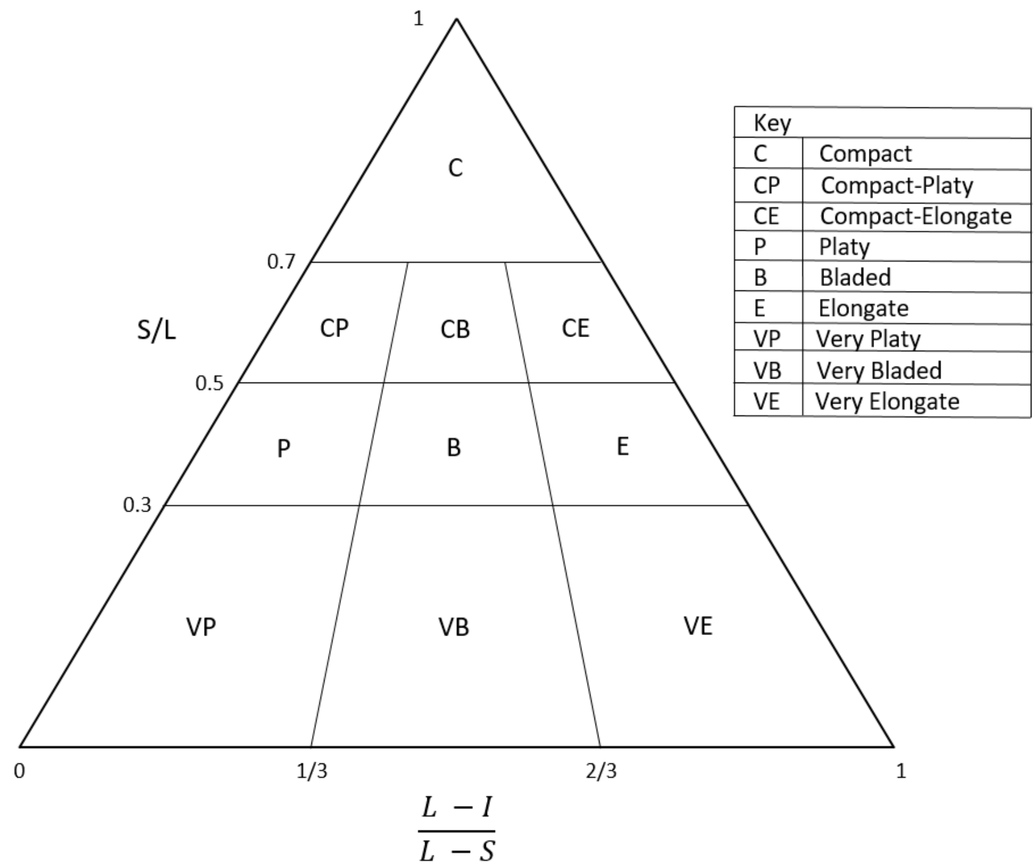

FIGURE 2.41: Form Diagram adapted from Sneed and Folk (1958) with key for form terms.

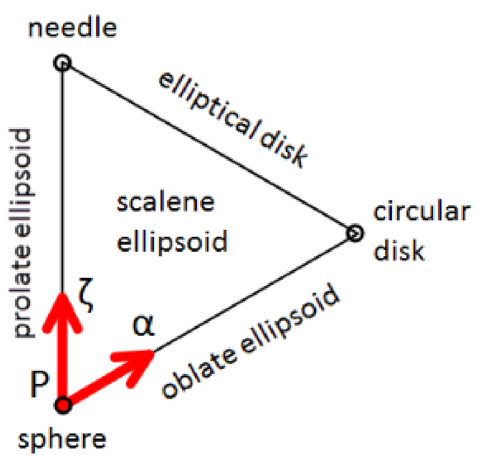

FIGURE 2.42: Elongation and Platiness plane with description of forms (Potticary et al., 2015).

as an index of flatness. However, Blott and Pye (2008) states this was more a measure of platiness and that true flatness is best described by the parameter S/I.

Alshibli and Cil (2018) defines form using S/L. This is equivalent to what Illenberger (1992) considers equancy. The simplicity of the form calculation in Alshibli and Cil (2018) shows that this is not a suitable measure as it completely ignores a lot of features of the particle, especially I.

Barrett (1980) reviewed measures for classifying form and found that the use of three orthogonal dimensions are not satisfactory for describing some forms. Triangular, rectangular and pentagonal cross-sections were highlighted. Barrett (1980) states that these forms can be distinguished by the number of sides that are present and therefore the number of sides is an aspect of form and not roundness. However, irregular, untooled rock shapes will have many sides and it will be hard to distinguish a quantity for this. Barrett (1980) suggests that the way form is defined excludes other aspects of shape such as roundness.

Circularity and Sphericity

Sphericity refers to the global form of the particle and reflects the similarity between L, I, and S (Cho et al., 2006). When discussing sphericity, it is common to think that a spherical shape is one which has equal dimensions in the three axis of breadth, length and width. However, using this method would mean that a cube could be described as spherical.

Wadell (1932) described the degree of sphericity of a particle, Ψ, as the ratio of the surface area of a sphere with the same volume as the particle, s_p, to the surface area of the particle, S_p.

$$\Psi = \frac{s_p}{S_p} \tag{2.17}$$

Wadell (1933) (as cited by Blott and Pye, 2008) transforms this into a two-dimensional quantification of a particle image using

$$\Lambda = \frac{c_p}{C_p} \tag{2.18}$$

where Λ is the degree of circularity, c_p is the perimeter of a circle of the same area as the particle shape and C_p is the actual perimeter of the particle shape. Measuring of sphericity using this method is shown in Figure 2.47. The maximum values of Ψ and Λ are 1, where such a value represents a sphere and circle respectively.

Barrett (1980) states a disadvantage of using the approach in Wadell (1933) (as cited by Blott and Pye, 2008) to characterise a particle is that sphericity is not just a parameter of shape but is also affected by angularity. In addition, it is impractical to measure the surface area of a soil particle, although this is much easier to do on the two-dimensional projection of one. Wadell (1933) (as cited by Blott and Pye, 2008) also suggested calculating circularity using a ratio of the diameter of a circle with the same area as the particle to the diameter of the smallest circumscribed circle which was named projection sphericity, Λ_P.

Riley (1941) proposed an index to measure circularity which was termed the inscribed circle sphericity Λ_I. In this method, the square root of the ratio of the largest inscribed circle diameter, D_i, to the smallest circumscribed circle diameter, D_c, is used as shown in Equation 2.19. An example of how this is determined is presented in Figure 2.43 with an indication of each diameter given.

$$\Lambda_I = \sqrt{\frac{D_i}{D_c}} \tag{2.19}$$

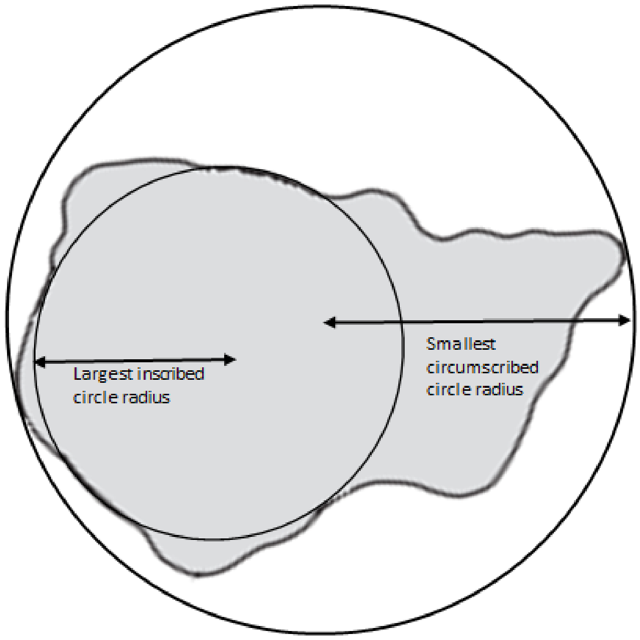

FIGURE 2.43: Method for measuring inscribed circle sphericity as described by Riley (1941) adapted from Blott and Pye (2008) with permission from John Wiley and Sons.

Roundness and Angularity

Angularity, or roundness, describes the scale of major surface features (Cho et al., 2006). It is typically estimated by measuring the sharpest corner or by obtaining a measure of convexity in the particle outline (Yudhbir and Abedinzadeh, 1991). Wadell (1932) described roundness as the curvature of the corners and edges of a particle compared to that of the overall particle shape and states that it is independent of sphericity. Initial studies into the roundness were made to make visual comparisons (Mackie, 1897 and Dunn, 1911 both as cited by Blott and Pye, 2008) but the first attempts to quantify roundness was made by Wentworth (1919) on sedimentary particles.

Wentworth (1919) suggested roundness was the ratio of the radius of curvature of the most convex part of the particle to half the longest diameter through that point. This is not necessarily the length of the particle. Wentworth (1922a) and Wentworth (1922b) (as cited by Kuenen, 1956) later revised this method so that roundness was calculated using the ratio of the radius of the sharpest corner to the mean radius of the particle. This is a fair method to measure roundness, but the sharpness of a single corner may not represent the grain as a whole, especially in fractured particles (Blott and Pye, 2008). Other variants have been proposed that use the ratio of the diameter of the curvature of the sharpest corner to the intermediate axis of the grain (Kuenen, 1956) or the diameter of the largest inscribed circle (Dobkins and Folk, 1970).

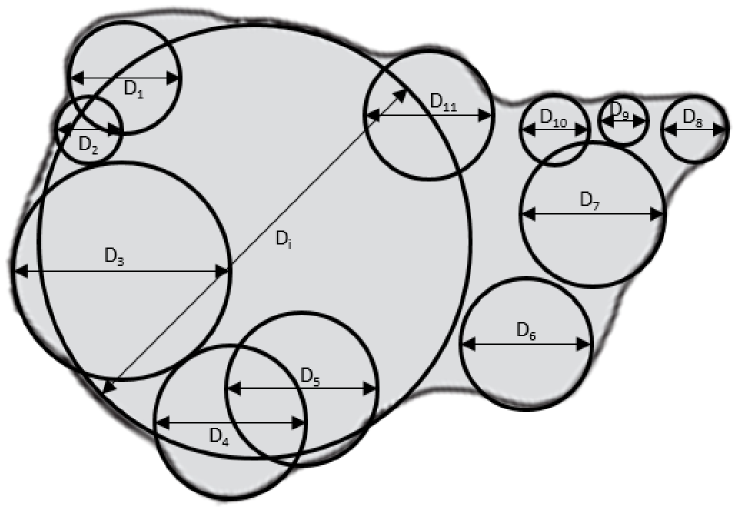

FIGURE 2.44: Diagram to show how measurements to calculate particle roundness using method proposed in Wadell (1932) are taken adapted from Blott and Pye (2008) with permission from John Wiley and Sons.

Wadell (1932) stated that the maximum degree of roundness is reached when the radius of curvature of a corner equals the radius of the maximum inscribed circle. Wadell (1932) proposed that the average curvature of the corners can be calculated by measuring the radius of all corners of a projection of the particle outline. The formula is given to find degree of roundness as

$$R = \frac{\sum\left(\frac{D_n}{N}\right)}{D_i} \tag{2.20}$$

Where D_i is the diameter of the largest inscribed circle, D_n is the diameter of curvature of any corner and N is the number of corners. Figure 2.44 demonstrates how this would be measured for a given particle outline. Each corner is analysed individually before a mean is taken to give the degree of roundness. It is understandable that the process of measuring the roundness of each corner can take time. Therefore, many researchers have produced visual charts for comparing the roundness of particles using Wadell's method to classify particles. These include Krumbein (1941), Powers (1953), and Russell and Taylor (1937). Roundness can be extended to be a three-dimensional measure by adopting spheres instead of circles for each corner (Barrett, 1980).

Lees (1964) showed that the measure of roundness is not able to differentiate between truly angular corners of different angles, since the radius of curvature of a circle fitted into an angular corner is nil irrespective of the size of the angle. Hence, Lees (1964) proposed a measure for any corner in the projected outline of a particle calculated using

$$A_{2D} = \sum_{i=1}^{n} (180^o - a_i)\frac{x_i}{r} \tag{2.21}$$

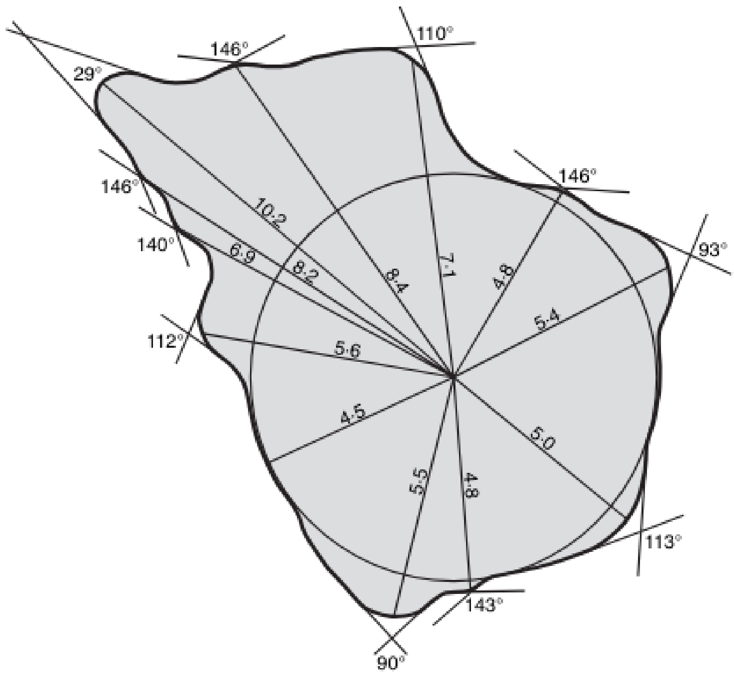

FIGURE 2.45: Measurements for calculating A using Equation 2.21 taken from Blott and Pye (2008) with permission from John Wiley and Sons.

termed the Degree of Angularity, A_{2D}, where a is the angle between planes bounding the corner, x is the distance of the top of the corner from the centre of the maximum inscribed circle, r is the radius of the maximum inscribed circle, and n is the number of corners. Measurements taken to determine angularity are presented in Blott and Pye (2008) and this is reproduced in Figure 2.45. The total degree of angularity for a three-dimensional shape, A_{3D}, is given by the sum of values A_{2D} for all the corners measured in each of the three orthogonal planes. Lees (1964) recognised that this method is very time consuming. However, it can be appreciated for a two-dimensional shape that the process is less so as only one plane is needed for this measurement.

Irregularity

The term "regular" is used to describe a shape with straight or smooth, continuously curving sides in two or three dimensions. The shape can be regarded as irregular if there are significant concavities and convexities on the surface. A gravel or soil particle can be described as irregular due to projections and indentations on the surface which can either be rounded or angular. A measure of particle irregularity has been developed to quantify the particle shape in two-dimensional images in Blott and Pye (2008). This is called the irregularity index, I_{2D}, and is found for a two-dimensional shape using

$$I_{2D} = \sum \frac{y - x}{x} \tag{2.22}$$

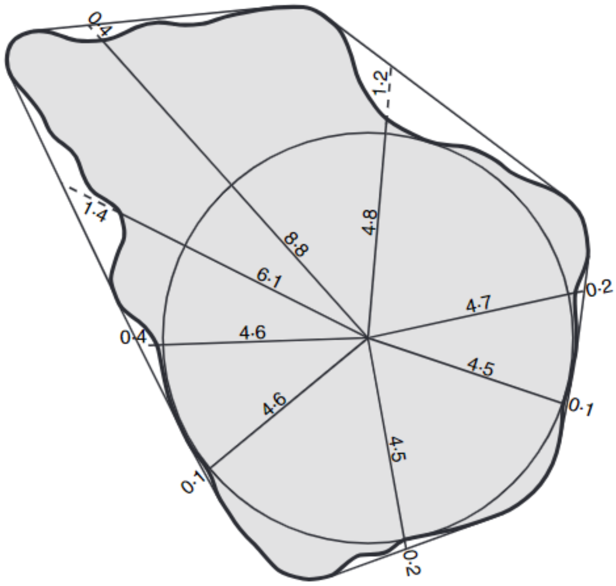

FIGURE 2.46: Measurements for calculating I_{2D} using Equation 2.22 taken from Blott and Pye (2008) with permission from John Wiley and Sons.

where x is the distance from the centre of the largest inscribed circle to the nearest point of any concavity and y is the distance from the centre of the largest inscribed circle to the convex hull. A measure of this index can be calculated for three-dimensions by summing the values of the projections of the particle from each orthogonal orientation, similar to angularity described by Lees (1964). This is referred to as I_{3D}. Figure 2.46 presents the method for calculating irregularity for a particle outline.

Whalley (1972) stated that surface texture is not resembled in a projected outline of a particle. However, Barrett (1980) states this is not true for crystalline rock particles. Additionally, Cho et al. (2006) describes roughness as the surface texture of a particle relative to the radius. It can be understood that a particle has a higher roughness if it has more irregularities. Following Barrett (1980) and Cho et al. (2006), irregularity is a measure of the roughness.

Convexity is another term used to describe the smoothness of a particle surface. Convexity, C, is given in Equation 2.23 as described by Li et al. (2013) where p_{hull} and $p_{particle}$ are the perimeters of the convex hull and the particle respectively. Li et al. (2013) states that convexity can range from 1 for a smooth particle and almost zero for a very rough one .

$$C = \frac{p_{hull}}{p_{particle}} \tag{2.23}$$

Yang and Luo (2015) describes convexity using a different method to Li et al. (2013). In Yang and Luo (2015), convexity is found as the ratio of the area of the particle (A) to the area of the convex hull that describes the particle (A+B). Figure 2.47 presents a particle with this calculation being performed.

Alshibli et al. (2014) measured surface texture of sand particles using an optical interferometry technique that led to particles being described through three-dimensional pixelated images. Root-mean-square (RMS) texture, R_q is found using the following

$$R_q = \sqrt{\frac{1}{MN}\sum_{i=1}^{M}\sum_{j=1}^{N} Z_{ij}^2} \tag{2.24}$$

where M and N are the number of pixels in the X and Y directions and Z_{ij} is the surface height at a specific pixel relative to the reference mean place. R_q represents the standard deviation of the surface heights (Alshibli et al., 2014). RMS texture is measured rather than average as it gives more significance to valleys and peaks in the image. Alshibli et al. (2014) successfully describes morphology of sand particles as well as glass beads. However, R_q is a three-dimensional measure and does not translate when analysing two-dimensional outlines.

Yang and Luo (2015) adopts four simplified shape parameters for characterising sand mixtures. These were sphericity, aspect ratio (AR), convexity, and overall regularity (OR). Sphericity and convexity have already been defined up to this point.

AR is defined by Equation 2.25 and is the ratio between D^{Fmin} and D^{Fmax}. D^F represents the Feret diameter, which is the distance between two tangents on opposite sides of the particle. Hence, D^{Fmin} and D^{Fmax} represent the minimum and maximum Feret distances respectively. Figure 2.47 indicates how AR can be calculated for a particle as presented in Yang and Luo (2015).

$$AR = \frac{D^{Fmin}}{D^{Fmax}} \tag{2.25}$$

Following the definition of AR, Yang and Luo (2015) goes on to define OR using the three terms of sphericity, aspect ratio and convexity. These are combined as follows.

$$OR = \frac{AR + \Psi + C}{3} \tag{2.26}$$

OR is used to try and characterise particle shapes in a collective manner and Yang and Luo (2015) uses this method to characterise a mixture of sands. Such a term could be adopted to describe two-dimensional particle shapes as each term can be found for an individual plane of a three-dimensional shape and Ψ can be replaced by Λ.

2.5.2 Fourier Descriptor Method

Ehrlich and Weinberg (1970) (as cited by Mollon and Zhao, 2012) proposes a method to yield a mathematical model of a two-dimensional soil grain based on discrete Fourier transforms in closed form. The contours of the grain are split into N_p points separated by a constant angle (θ_p, such that $\theta_p = \frac{2\pi}{N_p}$). Thus, each point is defined by an angle, θ_i, and a radial distance, r_i, which is the distance from a suitable centre to that point. Using Fourier theory, $r_\mathrm{i}(\theta_\mathrm{i})$, can be represented by the following series

$$r_\mathrm{i}(\theta_\mathrm{i}) = r_0 + \sum_{n=1}^{N}[A_\mathrm{n} cos(n\theta) + B_\mathrm{n} sin(n\theta)] \tag{2.27}$$

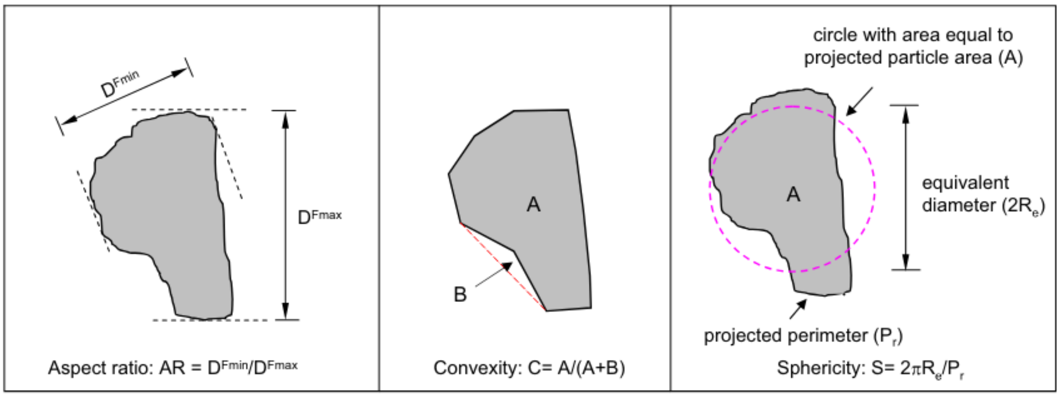

FIGURE 2.47: Definitions of aspect ratio (AR), convexity (C) and sphericity (S) from Yang and Luo (2015) used with permission from Elsevier.

where n is the number of the harmonic, N is the total number of harmonics, and A_n and B_n are coefficients giving the magnitude and phase for each harmonic. However, as stated by Bowman et al. (2001), the use of the closed form leads to the possibility of re-entrant angles where the radius intersects the particle outline twice. An example of this can be seen in Figure 2.48. As a result, two possible values of radius r are obtained at a given angle θ

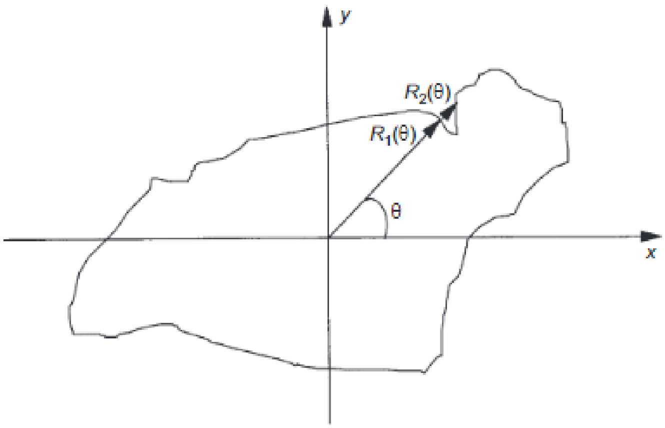

FIGURE 2.48: Example of re-entrant of the radius using Fourier analysis in closed form on a particle outline (Bowman et al., 2001) © Thomas Telford Ltd. Images used under Creative Commons Attribution-Non-Commercial 4.0 International Copyright (Creative Commons, 2013a).

Alternatively, Bowman et al. (2001) suggested the use of the Fourier descriptor method that was introduced by Clark (1981) (as cited by Bowman et al., 2001).

$$x_m + iy_m = \sum_{n=-N/2+1}^{N/2} (A_n + iB_n) \left[\cos\left(\frac{2\pi nm}{M}\right) + i \sin\left(\frac{2\pi nm}{M}\right) \right]$$

where x and y are coordinates of the particle outline, N is the total number of descriptors, n is the descriptor number, M is the total number of coordinates describing the particle, m is the index number of a point on the particle, A and B are coefficients for each descriptor and i denotes an imaginary number. Bowman et al. (2001) discusses how the Fourier descriptor method does not suffer from the re-entrant angle problem and that an accurate location of a centroid is not required.

The number of descriptors produced by the Fourier analysis is determined by the number of points chosen to describe the particle outline. Bowman et al. (2001) states that for 128 points, there are a possible N=128 Fourier descriptors ranging from -63<=n<=64. However, the value of these descriptors decays as these limits are approached and Bowman et al. (2001) suggests that the lower-order descriptors of n=-1 and n=1-4 can be used to describe the particle morphology. Analysis on various shapes conducted by Bowman et al. (2001) led to the effect of different shape descriptors and defined "signature descriptors" to have an effect of particle shape as listed in Table 2.7.

From this analysis, Bowman et al. (2001) refined their suggestion and stated that although n=+2 and n=+3 give additional information, the maximum signature descriptors required to approximate morphology are n=-1, -2, -3 and n=+1. Das (2007) suggested that Fourier descriptors n=+3 to n=+8 define the main irregularities of the particle contour whilst descriptors above n=8 can describe the roughness of the particle. These are also included in Table 2.7

Descriptor, n	Measurement of descriptor	Reference
-3	Squareness	Bowman et al. (2001)
-2	Triangularity	Bowman et al. (2001)
-1	Elongation, i.e. aspect ratio	Bowman et al. (2001)
0	Radius i.e. particle size	Bowman et al. (2001)
+1	Asymmetry or irregularity	Bowman et al. (2001)
+2	Second-order elongation term	Bowman et al. (2001)
+3	Second-order triangularity term	Bowman et al. (2001)
+3 to +8	Irregularities of the contour	Das (2007)
>+8	Roughness	Das (2007)

TABLE 2.7: Descriptors highlighted by Bowman et al. (2001) and Das (2007) and the effect they measure.

Bowman et al. (2001) shows that the shape descriptor, n, can be calculated from the amplitude of A_n and B_n. However, for comparison between differing sand grains, Bowman et al. (2001) explains that each descriptor should be normalised by the first descriptor value which is a measure of the radius of the particle. This normalised amplitude, D_n, is given for each harmonic, n, by

$$D_{\mathrm{n}} = \frac{\sqrt{{A_n}^2 + {B_n}^2}}{r_0} \tag{2.28}$$

A_n and B_n can be found by applying a discrete Fourier transform to $r_{\mathrm{i}}(\theta_{\mathrm{i}})$ that will give

$$A_n = \frac{1}{N} \sum_{i=1}^{N} \left[r_i \cos\left(i \cdot \theta_i \right) \right] \tag{2.29}$$

$$B_n = \frac{1}{N}\sum_{i=1}^{N}\left[r_i \sin\left(i \cdot \theta_i\right)\right] \tag{2.30}$$

It can be understood that D_0 will be equal to 1 as the amplitude of A_n and B_n will equal r_0 (Mollon and Zhao, 2012).

2.5.3 Generating Particle Shape from Fourier Descriptors

Mollon and Zhao (2012) reversed the concept of descriptors by using a spectrum to generate random particles using prescribed particle shape descriptors. This is the method that has been adopted in this research. Mollon and Zhao (2012) does this by defining only three values for shape descriptors. As explained previously, Bowman et al. (2001) and Das (2007) states that the most effective shape descriptors are within the range of n=-3 to n=+8. From these, it is known that D_0 is equal to 1. Mollon and Zhao (2012) states that D_1 corresponds to a shift of the grain contour with respect to a position point, O, and that this can be set to zero if the position of O is properly selected. D_2 is described to be extremely important to define the elongation of the particle. As for shape descriptors from D_3 and upwards, these are determined using

$$D_n = 2^{\alpha - \log_2(n/3) + \log_2(D_3)} \text{ for } 3 < n < 8 \tag{2.31}$$

$$D_n = 2^{\beta \cdot \log_2(n/8) + \log_2(D_8)} \text{ for } n > 8 \tag{2.32}$$

which determine a spectrum of the descriptors defined using D_2, D_3 and D_8. The reasoning for this is that Meloy (1977) showed that descriptor number decreases linearly when in a log-log scale in natural sands. The surface roughness of given sand can thus be described by only a slope and an intercept. An example of the sort of spectrum that would be produced is given in Figure 2.49. It should be noted that this is not in a log-log scale but the values for Fourier descriptors does decrease logarithmically. To simplify the analysis in Mollon and Zhao (2012), just descriptors D_2, D_3 and D_8 are taken for defining these slopes. α and β are values that describe these slopes and in the work conducted in Mollon and Zhao (2012) are taken to both equal -2. As deduced from information given in Bowman et al. (2001), Das and Ashmawy (2007), and Mollon and Zhao (2012), D_2, D_3 and D_8 represent Fourier descriptors for elongation, irregularity and roughness respectively.

From the spectrum determined by D_2, D_3 and D_8 and defined by Equation 2.31 and Equation 2.32, the reverse operation can be conducted to generate two-dimensional particle outlines with similar features. As features are described by the amplitude of A_n and B_n, Mollon and Zhao (2012) applies a degree of randomness by considering a phase angle, δ_n, for a given D_n defined by

$$\delta_n = tan^{-1}\left(\frac{B_n}{A_n}\right) \tag{2.33}$$

To create a random particle, a randomly assigned phase angle can be applied to each descriptor in the amplitude spectrum $\{D_n\}$ where n is greater than zero. Mollon and Zhao (2012) states that each of these random angles follows a uniform distribution

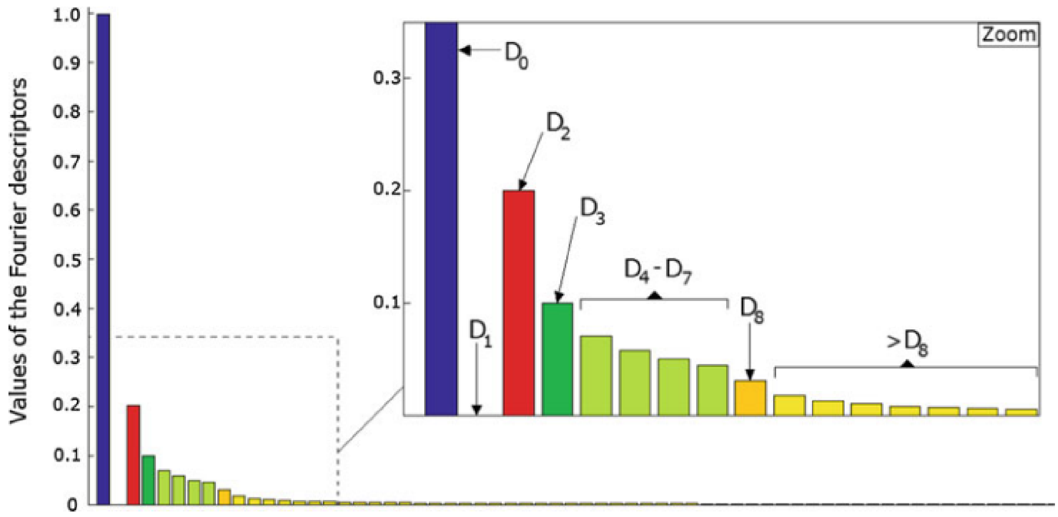

FIGURE 2.49: Illustrative normalised amplitude spectrum as presented in Mollon and Zhao (2012) reproduced with permission from SNCSC.

on the interval $[-\pi;\pi]$. The contour of the particle is found using Equation 2.27 where A_n and B_n are defined by

$$A_n = D_n.cos\delta_n \tag{2.34}$$

$$B_n = D_n.sin\delta_n \tag{2.35}$$

Placement of particles in a domain are determined by discretising the area into Voronoi cells which is based on the Voronoi tessellation approach described by Tillemans and Herrmann (1995) (as cited by Mollon and Zhao, 2012). Each cell is filled by a particle shape outline. An optimisation is conducted on how close each particle fills the cell compared to the targetted solid fraction which can be described as how much of the domain is made up of soil grains. From this, a layout of soil grains is created using just three Fourier Descriptors, D_2, D_3 and D_8. The effect that each of these descriptors is presented in Figures 2.50 and 2.51 which can also be found in Mollon and Zhao (2012).

Software for the generation of particles using the Fourier-Voroni method as described in Mollon and Zhao (2012) has been developed by Guilhem Mollon and is available from Mollon (2023). The programme is coded in MATLAB and generates 2D particle shapes, although a 3D version is readily available (Mollon and Zhao, 2013). The variety within the generated particles comes from the use of a random phase angle with the specified descriptors to find A_n and B_n as described in Equation 2.34 and Equation 2.35. The model also uses the Voronoi cell technique to create a realistic particle packing. It was considered that this could be adopted to create a packing structure of particles in this work before refining the placement. However, the arrangement of the particles produced leaves quite a high amount of voids between particles. Therefore this has not been adopted as a method for packing of particle outlines. Instead, the arrangements are created using the Fourier-Voronoi techniques and particle shapes are extracted. The Voronoi tessellation approach is

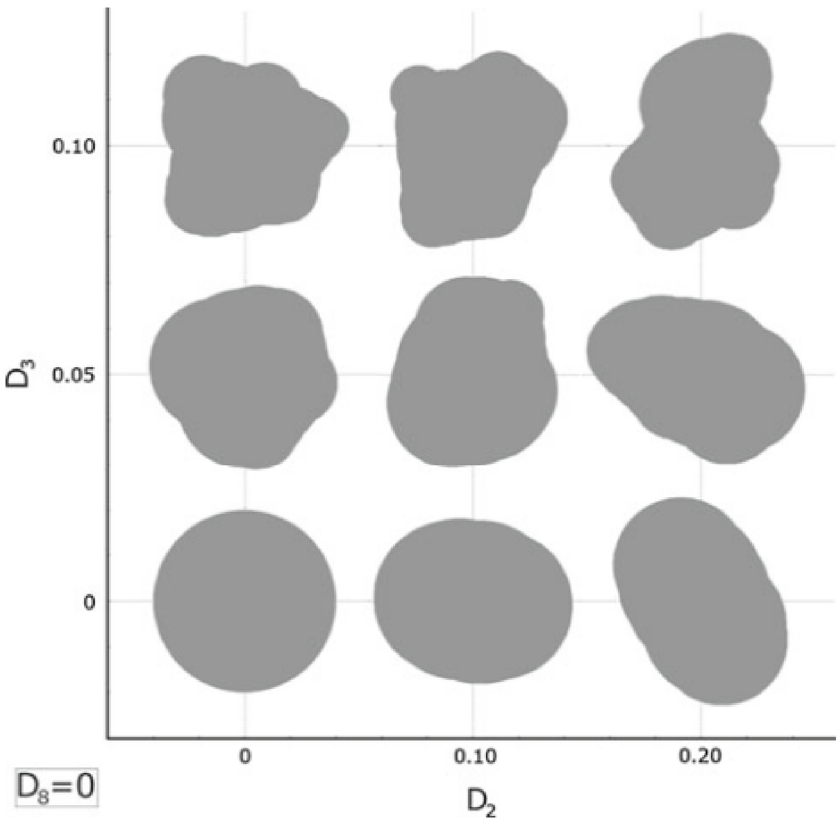

FIGURE 2.50: Effect of D_2 and D_3 on particle shape as presented in (Mollon and Zhao, 2012). Reproduced with permission from SNCSC.

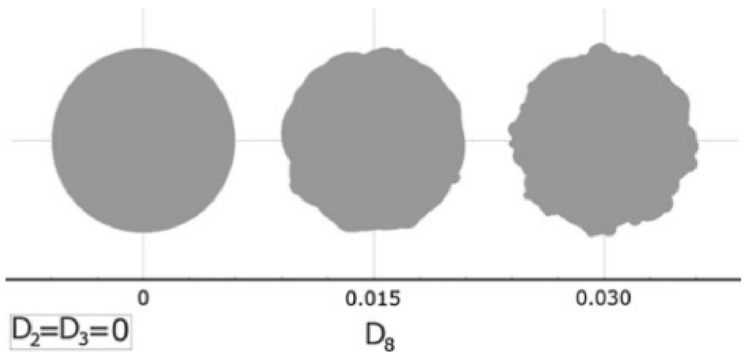

FIGURE 2.51: Effect of D_8 on particle shape as presented in Mollon and Zhao (2012). Reproduced with permission from SNCSC.

mentioned to outline the parameters adopted when creating shapes using the code in Section 3.6.1 but not further explored as it is not relevant to the types of shapes created.

2.5.4 Summary of Section 2.5

Section 2.5 describes different concepts for characterising particle shape as well as a method for generating two-dimensional particle outlines. The characterisation of particle shapes is beneficial for a selection process of particles for construction so that particles whose shape will lead to lower shear strengths of the structure can be discarded without an attempt to place them in the system. Meanwhile, the generation of two-dimensional particle shapes is beneficial as this is adopted to create the outlines that are packed in the algorithm described by Chapter 3.

Section 2.5.1 defines morphology of a particle and states that four aspects can be used to describe particle shape. These are form, sphericity, roundness, and irregularity. Each are defined in Section 2.5.1 with different methods presented for both two-dimensional and three-dimensional particle shapes.

Both Zingg (1935) and Sneed and Folk (1958) adopted plots to define the form of a particle. The description of the particle depends on where it lies on the plot. Both require all three measurements of L, I and S and therefore cannot be used for defining two-dimensional outlines unless thickness is assumed. Flatness again is a three-dimensional term that requires the thickness of the particle, which normally would be the parameter that is assumed for two-dimensional shapes. Potticary et al. (2016) defined platiness and elongation to describe the form of a particle but again uses L, I and S to define these parameters. However, Blott and Pye (2008) and Li et al. (2013) both define elongation using Equation 2.14 which omits S. Therefore, this can be adopted as a two-dimensional descriptor for the outline of particles.

Sphericity is inherently a three-dimensional shape as it compares particle shape to that of an ideal sphere. However, circularity is a two-dimensional version of this comparing particle shape to an ideal circle as defined in Wadell (1933) (as cited by Blott and Pye, 2008). Circularity is calculated using Equation 2.18. Maximum value of Λ is 1 with this representing an ideal circle. Wadell (1933) (as cited by Blott and Pye, 2008) also defined circularity as the ratio of the diameter of a circle with the same area as the particle to the diameter of the smallest circumscribed circle and called this projection sphericity. Riley (1941) defined inscribed circle sphericity using Equation 2.19. Both Λ_P and Λ_I can also be adopted to describe the circularity of two-dimensional particle outlines.

Roundness can be described using Equation 2.20 as proposed by Wadell (1932). This measures each corner of the particle and averages them to get the degree of roundness. This can be a time consuming process. As described by Barrett (1980), roundness can be extended to be a three-dimensional measure by adopting spheres instead of circles for each corner. Lees (1964) measured angularity, or in other words how far away from roundness a particle is, by the method described in Equation 2.21. Again, this method is also described to be time consuming. However, with the use of high-performance computational techniques, it is envisioned that the time to complete these calculations would not be equivalent to the time that was required when Wadell (1932) and Lees (1964) were published.

Surface roughness or surface texture can be described by the irregularity of the particle. This is typically defined as its difference from a convex hull that described the outline. These measures can be made for two-dimensional outlines of each plane and then be converted into a three-dimensional value. Therefore, the methods are suitable for describing two-dimensional particle outlines with the omission of the conversion step. I_{2D} is defined by Blott and Pye (2008) . Li et al. (2013) and Yang and Luo (2015) both described the term convexity using different methods, presented in Equation 2.23 and Figure 2.47 respectively. Aspect ratio is also defined by Yang and Luo (2015) using Equation 2.25. Yang and Luo (2015) then goes on to combined sphericity (or circularity), aspect ratio and convexity to describe overall regularity which is meant to give a general term to describe the particle shape.

Derivation of Fourier descriptors from two-dimensional particle shapes are discussed in Section 2.5.2. These can be adopted to describe the outline of a particle and are seen as an alternative method to the methods described in Section 2.5.1. Furthermore, Section 2.5.3 describes the method in which Fourier Descriptors can be used to generate particle outlines. This is described by Mollon and Zhao (2012) to create two-dimensional particle outlines from just three Fourer Descriptors (D_2, D_3, and D_8). Software that utilises this method is available from Mollon (2023) and this had been employed to create two-dimensional particle shapes that represent irregular, untooled rock as described in Section 3.6.1.

2.6 Conclusions from Literature

Granular material based walls that use particle sizes of gravel, cobbles and boulders as their construction material appear to be suitable for construction using earthen materials if a high strength is required. Examples of these are given in Section 2.2 of DSRW, retaining walls constructed by the Incans, and 16th-17th Centuary Japanese castle walls. Particularly with the Incan retaining walls and Japanese castles walls, minimal void is present in the structures with examples of these given in Figure 2.6b and Figure 2.8b. Snow (2001) provides a wide range of different DSRW constructions and a pattern of minimising voids in the structure is also clear from visual examination. These retaining walls rely on friction and interlocking for strength (Villemus et al., 2007). Therefore the internal configuration is relevant (Mundell et al., 2010). Unlike URE, water can flow through the rough interfaces (Vallejo and Fontanese, 2014) leading to minimal build up of pore water pressure. Also, the heavy particles used provide strength from their weight to prevent against sliding and overturning. The curved profile of Japanese castle walls should be noted here as it is another way to maximise shear strength (Utili and Nova, 2007). The heavier structures exhibit higher curves in the wall profile as observed by Fujioka (1969) and the work in Nishida et al. (2005) shows that this is to create compressive forces throughout the wall. Although this knowledge will not be utilised in this project as the focus is on 2D problems, it is important if a 3D problem is investigated in the future.

Section 2.2.4 explores current work into the area of autonomous construction using irregular particles by robot. These works tend to focus on the use of a heuristic to determine placement by how well a stone fits to the upper surface of the already placed particles (Furrer et al., 2017; Johns et al., 2020; Johns et al., 2023; Liu et al., 2021). Additional heuristics for the energy required to move the placed particle, lengths between newly placed objects and previously placed objects, deviation of the normal to the particle contact from the thrust line are considered as seen in Furrer et al. (2017). Further criteria were set out in Liu et al. (2021) to filter the number of candidate poses for testing to speed up computational time. These included ensuring the slope of the top surface must be inward and making sure the centroid height must be lower than the average of the centroid heights, as well as ensuring the deviation of the normal to the surface compared to the thrust line, the contact area of the particle with the surface, and the number of interlocking objects for the pose must be above the mean of all possible results. Johns et al. (2020) introduced a stability check that consisted of ensuring the horizontal and vertical dimensions of a stone are in a ratio greater than 0.5 when considering a pose with any poses not meeting this criteria being discarded to save on computational time. Furthermore, heuristics can be added from the information in Vivian (1976) for the construction of drystone walls by hand. The most important of these for this study is stones should rest on at least two other stones to reduce the number of runs in the wall.

From the reviewed literature, it can be stated that more angular and irregular particles will lead to increased ϕ values (Alshibli and Cil, 2018; Chan and Page, 1997; Cho et al., 2006; Koerner, 1970; Li et al., 2013; Miura et al., 1998; Selig and Roner, 1987; Vallerga et al., 1957; Xiao et al., 2019; Yang and Luo, 2015). In addition Vivian (1976) states that angular particles such as hard shales and schists that have flat sides due to cleavage are easier to build DSRWs with than stones which are rounded. Huu et al. (2017) showed that angular sands have a higher shear strength and show dilative behaviours at much lower relative densities than smoother sands. This is caused by the interlocking between aggregates created by their angular shape. The angular particles can be said to have a higher restriction on rotation and movement due to an increase in interparticle contacts and this is what is leading to a higher shear strength (Brandes, 2011; Li, 2013; Potticary et al., 2016). Santamarina and Cho (2004) agrees stating that the increased angularity will make it more difficult for particles to rotate. Guo and Su (2007) concluded that interlocking was more likely to occur in angular particles and this leads to an increase in shear strength. Rowe (1962) agrees, stating shear resistance is affected by interparticle friction, particle rearrangement, dilation and crushing in granular soils.

Furthermore for a DSRW, Villemus et al. (2007) showed that rotation of particles takes place when a wall fails. Interlocking of particles will prevent particle movement and rotation. The sangi-zuma pattern at the boundaries of Japanese castle walls (Figure 2.9) also provide evidence for this, as the overlaying pattern will mean more chance of particles interacting and interlocking with each other rather than blocks flush against each other on the same layer. It is envisioned that if waste rock is used as a construction material then angular particles will be utilised. However, as the construction material is limited by what is available if a focus on locally sourced materials is enforced, then a choice of material shape may not be possible. Therefore, selection of the particle by shape will not be considered for this project. Rather, by measuring other factors that contribute to interlocking - such as coordination number or surface area of particles in contact with other particles - this will constitute for not considering particle shape.

Higher mean coordination number of a system tends to lead to higher shear strengths (Ishigami et al., 1973; Oda, 1977). This is seen in the Incan retaining walls and Japanese castle walls. Utili and Nova (2007) stated the dispersed nature in which the different sizes of particles are positioned in the foundation for Japanese castle walls and foundations lead to the wall having a "cohesion" that is not normally found in granular material. This cohesion is created by the high coordination numbers around the larger stones. The higher coordination number helps spread the force through the system by providing more force chains (Fonseca et al., 2016; Muir Wood, 2008) as well as providing stability to particles (Alexander, 1998). As stated by Ueda et al. (2011), a high mean coordination number tends to lead to a lower void ratio and this is true in the Incan retaining walls and Japanese castle walls which have high coordination number and very low void ratio. Furthermore, Vivian (1976) suggests that in a DSRW stones should rest above at least two other stones when being placed to prevent runs within the wall, suggesting higher coordination numbers in the system will also prevent these runs from appearing.

Particle size will not be considered in this project. Although it is commonly reported that particle size affects shear strength (Alias et al., 2014; Holtz and Gibbs, 1956; Pakbaz and Moqaddam, 2012; Simoni and Houlsby, 2006; Wang et al., 2013), these changes in shear strength are actually due to other changes of the surface characteristics of the soil particles (Winterkorn, 1967). Many papers reported no significant change to shear strength with a change in particle size (Latha and Sitharam, 2008; Selig and Roner, 1987; Vallerga et al., 1957). The effect was especially highlighted in Azéma et al. (2017a) and Linero Molina et al. (2019), where PSD of a material was simulated but particle shape was kept consistent. Minimal effect on shear strength was seen when original shape was retained. However, when the shape was changed to more accurately represent change in particle shape that would occur for particles of the material in the scaled down size, the results gave a change in the shear strength of the system. Although it is reported for the Incan retaining wall examples that heavier particles lead to more stability due to their self weight, it is not known that particles of such a large size would be produced as waste rock or available as a locally sourced material close to site when constructing. Therefore, the use of much larger particles for stability from self-weight is not included in this study.

An increase in interparticle friction leads to higher values of shear strength (Thornton and Sun, 1993). The energy is dissipated through the system more and there is a decrease in sliding of the contacts between particles (Thornton, 2000; Santamarina and Cho, 2004; Suiker and Fleck, 2004). Santamarina and Cascante (1998) showed that surface roughness leads to an increase in critical state friction angle. From Equation 2.6 and Equation 2.7 it is known that this has an effect on maximum angle of shearing resistance. It can be hypothesised that the higher percentage of the soils surface in contact with other particles will lead to more chance of frictional forces being created. The minimal amount of void in the constructions discussed in Section 2.2.2 and Section 2.2.3 provides evidence of this theory as the high amount of friction between particles adds to the strength of the system (Villemus et al., 2007). More evidence is presented for this in Grillanda et al. (2021) and Santa-Cruz et al. (2021) where walls made from regular, rectangular blocks performed better than irregular blocks or blocks with imperfections in the bricks when tested by a tilting table method. This is due to less shear resistance because of the varying contact area. Additionally, the literature discussed in Section 2.2.4 (Furrer et al., 2017; Liu et al., 2021; Johns et al., 2020; Johns et al., 2023) designed with a heuristic approach that scored placement on its "goodness of fit", i.e. the maximum area of contact of the particle with the already placed stones. It is known that a more tightly packed structure will lead to higher strengths (Mogami, 1965; Moroto, 1982). Lodi et al. (1999a) and Wang et al. (2010) used the area of an item in contact with other items and the domain edges as a scoring criteria in solving the bin packing problem. Lodi et al. (1999a) states that this favour patterns that do not trap small areas of space which is also beneficial for reducing void ratio in the system. Solvers for jigsaws also relied on maximising the touching perimeter of jigsaw pieces, as seen in Section 2.4.4. The use of this as a scoring method for friction between particles can be adopted, as the higher area a particle has in contact with other particles will mean more chance for frictional forces to be produced.

High density and well-graded soils are typically considered to have high strength values (Duncan et al., 2014; Huu et al., 2017; Meyerhof, 1956; Meyerhof, 1976; Yan and Dong, 2011). However, as discussed in Section 2.3.5, the soil strength should not be directly linked to density or grading. Rather, a high density soil system will mean more particles are touching leading to a higher mean coordination number. Additionally, a system being well-graded will not necessarily lead to a high shear strength. If it is inferred that high density means low void ratio of a soil, it is known that this is affected by grading, compaction and particle shape (White and Walton, 1937; Shergold, 1953), all of which can be configured to increase coordination number. White and Walton (1937), Sohn and Moreland (1968), Lade et al. (1998), and Cubrinovski and Ishihara (2002) all proved that the inclusion of smaller particles can reduce voids so long as the inclusion of smaller particles do not displace the existing particles. This will lead to higher coordination numbers as well as potential for more frictional forces between particles. Therefore, low void ratio could be used as a criteria for assessing strength of a system as it will tend to lead to features that increase shear strength in granular materials. However, as stated by Mogami (1965), void ratio cannot be used on its own to describe the properties of granular material and the distribution of void is also needed to be known. Therefore void ratio alone cannot be used to analyse particle placement in a packing algorithm for creating a structure. Examples of heuristics trying to reduce void in a system are found in Section 2.4.5. Phon-Amnuaisuk (2015) focused on minimising the presence of unfilled tiles whilst Kostreva and Hartman (2004) and Böhm et al. (2005) minimised the gaps below the placed block as part of their criteria for optimising the Tetris problem as well as maximising the number of contacting sides of the tetrominoes. Both these criteria will help reduce void ratio in addition to increasing coordination number and interparticle friction.

Evidence for a particle being packed lower down in a system to increase stability is presented in Section 2.4. When discussing packings of spheres in Section 2.4.1, Graton and Fraser (1935) and Liu et al. (2015) both state that a sphere has a lower potential energy when lower down in a system with regards to gravity. Within the DSRW structures in Section 2.2.1, flatter stones are used for layers. By placing these pieces with their width horizontal this is reducing the potential energy of that piece. Additionally, heuristics for optimising space between particles in the bin packing problem and Tetris optimisation problem take advantage of packing particles further down in the system. Hifi and M'Hallah (2002), Jakobs (1996), and Liu and Teng (1999) take a bottom left approach. Wang et al. (2010) also prioritised the bottom-most position in their DBLF algoirthm. Kostreva and Hartman (2004) and Böhm et al. (2005) prioritised minimising the overall height of the structure when fitting Tetris shapes into a domain. This will naturally lower the potential energy of particles placed. Therefore, the height of the placed particle will be taken forward as a criteria for scoring particle placement. Stability of the system will need to be considered. Reducing the potential energy of particles by reducing the height will lead to better stability as well as reducing the creation of large wells of voids in the system as creation of thin canyons of void should be avoided with the inclusion of this criteria.

The suggested problem in this thesis is similar to that of the bin packing problem discussed in Section 2.4.3. This is shown to be NP-hard and this means that no algorithm can solve the problem in polynomial time is known as described in Section 2.4.2. It is common for these sorts of problems to be solved using a heuristic algorithm. Therefore an objective function with weighted criteria whilst following a heuristic approach will be utilised in this project. Examples of these heuristic approaches are found in Sections 2.4.3-2.4.5. Kostreva and Hartman (2004) and Böhm et al. (2005) are two examples of the use of a weighted function to score possible placements of tetrominoes in the Tetris problem. For this approach, each positioning and possible rotation is scored for placement and the best scoring result is taken forward. Algorithms discussed in Section 2.4.4 also used a heuristic approach of scoring each possible placement like in Woflson et al. (1988). With these scored heuristic approaches, it is possible to use a lookahead like in Goldberg et al. (2002) or for the offline approaches for bin packing. However, a large number of items will lead to extensive computational times as the permutations of the items' order of placement will be massive. On the other hand, only allowing a small amount of items to be packed at a time whilst testing all permutations of placement would greatly reduce the number of possible permutations and with it computational runtime. Research in the area of autonomous construction, discussed in Section 2.2.4, utilise heuristics to score placements and choose the most optimal solution (Furrer et al., 2017; Liu et al., 2021; Johns et al., 2020; Johns et al., 2023). Furthermore, Furrer et al. (2017) and Liu et al. (2021) make use of a weighted function for this heuristic approach to provide criteria that is deemed more suitable to the optimal solution. The position with the highest score is taken forward.

The possible criteria for a weighted function that will produce structures of high shear strength will be based on the discussed features that can affect shear strength. These are particle shape, coordination number, particle size, interparticle friction, void ratio, and height of placement in the system. Of those features, it has already been stated that particle shape and size will not be assessed due to the ability of the other features to describe their effect as well as the inability to predict the type of material that will be used if sourced locally. Therefore, the criteria taken forward will be

- Void ratio, or gaps created by placement of the particle in that position
- The potential energy, or height of the placement in the system
- Coordination number of the placed particle (at the time of placement)
- Area of contact of the particle with other particles and the domain edge, or the potential for frictional forces between particles

These four criteria will be adopted as the basis of an objective function for scoring placement of particles in a soil assembly with the purpose of creating a structure with high shear strength. As far as the author is aware, there is no current literature that provides a scoring heuristic for particle placement in a soil structure, either in 2D or 3D. The work in this project will take place in 2D but with the aim to enable it to be used for 3D scenarios in future work.

As it is envisioned that this construction would be completed robotically, other features highlighted in the literature review will influence the design of an algorithm which takes into account this approach. The robots seen in the research reviewed in Section 2.2.4 tend to use two or three-finger gripper to grasp stones and place items using a top-down approach. As such, the algorithm described in Chapter 3 will assume a top-down particle placement approach. A top-down method is also adopted in Jakobs (1996), Liu and Teng (1999), and Wang and Hauser (2019). This will help avoid collisions when placing particles. In addition, a stability check will be introduced as it is in Wang and Hauser (2019). The stability was modelled using contact points and a Coulomb friction model based on friction coefficient and a similar check can be completed in this project.

Furthermore, there is potential for the use of techniques to reduce runtime like in Cagan et al. (1998) where the domain and items were split into smaller resolutions for scoring before being scored at higher resolutions or Kong and Kimia (2001) where a coarse description of the edges of pieces were used to remove obvious non-matches before moving to a finer description. Alternatively, a top contour of the surface like in Bdolah and Livnat (2000) or Melax (2014) can be adopted. Unlike with the Tetris scenario, it is unlikely that rows of filled space will disappear. This, as well as the use of a top-down method, will mean that gaps below the surface will not be filled without the use of backtracking or an off-line approach. Therefore, a contour surface will be used to describe the potential placements of particles and further information below this may be disregarded when finding potential positions for particles.

Additionally, it is envisioned that there is potential to introduce a scheme that selects particles based on their suitability for packing in the structure. For example, if structure with high shear strength is required, particles that are angular may be selected based on the findings in Section 2.3.2 that soils made up of more angular particles tend to exhibit higher shear strengths due to interlocking. If this is the case, there is a requirement to characterise particles in some manner. Further discussion around this top can be found in Section 8.6. Section 2.5.1 explores these in detail for four terms that describe particle shape. These are form, sphericity (or circularity in the two-dimensional case), roundness and irregularity. Of the classification terms discussed, elongation (Blott and Pye, 2008; Li et al., 2013), circularity (Riley, 1941; Wadell, 1933 as cited by Blott and Pye, 2008), angularity (Wadell, 1932; Lees, 1964), convexity (Li et al., 2013; Yang and Luo, 2015), and aspect ratio (Yang and Luo, 2015) have potential to be adopted to describe two-dimensional shapes. There is also possibility for Fourier descriptors to be utilised which are introduced in Section 2.5.1 however this is not taken forward in this project. Alternatively, this concept can be reversed to use Fourier descriptors D_2, D_3 and D_8 to generate particle outlines as described in Section 2.5.3 (Mollon and Zhao, 2012). This is done in this project to generate two-dimensional outlines that represent irregular, untooled rock using software provided in Mollon (2023). Section 3.6.1 presents the methodology for this as well as particle outlines taken forward for packing by the algorithm described in Chapter 3.

Chapter 3

Methodology for Particle Packing

3.1 Introduction

3.1.1 Chapter Layout

Outlined in Section 2.4 were methods for packing items into a domain and the different heuristic approaches for minimising void in scenarios such as bin packing and Tetris playing methods. From the review, it is proposed that a packing algorithm can be developed that uses an objective function that includes weighted criterion for the scoring of placements of particles. In particular, a scoring system will be designed to pack particles into a structure that exhibits high shear strength. The development of such an algorithm is described in the following sections of this chapter. The work conducted follows on from that in Hoodless and Smith (2023) where the algorithm for placing irregular, untooled particles was not yet fully achieved. Further detail on the covered areas in Hoodless and Smith (2023) is given in addition to the evolution for the developed algorithm. A comparison between the methods here and those in Hoodless and Smith (2023) can be found in Section 3.12.2.

The algorithm is developed in the vector graphics language Asymptote. A brief description of Asymptote and its benefits is outlined in Section 3.2.1 with an explanation for the choice of this language. The algorithm is designed to pack Tetris particles for the Standard Tetris scenario described in Section 3.2.2. This is utilised as a test scenario to set up the algorithm as it is a simplified case of particle packing. In addition the aim for Tetris is to minimise the void ratio of the system which can very easily be quantified for analysis. Afterwards, an extension to facilitate packing of 2D soil particle shapes is added and new features are introduced to cut down on computational runtime as well as to include a stability check to ensure feasible packing is completed. This new scenario is described in Section 3.2.3.

Weighted criteria in an objective function are used to score placements of particles in the system, with the highest scoring placement determining where the particle is packed. The criteria are based on the literature review in Section 2.3 for features that affect shear strength in a granular material and those which are to be adopted in this project are outline in Section 2.6. These are stated in Section 3.5 along with a description and method for quantification in the algorithm. In this scenario, the criteria to describe soil strength are utilised but theoretically any criteria could be used as long as a way to quantify this is implemented into the program.

Section 3.6 describes the additional considerations that are implemented into the algorithm when moving to outlines of soil grains. Post development of the algorithm using the Tetris Scenario, the programme is taken forward to be utilised for shapes that represent outlines of irregular, untooled rock in the Soil Particle Scenario described in Section 3.2.3. The method for generation of these particle outlines is explored in Section 3.6.1. As rock particles are not confined to four orientations and a defined spacing between positions like in the Tetris Scenario it is necessary to redefine the orientations and spacings as well as the domain tests are conducted in which are discussed in Section 3.6.3 and Section 3.6.2 respectively.

It is shown in Section 3.6.5 that computational runtimes for irregular particles are massively increased compared to the simply defined tetrominoes. Therefore Section 3.7 introduces features which were implemented into the programme in order to increase the computational speed. Section 3.8 discusses the complexity of the algorithms. Additionally, Section 3.9 describes stability checks which were introduced to prevent placement on particles in unsuitable locations within the system.

Section 3.10 discusses how the different scenarios will be quantified to judge the effect of the objective function. For the Tetris Scenario, Section 3.10.1 describes how the void ratio of the system for the area underneath the placement surface can be used to show the efficiency of packing to create minimal gaps in the domain. For the Soil Particle Scenario, Section 3.10.2 considers how the shear strength of the system can be assessed without experimentally testing the resulting packing. The disruption of runs between particles is chosen as a suitable result that can be determined with a numerical value for comparison. The identification of runs and disruption by placed particles is described. Section 3.11 discusses how the algorithm handles finite-size and edge effects that can occur as well as irregular particles for packing.

Section 3.12 summarises the algorithm with the adopted features for the Soil Particle Test. Input parameters are specified in Table 3.6. This is used to collect the data presented in Chapter 6. Section 3.13 summarises the whole of Chapter 3, highlighting key points made in each section.

3.1.2 Outputs

With the production of an algorithm to produce soil structures of high shear strength, it is important to outline the aims that were set out at the start of this work. These are as follows

- Produce an algorithm that successfully packs particles into a domain. The particles and the domain can be specified to be any 2D shape so long as enough information is provided by the user.
- Design the algorithm to pack particles of irregular, untooled rock with the intention of designing a structure with a high shear strength. However, leave the possibility for the program to be extended or changed to be able to design to other criteria specified by the user if desired e.g. a high porosity structure for good drainage.
- Use the program to pack tetrominoes into a domain with an objective function targetting minimum void in the system as a test case. Carrying out this step will help develop the programme and identify issues that may be missed when just using soil particle shapes.
- Extend the program to move from packing simplified shapes such as the tetrominoes into being able to pack complex shapes such as soil particle outlines. With this will come the inclusion of feasibility checks such as a stability check

to ensure soil particles will remain in the positioned location with no dramatic collapse of the structure.

These aims were kept in mind whilst producing the program and it is hoped that each one specified is fulfilled in the following methodology.

3.2 Language and Testing Scenarios

3.2.1 Asymptote Programming Language

The work presented was conducted in the open-source vector graphics language Asymptote (Hammerlindl et al., 2014). Asymptote was developed to provide a standard for producing mathematical figures and technical drawings while using a high-level programming language (Bowman and Shardt, 2009) and has been chosen in this research as it can simultaneously perform complex mathematical operations and produce high quality images to display the results. The language uses syntax that is an adaption of C++ and Java so is easy to program in and also adopts ideas from Python such as named function arguments and array slices (Bowman and Hammerlindl, 2008). Inspiration is taken from an earlier drawing program called MetaPost and LaTeX typesetting for labels to ensure consistency across the document is also adopted (Hammerlindl et al., 2014). Asymptote is coordinate-based (Hammerlindl et al., 2014) which makes it suitable for the two-dimensional outlines of particle shapes that are described in Section 3.6.1 meaning the shapes can be easily transformed using the inbuilt functions of the language or manual calculation. The inbuilt functions are of use to this project - such as the intersectionpoints function which returns all coordinates where two lines intersect with each other - and therefore will not require being reproduced as they already exist. It should be noted that while this research is utilising Asymptote to produce 2D images, the language can be used for 3D graphics and could be adopted in future projects if three-dimensional particles are considered.

In summary, Asymptote has been chosen for this work because

- It is easy to use once an understanding of the language has been learnt.
- The language is coordinate-based which is suited for the two-dimensional outlines for particle shapes used in this research that are made up of coordinates.
- Complex mathematical operations can be performed in the script and there are already in-built functions to perform operations that will be needed.
- Asymptote produces high quality images for presenting the results of the script.

3.2.2 Tetris Scenario

For the simplified packing algorithm, the Standard Tetris scenario as introduced by Brzustowski (1988) will be taken forward. This is described in Section 2.4.5 but the key aspects are repeated here. The aim of the videogame Tetris is to fill rows of the domain and a score is achieved if a row is completed.

Tetrominoes are used as the particles for placement in the packing. These are made of four squares and each type is represented in Figure 2.38 in Section 2.4.5 as well as replicated here in Figure 3.1 along with the location of coordinates to create the shapes' outline. Particles are selected using the pull-from-bag technique as seen in the Tetris videogame. This is simulated by creating a list of the seven tetrominoes. The first particle is selected at random and positioned in the domain before being removed from the list of potential particles for placement. The process is continued until all seven initial particles are placed. The bag is then refilled with the seven different tetrominoes and the process continues until the targeted number of particles is placed or until the next particle cannot be placed in the domain. This was not originally adopted in the Standard Tetris scenario described by Brzustowski (1988) but is implemented into the work conducted here.

Each particle can be placed in four different rotational positions each separated by 90^o angles and have a spacing of 1 unit square for possible locations in the domain. This relates to the translations in the Tetris videogame. The program is given unlimited time to place particles, as in Brzustowski (1988), and no falling of particles for a given time frame is introduced.

Unlike with Tetris, completely filled rows will not be deleted in this scenario. When it comes to packing with soil particles in a real life situation, rows of soil will not miraculously delete themselves if there is no void in that row. Therefore, this is not replicated in the present project but it could be introduced if the aim of this research was to produce an optimised Tetris videogame playing method.

In the traditional Tetris videogame, a 10x20 square domain is used. However, in this scenario a 10x10 square domain is utilised. This is just to speed up the computational time as it will take less particles to fill the domain completely. The use of reduced domain size is commonly seen in the literature reviewed in Section 2.4.5 to describe the size of the state space (Carr, 2005). The produced results by these reduced domains are still good so therefore it can be taken forward in this project. An investigation into domain size is completed in Chapter 4.

3.2.3 Soil Particle Scenario

For the Soil Particle Scenario, 2D outlines of irregular, untooled rock are required. The generation of these outlines is described in Section 3.6.1. As particles are hypothesised to be of irregular, untooled quarry rock or CDW it is hard to know what shape these particles will be. Therefore a suitable selection will need to be determined qualitatively by visual inspection. Additionally, there is no defined number of orientations for the stones to be rotated by or a known location spacing to trial between potential positions. Domain size is also another unknown but a size that simulates an equivalent to the Tetris Scenario is adopted to retain similarity between the scenarios. These features are later discussed in Sections 3.6.3 and 3.6.2.

Unlike Tetris, rocks undergo gravitational forces through the centroid of the particle. As such, stability checks and conditions are introduced to prevent unstable positioning of objects. Further information on these stability checks are given in Section 3.9. As described in Section 2.2.4 a top-down approach is to be adopted which is equivalent to the Tetris Scenario.

With Tetris, particle selection is limited to one particle after the other as the game tries to catch out the player into placing tetrominoes in suboptimal positions. For a robot completing autonomous construction, it is determined that particles will be free for selection by the algorithm. Therefore more than one particle can be tested at a time and the optimal particle can be selected for placement. If all particles are available due to the free movement of the robot then still a limited number of particles should be made available for analysis to reduce the number of candidate poses as is seen in Johns et al. (2020) and Johns et al. (2023) where 20-40 stones are considered for placement at a time. Once all stones are placed or discarded, another 20-40 stones are scanned and placement for these is determined. Multiple particles for selection are not made available for the work in this project, but this could be implemented in future research. More discussion on this topic can be found in Section 8.4.1.

3.3 Tetris Scenario Initial Procedure

3.3.1 Defining Particles

Particles are defined by the user as a set of coordinates in the abscissa and the ordinate. By using this method, the particles can be defined by any shape with no limitations on being convex or concave. The coordinates are required to define a closed loop, i.e. the first and last coordinates must be of the same value. Also, coordinates of the outline are required to be listed in a clockwise order.

Tetris is chosen as the simplified method as these particles are only defined by a small number of coordinates at the corners. However, in this example, coordinates were used at each corner of the squares that made up the tetrominoes that lay on the outline of the particle shape. Each tetromino is displayed in Figure 3.1 with the coordinates that make up the outline of each shape. For irregular, untooled rock stones, a much larger number of coordinates is required to describe the details of the particles and to capture their surface features.

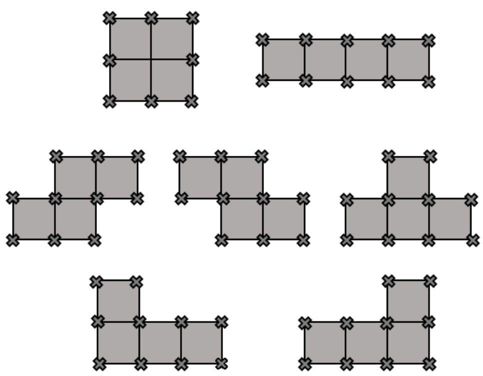

FIGURE 3.1: The 7 tetrominoes and the coordinates that describe the particles.

3.3.2 Particle Splitting

As each particle is defined by coordinates, these coordinates are used for the different functions of the program. Therefore, to decrease computational runtime the separation of the particle outline can be completed so only the coordinates that are required are utilised. Each particle is divided into its top line and bottom line which will help when it comes to the top down placement technique adopted for the testing scenarios as highlighted as a requirement in Section 2.6. The top line is the outline of the particle which is exposed at the top, i.e. no other section of the particle lies above it and therefore if an object is dropped then it could potentially hit this surface. The bottom line is the outline of the particle which is exposed at the bottom i.e. no area of the body of the particle lies below it and therefore if the particle was to be lowered downwards then this part of the particle is free to make contact with another object. In this manner, a convex particle outline is fully described by the top line and bottom line.

The bottom line is configured in a preprocessing step separate to the main algorithm of the program. The separation of the bottom line improves runtime as only the coordinates of the particle base are required when determining positioning in the domain. This is because of the top-down approach adopted for the construction method. Each coordinate that makes up the total particle outline is tested. A line is drawn vertically from the coordinate to an arbitrary line below the particle with ordinate value Z. If there is no intersection between this line and the outline of the particle, this coordinate is considered to be part of the bottom of the particle. This is seen in Figure 3.2(a). If the line does intersect the outline of the particle, a further check is required to see if this coordinate appears at a vertical edge-most boundary of the particle with another coordinate lying beneath it. An example of this is seen in Figure 3.2(b). This check is shown in Figure 3.3 for both Figure 3.2(b) and (c). For a particle, j, if the position of the i^{th} coordinate being measured is (x_{ij}, y_{ij}) then two further vertical lines are drawn at $(x_{ij} + a, y_{ij})$ and $(x_{ij} - a, y_{ij})$ where a is a value smaller than the horizontal distance between coordinates, named here as the distance of separation. If one of these lines does not intercept the outline of the particle - Figure 3.3(a) - then this can be considered an edge-most point and is classed as part of the bottom line. If both intercept with the particle outline - Figure 3.3(b) - then this is not considered part of the bottom line and is discarded, as would be the result of the check for the coordinate in Figure 3.2(c). If it were to exist that a near vertical edge that slopes outwards from top to bottom would occur, it is important that a is less than the horizontal distance between these two coordinates otherwise this coordinate will be falsely classed as a bottom coordinate when it does not make up the bottom line. The process for determining the bottom line can be summarised as

```
for particle j
    for each coordinate of bottom line, i
        CONNECT (x(i,j),y(i,j)) to (x(i,j),y(i,Z))
         if intersection with particle outline detected
            CONNECT (x(i,j)+a,y(i,j)) to (x(i,j)+a,y(i,Z))
            CONNECT (x(i,j)-a,y(i,j)) to (x(i,j)-a,y(i,Z))
            if one results with no intersection of particle outline
               return as bottom line coordinate
            end
        else
            return as bottom line coordinate
        end
    end
end
```

where Z is the ordinate value for the arbitrary line below the particle and $x(i,j)$ refers to the x position of the i^{th} coordinate of the shape outline for the j^{th} particle. The result of this process is presented in Figure 3.4.

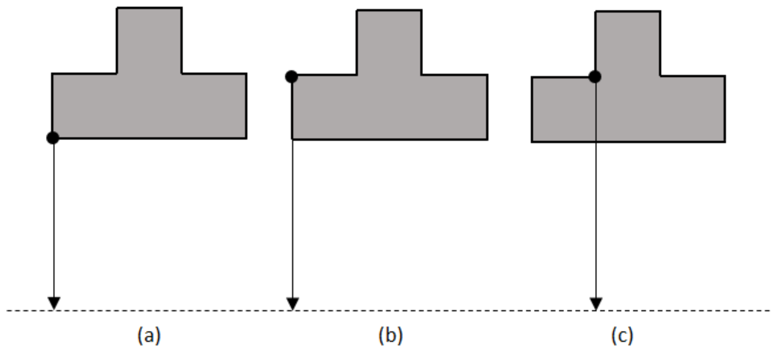

FIGURE 3.2: Examples of coordinates being tested for bottom of the particle detection.

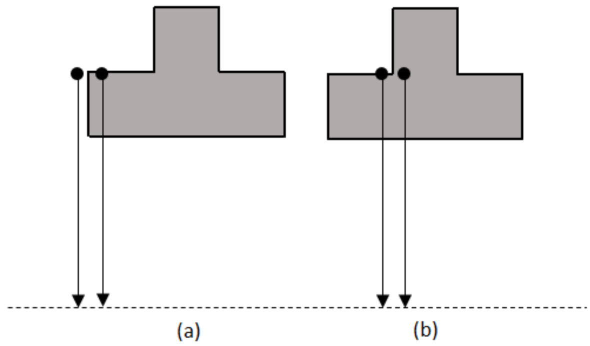

FIGURE 3.3: Examples of the second step of check for coordinates that intercept with particle outline to determine if edge-most coordinate.

The exact same method is then used to define the coordinates for the top line of the particle but with the arbitrary line positioned above the particle. However, whereas the bottom line was required for finding the position of the particle, the top line is required so that it can be attached to the placement surface in the domain, the reason for which is explained in Section 3.3.3. Because of this, an additional step is required to "drop" the surface where overhangs might occur in particles. This was not required for tetromino shapes rotated at 90^o but would be required if the particle was rotated by increments of 45^o for example. Figure 3.5 shows an example of a possible rotation of the "T" tetromino if increments of 45^o are desired. As a top-down method is being utilised, if a particle was being positioned on top of the T tetromino it is clear that the particle being placed would not rest on any part of the

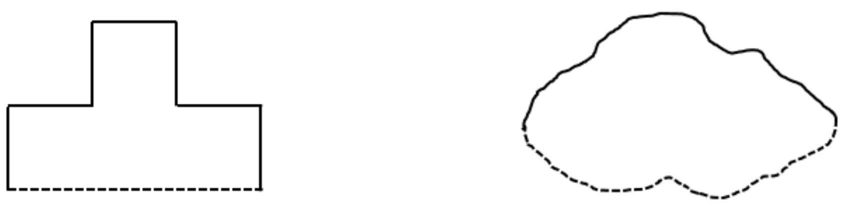

(A) (B)

FIGURE 3.4: Result of splitting of (a) T tetromino and (b) outline of untooled rock particle with bottom line indicated by dashed line.

tetromino apart from that which is outlined by the dashed line. Therefore the top line is designed to describe this shape whilst allowing for overhangs in the particle. Coordinates are listed in increasing abscissa for easy attachment to the placement surface in the domain. The calculation of the top line is completed once placement has been determined in the Tetris Scenario.

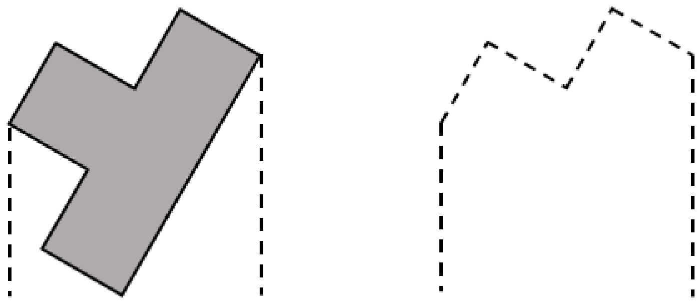

FIGURE 3.5: Example of the top line for a T tetromino with overhanging edges.

3.3.3 Domain Setup

The domain is the area in which particles can be placed. The outline of the domain is defined by coordinates that make up the shape similar to how particles are defined explained in Section 3.3.1. A square domain was used in these simulations, but it should be noted that any shape can be used so long as the area can be defined by coordinates. As with Section 3.3.2, the domain is split up into top and bottom outlines. As a square is used, it was not required for each coordinate to be tested as the outline for each is quite apparent. For the square shaped domain, a minimum coordinate is required as the designated point from which the domain is drawn and for operations to be conducted. In this study, this was taken as (0,0) with positive units reflecting translation along the width and height of the domain.

The bottom of the domain is described as the placement surface. The placement surface represents the features of the bottom of the domain and is where particles can be positioned for packing. Once a particle is placed, the top line of the particle is attached to the placement surface. This describes a new boundary for which subsequent particles can be placed. Figure 3.6 shows this action happening. The particle is in position to be placed above the domain and the distance that the particle needs to be lowered is calculated. The particle is shifted vertically by the lowering distance so that it is in position in the domain. The top line of the particle is then combined with the placement surface to create a new placement surface for particles to be positioned.

The top of the domain is utilised to detect when a particle placement is outside of the domain. If the particle intercepts with the top line of the domain, it is classed as outside of the boundaries set by the program and that placement is considered unfeasible.

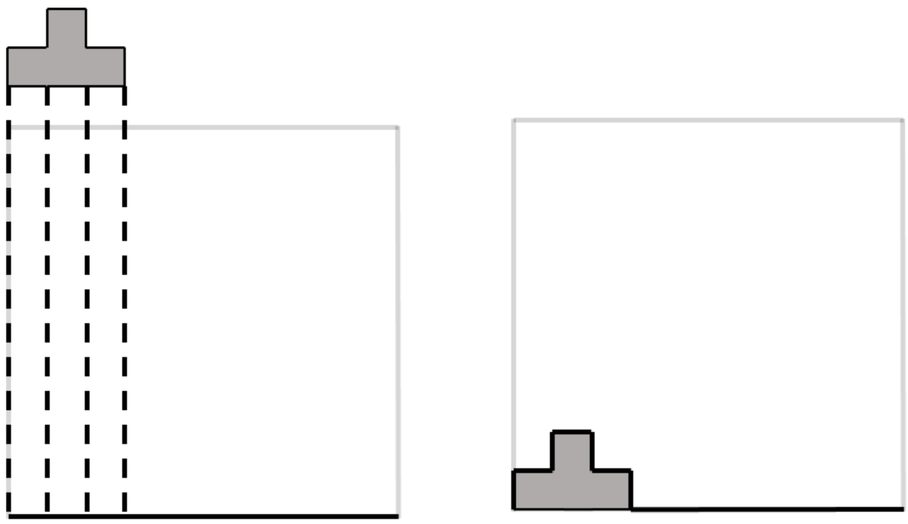

FIGURE 3.6: Particle being placed into a rectangular domain. The placement surface is shown as a solid black line before the placement of the particle and after the placement.

3.3.4 Initial Positioning

Another preprocessing step is to position the particle to be ready for positioning into the domain. This is achieved by moving the particle above and to the left-most position in the domain. An example of this is presented in Figure 3.6. The T tetromino is above the domain and at its left-most location possible whilst still being within the constraints of the domain's border. Because of this preprocessing step, the initial coordinates of the particle set out by the user are inconsequential so long as they accurately describe the particle shape and are to scale with the domain. The particle is then shifted along the abscissa by increments starting at an abscissa value equal to that of the minimum coordinate defined during setup of the domain. The position above the domain and the following positions after movement by these increments is from which the particle is lowered into the domain. Each final pose is scored using the heuristic described in Section 3.5.

3.3.5 Particle Order

A considered constraint on the algorithm is that full information of the all particles will not be known as is seen in Johns et al. (2023) where 40 particles were scanned and placed before moving on to the next 40 particles. Rather, a selection of particles is presented for placement. In the Tetris Scenario, this selection of particles will only ever consist of one particle as a player of Tetris cannot change particle and can only place what is presented by the videogame. Therefore the algorithm is limited to one particle and cannot place the next until the currently selected particle is positioned.

Particles are delivered in an order set out by the pull-from-bag technique as described in Section 3.2.2. This delivers each of the seven particles as a list in a random order. Using the pull-from-bag technique, no particle can be placed again within the same set of seven. For example, the T tetromino will be placed once in the first 7 particle placements, twice in the first 14, and three times in the first 21. The placement of the T particle is random within that set of seven so it is possible that two T tetrominoes could be placed subsequentially as the 7^{th} particle and the 8^{th} particle.

However, particles 9 through to 14 will not be a T tetromino as it has already been pulled from that bag of particles. The particle generation order for both the Tetris and Soil Particle Shape scenarios is arbitrary so long as this can be reproduced when comparing variables within the programme.

A complete order of particles for placement is set out at the start of the programme. The number of particles to be placed is set a maximum integer value. Lists of the seven tetrominoes are produced in random orders repeatedly until this targetted number is achieved. If this number is divisible by seven then each tetromino will occur the same number of times. If the maximum number is not divisible by seven then the number of tetrominoes taken from the last list produced will only equal that which will achieve the maximum number of particles to be placed. An example is set out as follows with Figure 3.7 providing visual aid. The method of ordering particles is referred to as the Tetris bag method.

1. The maximum number of particles to be placed is set to 10.
2. The first list of tetrominoes is produced ordering them randomly. This is represented in Figure 3.7a by the list labelled (1).
3. As the required number for the order list is 10, all of the tetrominoes are added to the order list in the order that they are generated.
4. The next list of the tetrominoes is produced, again in a random order. This is represented in Figure 3.7a by the list labelled (2).
5. As the required number to be added to the order list is 3, the first 3 tetrominoes are taken and added to the order list. The rest are discarded. This is represented in Figure 3.7b with the black particles being discarded.
6. The order list for delivery to the algorithm is now complete and consists of 10 tetrominoes in a random order. 4 of the tetrominoes will occur once and 3 of the tetrominoes will occur twice. Figure 3.7c shows an example of the produced order list of the 10 tetrominoes.

3.4 Development of Placement Method

3.4.1 Positioning Particles

A top-down method approach is adopted as it is envisioned this is the approach a machine or robot will place particles into position as suggested in Section 2.2.4. Additionally, this is what occurs in the Tetris Scenario. Therefore, particles can only be placed in a location where a clear vertical pathway can be followed for it to be lowered into. Lengths are measured between outlines similar to the method in Goldberg et al. (2002) when testing fits between pieces for the border of the jigsaw as described in Section 2.4.4. However whereas these were used to find a distribution of lengths that cluster tightly together around a median value, here the maximum distance that the particle can be lowered without overlap of the shapes is determined. These distances are determined between the bottom line of the particle and the top surface of the already placed particles in the domain. The omission of other coordinates is similar to Wang and Hauser (2019) where items were placed in a bin using a top-down heat map of the upper surface of the bin and a bottom-up heat map of the item, therefore ignoring features that are not required. Adopting only the placement surface is also similar to methods seen in Bdolah and Livnat (2000) and Melax (2014)

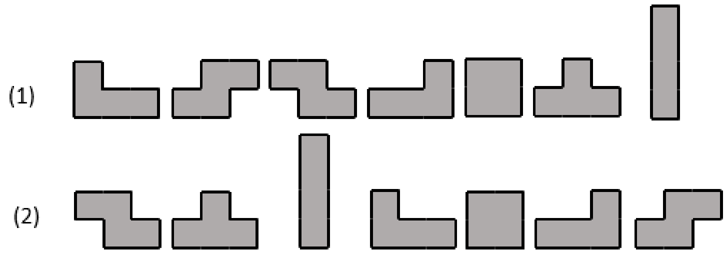

(A) Results of two order lists (1 & 2) produced from the pull-from-bag method when creating an order list confined by a maximum number of 10 tetrominoes

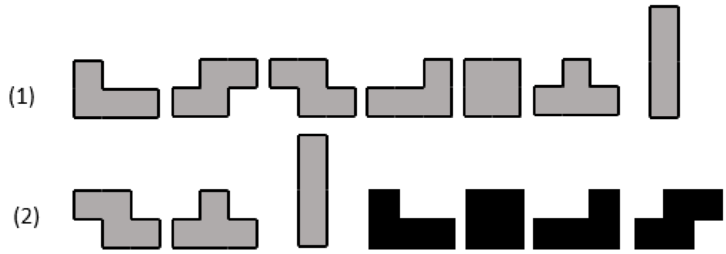

(B) All 7 tetrominoes are taken forward for the order list from Bag (1). The first 3 tetrominoes are taken from Bag (2) to achieve a number of 10 particles and the rest are discarded

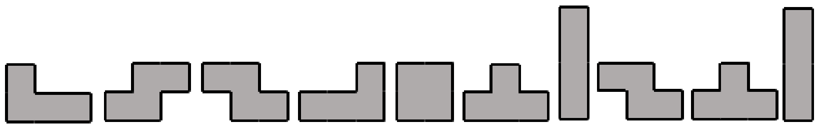

(C) The final list of particles in the order they will be placed by the algorithm

FIGURE 3.7: Steps outlined for producing an order list using the Tetris bag approach for 10 tetrominoes.

(see Section 2.4.5) where only the top contour in the Tetris domain were taken as possible locations of placement therefore ignoring information below this point.

Particles are tested at each rotation for each possible positioning as defined by increments set out by the user. For tetrominoes, this will translate to up to a maximum of ten horizontal placements for each of the four orientations of the particle given that the width of the domain is 10 units. The first lowering position at the left-most location above the domain is tested for placement. A score is given to this placement and then the next lowering position is trialled and scored. This is repeated for each position. The same process is then repeated for each orientation of the particle. The best scoring position is chosen and the particle is placed at this location for the determined orientation before the next particle is tested.

The sequence of steps for placement of the particle from it's position above the domain are as follows

1. Lengths are measured from each coordinate that makes up the bottom line of the particle to the placement surface. This is accomplished by finding the intercept of a vertical line drawn from each coordinate to below the domain with the placement surface line and calculating the distance.

2. Simultaneously, lengths are measured from the placement surface to the particle for all coordinates that fall below the particle. This is completed in a similar

fashion, with a vertical line drawn from the placement surface to above the particle.

3. Of all these lengths measured, the minimum value of these lengths is taken as the distance that the particle can be shifted downwards so that it is touching the base of the domain, and the particle is translated to this location.

4. The placement is scored using the Objective Function as described in Section 3.5.1

If Step 2 is not conducted, then details in the placement surface can be missed which in turn means that there can be instances where tetrominoes are positioned overlapping the already placed objects. An example of this is in Figure 3.8. For Figure 3.8a, the particle is lowered with the admission of Step 2. As can be seen, the detail of the bottom line is not detected and the particle is placed with an overlap of the already placed particles. With the inclusion of Step 2 as shown in Figure 3.8b, the detail of the bottom line is detected and the particle is placed without any overlap. For particle shapes in the given Tetris Scenario described in Section 3.2.2, the inclusion of defining the tetrominoes using coordinates at the outline for each square will prevent features of the bottom line not being detected. However, as the algorithm is desired to be used for particles of any shape designated by the user, it was important to include this feature.

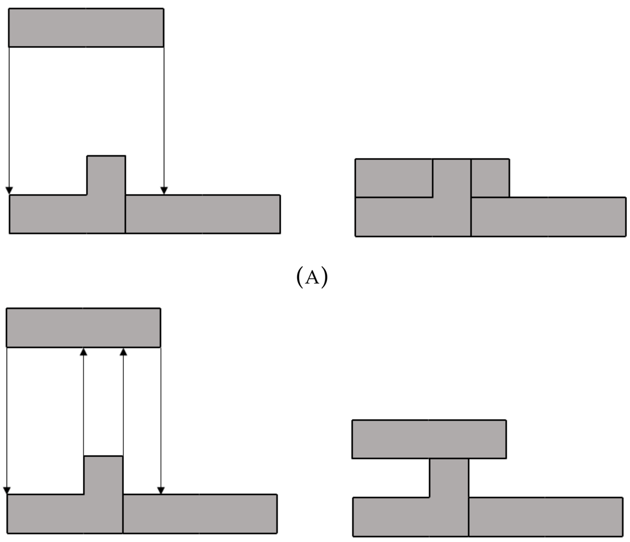

(A)

(B)

FIGURE 3.8: Placement of a particle following the placement procedure (A) without the inclusion of step 2 and (B) with the inclusion of step 2.

Particles are placed sequentially in the order specified. For the Tetris scenario, this will be determined by the Tetris bag method described in Section 3.3.5. Each horizontal position for each rotation of the particle is scored by the program using the objective function. The steps can be described as

```
for particle j
    for each rotation
        for each horizontal positioning
            for coordinates of bottom outline , i
                MEASURE (x(i,j),y(i,j)) to Placement Surface
            end
            distance1 == minimum distance measured
            for coordinates of Placement Surface below particle , k
                MEASURE (X(k),Y(k)) to particle outline
            end
            distance2 == minimum distance measured
                    if distance1 < distance2
                MOVE particle by distance1
            else
                MOVE particle by distance2
            end
           SCORE placement
        end
        CHOOSE position with highest score of each horizontal
        position as best score at this rotation
    end
    CHOOSE position with highest score of each rotation as
    best score of this particle
end
PLACE particle
```

for each particle, j, where (x, y) refers to the x and y coordinates of the bottom outline for particle j and (X, Y) refer to the coordinates of the placement surface. The nature of this method leads to computation runtimes which rely on the number of coordinates used to describe the particle and placement surface. As the definition of the particle increases, the runtime also increases. Therefore, it is expected that simulations placing Tetris particles will be much faster than simulations placing shapes that represent irregular, untooled rock. One of the driving factors for Tetris particles being used as verification for the algorithm is due to these fast runtimes. Figure 3.9 provides evidence for this as it is shown that the computational time of the algorithm increases as the number of coordinates used to describe the object being placed increases. The times for Figure 3.9 were calculated by packing 50 square particles of 5x5 units into a domain of 50x50 units. An example of the resulting packing is presented in Figure 3.10a. The number of coordinates to describe the object outline is the total quantity to define the whole perimeter of the square and includes left, right, top and bottom sides with an equal number of coordinates designated for each side.

The process continues until the targeted number of particles specified by the user are placed or the next particle cannot be placed. A particle cannot be placed if it is outside the boundaries of the domain. This is specified as outside of the domain rather than touching, as it is possible for particles to be touching the edge of the domain whilst still being classed as inside the domain. The check is performed by seeing if the outline of the particle at its final positioning and orientation intercepts with the line that describes the top of domain which is determined in the preprocessing steps as described in Section 3.3.3. As the outline can be touching, a tolerance is set on the

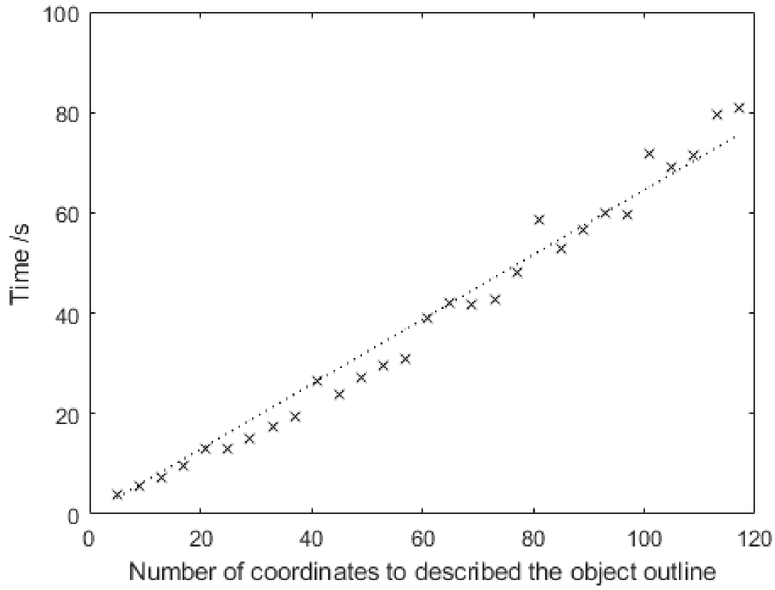

FIGURE 3.9: Times for the packing of squares of width 5 units in a domain of 50x50units with no rotation enabled and a location spacing of 1 unit. Times are calculated by running 30 simulations and taking the average and number of coordinates represents the quantity used to describe the perimeter of the square.

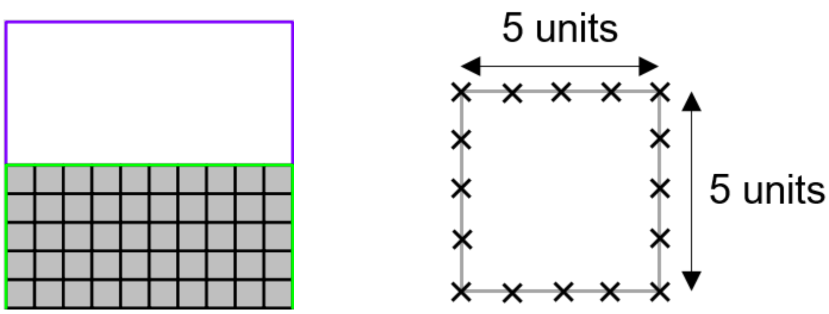

(A) (B)

FIGURE 3.10: (a) Outputted packing as produced by the Asymptote code for 50 squares of 5x5 units packed into 50x50 units domain using DBL heuristic. (b) Example of a 5x5 unit square made up of 16 coordinates.

coordinates to shrink the size of the particle very slightly. If the particle still intercepts with the line that describes the top of the domain then the particle is classed as outside of the domain and this position is classed as not viable.

For a square domain, it is possible to just state that the ordinates of the particle must not exceed the top of the domain. However the algorithm is to be designed to encompass any particle shape and any domain shape. Therefore it is necessary to perform an outside of the domain check in the manner outlined as this allows for the domain shape to be changed so long as coordinates can be used to describe the domain and identification of the top of the domain and the bottom of the domain are performed.

3.4.2 Straight Edge Corner Problem

An issue that arose when determining how far a particle should be lowered was when straight edges were present. This was a very common occurrence when using tetrominoes as it occurs when two corners meet when lowering the particle. Figure 3.11a shows an example of this where the particle does not fully lower to the bottom line and instead rests on the corner of the already placed particle. Instead, the particle should slide to be flush with the already placed particle. This is referred to as the Straight Edge Corner problem or SEC problem. To counter this problem, the distance the particle could be placed were found at $(x_{ij} + a, y_{ij})$ and $(x_{ij} - a, y_{ij})$ just as when determining the top line and bottom line of the particle in Section 3.3.2. Both distances are calculated and the largest of these distances is taken. The result of this can be seen in Figure 3.11b

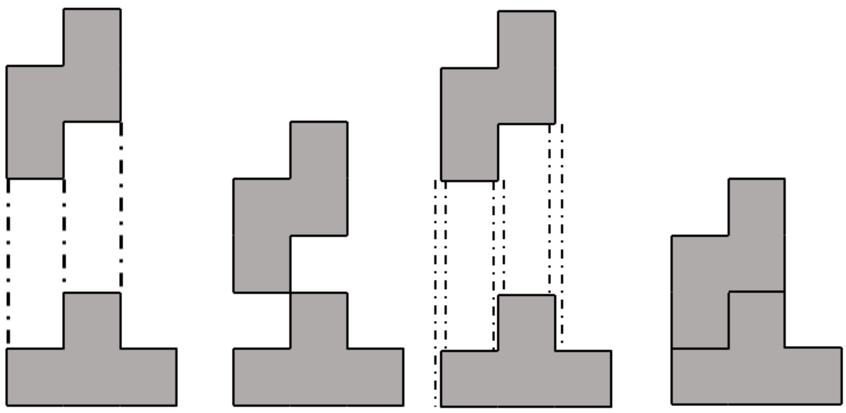

(A) (B)

FIGURE 3.11: Placement of a particle where SEC problems occurred (A) without the inclusion of measuring either side of the coordinate and (B) with the inclusion of measuring either side of the coordinate.

From the solution to the SEC problem presented in Figure 3.11a arose an additional issue that is presented in Figure 3.12a. Within this problem, two corners are coming into contact with each other. From the solution presented, the largest distance is being taken. This leads to overlapping of the particles as the program prioritises the most movement downwards without taking into account its own geometry.

The solution formed to overcome this was to shift the two starting coordinates for the measurement lines from $(x_{ij} + a, y_{ij})$ and $(x_{ij} - a, y_{ij})$ in the vertical direction to

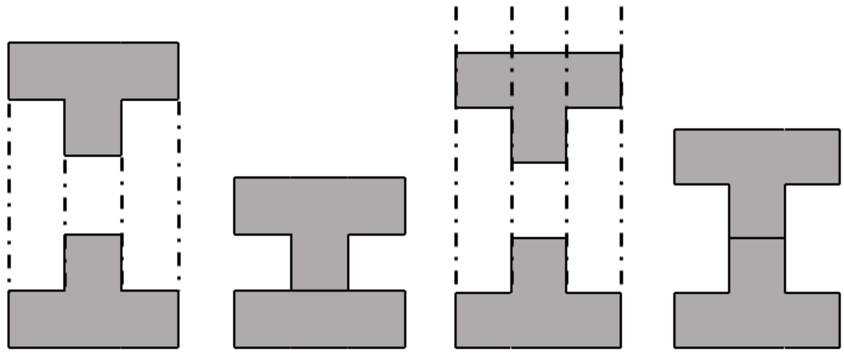

(A) (B)

FIGURE 3.12: Placement of particle where SEC problems occurred (A) with distances measured at $(x_{ij} + a, y_{ij})$ and $(x_{ij} - a, y_{ij})$ taking the largest distance as suggested to solve the problem in Figure 3.11 and (B) with the inclusion of searching for intersection points when measuring.

above the particle being placed. In this manner, the starting points would become $(x_{ij} + a, y_{ij} + P_{j,max} + 1)$ and $(x_{ij} - a, y_{ij} + P_{j,max} + 1)$ where $P_{j,max}$ is the maximum height of the particle. The line is then drawn down to below the placement surface. Intersections are calculated where the line crosses the particle outline and the placement surface.

Minimum y value for intersection with the particle outline and maximum y value for intersection with the placement surface are obtained and the distance is taken as their difference. This allows for Step 1 in the placement process described in Section 3.4.1. It is again repeated for when a SEC problem is detected for Step 2 using the same measurement lines. Providing a Cartesian coordinate system is in use and the operations of the program take place in a positive coordinate range, below the placement surface can be taken as $x = -1$ assuming that the domain is described by positive coordinates. The workings of these calculations is performed by the steps

```
for particle j at a given rotation and horizontal position
    for each coordinate of bottom outline i
        CONNECT (x(i,j),y(i,j)) to (x(i,j),-1)
        if number of intersections with placement surface == 1
            no SEC problem detected
        else if number of intersections with placement surface > 1
            SEC problem detected
            Distance1 = SEC(x(i,j), y(i,j), -1, max(y(i,j)))
        end
    end
    for each coordinate in the placement surface below particle k
        CONNECT (X(k),Y(k)) to (X(k),max(y(j))
        if number of intersections with bottom line == 1
            no SEC problem detected
        else if number of intersections with bottom line > 1
            SEC problem detected
            Distance2 = SEC(X(k), Y(k), max(y(j)), -1)
        end
```

```
    end
    Lowering Distance = min(Distance1 ,Distance2)
end

function SEC(x,y,b,t)
   CONNECT (x,t) to (x,b)
   if number of intersections with bottom outline > 1
      CONNECT (x+a,t) to (x+a,b)
      if number of intersections with bottom outline < 0
         p = minimum y intersection point with particle outline
         q = maximum y intersection point with placement surface
         MEASURE (x,p) to (x,q)
         distance1 = abs(p−q)
         end
      CONNECT (x−a,t) to (x−a,b)
      if number of intersections with bottom outline < 0
         p = minimum y intersection point with particle outline
         q = maximum y intersection point with placement surface
         MEASURE (x, p) to (x, q)
         distance2 = abs(p−q)
      end
   end
   return min(distance1 ,distance2)
end
```

This is performed upon a particle for each rotation and horizontal position to find the lowering distance with the inclusion of a check for SEC problems.

3.5 Scoring of Placement

3.5.1 Objective Function

Quantifying each candidate placement is required to determine the "best" positioning. This can be completed using a function that scores the placement based on the designated objective of the overall structure. Examples of this for placing untooled rock were seen in Furrer et al. (2017), Johns et al. (2020), Johns et al. (2023), Lambert and Kennedy (2012), and Liu et al. (2021) and were discussed in Section 2.2.4. Furthermore, heuristic functions were discussed that were used in the areas of bin packing (Section 2.4.3), jigsaw solving (Section 2.4.4), and Tetris optimisation (Section 2.4.5). A function of this style, named from now on as the Objective Function, can be utilised for scoring of placements for this algorithm based on the key features that will lead to the function that is desired.

Within this piece of work, it is desired that the structures produced are optimised for their functionality when it comes to shear strength. Therefore, criteria for particle placement used in the object function are based upon those discussed in Section 2.3 and highlighted in Section 2.6 that were stated to indicate a system that has a high shear strength. These are summarised again for the reader:

- Void ratio, or gaps created by placement of the particle in that position
- The potential energy, or height of the placement in the system

- Coordination number of the placed particle (at the time of placement)
- Area of contact of the particle with other particles and the domain edge, or the potential for frictional forces between particles

It desired that a minimum set of parameters are required to describe the system. The four adopted from Section 2.3 are seen as the minimum number. It could be argued that void ratio is not required as coordination number and area of contact can help describe this feature. However, as seen in Chapter 5 and Chapter 6, the quality of results is affected by the removal of this criteria.

From these criteria, an objective function can be produced. As this is the first stage of development for this heuristic approach, a first-order equation is adopted. Again, this helps reduce the number of parameters needed to be determined. How the objective function can be enhanced is discussed in Section 8.5. The objective function is described as

$$W_{ij} = C_V V + C_D D + C_T T + C_{CN} CN \tag{3.1}$$

where W_{ij} is the total weight (or score) for the i^{th} horizontal position and the j^{th} orientation of the particle, V, D, T, CN are the scoring criteria for void ratio, potential energy, contact area of the particle, and coordination number and C_V, C_D, C_T and C_{CN} are weighting coefficients applied to V, D, T and CN respectively. The objective function is applied to each position trialled. For the Tetris scenario, the highest scoring position for each orientation was taken forward. If more than one position possessed the highest score, the bottom-left most position was prioritised, taking precedent from Berkey and Wang (1987), Jakobs (1996), and Wang et al. (2010) who used a bottom-left or deepest-bottom-left heuristic when conducting binpacking. Out of these four scores at different orientations, the highest scoring position was taken again. Again, if multiple scores possessed the highest score, the bottom-left most position was taken forward.

In Sections 3.5.2-3.5.5, each of these criteria are described and the method of scoring is explained. All criteria are non-dimensional with the expectation that doing so will mean that particles of different shapes and sizes or described using a differing number of coordinates for the particle outline can be compared when scoring. Each criteria is given a different weighting which changes the effect that is implied upon particle placement. These were explored and suitable weightings were determined for both the Tetris scenario and Soil Particle scenario. The methodology for this is described in Chapter 4.

3.5.2 Void Ratio

Void ratio, e, in geotechnics is described as the ratio of volume of voids in a system compared to the volume of solids. As stated in Section 2.6, a low void ratio in the system tends to lead to other features that exhibit high shear strengths in soil structures. From the 2D domain in this programme, the void ratio can be described as

$$e = \frac{A_V}{A_S} \tag{3.2}$$

where A_V is the area of voids and A_S is the area of solids.

Each particle has a known area defined by the coordinates that make up the outline, so these can be totalled to equate to A_S. Calculations of A_V were conducted using the upper surface of the placed particles. The trapezium rule was utilised to find the area underneath the upper surface curve described by the coordinates of the upper surface. This gives the total area of the system, A_T. Then A_V can be determined by

$$A_V = A_T - A_S \tag{3.3}$$

The void ratio of the system could be calculated for each position as the geometries of the particles and the upper surface are known. The criteria, V, is described as

$$V = 1 - e \tag{3.4}$$

to reflect the relationship between void ratio and shear strength and produce lower scores when higher void ratios occur. It is simple to check that the calculation of void ratio is correct in the Tetris scenario as each square will relate to a fixed amount of void ratio. By counting the squares of void ratio and squares of solids in the system, a manual verification can be complete to ensure the correct values of void ratio are being produced.

While straightforward, a problem can arise from the definition of A_V in Equation 3.3. As the number of particles placed increases and the total area of solids increases there will be a decreasing effect on the score V. This is due to the area of void being created being kept to a minimum whereas the area of solid increases at a much higher rate with each additional particle placed. An example of this is illustrated in Figure 3.13. Due to this, two more methods for quantifying V were developed and compared.

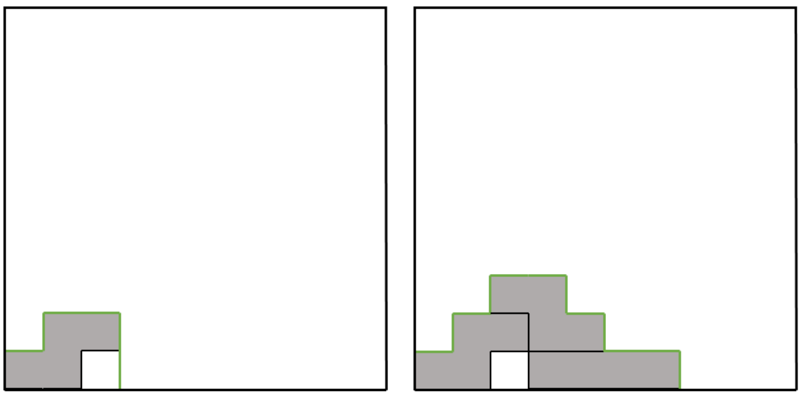

FIGURE 3.13: Example of decreasing effect of V as the number of particles in the system increases. Void ratios, e, equal 0.2 (left) and 0.077 (right) for the same amount of void present in the system. Green line represents placement surface under which e is calculated.

The first of these additional methods was to use a localised area of the system around the position of the particle rather than the whole system for calculating void ratio. From the minimum and maximum abscissa and ordinates, an extension is made to create this localised area. For testing purposes a localised area of 1.5 units - equivalent to 1.5 squares if a tetromino is made up of 4 squares - was taken. A distance of

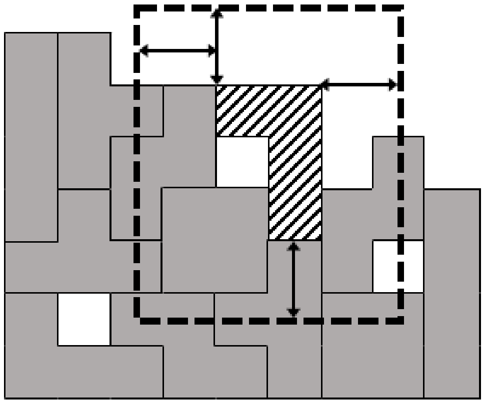

FIGURE 3.14: Example of a potential candidate placement of a tetromino in the Tetris Scenario with indication of extension of 1.5 squares from placed particle for the localised area calculation of void ratio.

1.5 squares was chosen so that gaps of a width of 1 square next to the particle being placed can be detected to avoid canyons forming in the system. An example of this is given in Figure 3.14. The area of investigation is created a distance of 1.5 squares from each side of the tetromino. Using information from the placement surface, a new area is created to describe the upper surface from the left-most side of the box indicated on Figure 3.14 to the right-most side. This extends down to the lower limit of the localised area, 1.5 squares below the lowest ordinate value. The area under this new upper surface is taken to describe the area of solids in the system. Therefore, the void present in the bottom-right of the localised area is not classed as void. This is a fair assumption as the placement of the particle does not create this void, only the void that is below its own placement. Therefore the scoring of the particle being placed should be not be based on void that it does not create within the system. A new score for a method using a localised area, V_{LE} can then be calculated by

$$V_{LE} = 1 - \frac{A_{VLE}}{A_{SLE}} \tag{3.5}$$

where A_{VLE} is the area of void created between the underside of the particle being placed and the upper surface line, and A_{SLE} is the estimated area of solids in the localised extension from the tetromino, described by the total area under the upper surface of the localised area.

The main note that should be added to this method is that any void created below the particle that is outside of the localised area is ignored. Therefore if a chasm of void is created by the particle through an overhang, the score is only based upon the void that is present in the localised area and V_{LE} will be higher than its expected value.

The third method for analysing void ratio for scoring utilised a technique that took the area of void created beneath the particle. To normalise this value, a ratio of the area created to the area of the particle was calculated. This new scoring method, V_{AB} can be described as

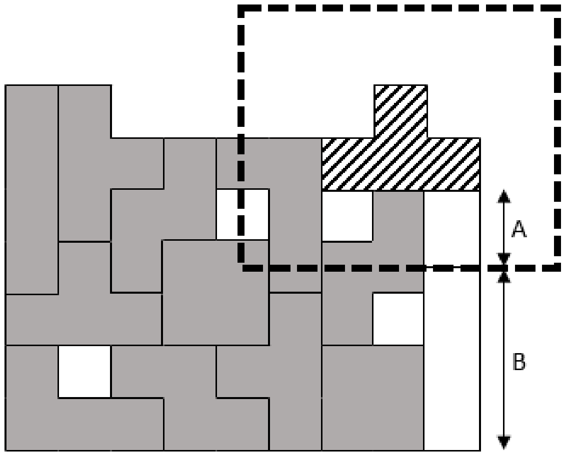

FIGURE 3.15: Example of a potential candidate placement of a tetromino in the Tetris Scenario where a canyon would be created. The length represented by A is the length for the area of void taken when calculating V_{LE}. Length A+B represents the length of the area of void taken when calculating V_{AB}.

$$V_{AB} = 1 - \frac{A_{VP}}{A_P} \tag{3.6}$$

where A_{VP} is the area of void created beneath the underside of the particle and the upper surface of the already placed particles and A_P is the area of the particle being placed. Unlike the method to calculate V_{LE}, this acknowledges all voids created below the particle and therefore any overhangs or creation of canyons in the system are accounted for. Figure 3.15 shows a case where canyoning occurs from placement, indicating the localised area (length A) that would be utilised and the area of void that would be excluded in the calculation of V_{LE} (length B).

Figure 3.16 presents data of 100 simulations of the Tetris Scenario through the form of violin plot. Figures 3.16a, 3.16c, and 3.16e are scored using an objective function with only a non-zero value for C_V out of the weighting coefficients in equation 3.1. Figures 3.16b, 3.16d and 3.16f have non-zero values for C_V and C_D and the coefficients of weighting are of equal value. The violin plots represent the frequency of a result by the width of the violin at that value of void ratio. Therefore, a wider width of the violin indicates a higher number of simulations that produced the result for that void ratio. Within the plots in Figure 3.16 are also the mean, median and quartile values for void ratio from the 100 simulations for each of the six scenarios. Figure 3.16e, although increasing in width from e=0 to e=0.1, has a shorter tail to its violin plot and has a lower mean value than objective functions using V or V_{LE}. Additionally, with the inclusion of D, lower void ratios are exhibited at a higher consistency than the other results. Therefore the use of V_{AB} is adopted in this work.

3.5.3 Depth of Placement

Many of the research papers explored previously in this thesis have taken the heuristic as suggested by traditional techniques of drystone wall construction to create structures in a layer by layer method (Johns et al., 2020; Johns et al., 2023; Liu et al., 2021). Furthermore it was shown in Section 2.6 that reducing the potential energy of the object being placed will increase stability (Furrer et al., 2017; Graton and Fraser,

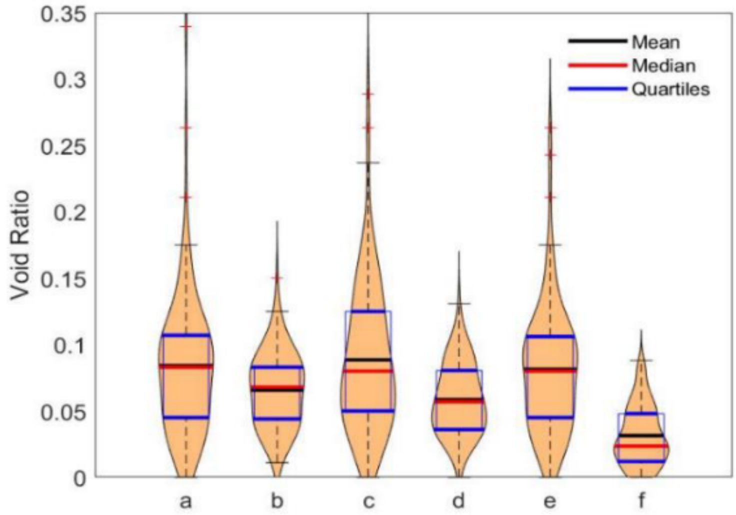

FIGURE 3.16: Violin plots with inset boxplots from Hoodless and Smith (2023), each representing results of 100 simulations for the Tetris Scenario using the different methods of quantifying the void ratio score using (a) V (b) V with D included in the objective function (c) V_{LE} (d) V_{LE} with D included in the objective function (e) V_{AB} (f) V_{AB} with D included in the objective function.

1935; Liu et al., 2015). In terms of helping to reduce void ratio, research in the areas of bin packing and Tetris optimisation took a bottom-left approach which prioritises placing the object towards the lowest depth possible (Hifi and M'Hallah, 2002; Jakobs, 1996; Liu and Teng, 1999; Wang et al., 2010). Böhm et al. (2005) and Kostreva and Hartman (2004) aimed to keep the height of the structure to a minimum for the Tetris Scenario and by introducing a scoring heuristic that prioritises the maximum depth it is thought that this can be achieved.

Criteria for scoring of depth, D relies on giving the object a higher score for being further down in the system. As such, this can be achieved by

$$D = \frac{D_{particle}}{D_{domain}} \tag{3.7}$$

where $D_{particle}$ is the depth of the particle in the domain measured by the distance from the top of the domain to the centroid of the particle and D_{domain} is the distance from the top of the domain to the bottom of the domain, i.e. the height of the domain. The ratio of $D_{particle}$ to D_{domain} was used to ensure dimensionless criteria so that comparison can be drawn between particles defined in different manners.

Initial runs of the programme indicated that towers of tetrominoes were created as leftmost positions were favoured if the score was equivalent to other candidate placements. The inclusion of D in the scoring criteria prevented these towers forming so long as C_D is large enough in relation to the other weighting coefficients to influence placement.

Like with the V having less of an effect on W_{ij} as more particles are placed, D will have less of an effect overall as the domain becomes full as $D_{particle}$ will tend towards zero. Other methods of quantifying D were considered. However, as the domain it is important that particles placed lower in the system are prioritised to ensure a layer-by-layer construction approach and to minimise the difference in height between the lowest and upmost points of the placement surface. The quantification of D is discussed in Section 8.5 and the effect that the chosen method had on results. As the domain is relatively small, it is thought that the calculation of D using method stated in Equation 3.7 is reasonable.

3.5.4 Contact Area

The contact area of the particle with other objects and the domain was highlighted as a potential scoring heuristic for a system where high shear strength is the objective in Section 2.6. More tightly packed structures will lead to higher strengths (Mogami, 1965; Moroto, 1982) and high amounts of friction adds to the strength of the system (Villemus et al., 2007). It is hypothesised that a larger area of contact between the particle and external surfaces will increase the chance for friction to occur. However, it is true that friction is caused by the roughness of the particles being used when packing and this is the main contributing factor to create friction. It can be understood that the more contacts a particle has with other particles and the domain the less area created beneath it and therefore less void initialised in the system.

Contact area was taken as the number of coordinates of the particle's outline in contact with the upper surface and the outline of the domain. Given that the lowering process of the particles stops as soon as the particle makes contact with the upper surface, often only a single direct contact is achieved. Tetrominoes did produce more than one point of contact creating a surface of contact between particles due to the touching faces being flush with each other but this was an unlikely scenario when moving to other shapes such as those representing untooled rock. Therefore a contact distance error, ϵ, was introduced. An extension from coordinates away from the particle was made. If this extension intersected with the upper surface or the domain then this point was classed as a contact point. Following the check for contact points, the score for contact area, T, was obtained by the process outlined here. The number of contact points is first found by

```
contact points = 0
for particle j at a given rotation and horizontal position
   for each coordinate of bottom outline i
      if x(i,j),y(i,j) intersects placement surface
      or x(i,j),y(i,j) intersects domain outline
         contact points = contact points + 1
      else if x(i,j)+CDE,y(i,j) intersects placement surface
           or x(i,j)+CDE,y(i,j) intersects domain outline
                contact points = contact points + 1
      else if x(i,j)−CDE,y(i,j) intersects placement surface
           or x(i,j)−CDE,y(i,j) intersects domain outline
                contact points = contact points + 1
     else if x(i,j),y(i,j)+CDE intersects placement surface
          or x(i,j),y(i,j)+CDE intersects domain outline
               contact points = contact points + 1
      end
   end
end
```

where CDE represents ϵ. Checks are made downwards as well as left and right of coordinates to check each possible direction a contact could be located. For the Tetris Scenario, ϵ was set to be 0.1. However, it should be stated that when ϵ was taken as 0 the same number of contact points were located due to contacts always sitting on the upper surface. T is then calculated by

$$T = \frac{n_T}{n_b} \tag{3.8}$$

where n_b is the number of coordinates in the bottom outline of the particle being placed and n_T is the number of coordinates in the bottom outline in contact with other particles and the domain. Intersection with the top of the domain was not classified as a contact point due to this top-down approach as well as this support not providing any resistance against particle slippage due to the direction of gravity. By totalling the number of contacts, this can be classed as an "area of contact". This value is made non-dimensional by creating a ratio to the total number of coordinates that make up the bottom outline, or the "area of the bottom of the particle", as shapes that are defined by more coordinates will naturally produce a higher n_T value for the same placement for two sets of coordinates that describe the same shape outline. n_b is taken rather than the total number of coordinates for the particle outline as only the bottom of the particle is utilised for placement as explained in Section 3.3.2 due to the top-down approach. Although T is referenced to as "area of contact" in this study, recognise this is actually a measure of the perimeter due to being performed in the two-dimensional plane.

It is expected that the higher number of contact points for a particle being positioned will indicate less void being created below the particle, especially in the Tetris Scenario. Therefore it is possible that T may be a secondary indication of V_{AB}. However, there is no consideration of the size of the void created below the particle. Instead, a contact point is indication of if void is directly below a coordinate with a higher score describing less coordinates that have void beneath them.

3.5.5 Coordination Number

Coordination number is the number of particles that are in contact with the particle being placed. The literature reviewed in Section 2.3.4 as well as the analysis of Incan retaining walls and Japanese castles in Section 2.2 provide evidence that a higher mean coordination number of a system of granular material leads to higher shear strengths exhibited. Therefore we introduce the parameter CN to the objective function.

Calculation of the coordination number was done by expanding the shape of the particle to be 5% larger in area around the centroid whilst in the placed position. If the outline of the expanded particle intersects with surrounding particles that are already placed in the system then these are deemed as touching and are totalled to be the coordination number. See Figure 3.17 for an example for a tetromino being positioned in a domain with already placed tetrominoes. The particle is surrounded by five others and gains a score of CN=5. Furthermore, the domain is classed as a placed particle and intersection with the outline of the domain is classed as a unique contact increasing the coordination number. Intersections are found using the inbuilt intersectionpoints function within Asymptote.

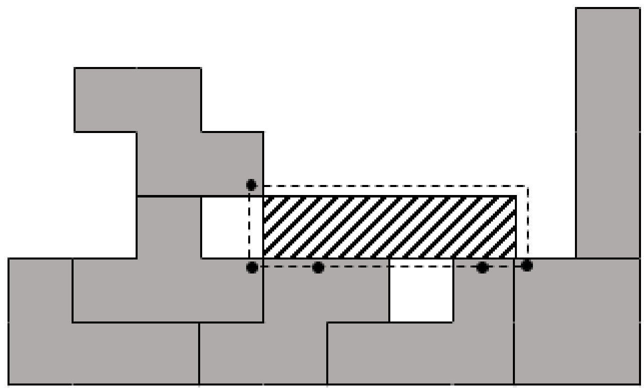

FIGURE 3.17: Example of the calculation of CN for a particle being placed (the hashed particle). The expanded particle outline is represented by the dashed line and touching tetrominoes are indicated by a black dot.

As CN is already a dimensionless number, this is taken as the unweighted score. It was considered to divide the coordination number by the number of particles in the surrounding area using a similar method to the localised area described in Section 3.5.2. However, it was considered that this penalised the particle for being near more particles rather than rewarding it for having a higher coordination number. For example, if a particle was near 10 particles but only had a coordination number of 2, it would score a value for CN of 0.2. If a particle was near 2 particles but only had a coordination number of 1 then this would score a value of 0.5 for CN even though a smaller coordination number is obtained.

As coordination number is calculated using the inbuilt intersectionpoints function in Asymptote it was necessary to lower the number of times this function is called to reduce computational time. In order to achieve this, the domain is split up into equal areas in a grid-like pattern as presented in Figure 3.18. When a particle is placed, the grids that it resides in is determined and the presence of the particle is recorded. For the next particle, the check for coordination number using the intersectionpoints is only completed for the grids within which the expanded particle shape sits in for that position, therefore omitting any particles that will definitely not contribute to coordination number.

Within Figure 3.18 there are already placed objects of a right elbow, left elbow and square tetrominoes. It is clear that the RE tetromino is positioned within grid locations of A1 and B1 for the specified naming system on the figure. The SQ tetromino resides only in the grid location D1. For the LE tetromino, the object clearly is situated in C1 and D1. However, the border of the tetromino sits on the border between grids B1 and C1. The particle could technically be classed to be in B1 as it is possible that other particles placed in B1 could lie next to the left elbow tetromino. Yet, as the expanded particle shape is utilised, the tetromino is not classed as within B1. If a tetromino placed in B1 does indeed touch the left elbow tetromino then the expanded particle shape will count as present in C1 and an intersection will be identified when analysing this area of the domain.

Figure 3.19 presents the cumulative time against the number of simulations ran for the Tetris Scenario for various separation of the domain into grids for storing particle location. These grid sizes are 1x1 (where no separation occurs), 2x2, 4x4 and 8x8

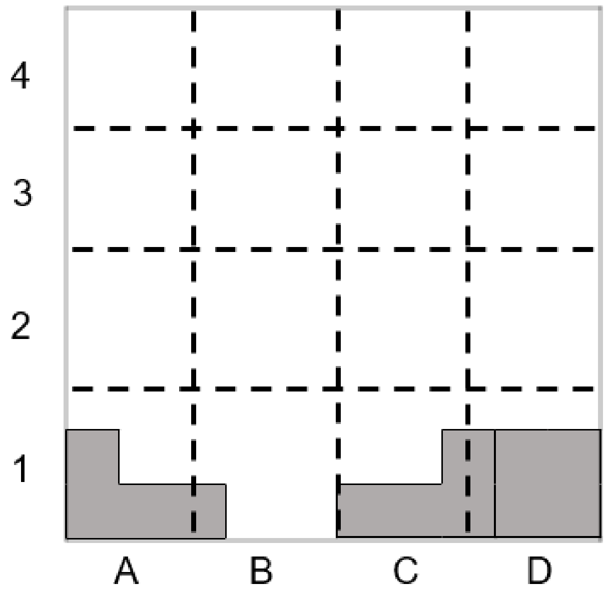

FIGURE 3.18: 10x10 square domain with split into equal areas of a 4x4 grid. Tetrominoes are placed for examples of scale and positioning.

sized grids. Each simulation is ran until the domain is "full" otherwise defined as the next tetromino to be placed has no viable position to fit without being outside of the domain. As the number of grids introduced increases the computational runtime also increases. It is clear that the time saved by not calculating intersections with each particle does not outweigh the time taken to store the particle information in each grid. However, it is thought that as the number of particles placed increases the time to find intersections with every particle will also increase. Therefore this step is introduced for future scenarios where the quantity of particles in the structure is much larger. The time to run an instance for a domain size of 100x100 squares placing 1000 tetrominoes is presented in Figure 3.20 for different numbers of separation of the grid. It is clear that the introduction of sectioning the domain does increase the computational speed when large number of particles are being analysed. For the current Tetris Scenario case, the gridsize can be set to 1 in the programme which will mean that no separation of the domain is completed.

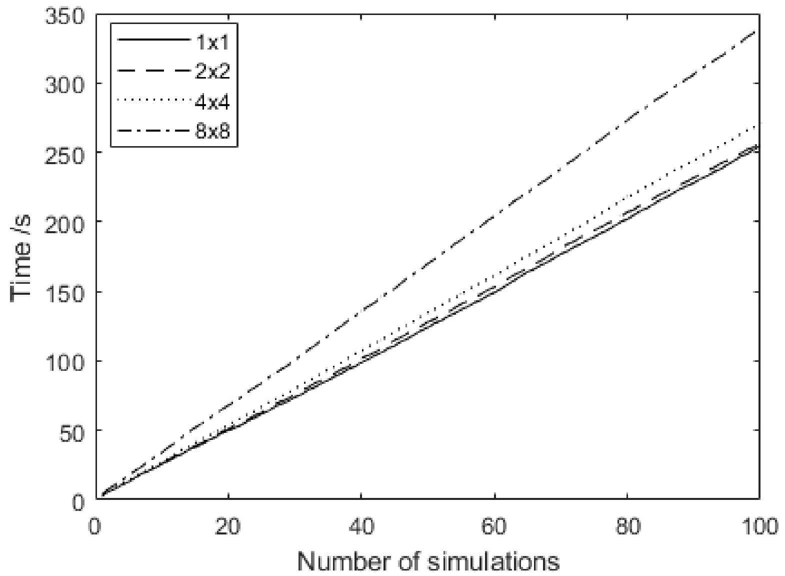

FIGURE 3.19: Cumulative time to run simulations up to 100 simulations. Tetris Scenario in a 10x10 square domain for varying separation of the domain into grids for storing particle location. Around 20 particles are placed in each simulation.

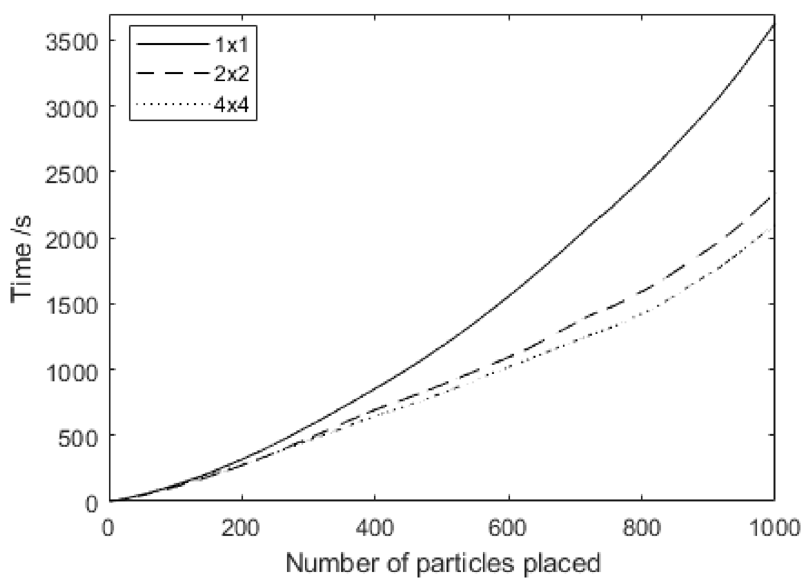

FIGURE 3.20: Cumulative time to place 1000 tetrominoes in a 100x100 square domain for varying separation of the domain into grids for storing particle location. Tetrominoes follow the same rules as Tetris Scenario with 4 orientations trialled at location spacings of 1 square.

3.5.6 Weighting Coefficient Values

Sections 3.5.2-3.5.5 describe the methods in which the criteria in Equation 3.1 are derived. The Tetris Scenario aims to create structures with minimal void ratio in the system. As such, in the objective function the weightings for each criteria can be adjusted to produce suitable results. In the previous work set out in Hoodless and Smith (2023), coefficients were tested manually by varying their value and running 100 simulations before analysing the resulting data by violin plots. Although results were achieved that exhibited low void ratios, it is not thought that an optimised value was achieved. A packing produced by this method is presented in Figure 3.21. A parametric study is conducted for C_V, C_D, C_T, and C_{CN} as explained in Chapter 4 and the values of these weighting coefficients are presented in Chapter 5.

Values for V_{AB}, D and T are all ratios that will range between 0 and 1. CN is defined by the number of surrounding particles and is therefore always an integer. Additionally, the value for CN is always a minimum value of 1 due to placement of a particle consistently being on either an already positioned particle or the base of the domain. This results in values of CN being greater than the other scoring criteria in the objective function. Therefore the expected value of C_{CN} is to be small relative to C_V, C_D and C_T. This would follow the work in Hoodless and Smith (2023) where coefficient values of C_V=5, C_D=1.25, C_T=0.4 and C_{CN}=0.01 were determined.

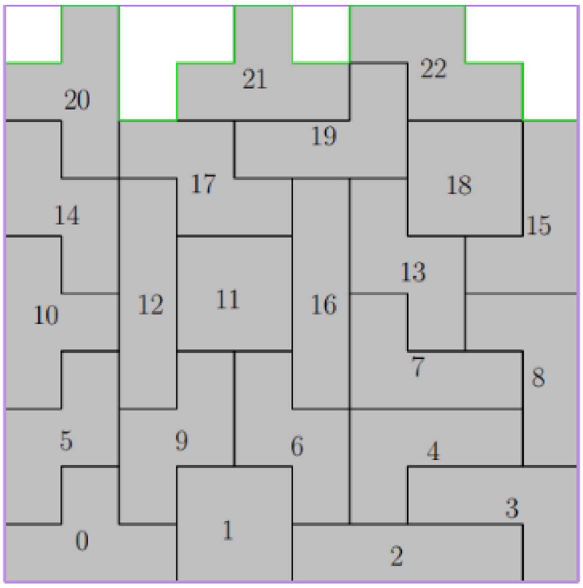

FIGURE 3.21: As presented in Hoodless and Smith (2023), single result of Tetris Scenario using coefficient values of C_V=5, C_D=1.25, C_T=0.4, C_{CN}=0.01 with the order of placement represented on top of each particle, the first placed particle indicated by 0

3.6 Soil Particle Scenario

3.6.1 Generating Particle Shape Outlines

Although the Tetris Scenario is useful for testing, the full use of a heuristic algorithm for determining placement of irregular, untooled rock can only be achieved if the simulated particles can represent real particle shapes. As the algorithm is currently designed to pack shapes in two-dimensions, the generation of particle outlines that have the characteristics of soil particles when presented as a two-dimensional shape is required.

Partice shapes for this research have been created using the Fourier-Voronoi method from Mollon and Zhao (2012) that is described in Section 2.5.3. Software is available from Mollon (2023). The code is based in MATLAB and is simple to use. It is possible to create different types of shapes using different combinations of Fourier descriptors. The effects of the shape descriptors were presented previously in Figures 2.50 and 2.51. From information in Bowman et al. (2001), Das and Ashmawy (2007), and Mollon and Zhao (2012) it is expected that D_2, D_3 and D_8 represent Fourier descriptors for elongation, irregularity and roughness respectively.

A further study was completed to produce the shapes that can be created by the code with different Fourier Descriptor input values. Results for some of the combinations trialled are presented in Figure 3.22-3.24. As expected, when D_2, D_3 and D_8 are all set to be zero (Figure 3.22) an arrangement of circles is produced in locations determined by the Voronoi tessellation approach. The target solid fraction - the targetted proportion of each cell covered by the particle - was set to be 0.7. This value is recommended to be less than or equal to 0.7 otherwise difficulties arise due to the biggest radius of the particle shape being greater than the smallest radius in the cell from the centre as described by Mollon and Zhao (2012).

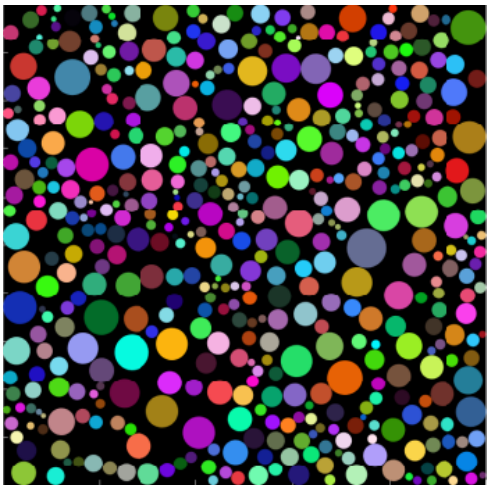

FIGURE 3.22: Products of the Fourier-Voronoi MATLAB code provided by Mollon (2023) for Fourier Descriptor values $D_2 = D_3 = D_8 = 0$.

As presented in Figures 3.23 and 3.24, an increase of the Fourier descriptors have the effects on the particle shape described in Mollon and Zhao (2012). An increase in D_8, represented by Mollon and Zhao (2012) in Figure 2.51, creates more noise to describe the particle edge increasing the roughness of the surface. From Figure 3.23c it can be seen that when D_8=0.04, the noise around the edge is very exaggerated. A value

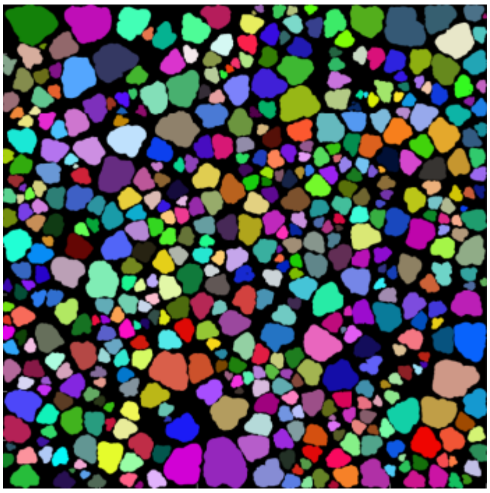

(A) $D_2 = 0.1$, $D_3 = 0.1$, $D_8 = 0.015$

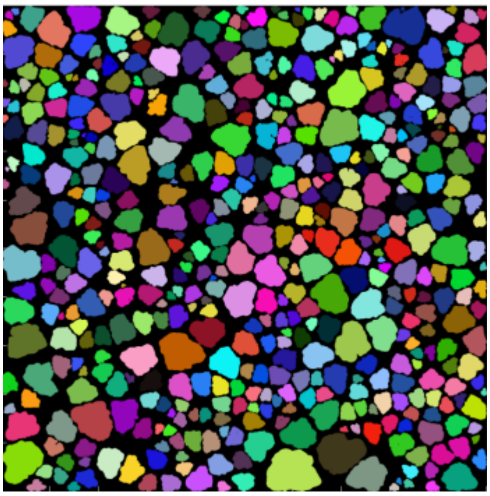

(B) $D_2 = 0.1$,$D_3 = 0.1$, $D_8 = 0.02$

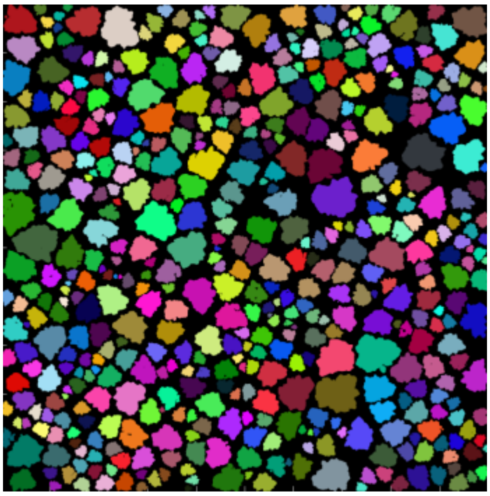

(C) $D_2 = 0.1$, $D_3 = 0.1$, $D_8 = 0.04$

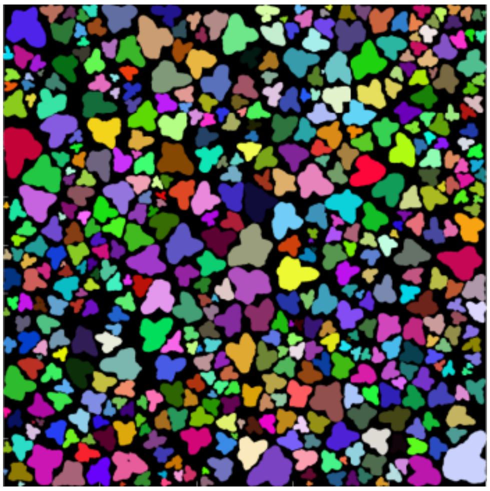

(D) $D_2 = 0.1$, $D_3 = 0.2$, $D_8 = 0.015$

FIGURE 3.23: Products of the Fourier-Voronoi MATLAB code provided by Mollon (2023) for different Fourier Descriptor values.

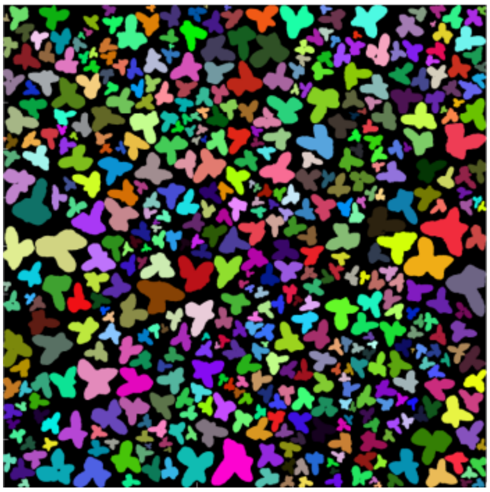

(A) $D_2 = 0.1$, $D_3 = 0.3$, $D_8 = 0.015$

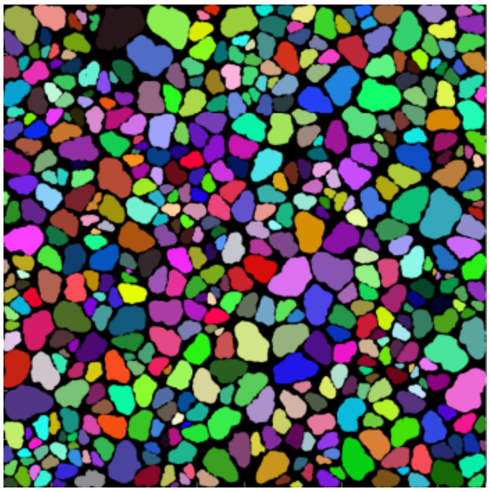

(B) $D_2 = 0.2$, $D_3 = 0.2$, $D_8 = 0.015$

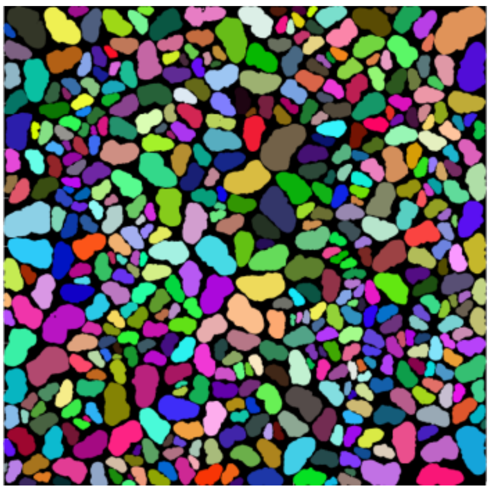

(C) $D_2 = 0.3$, $D_3 = 0.2$, $D_8 = 0.015$

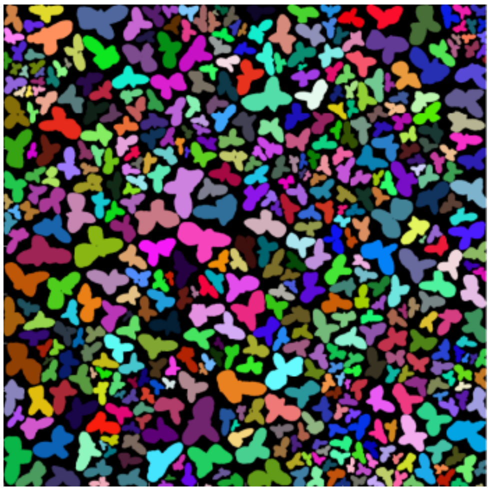

(D) $D_2 = 0.3$, $D_3 = 0.3$, $D_8 = 0.015$

FIGURE 3.24: Products of the Fourier-Voronoi MATLAB code provided by Mollon (2023) for different Fourier Descriptor values.

of D_8=0.02 (Figure 3.23b) is still quite exaggerated for the representation of quarry rock and stones that are envisioned for the use of this algorithm. D_2 increases elongation in the shape as described by Mollon and Zhao (2012) and shown in Figure 2.50. Past a value of D_2=0.2, the elongation of the particles becomes too high for representing untooled, rock particles. Increasing D_3 leads to a decrease from sphericity of the particle with the shapes generated possessing peninsula-like outcrops from the centre of the particle. An increase of D_2 in combination with D_3 (Figure 3.24b compared to Figure 3.23d) lessens this effect for D_2=D_3=0.2 but past this value the particle outlines start to exhibit peninsula-like outcrops again (Figure 3.24d where D_2=D_3=0.3).

Fourier Descriptor values of 0.2, 0.2, and 0.015 for D_2, D_3, and D_8 respectively were adopted when generating particles. This analysis has been completed by eye, however as discussed in Section 8.6.4 an improvement on this study would be to characterise untooled, irregular rock sampled from a quarry or mining facility to compare these shapes to or derive Fourier descriptors from.

An example of a distribution of particles produced can be seen in Figure 3.24b. These Fourier Descriptors were chosen as the particle shapes produced were irregular and therefore would test the method produced in Section 3.4 whilst also resembling the shapes of untooled rock stones. The target solid fraction (TSF) is the proportion of the cell created by the Voronoi tessellation that is filled by a generated particle and was set to 0.7 as recommended by Mollon and Zhao (2012). A value of 0.7 is given as an upper limit by Mollon and Zhao (2012) for generating particles. Values higher than this may not be reached due to fitting of the particle shape into a cell. This value had no effect on the types of particle produced apart from their size. Each particle's size is only related to the other particles as the sizes of the particles or of the domain can be scaled in the algoirthm. Therefore a value of TSF of 0.7 was selected as this produced the most particles in the MATLAB code provided by Mollon (2023). The value for TSF is given so that the study can be replicated if desired.

D_2	D_3	D_8	TSF
0.2	0.2	0.015	0.7

TABLE 3.1: Values taken forward in this study for producing particle outlines using the MATLAB code provided by Mollon (2023).

Particle Selection

To dismiss any particles that were undersized or oversized, an arbitrary radius limit between 3 and 7.5 units was chosen as this provided a good supply of particles from the outlines produced. An alternative could have been to take particles of unsuitable size and scale these to be within the suitable range. However, 500 soil grain outlines were generated by the Fourier-Voronoi code and it was also possible to produce more particles through more runs. Therefore this was not adopted in the method. Of the 500 particle outlines produced, 168 particle outlines were filtered by the radius limit. The first 100 of these 168 were taken forward to be used in the Soil Particle Scenario. Four particles produced for packing are presented in Figure 3.25 at the orientation given by the programme.

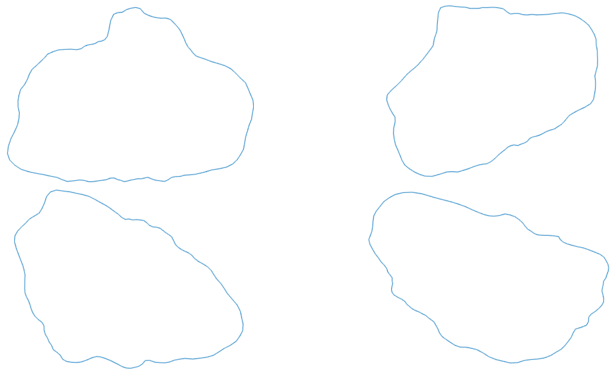

FIGURE 3.25: Outlines of particles selected for packing at the given orientation when produced by the MATLAB code provided by Mollon (2023).

3.6.2 Domain

The domain in which the algorithm described in Section 3.4 is utilised in outlines that represent two-dimension irregular soil grains is a 50x50 units square. The length of 50 units roughly equated to ten particles being placed in one course. This is similar to the width of the Tetris Scenario which allows for 10 squares width for placement of tetrominoes. In order to achieve this size of domain, the domain height was set to 50 and the domain width was set to 50 in the algorithm. Originally testing was conducted in a domain of size 75x75 units. This size was reduced to 50x50 units to reduce the runtime as less positions are trialled across the width of the domain.

3.6.3 Orientations and Spacings

Within Tetris, it is known that tetrominoes should be rotated by 90^o and a defined spacing of 1 square between potential positions should be adopted as set out by the scenario described in Section 3.2.2. For irregular, untooled rock shapes there is no determined number of orientations or distancing between placement with the number of potential positions ever increasing as the required definition of these values increases. Therefore the number of orientations and distance between placements will depend on the accuracy required for the placement. To start, the number of orientations was varied between 8, 16 and 32 and a location spacing of 1 unit was trialled. In Section 3.7.3, a new system for locating positions was introduced which change the way in which the number of orientations and spacing of locations are defined. As described in Section 3.5.4, a contact distance error, ϵ, of 0.1 units was adopted for determining contacts with the upper surface.

3.6.4 Particle Order

Particle order is again generated using the Tetris bag method described in Section 3.3.5. Given that 100 particles are taken forward from those generated using the method in Section 3.6.1 and the domain size described in 3.6.2, it is expected that 100 particles is an upper limit and that this number of particles will not be placed with roughly 50 particles predicted for placement in a domain of 50x50 units. Therefore, the particle order generated will be a list of 100 unique particles and none will be repeated in placing. However, the Tetris bag method is adopted for occasions where more than 100 particles are used, say if an investigation is conducted on increasing the domain to a size which can fit more than the 100 particles available for selection when packing. Again, the particle generation order for the Soil Particle Shape scenarios is arbitrary so long as this can be reproduced when comparing variables within the programme. Improvements on the algorithm would be to create a particle order that considers delivering particles based on the characteristics of the particle shape. This is further discussed in Section 8.6.3.

3.6.5 Computational Time

The computational time for the Tetris Scenario is quick, especially considering every potential position for each orientation is trialled. Table 3.2 presents the system information for the computer used in this study and Table 3.3 compares the computational runtime for packing in both scenarios. Comparing the time it takes to place 20 particles, the Soil Scenario takes significantly larger computational times compared to the Tetris Scenario. This is expected as not only does the Soil Scenario consider more candidate poses for each particle but also the number of coordinates to describe the untooled rock shape is vastly increased. In turn this leads to larger numbers of coordinates to describe the placement surface as particles are positioned in the system. The times currently outputted by the programme are too large for a real situation where a robot is placing stones. Realistically, the algorithm should not take 17 minutes to determine the location of 20 stones in a structure. Therefore methods to increase the computational speed of the programme are introduced in Section 3.7.

System Manufacturer	Dell
System Model	OptiPlex 7050
System Type	x64-based PC
Processor	Intel(R) Core(TM) i7-7700 CPU @ 3.60GHz
Cores	4
Logical Processors	8
RAM	16GB
Operating System	Microsoft Windows 10

TABLE 3.2: System information of the computer used in this study.

Scenario	No. particles	No. simulations	Total Time	Time per 20 particles
Tetris	20	100	257s	2.5s
Soil Particle	60	1	3061s	1020s
Soil Particle	20	4	3216s	804s

TABLE 3.3: Times to run simulations of Tetris Scenario and Soil Particle Scenario in a domain of 50x50 units for 16 orientations and location spacing of 1 unit.

Note, the computational runtime per 20 particles is quicker for placing 20 soil particle outlines than it is 60. This is because the placement surface increases in the number of coordinates it is described by. The inbuilt Asymptote "intersectionpoints" function - which is used when finding the distance to lower the particle - takes more time to perform when trying to intersect lines described by larger numbers of coordinates. Running four simulations of 20 particles is quicker per 20 particle due to the placement surface being reset to be described as two coordinates at the start of each simulation. For the scenario placing 60 particles the algorithm is continuing to place another 40 particles on a placement surface described by many more coordinates as the placement surface is now described by the top surface of the already placed particles. This is further explored in Section 3.7.2.

Table 3.2 is included to give context to the computational times presented in this thesis. It is clear that using a higher performing computer would lead to improved computational speeds. Indeed, it is expected that if this research is taken any further that a highspeed computer would be utilised. Other methods for improving computational speeds overall are given in Section 8.7.

3.7 Increasing Computational Speed

3.7.1 Particle Definition

Particles generated from the code provided by Mollon (2023) produce particles described by 129 coordinates for the outline of the shape. Each individual coordinate that is deemed to describe the bottom line or the top line are utilised when finding the lowering distance during placement. Therefore, the use of every single of these coordinates to describe the shape is a main cause of computational time in the system. Furthermore, the accuracy of describing a particle with such definition may not correlate to the level of accuracy that a machine may be able to visualise such a particle.

A method adopted to reduce the computational time of the algorithm is to use less coordinates to describe the particle shapes whilst still allowing for them to represent untooled, irregular rock. This was previously proven in Figure 3.9 of Section 3.4.1 Doing so allows for the speed to increase greatly when placing soil particles by the algorithm. This is discussed further in Section 6.2 and Section 6.3.

Figure 3.26 shows the outline of a particle represented by different quantities of coordinates. Figure 3.26a is the outline represented by all 129 coordinates that are originally produced by the particle shape generating code (Mollon, 2023). The outlines in Figures 3.26b-3.26f are represented by a decreasing amount of coordinates. As is seen in Figure 3.26, the general particle shape is well represented up until about 14 coordinates (10% of original) to describe the outline. Figure 3.26f uses 7 coordinates (5% of original) and the resulting outline is not recognisable to the original with a large section in the bottom right missing. Figure 3.26d and Figure 3.26e still resemble the outline of the particle. However, the features of the particle surface begin to lose definition which may be key is trying to depict the roughness of the particle. This roughness provides more precision for placement to ensure stability which is desired to be retained when representing the particle.

Going forward representing untooled, irregular rock shapes, a third (44) of the coordinates originally used to represent the outline will be adopted like in Figure 3.26c to ensure both the general outline of the particle and the finer surface details are retained. The use of non-dimensional criteria in the objective function means that this reduction in coordinates should not lead to a change to how particles are scored on placed. However, there will be some change to how particles are placed due to stability checks where perhaps locations of contact are not present when they would be if all coordinates were utilised to describe particle shape. A reminder is made that particles should be described by an enclosed loop and therefore it was ensured that the first and last coordinates in the vector describing the particle shape were equivalent.

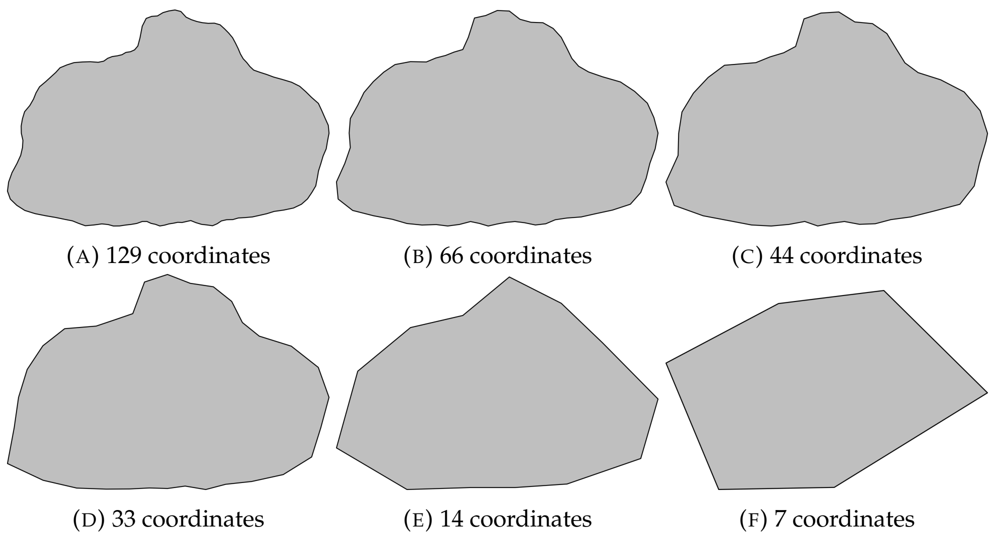

FIGURE 3.26: Outline of particle shape represented by (a) All the available coordinates for description (b) half of the coordinates (c) a third of the coordinates (d) a quarter of the coordinates (e) 10% of the coordinates. Each outline has the number of coordinates used to represent the shape displayed beneath.

3.7.2 Placement Surface Look Up Table

The computational time to place one particle appears to increase as the number of already placed particles increased up until the 10^{th} particle placement. From a visual inspection, this tended to be when the first course at the bottom of the domain had been filled. With each particle placed, the number of coordinates making up the placement surface increases as the outline of the particle is attached, with the original number of coordinates for the placement surface being two for the rectangular domain as described in Section 3.3.3. The reasoning for the increase in computational time is the use of the in-built intersectionpoints function in Asymptote. The use of this function detects where two paths intersect with each other. In order to do this, the function checks between every coordinate of the path leading to increasing computational times with the more coordinates being used to define the path. Once 10 particles are placed and the first course of the domain is full, the placement surface is described by an upper limit of coordinates and will not greatly increase past this value. Therefore the time taken to place a particle plateaus past this point.

To increase computational time it is clear that the path to describe the placement surface underneath the particle when being positioned needs to be shortened or the number of coordinates needs to be reduced. Therefore the placement surface was split up into partitions with equal numbers of coordinates and an upper and lower value for the abscissa. This was stored in a Look Up Table, a structure of data that the algorithm could easily access the information from. For the placement of a particle, the maximum and minimum abscissa for the object are taken. The sections of the surface that the object lies between are extracted from the Look Up Table and adopted as the placement surface for lowering the particle using the method described in Section 3.4.1. Figure 3.27 is an example of the separating of the placement surface with a particle about to be tested for placement in the top left above the domain. For this particle, coordinates for the two left-most partitions would be taken from the Look Up Table as it sits above these sections.

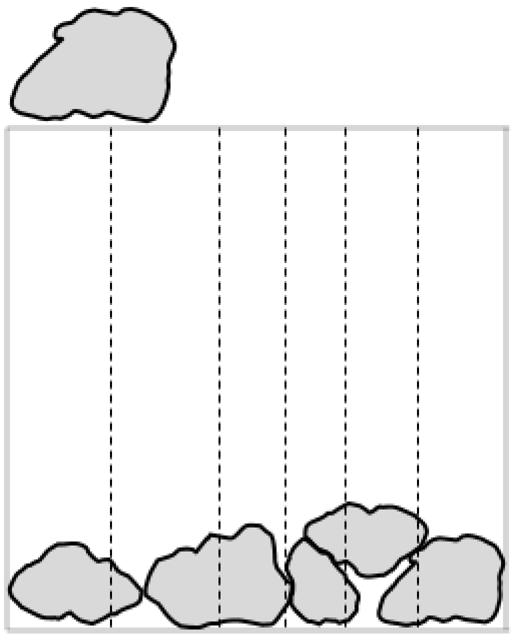

FIGURE 3.27: Example of the placement surface being split into different partitions and a particle about to be tested for placement in the top left above the domain. Notice the width of each partition is not uniform as it depends on the number of coordinates rather than the abscissa values.

Originally it was thought that there would be an optimal number of partitions made in the placement surface. Figure 3.28 shows the computational run times in seconds for a different number of partitions in the placement surface. The scenario that this test was conducted in was the soil particle scenario for a domain of 50x50 units placing 20 particles at 32 different orientations and a location spacing of 1 unit. As can be seen in Figure 3.28, the number of partitions decreases until it plateaus at around a value of 40 before increasing. However, Figure 3.29 show results for similar set ups but for a 25x25unit domain and a 75x75unit domain. Although full testing of the 75x75unit domain was not complete due to the computational time, it is clear to see that these times plateau at different values than the number of partitions equalling 40 - at around 20 partitions for Figure 3.29a and around 50 partitions for Figure 3.29b. Therefore, the optimal value must depend on a different factor.

An investigation was completed into the size of each partition given that the computational speed of the intersectionspoints function depends on the number of coordinates. Figure 3.30 shows results of the average time placed per particle after the 10^{th} particle has been placed and the average number of coordinates in each partition. Average time after the 10^{th} particle was chosen as this was when the bottom coarse was filled and the placement surface should be at an upper limit of coordinates in length. The coordinates were split up to have an equal quantity in each partition so this average was calculated by dividing the number of coordinates in total by the number of partitions in the surface.

From Figure 3.30 it can be determined that there is an optimal number of coordinates in each partition for the optimisation of the number of partitions. This value is around 10 coordinates per partition. Therefore, the separation of the placement surface was changed. Rather than specifying a number of partitions, the number of

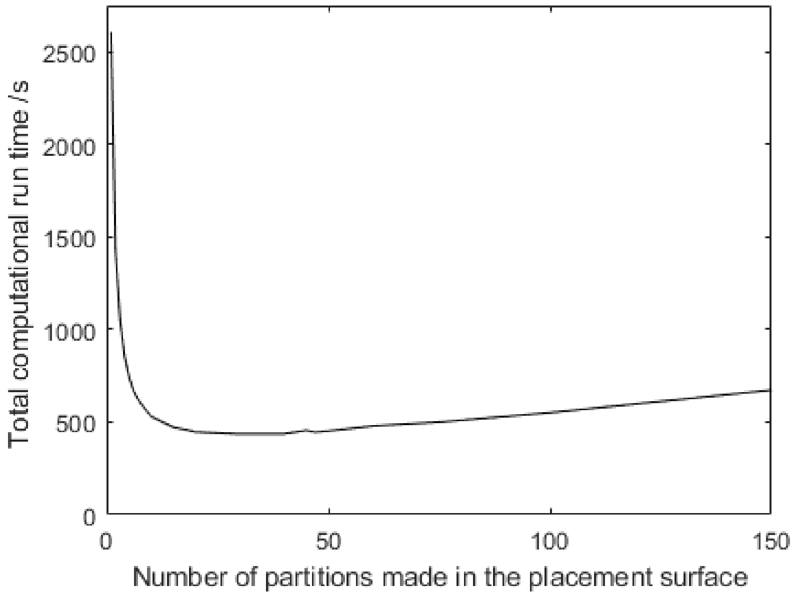

FIGURE 3.28: Total computational run time for 50x50unit domain placing 20 particles at 32 orientations and a location spacing of 1 unit in the Soil Particle Scenario for different numbers of partitions made in the placement surface.

partitions is determined by the number of coordinates in the placement surface. A section of the placement surface made up of 10 coordinates is put into each partition and then taken from the Look Up Table when the particle is being placed above this section. Figure 3.31 compares the computational time for splitting the placement surface into sections of 10 coordinates to the original scenario without this implemented. It can be determined that the computational speed is vastly increased as the time is 20% that of the original.

3.7.3 Reducing Candidate Positions Tested

The computational runtime of the algorithm is heavily influenced by the number of positions and orientations attempted for finding the optimal placement. A lower number of orientations and a higher value of location spacing can be adopted to increase speed but at the expense of the accuracy of placement. Instead, it is possible to use smaller resolutions for scoring before moving to higher resolutions like in Cagan et al. (1998) or use a coarse description of the object's outline to remove obvious non-matches as described in Kong and Kimia (2001). These were discussed in Section 2.4.3 and Section 2.4.4 respectively. As such, a method to reduce the resolution was adopted. Both the next selected particle and the domain with positions of already placed particles are discretised into binary matrices for which size depended on the specified resolution. An example of this is given in Figure 3.32. A resolution value is set in the programme. If this was a value of 0.5, a domain of 50x50 units would be converted into a 100x100 matrix and a particle with maximum width and height of 6 and 7 would be converted into a 12x14 matrix. In the matrix, squares which have no presence of a particle are classed as empty and given a value 0 whereas squares which do are classed as full and given a value of 1. An example of the discretised domain with two particles already placed is represented in Figure

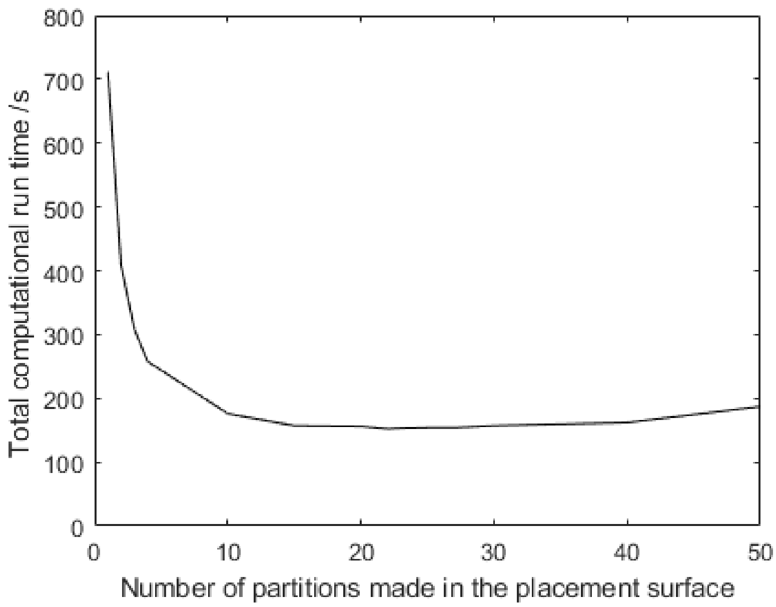

(A)

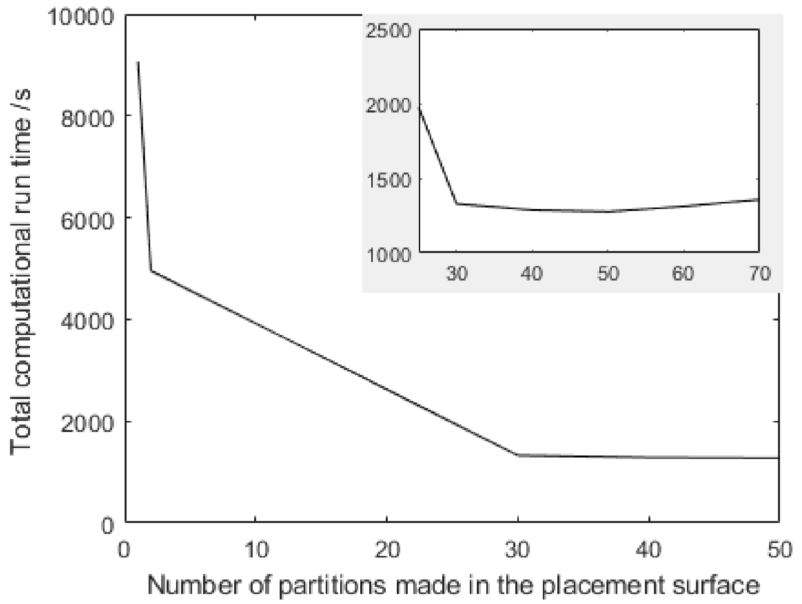

(B)

FIGURE 3.29: Total computational run time placing 20 particles at 32 orientations and a location spacing of 1 unit in the Soil Particle Scenario for different numbers of partitions made in the placement surface for (a) a 25x25unit domain and (b) a 75x75unit domain with zoomed in part of data inset into the figure.

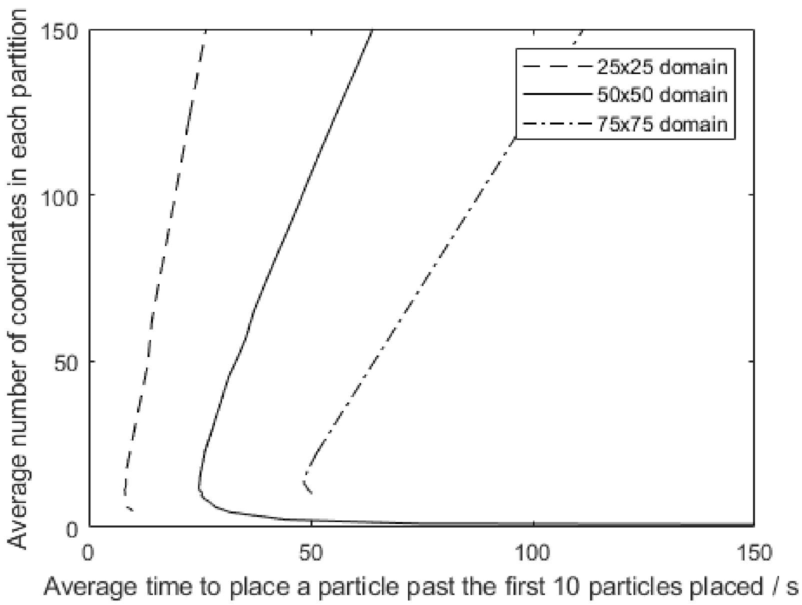

FIGURE 3.30: Average computational speed to determine particle position past the 10th particle placed against the average number of coordinates in each parition for domain sizes of 25x25units, 50x50units and 75x75units. Soil Particle Scenario adopted for 20 particles at 32 orientations and a location spacing of 1 unit.

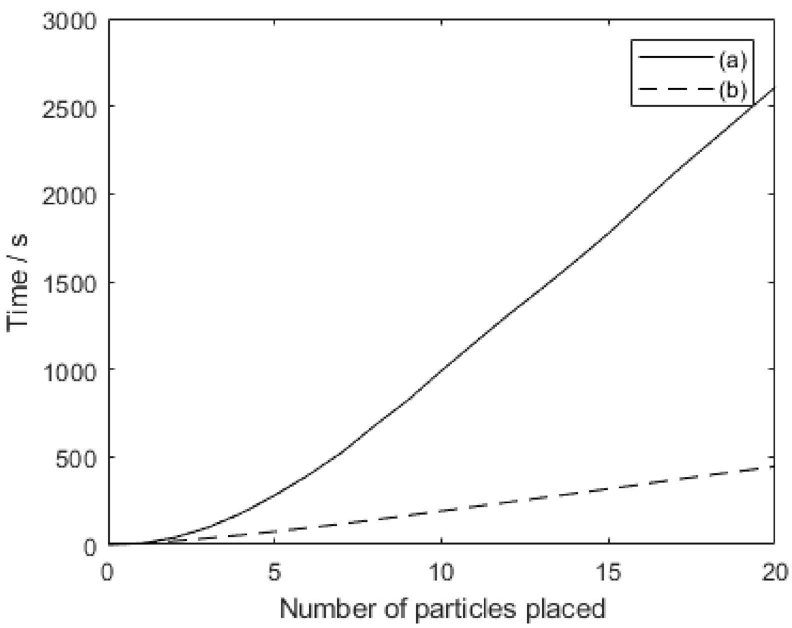

FIGURE 3.31: Computation speed to place 20 particles. Soil Particle Scenario in a 50x50unit domain at 32 orientations and a location spacing of 1 unit for (a) no splitting of placement surface and (b) splitting of placement surface optimised to have 10 coordinates in each partition.

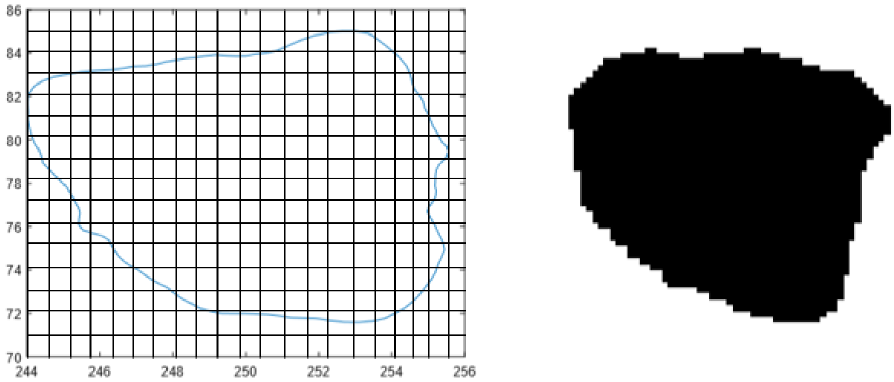

(A) (B)

FIGURE 3.32: (a) Discretisation of particle at a resolution of 0.5 units per square (b) Result of discretisation

FIGURE 3.33: Example of domain with two particles placed discretised. Information is stored in binary form with designations of 0 (black squares) and 1 (white squares) for empty space and filled space respectively.

3.33 The matrix of the particle is tested along the placement surface within the domain to locate possible positions for the particle. Fittings are classed as suitable if the product of both matrices is equal to zero. If the particle does not fit, the resulting product will be a non-zero value and this location is omitted. By doing this process, the number of possible placements is reduced as it automatically excludes positions where the particle will not fit. The discretised matrix of the domain is expanded to include the edge and these are classed as filled material and equal to 1. The size to represent the border is specified. For example, if a size of 2 is selected for resolution of 0.5, a 50x50 unit domain would be converted to a 104x104 matrix where the central 100x100 squares represent the domain and the perimeter of 2 squares represent the border.

The approach adopted to discretise the particles into squares of filled and unfilled space creates a new problem for when should a square that has some material within it be classed as filled. It is common within mathematics to adopt an approach that states that if more than or equal to half the area of the square is filled that the square should be classed to be filled. In this work, it is adopted that if the square has any material within it it is classed as filled. The accuracy of the placement algorithm will come down to the accuracy of the equipment used to image material. By accepting all squares with material in as filled a tolerance is allowed for any inaccuracies of measurements and will prevent extremely tight placements being tested when it may be that in reality the object will not be able to be positioned in the determined location due to unregistered dimensions. Additionally, it should be considered that the method of placement by robot will involve some form of gripper. Whilst the addition of the gripper on the sides of the stones have not been considered when lowering the particle, taking the conservative approach for filling discretised squares with any amount of material in them accounts for this slightly.

By completing the previous step, there are still a large number of candidate positions for different orientations of the particle to be placed. To further reduce this, a filtering system can be introduced like the one in Johns et al. (2020) where a minimum ratio of width to height for a particle at a given orientation was set to 0.5 as discussed in Section 2.2.4 and any poses not meeting this criteria are discarded to save on computational time. Furthermore, the use of a hierarchical filtering approach as seen in Liu et al. (2021) can be adopted. However, rather than filtering out potential positions, an order list is created by prioritising different features of the position. These ordering list criteria are described as the following.

Discretised particle score

Particles are evaluated using the objective function discussed in Section 3.5 with criteria of void ratio, depth of placement, contact area, and coordination number. This is complete whilst in their discretised form so this is thought to be a rough estimate and not the final score for the placement. Each criteria is calculated using the stated method and a weighting coefficient is applied to each score.

- Void Ratio: the discretised number of squares that are empty between the particle and the placement surface are counted (A_{VP}). This is put into a ratio with the number of filled squares that make up the discretised particle (A_P). As with the scoring for void ratio in Section 3.5.2, V_{AB} is determined by $1 - \dfrac{A_{VP}}{A_P}$ as seen in Equation 3.6.
- Depth of placement: the number of squares the particle is lowered in the discretised domain is converted to a length which is taken as $D_{particle}$. D is then determined using equation 3.7 in Section 3.5.3 taking D_{domain} as the length of the domain in squares excluding the perimeter representing the boundaries.
- Contact area: the perimeter of the discretised object is located and checked to see if this is touching a filled square in the discretised domain. If it does, then this is marked as a contact point. T is calculated as a ratio of number of contact points to the number of squares that make up the perimeter in the discretised particle.
- Coordination number: as with contact area, the perimeter of the discretised object is located. If a contact point is located then this is compared to a matrix of the domain where each different particle is given a unique number greater than 1 as its value to indicate a full square. If the value in this matrix is non-zero and a number that has not been detected before, this is counted as contact with a "new" particle. Coordination number, CN, is the total number of contacts with "new" particles. The boundary of the domain is also taken into account and given a value of -1.

These scores are applied to Equation 3.1 with their corresponding weighting and a score can be given to each placement for each orientation trialled. The candidate positions are ordered into decreasing score for this ordering criteria.

Depth in the system

The ordering criteria for depth in the system sorts placements into increasing distance from the bottom of the domain to the centre of the particle, with the lowest depth being prioritised. The depth of placement is determined as previous with the discretised length lowered converted into a distance value. This ordering criteria is adopted if positions are jointly scored on the discretised particle score.

Left-most position

The left-most position ordering criteria sorts placements into increasing location in the abscissa and therefore prioritises the left-most location in the domain out of the poses. This is adopted if positions possess the same discretised particle score and depth in the system criteria.

Area beneath the particle to width ratio

Area beneath the particle is calculated as the amount of empty space below the particle for a given orientation to a horizontal line below the particle. This does not take into account the placement surface for where the particle is being positioned. However, it is a quick way of judging how much void will be created without having to clearly define the placement surface in the discretised system. The area beneath the particle is then defined as a ratio with the particle width to prevent slender particles being prioritised as this would create a smaller amount of void than wider particles. It is thought that this ordering criteria will mainly prioritise orientations which are mainly flat and parallel to the horizontal, aligning to the suggested method of building a drystone wall in Vivian (1976) which recommended using flatter stones. Again, the ordering criteria described here is only adopted if positions have joint values for all previous ordering criteria.

Width to height ratio

As with Johns et al. (2020) a width (d) to height (h) ratio criteria is applied such that

$$\frac{d}{h} > 0.5 \tag{3.9}$$

Any orientations that possess a $\frac{d}{h}$ value below 0.5 are discarded and not considered a candidate position. Additionally $\frac{d}{h}$ is adopted as the final ordering criteria, with those orientations that have a higher width-to-height ratio being prioritised. This ordering criteria is required if two or more possible placements are joint for all other criteria.

The number of candidate positions considered

From the application of the above criteria, an order list of candidate positions is provided. Taking the whole list of candidate positions would take massive computational times. For example, a particle being placed in the Soil Particle Scenario at a resolution of 0.5 at 32 orientations produced over 35,000 potential positions which would require scoring. It is considered that only the "best" candidate positions can be taken forward for positioning like seen in Woflson et al. (1988) who took the 200 best solutions through to the next step for trialling when fitting jigsaw pieces.

To determine the number of candidate positions to be taken forward for consideration, a study was conducted with what is thought to be an oversized amount of candidate numbers tested. Initially, the first 100 positions produced by the order list after applying a hierachical filtering approach are tested. Next, 1000 positions from the order list being tested was trialled. This was completed in the Soil Particle Scenario for 16 and 32 orientations using a resolution value of 0.5. Figure 3.34 shows the cumulative frequency for the numerical position in the order list of the final chosen candidate position for both 100 and 1000 candidates tested. For each tested scenario, the cumulative frequency for the numerical position in the order list increases at a higher rate at lower numerical positions. For 100 positions, the gradient of the lines is always quite steep whereas for 1000 positions the rate of increase does start to decline as the numerical position in the order list becomes greater. It should be noted that for 100 positions tested, the number of particles placed was set to 50 whereas for 1000 positions tested the algorithm was set to place particles until the next particle could not be placed within the domain and this is why the cumulative frequency for these results is larger.

Figure 3.34 suggests that testing up to a numerical position in the order list of around 80 would be optimal as this is when the rate of increase for cumulative frequency starts to decline for the scenario where 1000 positions were trialled. However, using this many trials will lead to long computational times. In the scenarios where 100 positions were trialled, computational runtimes of 4.6 hours and 3.6 hours for 16 orientations and 32 orientations respectively were outputted. The reasoning for 32 orientations taking less computational time is discussed in Section 3.7.4. Instead, the number of candidate positions analysed for placement will be reduced to 30 where the decline in rate of increase for cumulative frequency is not as pronounced but the effect on computational runtimes is not as large.

3.7.4 Improving Accuracy of Placement

Initially, the number of orientations is limited for values between 8, 16 and 32 different orientations and location spacing as 1 unit between horizontal positions across the domain. This was due to the computational runtimes exhibited by the algorithm. However, by limiting to these smaller resolutions of placement, positions for placement may be missed and more gaps may appear between materials. The introduction of the discretised search results in less locations being tested. Therefore, an increase in accuracy of placement can be made. Again, this will speed up computational runtime and becomes a question between accuracy of placement and the required speed at which the algorithm will need to run.

As such, a refined orientation of the particle and location spacing are introduced when analysing the candidate positions. The orientations for each position is set to a small angular value at which the particle is rotated by. For an example of the initial number of discretised rotations being 4 and the refined angular value being 10^o, the starting particle orientation can be classed as having being rotated at 0^o for a candidate position. As the number of discretised rotations is 4, the particle is tested at a difference of 90^o. Therefore, the particle is rotated a further 10^o from the 0^o until it reaches a rotation of 90^o from its original orientation. In this manner, the particle will be tested at 10 different orientations (0^o, 10^o, 20^o, 30^o, 40^o, 50^o, 60^o, 70^o, 80^o, 90^o).

The refined location spacing is required to be that of a value that is lower than the spacing between squares when the particle is discretised. For example, if a resolution

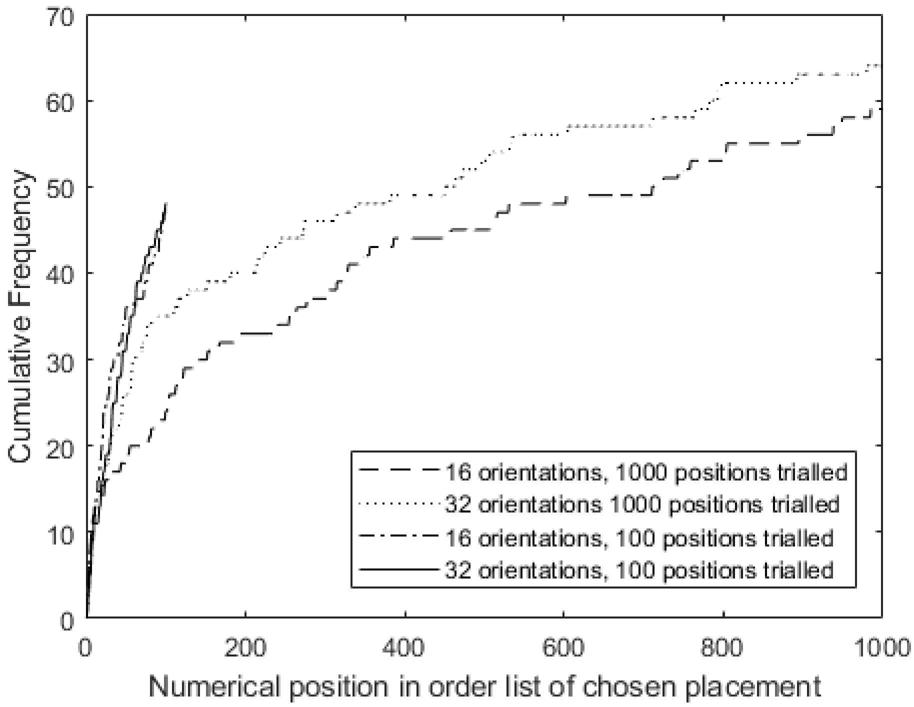

FIGURE 3.34: Cumulative frequency for the numerical placement in the order list of positions for the final position chosen by the algorithm. Resolution adopted in test is 0.5 with weighting coefficients of $C_V = 6$, $C_D = 2$, $C_T = 1$, $C_{CN} = 0.05$.

is set to be 0.5, each square is a width of 0.5 units. Thus, the refined location spacing is limited to a maximum value of 0.5. More than this and the spacings will be greater than that trialled in the discretised scoring described in Section 3.7.3. The number of horizontal locations trialled will depend on the resolution, the width of the particle and the domain size, as well as the value of refined location spacing.

3.7.5 Improved Computational Runtime

For the studies in this thesis, a resolution of 0.5 was adopted as this was found to be a good level between still describing the particle shape whilst reducing the runtime of the algorithm. A resolution of 0.5 describes each unit length of the particle being described by two squares in the discretised form. Therefore, some level of overall shape is still present rather than particles just being described by a simple rectangle.

Figure 3.35 presents runtimes for the algorithm (with some steps to reduce computational time not get added) for packing 30 soil particles into a domain of 50x50 units. The number of rotations trialled in the discretised step is seen to reduce run time as its own value is increased. Multiple differences between orientation are specified as MO and values for 5.625^o, 10^o and 11.25^o were tested. As the number of rotations is increased, the computational time decreases. This is due more orientations being trialled in the discretised method which is much faster and less accurate approach to scoring placement. This means less rotations are scored when positioning the particle described by coordinates and larger MO values means fewer orientations that are trialled.

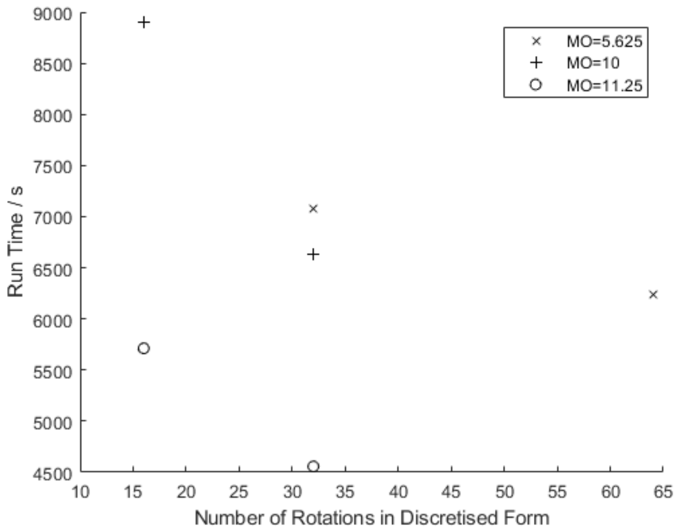

FIGURE 3.35: Run time for different rotations in the discretised form for the Soil Particle Scenario packing 30 particles at a discretisation resolution of 0.5 and defined location spacing of 0.1. Multiple values for defined angle of orientation are shown and reference to as MO in the legend.

The fastest speed is seen at the number of rotations equalling 64. This would describe a difference of 5.625^o between rotations in the discretised scoring approach, meaning that only one orientation is tested when trialling candidate poses. As stated, the discretised method is less accurate for scoring particles and therefore it is required to reduce the number of rotations applied to the discretised particle. As a result, the number of rotations applied is chosen to be 16 as this gives a good balance between utilising the more accurate scoring method whilst using the discretised system to speed up computational speeds. This allows for a defined angle of orientation of 5.625^o and a defined location spacing of 0.2 to be selected to precisely locate positions for particles.

The computational runtime for the Tetris Scenario remains unchanged as the new features described for the Soil Particle Scenario were not implemented into the code for packing tetrominoes. For a 10x10 square domain being packed until the next particle delivered to the algorithm cannot be placed the computational runtime was seen to be on average 3.7 seconds with roughly 30 particles being packed.

For the Soil Particle Scenario using

- 0.5 resolution for discretisation
- 16 rotations of the discretised particle
- 5.265^o for the defined rotation
- 0.2 units for the defined location spacing
- trialling 30 candidate poses for locating positioning

the total runtime to place 40 particles is found to be 2670 seconds. Taking the time for 30 trialling candidate poses and extending, testing of all 35,000 candidate poses for the example seen in Section 3.7.3 would take 36 days to complete. This highlights

Scenario	Particles packed	Total Runtime	Runtime per particle
Tetris	∼30	3.7s	∼0.12s
Soil Particle Scenario	40	2670s	67s

TABLE 3.4: Runtimes for the Tetris Scenario and Soil Particle Scenario with the introduction of techniques to increase computational speed for the Soil Particle Scenario. Time for Tetris Scenario taken from average of 100 runs, time for Soil Particle Scenario taken from average of 25 runs.

the importance of introducing the reduction of candidate poses trialled and the use of the hierarchical filter.

3.8 Computational Complexity

The computational complexity of the Soil Particle Scenario algorithm can be described to be affected by multiple input variables for the programme. Specifically, the input variables that affect computational runtime are given in the list below.

- The number of particles to be placed in the system
- The number of coordinates used to define the particle
- The width of the domain
- The number of rotations for which the particle is tested in the discretised system
- The resolution at which the discretised fitting is tested
- The angle of orientation at which the particle is rotated for positioning in the defined method
- The location spacing between tested positions of the particle in the defined method
- The number of candidate positions considered

All these variables change the computational runtime and it is expected that each increases the computational runtime linearly as the variable is increased. This is due to the brute force nature of the code with the number of operations being repeated depending on the variable. For example, if the number of particles placed in the system is increased then the code is repeated an equivalent number of times to the increase in the number of particles. If the number of coordinates used to define each particle is decreased, the number of times the operations for calculating how far the particle can be lowered in the system also decreases linearly to the decrease in coordinates. Equivalently for the Tetris Scenario, this is expected to also exhibit a linear relationship for the variables that relate to this stage of the algorithm. A reminder that the Tetris Scenario omits the discretised search seen in the Soil Particle Scenario algorithm. Therefore, the variables that apply for the Tetris Scenario are the number of particles placed, the number of coordinates used to define the particles, the width of the domain, the number of rotations of the particle and the location spacing between tested positions.

Attention should be brought to how the number of candidate positions considered affects computational runtime. It is true that this would follow a linear relationship as an increase in candidate positions tested leads to an equivalent number of operations having to be repeated in the algorithm. However, if no viable candidate position is found then more candidate positions are tested until a viable solution is found. It was determined in Section 3.7.3 that a suitable number of candidate positions to be trialled could be taken to be 30. However, in the worst case scenario, the whole list of candidate positions may need to be tested before a suitable positioning is found. In this case, it can be described that the algorithm is not being affected by the suggested number of candidate positions tested. Rather, this number is determined by the input variables of the resolutions and the number of orientations tested in the discretised system. Note that this is for the worst case scenario and for typical use of the code that the computational time should increase linearly with an increase in the number of candidate positions trialled.

The main limitation of the algorithm is the large computational times to determine where a particle should be placed. This is due to the brute force nature of the algorithm, testing each position (or the number of candidate positions suggested for testing) and choosing the best option. Methods for increasing the computational speeds are suggested in Section 8.7. Additionally, the use of a high-performance computer compared to the hardware used in this study (see Table 3.2) would mean faster runtimes can be achieved.

3.9 Stability Checks

3.9.1 Introduction

Placements of individual particles in a precision structure relies on the particle staying in that position once placed. Therefore, a stability check was introduced to try and ensure this. The Tetris Scenario did not require a stability check as tetrominoes do not experience normal gravitational rules and there was no intention to test these shapes experimentally. Rather these shapes were for initial validation of the code. The stability checks introduced checks for sliding and for toppling of the particle by rotation as described in Section 3.9.2 and Section 3.9.3 respectively. Section 3.9.4 describes how particles that are close to being unstable are detected and also omitted as a solution for position.

3.9.2 Sliding

A sliding check was first introduced for this algorithm in Hoodless and Smith (2023). In this work, sliding was assumed to occur above an angle of 31^o as an estimate for the supposed material according to Buffington et al. (1992). However, a more sophisticated approach is required as sliding will depend not only on the friction between particles but also the weight of the particle being placed. A mechanics analysis of an object on a slope can be used to find the force due to weight in the direction of the slope and the frictional force acting in the opposite direction. Figure 3.36 shows this with the forces acting on the object. If the weight of the object, W, is

$$W = mg \tag{3.10}$$

where m is the mass of the object and g is the gravitational acceleration experienced by the object, then the forces due to weight in the direction of the slope and perpendicular to the slope can be known to be equal to $W\sin\theta$ and $W\cos\theta$ respectively.

$W\sin\theta$ is the magnitude of the force acting in the direction the particle will slide if unstable and can be described as F

$$F = mgsin\theta \tag{3.11}$$

where θ describes the angle of the slope. Frictional force, F_r on the object can then be described to be

$$F_r = \mu Wsin\theta \tag{3.12}$$

where μ is the coefficient of friction for the interface between the object and the slope.

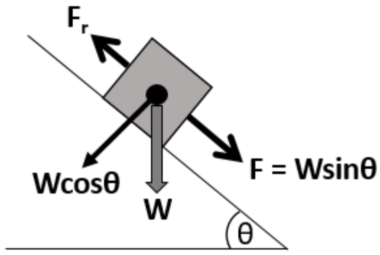

FIGURE 3.36: Mechanical analysis of a box on a slope and the forces that the box experiences.

If F>F_r, then the force acting on the particle is deemed enough to create a sliding failure. An example of sliding failure between two particles is presented in Figure 3.37a. The gradient of the slope means that the value of F is greater than the friction between the two particles and the particle slides down the system. Figure 3.37b presents a case where the particle would be stable. It can be understood that the value of θ is much less than the previous example and therefore the value for F will significantly decrease. In this scenario, F_r>F and the particle is stable in its position.

Locations for contacts for determining θ were taken from the method for detecting contact in Section 3.5.4 where a contact distance error, ϵ was introduced. Contact locations were split into two - left and right of the centre of the particle - and ranked by how close they were to the centroid. The closest to the centroid but greater than a distance of 2ϵ away were taken as coordinates for determining the slope of the angle. This was then taken forward for the sliding check in the stability calculations.

The coefficient of friction for the system depends on the friction between the two interfaces. This was difficult to determine without performing laboratory tests on trial materials. Instead, a study of the literature was conducted for modelling of particles. Table 3.5 shows the values that are used in various projects where DEM has been used to model particle interaction. These vary from 0.35 to 0.5 for particle-to-particle interaction. Note, the citations that have used 0.35 as a value come from journals that are concerned with powder mechanics looking at the behaviour of agglomerates, whereas the others come from areas of research to do with soils and geotechnics. Hence, a coefficient of friction of 0.5 has been adopted in this study. For laboratory tests to verify the algorithm described in Chapter 7, coefficient of friction between particles will need to be determined before collecting results of the algorithm to ensure particles are placed in stable positions.

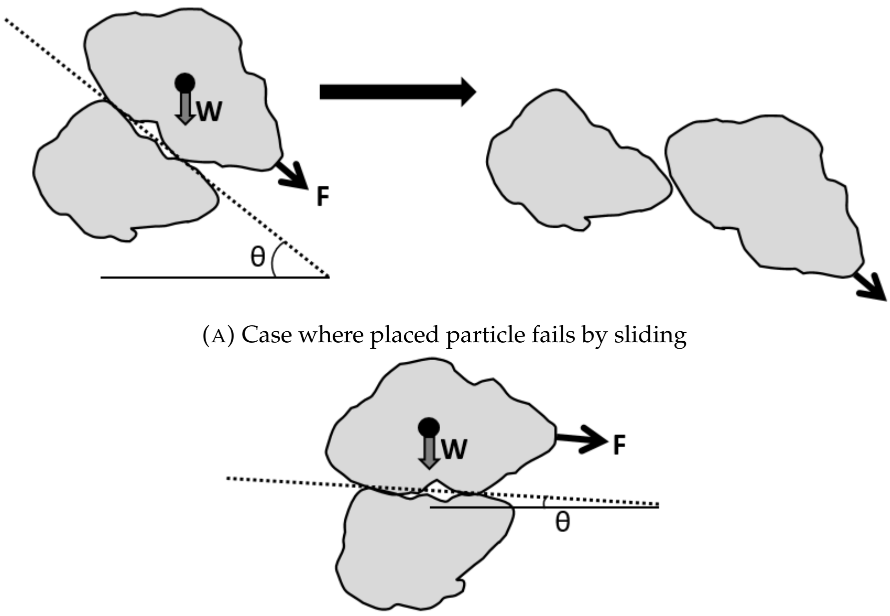

(A) Case where placed particle fails by sliding

(B) Case where particle is in a stable final position and does not fail by sliding

FIGURE 3.37: Examples of sliding checks for a particle placed on top of another.

In Johns et al. (2020) and Johns et al. (2023), gneiss boulders were used for construction of the walls. Assuming a similar material is used in this study, a particle density of 2900kg/m^3 can be taken. This value is derived from those reported in literature (Dorren and Seijmonsbergen, 2003; Oldenburg et al., 2017; Smithson, 1971; Subrahmanyam and Verma, 1981; Tenzer et al., 2011). As the present study is conducted in two-dimensions, it is required to convert this density to a two-dimensional value to ensure forces of weight of the particle are correctly estimated in the programme. As there are no particles of known weight, the stones used in Johns et al. (2020) are taken to help with this study. The mass of the stones used in Johns et al. (2020) are described have an average mass of 757 kg between a range of 230-1584kg. From this information, a 2D conversion factor can be calculated from

$$c_f = \frac{757}{\rho A_m} \tag{3.13}$$

where c_f is the conversion factor, 757 represents the average weight from Johns et al. (2020), ρ is the particle density (taken as 2900kg/m^3 to represent gneiss stones), and A_m is the median area of the 100 particle shapes generated using methods described in Section 3.6.1. A value of c_f=0.0113m was determined given the variables presented. In the algorithm, the weight of each particle is then determined by

$$W_p = c_f \rho g A_p \tag{3.14}$$

where W_p is the weight of particle and A_p is the area of that particle.

Reference	μ	Simulation	Dimensions
Cundall and Strack (1979)	0.45 for disc-to- disc 0.17 for disc-to-wall	Circular discs	2D
Thornton et al. (1996)	0.35	Circular discs	2D
Cheng et al. (2003)	0.5	Spheres	3D
McDowell and Harireche (2002)	0.5	Spheres	3D
Mishra and Thornton (2001)	0.35	Spheres	3D
Yan and Dong (2011)	0.5 for Spheres 0 for Wall Boundaries	Spheres	3D

TABLE 3.5: Values of μ in DEM from various sources in the literature.

3.9.3 Toppling

A stability check within this algorithm for toppling of the particle was also first introduced in Hoodless and Smith (2023). Again, contact points of the particle with the placement surface were split into two categories of being positioned to the left of the centroid or to the right of the centroid. If all contacts were in one of these categories with no contact points in the other, then this could be taken as an unstable position and described to fail by toppling. An example of a toppling is presented in Figure 3.38a. The contact points both lie to the right of the centroid. If there was a contact point to the left of the centroid, as seen in Figure 3.38b, then the particle would be unable to topple and would be stable in this position.

3.9.4 Avoiding Close-to-Unstable Positions

Figure 3.39 presents a particle positioned on a flat surface. The centroid of the particle is indicated by the circle inside of the object's outline and the position of this in the horizontal axis is indicated by a dashed line. For this object at this position and orientation, the placement would be deemed stable according to the stability checks described in Sections 3.9.2 and 3.9.3. However, it is clear that the particle could very easily fail by toppling if a slight force is placed upon the particle. Indeed, the accuracy of placement by a robot or human may not even be able to balance the particle in this position. This positioning of the particle can be deemed as "close-to-unstable". In order to avoid scenarios like the one presented in Figure 3.39, two more criteria when conducting the stability check for toppling are introduced.

The first of these criteria is to ensure that the contact points are distanced away from the centroid of the particle. A lower bound limit of 5% of the maximum particle width for distance away from the centroid was set for contact points to be suitable. 5% of the particle width gave a good improvement when looking at final positions of particles in the system. The value was taken as a percentage of particle width as this ensured that smaller particles would not face an issue of not having a suitable location due to their width being less than any fixed value set. The second criteria was to ensure that the distance between the left and right contact for the particle between the surface was at least 20% of the maximum particle width. Again, this was to try and avoid positions like that seen in Figure 3.39 and to prevent top-heavy orientations being placed. Additionally, the ordering of decreasing H/L as a placement filter described in Section 3.7.3 also acted as additional measure for avoiding these close-to-unstable positions.

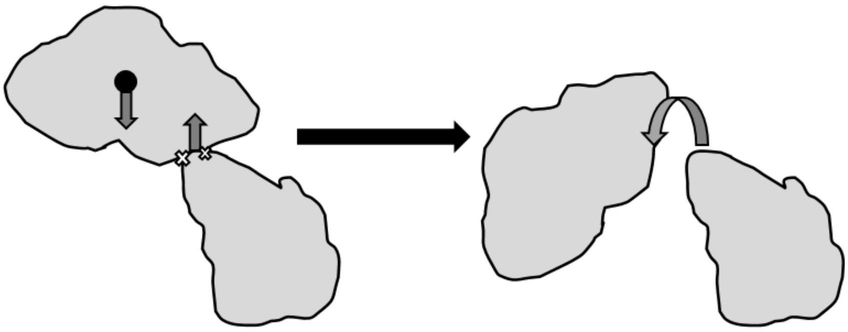

(A) Case where particle fails by toppling

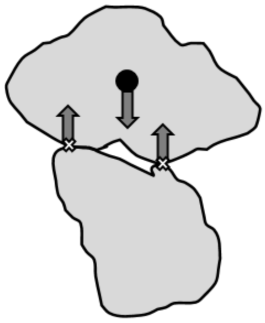

(B) Case where particle is placed in a stable position and does not fail by toppling

FIGURE 3.38: Examples of toppling checks for a particle placed on top of another

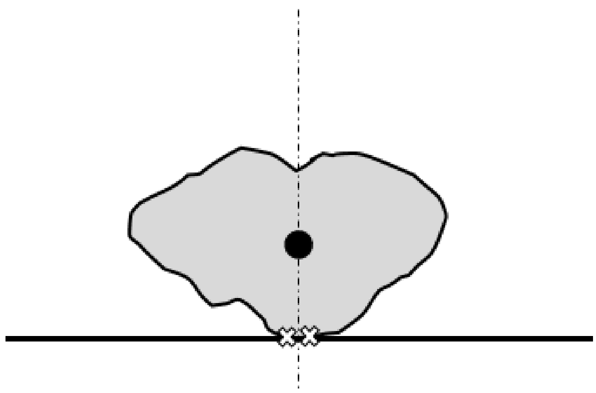

FIGURE 3.39: Example of particle that passes toppling stability check but be an unstable or close-to-unstable particle positioning

3.9.5 Results of Stability Checks

If a candidate pose passes all stability checks it is deemed as a suitable final position and is scored using the objective function. If one of the stability checks is failed, the position is classed as not suitable. As described in Section 3.7.3, only the first 30 candidate positions in the filtered ordering list are trialled to increase the computational speed of the programme. Although unlikely, it is possible that all candidate positions fail the stability checks outlined. In this case, the programme will continue to test candidate poses from the ordered list of positions until a position and orientation which passes the stability checks is found. If all positions for all orientations are failed, then the particle is discarded and the next particle is trialled. Due to the high number of candidate poses, this could output very large computational times. However, a suitable position is usually determined with the first 30 candidate positions trialled. For future work it may be necessary to discard the particle after a certain number of positions are tested rather than testing all possibilities as the particle being analysed may be unsuitable. This is discussed in Section 8.4.2.

3.10 Quantifying Results

3.10.1 Tetris Scenario

As stated in Section 3.2.2 the aim of the videogame Tetris is to fill rows of domain whilst the player receives a score when each row consists of only blocks of the tetromino shapes. Therefore, it can be stated that the aim of the game is to produce the least amount of voids in the system as possible. Due to rows not being deleted in the system when complete in this study, the void ratio of the final structure is suitable for judging the packing ability of the algorithm with a specified combination of weighting coefficients.

Void ratios for each simulation of packing are recorded for the Tetris Scenario. Results are produced for different combinations of weighting coefficient. The mean of these values is taken for a given sample size, the number of which is discussed in Chapter 4, for comparison between other coefficient combinations. Void ratio is determined as the ratio of the area of voids located beneath the placement surface to the area of placed tetrominoes in the domain.

3.10.2 Soil Particle Scenario

For the Soil Particle Scenario, the objective function is designed to achieve structures which exhibit high shear strengths. Section 2.3.7 provides evidence that low void ratio in a soil structure can indicate higher shear strengths. However it is stated that void ratio alone is not suitable. Additionally, as void ratio is a variable in the objective function to then use this as a final measure of shear strength may lead to the oversizing of C_V. Instead a new measure needs to be adopted to help quantify shear strength when comparing combinations of weighting coefficients.

A way in which shear strength may be quantified could perhaps be derived from a suggestion for the construction of drystone walls in Vivian (1976). As stated in Section 2.2.1, Vivian (1976) recommends to place stones above where two in-situ stones meet to reduce the number of runs in the system. Not only will this help prevent rotations of particles in the system but it can be understood that it will naturally result in higher coordination numbers. Coordination number tends to lead to higher shear strength as shown in Section 2.3.4 as forces are more readily transferred meaning better distribution in the soil system (Fonseca et al., 2016; Muir Wood, 2008) whilst particles with low coordination numbers can be unstable and not contribute to the overall strength (Oda, 1977). Disrupting runs is not included within the objective function yet the inclusion of T and CN should encourage placements of particles as they lead to larger coordination numbers and areas of contact with already placed particles.

The formation of running joints are identified in the algorithm when two particles are placed next to each other. If the edges of the particles are within sufficient distance of each other, this is classed as a run. However, it is difficult to determine what is "sufficient distance". There is a balance required between a particle creating runs with other particles when it is clear that another particle may be placed between them and runs not being detected when particles are placed. Particles between 3 and 7.5 units were selected for placement as discussed in Section 3.6.1. Therefore, a maximum gap of 3 units was adopted for a gap to be considered a run. Any larger than this, and a particle would not be able to be placed above it and rather could be placed inbetween, creating two potential runs with the surrounding particles. At the same time, the original run could be classed as disrupted when really it should not have existed to begin with. If the number of disrupted runs is adopted as a method to quantify the fit of the structure, it is important to not gain false readings such as what would occur in this scenario. From visual inspection of the results, this maximum gap value located runs which could be filled by particles either by their narrower side or just part of the particle. Therefore the maximum gap was reduced to 2 units as this gave more reliable identifications of runs.

An example of a particle being placed in the domain is presented in Figure 3.40. The start of running joints are indicated as circles on Figure 3.40 and the horizontal position is indicated by a dashed line. As can be seen, the particle interrupts two runs between already placed particles in the system. The run which lies at the middle of the particle is clearly underneath the to-be-placed particle and can be classed as disrupted. The run that lies to the left of the particle is only disrupted by a fraction of the particle's area and is very close to the left-most border. The particle here would not provide much resistance against this running joint progressing up through the structure. Therefore, it is required to include a condition to ensure enough of the particle lies above the run for it to be classed as disrupted. Therefore the condition

$$0.75 > \frac{x_{pl} - x_r}{x_{pl} - x_{pr}} > 0.25 \tag{3.15}$$

is introduced where x_r is the abscissa of the run and x_{pl} and x_{pr} are the left-most and right-most abscissa of the particle being placed in the domain. This condition follows from the need for a "significant amount" of overlap from placed particles on below runs as stated in Adcock (2012). From this condition, it is required that 25% of the particle's width must lie over the run to count as disrupted. This is an estimate of what a "significant amount" of overlap would be as no value was stated by Adcock (2012). If the particle overlaps the run outside of the condition in equation 3.15 then the run is considered to be continued up to the nearest side of the particle to the run. This is shown in Figure 3.40 as the running joint is relocated to be to the left side of the recently placed particle.

In the algorithm, when particles are placed, runs will either be recorded between in-situ particles in the course as the middle distance between the two, discarded if the to-be-placed particle disrupts the run or shifted to be to the side of the placed particle it is closest to if Equation 3.15 is not satisfied. Similar to the location of particles described in Section 3.5.5, locations of runs are stored in relation to where they are located in the domain and loaded when the particle placement is in that section.

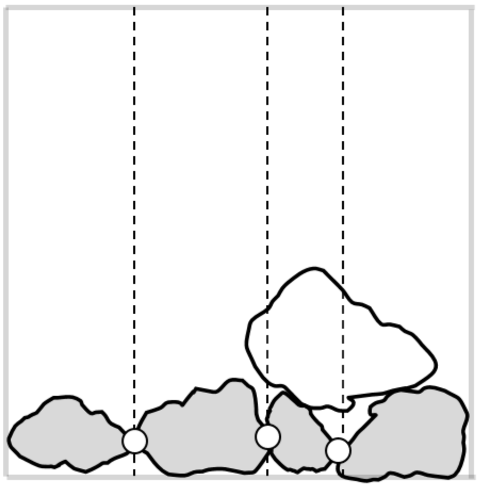

(A)

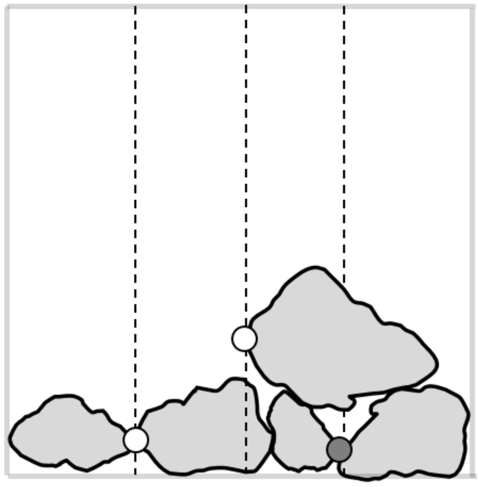

(B)

FIGURE 3.40: Placement of particle in a domain with the locations of running joints between particles indicated as circles with unfilled and filled circles representing undistrubed and disrupted running joints respectively and dashed line representing horizontal location of running joints. The domain is displayed (a) before the particle is placed (represented by unfilled particle) and (b) after the particle is placed.

3.11 Effects of Domain and Particle Size

As the algorithm is essentially solving a bin packing problem that is based on geometry rather than any physical calculations, it is thought that minimal edge effects will arise in the programme. This might be the case if the domain that particles are packed into has a big effect on any of the weighting criteria. For example, if a domain made up of many coordinates is allowed to contribute to T then this will lead to particles tending to be packed next to the edge of the domain if a non-zero value for C_T is chosen. As a result, the way in which criteria are measured is set to not be greatly affected by the domain. V_{AB} is based on space underneath the placement surface and is therefore not affected by the domain as the shape of the domain does not change from its original definition. Again, D is based on the depth of the particle in the domain and is therefore not affected by the domain as the shape of the domain does not change. T is calculated without consideration of the edges of the domain by only considering the placement surface and rather is affected by how the particle is defined. CN allows for the domain to be classed as a coordination for the placed particle but only up to a maximum value of 1.

Touching of the sides of the domain also allows for contact points of the particle to be detected for the stability check. This can be removed to simulate packing of an area that is not a box where contact with edges cannot be found if required. For these simulations, detection of contact points with the sides of the domain remains to allow for more stable positions for particles.

The size of the domain is explored for the Tetris Scenario in Section 4.3.4 where it is shown that increasing the domain size from 10x10 squares to 20x20 squares has little effect to the method of packing by the algorithm. A similar study is not completed for the Soil Particle Scenario due to computational times required to do this, but it is thought that the size of the domain is suitably large to avoid any finite-size effects. From visual inspection of the results in Chapter 6 it is concluded that these did not occur. It is thought that the given reasons above will help avoid these sorts of problems from occuring.

It is possible that if the size of the particle is large or irregular, this may mean increased amounts of void occurring at the edges of the domain where particles cannot fit properly. Therefore, this will lead to other placements being prioritised if C_V is a non-zero value and it will be unlikely that these placements are chosen. In this case, the algorithm is being affected as it may lead to suitable placements near the edges of the domain not being detected due to the size of the particle being too large for the given domain size.

If the particle can fit within the domain at a suitable location, the size of the particles should also have no effect on the packing algorithm. This is due to the algorithm being based on geometrical calculations rather than any physical parameter. If these particles are made up of more coordinates, then this will mean that a longer computational time will be required to find a suitable particle placement. However as V_{AB}, D and T are calculated using ratios, placement is determined by a method that allows for any size particle to be placed so long as it fits within the domain. CN is calculated as the number of surrounding particles to the placed particle. Therefore, if a bigger particle is placed then a larger CN value is possible due to this increased size. However as shown in Section 2.2.2 and Section 2.3.4, a larger coordination number assists in the transfer of forces in a system and is a desired feature in the system if the function of the packing is to have a high shear strength. CN also depends on the number of other particles that are already packed in the system.

In future scenarios it may occur that unusual and very irregular shapes may want to be adopted for a study using the algorithm. For example, particles which have gaps in the middle of the particle as can be seen in Figure 3.41. As the algorithm packs in two-dimensions using a top-down approach this means that there should not be a problem so long as the particle is correctly defined by a top line and bottom line. In effect, the hollow middle of particle can be ignored. However, a new characteristic for the particle would need to be developed indicating how much of the particle is made of void for calculating the final void ratio of the system if these hollow sections are to be taken into account.

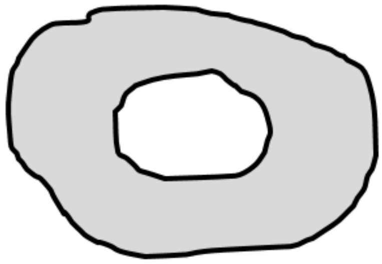

FIGURE 3.41: Example of irregular particle shape with hole in centre.

3.12 Summary of Algorithm

3.12.1 Algorithm Description

The algorithm set out in Sections 3.3-3.10 is finalised and a summary is given here. Set up of the algorithm is completed using tetrominoes and outlines that represent irregular, untooled rock. However it is envisioned that any two-dimensional shape can be packed so long as the outline is described by a closed-loop of coordinates in clockwise order of the abscissa and ordinate. The algorithm is written in Asymptote to take advantage of the coordinate-based language and produce high quality images for presenting the results.

For the Soil Particle Scenario, particles that represent irregular, untooled rock are generated by the Fourier-Voronoi method which is described in Section 2.5.3 using the MATLAB code sourced from Mollon (2023). The code outputs these shapes as coordinates of the outline. Investigation into the shapes that are produced can be found in Section 3.6.1. The Fourier Descriptors and Target Solid Fraction adopted are D_2=0.2, D_3=0.2, D_8=0.015, and TSF=0.7. Particle diameters of 3 to 7.5 units were selected which led to 168 possible particles for placement. Out of these, the first 100 were chosen for packing by the algorithm. Tetrominoes were specified as a set of coordinates manually for each of the seven different shapes.

Figure 3.42 is a workflow chart of the algorithm showing the order in which each step is conducted. Input parameters are presented in Table 3.6 with either the value used in this study for the Soil Particle Scenario or an example value if the parameter is not fixed. Placements are scored using the objective function, which is repeated here in Equation 3.16 and is based on void created in the system by the placement, depth of placement, touching area of the particle with other particles and the domain boundary, as well as coordination number. V_{AB} is adopted for scoring the void created in the system.

$$W_{ij} = C_V V_{AB} + C_D D + C_T T + C_{CN} CN \tag{3.16}$$

Placements are scored twice, once as a discretised particle as a quick scan for candidate positions. These are ranked and the top 30 candidate positions are taken for testing. If these finalised placements are unsuitable, further candidate positions are taken until a suitable solution is found. Then further placements are scored with a refined location spacing between laterial positions and further orientations of the particle outline tested. The best scoring position is taken as the solution for placement of that particle, and the next particle is tested. The programme ends when the specified number of particles are placed or no viable solution is identified.

Parameter	Value	Fixed or varied	Section
Domain height	50	Varied	3.6.2
Domain width	50	Varied	3.6.2
Number of particles to be placed	50	Varied	3.6.4
Number of particles available	100	Fixed	3.6.4
Initial number of orientations of particle	16	Varied	3.6.3
Minimum domain coordinates	(0,0)	Fixed	3.3.3
Particle permutations	1	Fixed	8.4.1
Defined location spacing	0.2	Varied	3.7.4
Defined angle of orientation	5.625^o	Varied	3.7.4
Expanding factor	5%	Fixed	3.5.5
Contact Distance Error, ϵ	0.1	Fixed	3.5.4
Grid size	1	Fixed	3.5.5
Stability Check Activated	"Yes"	Fixed	3.9
Coefficient of friction	0.5	Fixed	3.9.2
Particle density	2900kgm^3	Fixed	3.9.2
c_f	0.0113m	Fixed	3.9.2
Gravitational acceleration	9.81 ms^{-2}	Fixed	3.9.2
Height to width ratio	0.5	Fixed	3.7.3
Percentage from touch	5%	Varied	3.9.4
Resolution for discretisation	0.5	Varied	3.7.3
Size of border in the discretised domain	2	Fixed	3.7.3
Number of candidate positions tested	40	Varied	3.7.3
C_V	1	Fixed	3.5.2
C_D	1	Varied	3.5.3
C_T	1	Varied	3.5.4
C_{CN}	1	Varied	3.5.5

TABLE 3.6: Table of input parameters for the algorithm with a suggested value, whether this was fixed or varied during testing for the Soil Particle Scenario and the section of the thesis where this parameter is discussed.

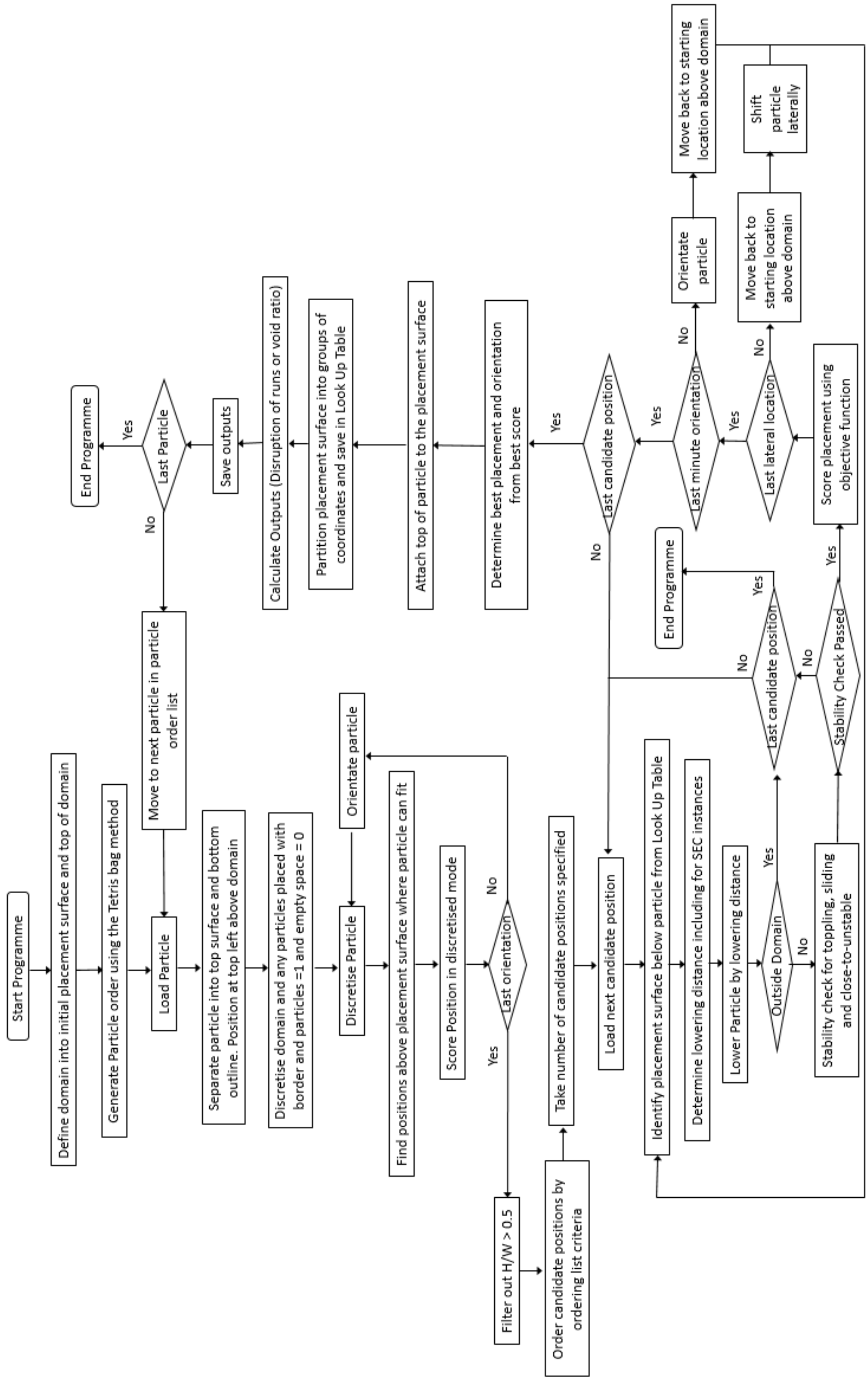

FIGURE 3.42: Workflow chart for the algorithm packing two-dimensional shapes using the methods described in Chapter 3.

3.12.2 Comparison to Previous Work

Method of Previous Work

Hoodless and Smith (2023) previously investigated the Tetris Scenario to determine the optimal combination of weighting coefficients for packing tetrominoes. Values of weighting coefficients were activated individually and tested by trial and error. Tetrominoes were packed into a 10x10 square domain until the next tetromino cannot be placed. 100 simulations were completed for each coefficient combination.

Coefficients were activated individually by being set to a value of 1 starting with C_V. Next, C_D was activated. This value was then raised and lowered to see the effect of outputted void ratios. Values of C_V were not fixed to 1 like they are in this study. Therefore C_V was increased rather than adopting smaller values of C_D, C_T, and C_{CN}. The method for determining coefficients of weighting is further explored in Section 4.6.

Differences

Results from Hoodless and Smith (2023) were found using a version of the algorithm which worked in a same manner to the one described in Chapter 3, however with a less-defined manner for determining the stability of particles. Methods described in Sections 3.3.1-3.5.1 are equivalent to that described in Hoodless and Smith (2023).

As stated, the way in which stability of particles is determined in Hoodless and Smith (2023) is less developed method as to that described in Section 3.9. In Hoodless and Smith (2023), a sliding angle is given and any contacts between particles that exceeds this angle is deemed unstable. This differs from that in Section 3.9.2 which uses a mechanics analysis to determine the force on the particle due to gravity and the frictional force between particles. This is relevant for the investigation into soil particles and does not have an effect on the results for Tetris particles as stability checks were not performed for these objects.

3.12.3 Examples of Packing Outputs

Results for both the Tetris Scenario and Soil Particle Scenario are presented here to give examples of what is achieved by the algorithm for both cases. The coefficients selected are those that are determined using the methods described in Chapter 4. Full exploration on how these results were achieved are described in Chapter 5 and Chapter 6 for the Tetris Scenario and the Soil Particle Scenario respectively.

Tetris Scenario

Figure 3.43 presents two examples of packing for the Tetris Scenario using coefficients C_V=1, C_D=1.6, C_T=0.4 and C_{CN}=0.045. This is found in Chapter 5 to be the optimal coefficient combination for the Tetris Scenario. The packings for the two results create minimal void. Locations where void occurs are in positions where the next particle in the sequence could not be placed without creating void. For example, Particle 0 in Figure 3.43b would create void beneath it no matter the location or rotation of the particle. As stated, further discussion of the results from the Tetris Scenario are presented later in this thesis.

Similar to bin packing, the Tetris Scenario represents a case where items are being packed into a domain with the aim to minimise void space. Potential arises for the

Tetris Scenario to be adopted as a method for solving the bin packing problem. This topic is further explored in Section 8.9.1.

Soil Particle Scenario

Figure 3.43 presents two examples of packing for the Tetris Scenario using coefficients C_V=1, C_D=6, C_T=0.5 and C_{CN}=10. Note that this combination of coefficients is not deemed to be the optimal solution in Chapter 6. Again, further discussion of the results from the Soil Particle Scenario are presented later in this thesis.

As with the results for the Tetris Scenario presented in Figure 3.43, the results for the Soil Particle Scenario in Figure 3.44 also present a scenario where items are being packed into a domain. The purpose for this could be to minimise void ratio, however in this case the objective function is to try and maximise the strength of the structure. However, it could be considered that the algorithm could be used as a bin packing solution for irregular shapes with some fine tuning. Furthermore, the outputted results represent the packing of soil particles. Hence, it should be highlighted that this approach has potential to be adopted for specimen generation of soil particles. This topic is discussed in Section 8.9.2 with reference to DEM modelling research.

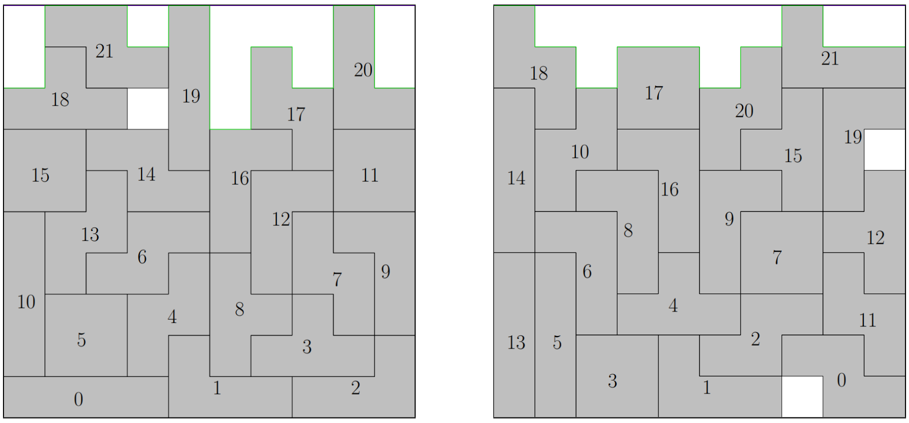

(A) e=0.011 (B) e=0.023

FIGURE 3.43: Packings for the Tetris Scenario using coefficients C_V=1, C_D=1.6, C_T=0.4 and C_{CN}=0.045.

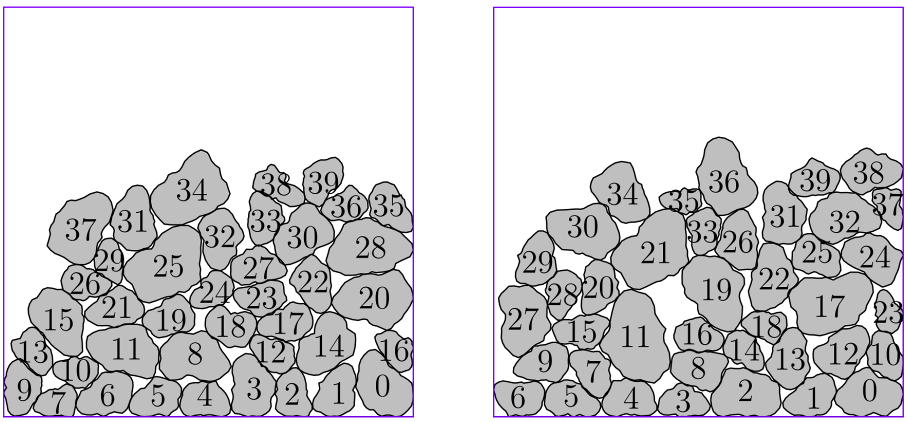

(A) Running joints disrupted=25, e=0.017 (B) Running joints disrupted=26, e=0.020

FIGURE 3.44: Packings in the Soil Particle Scenario for coefficients C_V=1, C_D=6, C_T=0.5, C_{CN}=10.

3.13 Summary of Chapter

The development of a method for packing tetrominoes and in turn outlines of particles that represent untooled, irregular rock is described in Chapter 3. This placement algorithm is to be adopted and results are presented in Chapter 5 and Chapter 6 for the Tetris Scenario and Soil Particle Scenario respectively. Desired aims for the algorithm are described in Section 3.1.2 with an emphasis put on adaptability of the program. For example, it is desired that any type of 2D particle could be packed whilst allowing for the objective function to be changed to allow for other criteria for scoring as specified by the user. The language that the program is developed in is Asymptote, an open-source vectors graphics language adapted from C++ and Java. Asymptote and the benefits of its use are briefly described in Section 3.2.1. Following this, the two packing scenarios are described in Section 3.2.2 and Section 3.2.3. These are the Tetris Scenario (packing of tetrominoes to emulate the Tetris video game) and the Soil Particle Scenario (the packing of 2D outlines that represent irregular, untooled rock).

Section 3.3 describes initial steps that are performed before the placement of particles is completed. Defining particles using a system of coordinates describing the abscissa and ordinates is described in Section 3.3.1. The algorithm allows for both convex and concave particles to be described so long as the particle is a closed loop and that first and last coordinates identical whilst being described in a clockwise order. Section 3.3.2 describes the splitting of the particle into the bottom line and top line in order to increase computational speed when performing the placement process. Setting up of the domain, again by a description of coordinates in the abscissa and ordinates, is described in Section 3.3.3 whilst the requirement of positioning particles above the domain to the top-left before placement is performed is described in Section 3.3.4. In the final part of Section 3.3, determining the order of placement for the particles is described in Section 3.3.5. This adopted the "pull-from-bag" method that is found in the Tetris videogame.

Section 3.4.1 focuses on the placement method adopted by the algorithm. A top-down method is adopted as specified by the conceptual design in Section **??**. This consists of calculating the maximum distance a particle can be lowered without overlapping existing particles or the boundaries of the domain. This utilises the bottom line of the particle as well as the placement surface below the particle. As a result, larger number of coordinates to describe the particle results in larger computational times as shown in Figure 3.9. With the placement of tetrominoes, Straight Edge Corner (SEC) problems occur where overlapping of particles takes place. Section 3.4.2 investigates these and two solutions are found.

The placement method finds multiple locations for the particle to be situated. Therefore a method to score each option is required leading to the production of the objective function in Section 3.5.1. Equation 3.1 describes the objective function and this is based upon the four criteria of void ratio, potential energy, coordination number, and area of contact as derived from the literature review in Section 2.3. Each of these is assigned a weighting coefficient parameter that is required to be found. As each additional parameter will require derivation, it is important to try and keep the number of parameters to a minimum. Therefore the equation is kept to be a first-order equation whilst only four criteria are specified for scoring. The four criteria are explored in Sections 3.5.2-3.5.5. Each criteria is non-dimensional so that the scoring method could be used for any type of particle described by a set of coordinates in a closed loop.

As discussed in Section 3.5.2, Traditional methods for calculating void ratio using the area of void in the system compared to the area of solids leads to the scoring of V to have less of an impact as more particles are placed. Therefore, a new method for scoring the void in the system is adopted that utilises A_{VP} and A_P. This ensures that the effect of V does not diminish as the quantity of particles increases. Section 3.5.3 shows that the inclusion of a depth parameter is beneficial to the packing of tetrominoes for reducing final void ratio and that this can be normalised by the total height of the domain. The method for scoring T is described in Section 3.5.4. This is done by quantifying the area in contact with other particles and domain by totalling the number of coordinates in the bottom line that are in contact with already placed particles as well as the domain boundaries. This is normalised by the total number of coordinates that make up the bottom line. It should be noted that as T indicates the area of the particle in contact with other objects that this can also be taken as a secondary sign for void created below the particle, although without any consideration of the area of void created. Furthermore, coordination number and how this is quantified is discussed in Section 3.5.5. This is completed by increasing the area of the particle in-situ and finding intersection points with surrounding particles. Coordination number is already a non-dimensionalised criteria. Due to this, CN is expected to be a much larger value that V, D, and T and therefore it is expected that C_{CN} will be a smaller value compared to the other weighting coefficients.

Section 3.6 begins to discuss the placement of irregular, untooled rock particles. The features previously described in Chapter 3 are sufficient to pack tetrominoes in the Tetris Scenario. However, it was discovered that additional features were required for the Soil Particle Scenario to improve the algorithm.

The procedure for generating particle outlines by the Fourier-Voronoi method using the MATLAB code provided by Mollon and Zhao (2013) is outlined in Section 3.6.1. It is desired that these particles are to represent untooled rock. From visual analysis, Fourier Descriptors of 0.2, 0.2, and 0.015 for D_2, D_3, and D_8 respectively were adopted. An improvement for this study would be to derive the Fourier Descriptors from actual untooled rock particles as discussed in Section 8.6.4. A TSF value of 0.7 was used within the code when generating the particles. From the produced particles, those with a radius limit between 3 and 7.5 units were selected for the packing process. This produced 168 particles. From this, the first 100 were taken as this was a sufficient amount of particles for packing within the domain, which was set to be 50x50 units as described in Section 3.6.2.

Differences between the Tetris Scenario and Soil Particle Scenario were highlighted in Section 3.6.3 and Section 3.6.4. The particle order will no longer require a Tetris-bag method as 100 particles is seen to be much larger than the required particles to fill the domain although this feature is kept for scenarios where this may not be the case. Additionally, Tetris only requires for particles to be rotated by 90^o with a defined spacing of 1 square in a domain of 10 square width. For the Soil Particle Scenario, numerous orientations and spacings between placement locations are possible. As a result of this, it was required to increase the computational speed which Section 3.7 explores. Decreasing the number of coordinates defining the particle and partitioning the placement surface into smaller sections of coordinates are both described in Section 3.7.1 and Section 3.7.2 respectively. It was shown that partitioning the placement surface into groups of 10 coordinates each was optimal for increasing computational speed.

An additional method for reducing the computational speed is to reduce the number of positions and orientations trialled for final placement in the algorithm. Section 3.7.3 investigates reducing the number of candidate positions similar to the work in Kong and Kimia (2001) (discussed in Section 2.4.3) whilst using a coarser description of the domain and particle which was highlighted as an approach used in Cagan et al. (1998) (discussed in Section 2.4.4). This was completed by discretising the domain and particles into binary matrices, the size of which is given by a specified resolution. In this discretised method, particles are scored using the criteria from the objective function with less accuracy than the non-discretised method. From this, poses are ordered using a filtering approach as seen in Johns et al. (2020) and Liu et al. (2021). The order in which the candidate poses are ordered are

1. Objective function score determined in the discretised system
2. Depth in the system
3. Left-most position
4. Area beneath the particle to width ratio
5. Width to height ratio, with particles at an orientation where the width to height ratio is less than 0.5 considered unsuitable for placement and being discarded

From this list, it was determined from Figure 3.34 that the optimal number of candidate positions to trial for placement using the method described in Section 3.4.1 is 30. This is where a decline in rate of increase for cumulative frequency can start to be seen whilst the effect on computational runtimes from the number of candidate positions taken forward is not as large.

Section 3.7.4 discusses the ability to trial more refined orientations and spacings between placement locations to improve the accuracy of results in the Tetris Scenario due to the increase in computational times of the program. In Section 3.7.5 it is described that a good balance between increased speed and number of orientations trialled using the more developed scoring method rather than doing this in the discretised system is needed. It is suggested that this comes by testing 16 orientations in the discretised system at a resolution of 0.5 whilst using a defined location spacing and defined angle of orientation of 0.2 units and 5.625^o respectively.

The introduction of removing particles with a width to height ratio less than 0.5 adds an aspect of stability when placing particles. However, it is required for stability of the final position to be tested to ensure that particles will not collapse immediately after placement. The stability checks that are performed when placing particles are described in Section 3.9. These include sliding (Section 3.9.2), toppling (Section 3.9.3) and the avoidance of particles that are deemed close-to-unstable (Section 3.9.4). A requirement of this was to define the coefficient of friction, μ, as well as the density of the untooled rock particles and a 2D conversion factor for converting the density of rock into a two-dimensional representation. Gneiss boulders were assumed to be the material as this is the printing material used in Johns et al. (2020). Therefore the density of the material is taken as 2900kg/m^3. From the average weight of the boulders used in Johns et al. (2020), a value of c_f=0.0113m was determined and hence the weight of the particles used for placement can be calculated following Equation 3.14.

The method for quantifying results is described in Section 3.10. The results of the Tetris Scenario can be quickly analysed using the void ratio of the system as stated in Section 3.10.1 as this is the main objective of the Tetris videogame. Due to rows not being deleted in the system when complete in this study, the void ratio of the final structure is suitable for judging the packing ability of the algorithm with a specified combination of weighting coefficients. As discussed in Section 3.10.2, the Soil Particle Scenario has an objective to maximise the shear strength of the structure. Is is difficult to quantify without testing of the structure either numerically or physically. Due to the large number of results that will be produced, it is required to have some sort of method to quantify the shear strength. As a measurable value the number of runs disrupted by particles being placed is adopted. This is derived from the suggestion by Vivian (1976) for the construction of drystone walls indicating that the presence of running joints leads to faults in the structure. Additionally, void ratio is taken as a secondary measure as this tends to indicate higher shear strengths as discussed in Section 2.3.7. The way in which the formation of runs are identified in the structure during placement as well as the disruption of running joints are described in Section 3.10.2.

In Section 3.12, the main aspects of the Soil Particle Scenario algorithm are summarised for the reader. This is done with the aid of Figure 3.42 which is workflow chart showing the order in which each step is conducted. Table 3.6 presents input parameters for the program with suggested values. Whether this value was varied or fixed is also indicated. Section 3.12.3 presents example outputs of the algorithm for the Tetris Scenario and the Soil Particle Scenario with suggestion that these approaches could be adopted as bin packing solutions and a specimen generation method. This is further discussed in Section 8.9.1 and Section 8.9.2 respectively.

Chapter 4

Determining Sample Size and Weighting Coefficients

4.1 Introduction

Along with producing results for packings of tetrominoes and soil particles, the problem arises of knowing how many simulations are required to accurately represent a true result of the method. Running a large number of simulations for a given scenario will lead to a more accurate representation of the range of results that can be achieved. However, computational time will be increased. Alternatively, decreasing the number of simulations will lead to faster runtimes at the expense of accuracy and too few simulations may give an incomplete understanding of any outputs. The aim of this chapter is to understand and reflect on initial data received by the placement method described in Chapter 3. Statistical analysis will be performed to determine the number of simulations suitable when trying to determine the optimal set of coefficients for the weighted objective function described in Section 3.5. Furthermore, it is desired that a methodology for determining the combination of weighting coefficients that provide optimal solutions for the Tetris Scenario and Soil Particle Scenario can be described. It is envisioned that these procedures can be followed to reliably find values of coefficients that result in values for scoring criteria which bring forward the most optimal packing structures relating to the overall objective for the structure.

To determine the effect of the number of tests on the confidence of results, two scenarios will be tested and are described in Section 4.2. Simulations will be completed based on the Deepest Bottom Left (DBL) heuristic as outlined by Wang and Hauser (2019). Later, the weighted objective function outline in Section 3.5 will be implemented and a broader understanding of the variability of results will be analysed using all objective function parameters.

Section 4.3 discuses how the sample size required to accurately represent the population data will be determined. This is completed by firstly discussing statistical rules around the subject before looking at the confidence interval and distributions of the results from the simulations outlined in Section 4.2. Additionally, an investigation into the effect of domain size used is completed in Section 4.3.4.

Section 4.4 discusses the methodology adopted when determining weighting coefficients. This is completed by taking a broad range of coefficients before analysing located areas where a minima may occur. Section 4.4.2 investigates the effect of using a fixed seed for generating particle order for each combination of weighting coefficient compared to randomly generating new particle orders for each simulation. In

Section 4.4.3, the mean filter and Gaussian filter are introduced for smoothing the datasets of mean void ratio generated by the algorithm in the Tetris Scenario. Section 4.4.4 and Section 4.4.5 investigate the effect of applying Gaussian filter on the search areas for determining the optimal solution as well as the effect on the values located at the edges of the dataset.

Carrying on from Section 4.3, Section 4.4.6 investigates the effect of sample size on the variation of results between different weighting coefficient combinations. The sampling frequency, otherwise known as the size of the increments between coefficient values, is also explored. Higher sample size and sample frequency are described to increase the accuracy of the obtained results at the expense of higher computational speeds.

A procedure for locating the optimal solution for the Tetris Scenario and Soil Particle Scenario is described in Section 4.5 providing information on initial investigations that should be considered before refining the search in areas of interest where optimal solutions may be located. A suitable starting range of coefficients to investigate are given with suggested sample size to be utilised. The procedure is followed in Chapter 5 and Chapter 6 where results of the Tetris Scenario and Soil Particle Scenario are presented respectively.

The conclusions from this study into determining the required sample size when investigating weighting coefficients are summarised in Section 4.7. The sample sizes that will be utilised when running simulations and analysing the results are stated as well as key points to take forward for the Tetris Scenario and Soil Particle Scenario results. Further studies for the Soil Particle Scenario are highlighted to be taken forward for the work conducted in Chapter 6.

4.2 Testing Scenarios

4.2.1 DBL

The DBL Scenario describes the packing of objects in the deepest-bottom-left heuristic. In this method, the deepest location in terms of height will be selected with the left-most location being selected if positions have equivalent height. The depth for a given placement is quantified by the depth of the centre of mass for that particle. The DBL heuristic was outlined by Wang and Hauser (2019) and discussed in Section 2.4.3.

4.2.2 Weighted Objective Function

Packing of tetrominoes using the weighted objective function described in Section 3.5 utilises the criteria set out for creating structures with a high shear strength. As the coefficients of weight are not yet determined, the method for determining is conducted on tetrominoes because of the quicker computational speeds before moving to shapes that represent untooled rock. The decreased runtime for tetrominoes is due to the minimal number of coordinates utilised to describe the outline. This scenario follows that set out in Section 3.2.2 for the standard Tetris scenario using 4 orientations of the particles with a location spacing of 1 square in a 10x10 square domain. However, variations on the domain size are used when conducting the investigations in the Section 4.3.

4.3 Determining Sample Size

4.3.1 Rules for Determining Sample Size

Determining the require sample size is a key part to any study, with the size selected being able to accurately represent the whole population of possible results. Sample size in this discussion is the number of simulations or runs of the algorithm to compare the results rather than the number of particles. In this case, the accuracy of the results is weighed against the cost of run time for the data collection. It is impossible to have a true understanding of population of data without performing a full "census" or, in other words, by performing a mass of tests to try and produce all forms of results possible. From central limit theorem, the mean of a sample of data will have a higher precision for estimating the mean of that actual population as the sample size increases.

A rule of thumb in statistics is that a sample size of 30 is seen as the minimum number to represent the whole of a population (Chang et al., 2006). Hogg et al. (2014) states that generally a sample size greater than 25-30 will give good approximations of the population data and if the distribution of data is symmetric, unimodal, and of the continuous type, then a sample size of 4 or 5 can yield an adequate approximation. However, the variability of the results produced by the algorithm in Chapter 3 is very great and can depend entirely due to the number of variables being investigated or the sequence that particles are presented.

4.3.2 Confidence Interval

Confidence Interval (CI) was introduced by Neyman (1937) and is the probability (P) that a result will fall between a set of values for a certain percentage chance. Benefits of confidence intervals are described in Hazra (2017) to be that it is more dependable than forming conclusions based on the P value and an indication of the precision of the observation is acquired. The narrower the CI of a sample statistic, the more reliable is the estimation of the underlying population parameters. Confidence Interval can be calculated using the formula

$$CI = z * \frac{\sigma_p}{\sqrt{n}} \tag{4.1}$$

where CI is confidence interval, z is the confidence level, σ_p is standard deviation of the population (or if this is unknown, the standard deviation of the sample distribution), and n is the sample size . A confidence interval of 95% is the most commonly used in the field of science (Hazra, 2017). This is traditionally described to be two standard deviations above and below the mean value in a population that can be represented by a normal distribution. A confidence level for a CI of 95% is determined to be 1.96 for a normal distribution, as determined in confidence level tables which were first produced by Kramp (1799).

The confidence interval for tests using the Deepest-Bottom-Left heuristic, as outlined in Section 4.2.1, for the Tetris scenario is plotted for different sample sizes in Figure 4.1 using Equation 4.1. The population size consisted of results from 1000 runs of different permutations of tetrominoes from the Tetris bag. Void ratio of the system created using the Deepest-Bottom-Left heuristic is taken as the final output to analyse the packing structure. The mean and standard deviation of the population was 0.1036 and 0.0350 respectively. A z value of 1.96 was taken to represent a confidence level of 95%. The distribution of this data is presented in Figure 4.2. It can be understood from Equation 4.1 that, although values of CI may differ in magnitude, the shape of the plot will not change if z and σ_p are of different values. The exponential curve on the plot shows that there are diminishing returns with increasing the sample size, whereas an increase leads to a large reduction of CI to begin with. Past the inflection point at n=15 the decreases in CI is at a much slower rate. From the plot in Figure 4.1 it can be determined that past a sample size of 50 there will be no beneficial gain from an increase in sampling when considering the increase in computational time that this will lead to. It is clear that a sample size of 30 adheres to the rule of thumb number of samples taken. Past sample size n=9, the gradient for reduction in CI is a lot less steep. Therefore, if quick and less accurate results are desired, it may be good to use a sample size of 9 for this. For example, if a general idea of the effects of the parameters are desired, it may be best to use a value of n=9 before refining this in areas of interest with a larger sample size of n=30.

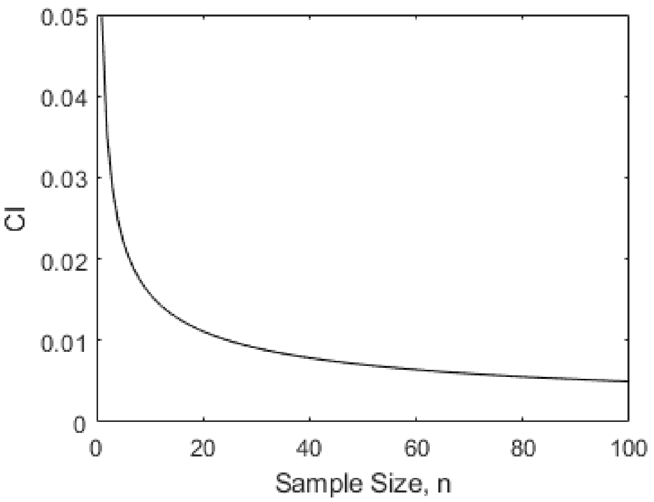

FIGURE 4.1: Confidence Interval for Tetris scenario using Deepest-Bottom-Left heuristic.

4.3.3 Distribution Shape and Sample Distribution

To determine the required sample size, a population of data was necessary to compare these results to. Placement of particles with randomised particle selection using the Tetris bag method (described in Section 3.3.5) were ran to simulate 1000 tests to ensure a full range of possible results greatly exceeding the suggested value of n=30 from Section 4.3.1. Figure 4.2 is the distribution of 1000 simulations of the DBL heuristic. The distribution in Figure 4.2 can be described as normal. However, in this heuristic there is no weighting for minimum void present. For weighting coefficients in the objective function that prioritise minimum void, it is expected that this would create a skewing of the data. Indeed this is true as is represented in Figure 4.3 which is the distribution of 1000 runs for the coefficients C_V=1, C_D=0.75 C_T=0.3 and C_{CN}=0.045. The mean of the data in Figure 4.3 is 0.0317 and this can be viewed as the population mean. The majority of results tend towards a void ratio of 0 as this is what the objective function is trying to achieve. Therefore the data cannot be described as a normal distribution.

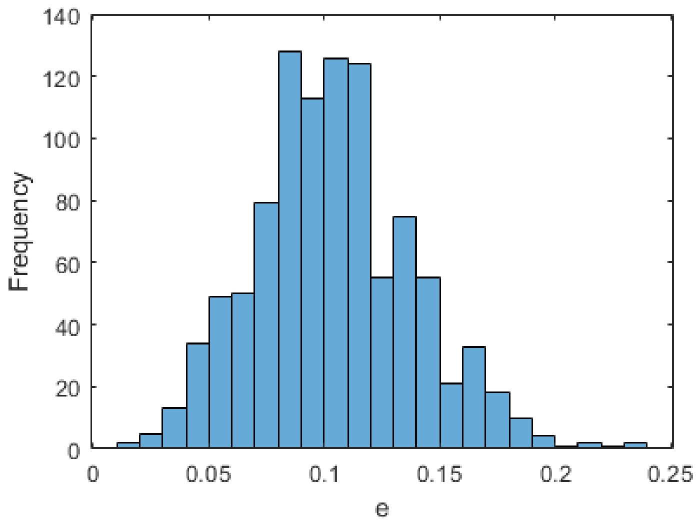

FIGURE 4.2: Distribution of tetrominoes packed using the DBL heuristic in a 10x10 square domain for 1000 simulations.

However, as the mean of the data is being used in the analysis, it is possible to achieve an accurate result from a sampling distribution. This is achieved by taking n samples from the population of Figure 4.3 multiple times. This will produce a normal distribution of possible mean values that can be achieved from the population data for that sample size. Figure 4.4 is an example of the sample distribution, showing the distribution of results for 5000 instances of random samplings for a sample size of n=30. From visual inspection, the data can clearly be described by a normal distribution. The mean of Figure 4.3 is 0.0316, which closely represents the population mean of 0.0317. As the data in Figure 4.3 is normal, it is possible to now analyse the data using Gaussian descriptors such as standard deviation. Note, these descriptions now refer to the mean of the values rather than being a description of the actual data set.

Values of n were varied from n=4 to n=100. n results were taken randomly from the population data to create a sample dataset. The mean value of the sample dataset is calculated and this is repeated 5000 times for each value of n. Figure 4.4 is the results of the 5000 samples for n=30 from the dataset displayed in Figure 4.3. Random sampling was completed 5000 times because, as central limit theorem states, the distribution of data will tend to a normal distribution with the more repeats of sampling leading to higher accuracy compared to a "true value" of the population mean. Inspection of Figure 4.4 confirms this. Figure 4.5 shows results of the sample dataset means for n=4 to n=100 with all 5000 acquired means plotted for each n value. As n increases, the values of the sample dataset become closer to the mean value of 0.032 for the population (which is indicated by the horizontal dashed line). These values oscillate with each simulation of data sampling giving a large variety of results. This variance decreases as n increases as indicated by the onset upper and lower limits which represent the range in which 95% of values lie for the given n which is equivalent to the CI being considered. Once again, the confidence interval is the range in which a value has a probability - the confidence level - for falling between. A CI of 95% can be predicted using $\pm 2\sigma_p$ from the mean.

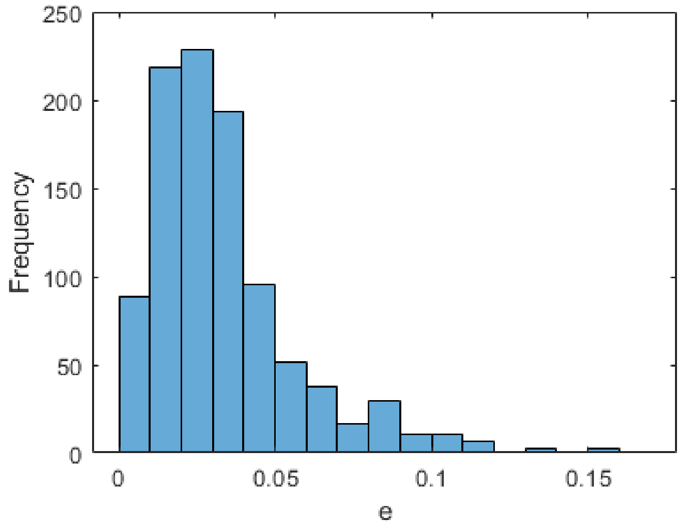

FIGURE 4.3: Distribution of data of 1000 tests ran with coefficients C_V=1, C_D=0.75 C_T=0.3, and C_{CN}=0.045 for resulting values of void ratio, e, in a domain of 10x10 squares.

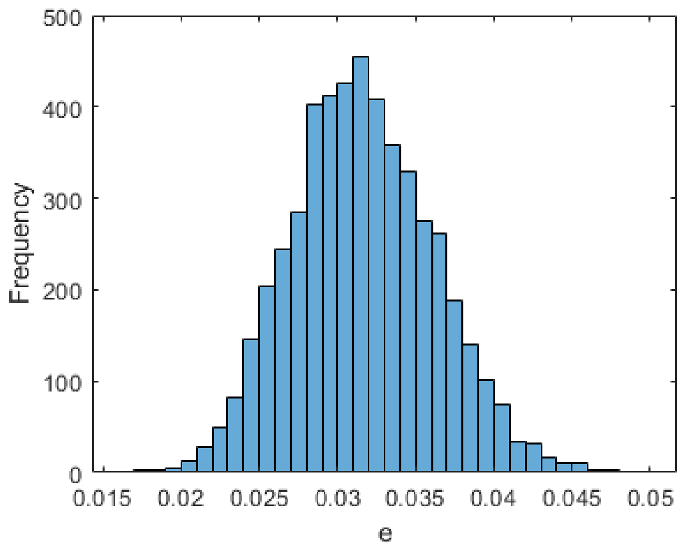

FIGURE 4.4: Distribution of mean e values for n=30 samples from data presented in Figure 4.3 repeated 5000 times.

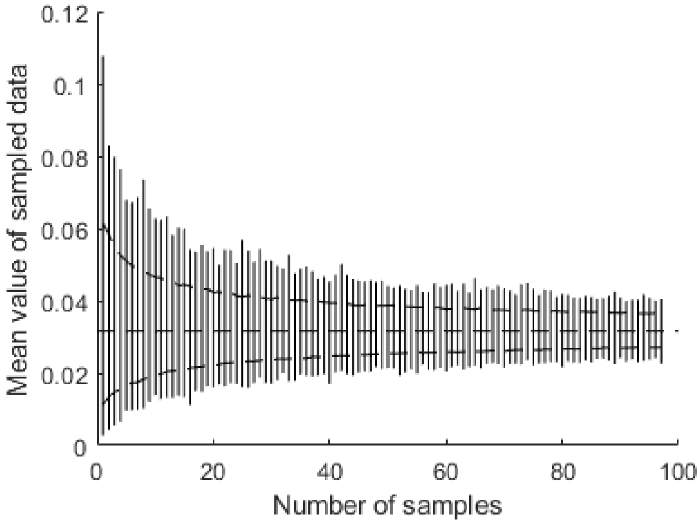

FIGURE 4.5: Mean value of each distribution of data like in Figure 4.3 for each value of n from n=4 to n=100. Onset are values that show the range that 95% of values lie between and a horizontal line that represents population mean.

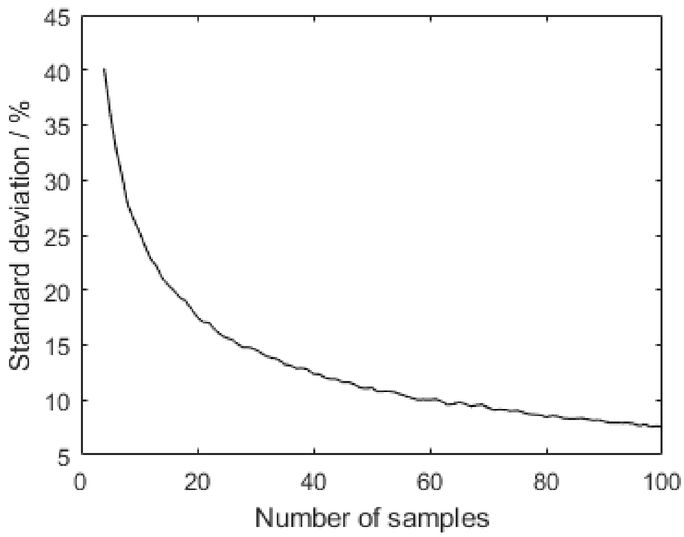

FIGURE 4.6: Standard deviation as percentage of the total void for different sample sizes, n, for Tetris Scenario with coefficients C_V=1, C_D=0.75 C_T=0.3, and C_{CN}=0.045 in a domain of 10x10 squares.

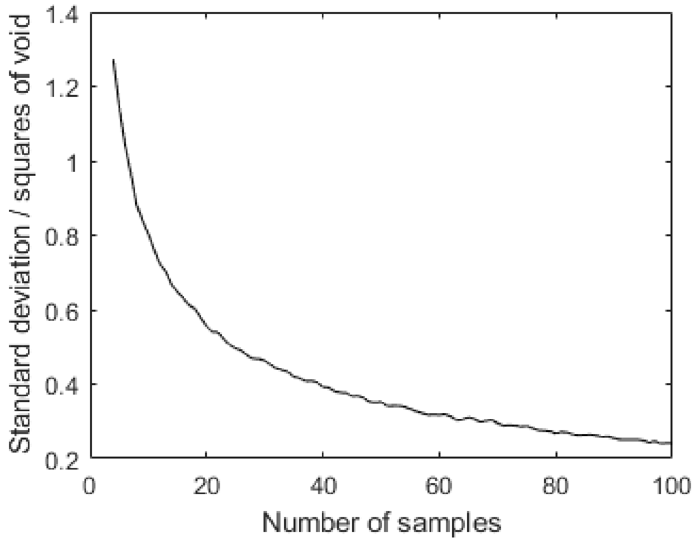

FIGURE 4.7: Standard deviation as Tetris squares of void in percentage for different sample sizes, n, for Tetris Scenario with coefficients C_V=1, C_D=0.75 C_T=0.3, and C_{CN}=0.045 in a domain of 10x10 squares.

Figure 4.6 indicates the standard deviation of the sample as a percentage of the total void in the system determined by

$$\sigma_{\%} = \frac{\sigma_p}{A_V} * 100 \tag{4.2}$$

where A_V is the area of voids in the packed structure below the placement surface. For n=30, a σ_p of 0.0046 was calculated. This is 14.5% of the total void that is present in the system. If a confidence level of 95% is desired then $2\sigma_p$ either side of the mean leads to CI being 0.0317 $\pm$ 0.0092. This would mean that the CI would lie between a range of 58% of the void in the system. This appears to be a large variance from the mean value and can lead to high amounts of uncertainty. However, in the Tetris scenario, the minimum amount of void that can be created when a particle is placed (without the value being zero) is 1 squares worth of void. If the void in the system is considered as squares of void, a different picture of the scenario is created. The mean value of void for the data from Figure 4.4 is approximate to 3.7 squares of void present in the final packing structure. This is a very small value of the system, given that the maximum number of squares in the domain is 100. Additionally, from Figure 4.7, it can be determined that the standard deviation now becomes a value of 0.46 squares leading to a CI of 3.7$\pm$ 0.92 squares. Alternatively, this could be viewed as there is a 95% probability that the mean of a sample for n=30 will lie in the range of 2 squares (when rounded to the nearest square) around the actual mean value. As it is not possible to have a change from void ratio smaller than 1 square in the Tetris scenario, this appears to be more than sufficient for the range of CI.

A check was completed to ensure that the confidence interval was correctly predicting 95% of the mean values achieved from sampling. For the full 5000 means from sampling for each n value, the 2.5th and 97.5th percentile was calculated. The range for these values are presented in Figures 4.8 and 4.9. The determined range for the confidence interval for a confidence level of 95% is 56% of the total void, or 1.77 squares. This compares nicely to the CI range of 58% or 1.84 squares gained from

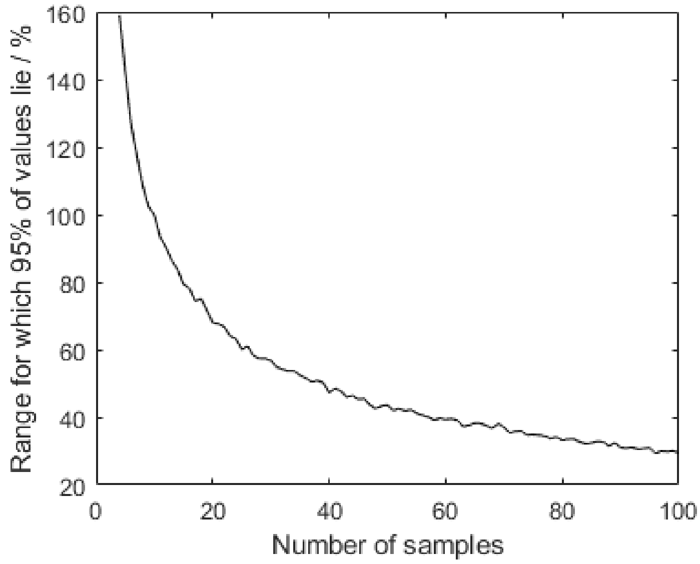

FIGURE 4.8: Range for which 95% of mean values lie when 5000 samples are taken with a sample size of n as percentage of the total void for Tetris Scenario with coefficients C_V=1, C_D=0.75 C_T=0.3, and C_{CN}=0.045 in a domain of 10x10 squares.

Figures 4.6 and 4.7. In comparison, n=9 shows CI range of 3.7± 1.6 squares meaning a range of around 3 squares for 95% of values to lie between. For the increased computational speed that running 9 simulations of a sequence of coefficients brings compared to 30 it could be worth using n=9 and then using more simulations (n=30) when more acccurate results are required.

n	$\sigma_{\%}$	σ_{square}	CI (squares)
5	36.2	1.1	±2.3
9	26.7	0.85	±1.6
15	20.6	0.65	±1.3
20	17.5	0.55	±1.1
30	14.6	0.46	±0.92
40	12.3	0.39	±0.76
50	11.0	0.35	±0.68
100	7.7	0.24	±0.48

TABLE 4.1: Standard deviation for the resulting means of the 5000 sample datasets with different values of n for Tetris Scenario with coefficients C_V=1, C_D=0.75 C_T=0.3, and C_{CN}=0.045 in a domain of 10x10 squares.

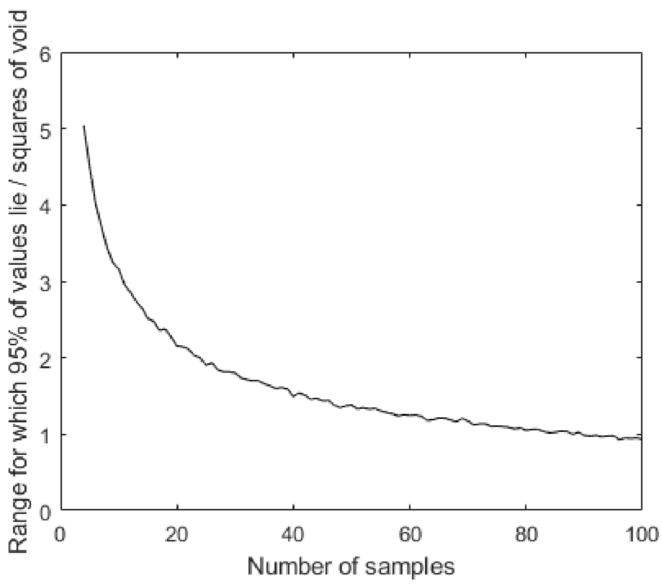

FIGURE 4.9: Range for which 95% of mean values lie when 5000 samples are taken with a sample size of n as Tetris squares of void for Tetris Scenario with coefficients C_V=1, C_D=0.75 C_T=0.3, and C_{CN}=0.045 in a domain of 10x10 squares.

4.3.4 Domain Size

It is required to confirm that the domain size of 10x10 squares is sufficient to lead to all possible results for voids created when packing and that the size of the domain is not a limiting factor. The DBL packing heuristic was repeated for a domain of 20x20 squares to see if there is any change to the distribution produced. The histogram of results for 1000 packings is presented in Figure 4.10. In the previous simulations for a 10x10 square domain, the number of particles placed was set to 35 as this greatly outnumbered the total number of particles that could fit into the domain. For the 20x20 square domain, this particle limit had to be increased to 100. As can be envisioned, the computational runtime of the simulation was increased dramatically as, not only were more positions trialled, but also more particles had to be placed. Table 4.2 presents computational runtimes for the different domain sizes. The distribution of the results again take the form of a normal distribution as can be seen in Figure 4.10.

Domain size	Number of simulations	Time	Time per simulation
10x10	1000	41 mins	2.5s
20x20	1000	522 mins	31.3s

TABLE 4.2: Time to complete packing for different domain sizes under the Tetris Scenario using the DBL heuristic.

Table 4.3 presents mean values and σ_p for the distributions investigated for a change of domain size. The void ratios produced from the packing of the 20x20 square domain are lower than presented in Figure 4.2. This is most likely due to there being a wider domain base lead to more possible positions for particle placement. The placement of the particle is being scored on the position of the centre of mass of the tetromino, so a larger base - e.g. T shape tetromino when the three squares of that make up the top of the T are faced downwards - will lead to a lower centre of gravity. The wider the domain, the more chance there will be a (3-square width

Heuristic	Domain Size / squares	Mean Void Ratio	σ_p
DBL	10x10	0.1036 (10.4 squares)	0.0350 (3.5 squares)
DBL	20x20	0.0774 (30 squares)	0.0137 (5.5 squares)
Objective Function	10x10	0.0317 (3.2 squares)	0.0254 (2.5 squares)
Objective Function	20x20	0.0082 (3.3 squares)	0.0079 (3.2 squares)

TABLE 4.3: Statistical data from 1000 simulations of DBL-heuristic and the objective function with weighted coefficient values of C_V=1, C_D=0.75 C_T=0.3, and C_{CN}=0.045 for 10x10 domain and 20x20 domain.

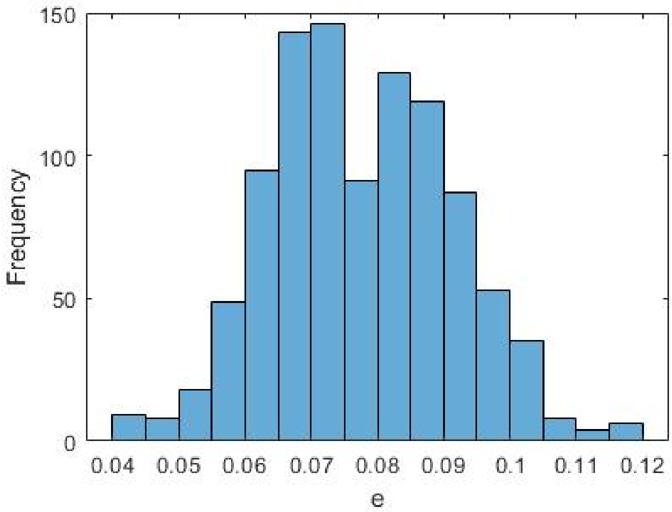

FIGURE 4.10: Distribution of tetrominoes packed using the DBL heuristic in a 20x20 square domain for 1000 simulations.

for the T shape) position for this particle to be placed. However, the DBL heuristic does not prioritise minimising void, so therefore the mean void ratio from the 20x20 domain DBL simulations is not vastly smaller than the 10x10 domain as filling gaps is not being prioritised. σ_p for the 20x20 square domain is much smaller than that of the 10x10 domain. The order of particles will have a greater effect on the 10x10 domain as there are limited placements for the particle to be positioned so it is more likely that a void will be created beneath the particle.

In addition, a comparison for weighting coefficients in the objective function of C_V= 1, C_D=0.75 C_T=0.3, and C_{CN}=0.045 was completed for a domain of 10x10 squares and a domain of 20x20 squares. The data for the domain of 10x10 squares has already been discussed in Section 4.3.3 and Figures 4.3-4.9. 1000 simulations filling a domain of 20x20 squares was completed for comparison. Figure 4.11 presents the resulting void ratios obtained from these simulations. As can be seen, the mode value has a much higher frequency than in the previous data set. The likelihood for this is that the bigger domain leads to more potential positions for particles similar to the DBL-heuristic case. The range in particle shape only varies to be seven different options all of which are orthogonal. Therefore, the chance that a placement can be without leaving void below the particle is much more achievable than with irregular shapes. This is also demonstrated by the much lower values of void ratio seen in the results for Figure 4.11. The process of creating the sample distribution was repeated for the data in Figure 4.11 and this produces the histogram presented in Figure 4.12. Void ratios are much closer to zero due to the volume of total solids in the system

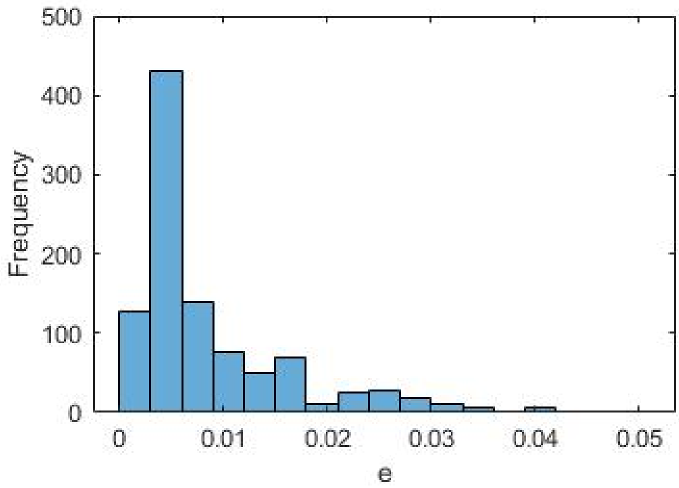

FIGURE 4.11: Distribution of results for 1000 runs using weighted coefficients C_V= 1, C_D=0.75 C_T=0.3 and C_{CN}=0.045 for resulting values of void ratio, e, in a domain of 20x20 squares.

being much higher as there is a larger number of placed particles. Figure 4.13 takes a very similar shape to Figure 4.5. Therefore it can be determined that the sample distribution of results for both domain sizes each have a reduction in variability for the mean value as sample size increases.

From examining the standard deviation of the sample distribution for n=30 for a domain of 20x20 squares, it can be seen that σ_p is equivalent to 1.38x10^{-3}. This is equivalent to 16.9% of the total void of the system or 0.55 squares of void as derived from Figure 4.14 and Figure 4.15. When compared to the standard deviation of 1000 simulations in the 10x10 domain of 14.5% and 0.46 squares, it can be seen that these values are alike. Given the increase in runtime between the two scenarios, any accuracy gained from increasing the domain size does not outweigh the additional computational cost considering the similarity between the results. Therefore, the domain size of 10x10 squares is taken as a sufficient representation of the packing procedure. This also nicely lines up with the domain width being equivalent to the 10 square width found in Standard Tetris case.

The domain size for the Soil Particle Scenario is set to be 50x50 units large. From initial packings, it was seen that around 10 particles are placed at the base of domain. As soil particle outlines are fairly uniform it can be assumed to be simulated in the Tetris Scenario as a SQ tetromino. Therefore, this 50x50 unit domain in the Soil Particle Scenario can be said to represent a 20x20 square domain for the equvialent size in the Tetris Scenario. Taking this whilst also attempting to not fill the domain by more than half the volume means it can be assumed that a 50x50 unit domain size is suitable.

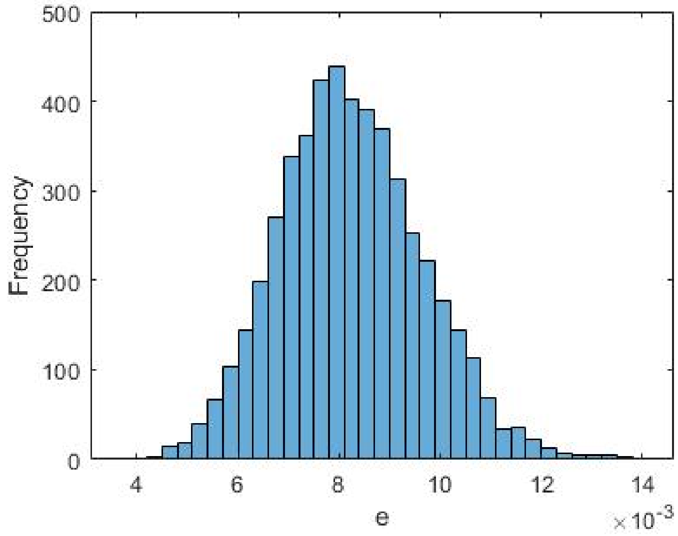

FIGURE 4.12: Distribution of mean e values for n=30 samples from data presented in Figure 4.11 repeated 5000 times.

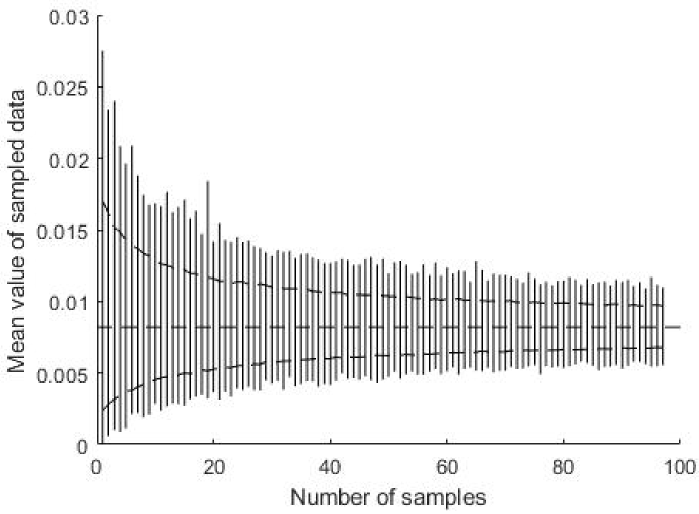

FIGURE 4.13: Mean value of each distribution of data like in Figure 4.12 for each value of n from n=4 to n=100. Onset are values that show the range that 95% of values lie between and a horizontal line that represents population mean.

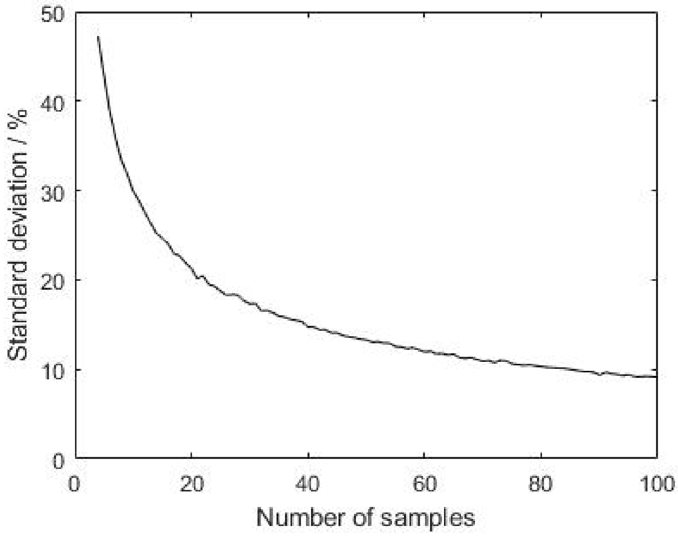

FIGURE 4.14: Standard deviation as percentage of the total void for different sample sizes, n, in a 20x20square domain packing using weighting coefficients of C_V=1, C_D=0.75 C_T=0.3, and C_{CN}=0.045.

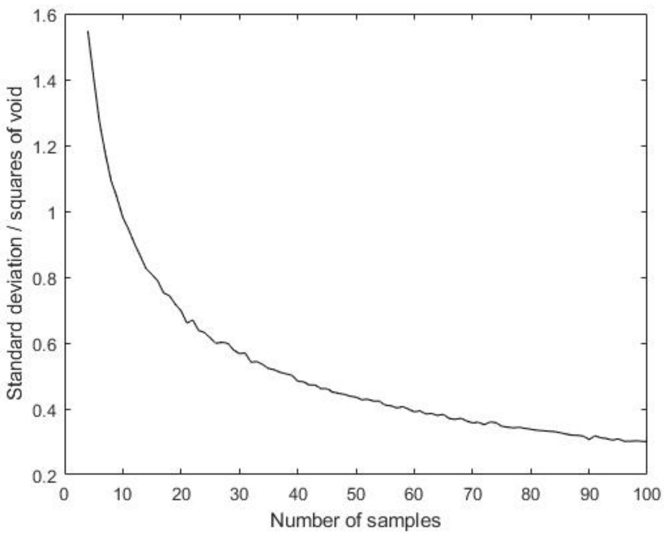

FIGURE 4.15: Standard deviation as Tetris squares of void for different sample sizes, n, in a 20x20square domain packing using weighting coefficients of C_V=1, C_D=0.75 C_T=0.3, and C_{CN}=0.045.

4.3.5 Summary

In Section 4.3.2, examining Figure 4.1 led to the conclusion that for quick, broad testing of lots of coefficient combinations then sample size n=9 is suitable with a sample size n=30 being used for more accurate analysis in areas of interest. This agrees with the rule of thumb of using n=30 to represent a dataset (Chang et al., 2006; Hogg et al., 2014) as discussed in Section 4.3.1. Section 4.3.3 presents an investigation into the DBL scenario and Tetris scenario using weighted coefficients. The DBL heuristic exhibited a normal distribution of results whereas the weighted coefficients did not due to their objective to achieve minimal void ratio. However, a normal distribution was achieved with the mean result of sampled data. It was shown that for n=30, a 95% CI could be represented by 3.7$\pm$ 0.92 squares. As the smallest possible non-zero value of void that can be created is 1 square, this is definitely a reasonable range for results to lie between.

The investigation into the size of the domain being sufficient enough not to cause limitations on the results from simulations was conducted in Section 4.3.4. Packings conducted in a domain of 20x20 squares exhibited similar distributions for both the DBL and the use of an objective function with weighting coefficients of C_V=1, C_D=0.75 C_T=0.3, and C_{CN}=0.045. For results using the objective function, it was shown that both the mean and 95% confidence interval are of equal measure in terms of percentage of the total area and Tetris squares of void created. As these are similar, any accuracy gained from increasing the domain size does not outweigh the additional computational cost.

The results of from Section 4.3 provide proof that a value of n=30 is a suitable sample size to take when investigating the coefficients of weight for the objective function. As stated, this leads to a suitable representation of the possible population data. However, as shown in Section 3.6.5, computational runtimes for the Soil Particle Scenario are much larger than for tetrominoes in the Tetris Scenario. Therefore, a lower n value will be used to get a broad understanding of the effects of coefficients. As determined in Section 4.3.2 and Section 4.3, n=9 is a suitable sample size for this in the Tetris Scenario.

4.4 Investigation of Weighting Coefficients

4.4.1 Representation of Results

To determine the weighting coefficients within the objective function, an optimised value is required. It is possible to do this for the Tetris Scenario by varying the coefficients of weight and following a minimum value of mean void ratio (MVR) from the test result. However, this can lead to resting in a local minimum. To avoid this, a wide range of coefficients are investigated. The methodology for this process is analysed in this section to give reasoning and justification for the process completed. As discussed in Section 4.3.3, a sample size of 30 is reasonable to take forward when it comes to computational time versus the confidence that the outputted values represents the population of results that could be exhibited by the simulations. However, as a wide range of coefficients are tested to begin with, a lower sample size will be desired such as n=9. In Section 4.4, it will be explored as to whether the use of a lower sample size can reasonably represent the whole picture of the data before using a higher sample size to narrow down on an exact result.

Three-dimensional surface plots of mean void ratio from n samples for different weighting coefficients are investigated for the Tetris scenario described in Section 3.2.2. As the objective function consists of four criteria each with a weighting, C_V was set to a fixed value. Surface plots for fixed values of C_D are then used to represent the data.

4.4.2 Fixed Seed vs Random Seed

During the investigation of determining the correct weighting coefficients for the Tetris Scenario, it became apparent that there were two methods that could be adopted for the investigation. The first was to completely randomise the particle order generated by the Tetris bag method whereas the second was to set the seed at the beginning of each set of weighting coefficients so that the order of particles were the same for each set of weighting coefficients investigated. Figure 4.16 are the results of mean void ratio for varying weighting coefficients for C_T and C_{CN} between values of 0 to 1 by increments of 0.1 with a sample size of n=9. Three plots are represented as C_D was varied from 0 to 1 with increments of 0.25. These plots are for results where C_D=0, C_D=0.5 and C_D=1 in Figures 4.16a, 4.16b and 4.16c respectively. No seed for random number generation was set in the programme and the particle order is unique for each simulation.

Figure 4.17 is a replication of this procedure. However, for these tests, a seed for the generation of particles from the Tetris bag was set before the investigation into each set of coefficients. This ensured that each set of 9 tests would have the same 9 permutations of particle delivery order. For example, if the first test for weighting coefficients C_V=1, C_D=1, C_T=1, C_{CN}=0.5 has particles delivered in an order of 1,2,3,4,5,6,7 (with each number indicating a different type of particle) and then the second test had particles delivered in the order of 7,6,5,4,3,2,1 then the first and second test of all other sets of coefficients (e.g. C_V=1, C_D=1, C_T=1, C_{CN}=1) would have identical orders delivered for the respective tests.

From the comparison of Figure 4.16 and Figure 4.17, it can be seen by fixing the particle delivery order that the surface plot becomes much more consistent for slight changes to the combinations of weighting coefficients and there is less variability between datasets which are closer to each other in terms of space on the plots. Figures 4.18 and 4.19 are replications of the same scenarios with a sample size of n=30 for a randomised generation of particles and a fixed seed respectively. Comparison between these figures produces the same observation that using a fixed seed produces much more similar data for coefficient values that are close to each other. This is because changing the particle order introduces a new variable that can affect the results of the tests. The order that particles are delivered is important as voids will only be filled if the shape of the tetromino can fit into any gaps. It is best to keep this consistent when comparing different coefficients of weight. Therefore, the investigation of coefficients will be conducted using a fixed seed to remove an extra element of unpredictability.

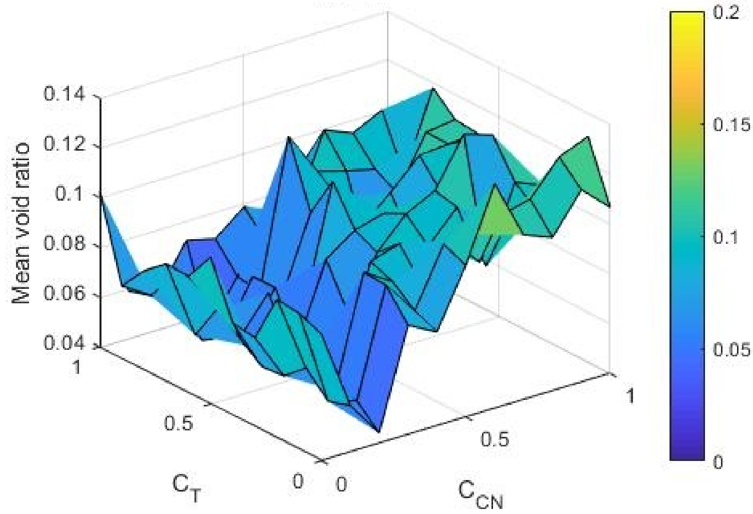

(A) $C_D = 0$

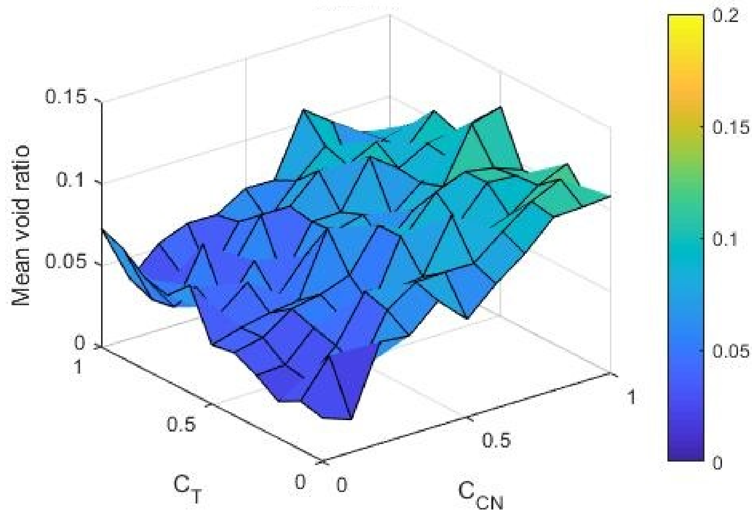

(B) $C_D = 0.5$

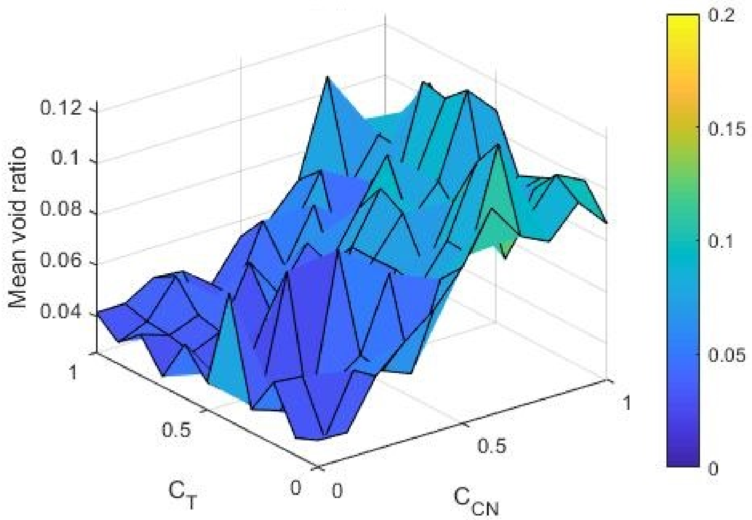

(C) $C_D = 1$

FIGURE 4.16: Surface plot for different coefficients and the resulting mean of the void ratios for a sample size of 9 with randomised generating Tetris bag particle ordering.

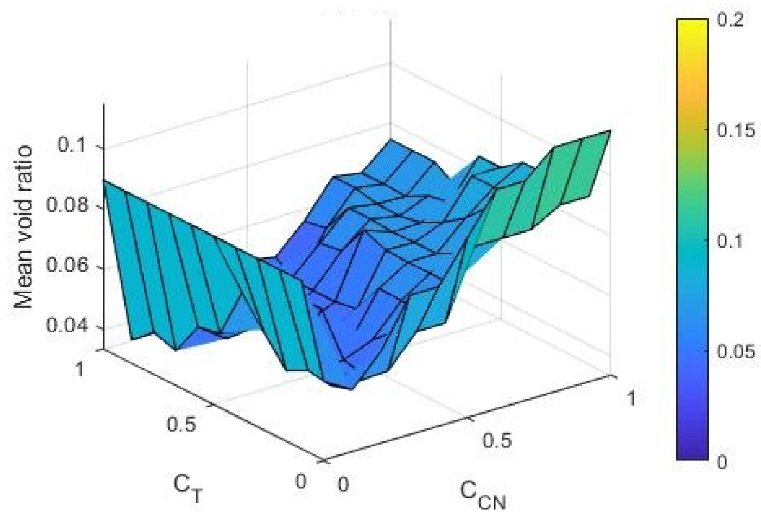

(A) $C_D = 0$

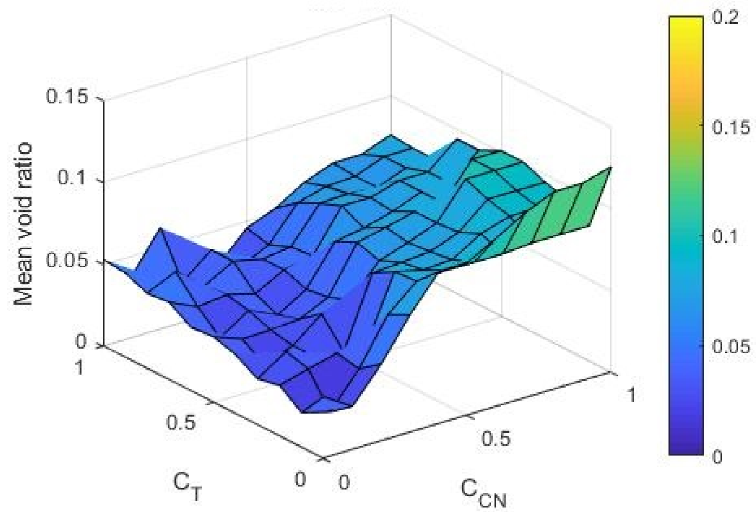

(B) $C_D = 0.5$

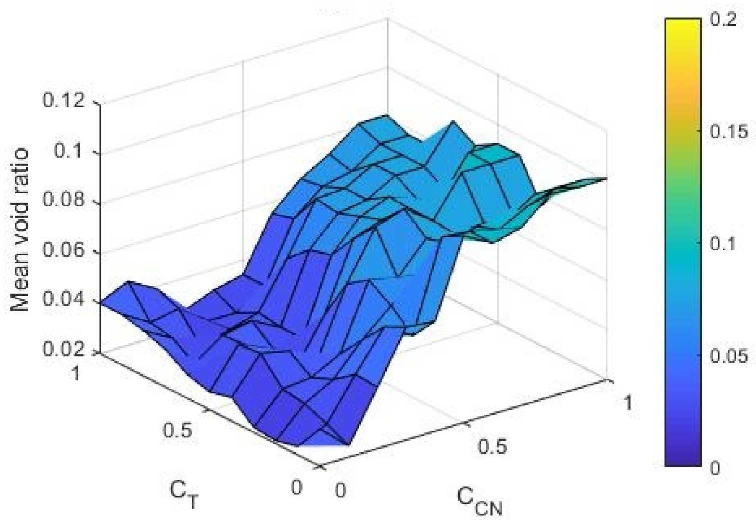

(C) $C_D = 1$

FIGURE 4.17: Surface plot for different coefficients and the resulting mean of the void ratios for a sample size of 9 with fixed seed for generating Tetris bag particle ordering.

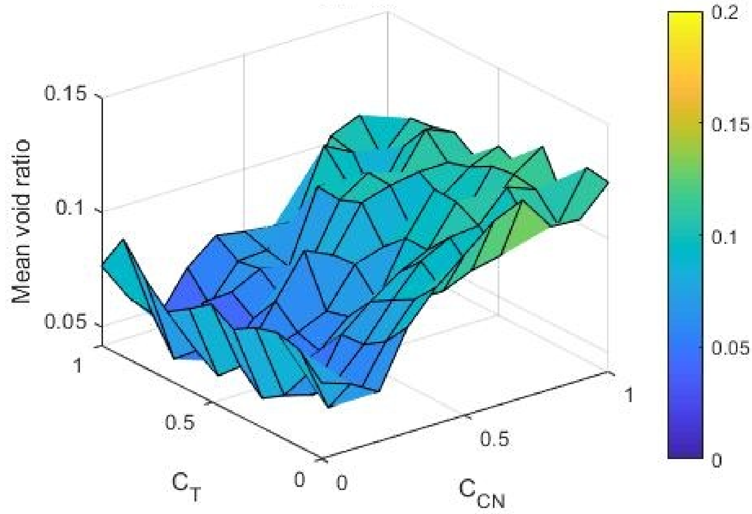

(A) $C_D = 0$

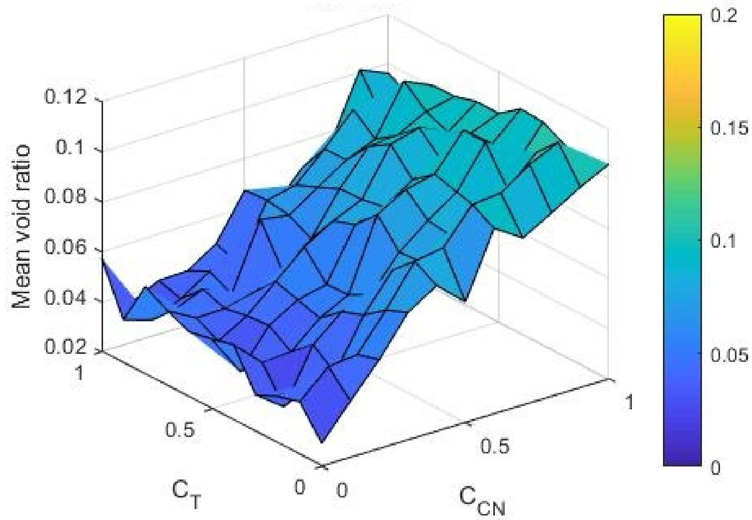

(B) $C_D = 0.5$

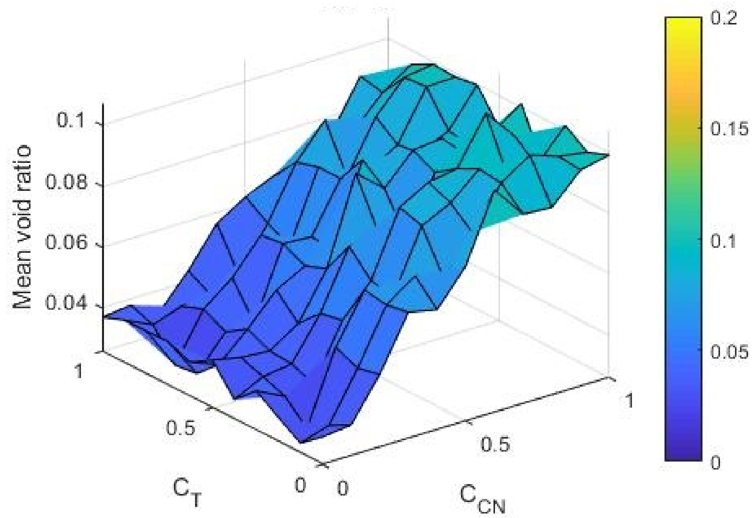

(C) $C_D = 1$

FIGURE 4.18: Surface plot for different coefficients and the resulting mean of the void ratios for a sample size of 30 with randomised generating Tetris bag particle ordering.

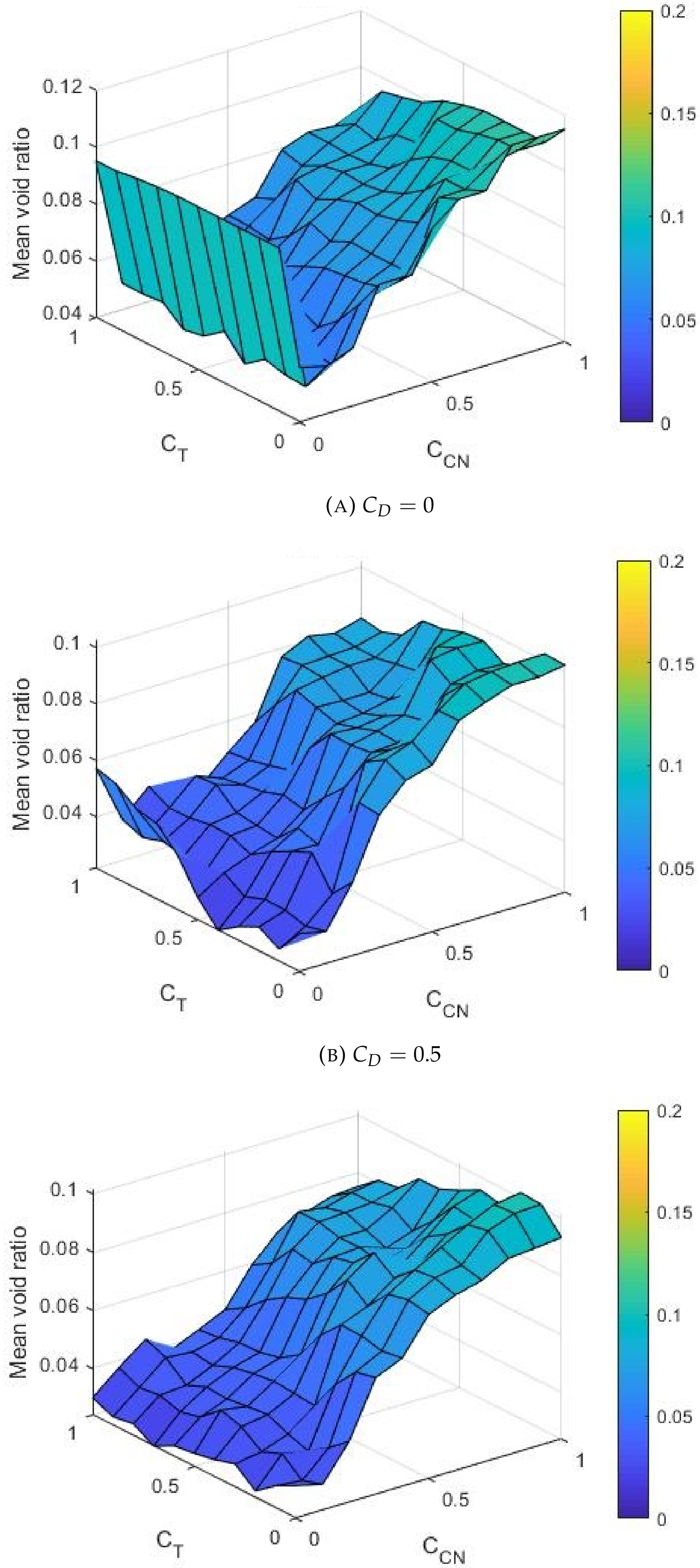

(A) $C_D = 0$

(B) $C_D = 0.5$

(C) $C_D = 1$

FIGURE 4.19: Surface plot for different coefficients and the resulting mean of the void ratios for a sample size of 30 with fixed seed for generating Tetris bag particle ordering.

4.4.3 Smoothing of the Surface Plots

Even with a fixed seed for randomising the particle order for each new set of coefficients, the curve of the surface plot is still undulating and it is difficult to distinguish true minima and maxima. This is seen in Figure 4.17 and Figure 4.19. As a result, smoothing of the surface plot was conducted using a mean filter and Gaussian filter method. These filters are applied to the surface of the plot and calculate new mean void ratio values using a weighted function applied to a sample area around the datapoint selected. Results of the filters applied to the data in Figure 4.17 are displayed in Figure 4.22 for the application of a mean filter and Figure 4.23 for the application of a Gaussian filter.

The mean filter, or box filter, is one of the most commonly used filters in graphics (Pharr et al., 2016). The filter works by averaging all values in a sampled square around the selected datapoint. The filter applied is shown in Figure 4.20 and it can be seen that an equal weighting is given to datapoint being analysed and each surrounding value.

$\frac{1}{9}$	$\frac{1}{9}$	$\frac{1}{9}$
$\frac{1}{9}$	$\frac{1}{9}$	$\frac{1}{9}$
$\frac{1}{9}$	$\frac{1}{9}$	$\frac{1}{9}$

FIGURE 4.20: Mean Filter applied to curve for smoothing.

The Gaussian filter is similar to the mean filter in terms of use. However, rather than averaging the sample values, the Gaussian kernel represents that of a Gaussian distribution (Fisher et al., 2008). The calculation for a Gaussian distribution is completed using Equation 4.3 (Sorenson and Alspach, 1971) where x and y are coordinates in space on the filter and σ_p is the standard deviation of the distribution, taken as 1 in this case. Equation 4.3 is used to create the filter values which are applied as a weight to the relevant sample values. The weights in the filter are divided by their sum. This is also known as the Gaussian sum approximation.

$$G(x, y, \sigma_p) = \frac{1}{2\pi\sigma_p^2} e^{-\frac{x^2+y^2}{2\sigma_p^2}} \tag{4.3}$$

For the mean filter, the larger the filter the more influence values that lie further away from the datapoint being analysed will have on the filtered result. For example, if a mean filter of size 5x5 is chosen for application on the dataset in Figure 4.17 then all values in this 25 square grid will be multiplied by $\frac{1}{25}$. Therefore it is best to tend towards a smaller filter otherwise values may become too similar to each other once filtered and the shape of the surface plot becomes less meaningful. As the Gaussian filter is based on a Gaussian distribution, values lying further from the datapoint being analysed will have less effect on the filtered result. Due to this, a mean filter of size 3x3 (Figure 4.20) was adopted whilst a Gaussian Filter of size 5x5 is utilised due to the decreasing effect for values from the centre to the edge of the filter.

A problem occurs when applying the filter at the edge of the datasets and there is not a credible value for every square in the filter. When this occurs, zero-padding

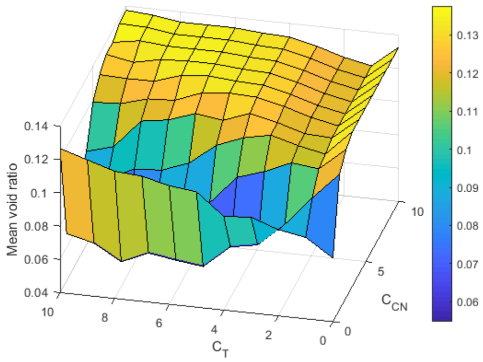

(A)

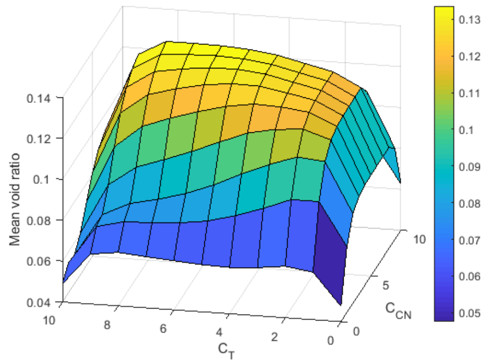

(B)

FIGURE 4.21: Surface plot of MVR results for n=50 when C_V=1 and C_D=0 with C_T and C_{CN} ranged from values of 0 to 10 by increments of 1. Shown is (a) the data with no filter applied and (b) Data with the Gaussian filter applied without the application of Equation 4.4 and therefore zeropadding is present.

is used at the boundaries of the matrix. For example, if the filter in Figure 4.20 was being applied to the left side of the dataset in Figure 4.19c then it does not have valid numerical results for the left side of the filter. These values would be take as zero values. This allows the filter to be applied to the whole dataset and return a matrix of the same size but it should be noted when considering values that are calculated using this "fix" in the analysis. However, values where zero-padding occurs are under predicted especially at corners where the majority of values the filter is applied to are null. Figure 4.21 presents an example of this where Gaussian filter is applied to the dataset in Figure 4.21a. The resulting surface plot in Figure 4.21b have values at edges which are much lower than the actual values at edges before filtering.

To avoid the problem of zeropadding leading to ignoring edge values, the convolution of the filter and the dataset for a given surface plot can be adapted using

$$\frac{M * G}{J * G} \tag{4.4}$$

where M is the matrix of MVRs for that surface plot and J is a unit matrix of equivalent size to M where every value in J is equal to one. Following Equation 4.4, $J * G$ indicates the portion of the Gaussian filter than is being applied to a datapoint in M. As the sum of all values in G equals one, the ratio of the portion of G applied to M can be taken to find an equivalent value assuming filter values scaled up to total one were utilised. This results in a value that better represents the edges of the surface, although care is still required at these points as a high level of approximation is seen. Comparing Figure 4.22 and 4.23 shows the effect of Equation 4.4 as edge values are no long much lower than other datapoints in the surface plot.

From Figures 4.22 and 4.23 compared to Figure 4.17, the smoothing of the curve leads to easier analysis of the total shape of the curve and the location of minimum when following the surface of the plot. From visual inspection, the Gaussian filter and mean filter both produce curvature for the plots with good effect. Out of the two, the Gaussian filter is selected to be taken forward with the investigation into determining the weight coefficients to give the optimal solution for the Tetris Scenario. The reason for this is the layout of the filter applying a decreasing effect from the centre of the filter towards the edge spaces when compared to the mean filter which applies the same value to each datapoint. Using the Gaussian filter will lead to less effect from datapoints which have large spikes away from values exhibited in other weight coefficients.

It is thought that no filter will be taken forward for the results of the Soil Particle Scenario in Chapter 6. This is due to the increased computational times meaning a smaller frequency of datapoints tested for different coefficients of weighting. As stated, zeropadding occurs when filters are applied to areas of no values which may produce negative effects on the surface plots of the search areas. If a large number of datapoints are available for collection and a filter can be applied, a Gaussian filter is adopted in the approach.

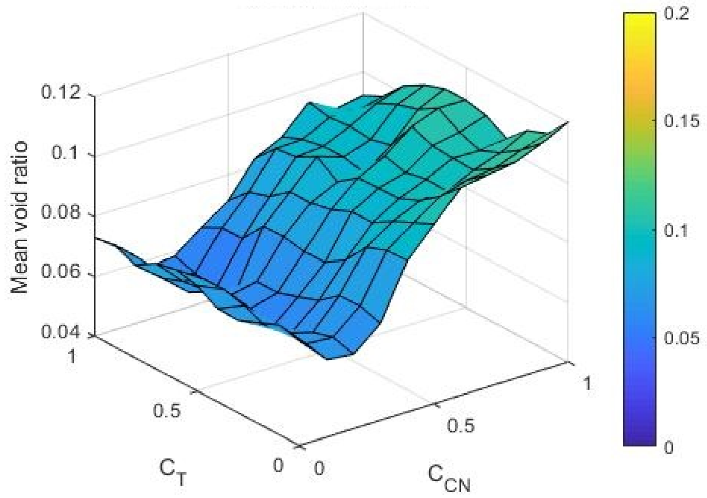

(A) $C_D = 0$

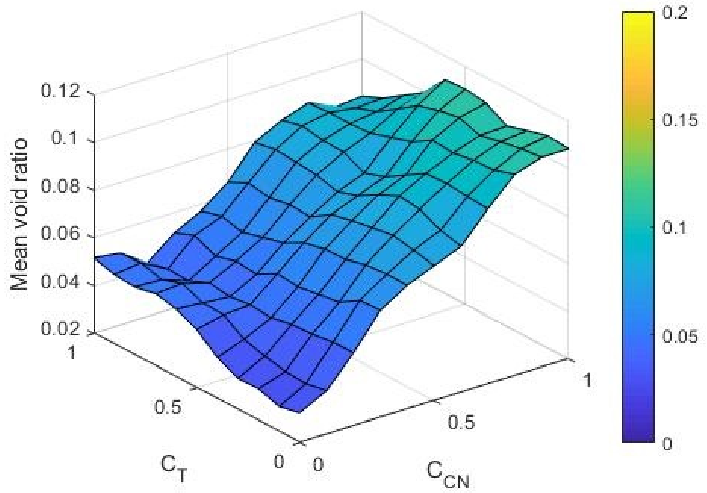

(B) $C_D = 0.5$

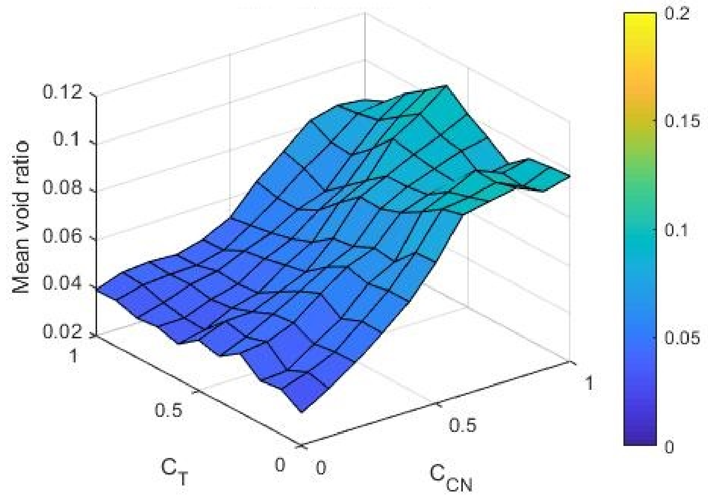

(C) $C_D = 1$

FIGURE 4.22: Surface plot for different coefficients and the resulting mean of the void ratios for a sample size of 9 with fixed seed for generating Tetris bag particle ordering with mean filter applied for curve-smoothing.

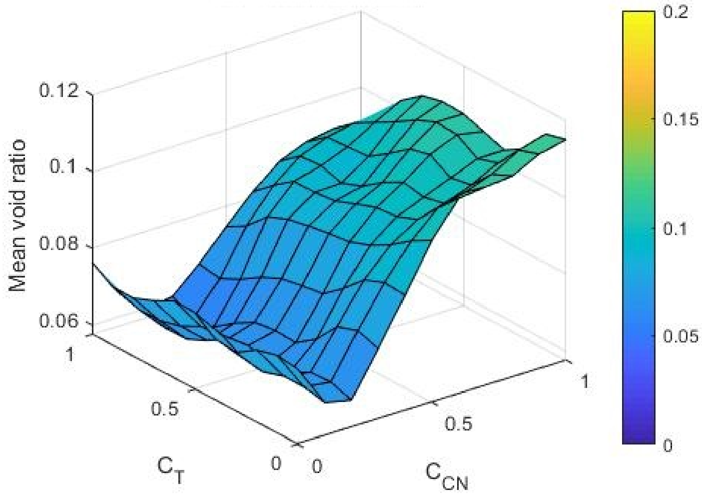

(A) $C_D = 0$

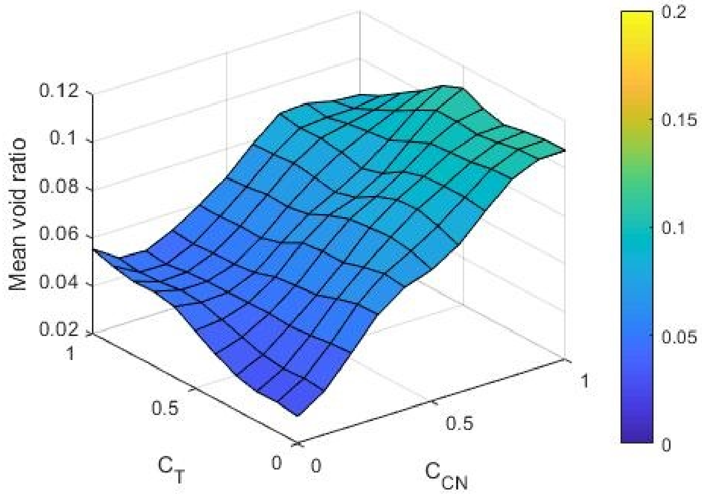

(B) $C_D = 0.5$

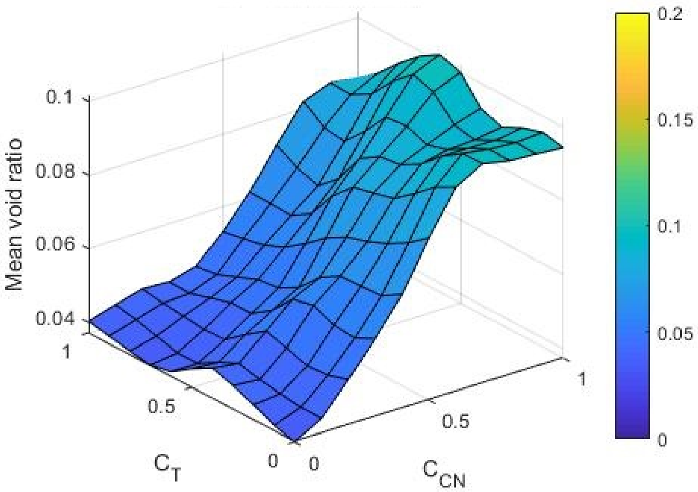

(C) $C_D = 1$

FIGURE 4.23: Surface plot for different coefficients and the resulting mean of the void ratios for a sample size of 9 with fixed seed for generating Tetris bag particle ordering with Gaussian filter applied for curve-smoothing.

4.4.4 Effect of Gaussian Filter on Results

As the Gaussian filter accounts for data in a given area rather than just a single point, the location of the minimum MVR for search areas with the filter applied represents a region in which multiple values are low. When the data is taken without the filter, it is identifying locations where the minimum MVR is achieved but these can occur where surrounding values are still relatively large. Therefore, the data in these areas are sensitive to change in the coefficients of weighting.

An example of the sensitivity in results for non-filtered data is shown in Figure 4.25. Figure 4.25a and 4.25b present surface plots for combinations of C_T and C_{CN} for C_D=0 with fixed value C_V=1 and their resulting MVR for packing in the Tetris Scenario. Coefficients were varied from values of 0 to 10 at increments of 1 and a sample size n=50 was adopted. The point highlighted in Figure 4.25a of C_T=8 and C_{CN}=1 is the location of the lowest MVR for all coefficient combinations when C_D=0 as indicated on Figure 5.11b and MVR=0.055 at this point. This located value can be considered sensitive as demonstrated by Figure 4.24a. A change in the coefficient values can considerably change the value of MVR produced. In comparison, the same location is identified for the data with Gaussian filter applied whose plot is presented in Figure 4.25b. From Figure 4.24b, it can be seen that the change in results are much less sensitive in comparison. Therefore it can be concluded that applying the Gaussian filter may mean that an absolute minimum value is missed but the outputted coefficients of weight will be less sensitive to slight changes in their value.

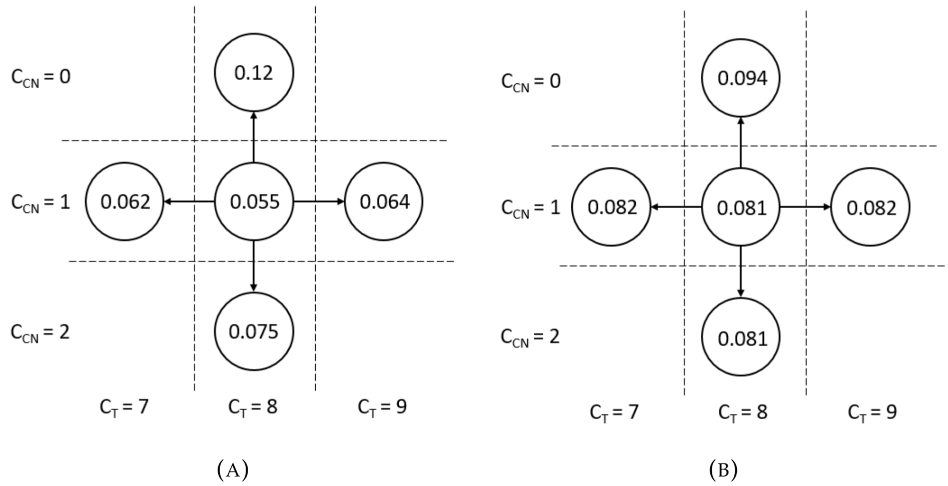

FIGURE 4.24: Central value indicates the value of MVR produced by the algorithm in the Tetris Scenario for a sample size n=50 for weighting coefficients C_V=1, C_D=0, C_T=1, and C_{CN}=9. Surrounding values indicate the values when an increase or decrease of 1 is applied to coefficients C_T and C_{CN} in datasets where (a) no filter is applied and (b) the Gaussian filter is applied.

Another example of sensitivity in results is presented for the Tetris Scenario with sample size n=50. Surface plots for combinations of C_T and C_{CN} for C_D=5 with fixed value C_V=1 are shown in Figure 4.26 for unfiltered MVR results and MVR results with Gaussian filter applied. In Figure 4.26a it can be determined that the lowest MVR is achieved at C_T=2 and C_{CN}=0. However, for the results once Gaussian filtering has been completed, the lowest MVR is achieved at C_T=4 and C_{CN}=0 The difference in MVR between (C_T=2,C_{CN}=0) and (C_T=4,C_{CN}=0) for Figure 4.26a is relatively large compared to differences in other locations with the MVRs for these locations

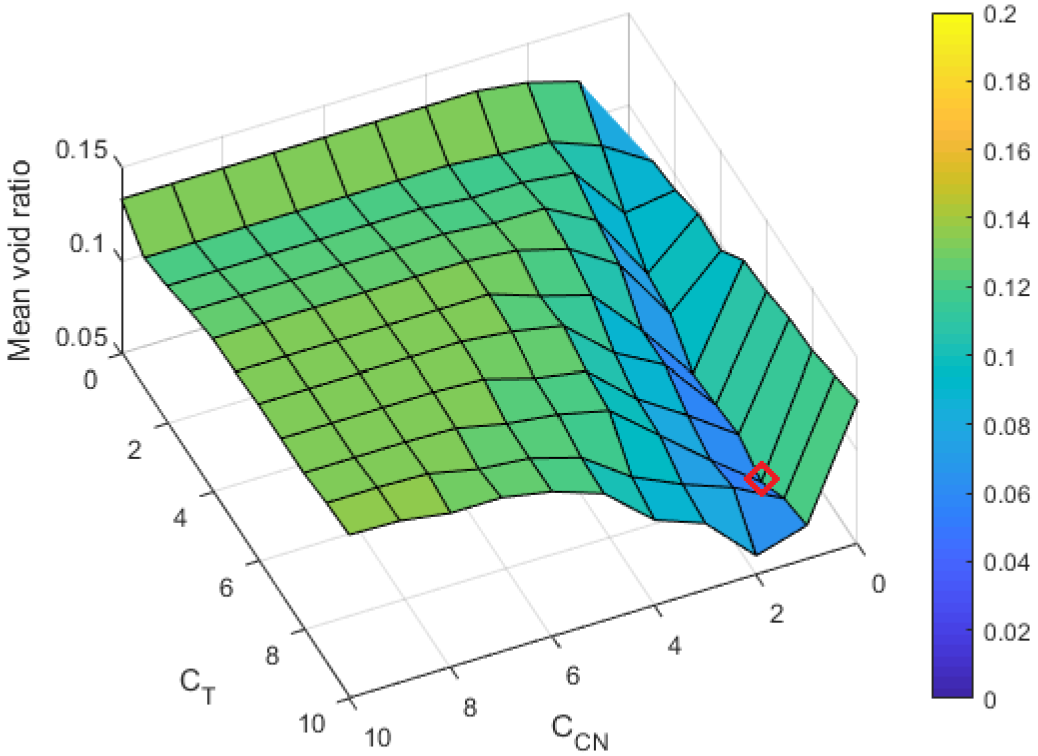

(A)

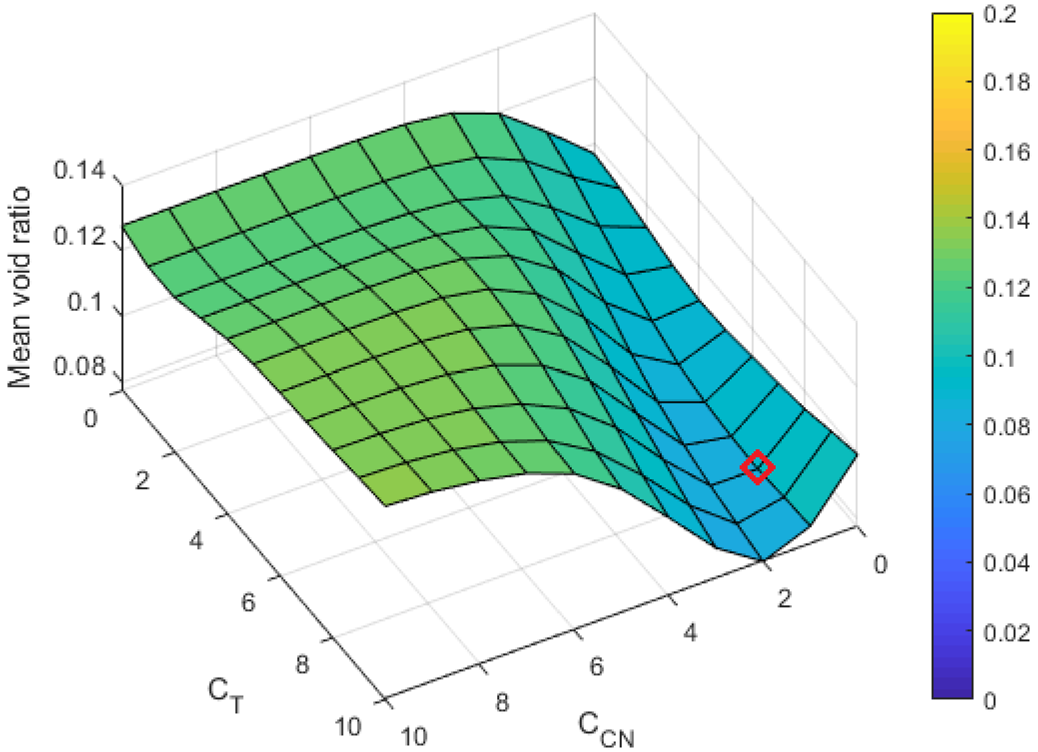

(B)

FIGURE 4.25: Surface plots of MVR results for n=50 in the Tetris Scenario for different C_T and C_{CN} values varied from 0 to 10 at increments of 1 with C_V=1 and C_D=0 for (a) the unfiltered MVR results and (b) the MVR results with Gaussian filter applied.

being 0.037 and 0.045 respectively. Therefore, if (C_V=1, C_D=5, C_T=4, C_{CN}=0) was chosen as the optimal weighting combination, this would be an incorrect solution for producing the minimum amount of voids in the Tetris Scenario. This is the risk of using the Gaussian filter.

However, values closer to the datapoint being analysed should affect the calculated MVR more due to the Gaussian style distribution of values in the filter. By selecting the lowest MVR for Gaussian filtered data, it is thought that a weighting combination will be selected that is closest to the optimal solution whilst being less sensitive to changes as seen in Figure 4.25. A check on unfiltered data can be completed to ensure this is the case. Additionally, increasing the sampling frequency for the search area will result in more datapoints around any optimal solution that may be missed. If these results are similar to this value, then the increase area of results closer to an optimum will still be able to be located even with the application of a Gaussian filter.

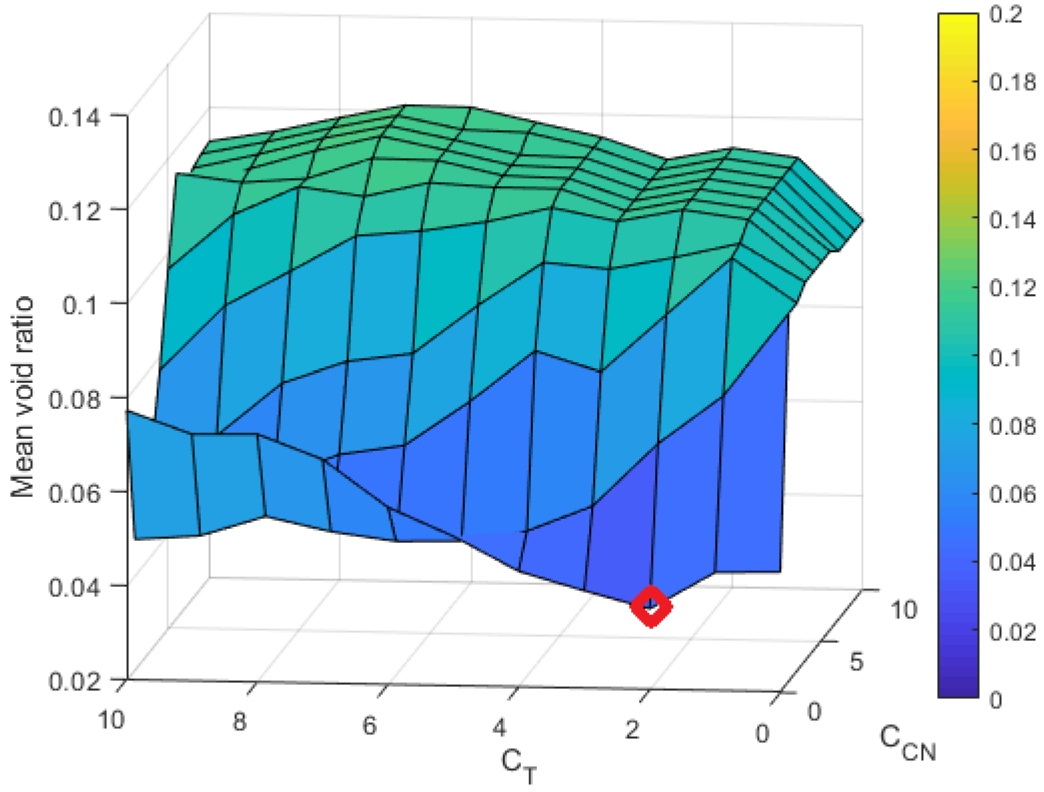

(A)

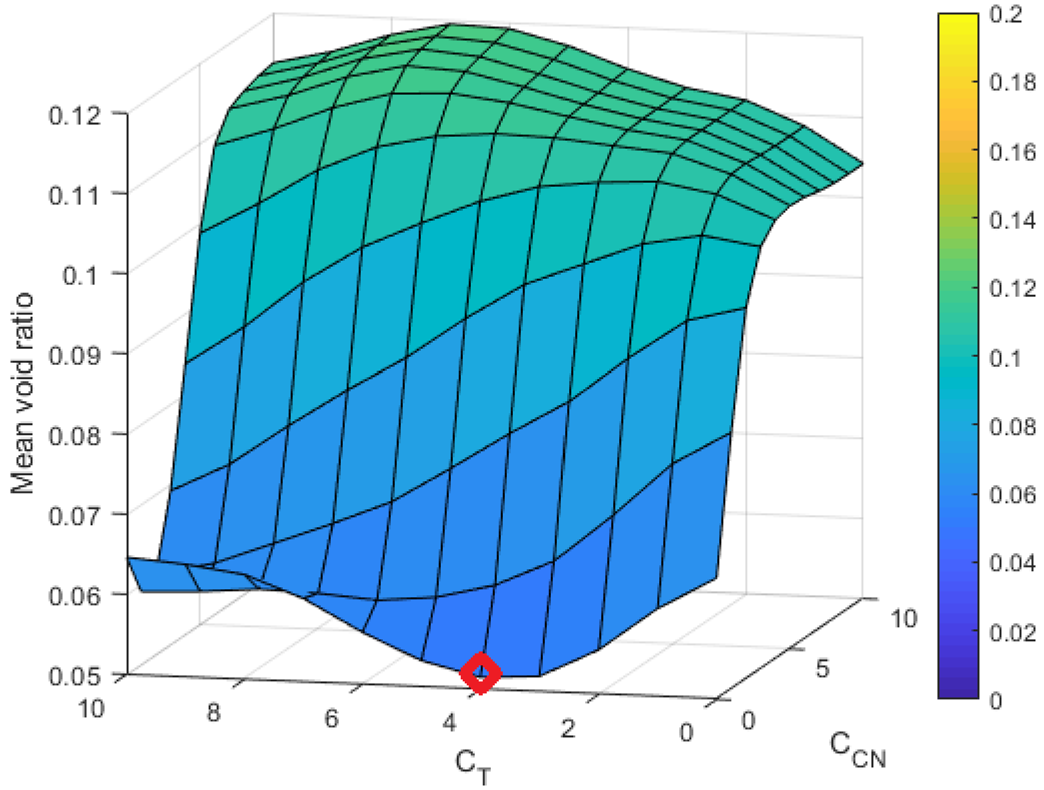

(B)

FIGURE 4.26: Surface plots of MVR results for n=50 in the Tetris Scenario for different C_T and C_{CN} values varied from 0 to 10 at increments of 1 with C_V=1 and C_D=0 for (a) the unfiltered MVR results and (b) the MVR results with Gaussian filter applied.

4.4.5 Effect of Gaussian filter at the Surface Edge

An issue occurs with the data at the edges of the surface plots due to zero-padding when applying the Gaussian filter as described in Section 4.4.3. An example of this is can be seen between Figure 4.30a and Figure 4.31a located in Section 4.4.6. The value at (C_T=0, C_D=0) in Figure 4.30a drops suddenly and indicates a trend towards a minimum value. This value of MVR for the equivalent location in Figure 4.31a does not have as much variance from other values and as a result the drop in the surface is not as pronounced. At edges and corners where the trend of the surface plot is decreasing, the surrounding higher values leads to an overprediction for the datapoint due to the scaling of their effect to avoid zero-padding. As a result, the lowest MVR value may occur at these edges but is unable to be located when Gaussian filter is applied.

It is important to consider these values at the edge as for most of the search areas this can represent where at least one of the coefficients of weighting is zero meaning the omission of that criteria from the objective function. There are two possible solutions. The first is to increase the frequency around the edges of the surface so that there are more values of a similar magnitude when applying the Gaussian filter. However, this will increase computational time.

The second is to expand the datasets to include negative coefficients of weighting values. Figure 4.27 shows an example for the minimum MVR value located for search area where C_V=1 and C_D=3.5 and C_T and C_{CN} were ranged between 0 to 10 at increments of 0.5 and n=9. The surface plot for these results are presented in Figure 5.13a in Section 6. Figure 4.27 extends the search area into negative values for coefficients of weighting as the minimum MVR was located at an edge point. A clear channel has formed in Figure 4.27a for C_{CN}=0 with a big increase in values of MVR for negative C_{CN}. These values are taken into account when the Gaussian filter is applied, and actually the MVR for this region is larger than that displayed in Figure 5.13b for the equivalent location. Therefore, including negative coefficient values whilst still applying the Gaussian filter is not the solution to the problem of analysing values at the edge of the dataset.

Instead, the raw data should be analysed separate to data with Gaussian filter applied for coefficients around the edge of datasets, especially those with zero values for coefficients. Visual inspection of unfiltered datasets are conducted for these areas to ensure that omission of criteria in the objective function is sensible. If a value is located at a non-zero edge, the search area can be expanded to see if the surface plots continue to trend towards an optimal solution outside of the investigated range.

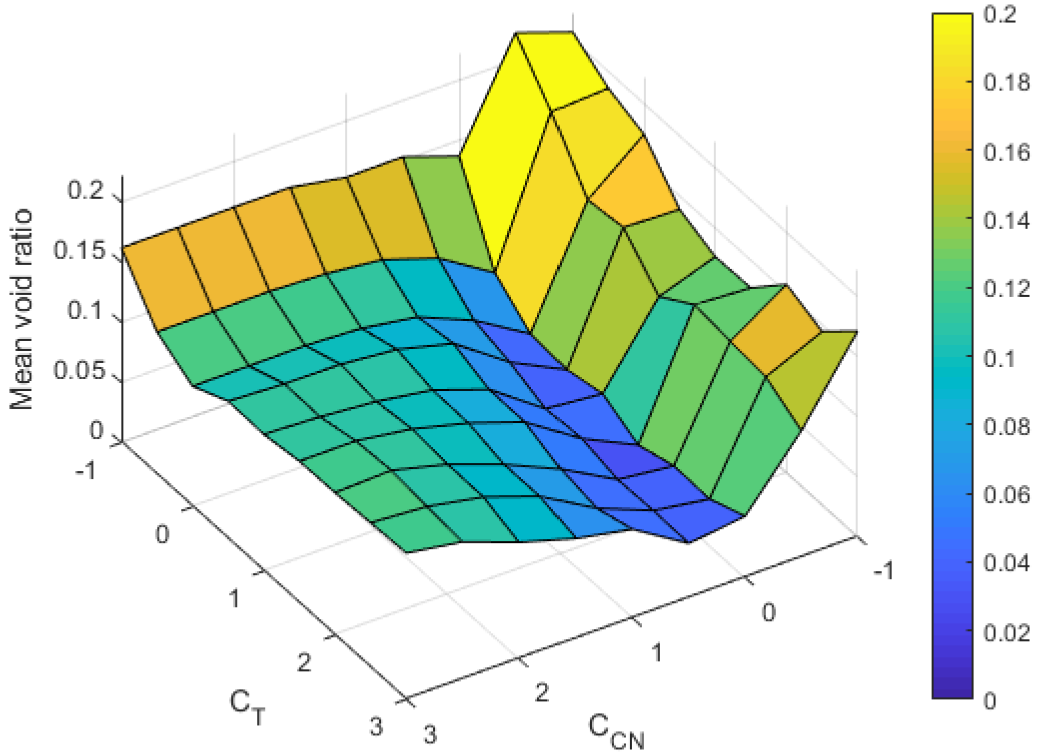

(A)

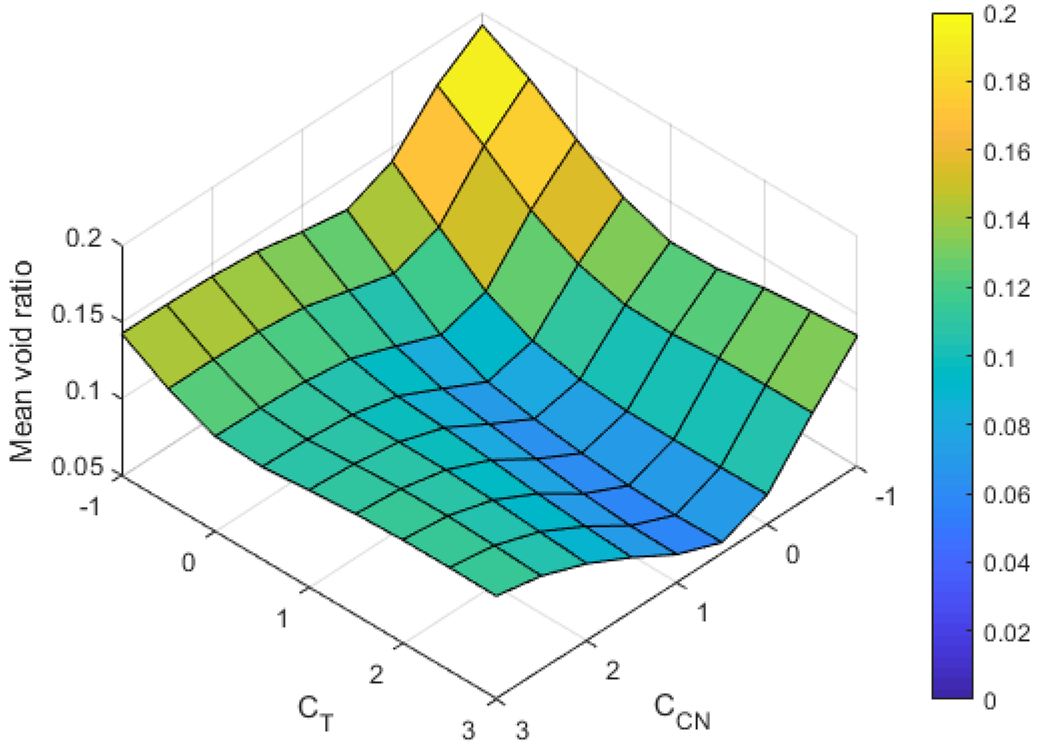

(B)

FIGURE 4.27: Surface plots of MVR results for n=30 in the Tetris Scenario for different C_T and C_{CN} values varied from -1 to 3 at increments of 0.5 with C_V=1 and C_D=3.5 for (a) the raw MVR results and (b) the MVR results with Gaussian filter applied.

4.4.6 Varying Sample Size and Sampling Frequency

Discussed in Section 4.3 is the sample size required to accurately estimate the population data when conducting simulations of packing particles for determining weight coefficients. It was concluded that n=9 can be adopted to get a broad visual of the plots of coefficients whilst n=30 can be adopted for more accurate results areas of interest.

Figures 4.28-4.33 present surface plots of results for mean void ratio for weighted coefficient values of 0-10 for C_D, C_T, and C_{CN} increasing by increments of 1. Three results for C_D are included for values of 0, 5 and 10. C_V is equal to 1 and is kept constant. Figure 4.28, Figure 4.29 and Figure 4.30 present data for n=9, n=30 and n=50 respectively with no filter applied to the surface whilst Figure 4.31, Figure 4.32 and Figure 4.30 present data for n=9, n=30 and $n = 50$ respectively with the Gaussian filter described in Section 4.4.3 applied. The difference between n=9 and n=30 suggests that as the sample size is increased, more features of the surface plot are observed. This is further proved as n is increased to 50. When the Gaussian filter is applied, these features are smoothed and the plots appear more similar. It is clear the minimum void ratio is located in approximately the same area with a trend towards the location (C_T=1, C_{CN}=10) for each plot. As these minimum are located in similar areas, it is justified to use a lower sample size of n=9 for locating the rough area of minima. Any minima missed will be spikes in data. To locate these spikes would require higher sample sizes which in turn leads to longer computational times.

Figure 4.34 and Figure 4.35 show the effect of increasing the sampling frequency. The conditions for sampling are equivalent to the results in Figure 4.28 and Figure 4.31 but with increments of 0.5 between coefficient values. For Figure 4.34 where no smoothing filter is applied to the data surface, more spikes in values from compared to surrounding values are apparent. Applying the Gaussian filter, as shown in Figure 4.35, smooths these spikes and represents data that is more similar to Figure 4.31 with minima being located in roughly the same area again. However, there are more surface features present. From this analysis, it can be concluded that a higher sampling frequency leads to more accurate descriptions for varying weighting coefficients. Again, the increased sampling frequency will lead to longer computational times as more simulations are required due to the larger number of weighting coefficient combinations.

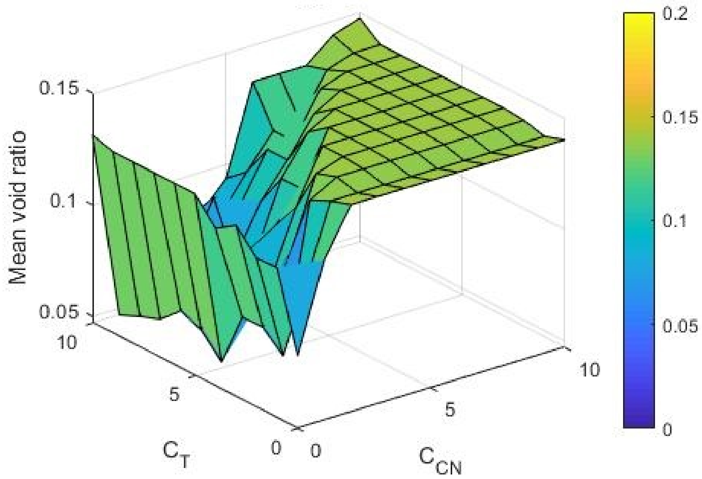

(A) $C_D = 0$

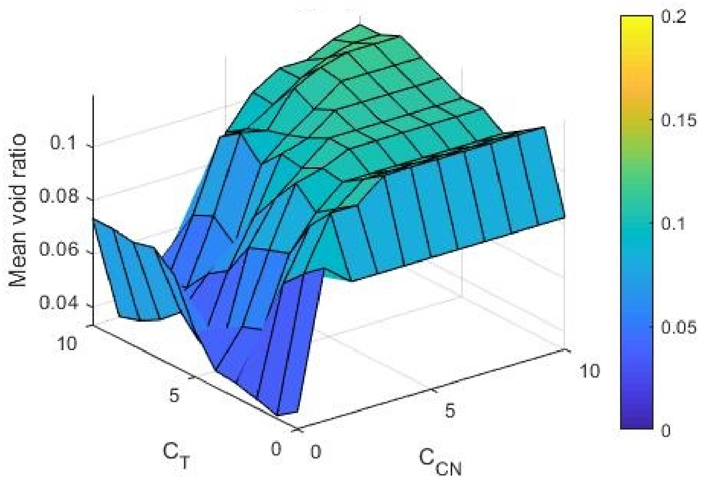

(B) $C_D = 5$

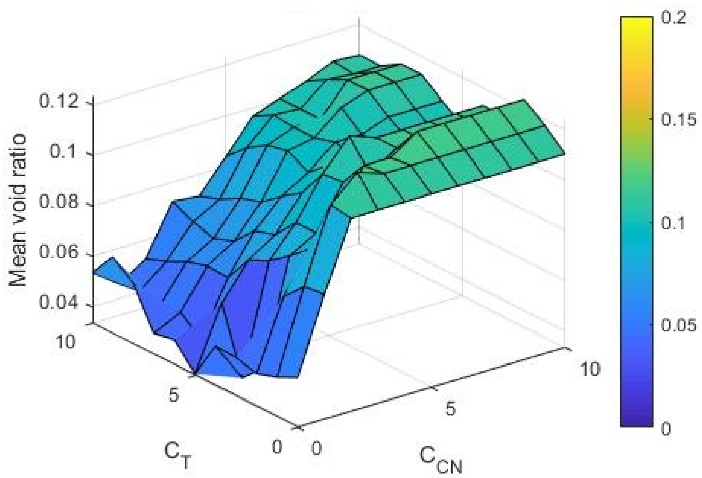

(C) $C_D = 10$

FIGURE 4.28: Surface plot for different coefficients and the resulting mean of the void ratios for n=9 with fixed seed for generating Tetris bag particle ordering with no filter applied ranging from 0-10 for coefficient values.

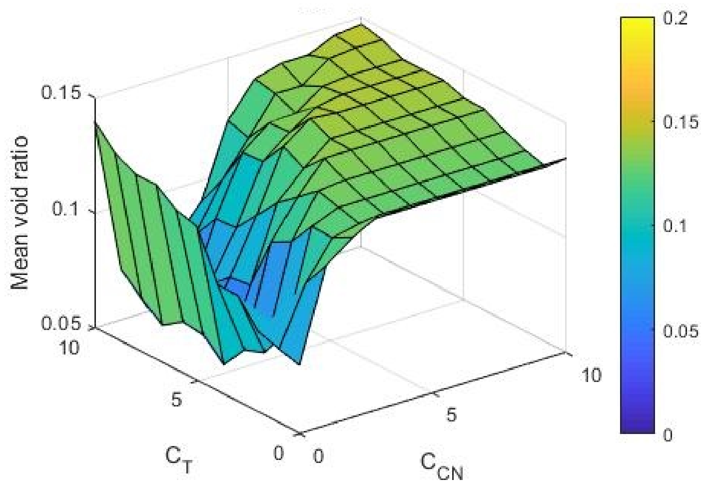

(A) $C_D = 0$

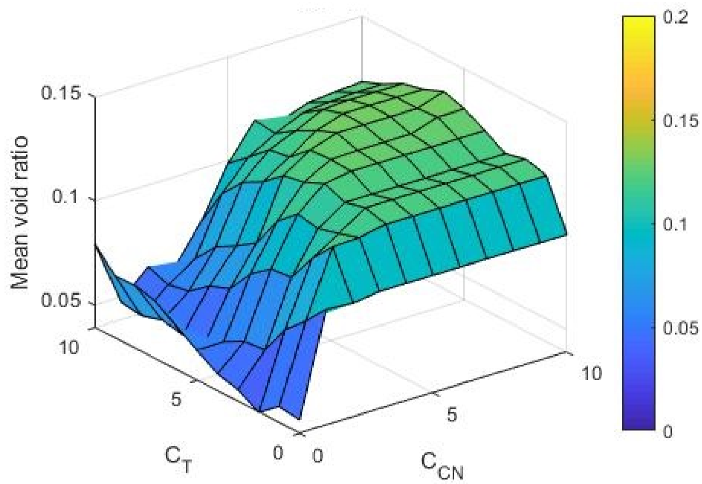

(B) $C_D = 5$

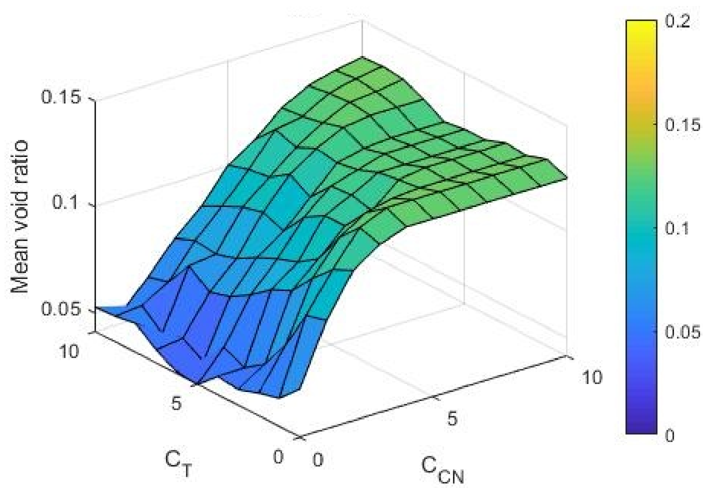

(C) $C_D = 10$

FIGURE 4.29: Surface plot for different coefficients and the resulting mean of the void ratios for n=30 with fixed seed for generating Tetris bag particle ordering with no filter applied ranging from 0-10 for coefficient values.

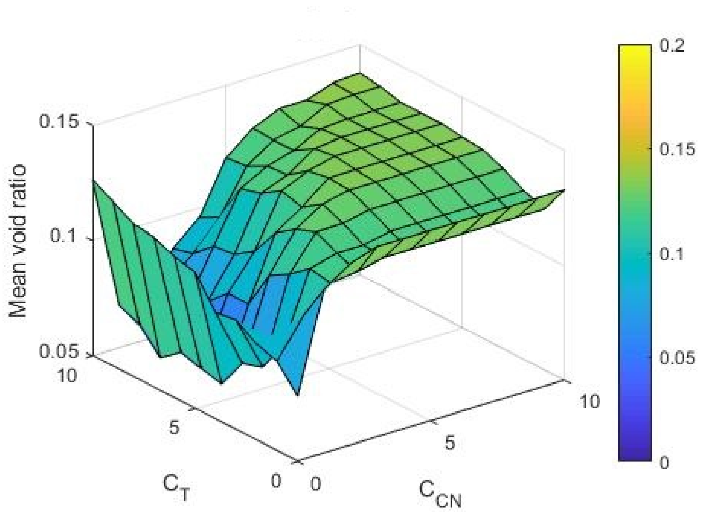

(A) $C_D = 0$

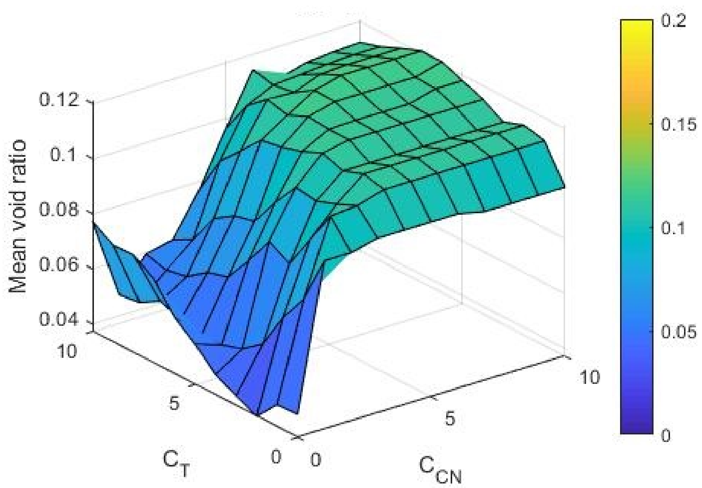

(B) $C_D = 5$

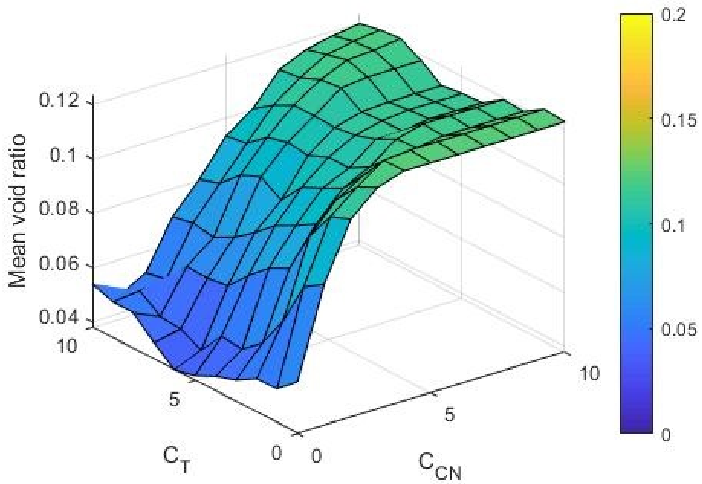

(C) $C_D = 10$

FIGURE 4.30: Surface plot for different coefficients and the resulting mean of the void ratios for n=50 with fixed seed for generating Tetris bag particle ordering with no filter applied ranging from 0-10 for coefficient values.

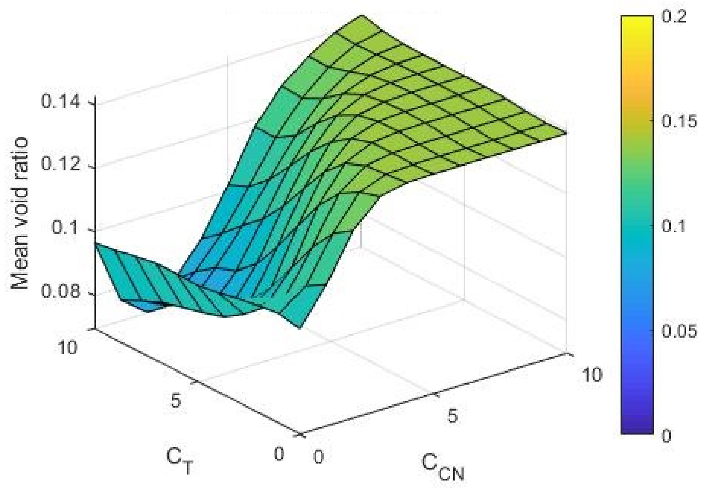

(A) $C_D = 0$

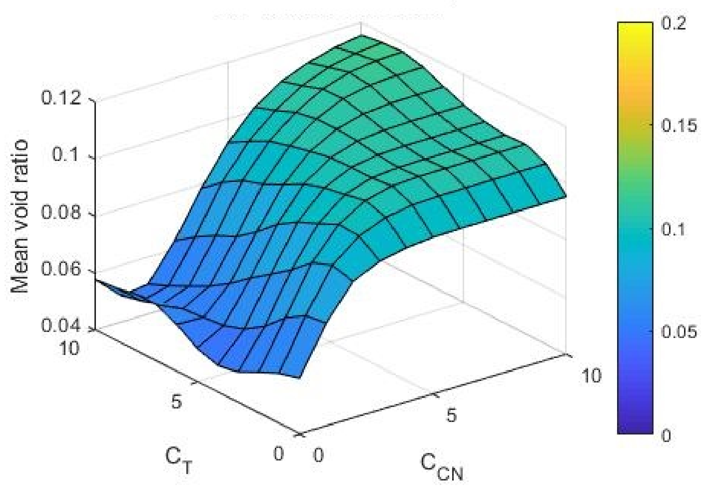

(B) $C_D = 5$

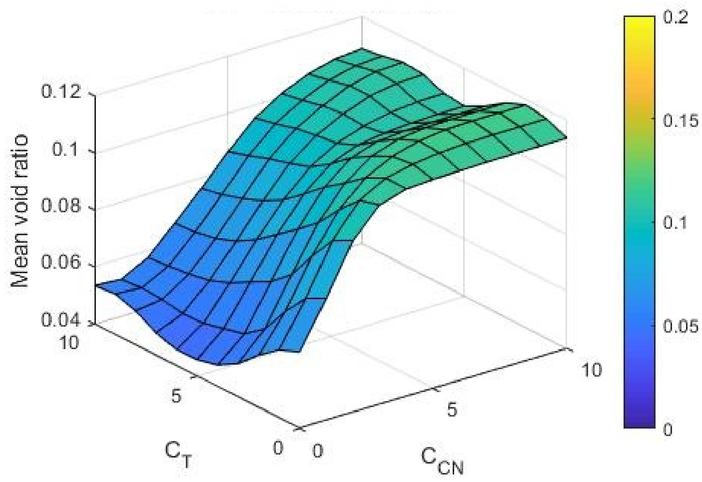

(C) $C_D = 10$

FIGURE 4.31: Surface plot for different coefficients and the resulting mean of the void ratios for n=9 with fixed seed for generating Tetris bag particle ordering with Gaussian filter applied for smoothing ranging from 0-10 for coefficient values.

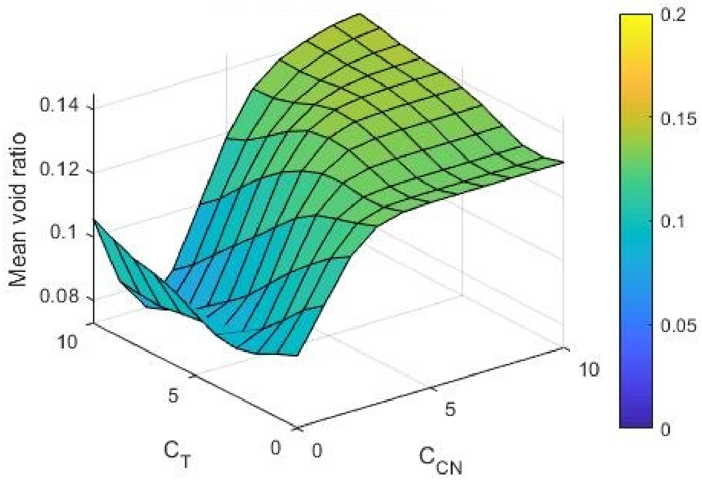

(A) $C_D = 0$

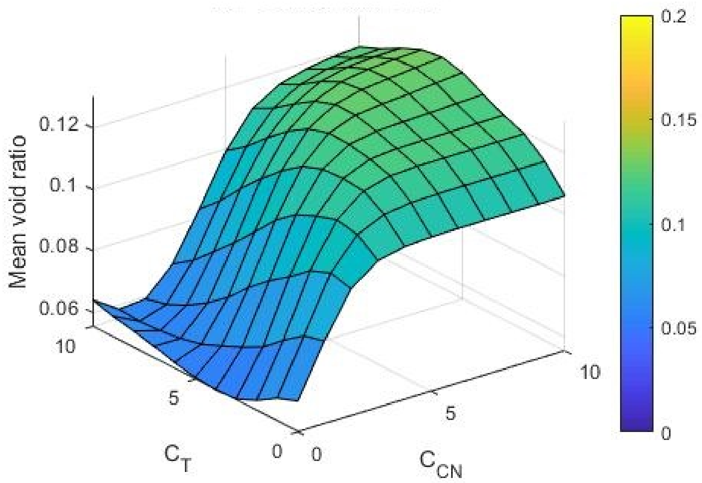

(B) $C_D = 5$

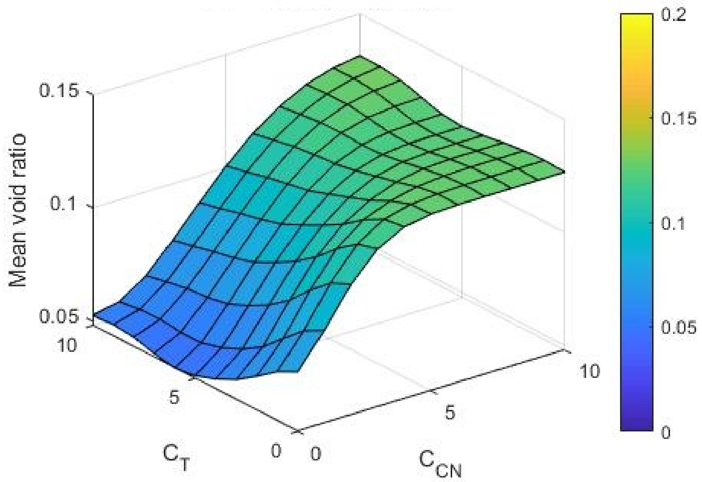

(C) $C_D = 10$

FIGURE 4.32: Surface plot for different coefficients and the resulting mean of the void ratios for n=30 with fixed seed for generating Tetris bag particle ordering with Gaussian filter applied for smoothing ranging from 0-10 for coefficient values.

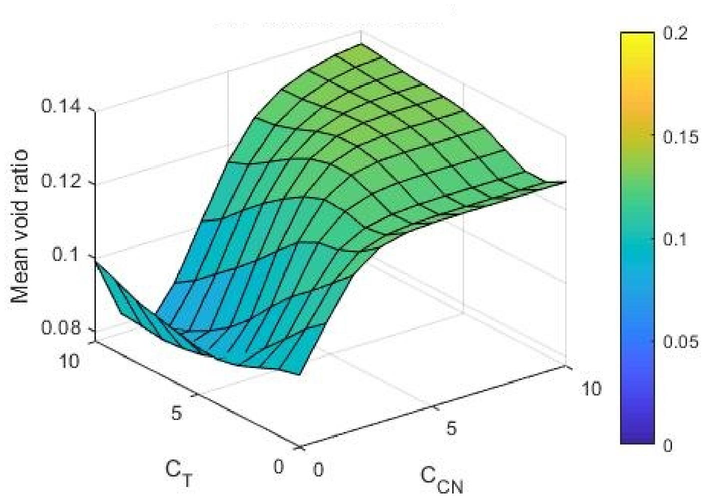

(A) $C_D = 0$

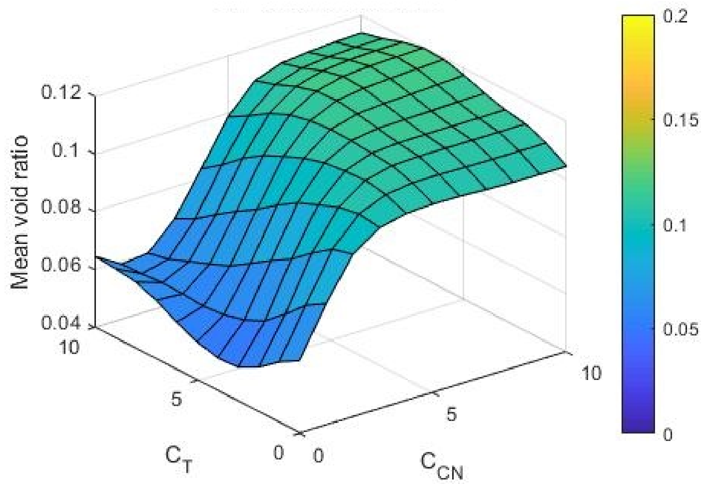

(B) $C_D = 5$

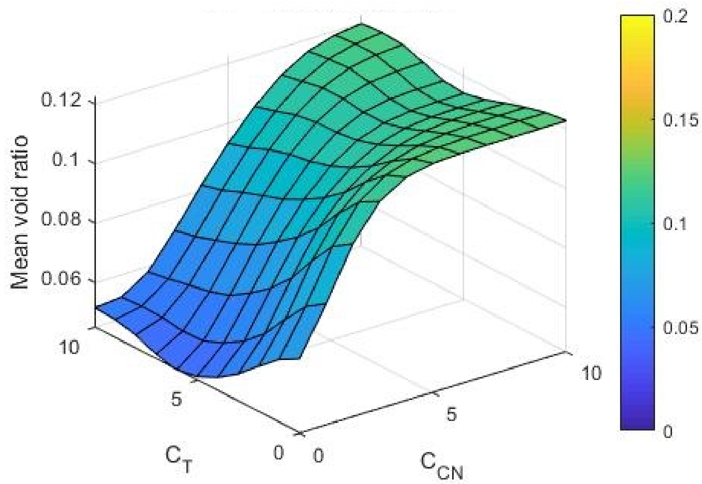

(C) $C_D = 10$

FIGURE 4.33: Surface plot for different coefficients and the resulting mean of the void ratios for n=50 with fixed seed for generating Tetris bag particle ordering with Gaussian filter applied for smoothing ranging from 0-10 for coefficient values.

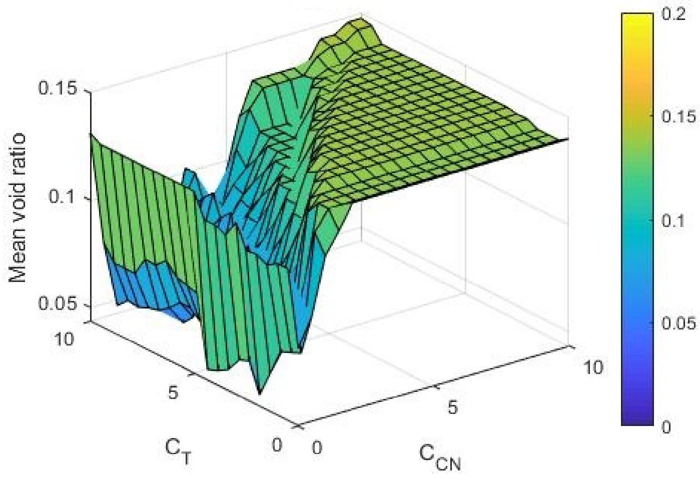

(A) $C_D = 0$

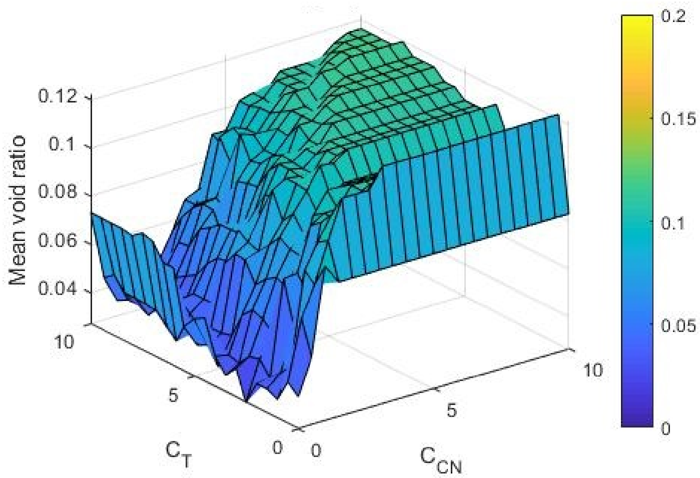

(B) $C_D = 5$

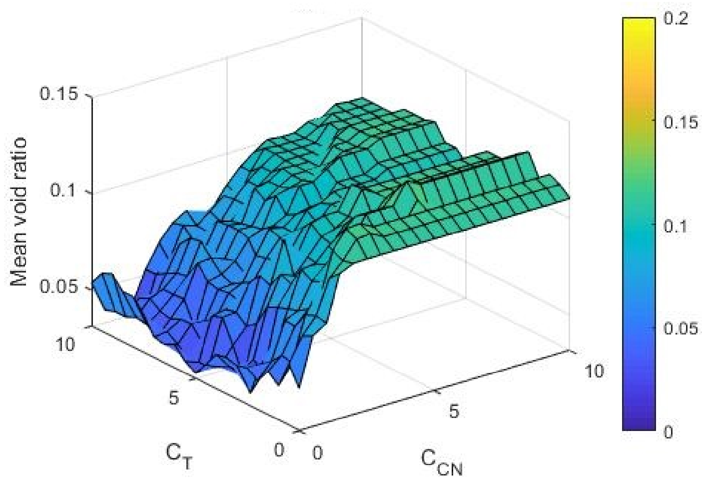

(C) $C_D = 10$

FIGURE 4.34: Surface plot for different coefficients and the resulting mean of the void ratios for n=9 with fixed seed for generating Tetris bag particle ordering with no filter applied ranging from 0-10 for coefficient values with sampling frequency of 0.5 between coefficients.

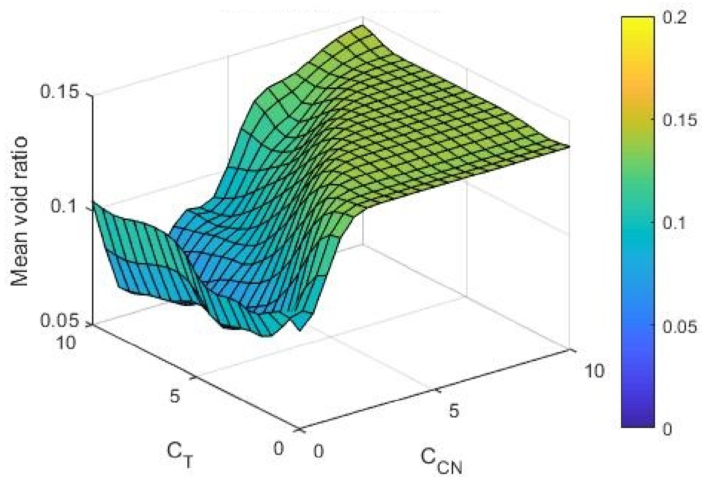

(A) $C_D = 0$

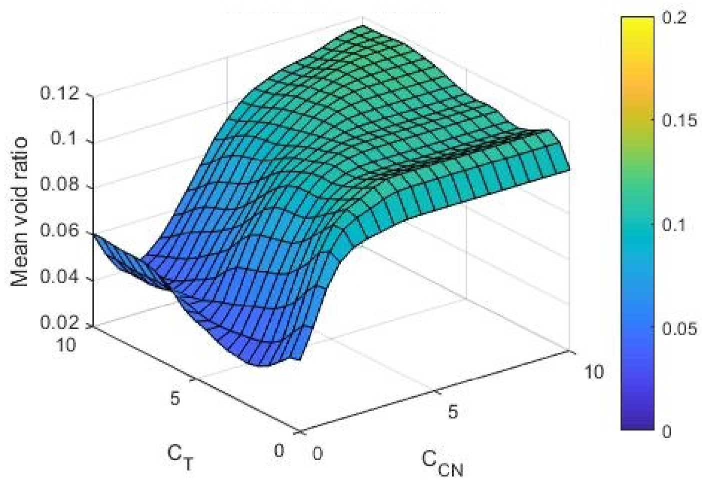

(B) $C_D = 5$

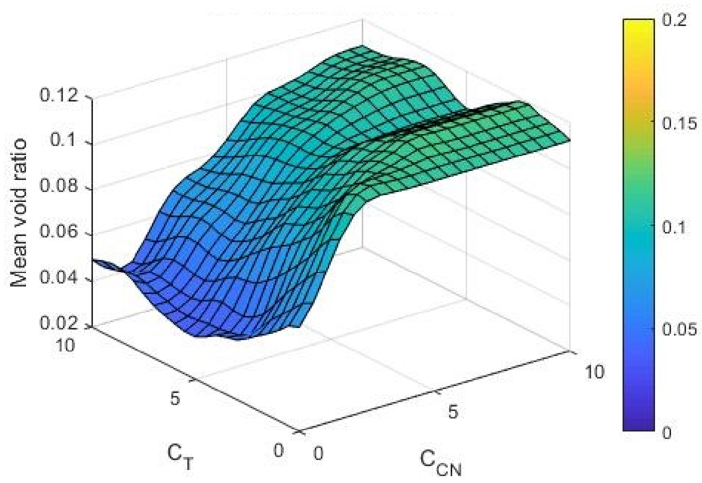

(C) $C_D = 10$

FIGURE 4.35: Surface plot for different coefficients and the resulting mean of the void ratios for n=9 with fixed seed for generating Tetris bag particle ordering with Gaussian filter applied ranging from 0-10 for coefficient values with sampling frequency of 0.5 between coefficients.

4.4.7 Summary

Section 4.4 has described the methodology for the investigation of weighting coefficients in the objective function. The use of a consistent particle order for each combination of weighting coefficients is required as shown in Section 4.4.2. This will produce a random particle order from the Tetris Bag method for each simulation for a set of weighting coefficients but ensure that simulations for all other coefficient combinations are produced using identical particle orders. Implementation of this method removes an extra variable as particle order effects the end result of the packing as particles are packed in the sequence they are delivered to the algorithm in the Tetris Scenario.

Smoothing of the plot was investigated using mean filter and Gaussian filter in Section 4.4.3. It was determined that a Gaussian filter will be adopted due to the decreasing effect of datapoints when moving away from the centre of the filter. The Gaussian filter is described using Equation 4.3 and a 5x5 filter is adopted. If a mean filter was to be adopted, it is suggested that a size of 3x3 is adopted due to each datapoint being of equal weighting when applying the filter. The application of the filter to the search area leads to zero-padding at the edges of these datasets where values are massively underpredicted. As a result, a ratio of the convolution of the MVR and the Gaussian filter to the convolution of a unit matrix to the Gaussian filter can be taken as presented in Equation 4.4. This scales the values in the Gaussian filter for edgepoints so that the sum of filter values is equal to one negating the effect from zeropadding. Section 4.4.4 and Section 4.4.5 explored the effect of the Gaussian filter when applied to surface plots. Section 4.4.4 showed that by applying the Gaussian filter, false optimums which may lead to a optimal solution but will be very sensitive to any type of change to the packing can be avoided. This may lead to missing locations of optimal solutions but it is thought that by increasing sampling frequency these locations will be located. Meanwhile Section 4.4.5 described that even though datapoints at the edge are a fairer visualisation of the actual value compared to when Equation 4.4 is not applied, datapoints located on the edge are still misrepresented and should be analysed by taking the unfiltered data for these areas of the search area. Overall, it is concluded that the Gaussian filter of matrix size 5x5 can be adopted forward but care must be taken with application to the datasets in certain scenarios.

Sample size and sample frequency are both explored in Section 4.4.6. From the analysis of Figures 4.28-4.35 it can be established that larger sample sizes at more frequent intervals between coefficients will lead to a more accurate picture of the mean void ratio surface plots for different combinations of weighting coefficients. However increasing these variables leads to an increase in computational time.

4.5 Process for Locating Optimal Weighting Coefficients

A procedure for the investigation into determining the optimal solution for combination of weighting coefficients for the Tetris Scenario and Soil Particle Scenario is presented in this section to describe to the reader how coefficients of weighting can be determined to find an optimal solution.

For the Tetris Scenario, the objective is to minimise void ratio of the system. Therefore, results of the mean void ratio (MVR) of the packings are taken to indicate the efficiency of the algorithm. The objective in the Soil Particle Scenario is to optimise packing so that a maximum shear strength is achieved. Whilst void ratio can be an indication of shear strength of a structure it is stated it cannot be used to describe the structure alone and that another measure is required (Mogami, 1965). The number of running joints disrupted when filling the domain can be taken as a sign of strength (Vivian, 1976) as discussed in Section 3.10.2. Therefore, both results for MVR and mean number of running joints disrupted (MRJ) are examined for locating the optimal solution. A verification method for testing of shear strength for the produced structures is explored in Chapter 7. Stated in Section 4.4.2 was that a fixed seed is to be used for generating particle order. This is to ensure that packings are conducted with the same particle order delivery to prevent this becoming a study into particle order.

As determined in Section 4.3, a sample size of 30 gives a good estimation for the population of data as has been trialled with the Tetris Scenario. It has been suggested that initial searchs when n=9 are used to explore the results of different combinations of coefficients. Once areas of possible optimal solutions are located, a sample size of n=30 can be utilised as this gives a better representation of the possible results from packing. This is taken forward for the Tetris Scenario. However, the computational runtime for the Soil Particle Scenario is much greater. It is thought that taking samples of nine packings for every combination of coefficients in the search areas will lead to a vast amount of time required. Furthermore, taking n=30 to further define the search area is unfeasible. Therefore, it is suggested a lower sample size is adopted. It can be understood that the packing of tetrominoes will be affected greatly by particle delivery order. For the Soil Scenario, this is not the case as most outlines resemble a similar form and there are no drastic kinks or elbows in the overall shape. As a result, a sample size of n=3 is to be taken for the investigation into the search areas with an increase to value of sample size adopted when locating optimal solutions later on in the investigation.

Initial testing of the algorithm for each coefficient in the objective function is to be completed. Doing so will give an understanding of the effect of each criteria in relation to the overall packing. The method to determine this will be to set all values of coefficients to zero. Then, each criteria can be activated individually by setting its matching coefficient to a value of one. Furthermore, effects of the criteria when it is the dominating parameter in the objective function can be explored by oversizing the coefficient of weighting i.e. ensuring that the product of the criteria and its matching coefficient (for example, $C_V V_{AB}$) is much larger than all other coefficient and criteria products.

From here, the investigation into an optimal solution can begin. To achieve a broad range of coefficient values, the search area from 0 to 10 for each coefficient that is to be varied is explored using relatively large increments between coefficient values. For the cases of the Tetris Scenario and Soil Particle Scenario, it is suggested that a value of 10 is suitable to detect when a scoring criteria becomes dominant in the objective function. Therefore larger values should not be required unless suggested by the search area. If indication of an optimum solution at a larger value for the coefficient is experienced, the range of coefficients past the maximum value will be expanded to investigate this area. Note, C_V is to be fixed at a value of 1 so that this becomes an investigation into three parameters rather than four. Doing so allows for three-dimensional surface plots to be adopted for analysing results. C_V is chosen to be fixed to a value of 1 due to the findings from Section 2.3.7 showing that a low void ratio is an indication of high shear strength.

Areas of interest where an optimal solution can be found are to be refined to better locate this value. This is done in two ways. The first is to increase the sampling frequency to help indicate any solutions that may have been missed due to increments between values being too large. The second is to increase the sampling size so that the MVR and MRJ become more accurate representations of the population. Again, possible optimal solutions can be located in the search areas.

So far, values are searched between 0 to 10 whilst C_V=1. If the score for V_{AB} being larger relative to D, T and CN in the objective function leads to an optimal solution, it is required to explore values where C_V is larger than C_D, C_T and C_{CN}. Hence, the search area between coefficient values of 0 to 1 is explored at an increment of 0.1 and MVR and MRJ values are investigated to locate if an optimal solution lies in this range. Again, areas of interest where optimal solutions can be located should be refined by adopting a higher sampling frequency and a larger sampling size.

Refinement in areas of suspected optimal solutions can be continued until a final solution can be determined. The sensitivity between small changes in coefficient is not yet known so the level of detail required is hard to say. However, from initial studies for the Tetris Scenario it is suspected for Chapter 5 that resulting MVRs will have high levels of sensitivity between coefficient combinations. It is suggested to the reader than refinement can culminate when surround values of the search area do not vary significantly from the optimal solution. In the Tetris Scenario, the minimum difference between the void in the system is one square which relates to a difference of 0.011 if the rest of the domain is assumed to be filled with tetrominoes. Therefore if surrounding values vary less than this, it is suggested that searching for higher accuracies in the value representing coefficients of weighting has become an exercise in superfluity.

Packings of the determined solution should be examined to determine if packings produced do indeed appear to be optimal. A comparison between these and packings which are produced by random placement of particles can be done to show that this does improve packing in terms of the objective. Furthermore, the results can be compared to systems that are packed using the DBL-heuristic described in Section 2.4.3 as a binpacking solution. This will help analyse results against scenarios where particles are placed following a differing controlling factor rather than the controlling factor being randomness. Doing so will provide evidence that the method for packing suggested is an improvement on what exists already.

To summarise the following steps should be taken to conduct an investigation into determining the weighting coefficients for the objective function.

1. Investigate each parameter in the objective function separately.
2. Search areas for coefficients between 0 to 10 at a smaller sample size (n=9 and n=3 for the Tetris Scenario and Soil Particle Scenario respectively) whilst keeping C_V=1 as a constant.
3. Refine the search adopting either a higher sampling frequency or sample size in areas of interest, investigating higher values of coefficients if the analysis of the surface plots suggests an optimal solution could be located past the coefficients already investigated.
4. Search areas for coefficients between 0 to 1 similar to Step 1.
5. Again, refine the search in areas of interest for these plots.

6. Identify possible optimal solutions in the search areas investigated and refine in these areas further to distinguish locations of optimal solutions. It is suggested that refinement can end when differences between surround values are not significant

7. Analyse packing structures to ensure an optimal solution has been found and compare these to results from other methods of packing

4.6 Comparison of Methods to Previous Work

Hoodless and Smith (2023) present results from a very early stage exploration into the coefficients of weight for the developed algorithm for particle placing. As stated in Section 3.12.2, results from Hoodless and Smith (2023) were found using a version of the algorithm which worked in a same manner to the one described in Chapter 3, however with a less-defined manner for determining the stability of particles.

The methods for determining weighting coefficients presented in Hoodless and Smith (2023) differ from those in this chapter. One difference is the use of a fixed seed for random number generation when creating particle order was not adopted. Section 4.4.2 explored the importance of having a fixed seed rather than a random seed. However, as Hoodless and Smith (2023) completed 100 runs for calculation of the final results, it is fair to assume that this represents the population of possible results rather than just a sample of that population.

Another difference in Hoodless and Smith (2023) from that described here is the method in which the coefficients of weighting are determined. In this chapter, the methods described are going to be adopted whilst fixing C_V to a value of 1. Hoodless and Smith (2023) employs a method of initiating each coefficient value separately and determining the effect on the resulting MVRs from 100 runs. Values were changed to see if they have a positive effect on results. Rather than using a search area to investigate the effect of different coefficients as described in Section 4.4, values were changed by small quantities until they no longer have a positive effect on MVR.

Each coefficient is being introduced individually with the absence of a search area of coefficient combinations explored. This created a sort of "settling" of coefficient values around a certain area. For example, Table 5.1 in Section 5.2.2 shows the range of coefficients explored for the results in Figure 5.1. As C_D is activated, a value of C_V=5 is reached. Testing of values away from this number is not performed. Therefore it is clear that the final combination of weighting coefficients being located at a local minimum is possible. This is why the method of plotting MVR as a surface plot as decribed in Section 4.4 with a wide range of coefficient values is adopted to avoid local minima being reached.

Following this method, it is possible that local minima are reached rather than a true minimum value. However, a higher level of precision can be used on the values of weighting coefficient without massively increasing the number of weighting coefficient combinations to be explored. In the methods adopted in this chapter, a higher level of precision is equivalent to increasing the sampling frequency for the surface plots as seen in Section 4.4.6 which leads to longer computational times.

4.7 Summary of Chapter

Determined in Section 4.3 was the methodology to use a combination of smaller sample sizes to create a broad picture of the datasets for the different combination of weighting coefficients before moving to a larger sample size to further analyse areas of interest. Further proof for this is presented in Section 4.4.6 where it was shown that, although larger sample sizes show more features to the surface plot, the general shape of the plots are similar and tend towards a minimum value within the same range of weighting coefficients. As stated in Section 4.3.1, it is common rule of thumb in statistics to take a sample size of 30 to represent a whole population (Chang et al., 2006). Section 4.3.2 investigated the confidence interval for the DBL heuristic and determined in Figure 4.1 that a sample size of n=9 could be taken to gain a general idea of the search area of solutions before refining to n=30. Section 4.3.3 further reinforced this by investigating the results of taking a sample distribution from results of the Tetris Scenario where 1000 runs for the coefficients C_V=1, C_D=0.75 C_T=0.3 and C_{CN}=0.045 were completed. For a 95% CI, n=30 will produce mean results $\pm$0.92 squares of void away from the population's MVR. n=9 produces mean results $\pm$1.6 squares of void away from the population's MVR. Therefore the determined ranges for CI=95% is $\sim$2 and $\sim$3 squares of void produced in the structure for n=30 and n=9 respectively.

Section 4.3.4 explored the effect on increasing the domain size for the Tetris Scenario. Results for void ratio decreased but this is expected as the total solids in the system is increasing whilst the algorithm is still trying to reduce the number of voids. Furthermore, more possible positions leads to more chances of the placed particle not creating voids in the system. Distributions for 10x10 square domains and 20x20 square domains exhibited similar shapes and therefore it is concluded that a 10x10 square domain is of sufficient size although an increase in σ_p is observed showing that a wider variety of results are produced. Any missed features or boundary effects are not necessarily worth the increase in computational time when a 10x10 square sized domain is still suitable. For the Soil Particle Scenario, it is thought a 50x50 unit domain will be large enough as this is roughly equivalent to a 20x20 square domain in the Tetris Scenario.

For the determining of weighting coefficients, Section 4.4.2 showed that a consistent particle order for each combination of weighting coefficients is required, with the particle order being different for each simulation in that weighting coefficients combination. By introducing this, the variable of particle order is removed. An investigation into the particle order is a different focus to the work that is being complete in this thesis and would involve more analysis on the particle shapes used for the outlines that represent irregular, untooled rock.

Smoothing of the curve that represents the search area is completed in Section 4.4.3 through the application of a mean filter and a Gaussian filter. It is determined that the Gaussian filter described by Equation 4.3 should be adopted in this study. The size of this filter is to be a 5x5 matrix. Hence, this will be used when investigating datasets of weighting coefficients. As shown in Section 4.4.3, zero-padding affects the edges of the datasets analysed when a filter is applied. As a result, the convolution of the MVR results and the Gaussian filter can be taken in ratio to the convolution of a unit matrix to the Gaussian filter as described by Equation 4.4. This scales the values in the Gaussian filter for edgepoints so that the sum of filter values is equal to one negating the effect from zeropadding. This resulted in values at the edge in search areas with Gaussian filter applied giving a better representation of the values found in surface plots with no filter applied. The Gaussian filter will be taken forward for the Tetris Scenario. However, it is considered that due to computational times it may not be possible to provide enough datapoints for meaningful application of the filter in the Soil Particle Scenario. If enough datapoints are available for application of a filter, Gaussian filter will be selected. Otherwise, no filter will be applied.

Section 4.4.4 and Section 4.4.5 investigated the effect of applying the Gaussian filter to the surface plots of MVR results for the overall shape and at edgepoints in the dataset respectively. As detailed in Section 4.4.4, application of the Gaussian filter may lead to optimal solutions being missed if sampling frequency is set to be at relatively large increments. However, application of the filter helps prevent locating false optimums where there is high sensitivity of results due to slight changes of coefficient value. With an increased sampling frequency, more datapoints in the search area will lead to a clearer definition of the surface plot and optimal values that may be missed when applying the Gaussian filter will be present. Furthermore, Section 4.4.5 showed that for datapoints at the edge of surface plots the unfiltered datapoint should be analysed as the values present in Gaussian filtered surface plots are affected by a lack of information from the surrounding boundaries. Although Equation 4.4 leads to a better representation of the value that can be found at edges, the value is still a misrepresentation of the true result found at these locations.

As discussed in Section 4.4.6, increasing sample size and the frequency of points at which solutions are found for the search area improves the accuracy of the results. However, increasing these leads to a sacrifice on computational speed as many more simulations of the algorithm are required. Therefore it can be stated that lower sampling frequencies can be adopted when creating a broad picture of the dataset with higher frequencies adopted in areas of interest. Additionally, initial studies can be taken using a lower sampling size before moving forward with a larger sampling size.

The process followed for locating optimal weighting coefficients is laid out in Section 4.5. Here it is described to start with an initial study between coefficient values of 0 to 10 with a smaller sample size and sampling frequency. From here, refinement can be conducted at areas of interest where optimal solutions are suspected by increasing sample and sample frequency. Additionally, coefficients between 0 to 1 should be investigated due to C_V being fixed to a value of one to investigate solutions when $C_V VAB$ has a higher contribution in the objective function relative to other scoring criteria. Again, areas of interest can be searched at a higher sampling frequency and sample size to gain more information about these areas. An optimal solution can be located through further refinement until a suitable solution is achieved. Packing structures can then be analysed and compared to other results and heuristics such as the DBL-heuristic or randomly placed particles.

The methodology outlined in this chapter differs from previous work presented in Hoodless and Smith (2023). In Hoodless and Smith (2023) for the Tetris Scenario, coefficients were varied individually and changed depending on their effect to MVR. As stated it is likely that this falls into a local minimum which the method developed here attempts to avoid.

To summarise the key points of this chapter

- For the Tetris Scenario, sample size of n=9 will be adopted for quick results to get an idea of the results from different weighting coefficient combinations. n=30 will then be used for further details on areas of interest (which is where local minima occurs for the Tetris Scenario).
- Smaller sampling frequencies (so larger increments between values of weighting coefficients) will be used initially with the frequency being increased for further details in areas of interest.
- It has been shown that a domain size of 10x10 squares is suitable for the Tetris Scenario. As the Soil Particle Scenario is filled to halfway up the domain, it is assumed that the equivalent domain size of 50x50 units will be suitable.
- A consistent particle order is used for each combination of weighting coefficients with each simulation in the combination having unique particle orders (unless the particle order generated by the Tetris bag method is repeated). This is achieved by fixing the seed for generating random numbers at the start of the algorithm.
- A Gaussian filter will be used to smooth datasets for the Tetris Scenario when analysing the results. Care is to be taken when identifying values at edge-points.
- Investigation of the search area will start by investigating coefficients in the range of 0 to 10 whilst C_V=1 before refinement at areas of interest where an optimal solution may lie. Additionally, the range between 0 to 1 where $C_V V_{AB}$ has more affect on the objective function are to be investigated and refinement conducted in areas of interest.

It is anticipated that the increased computational runtimes of the Soil Particle Scenario may not allow for a sample size of n=9 and n=30 to be adopted for the collection of results. Additionally, it is unlikely that the sampling frequency will allow for a large range of datapoints in the search area. Therefore application of a filter may be detrimental to analysing the results due to zeropadding and it is also anticipated that this will be omitted from study in Chapter 6. If time allows, these sample sizes will be taken forward and Gaussian filter will be applied to datasets.

Chapter 5

Results of the Tetris Scenario

5.1 Introduction

In this chapter, results of the Tetris Scenario produced by the methods described in Chapter 3 following techniques in Chapter 4 are determined and presented. Section 5.2 describes the results produced in Hoodless and Smith (2023) where combinations of weighting coefficients were varied manually with a sensitivity study being conducted. A minimum outputted void ratio for 100 runs were found for different weighting coefficient combinations and it was determined weighting coefficients of C_V=5, C_D=1.25, C_T=0.4, and C_{CN}=0.01 produced the lowest mean void ratio of all tested combinations. Although this may be a valid result for the minimisation of void ratio in the system, it is possible that this combination is a local minimum and that there could be a more optimised solution. Therefore, the methodology described in Section 4.4 is adopted for determining the optimal combination of coefficients. Whilst C_V is kept constant, a broad range of different combinations of weighting coefficients are tested and results of the mean void ratios are plotted using three-dimensional surface plots for different values of C_D. As determined in Section 4.4, initial samples of n=9 tests are taken before a sample size of n=30 is used for more detailed analysis to find the optimised combination of weighting coefficients for minimum void ratio. The results from Hoodless and Smith (2023) act as verification of the method and the Tetris Scenario is adopted to show that the packing algorithm is effective on a simplified example.

Section 5.3 explores the effect of each scoring criteria in the objective function described in Section 3.5.1. C_V, C_D, C_T, and C_{CN} are each investigated individually in Sections 5.3.2-5.3.5 to determine their influence on placement either as a single criteria or in combination with the other criteria when oversized. This shows the influence of each step in the objective function when packing tetrominoes to minimise voids. The produced packing structures are shown and mean void ratios are presented for the sample size n=30.

Section 5.4 begins the analysis of the produced mean void ratios (MVRs) for different weighting coefficient combinations by ranging coefficients from 0 to 10 for C_D, C_T and C_{CN} as suggested in Section 4.5. C_V is kept at a constant value of one. From here, refinement of the search area is completed for the equivalent ranges by increasing the sampling frequency. A potential area where an optimal solution may be located is highlighted.

From the investigations conducted in the previous section, Section 5.5 refines the sampling frequency down to determine the location of a solution to produce minimum void ratio in the Tetris Scenario. The area of interest is further investigated, as well as the search areas for coefficient values not considered such as much larger (Section 5.5.2) and values where $C_V V_{AB}$ has more of an effect in the objective function by taking values of C_D, C_T, and C_{CN} from between 0 and 1 (Section 5.5.4). Following this, a combination of weighting coefficients is found as a solution to provide optimal packing in the Tetris Scenario. Locations of an optimal solution are suggested at the end of this section.

Section 5.6 displays the packing results of the weighting coefficient combination determined to produce the best packing structures from tetrominoes by the method followed in Section 5.4. These are compared to the packing results from Hoodless and Smith (2023) using the weighting coefficients (C_V=5, C_D=1.25, C_T=0.4, C_{CN}=0.01) as well as another potentially optimal solution that was located for different combination of weighting coefficients. Section 5.7 compares the packings to controls of the DBL heuristic approach to packing and randomly placed particles to show that the algorithm performs better than alternative approaches.

The chapter is summarised in Section 5.8 and the determined combination of weighting coefficients to provide optimal packing structures in the Tetris Scenario is repeated.

5.2 Results of Previous Work

5.2.1 Introduction

Work on the optimal combination of weighting coefficients has been conducted already in Hoodless and Smith (2023). Differences between the method in Hoodless and Smith (2023) and those proposed in Chapter 3 and Chapter 4 are previously stated in Section 3.12.2 and Section 4.6 respectively.

The main difference between Hoodless and Smith (2023) and the work here is that Hoodless and Smith (2023) employs a method of initiating each coefficient value separately and determining the effect on the resulting MVRs from 100 runs. Values were changed to see if they have a positive effect on results. Rather than using a search area to investigate the effect of different coefficients as described in Section 4.4, values were changed by small quantities until they no longer have a positive effect on MVR. As described in Section 4.6, this can lead to a higher precision for the values of the coefficients. However, it is possible that the resulting weighting coefficients provide results for a local minimum and that the true minimum has been missed. Therefore, the methods described in Chapter 4 are adopted in this study to try and avoid this possibility.

Section 5.2.2 discusses the results achieved in Hoodless and Smith (2023) for the different coefficients of weighting explored. As stated, the combination of weighting coefficients determined as the optimal solution was C_V=5, C_D=1.25, C_T=0.4, and C_{CN}=0.01. This is most likely to occur at a local minimum and further study of the search area is required.

5.2.2 Weighting Coefficient Combination

Figure 5.1 presents the results from Hoodless and Smith (2023) as violin plots with the mean, median and quartiles for the 100 runs indicated on the each plot. Table 5.1 indicates the relating combinations of weighting coefficients for each labelled plot.

As shown in Figure 5.1, the void ratios produced by just the inclusion of C_V have a much larger range than those with the inclusion of other weighting coefficients. By also introducing a non-zero value for C_D the maximum void ratios reached for the 100 simulations tested massively reduces. This is thought to be due to the decrease in chance of canyoning during packing as is highlighted in Section 5.3.3

From analysis of Figure 5.1, it is determined in Hoodless and Smith (2023) that C_V is the largest coefficient of those explored followed by C_D. C_{CN} is the smallest of the weighting coefficients. This is due to the fact that the score for D in the objective function from coordination number is much larger compared to other contributors to scoring of placement as this is measured by the number of touching particles whilst the other scoring methods are measured as a ratio.

Hoodless and Smith (2023) determines that combination O is the optimal weighting coefficient combination from those explored in the paper. As stated in Hoodless and Smith (2023), combination O gave the highest frequency of results closest to zero void ratio. This is represented by the overlying box plot that shows the mean, median and lower quartile values being closer to zero void ratio than combinations A-H. The mean is lower than values for the similar plots of combinations K-P. Therefore, the determined coefficients are C_V=5, C_D=1.25, C_T=0.4, and C_{CN}=0.01.

Letter	C_V,C_D,C_T,C_{CN}	Letter	C_V,C_D,C_T,C_{CN}
A	1,0,0,0	I	5,2,0.4,0
B	1,1,0,0	J	5,2,0.4,1
C	1,2,0,0	K	5,2,0.4,0.01
D	2,1,0,0	L	5,2,0.4,0.05
E	5,2,0,0	M	5,2,0.4,0.02
F	5,2,1,0	N	5,1,0.4,0.01
G	5,2,2,0	O	5,1.25,0.4,0.01
H	5,2,0.5,0	P	5,1.75,0.4,0.01

TABLE 5.1: Values of coefficients for data plotted in Figure 5.1.

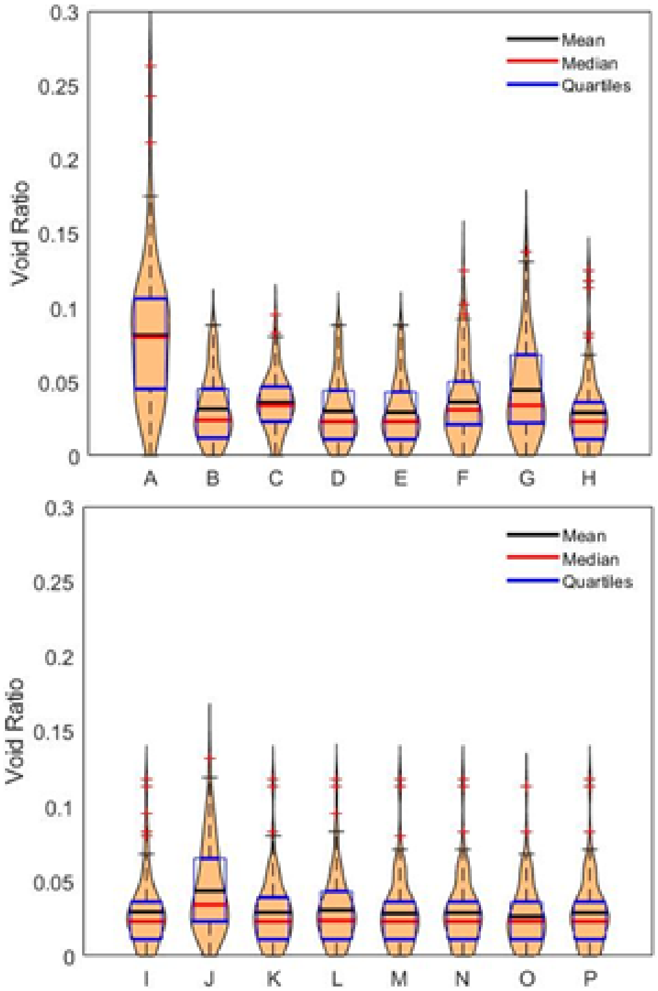

FIGURE 5.1: Violin plots for results of 100 runs for the packing of tetrominoes for different coefficients of weighting combinations with mean, medium and quartiles indicated on the plot. Results originally presented in Hoodless and Smith (2023).

5.3 Effects of Changing Coefficient Values

5.3.1 Varying Coefficients

In this section, an investigation into the effect of each coefficient on the final void ratio of the structures for the Tetris Scenario is investigated. The effect of each coefficient is explored as a collective in Figure 5.2 which shows the results of mean void ratio derived using a sample size of n=30. Separately, each coefficient of C_D, C_T, and C_{CN} is varied from 0 to 10 at increments of 1 whilst the other coefficients are kept at a value of 1. For all the results in Figure 5.2, C_V=1 and was set as a constant. The results of each criteria in the objective function are discussed in relation to the other criteria. MVR results of each variable when oversized - this is to say that the value of the coefficient is set to be very large whilst all other coefficients remain constant at a value of 1 - are expected to be where values plateau if Figure 5.2 was to continue to infinity. These values are presented in Table 5.2.

Additionally, each criteria was tested independently with no effect of other criteria to investigate their individual effect of determining placement of tetrominoes. This is done by activating each coefficient individually by setting it to a value of 1 whilst all other coefficients are kept at a zero value. Results of these are presented in Figures 5.4-5.8 with the MVR for a sample size of n=30 presented for each in Table 5.2.

Variable activated	MVR	MVR (Oversized)
V_{AB}	0.0797	0.0396
D	0.1067	0.0983
T	0.1564	0.1282
CN	0.3878	0.1275

TABLE 5.2: Mean void ratios for a sample size of n=30 for the individual criteria of the objective function either as a single variable or when the variable is oversized to be 100 whilst all other variables are set to 1.

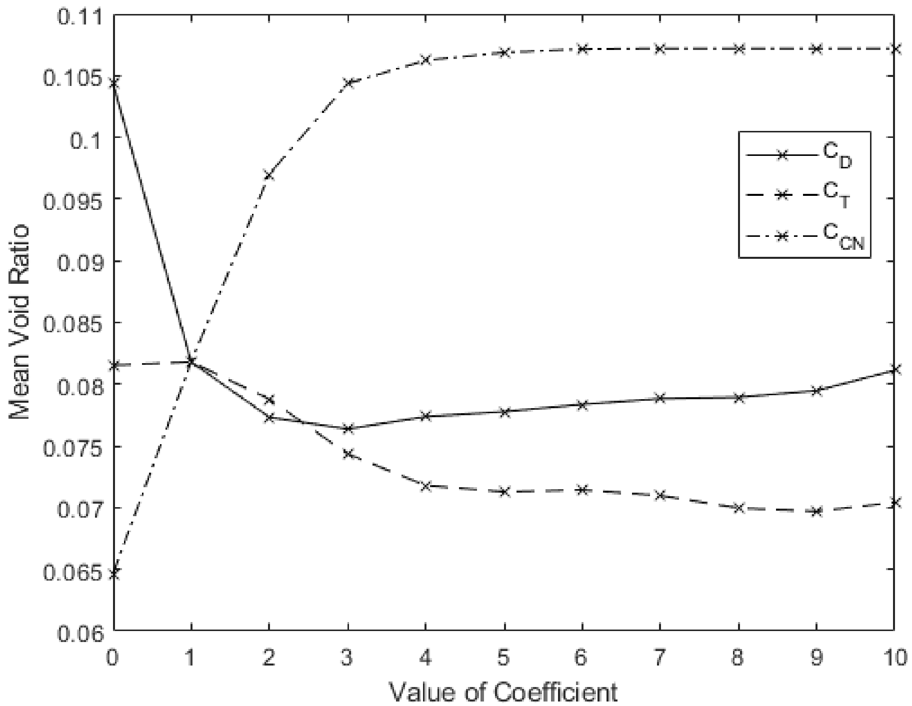

FIGURE 5.2: Values of mean void ratio for the varying of coefficient values. Each value of coefficient varied from 0 to 10 at increments of 1 whilst the rest are fixed at a value of 1. C_V=1 for all plots. Gaussian filter applied to data.

5.3.2 Effect of V_{AB}

It is planned that C_V=1 is taken as a fixed value for all other coefficients to be standardised against. Therefore, it is required to ensure that C_V has a positive effect on minimising void ratio. Figure 5.3 shows the effect of C_V by investigating resulting mean void ratios for when C_V is zero or a non-zero value. The MVR in Figure 5.3 indicates the lowest possible mean void ratio for each combination of weighting coefficients trialled when C_V is fixed and C_D is the value indicated by the x-axis. C_T and C_{CN} were ranged from a value of 0 to 10 at an increment of 1 between coefficient values. The coefficients for this resulting MVR are presented in Table 5.3. MVR is consistently lower for the scenario where C_V=1 and therefore it can be concluded that V_{AB} has a positive effect in the objective function for minimising void ratio. Clearly this is logical as it introduces a criteria for positioning that is equivalent to to the desired outcome.

If V_{AB} is separated to be the only variable in the objective function (i.e. C_V=1 and all other weighting coefficients are set to zero) then placements are being scored only for creating no space beneath them. Figure 5.4 shows an example of this. In the figure particles are numbered in the order for which they were placed with 0 indicating the first tetromino. From analysis of the particle order, voids appear in the system where the tetromino being placed must create void regardless of the final position in the domain. Although a different particle could have filled these spaces, there is no permutation of particle sequence for the tetromino to be swapped for another. Additionally, to the right of the domain it can be seen that canyoning has occurred. As no particle fits within this canyon, placements that cap this area will create void a large amount of void. Therefore, other positions are prioritised. As the domain fills up with particles, this canyon on the right of the domain grows in size to the point where a particle placement here will create a much greater amount of void in comparison to being placed there earlier. A Bar tetromino would fill this gap, but this is not the next particle to be produced in the particle order. Instead a LK tetromino is attempted for placement which cannot fit in the remaining space. The previous B-tetromino to be placed was Particle 11 which was used to fill the space to the left of the domain where another canyon had formed. An additional heuristic is required to fill these spaces and avoid this situation.

Note, a suitable placement of Particle 6 in Figure 5.4 would have been to the right of Particle 5 and rotated by 90^o as this would have filled this space whilst creating no voids. The Tetris Scenario was tested before the ordering of potential placements was introduced (described in Section 3.7.3). Therefore, the identification of the bottom-left most position has not been included in the code and rather the first position to produce the lowest score is selected. This tends to be to the left of the domain rather than towards the bottom and the first orientation tested is prioritised. Introducing the bottom-left heuristic to determine between jointly scored positions would produce better results to the programme as a Tetris solving algorithm. This is equivalent to introducing a slight scored for D by making C_D a non-zero value which is much less than C_V.

It was thought that the inclusion of D in the objective function will automatically solve this issue as deeper locations will be chosen, however the case of all coefficients being of zero value except C_V has highlighted that this will only be the case if C_D is a non-zero value. This is shown in Figure 5.5 where C_D, C_T, and C_{CN} are designated as a value of 1 and C_V=100 to create an oversizing effect on V_{AB} in the objective function. The particle delivery order to the programme is identical to Figure 5.4. More particles are placed in the system as the programme ends when the next particle cannot be placed (so Figure 5.4 terminated earlier than Figure 5.5). As can be seen, the canyonying effect that is seen in Figure 5.4 no longer occurs. Additionally, the decrease for MVR when n=30 presented in Table 5.2 shows that the introduction of the other variables in the objective function have a positive effect on creating low-void structures in the Tetris Scenario.

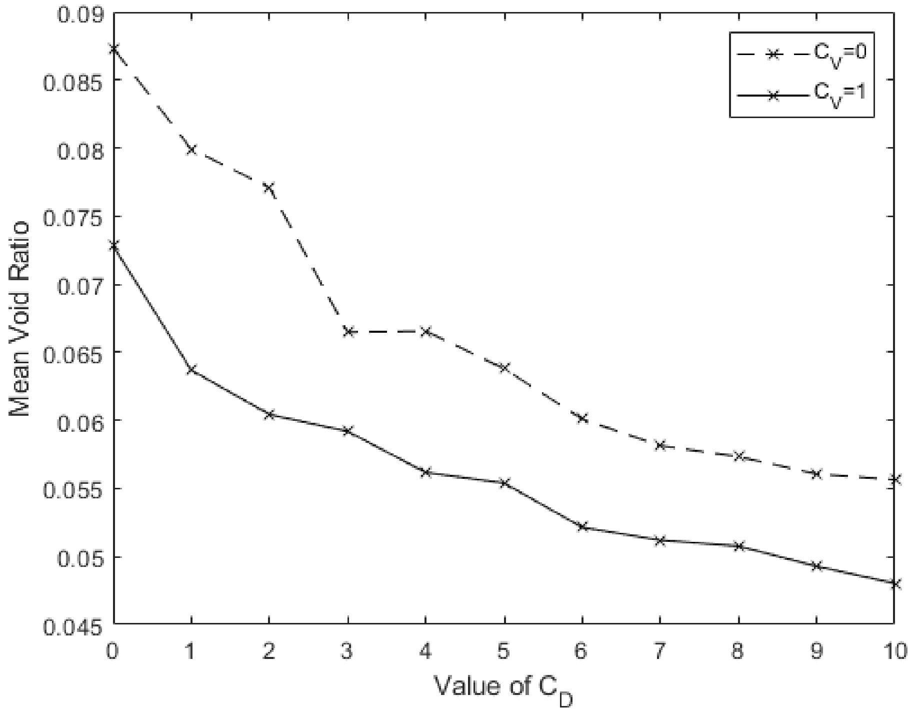

FIGURE 5.3: Lowest MVR value from surface plots of coefficients C_T, C_{CN} and mean void ratio for different C_D values with $C_V = 0$ and $C_V = 1$ represented. C_D, C_T, C_{CN} between 0 to 10 by increments of 1. Gaussian filter is applied to results.

C_V	C_D	C_T	C_{CN}	MVR	C_V	C_D	C_T	C_{CN}	MVR
0	0	10	2	0.0873	1	0	10	2	0.0728
0	1	10	2	0.0799	1	1	0	0	0.0637
0	2	8	1	0.0771	1	2	0	0	0.0604
0	3	8	1	0.00665	1	3	2	0	0.0592
0	4	9	1	0.0666	1	4	3	0	0.0562
0	5	5	0	0.0638	1	5	4	0	0.0554
0	6	5	0	0.0601	1	6	4	0	0.0521
0	7	7	0	0.00581	1	7	5	0	0.0512
0	8	7	0	0.00573	1	8	5	0	0.0508
0	9	6	0	0.00561	1	9	5	0	0.0493
0	10	9	0	0.0556	1	10	6	0	0.0480

TABLE 5.3: Combinations of weighting coefficients that resulted in the lowest MVR values for the data presented in Figure 5.3 for unfiltered data (left) and Gaussian filtered data (right).

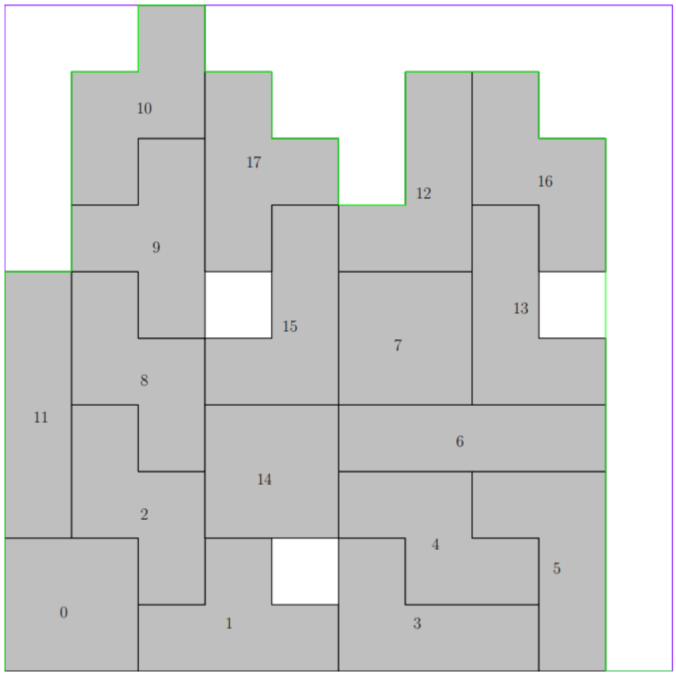

FIGURE 5.4: Results of the algorithm in the Tetris Scenario for weighting coefficients of C_V=1 and C_D=C_T=C_{CN}=0. Void ratio of the system is 0.042.

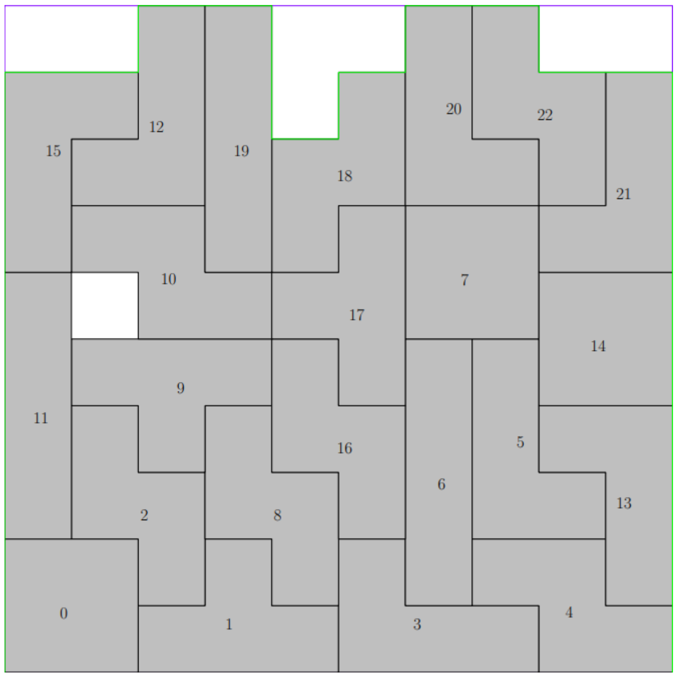

FIGURE 5.5: Results of the algorithm in the Tetris Scenario for weighting coefficients of C_V=100 and C_D=C_T=C_{CN}=1. Void ratio of the system is 0.011.

5.3.3 Effect of D

Figure 5.6 presents the results of packing a particle order produced by the Tetris bag method equivalent to Figure 5.4 where D is the only variable activated in the objective function. As expected, tetrominoes are packed at the lowest point possible in the domain. As depth is calculated by the centre of gravity of the particle, orientations of particles are selected which are "bottom heavy". For example, Particle 1 is a T-tetromino placed with a base of 3 squares touching the base of the domain. This is not due to any need to minimise void ratio but rather because the central point of the particle is lower than the other three possible orientations. Additionally, B-tetrominoes like Particles 6, 11 and 19 prioritise being placed flat rather than length ways. Almost the opposite problem to Figure 5.4 is occurring as there is no possibility of canyons forming. Therefore, B-tetorminoes will not get chance to fill these sorts of gaps.

As indicated in Table 5.2, MVR is again reduced with the inclusion of other variables with C_D=100 set to oversize the effect of D. However, the reduction to void ratios produced is not as dramatic as with V_{AB}.

With relation to the other variables in the objective function, D appears to have a positive effect in terms of minimising void ratio. Figure 5.2 indicates this as MVR decreases between C_D=0 to around C_D=3. From here, the value fluctuates a little but it can be determined by the value of MVR for when D is oversized in Table 5.2 that MVR will tend to a value of 0.095.

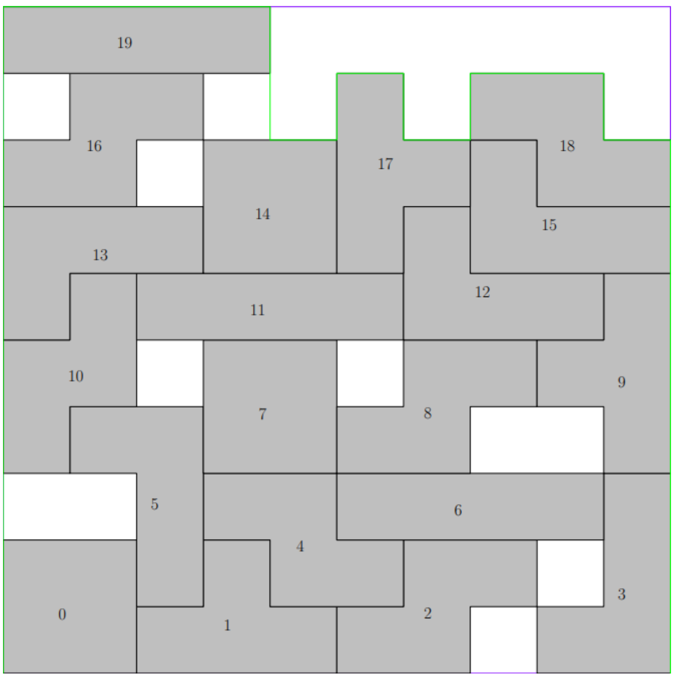

FIGURE 5.6: Results of the algorithm in the Tetris Scenario for weighting coefficients of C_D=1 and C_V=C_T=C_{CN}=0. Void ratio of the system is 0.138.

5.3.4 Effect of T

T in the objective function applies a score for positions that produce the most contact area with other tetrominoes or the domain boundary. Figure 5.7 presents the results for a case where C_T=1 and C_V=C_D=C_{CN}=0 for the equivalent particle order as Figure 5.4. Particles are placed in the system to optimise contact with other particles. However, some positions clearly do not provide the most contact area.

For example, the placement of Particle 6. Particle 6 produces much more contact area with Particles 1, 2 and 4 if rotated by 90^o to its current orientation. The reasoning for placements such as this are due to T being defined as the ratio of coordinates in contact with the placement surface to the total coordinates that make up the bottom of the particle. For Particle 6, its current position produces a value of T equivalent to 1 as all coordinates of the bottom outline are in contact with the placement surface. If the particle is placed at the proposed rotation of 90^o, an overhang will occur meaning that the produced value of T is less than 1. In this way, T almost acts as another V_{AB} variable as if a T value of 1 is produced, then the value of V_{AB} will also be 1 as no void is created below the particle. This was previously suggested in Section 3.5.4. In canyoning scenarios like that in Figure 5.4, T will not be able to account for the area of void created below the particle, so it is more likely that a position above such a canyon is selected. This could be beneficial as it may avoid canyoning occurring in the system whilst a detrimental effect may occur if a particle is placed over the canyon once it has built up.

Again, MVR is reduced with the inclusion of other variables when T is oversized by applying coefficients of C_T=100 and C_V=C_D=C_{CN}=1. Although there is a noticeable difference in the void ratios, the value is not reduced as much as with V_{AB}. As stated for V_{AB}, the inclusion of the other variables counters the canyoning effect from occurring. T does not have an issue with canyoning as the quantity of void created below the particle is not took into account when scoring the placement. Therefore, the reduction in MVR is not as significant as this issue is not being resolved in the same way that it is with oversizing V_{AB}.

Evidence for T acting as an alternative V_{AB} value is present in Table 5.3. When C_V=0, higher values of C_T are acquired for the combination that produces the lowest MVR. Therefore it can be concluded that T is being used as a substitute version of V_{AB} in the objective function to result in lower void ratios. This would also explain why MVR values are higher when C_V=0 due to, as previously discussed, T not considering the quantity of void being created beneath the particle when determining placement. Therefore earlier on in the packing, tetrominoes may be placed that avoid creating void but then later on cap these areas regardless of the size of void created below.

When combined with the other variables in the objective function, Figure 5.2 shows that MVR decreases as C_T increases until a value of 8. From here, MVR starts to increases slightly. It is thought from the oversizing of C_T in Table 5.2 that this will continue to increase until a value of around 0.12. This is due to the effect of T outweighing that of V in the objective function meaning that overhangs and capping of canyons are more likely to occur. Initially, between C_T=0 to C_T=1, it appears that T causes a slight increase in void ratio of the packed systems. It is thought that this is due to V having more effect in the scoring of placement so more canyoning is occurring before the effects of D, T, and CN overcomes this.

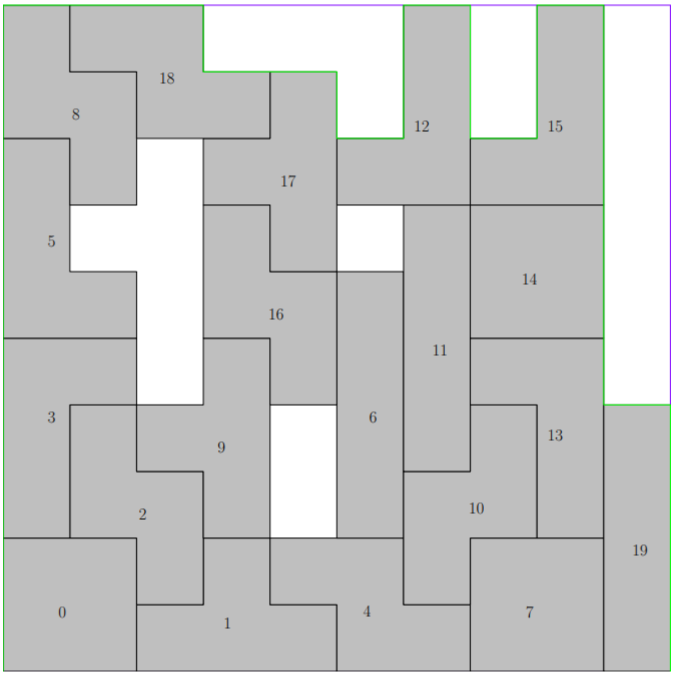

FIGURE 5.7: Results of the algorithm in the Tetris Scenario for weighting coefficients of C_T=1 and C_V=C_D=C_{CN}=0. Void ratio of the system is 0.10.

5.3.5 Effect of CN

The effect of activating CN as a single variable in the objective function is shown in Figure 5.8. Again, the particle order delivered to the algorithm is the same sequence as that in Figure 5.4 The positioning of particles to prioritise coordination number can be seen to be quite detrimental to the packing in terms of minimising void ratio. Large gaps appear as particles are placed that give overhangs. This is partially due to the lack of ordering potential placements and particles that have equivalent scores are being placed by the first location found to produce that score.

As with C_V, the inclusion of other variables in the objective function leads to much improved results. Figure 5.9 presents the same packing for C_{CN}=100 and C_V, C_T and C_{CN} set to values of 1 to create an oversizing effect for CN in the objective function. Fewer gaps and overhangs are produced by the algorithm and it is presented in Table 5.2 that the MVR is much lower when the other variables are included in the objective function.

From Figure 5.2, it appears as though increasing the effect of CN has a detrimental relationship on MVR produced. The value of MVR increases before becoming a constant value of 0.115 for C_{CN}=5 and higher. The constant MVR past C_{CN}=5 is due to CN having no larger impact on the objective function. It can be considered that CN has become the dominant factor when determining positioning of the tetromino. At some value for the coefficient, each of C_D, C_T, and C_{CN} will become the dominant factor in the objective function if all other coefficients are kept as 1. CN achieves this at a lower value for C_{CN} due to coordination number being a much larger value than scorings for V, D, and T. Although the coefficient value for which this occurs has not been investigated for each parameter, the score for MVR in Table 5.2 when each coefficient is oversized individually gives the MVR that is produced when each variable is dominant. It should be noted that the difference in values of MVR past

C_{CN}=5 and the value in Table 5.2 are due to the Gaussian filter being applied to the data presented in Figure 5.2.

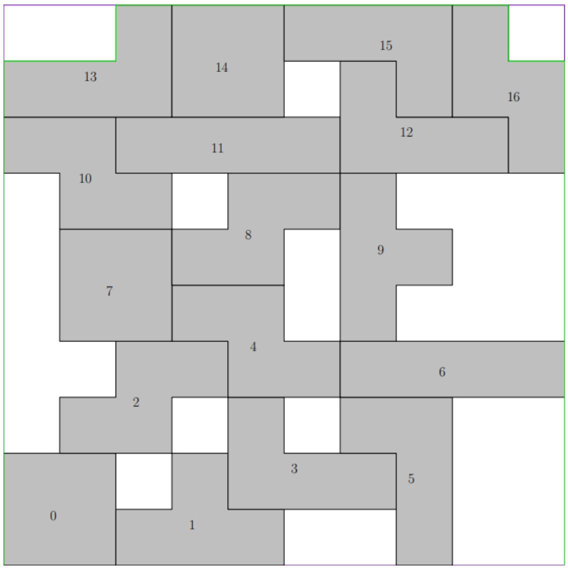

FIGURE 5.8: Results of the algorithm in the Tetris Scenario for weighting coefficients of C_{CN}=1 and C_V=C_D=C_T=0. Void ratio of the system is 0.426.

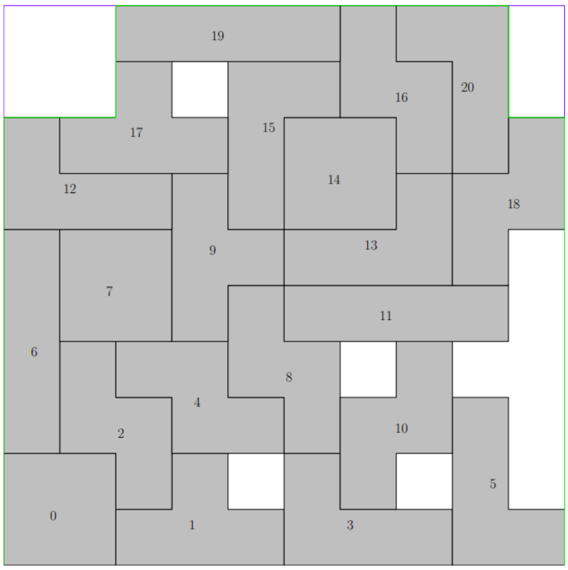

FIGURE 5.9: Results of the algorithm in the Tetris Scenario for weighting coefficients of C_{CN}=100 and C_V=C_D=C_T=1. Void ratio of the system is 0.119.

5.4 Analysing Results for Different Weighting Coefficient Combinations

5.4.1 Initial Study

Presented in this section are results from surface plots of MVR for different combinations of weighting coefficients. As Chapter 4 involved analysing the nature of these results, some additional information is already known when these tests may not have been completed if the task was being started again. For example, data for a sample size of n=50 were presented in Figures 4.30 and 4.33 in Section 4.4.6 when it has been determined that a maximum sample size of n=30 is sufficient. Advantage will be taken of this already produced data for determining the weighting coefficient combination for producing minimum void ratios in the Tetris Scenario rather than dismissing these trial tests.

As stated in Section 4.5, the study is to begin by conducting a search between coefficient values of 0 to 10 for C_D, C_T and C_{CN} whilst C_V is kept to a constant value of 1. Figure 5.11 presents the lowest MVR achieved for different values of C_D when C_T and C_{CN} were varied between 0 to 10 at increments of 1 whilst C_V is kept at a constant value of 1. Results are presented for the data with Gaussian filter applied as described in Section 4.4.3 as well as with the exclusion of the filter. Lower MVRs are achieved earlier in the plot at lower values of C_D for the data with no filter applied whereas when the Gaussian filter is adopted the MVR tends to continue to decrease as C_D increases. It is clear from the unfiltered data that 10 is a reasonable range of coefficients to go up to as the results show no signs of producing MVRs as low as located at C_D=1. However, a study into coefficients greater than this range is conducted in Section 5.5.2 as proof of this theory. This is present for the Tetris Scenario because of the faster computational speed for packings to be completed and is not repeated for the Soil Particle Scenario.

The difference between MVR results in Figure 5.11a and Figure 5.11b suggest that application of the Gaussian filter is leading to an optimal solution being missed in the range of C_D=1 which can be detected for the unfiltered data. Section 5.4.2 investigates changing the sampling frequency for the whole of the already explored search areas. However, it is to be highlighted that Figure 5.11a indicates a potential optimal solution at C_D=6 whereas none would be identified for an area around C_D=1.

Results of for n=9, n=30 and n=50 for coefficients in the range of 0 to 10 whilst C_V=1 have already been collected from the work done in Chapter 4 when determining a methodology for the identifying the combination of weighting coefficients that lead to an optimal solution. Consideration of the difference in value of MVR achieved for sample sizes of n=9 and n=50 shows that results with n=9 are lower than those for n=50. The explanation for this trend is that the particle orders produced in the first nine tests is a sequence that leads to tighter packing on average compared to the particle orders produced by the Tetris bag method after this. As n=50 is greater than the determined value of n=30 for representing the population data, it can be concluded that the MVRs produced in Figure 5.11b are a fairer representation of the void ratios that can be produced than those in Figure 5.11a.

As for when n=30, Figure 5.10 shows the values of lowest MVR found in the surface plots for this sample size. When compared to Figure 5.11b, it can be concluded that the layouts are similar, especially for the Gaussian filtered data. Therefore, this confirms that it is justified to take a sample size of n=30 as determined in Section 4.3.

Table 5.4 contains the coefficients of weight for which these minimum MVR values were found. These are equivalent to the coefficient combinations presented in Table 5.3, again confirming that n=30 is a reasonable sample size to employ.

Note that Figure 5.10 and Figure 5.11 show the lowest MVR value for surface plots of different C_D values in the same range of C_T and C_{CN} of between 0 and 10. These lowest MVR values do not necessarily relate to being located at the same C_T and C_{CN} and could in fact be located at opposite sides of the surface plot. Proof of this can be seen in Table 5.4 where the location of the lowest MVR values for each surface plot is presented. This is highlighted here as similar plots are seen throughout this thesis when locating optimal coefficient values. Furthermore, on each figure two results are presented. These are the lowest MVR values for when Gaussian filter is applied and for when no filter is applied. It can be seen that the lowest MVR values when Gaussian filter is applied are typically higher than when no filter is applied. The nature in which the Gaussian filter affects the surface plots is to remove any big spikes in data to avoid areas of sensitivity as described in Section 4.4.4. Therefore it is expected that the lowest MVR value when Gaussian filter is applied would be larger than when no filter is applied as the Gaussian filter is reducing the size of any spikes in the data. Again, this is to prevent the optimum coefficients of weighting location being determined in an area of high sensitivity where a slight change in coefficient could greatly affect the produced results.

C_V	C_D	C_T	C_{CN}	MVR
1	0	10	2	0.0711
1	1	0	0	0.0632
1	2	0	0	0.0590
1	3	2	0	0.0559
1	4	3	0	0.0539
1	5	4	0	0.0515
1	6	4	0	0.0490
1	7	5	0	0.0479
1	8	5	0	0.0471
1	9	5	0	0.0461
1	10	6	0	0.0448

TABLE 5.4: Combinations of weighting coefficients that resulted in the lowest MVR values for the Gaussian filtered data presented in Figure 5.10.

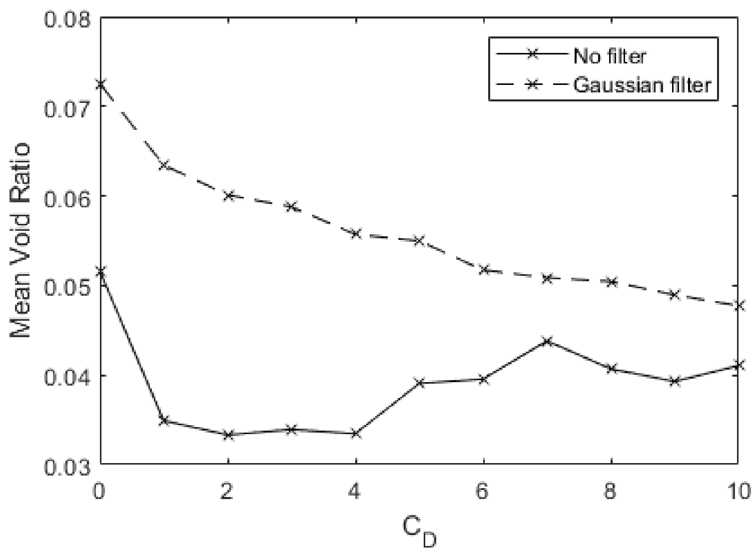

FIGURE 5.10: Lowest Mean Void Ratio achieved for different combinations of weighting coefficients for C_V=1 and C_D, C_T and C_{CN} varied from 0 to 10 at increments of 1. Data is presented as the lowest MVR for the given C_D value. Sample size of n=30.

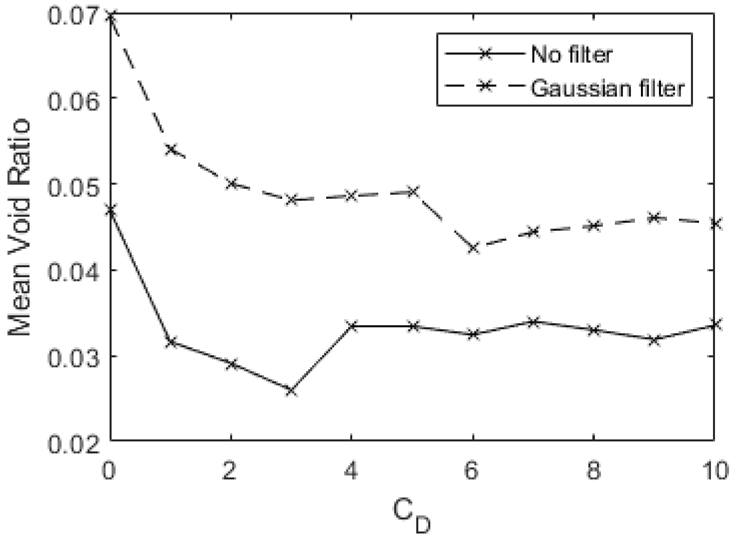

(A)

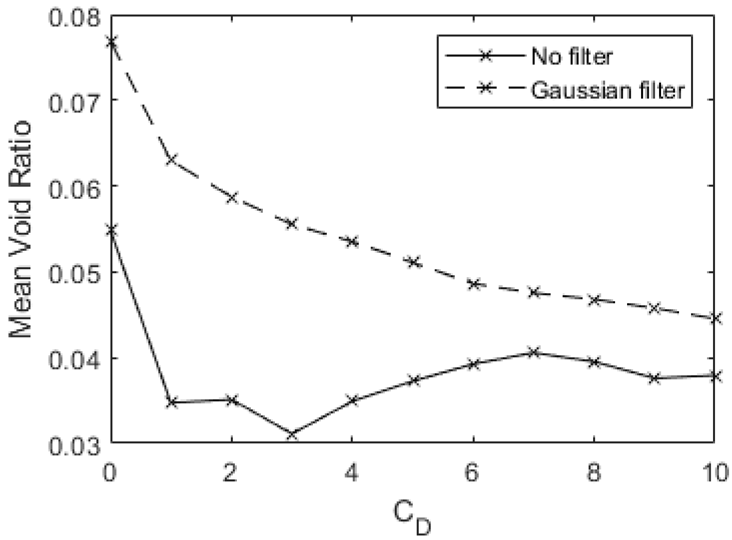

(B)

FIGURE 5.11: Lowest Mean Void Ratio achieved for different combinations of weighting coefficients for C_V=1 and C_D, C_T and C_{CN} varied from 0 to 10 at increments of 1. Data is presented as the lowest MVR for the given C_D value. Sample size of (a) n=9 and (b) n=50 for the Tetris Scenario is presented for data with no filter applied and Gaussian filter applied.

5.4.2 Increasing Sampling Frequency

The lowest MVRs achieved for different C_D values for a sampling frequency of 0.5 are seen in Figure 5.12. Coefficients C_D, C_T, and C_{CN} were varied from 0 to 10 whilst C_V was kept at a constant value of 1. The produced MVRs are lower than that in Figure 5.11a due to the higher frequency of datapoints. The greater number of solutions investigated has led to definition of more of the search area and location of lower MVRs have been found. Furthermore, the increase in datapoints leads to the Gaussian filter being applied to surrounding values which are more similar to the datapoint being analysed in terms of magnitude than previously as increments between coefficients of weighting are smaller. With an increase in frequency it is expected that there is an increase in accuracy. The filter being applied to values which are more similar will not affect the determination of suitable weighting coefficients.

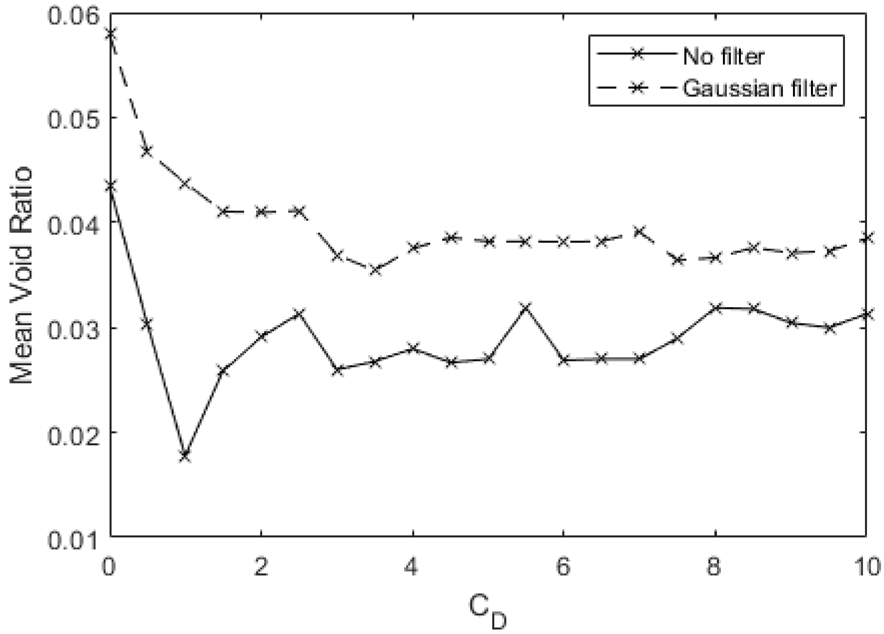

FIGURE 5.12: Lowest Mean Void Ratio achieved for different combinations of weighting coefficients for C_V=1 and C_D, C_T and C_{CN} varied from 0 to 10 at increments of 0.5. Data is presented as the lowest MVR for the given C_D value. Sample size of n=9 for the Tetris Scenario is presented for data with no filter applied and Gaussian filter applied.

In Figure 5.12, the lowest MVR appears at C_D=1 for the data with no filter applied whereas this occurs at C_D=3.5 when a Gaussian fitler is applied. Figure 5.13 shows the plots of coefficients C_T and C_{CN} for when C_V and C_D=1. As can be seen, the lowest MVR for Figure 5.13a is located at a spike downwards for coefficients of (C_T=0.5,C_{CN}=0). As discussed in Section 4.4.4, this sudden drop in results means that this point is sensitive to any change. Additionally, the sample size of n=9 means that this is not a full representation of the whole population data as discussed in Section 4.3. A higher sampling size for the search areas presented in Figure 5.13 was not complete due to computational times required to collect this data as the range of coefficients is large.

The variability in results are highlighted in Figure 5.15a where the general trend of the data is for MVR to decrease as C_{CN} decreases. However, clear spikes in the results are present in this surface. Again, this is most likely due to a small sample size of n=9 being selected. As demonstrated in Section 4.4.4 and Figure 5.15b, the Gaussian filter accounts for these variabilities.

From analysis of Figure 5.12, it is suggested that the combination of weighting coefficients that leads to an optimal scoring technique for packing tetrominoes to minimise void ratio is in the range of C_D=3.5. Figure 5.14 presents the surface plots of this coefficient range. Both Figure 5.14a and 5.14b have a minimum value located in the same location at (C_T=2.5,C_{CN}=0). This agrees with the hypothesis proposed in Section 4.4.4 that by selecting the lowest possible MVR for data with the Gaussian filter applied then this should lead to a suitable result for the equivalent combination of coefficients for the data with no filter applied. Therefore, values for C_V, C_D, C_T, and C_{CN} of 1, 3.5, 2.5 and 0 respectively appear to be an optimal solution

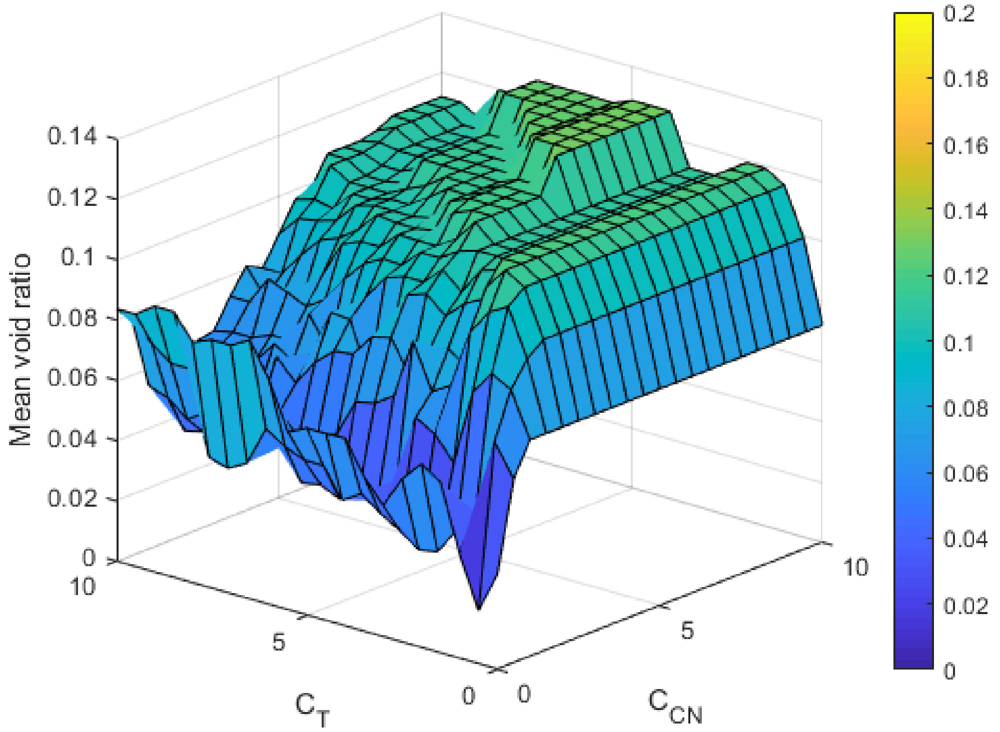

(A)

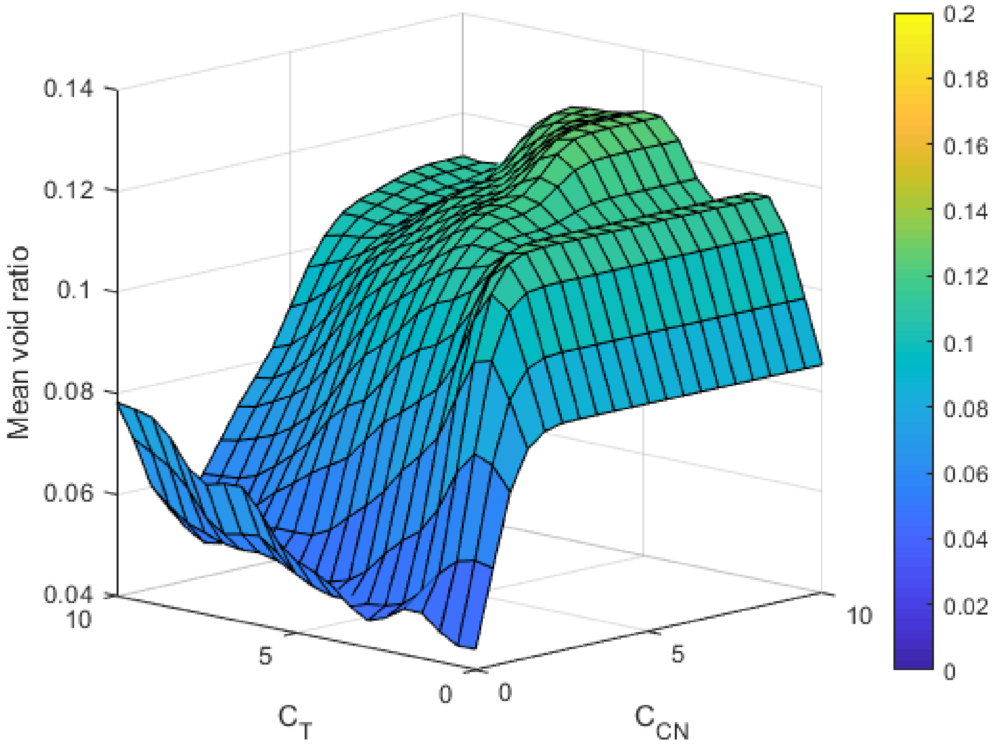

(B)

FIGURE 5.13: Surface plots of MVR results for n=9 in the Tetris Scenario for different C_T and C_{CN} values varied from 0 to 10 at increments of 0.5 with C_V=1 and C_D=1 for (a) the raw MVR results and (b) the MVR results with Gaussian filter applied.

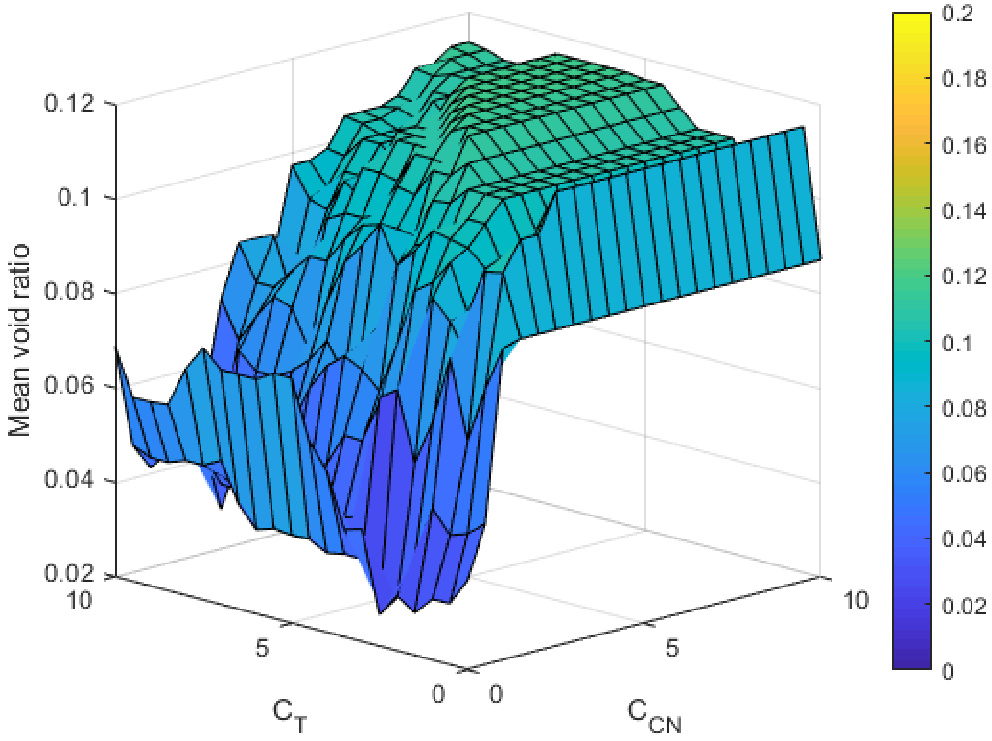

(A)

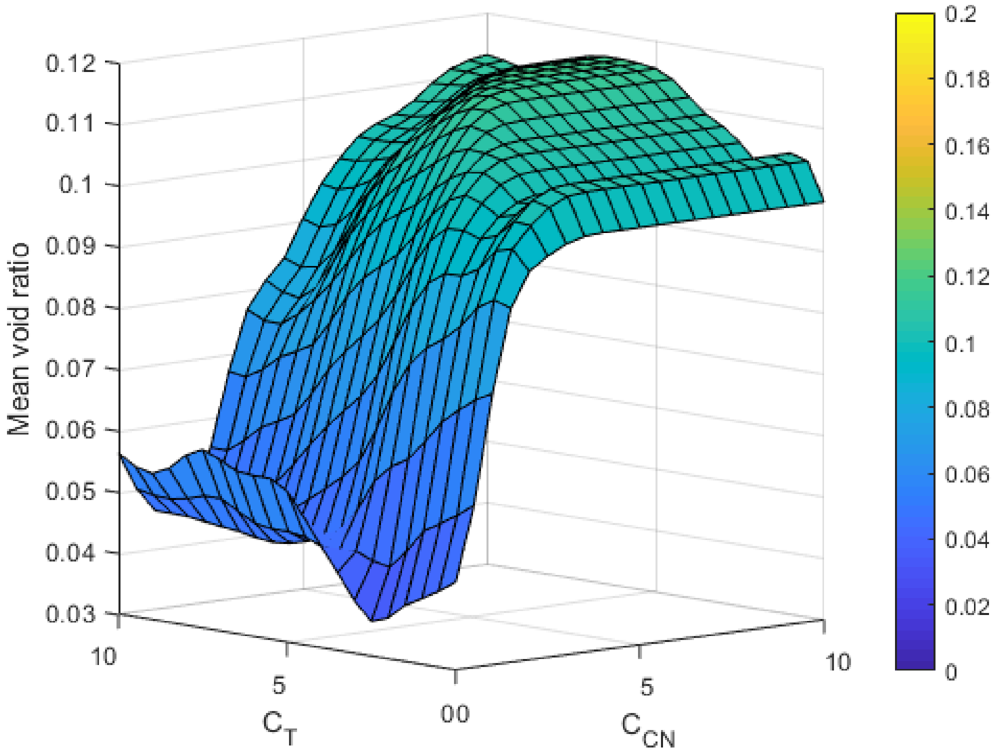

(B)

FIGURE 5.14: Surface plots of MVR results for n=9 in the Tetris Scenario for different C_T and C_{CN} values varied from 0 to 10 at increments of 0.5 with C_V=1 and C_D=3.5 for (a) the raw MVR results and (b) the MVR results with Gaussian filter applied.

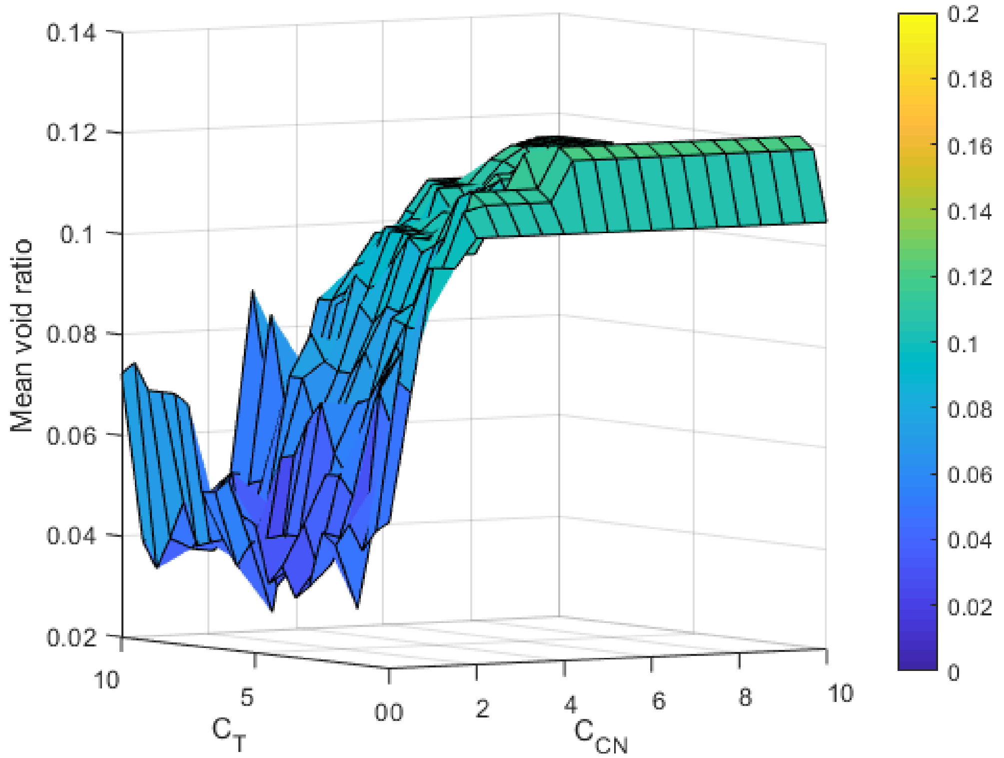

(A)

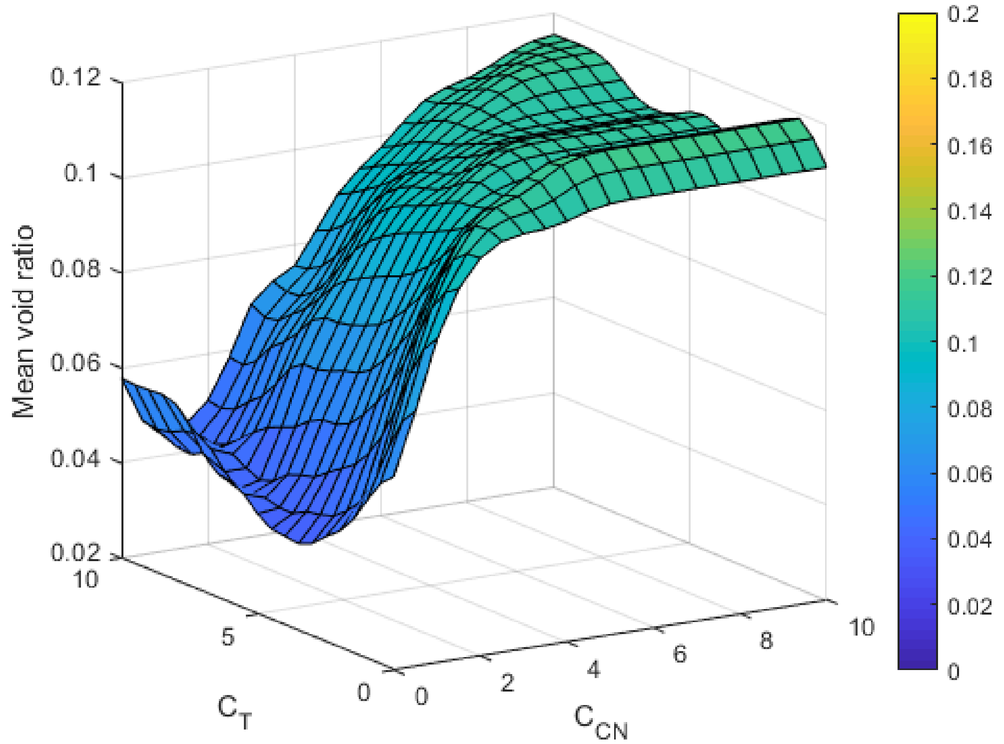

(B)

FIGURE 5.15: Surface plots of MVR results for n=9 in the Tetris Scenario for different C_T and C_{CN} values varied from 0 to 10 at increments of 0.5 with C_V=1 and C_D=6.5 for (a) the raw MVR results and (b) the MVR results with Gaussian filter applied.

5.5 Identifying Coefficients for a Viable Solution

5.5.1 Introduction

As suggested in Section 5.4.2, values for C_V, C_D, C_T, and C_{CN} of 1, 3.5, 2.5 and 0 appear to be an optimal solution when using the packing algorithm for the Tetris Scenario. Indeed, from the values presented in Table 5.4 it can be derived that C_{CN}=0 as all but one solution has a zero value for this coefficient. As discussed in Section 4.4.5, it is required to analyse datapoints with a coefficient value of zero using no filter as the effect of the filter can lead to these locations not being detected as minimums.

So far in Chapter 5, the range of weighting coefficients investigated have been between 0-10 at different sample sizes and sampling frequencies. It has been stated that coefficient values above 10 are not required for investigation. Proof of this is found in Section 5.5.2 where the value of C_D is extended past the limit of 10 show that coefficients larger than 10 do not lead in a trend towards an optimal solution. Also, finer exploration and refinement of the search area for (C_V=1, C_D=3.5, C_T=2.5, C_{CN}=0) is conducted in Section 5.5.3 to see if an optimal value lies in this range when a higher sampling frequency is adopted. Furthermore, it is required to focus on the search area where values are less than 1. The reason for such investigation is due to fixing C_V to a value of 1. In the cases explored so far, all coefficients have a bigger impact on placement when compared to $C_V V_{AB}$ in the objective function. Therefore in Section 5.5.4, the search area around the smaller values are investigated.

5.5.2 Searching Larger Coefficient Values

It has been stated that values of coefficients greater than 10 will not lead to an optimal solution for packing. Evidence for this is found in Section 5.3 where each scoring criteria was oversized to be the dominant contributor in the objective function. None of the produced MVR values lie below the lowest MVR values presented in Figures 5.10-5.15. However, it should be acknowledged that so far a limitation on the search area has been set with no verification past these limits. Therefore, this section exists to offer proof that this is true. Search of this area has been conducted in the Tetris Scenario due to the increased computational time compared to the Soil Particle Scenario. No investigation for the Soil Particle Scenario is to be completed unless the produced data indicates an optimal solution past coefficient values of 10 for C_D, C_T and C_{CN}.

As seen in Figure 5.3, C_D appears to have a decreasing effect on MVR as it is increased. Therefore, to ensure reliability of results, larger values of C_D were tested. Figure 5.16 shows the lowest MVR achieved for each C_D value from 0 to 25. Table 5.5 indicates the ranges of the coefficients investigated and the increment used between values. As C_D is increased, the lowest MVR value does not show any indication of repeating a value similar to that experienced at C_D=3.5. Therefore it can be stated that this location is a viable solution when looking for minimum void ratio created in a system for Tetris shapes and that a more optimal solution does not exist for coefficients of C_D greater than 10.

From Figure 5.11b, Figure 5.10, Figure 5.12 and Figure 5.16 it is determined that it is very unlikely that a minimum MVR value is found for coefficient values past the typical range explored of 0 to 10. Further evidence for this are the values of MVR presented in Table 5.2 for the oversized coefficient values. MVR for when each coefficient is oversized equates to a value greater than the lowest MVRs determined in

C_D range	Increments	C_T range	Increments	C_{CN} range	Increments
0-10	0.5	0-10	0.5	0-10	0.5
11-17	2	0-10	2	0-10	2
17-25	1	0-10	2	0-10	2

TABLE 5.5: Values of coefficient ranges and incremental steps used between them for the data plotted in Figure 5.16.

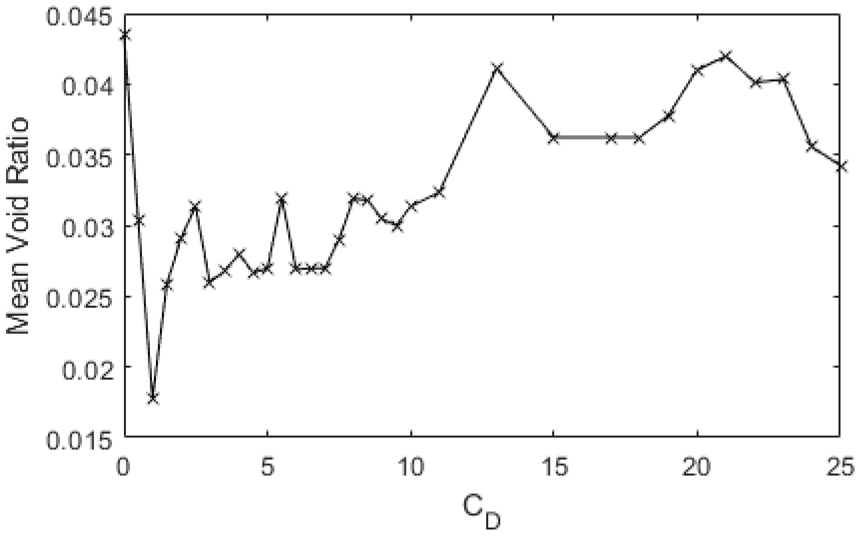

FIGURE 5.16: Lowest MVR values detected in plots of C_T and C_{CN} for different C_D values. C_V=1 for all plots. Sample size of n=9 is adopted. Table 5.5 indicates the ranges of coefficients and incremental values adopted.

the search areas investigated. It is expected that the optimal values of each coefficient are much less than 10 as suggested by Figure 5.12 and therefore the limitation set of up to a coefficient value of 10 is reasonable.

5.5.3 Searching Coefficient Values Around the Current Result

Searching of results around (C_V=1,C_D=3.5,C_T=2.5,C_{CN}=0) is required to ensure that this is a true optimum value. The search around this area was only completed at a sample size of n=9 for sampling frequency of 0.5 increments in Section 5.4.2. Here, the sample size is increased to represent the population of data fully. Table 5.6 presents the minimum MVR location identified in Figures 5.14 and the value for MVR when the sample size is n=30. Gaussian filter is not applied to the values in Table 5.6 due to the locations being found at the edge of the dataset for C_{CN}=0. n=9 does not fully representing the whole population and the MVRs produced are slightly underpredicted as discussed in Section 5.4.1. In fact, from the scan of n=30, the location of the minimum is actually determined to be located at (C_V=1,C_D=3.5,C_T=1.5,C_{CN}=0). The MVRs for the different samples sizes for this location are also presented in Table 5.6.

Another possible location for a solution at (C_V=1, C_D=1, C_T=0.5, C_{CN}=0) was found in Figure 5.13a when the sample size was n=9. Further investigation into (C_V=1, C_D=1, C_T=0.5, C_{CN}=0) with a sample size of n=30 was completed and the result for this is presented in Table 5.6. The difference in MVR for the sample size of 30 is

Coefficient combination	MVR for n=9	MVR for n=30
(C_V=1,C_D=3.5,C_T=2.5,C_{CN}=0)	0.0268	0.0386
(C_V=1,C_D=3.5,C_T=1.5,C_{CN}=0)	0.0291	0.0302
(C_V=1,C_D=1,C_T=0.5,C_{CN}=0)	0.0178	0.0317

TABLE 5.6: MVR value for the given coefficient combination for n=9 and n=30. Gaussian filter not applied to data.

much greater than that of n=9. The value of MVR for this location when n=9 is lower than for (C_V=1,C_D=3.5,C_T=1.5,C_{CN}=0) whilst at n=30 the opposite is found. It is suggested that this is due to the particle delivery order of the first nine runs coincidently leading to lower mean values for (C_V=1, C_D=1, C_T=0.5, C_{CN}=0) compared to other combinations of weighting coefficients. Adopting n=30 leads to more accurate representation of the population data. Although it is important to be careful for combinations of weighting coefficients when one or more are of a zero value, it can be shown that this sudden decrease is due to the sample size not being large enough when collecting the data.

Figure 5.17 completes the investigation surrounding the location (C_V=1, C_D=3.5, C_T=2.5, C_{CN}=0) where MVR was found to be minimum by exploring the search area around this point. C_V and C_{CN} were kept constant at values of 1 and 0 respectively whilst C_D and C_T were varied at increments of 0.1. A finer resolution than this was not investigated due to the difference in MVR being small. It is thought that at this point, the difference in packing is due to the combination of coefficients being more suitable to the particle order of the 30 runs than more suitable for gaining low void ratios regardless of particle order.

Figure 5.17a shows the results with no filter applied whereas Figure 5.17b presents these results with the Gaussian filter applied. For Figure 5.17a, there is a spike of minimum void located at (C_V=1, C_D=3.8, C_T=2, C_{CN}=0) with MVR=0.027. However, this is surrounded by results which are relatively larger. As stated in Section 4.4.5, it is necessary to take the results with Gaussian filter applied if the result does not lie on the boundary of the plot.

From Figure 5.17b it can be determined that (C_V=1, C_D=3.3, C_T=1, C_{CN}=0) is the optimal set of coefficients from those investigated by the utilised sampling frequencies and ranges explored. MVR value at this point is 0.316.

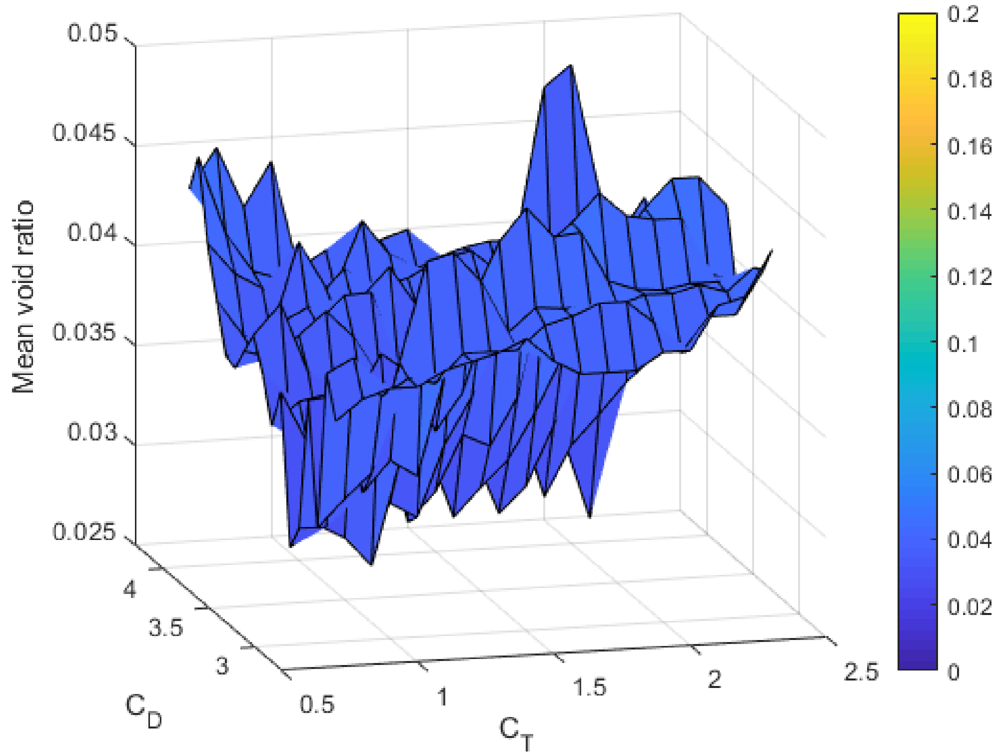

(A)

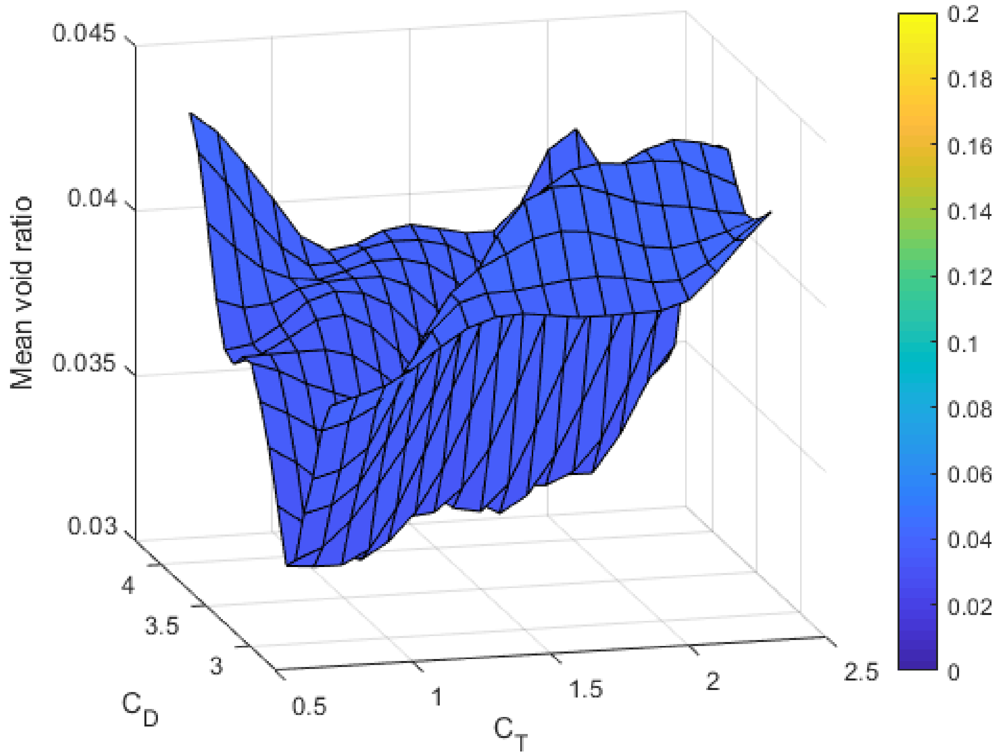

(B)

FIGURE 5.17: Surface plots of MVR results for n=30 in the Tetris Scenario for different C_D and C_T values varied from 2.7 to 4.3 and 0.7 to 2.3 respectively at increments of 0.1. C_V=1 and C_{CN}=0 for (a) the raw MVR results and (b) the MVR results with Gaussian filter applied.

5.5.4 Searching Smaller Coefficient Values

It has been determined that a range of coefficients past values of 10 is not required but it is also a necessity to check MVR values for coefficients where C_V is in the same order of magnitude. Following Hoodless and Smith (2023) it can be seen that if C_V is not fixed to a value of 1 then it tends to be larger than the other coefficients in the objective function. Additionally, as the objective for the Tetris Scenario is to produce packings which have minimum void ratio, it is clear that having C_V as the main contributor to scoring will potentially lead to a more optimum solution although this is not necessarily true.

Figure 5.18 presents the lowest MVR values for different C_D values when coefficients are varied from 0 to 1 at increments of 0.1, whilst C_V is fixed at a value of 1. The values of the weighting coefficients and the resulting MVR when Gaussian filter is applied is presented in Table 5.7 for both the unfiltered data and that with Gaussian filter applied. For both, values of MVR are lower than that found at (C_V=1, C_D=3.3, C_T=1, C_{CN}=0). Therefore, it is likely that the true optimal value lies in a range where coefficients C_D=3.3 and C_T=1 are not as large as suggested. Additionally, C_{CN} of 0.1 appears at the lowest MVR points for data with no filter applied. This suggests that CN may have a positive effect on packing when trying to minimise void ratio and C_{CN} is in fact not of zero value. Instead the sizes of C_{CN} investigated are too large and leading to a negative effect as when CN is the dominating factor this leads to a negative influence on void ratio as shown in Section 5.3.

It is important not to set false limits by only investigating this search area up to a limit of 1 as has been done for the investigation of the search area for Figure 5.18. Figure 5.20 presents the lowest MVR results for different C_D values ranging from 0 to 2 increasing at increments of 0.25. The MVR results were found in plots of C_T against C_{CN} where each were also ranged from 0 to 2 increasing at increments of 0.25. The resulting lowest MVR values seen in Figure 5.20 suggest that an optimal solution may be around the search area for C_D=1.5 as this is where the lowest MVR value from the Gaussian-filtered data is located.

It should be noted that results in Figure 5.18 and Table 5.7 as well as Figure 5.20 consist of being calculated from a sample size of n=9 and are most likely underestimated as was found in Section 5.5.3. Figure 5.19 presents lowest MVR values for different C_D values when coefficients are varied from 0 to 1 for a sample size of n=30. C_D was increased by increment of 0.25 whilst C_T and C_{CN} were increased by increments of 0.1. Comparing Figure 5.18 and Figure 5.19 confirms that the value of MVR is being underestimated when n=9, however Figure 5.19 does still suggest that the true optimal combination of weighting coefficients lies within a range away from (C_V=1, C_D=3.3, C_T=1, C_{CN}=0) as values fall below an MVR of 0.316.

It is required that smaller values of each coefficient in relation to C_V=1 are explored. Figure 5.21 presents MVR results produced by varying C_D from 0 to 1.5 by increments of 0.15, C_T from 0 to 0.5 by increments of 0.05, and C_{CN} from 0 to 0.1 by increments of 0.01. This is produced by plotting the lowest MVR value obtained from surface plots of C_T and C_{CN} for that value of C_D. Table 5.8 contains the C_T and C_{CN} values for the lowest MVR results for each C_D value investigated for both the unfiltered and Gaussian filtered results. From Figure 5.21, minimum values appear at C_D=0.6 and C_D=1.5 for the Gaussian filtered MVR values, whilst C_D=0.6 appears to be a minimum when no filter is applied. Figure 5.23a and Figure 5.23a display these surface plots respectively. From these plots and the coefficients presented in

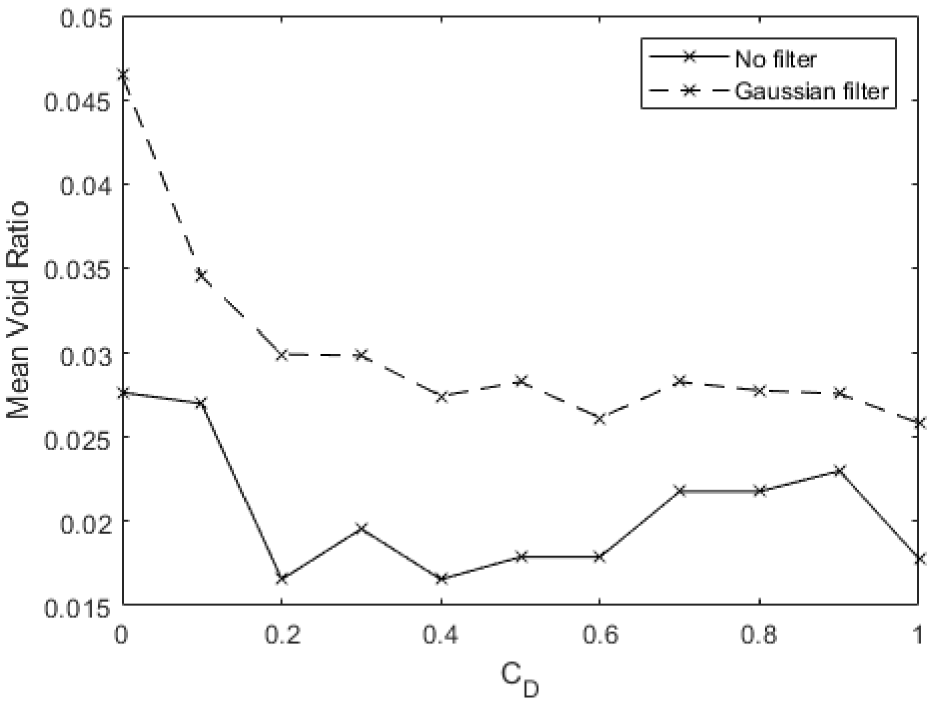

FIGURE 5.18: Lowest MVR values detected in plots of C_T and C_{CN} for different C_D values. C_V=1 for all combinations investigated. C_D, C_T, and C_{CN} varied from 0-1 at increments of 0.1. Sample size of n=9 is adopted.

		No filter			Gaussian filter		
C_V	C_D	C_T	C_{CN}	MVR	C_T	C_{CN}	MVR
1	0	0.7	0.1	0.277	0.8	0.2	0.0464
1	0.1	0.4	0.1	0.270	0	0	0.0345
1	0.2	0.1	0	0.0166	0	0	0.0299
1	0.3	0.6	0.1	0.0196	0.1	0	0.298
1	0.4	0.2	0	0.0166	0.2	0	0.0275
1	0.5	0.1	0.1	0.0179	0.1	0	0.283
1	0.6	0.1	0.1	0.0179	0.2	0	0.0261
1	0.7	0.2	0.1	0.0218	0.3	0	0.0283
1	0.8	0.2	0.1	0.0218	0.3	0	0.0278
1	0.9	0.2	0.2	0.0230	0.4	0	0.0276
1	1	0.5	0	0.0178	0.4	0	0.0258

TABLE 5.7: Values of coefficients for lowest MVR for each C_D value investigated in Figure 5.18 for data with no filter and Gaussian filter applied.

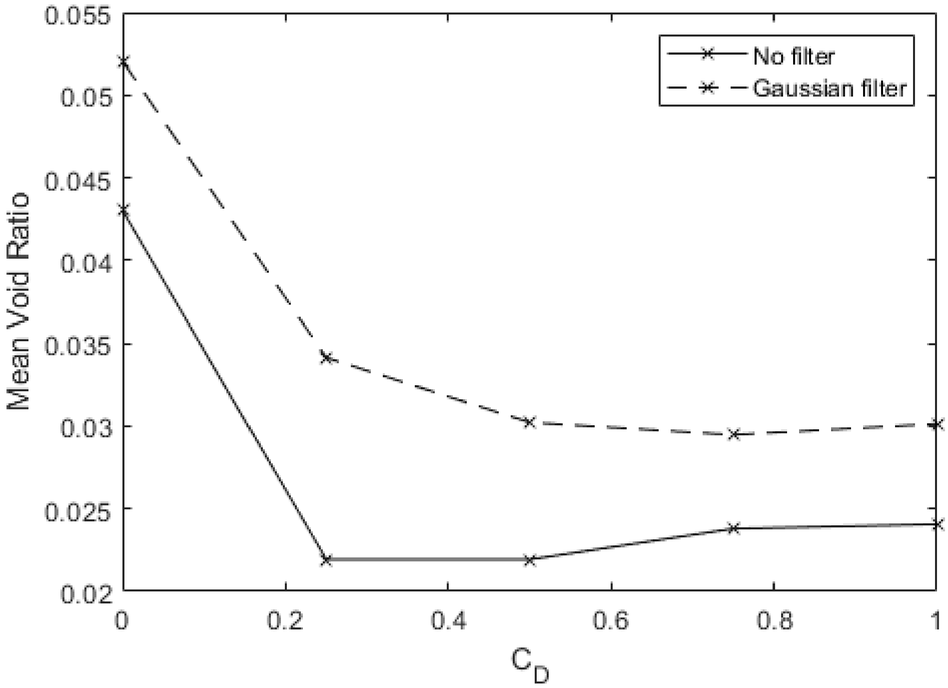

FIGURE 5.19: Lowest MVR values detected in plots of C_T and C_{CN} for different C_D values. C_V=1 for all combinations investigated. C_D varied from 0-1 at increments of 0.25. C_T, and C_{CN} varied from 0-1 at increments of 0.1. Sample size of n=30 is adopted.

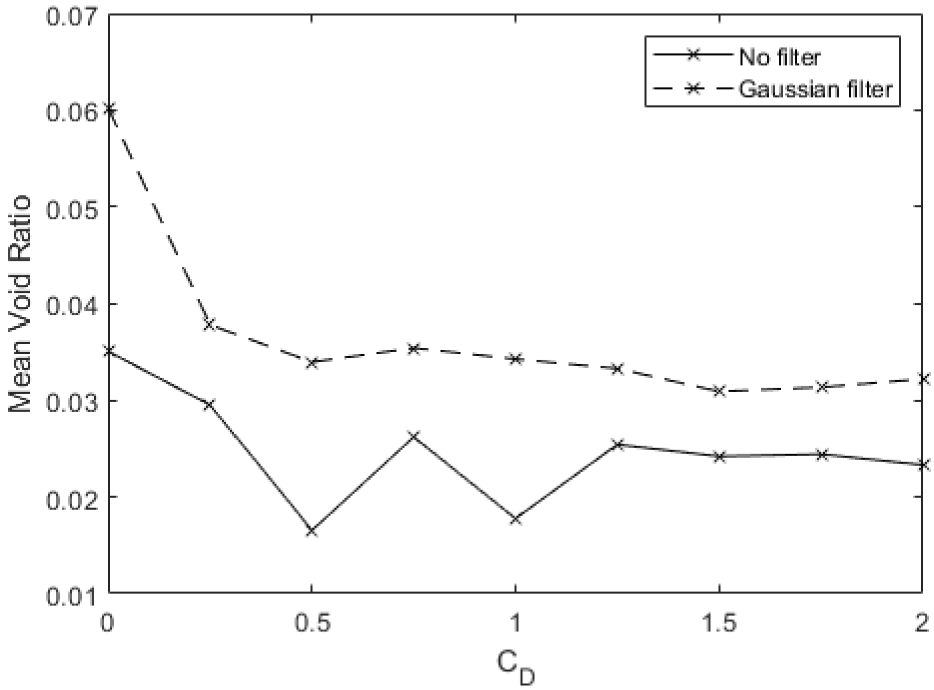

FIGURE 5.20: Lowest MVR values detected in plots of C_T and C_{CN} for different C_D values. C_V=1 for all combinations investigated. C_D, C_T, and C_{CN} varied from 0-2 at increments of 0.25. Sample size of n=9 is adopted.

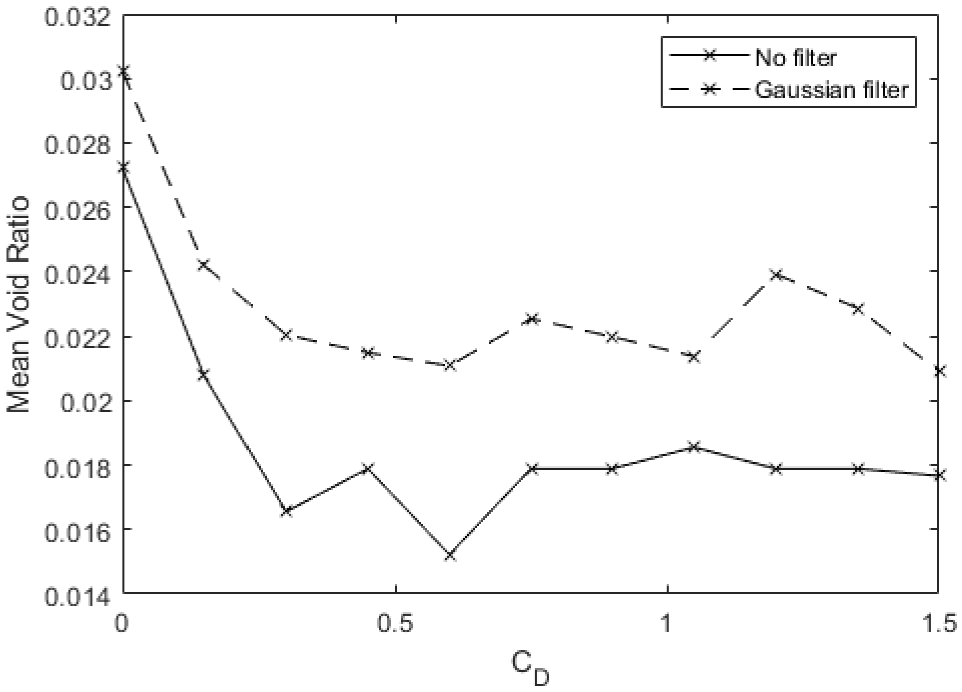

FIGURE 5.21: Lowest MVR values detected in plots of C_T and C_{CN} for different C_D values. C_V=1 for all combinations investigated. C_D varied from 0-1.5 at increments of 0.15. C_T varied from 0-0.5 by increments of 0.05. C_{CN} varied from 0-0.1 at increments of 0.01. Sample size of n=9 is adopted.

Table 5.8, further inspection is required with an extension of the search areas. The parameters used for this extended search are presented in Table 5.9.

Lowest MVR results for the coefficients explored in Table 5.8 are presented in Figure 5.22. Again, the results suggest a minimum value at C_D=0.6. Figure 5.25 presents the surface plots for C_D=0.5, C_D=0.6, and C_D=0.7 from the search using coefficient ranges outlined in Table 5.9. Inspection of the results identifies two areas of MVR values that approach a minimum. There are around (C_T=0.15, C_{CN}=0.09) and (C_T=0.3, C_{CN}=0.02) A refined search of these areas is completed adopting a sample size of n=30 for a better representation of the possible MVR results. The range of coefficients explored and the increments adopted are presented in Table 5.10. The range selected encompasses both areas of interest and the sample size of n=30 selected will provide MVR values that represent the population of data.

Additionally, the search areas for C_D=0.8 to C_D=1.7 adopting the coefficients in Table 5.9 provided more areas of interest. These were mainly at (C_T=0.5, C_{CN}=0.1) and (C_T=0.2, C_{CN}=0.02) for C_D values above 1.1 and (C_T=0.4, C_{CN}=0.02) for C_D values below 1.1. From these, the ranges presented in Table 5.11 were investigated as it encompasses the areas of interest. Again, n=30 is adopted to provide a better representation of the population of data for MVR.

Figure 5.26a and Figure 5.26b show the lowest MVR results for the range of coefficients searched using parameters set out in Table 5.10 and Table 5.11 respectively. The data suggests that an optimal solution can be found at C_D=1.6 for Gaussian filtered data and C_D=0.6 for unfiltered data. Without further exploration, it could

		No filter			Gaussian filter		
C_V	C_D	C_T	C_{CN}	MVR	C_T	C_{CN}	MVR
1	0	0.5	0.07	0.0272	0.5	0.07	0.0306
1	0.15	0.5	0.07	0.0208	0.05	0.06	0.0243
1	0.3	0.15	0	0.0166	0.5	0.06	0.0220
1	0.45	0.1	0.08	0.0179	0.2	0.07	0.0219
1	0.6	0.3	0.03	0.0152	0.15	0.1	0.0206
1	0.75	0.35	0.03	0.0179	0.35	0.03	0.0225
1	0.9	0.45	0.04	0.0179	0.45	0.04	0.0218
1	1.05	0.5	0.04	0.0186	0.5	0.04	0.0223
1	1.2	0.5	0.09	0.0179	0.5	0.09	0.0237
1	1.35	0.5	0.09	0.0179	1.5	0.02	0.0229
1	1.5	0.2	0.02	0.0177	0.2	0.02	0.0209

TABLE 5.8: Values of coefficients for lowest MVR for each C_D value investigated in Figure 5.21 for data with no filter and Gaussian filter applied.

Coefficient	Range	Increments
C_D	0.4-0.9	0.1
C_T	0-0.75	0.05
C_{CN}	0-0.18	0.01
C_D	0.8-1.7	0.1
C_T	0-0.7	0.05
C_{CN}	0-0.1	0.01

TABLE 5.9: Coefficients adopted for further investigation of search area for C_D values ranging from 0.4 to 1.7. C_V was kept constant at a value of 1 and a sample size of n=9 was adopted.

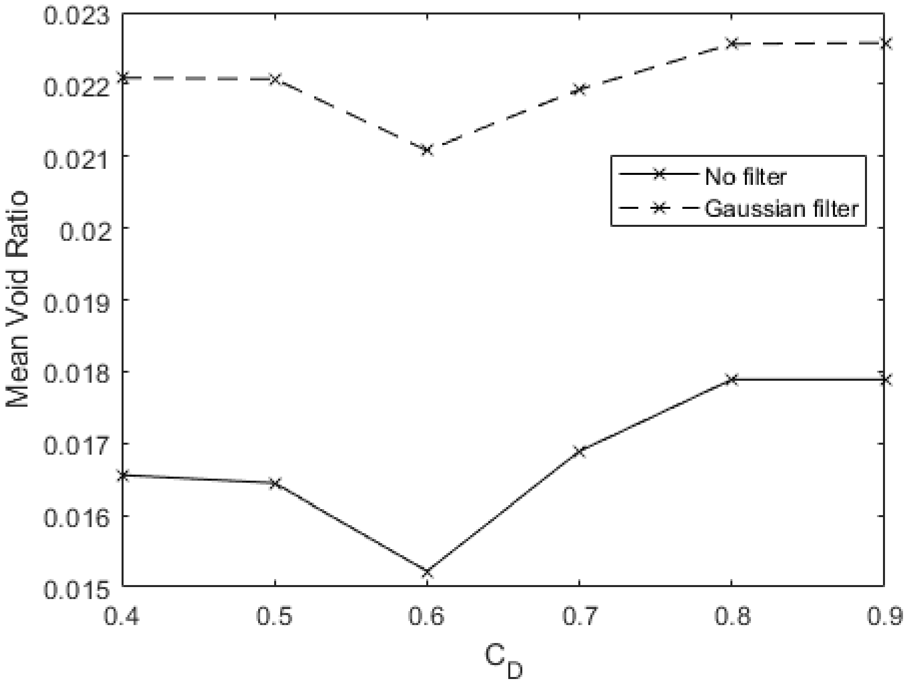

(A) 0.4-0.9

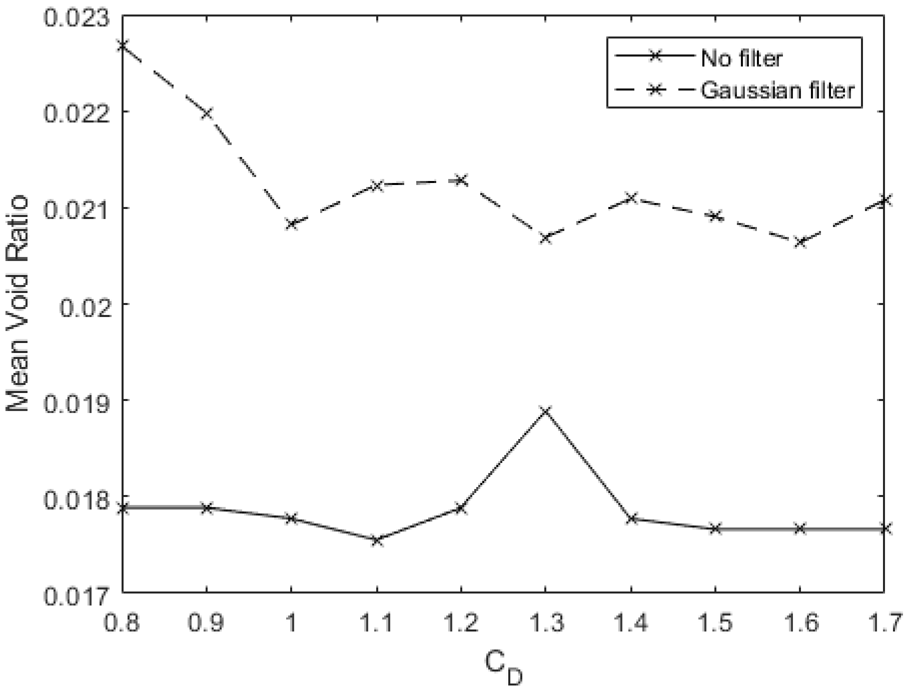

(B) 0.8-1.7

FIGURE 5.22: Lowest MVR results for coefficients presented in Table 5.8.

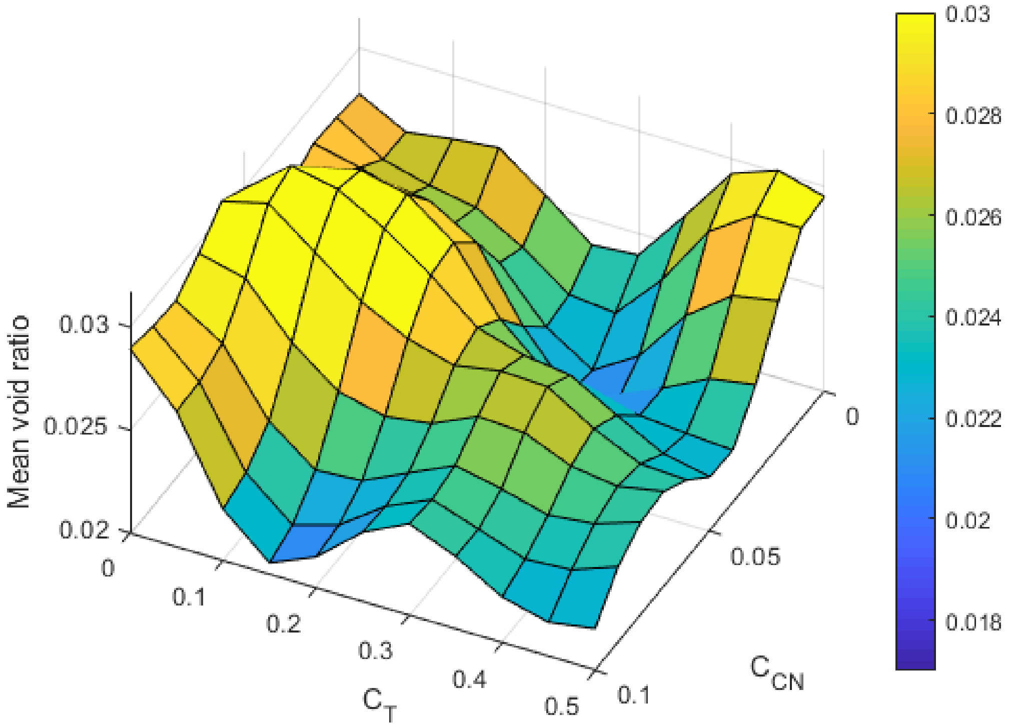

(A)

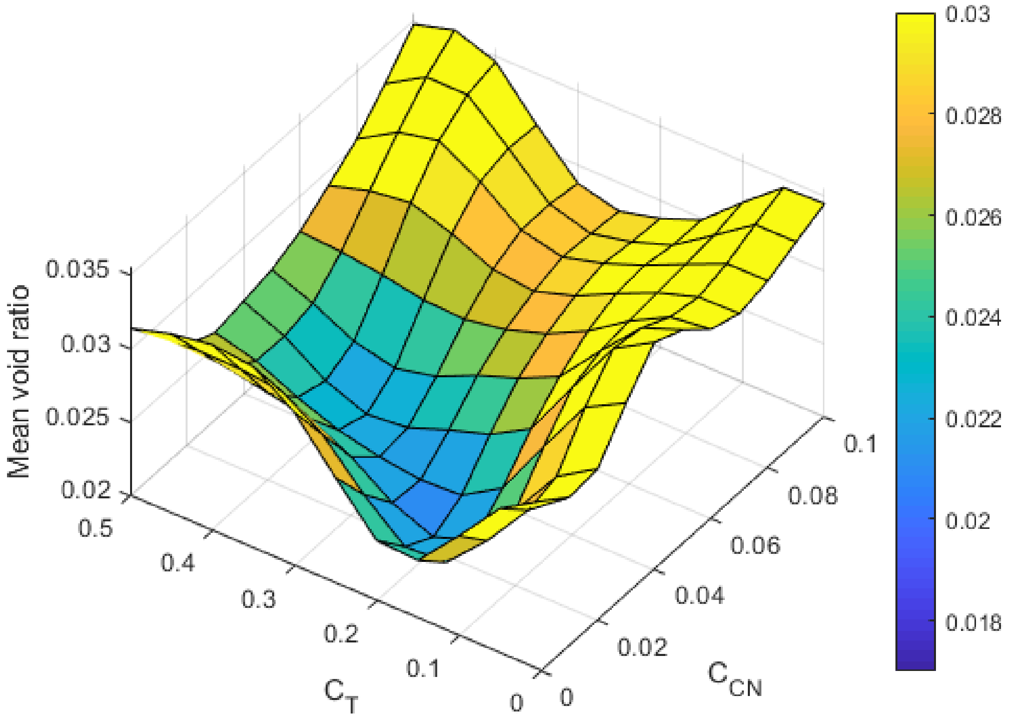

(B)

FIGURE 5.23: smaller-further-cd=1.5.png

FIGURE 5.24: Surface plots of MVR results for n=9 in the Tetris Scenario for different C_T values varied from 0 to 0.5 at increments of 0.05 and C_{CN} values varied from 0 to 0.1 at increments of 0.01. C_V=1 and Gaussian filter is applied to the search area. Plots present search areas for (a) C_D=0.6 (b) C_D=1.5

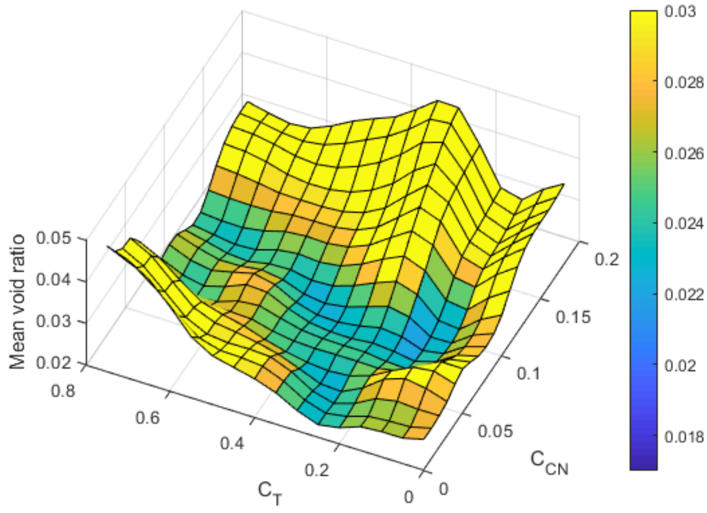

(A)

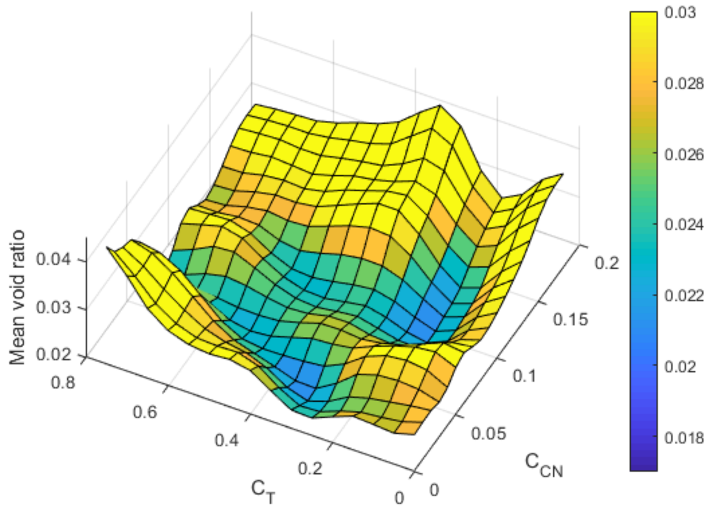

(B)

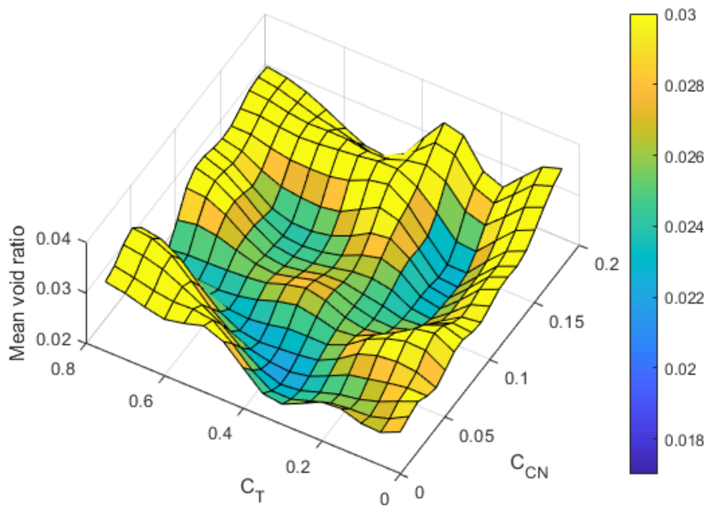

(C)

FIGURE 5.25: Surface plots of MVR results for n=9 in the Tetris Scenario for coefficient values specified in Table 5.9. C_V=1 and Gaussian filter is applied to the search area. Presented are C_D values of (a) 0.5 (b) 0.6 and (c) 0.7

Coefficient	Range	Increments
C_D	0.4-0.7	0.1
C_T	0.2-0.6	0.05
C_{CN}	0-0.12	0.01

TABLE 5.10: Coefficients of weighting for further search around suspected optimal solution at C_D=0.6 with range of coefficients investigated and increments between values. C_V=1 kept as constant value and n=30 sample size is applied.

Coefficient	Range	Increments
C_D	0.8-1.7	0.1
C_T	0.2-0.7	0.05
C_{CN}	0-0.1	0.01

TABLE 5.11: Coefficients of weighting for further search around suspected optimal solution at C_D=1.5 with range of coefficients investigated and increments between values. C_V=1 kept as constant value and n=30 sample size is applied

be assumed that the solution at C_D=1.6 should be taken forward. However, Figure 5.27 presents the surface plots of MVR for C_D=0.6 between the range of C_T and C_{CN} values specified in Table 5.10. The lowest value of MVR is located at (C_T=0.25, C_{CN}=0.02). Because the Gaussian filter applied is a 5x5 sized square, the relatively larger values experienced at C_T=0 affect this result making it larger. Figure 5.28a is a top view of the search area with values affecting (C_T=0.25, C_{CN}=0.02) when Gaussian filter is applied. The MVR values for C_T=0 - which are included when Gaussian filter is applied - are relatively high compared to the rest of the surrounding values, as can be seen in Figure 5.27. This is not the case for the lowest MVR value for C_D=1.6 which was located at (C_T=0.5, C_{CN}=0.05) for the unfiltered data. Figure 5.28b indicates the position of (C_T=0.5, C_{CN}=0.05) and the datapoints affecting this value in the Gaussian filter. Although relatively larger values of MVR are affect this datapoint, these are not at a range where the coefficients are zero values. Therefore the values affecting the datapoint are not large due to the omission of a criteria in the objective function but rather due to the combination of coefficients producing larger void ratios when packing tetrominoes.

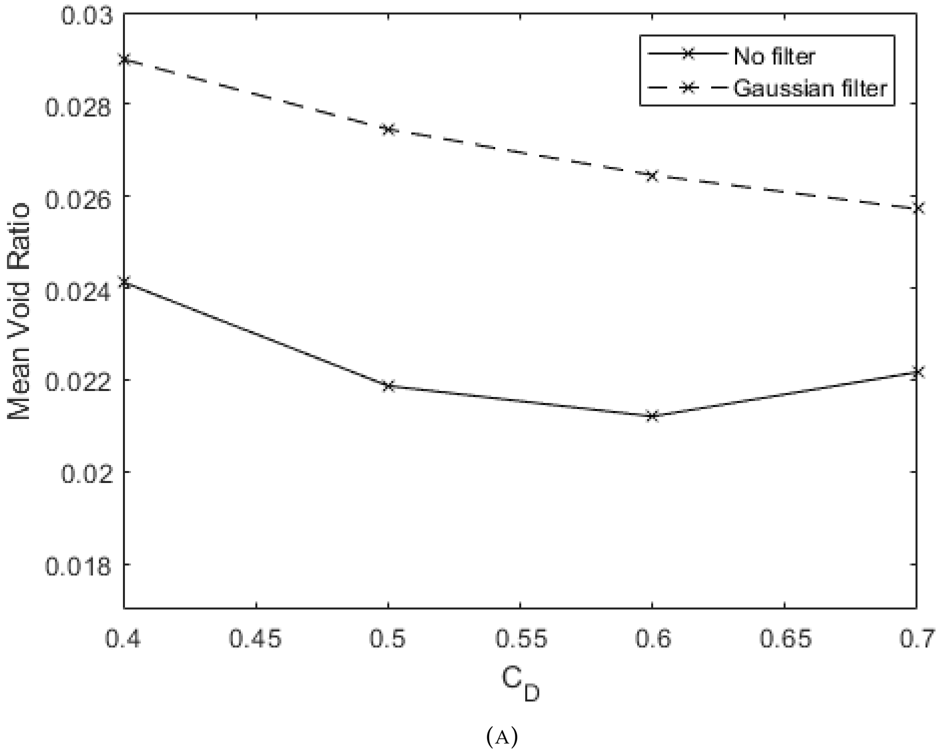

FIGURE 5.26: Values for lowest MVR at different C_D values when C_V=1 and C_T and C_{CN} are ranged from parameters specified in (a) Table 5.10 (b) Table 5.11.

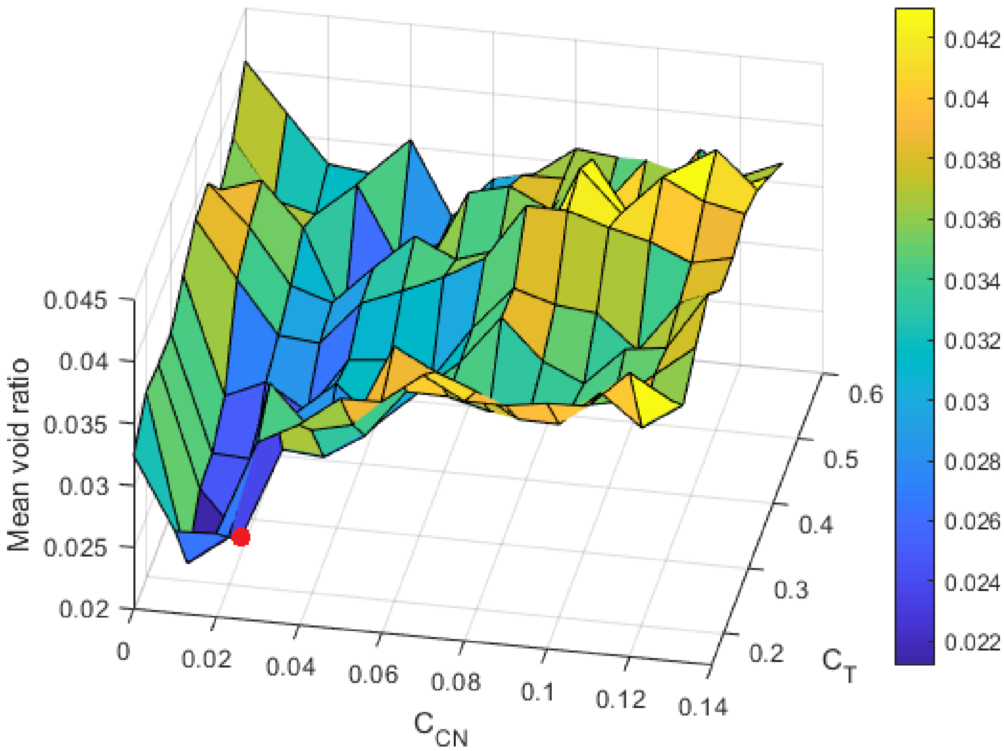

(A)

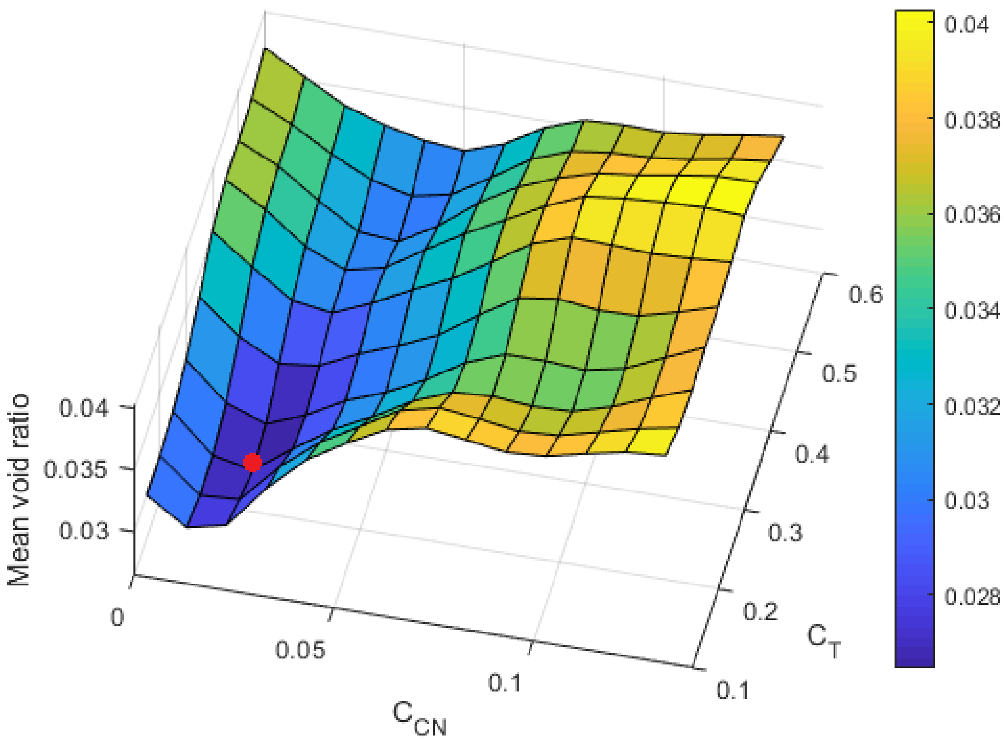

(B)

FIGURE 5.27: Surface plots of MVR values for C_V=1 and C_D=0.6 for ranges of C_T and C_D specified in Table 5.10 (a) with no filter applied (b) with Gaussian filter applied. Lowest value of MVR is indicated by red circle.

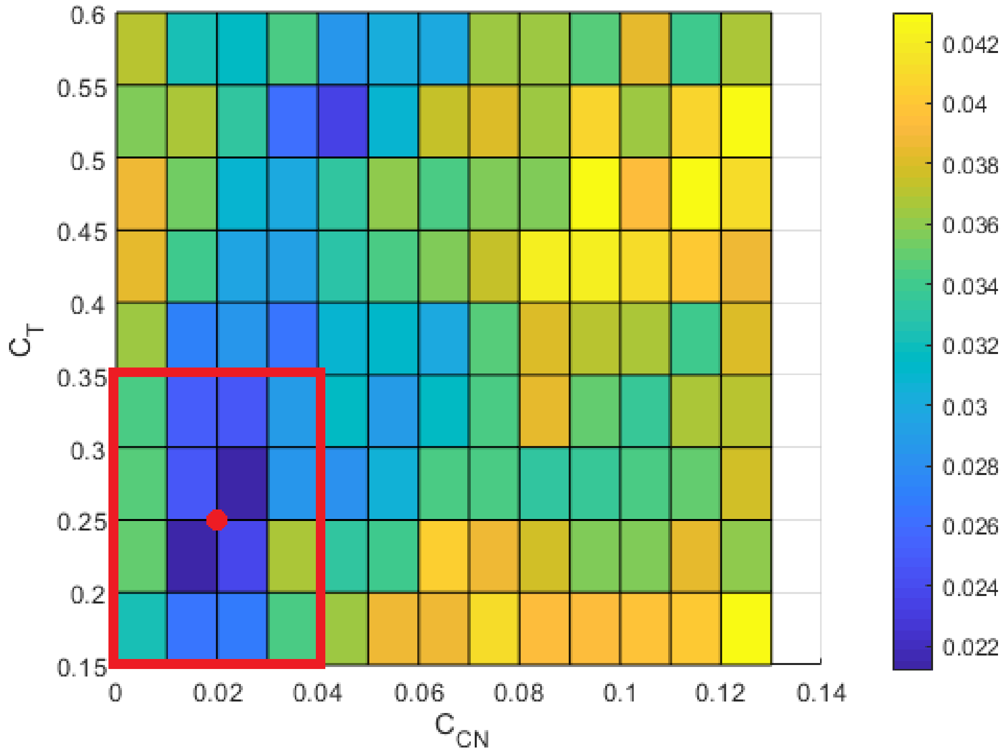

(A)

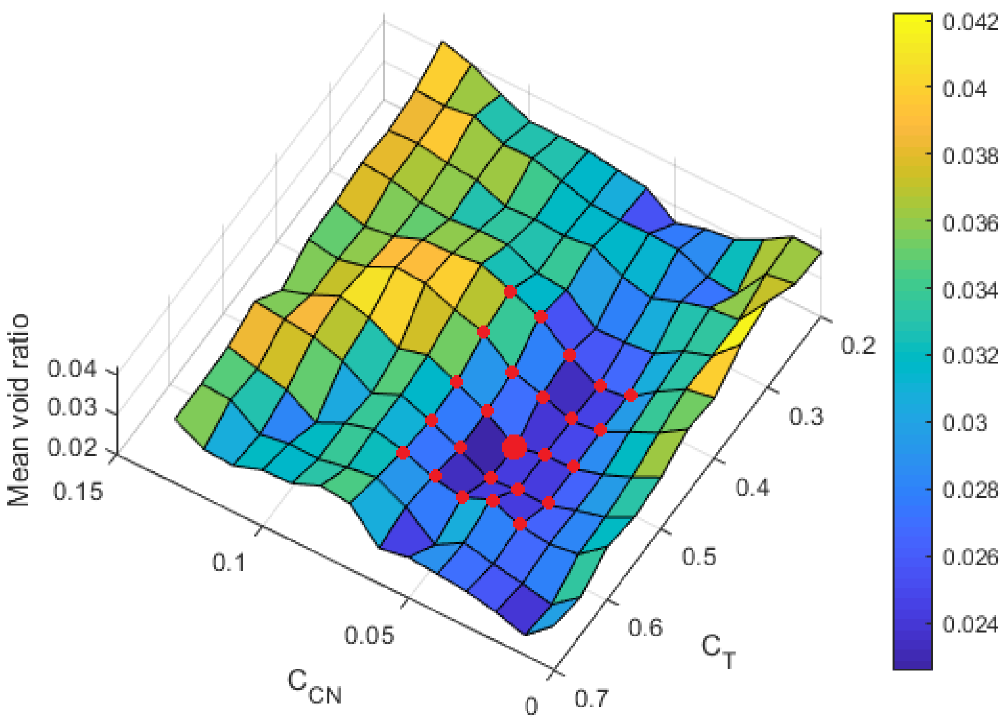

(B)

FIGURE 5.28: Surface plots of MVR values for (a) C_V=1 and C_D=0.6 for ranges of C_T and C_D specified in Table 5.10 with lowst MVR indicated by circled point and the area of datapoints taken for application of the Gaussian filter indicated by the surrounding box (b) C_V=1 and C_D=0.0.9 for ranges of C_T and C_D specified in Table 5.10 with lowst MVR indicated by larger circled point and the area of datapoints taken for application of the Gaussian filter indicated by surrounding smaller circles.

Exploration around the point of (C_V=1, C_D=0.6, C_T=0.25, C_{CN}=0.02) is completed with a finer resolution of datapoints around this location to prevent the effect of C_T=0. Increments between C_T of 0.005 were utilised rather than 0.01 to increase the number of datapoints between (C_V=1, C_D=0.6, C_T=0.25, C_{CN}=0.02) and the boundary of the search area. The surface plot of these datapoints can be seen in Figure 5.29a. When Gaussian filter is applied without the exclusion of values for CT=0, the resulting MVR is lower than that produced in Figure 5.27b. This investigation with a refined resolution of datapoints was also completed for (C_V=1, C_D=1.6, C_T=0.5, C_{CN}=0.05) to ensure equivalent resolutions have been performed on both locations and the surface plot for C_D=1.6 is presented in Figure 5.29b.

In Table 5.12 are the lowest MVR values located on Figure 5.29a and Figure 5.29b. Similar to Figure 5.26, the lowest MVR is lower for C_D=0.6 for the unfiltered data and lower for C_D=1.6 for the Gaussian filtered data. As discussed in Section 4.4.4 the Gaussian filter data should be examined for selection of an optimal combination of weighting coefficients given that the result will be less sensitive to changes given the utilisation of an area of results around the location. At C_D=1.6 the lowest MVR value for the Gaussian filtered data is actually located at (C_V=0.4, C_{CN}=0.045). As stated, the Gaussian result should be taken as it is should be less sensitive to slight changes as determined in Section 4.4.4.

Therefore, the solution taken forward for the Tetris Scenario for the combination of weighting coefficients is (C_V=1, C_D=1.6 C_V=0.4, C_{CN}=0.045). The MVR for the unfiltered data at (C_V=1, C_D=1.6 C_V=0.4, C_{CN}=0.045) 0.023833 is and for the Gaussian filtered data is 0.024196. Results of the packings are presented in Section 5.6.

		No filter			Gaussian filter		
C_V	C_D	C_T	C_{CN}	MVR	C_T	C_{CN}	MVR
1	0.6	0.2	0.015	0.021133	0.2	0.015	0.024390
1	1.6	0.5	0.05	0.022567	0.45	0.04	0.024196

TABLE 5.12: Values of the lowest MVR and their location for surface plots of C_D=0.6 varying C_T from 0 to 0.6 at increments of 0.05 and C_{CN} from 0 to 0.08 at increments of 0.005 and C_D=1.6 varying C_T from 0 to 1.7 at increments of 0.05 and C_{CN} from 0 to 0.075 at increments of 0.005.

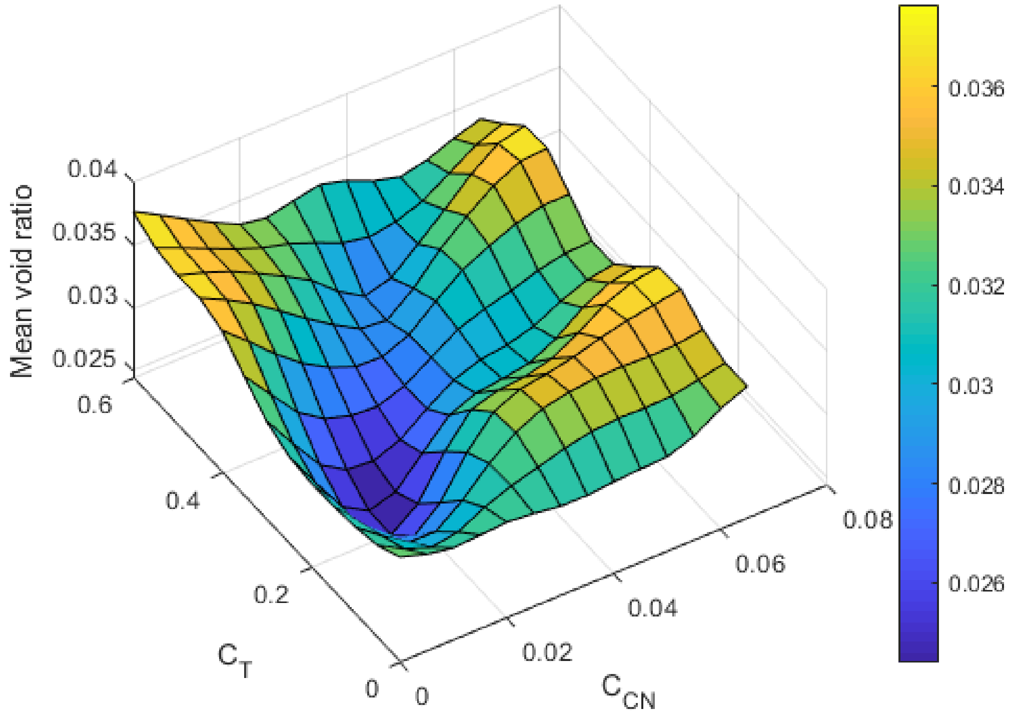

(A)

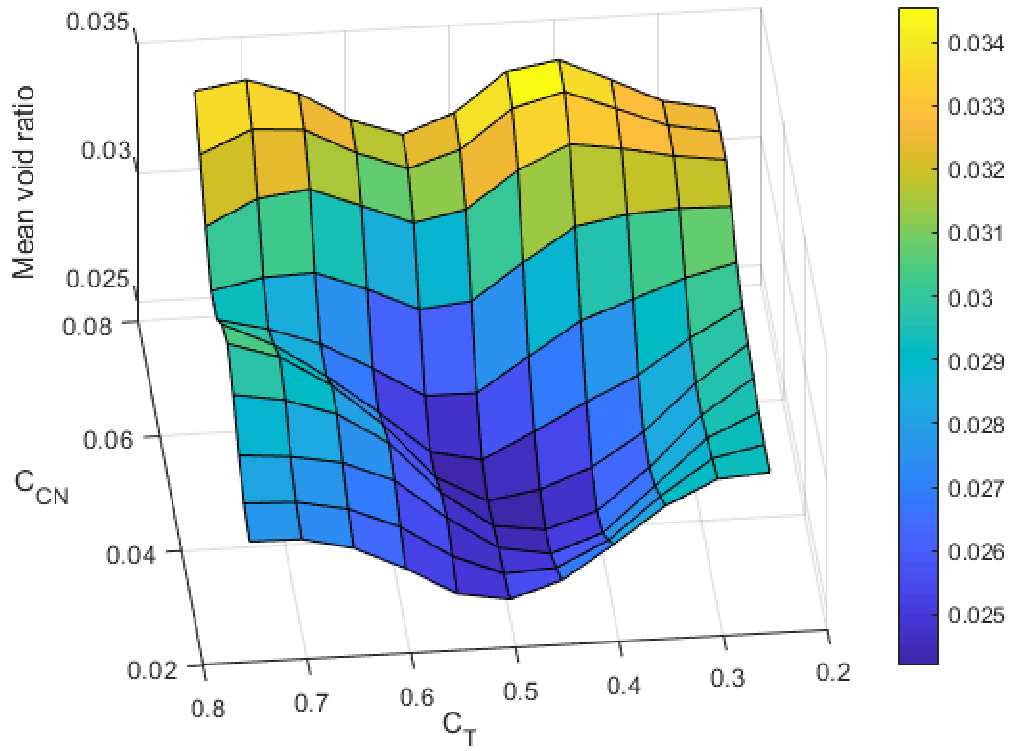

(B)

FIGURE 5.29: Surface plot of MVR values when C_V=1 for (a) C_D=0.6 varying C_T from 0 to 0.6 at increments of 0.05 and C_{CN} from 0 to 0.08 at increments of 0.005 (b) C_D=1.6 varying C_T from 0 to 0.7 at increments of 0.05 and C_{CN} from 0 to 0.075 at increments of 0.005.

5.6 Results of Weighting Coefficient Combinations

Figures 5.30a-5.44a presents packings of tetrominoes using the algorithm produced in Chapter 3 under the Tetris Scenario. Coefficients of weighting are taken as (C_V=1, C_D=1.6 C_V=0.4, C_{CN}=0.045). Equivalent packings for coefficients of weighting taken as (C_V=5, C_D=1.25 C_V=0.4, C_{CN}=0.01) as per Hoodless and Smith (2023) are also present in Figures 5.30b-5.44b with equivalent particle packing order produced using the Tetris bag approach.

For n=30, void ratio of the final packing for (C_V=1, C_D=1.6 C_V=0.4, C_{CN}=0.045) and (C_V=5, C_D=1.25 C_V=0.4, C_{CN}=0.01) were equivalent for 11 cases. In 5 of the packings, (C_V=5, C_D=1.25 C_V=0.4, C_{CN}=0.01) from Hoodless and Smith (2023) produced a lower void ratio than (C_V=1, C_D=1.6 C_V=0.4, C_{CN}=0.045). (C_V=1, C_D=1.6 C_V=0.4, C_{CN}=0.045) produced lower void ratio for 14 of the cases.

For n=100, void ratio of the final packing for (C_V=1, C_D=1.6 C_V=0.4, C_{CN}=0.045) and (C_V=5, C_D=1.25 C_V=0.4, C_{CN}=0.01) were equivalent for 29 cases. In 32 of the packings, (C_V=5, C_D=1.25 C_V=0.4, C_{CN}=0.01) from Hoodless and Smith (2023) produced a lower void ratio than (C_V=1, C_D=1.6 C_V=0.4, C_{CN}=0.045). (C_V=1, C_D=1.6 C_V=0.4, C_{CN}=0.045) produced lower void ratio for 39 of the cases.

In general, packings for (C_V=1, C_D=1.6 C_V=0.4, C_{CN}=0.045) outperform the result of (C_V=5, C_D=1.25 C_V=0.4, C_{CN}=0.01) from Hoodless and Smith (2023) as indicated by the results for MVR in Table 5.13 for n=30 and n=100. Although Section 4.3 found that n=30 is a fair representation of the population data, here n=100 was taken to further ensure that the population of data is being represented rather than just a sample.

Location	MVR (n=30)	MVR (n=100)
(C_V=1, C_D=1.6 C_V=0.4, C_{CN}=0.045)	0.0223	0.0271
(C_V=5, C_D=1.25 C_V=0.4, C_{CN}=0.01)	0.0281	0.0283
(C_V=1, C_D=0.6 C_V=0.2, C_{CN}=0.015)	0.0211	0.0260

TABLE 5.13: Mean of void ratios results taken when a sample size of n=30 and n=100 are adopted.

The number of instances for outperformance being relatively similar at 32 and 39 from packings when taking n=100 suggest that the two combinations of coefficients perform at an equivalent level. Inspection of Figures 5.30-5.44 shows that for (C_V=5, C_D=1.25 C_V=0.4, C_{CN}=0.01) there is tendancy for canyons to be created as was described in Section 5.3.2 when V_{AB} was the only activated criteria in the objective function. Figure 5.30b, Figure 5.33b, Figure 5.37b and Figure 5.44b are examples where this has occurred either on a minor scale or with resulting relatively large canyon. The want to not create void in the system from the effect of $C_V V_{AB}$ in the objective function means canyoning can occur. If a tetromino is to then later be placed above this canyon (e.g. Particle 22 in Figure 5.30b or Particle 21 in Figure 5.44b) then this leads to larger amounts of void being formed that if just a single block of void being created earlier in the packing sequence.

Furthermore, the canyoning effect leads to instances like Figure 5.33b and Figure 5.37b where canyons have formed but there is not enough space for a particle to be placed above it. As void ratio is calculated taking only the area below the surface line, this leads to lower void ratios being reached. Take Figure 5.33b. If a square particle was next to be delivered in the particle order and was placed to the left of

Particle 21, this would mean an additional three squares of void would be included in the void ratio calculation. Therefore, e=0.056 for the system suggesting that (C_V=1, C_D=1.6 C_V=0.4, C_{CN}=0.045) has outperformed (C_V=5, C_D=1.25 C_V=0.4, C_{CN}=0.01) rather than producing equivalent packings.

Additionally in Table 5.13, MVR for n=30 and n=100 is shown for (C_V=1, C_D=0.6 C_V=0.2, C_{CN}=0.015). From the values, it appears that this combination of coefficients is actually the optimal solution for the Tetris Scenario. Packings produced using this combination were equivalent for Figures 5.30-5.44 as indicated in Table 5.14 except for Figure 5.38, Figure 5.41, Figure 5.42 and Figure 5.44. The packings for these particle orders using coefficient values of (C_V=1, C_D=0.6 C_V=0.2, C_{CN}=0.015) are presented in Figure 5.45.

Figure	Equivalent to (a)	Equivalent to (b)
5.30		✓
5.31	✓	
5.32		✓
5.33		✓
5.34	✓	✓
5.35	✓	
5.36	✓	✓
5.37		✓
5.39		✓
5.40	✓	✓
5.43	✓	

TABLE 5.14: Packing structure of (C_V=1, C_D=0.6 C_V=0.2, C_{CN}=0.015) equivalent to packing structure of (a) (C_V=1, C_D=1.6 C_V=0.4, C_{CN}=0.045) and/or (b) (C_V=5, C_D=1.25 C_V=0.4, C_{CN}=0.01) as indicated by the relevent figure reference.

For n=100, void ratio of the final packing for (C_V=1, C_D=1.6 C_V=0.4, C_{CN}=0.045) and (C_V=1, C_D=0.6 C_V=0.2, C_{CN}=0.015) were equivalent for 47 cases. (C_V=1, C_D=0.6 C_V=0.2, C_{CN}=0.015) produced a lower void ratio than (C_V=1, C_D=1.6 C_V=0.4, C_{CN}=0.045) for 25 of the packings. (C_V=1, C_D=1.6 C_V=0.4, C_{CN}=0.045) produced lower void ratio for 28 of the cases. These results suggest an equivalent level of packing as was hypothesised when comparing (C_V=5, C_D=1.25 C_V=0.4, C_{CN}=0.01) to (C_V=1, C_D=1.6 C_V=0.4, C_{CN}=0.045).

Similar to (C_V=5, C_D=1.25 C_V=0.4, C_{CN}=0.01), Figure 5.45 shows instances where canyoning is occurring in the packing structures for (C_V=1, C_D=0.6 C_V=0.2, C_{CN}=0.015). Yet again where canyoning is present without the capping of a particle above it, this void is therefore not included as below the surface line and is not included in the void ratio calculation. This is arbitrarily lowering the MVR of the results. Further proof of this is seen in Table 5.13. The MVR result is much lower for n=30 as compared to n=100 for (C_V=1, C_D=0.6 C_V=0.2, C_{CN}=0.015). It is likely that the additional packings included for calculating MVR have more instances where canyons are capped by a final particle and therefore voids are larger than experienced in the first 30 packing structures.

From examination of the packings, it is determined that coefficients of weighting (C_V=1, C_D=1.6 C_V=0.4, C_{CN}=0.045) are to be taken forward for the objective function

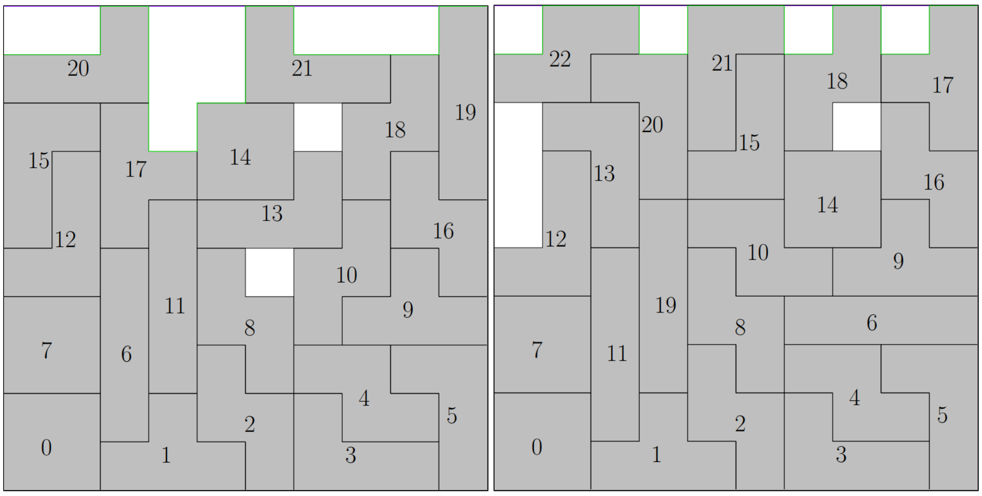

(A) e=0.023 (B) e=0.043

FIGURE 5.30: Packing result for combination of weighting coefficients (a) (C_V=1, C_D=1.6 C_V=0.4, C_{CN}=0.045) (b) (C_V=5, C_D=1.25 C_V=0.4, C_{CN}=0.01).

for the Tetris Scenario. Packings produced are less likely to experience canyoning when compared to (C_V=5, C_D=1.25 C_V=0.4, C_{CN}=0.01) and (C_V=1, C_D=0.6 C_V=0.2, C_{CN}=0.015). It is thought that this is due to C_D being a higher value relative to C_V. The positioning tends to try and position particles closer to the domain base rather than avoiding creating any area of void. As a result, canyons are less likely to occur later on in the packing.

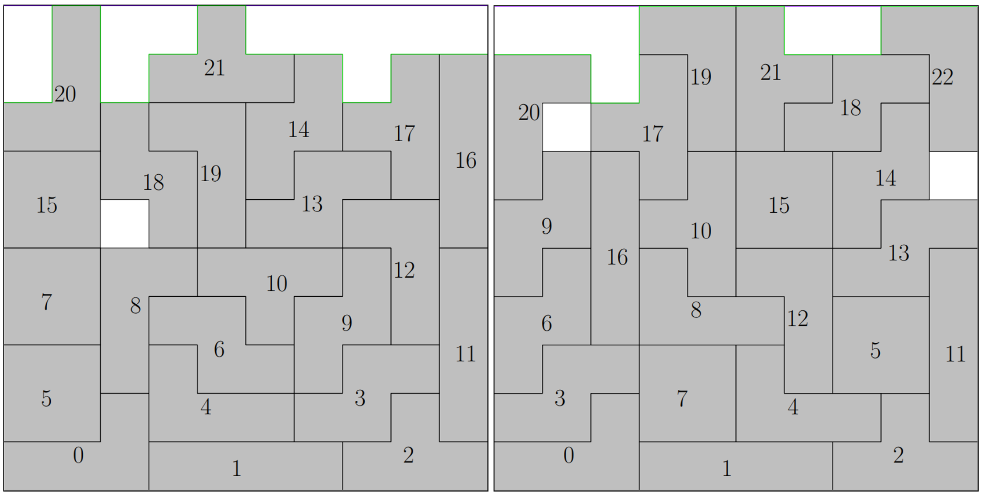

(A) e=0.011 (B) e=0.022

FIGURE 5.31: Packing result for combination of weighting coefficients (a) (C_V=1, C_D=1.6 C_V=0.4, C_{CN}=0.045) (b) (C_V=5, C_D=1.25 C_V=0.4, C_{CN}=0.01).

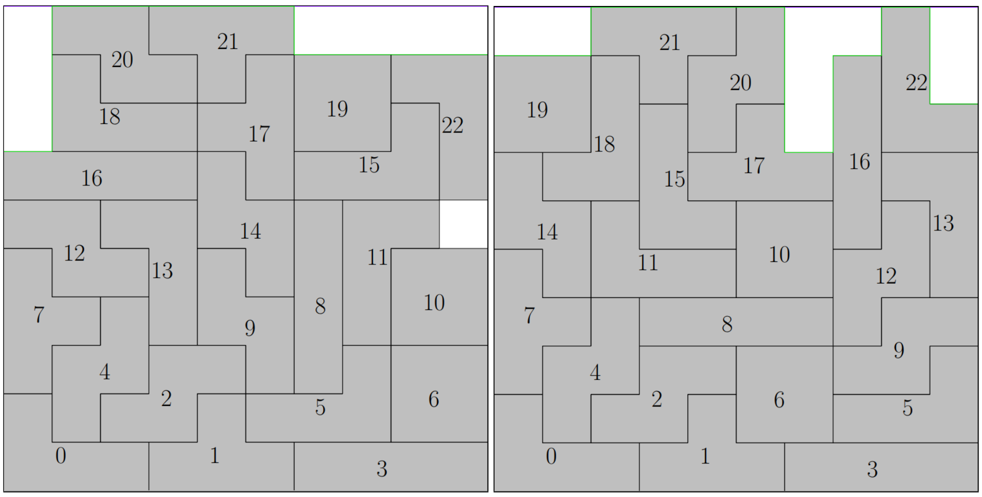

(A) e=0.011 (B) e=0

FIGURE 5.32: Packing result for combination of weighting coefficients (a) (C_V=1, C_D=1.6 C_V=0.4, C_{CN}=0.045) (b) (C_V=5, C_D=1.25 C_V=0.4, C_{CN}=0.01).

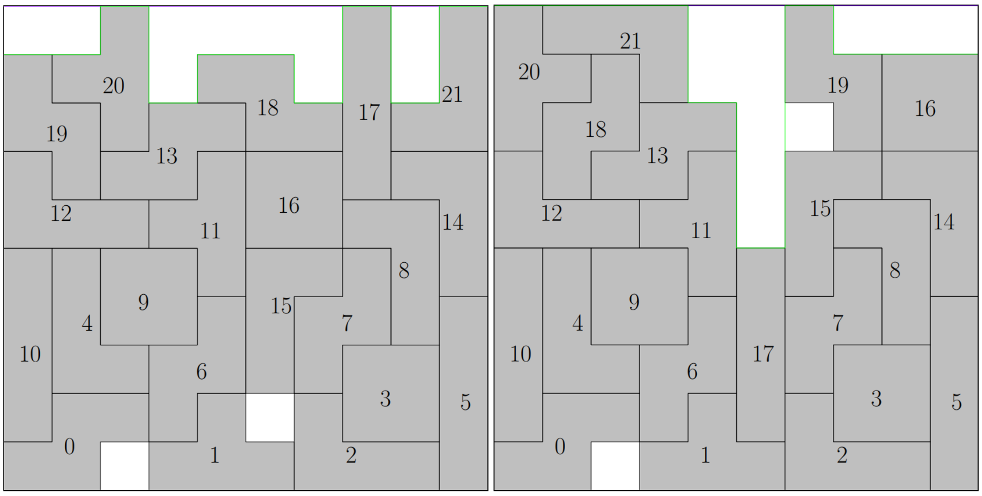

(A) e=0.023 (B) e=0.023

FIGURE 5.33: Packing result for combination of weighting coefficients (a) (C_V=1, C_D=1.6 C_V=0.4, C_{CN}=0.045) (b) (C_V=5, C_D=1.25 C_V=0.4, C_{CN}=0.01).

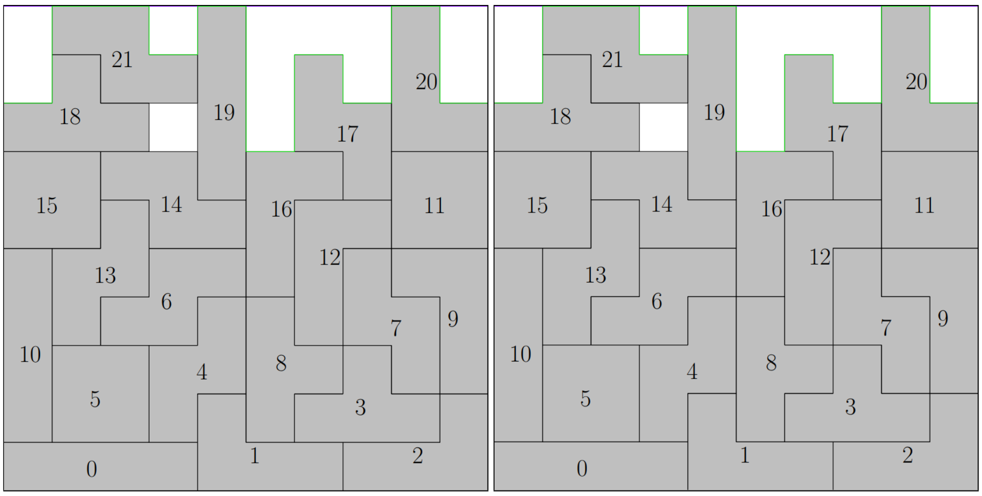

(A) e=0.011 (B) e=0.011

FIGURE 5.34: Packing result for combination of weighting coefficients (a) (C_V=1, C_D=1.6 C_V=0.4, C_{CN}=0.045) (b) (C_V=5, C_D=1.25 C_V=0.4, C_{CN}=0.01).

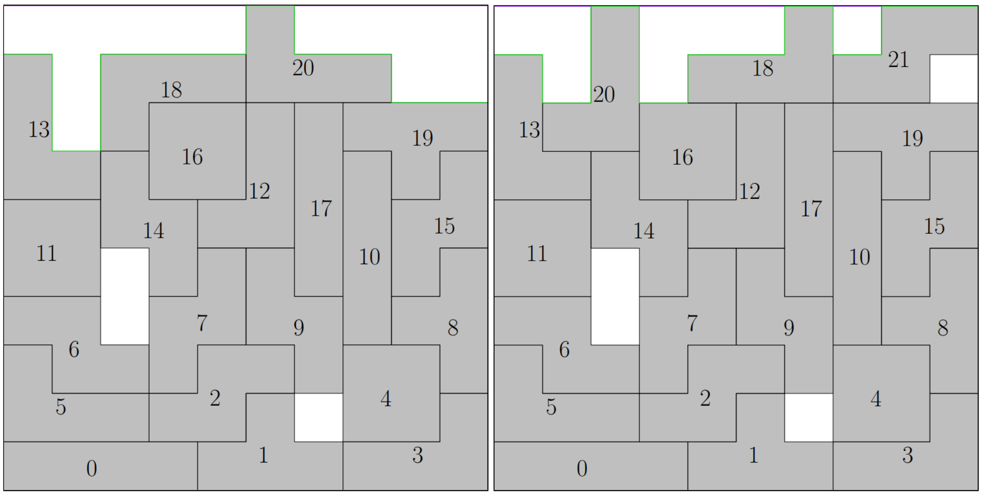

(A) e=0.036 (B) e=0.045

FIGURE 5.35: Packing result for combination of weighting coefficients (a) (C_V=1, C_D=1.6 C_V=0.4, C_{CN}=0.045) (b) (C_V=5, C_D=1.25 C_V=0.4, C_{CN}=0.01).

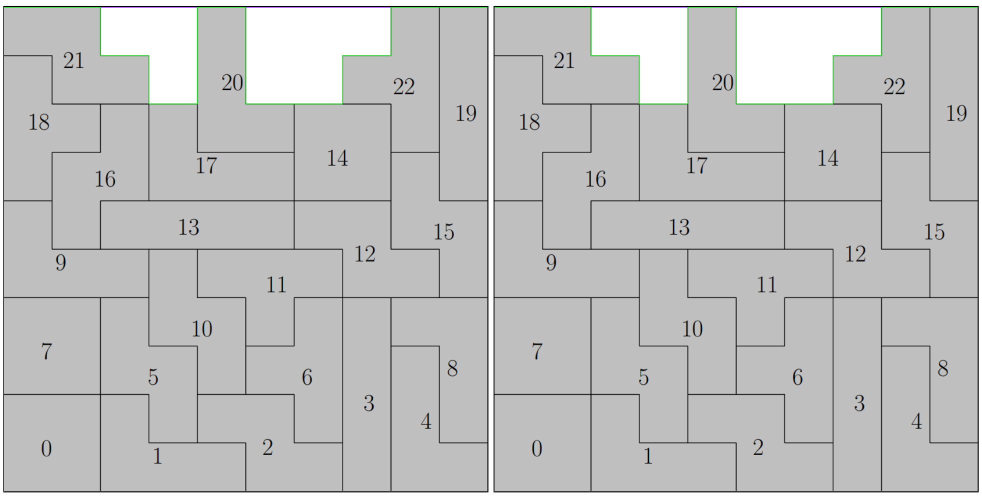

(A) e=0 (B) e=0

FIGURE 5.36: Packing result for combination of weighting coefficients (a) (C_V=1, C_D=1.6 C_V=0.4, C_{CN}=0.045) (b) (C_V=5, C_D=1.25 C_V=0.4, C_{CN}=0.01).

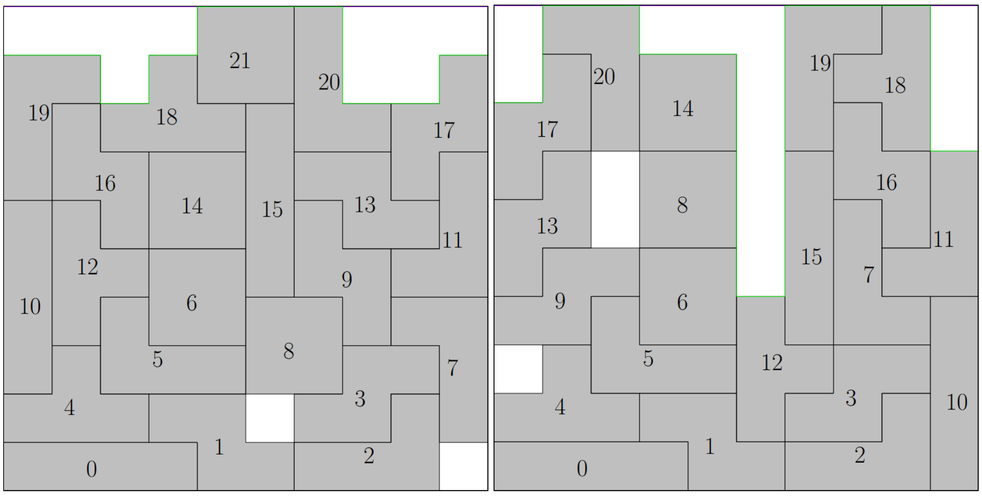

(A) e=0.023 (B) e=0.036

FIGURE 5.37: Packing result for combination of weighting coefficients (a) (C_V=1, C_D=1.6 C_V=0.4, C_{CN}=0.045) (b) (C_V=5, C_D=1.25 C_V=0.4, C_{CN}=0.01).

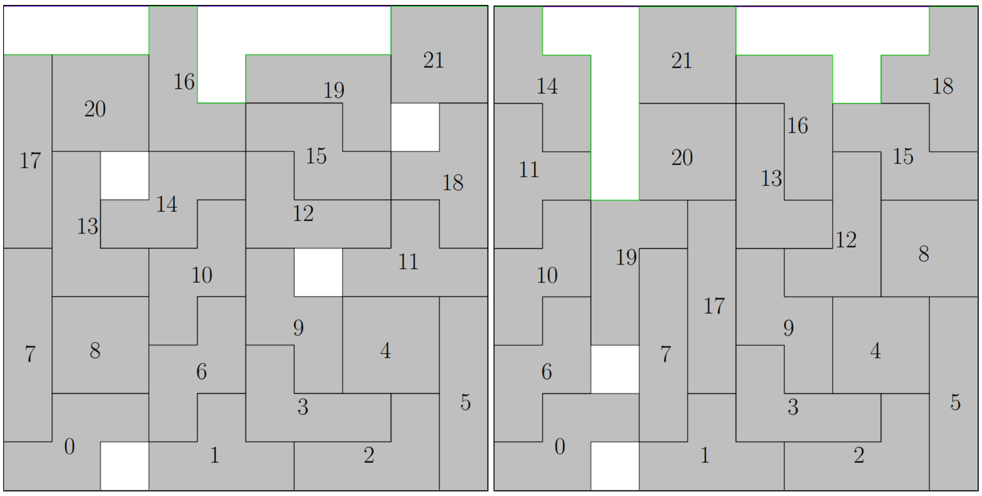

(A) e=0.045 (B) e=0.023

FIGURE 5.38: Packing result for combination of weighting coefficients (a) (C_V=1, C_D=1.6 C_V=0.4, C_{CN}=0.045) (b) (C_V=5, C_D=1.25 C_V=0.4, C_{CN}=0.01).

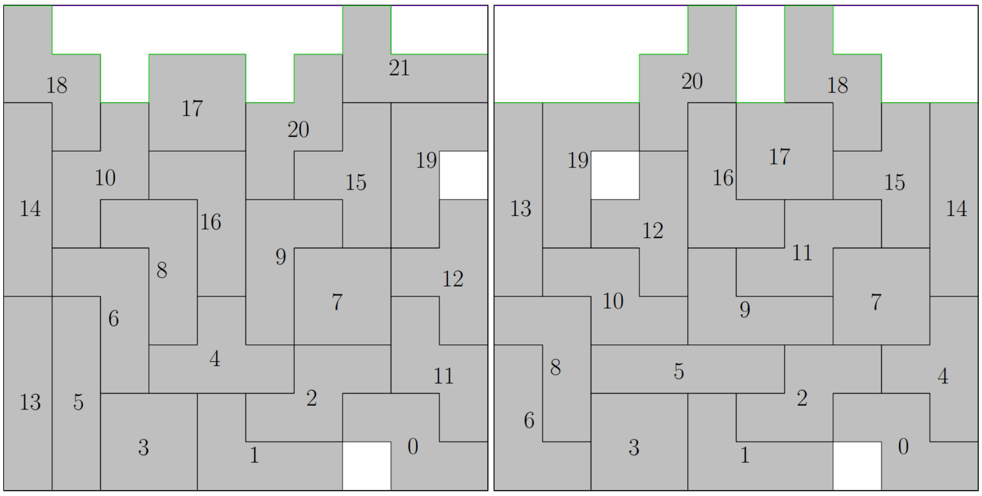

(A) e=0.023 (B) e=0.024

FIGURE 5.39: Packing result for combination of weighting coefficients (a) (C_V=1, C_D=1.6 C_V=0.4, C_{CN}=0.045) (b) (C_V=5, C_D=1.25 C_V=0.4, C_{CN}=0.01).

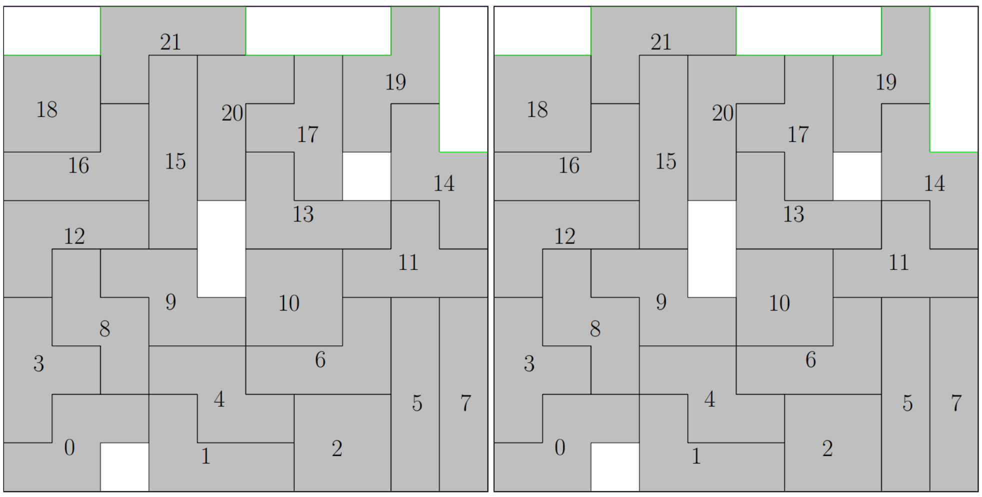

(A) e=0.045 (B) e=0.045

FIGURE 5.40: Packing result for combination of weighting coefficients (a) (C_V=1, C_D=1.6 C_V=0.4, C_{CN}=0.045) (b) (C_V=5, C_D=1.25 C_V=0.4, C_{CN}=0.01).

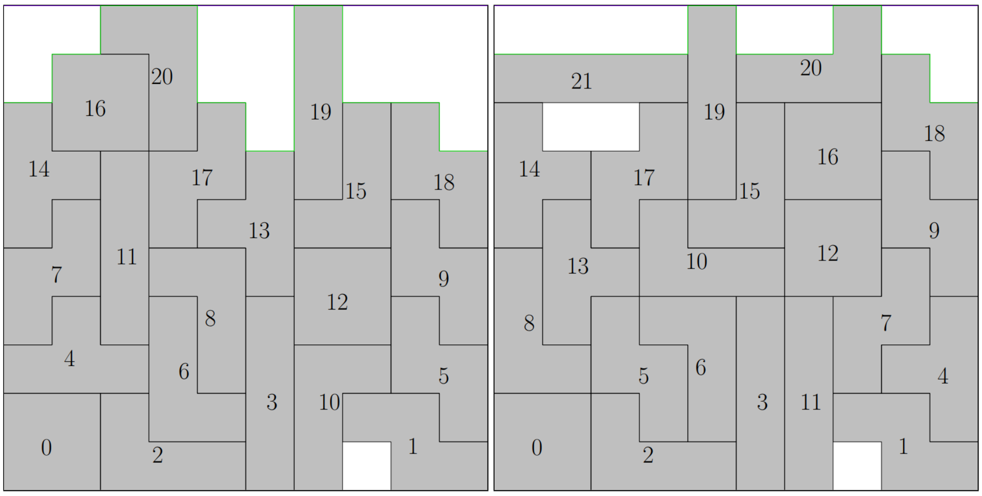

(A) e=0.012 (B) e=0.034

FIGURE 5.41: Packing result for combination of weighting coefficients (a) (C_V=1, C_D=1.6 C_V=0.4, C_{CN}=0.045) (b) (C_V=5, C_D=1.25 C_V=0.4, C_{CN}=0.01)

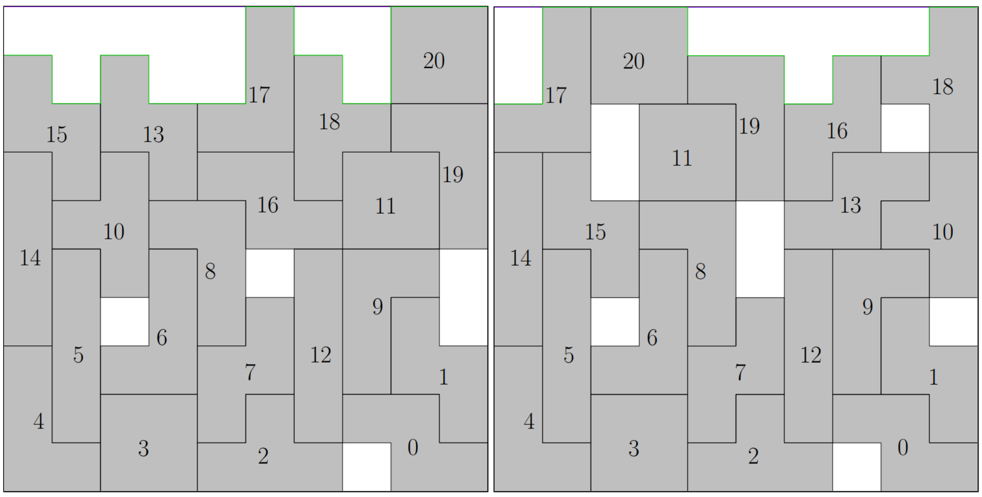

(A) e=0.06 (B) e=0.095

FIGURE 5.42: Packing result for combination of weighting coefficients (a) (C_V=1, C_D=1.6 C_V=0.4, C_{CN}=0.045) (b) (C_V=5, C_D=1.25 C_V=0.4, C_{CN}=0.01).

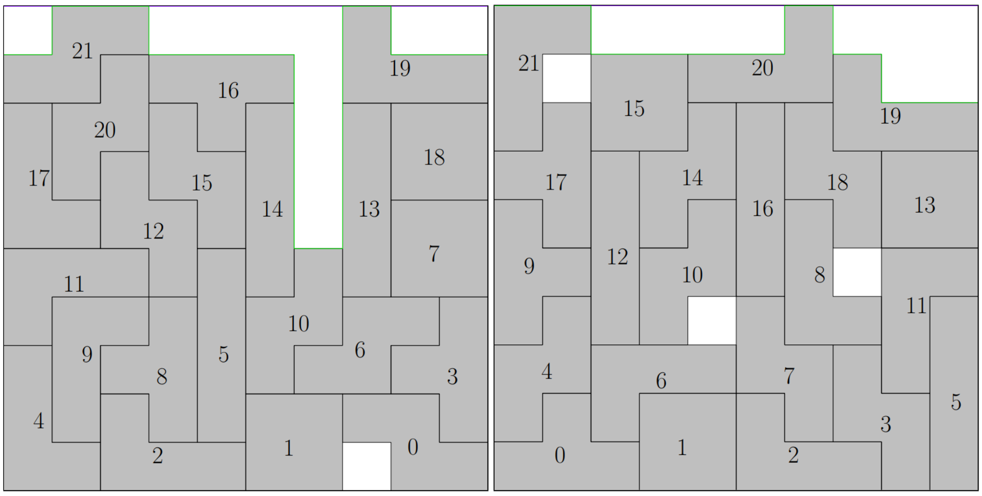

(A) e=0.011 (B) e=0.011

FIGURE 5.43: Packing result for combination of weighting coefficients (a) (C_V=1, C_D=1.6 C_V=0.4, C_{CN}=0.045) (b) (C_V=5, C_D=1.25 C_V=0.4, C_{CN}=0.01).

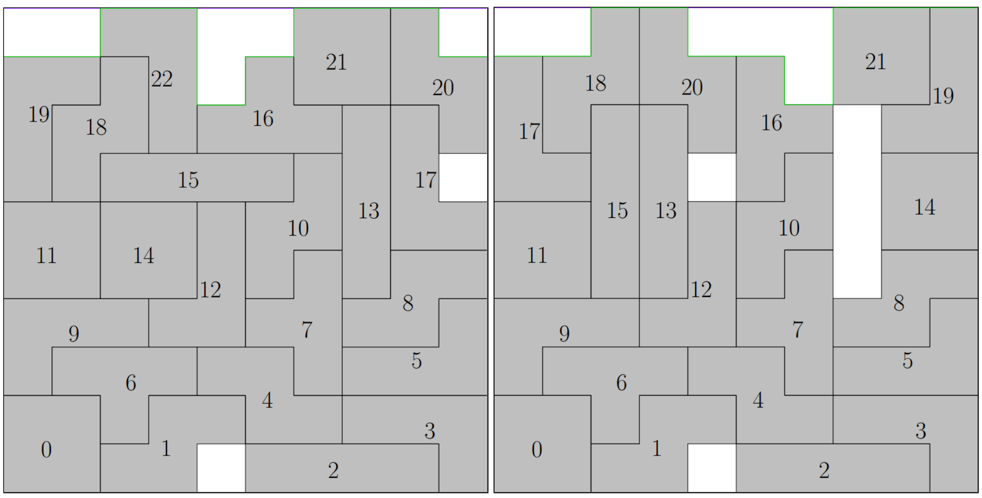

(A) e=0.022 (B) e=0.068

FIGURE 5.44: Packing result for combination of weighting coefficients (a) (C_V=1, C_D=1.6 C_V=0.4, C_{CN}=0.045) (b) (C_V=5, C_D=1.25 C_V=0.4, C_{CN}=0.01).

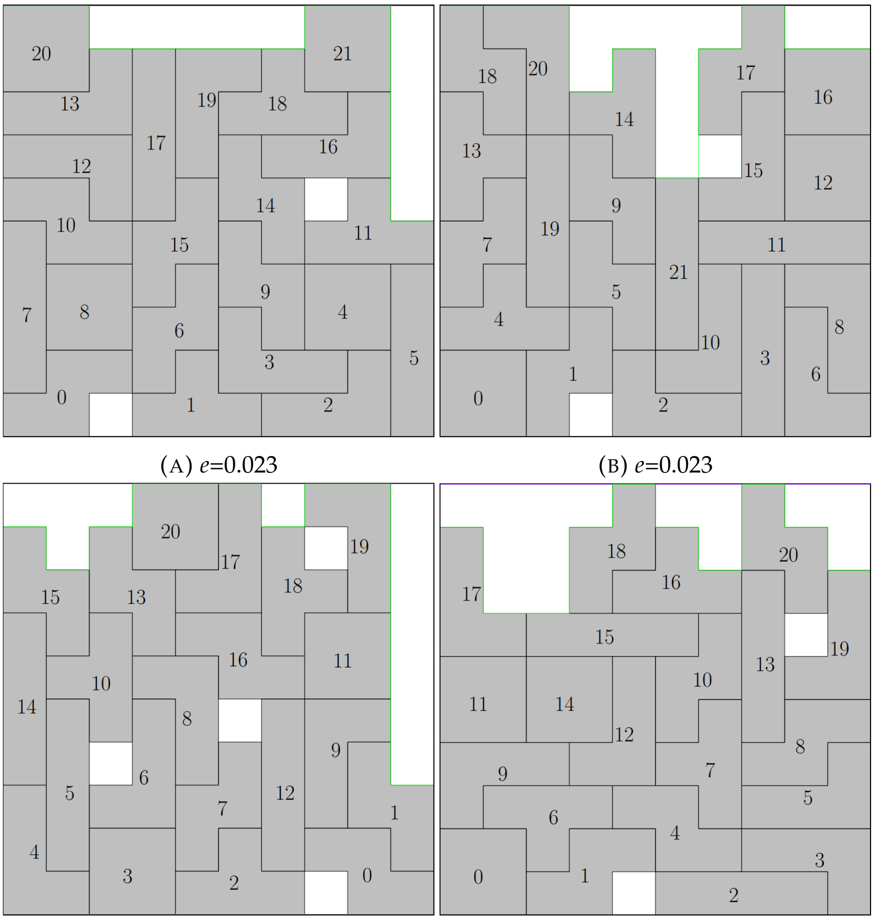

(A) e=0.023 (B) e=0.023

(C) e=0.048 (D) e=0.024

FIGURE 5.45: Packing structures for weighting coefficients (C_V=1, C_D=0.6 C_V=0.2, C_{CN}=0.015) for equivalent particle order to (a) Figure 5.38 (b) Figure 5.41 (c) Figure 5.42 and (d) Figure 5.44.

5.7 Results of DBL Heuristic and Randomly Packed Structures

As stated in Section 4.5, it is required that results are compared to a control to ensure the method of packing is an improvement on what already exists. Two controls are produced for comparison with the obtained optimal solution using weighting coefficients (C_V=1, C_D=1.6 C_V=0.4, C_{CN}=0.045) and the algorithm described in Chapter 3. These are the DBL-heuristic for bin packing and randomly packed tetrominoes into the domain.

The DBL-heuristic is previously introduced in Section 2.4.3 and is used by Wang and Hauser (2019) as a Deepest-Bottom-Left Fit for packing items into a bin. The heuristic follows that items are to be packed at their the deepest location in the bin, followed by the left-most location. A similar process has been adopted here for packing tetrominoes in the 10x10 square domain. The packing is conducted by locating the tetromino in the deepest location, followed by the left-most location with an additional clause that a rotation in this location should be prioritised if it produced no void below the particle. This ensures that particles are not placed at a random orientation and comply in some way to the objective of minimising void ratio. Therefore, the heuristic is actually a DBL-R heuristic as it takes into account rotation of the particle. However, this will referred to as the DBL heuristic from here on.

Randomly packed particles are done so by letting the algorithm select a position for tetrominoes at any location at any orientation. Results of these packings exhibited void ratios well above those seen for solutions using a heuristic. As a result, another approach was taken scoring placement using the objective function with coefficients (C_V=5, C_D=1.25 C_V=0.4, C_{CN}=0.01) as were determined in Hoodless and Smith (2023) and for coefficients (C_V=1, C_D=1.6 C_V=0.4, C_{CN}=0.045). However, a random lateral location is selected and the highest scoring rotation is taken forward. Coefficients equivalent to and different to the optimal solution were investigated to see if this any similarities would lie between (C_V=1, C_D=1.6 C_V=0.4, C_{CN}=0.045) and its random counter part which do not exist in random packings adopting (C_V=5, C_D=1.25 C_V=0.4, C_{CN}=0.01). These random packings are referred to as

- RAND: The totally random technique where lateral position and rotation are both random
- RAND-OF1: Where lateral location is randomised and objective function is employed to score the best rotation for this location using coefficients (C_V=1, C_D=1.6 C_V=0.4, C_{CN}=0.045).
- RAND-OF2: Where lateral location is randomised and objective function is employed to score the best rotation for this location using coefficients (C_V=5, C_D=1.25 C_V=0.4, C_{CN}=0.01) which were determined in Hoodless and Smith (2023).

Table 5.15 presents the MVR results for the DBL heuristic and the randomly packed structures RAND, RAND-OF1 and RAND-OF2 for sample sizes n=30 and n=100. The results using the objective function and coefficients (C_V=1, C_D=1.6 C_V=0.4, C_{CN}=0.045) are also repeated in Table 5.15 under Objective Function.

MVR results for (C_V=1, C_D=1.6 C_V=0.4, C_{CN}=0.045) are a massive improvement on the structures which are constructed by random placements, RANDOF-1 and

Heuristic	MVR (n=30)	MVR (n=100)
RAND	0.6343	0.6560
RAND-OF1	0.2589	0.2483
RAND-OF2	0.2267	0.2203
DBL	0.0700	0.0707
Objective Function	0.0223	0.0271

TABLE 5.15: MVR results for heuristics explored as controls for n=30 and n=100 with results for the objective function using coefficients (C_V=1, C_D=1.6 C_V=0.4, C_{CN}=0.045) for comparison.

RANDOF-2 included. Additionally, the use of the objective function with these coefficients appears to improve on the packing following the DBL heuristic. Figure 5.46 and Figure 5.47 present packing results from the use of the DBL heuristic and random selection of placement respectively.

5.8 Summary

Following the methodology presented in Chapter 4, a weighting coefficient combination of (C_V=1, C_D=1.6 C_V=0.4, C_{CN}=0.045) was determined. It has been shown from comparison with results that are produced from the coefficient combination of (C_V=5, C_D=1.25, C_T=0.4, C_{CN}=0.01) determined in Hoodless and Smith (2023) that (C_V=1, C_D=1.6 C_V=0.4, C_{CN}=0.045) generally leads to better packing of the tetrominoes. Although MVR for $n = 30$ and n=100 is lower for coefficients (C_V=1, C_D=0.6 C_V=0.2, C_{CN}=0.015), this is due to canyoning occurring in the packing with the absence of a capping particle to include this void in the final void ratio of the system.

The effect of each criteria in the objective function was investigated in Section 5.3. Independent to other criteria, V_{AB} produced the lowest MVR values when compared to D, T, and CN. In addition, when the value of the coefficient is oversized compared to the others (e.g. C_V=100 whereas C_D=C_T=C_{CN}=1), V_{AB} also exhibits the lowest MVR values compared to the other criteria. This is reasonable as V_{AB} scores placements on minimising void ratio in the system. The introduction of D, T and CN stop canyoning whilst packing as shown in Figures 5.4 and 5.5.

It was seen when V_{AB} was not included in the objective function that values of C_T at the location of the lowest MVR was increased. This is due to T being defined by a method where particles are scored higher if they have more area in contact with other particles. As tetrominoes are flat-to-flat edges, this leads to almost having the same effect as V_{AB}, although T does not account for the size of the void created beneath the particle. Therefore T acts as a substitute criteria for V_{AB}.

The introduction of D and T in the objective function both have a positive influence on MVR, producing lower values when included. From the investigation, CN has a detrimental influence. However, as seen with the value of C_{CN}=0.01 for the final solution from Hoodless and Smith (2023), this may be due to the sampling frequency not being defined enough to see effects when this value is much lower than the other coefficients.

Section 5.4 begins the process of determining the optimal combination of weighting coefficients by exploring C_D, C_T, C_{CN} between the range of 0 to 10 whilst C_V=1 is kept as a constant. Results are analysed using MVR values for the unfiltered and

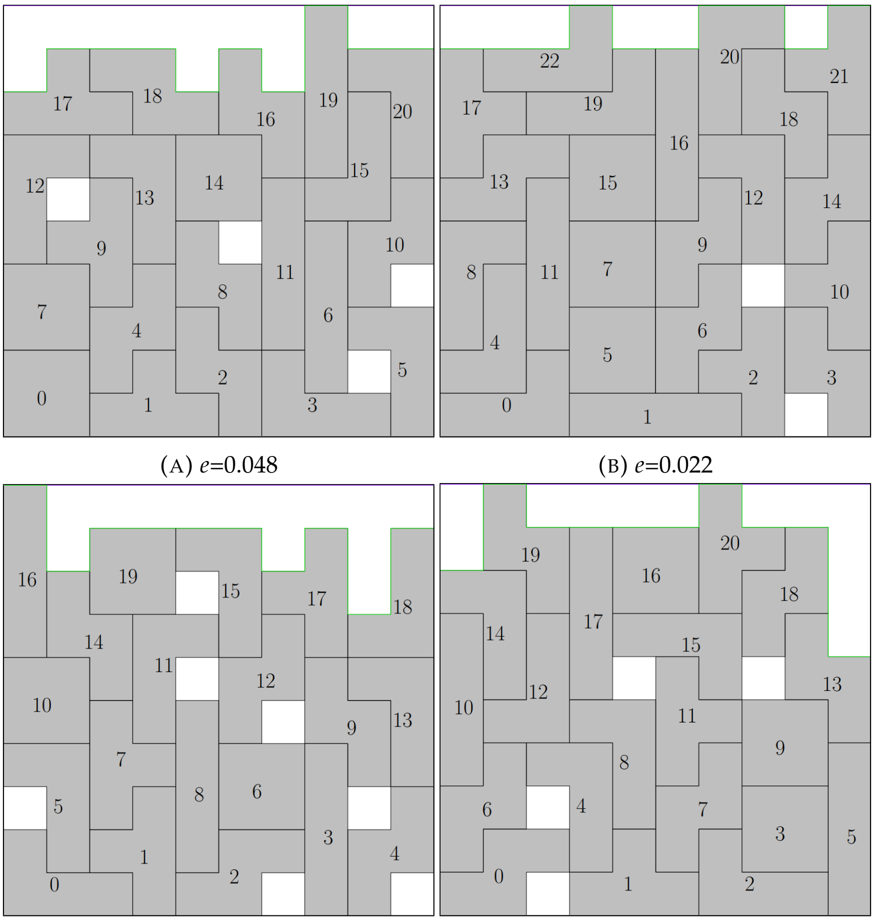

(A) e=0.048 (B) e=0.022

(C) e=0.088 (D) e=0.048

FIGURE 5.46: Packing structures following DBL-heuristic for equivalent particle order to (a) Figure 5.30 (b) Figure 5.31 (c) Figure 5.32 and (d) Figure 5.33.

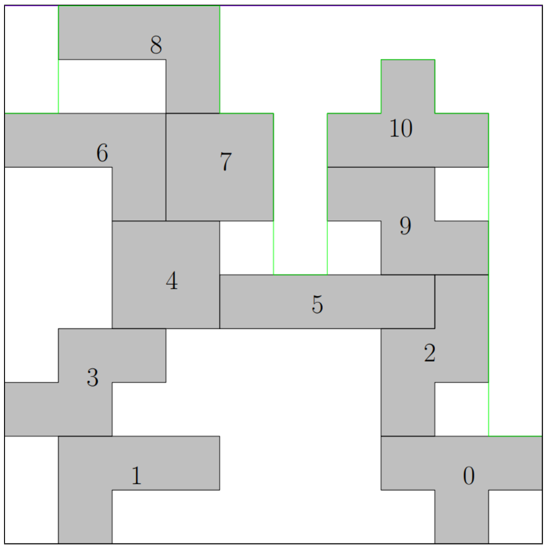

(A) e=0.048

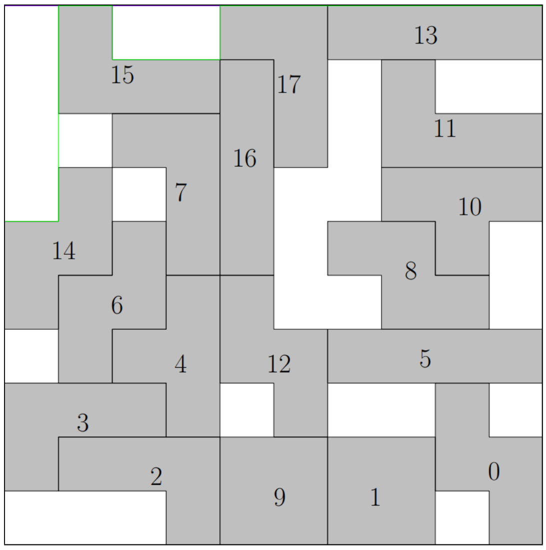

(B) e=0.022

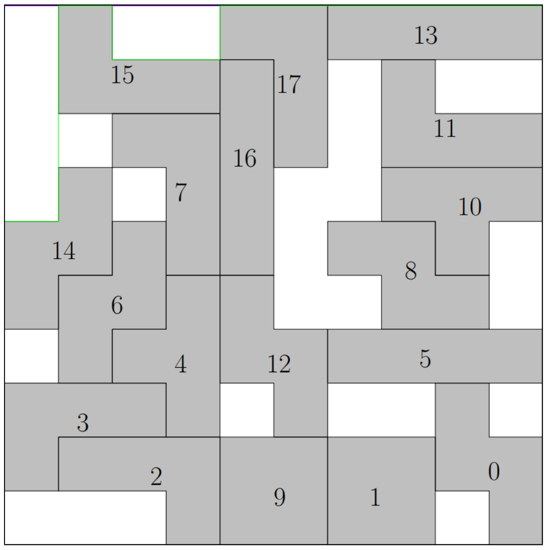

(C) e=0.088

FIGURE 5.47: Packing structures following random packing determined by (a) RAND (b) RAND-OF1 (c) RAND-OF2.

filtered data and the location of lowest MVR values found for each search area when C_D is varied are presented. n=9, n=30 and n=50 results were all presented as these had already been collected from studies when determining the required sample size in Chapter 4. These results provided further evidence that n=30 is a reasonable sample size to take to represent the whole population of possible void ratios when packing as was originally found in Section 4.3.

Refinement of the search area was conducted in Section 5.4.2 by increasing the sampling frequency i.e. using smaller incremental values between the values of the coefficients. An incrememnt value of 0.5 was adopted for the same range of 0 to 10 as seen in Section 5.4. Due to fast computational speeds of the algorithm for the Tetris Scenario, it was possible to do this for the whole range already explored. Further detail for the location of an optimal solution was obtained with values of MVR suggesting this lies around C_D=3.5 when analysing the Gaussian filtered data and C_D when analysing the unfiltered data. C_D=3.5 was adopted for further exploration as the value of lowest MVR for C_D=1 was seen at a local minimum with relatively large values for the surrounding datapoint meaning this combination is very sensitive to change.

Section 5.5 furthers the refinement of the search area as well as exploring coefficients of different magnitudes in comparison to C_V. It has already been stated that coefficient values of 10 should be large enough to create dominant scoring criteria in the objective function. Section 5.5.2 utilises the faster computational speeds when packing during the Tetris Scenario to provide evidence for this by increasing coefficient values. No indication of a optimal solution is provided by this investigation as was expected. This study is conducted here to provide evidence that this is not required for the Soil Particle Scenario, where computational runtime is much larger.

Section 5.5.3 refines the search area around the suspected minimum in the range of C_D=3.5. A solution that provides the lowest MVR value is located at (C_V=1, C_D=3.3, C_T=1, C_{CN}=0) where MVR=0.316 when n=30. Meanwhile, Section 5.5.4 explores search areas where coefficients range from 0 to 1 to allow $C_V V_{AB}$ to become more dominant in the objective function. Values of MVR exhibited are much lower than 0.316 as determined at (C_V=1, C_D=3.3, C_T=1, C_{CN}=0). Therefore, it is known that an optimal solution actually lies in this range and further exploration of the search area around these points are conducted. Two possible optimal solutions are located for the range of C_D=0.6 and C_D=1.5 which are studied further.

From the process of refining coefficient values by adopting a smaller increment, two locations are determined that could potentially be optimal solutions for combinations of weighting coefficients for packing tetrominoes with the objective to minimise void ratio. These are located at (C_V=1, C_D=0.6, C_T=0.25, C_{CN}=0.02) and (C_V=1, C_D=1.6, C_T=0.4, C_{CN}=0.045) where MVR=0.0211 and MVR=0.0226 for the unfiltered data. Of these, (C_V=1, C_D=1.6, C_T=0.4, C_{CN}=0.045) provides the lowest MVR for the Gaussian filtered data, which was 0.0242 compared to 0.0244 for (C_V=1, C_D=0.6, C_T=0.25, C_{CN}=0.02). Therefore it is suggested that this is to be the optimal solution as it will be less sensitive to change as was discussed in Section 4.4.4.

Results for packings adopting coefficients of (C_V=1, C_D=1.6, C_T=0.4, C_{CN}=0.045) are presented in Section 5.6 with the equivalent particle delivery order using coefficients (C_V=5, C_D=1.25 C_V=0.4, C_{CN}=0.01) as was determined as the solution in Hoodless and Smith (2023). The solution that is suggested in this work was shown to outperform that from Hoodless and Smith (2023). Figures 5.30-5.44 are the packings using both of these coefficient combinations. Furthermore, results of (C_V=1, C_D=0.6, C_T=0.25, C_{CN}=0.02) were also presented using the equivalent particle order as Figures 5.30-5.44. It was found that packings for this combination matched those from (C_V=1, C_D=1.6, C_T=0.4, C_{CN}=0.045) and (C_V=5, C_D=1.25 C_V=0.4, C_{CN}=0.01) as indicated in Table 5.14 except for four of the packings presented. These can be found in Figure 5.45.

Comparison of the number of instances that (C_V=1, C_D=1.6, C_T=0.4, C_{CN}=0.045) outperformed, was outperformed or produced equivalent void ratio results with regards to (C_V=5, C_D=1.25 C_V=0.4, C_{CN}=0.01) and (C_V=1, C_D=0.6, C_T=0.25, C_{CN}=0.02) suggest that the packings overall have similar levels of efficiency. This was suggested when looking at results for a sample size of 30 as well as a sample size of 100. However, results for (C_V=5, C_D=1.25 C_V=0.4, C_{CN}=0.01) and (C_V=1, C_D=0.6, C_T=0.25, C_{CN}=0.02) showed canyoning in their packings without the presence of a capping particle. Therefore, these gaps were not included in the final void ratio of the system. It is determined that (C_V=1, C_D=1.6, C_T=0.4, C_{CN}=0.045) is a more suitable solution as canyoning was not present when viewing results produced by the algorithm.

Controls for packing are produced in Section 5.7. These employ the DBL heuristic as well as random placement of particles, either at a random orientation or orientation determined by the algorithm from Chapter 3 using coefficients (C_V=1, C_D=1.6, C_T=0.4, C_{CN}=0.045) or coefficients (C_V=5, C_D=1.25 C_V=0.4, C_{CN}=0.01). Packings analysed in Section 5.6 massively outperformed cases where particles are placed randomly, even when scoring of the placement to determine orientation is used. Packings using the DBL heuristic showed better results compared to random packings, yet MVR results were still much greater than those exhibited in Section 5.6.

To conclude, from the exploration of the search area for MVR results produced when packing tetrominoes in the Tetris Scenario with the objective to minimise void ratio, it can be stated that coefficient combination (C_V=1, C_D=1.6, C_T=0.4, C_{CN}=0.045) provides the best results of all combinations investigated. Study of the packings shows that these outperform other suggested combinations for optimal solutions as well as control heuristics tested. For n=30 and n=100, values of MVR=0.0223 and MVR=0.0271 are produced with the omission of Gaussian filter to the search area. (C_V=1, C_D=1.6, C_T=0.4, C_{CN}=0.045) was located in the search area with an MVR=0.0242 when C_D=1.6 and C_T was ranged from 0 to 0.7 at increments of 0.05 and C_{CN} was ranged from 0 to 0.1 at increments of 0.005.

Chapter 6

Results of the Soil Particle Scenario

6.1 Introduction

In this section, results of packing in the Soil Particle Scenario are presented. MVR is to be taken as an indication of high shear strength structures. However, as stated by Mogami (1965), this cannot be taken alone and another parameter is required. Therefore, the number of running joints disrupted in the system (MRJ) is also taken. This was derived as a suitable quantity in Section 2.2.1. Results for both are analysed, with MRJ being prioritised as indication of high shear strength.

The layout of the chapter is as follows. Section 6.2 describes the necessary changes to the method from those stated in Chapter 4. This is due to the increased computational speeds of the algorithm when defining irregular objects compared to the simple tetromino shapes.

Section 6.3 investigates the effect of changing the coefficient values in the objective function on the packing of the structures. Each variable in the objective function. This is completed by changing the value of the coefficient. Each parameter is examined individually by setting its coefficient to a value of one and all other coefficients to a value of zero. Furthermore, the oversized effect is investigated by setting the coefficient for the parameter to be a value of 100 and all other values are set to 1. Section 6.3.3 completes this study and presents packings for these cases.

The analysis of combinations of weighting coefficient is found in Section 6.4. Results of MRJ and MVR are analysed and areas of interest are investigated further where it is suggested optimal solutions may lie. From examining these packings, further studies are found in Section 6.4.2 where the effect of $C_V V_{AB}$ in the objective function is increased.

In Section 6.5, packings using the coefficients obtained from Chapter 5 found to be possible optimal solutions for the Tetris Scenario are produced. These are to be compared to. Furthermore, control samples are produced in Section 6.6 to provide evidence that the method of packing by the algorithm is suitable for positioning soil particles in the domain.

6.2 Required Changes to Method

6.2.1 Sample size and Sampling Frequency

With the inclusion of additional rotations and a finer spacing between lateral locations tested as suggested in Section 3.7.4, the time to run a simulation of particle placement greatly increased. The computational runtime for a single run increased to around 2.5 hours. Therefore, it is not feasible to do as many runs as previously seen in Chapter 5. Therefore, in this section a sample sizes of n=3 are adopted. If there were no time restraints for this project then sample sizes of n=9 to n=30 could be investigated as suggested in Chapter 4.

Additionally, it is known that larger quantities of coefficients explored with a higher frequency of data points will lead to higher accuracy of the results. Again, due to time limitations this is not possible. If there were no time restraints for this project then a higher sampling frequency could be adopted with a greater exploration of the search area. Because of the reduced number of datapoints, this leads to omission of the Gaussian filter. Such a method would lead to zeropadding on most results in the search area.

6.2.2 Definition of Particles

To further reduce the computational time required, the number of coordinates used to describe the particle was decreased. Originally, 129 coordinates were utilised for the particle outline. However, it was found that the particle could be described with a third of the coordinates whilst still resembling a similar shape so long as the particle remains a closed loop. This was originally discussed in Section 3.7.1. The use of non-dimensional criteria in the objective function means that this reduction in coordinates should not lead to a change to how particles are scored on placed. However, there will be some change to how particles are placed due to stability checks where perhaps locations of contact are not present when they would be if all coordinates were utilised to describe particle shape.

An example of this is seen in Figure 6.1. Both packings are of the same particle order for when coefficients are set to zero values with parameters defined by the values stated in Table 6.1. Positioning of the particles in their final placement differs when comparing Figure 6.1a where outlines were defined using the total number of coordinates to Figure 6.1b where outlines were defined using a third of the total number of coordinates. As mentioned this is because less stable positions are able to be identified by the reduction of coordinates. Contact of the particles with the domain and other particles are determined at each coordinate of the particle and the surface line. Therefore, the less coordinates that are utilised for defining particles the less chance of identifying a stable position. This limits the number of possible placements leading to lower efficiency at packing. For the current project, it is more important to increase computational speed for an initial investigation rather than producing very accurate and precise packings.

6.3 Effects of Changing Coefficient Values

6.3.1 Investigation Parameters

In this section, an investigation into the effect of each criteria in the objective function described in Section 3.5.1 is carried out. Results of the void ratio of the structures for the Soil Particle Scenario is investigated, similar to Section 5.3 for the Tetris Scenario. As stated by Mogami (1965), void ratio cannot be used on its own to describe the properties of granular material. Therefore the identification of runs in the structure has been completed and the number of runs that are disrupted in the structure are presented such as described in Section 3.10.2. It is important to understand the effect of each criteria in the objective function to determine if the inclusion of these parameters has a positive effect on resulting packings.

Input parameter values selected for the algorithm described in Chapter 3 that were selected for the study in the investigation here are presented in Table 6.1.

Number of particles placed	40
Number of particles available for selection	100
Number of rotations in the discretised placement	16
Spacing between placement in the refined phase	0.2 units
Rotation applied in the refined phase	5.625^o
Resolution	0.5
Number of candidate positions trialled	30

TABLE 6.1: Parameters adopted for the study in this chapter, as determined in Section 3.7.5.

6.3.2 Zero Value for Coefficients

When particles are placed with no scoring of placement, i.e. coefficients of weighting are all set to be zero values, the candidate positions that are trialled for placement are based upon the remaining categories in the priority order analysed during the discretised particle positioning in Section 3.7.3. These prioritise

1. the score achieved when completed for the discretised particle and domain - for which this value is always zero as no criteria are activated in the objective function
2. depth in the system
3. the left-most position
4. area beneath the particle to the width of the particle ratio
5. width to height ratio

in the order they are stated.

Therefore, a bottom-left heuristic is adopted followed by the prioritising of the minimum amount of void created below the placement and then followed by the particle being placed so that it's height is minimised. After the discretised placement phase, the refined placement phase will have no effect on placement except for removing positions which are determined to be unstable via the method described in Section 3.9. The first stable position is chosen from the sorted candidate positions.

Figures 6.1-6.4 show some results of the placement of the rock particles with coefficients of weight set to equal zero values. 40 particles are placed in a domain of 50x50 units. The parameters used for the run are seen in Table 6.1. In total, 5 runs were performed for the case where all coefficients were set to a zero using all available coordinates for describing the shape outline. Particles are placed in courses such as a bottom-left heuristic would attempt to follow, building up in a layer-by-layer process. In this scenario it is clear that void beneath the particle is not being prioritised with particles standing on just one point of their outline. This is especially highlighted in the lowest course in the domain, usually consisting of the first 9 particles placed.

The envisioned result here is that the particles would be flatter due to criteria 3 and 4 in the priorities list from the discretised particle scoring. It is believed that as priority criteria 2 is trying to place the particle at the position with the lowest abscissa value possible, this is causing particles to be stood tall as this results in the centre of gravity to be closest to the left-hand side. Therefore the effects of priority 3 and 4 are being ignored unless multiple rotations exist where the centre of mass is positioned at the same x-coordinate. The results are reasonable for a DBL heuristic for bin packing, but in terms of sensible packings of irregular, untooled rock particles the algorithm suffers from a lack of placement scoring using the objective function.

Figure 6.1b is the packing of equivalent particle order to Figure 6.1a with particle outlines defined by a third of the total coordinates available. Section 6.2.2 discussed the difference between packings is due to fewer detections of contact points meaning fewer stable positions are determined. However, it can be shown that the manner in which the packing arrangements are achieved is through a similar fashion just with the difference that the system in Figure 6.1b is less tightly packed compared to Figure 6.1a. The packings investigated in Section 6.3 are defined using all available coordinates. However, packings when completing exploration of the search area are achieved adopting a third of coordinates to describe the particle outline. A comparison will be made in Sections 6.3.3 to determine if this changes the end result of packings by the algorithm of equivalent coefficient values.

For the five simulations conducted taking all available coordinates MVR=0.2750 and MRJ=21.6 as indicated in Table 6.2 where a packing with all coefficients of weighting set to zero is indicated as "none".

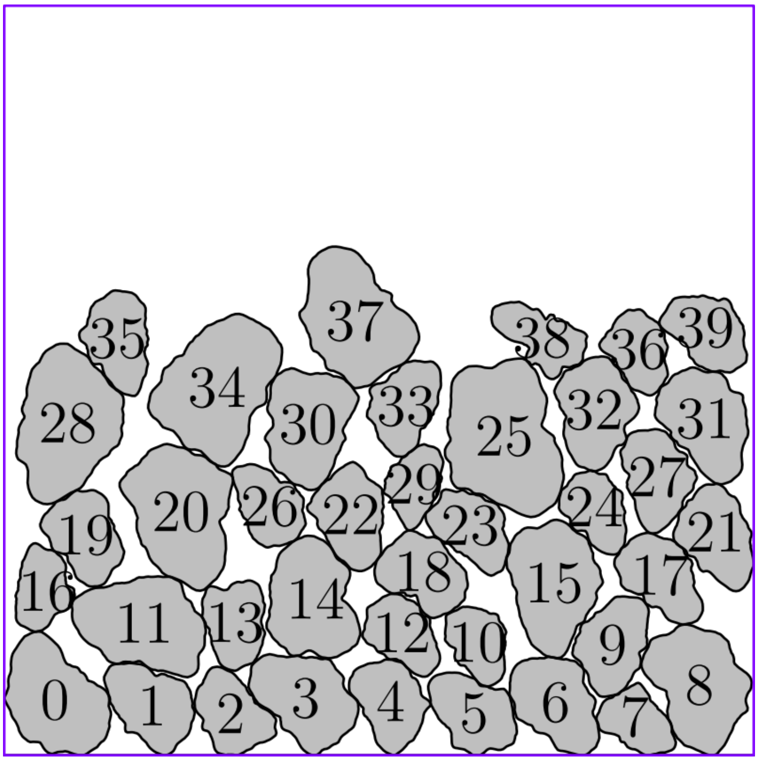

(A)

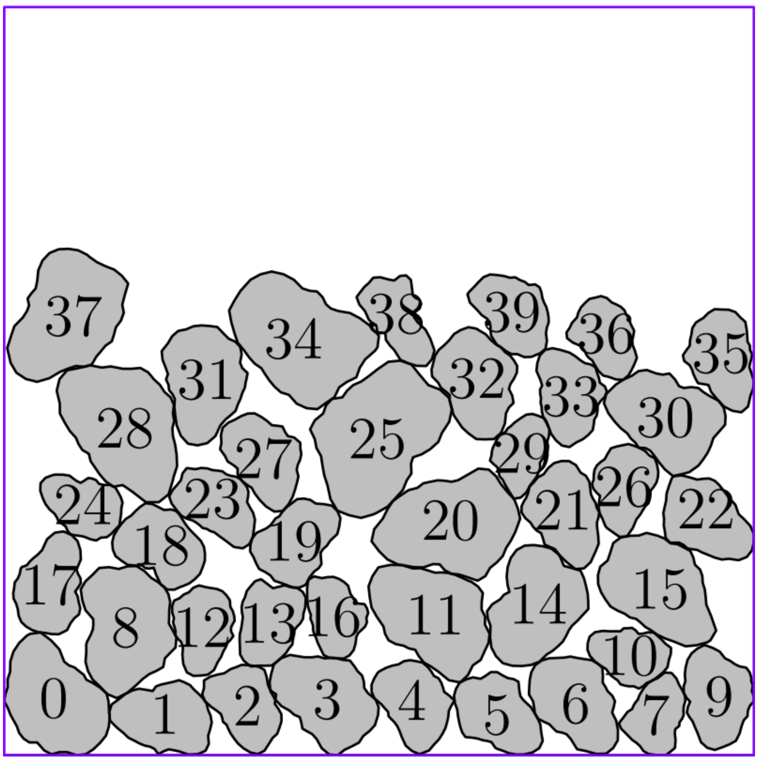

(B)

FIGURE 6.1: Packing of 40 rock particle outlines in a 50x50 unit domain with coefficients of weighting set to zero values for particles represented by (a) all 129 coordinates (b) a third of coordinates.

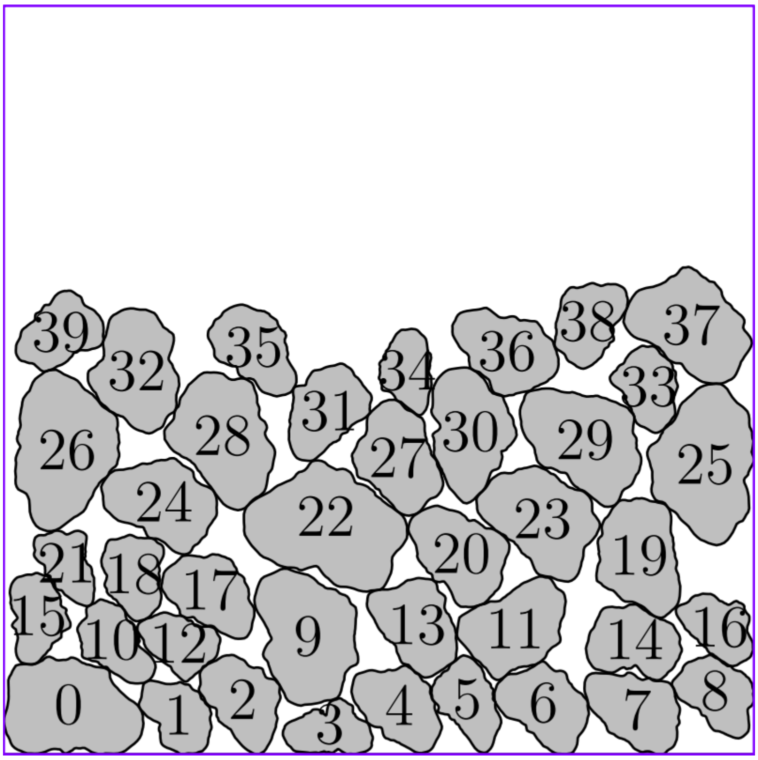

FIGURE 6.2: Packing of 40 rock particle outlines in a 50x50 unit domain with coefficients of weighting set to zero values.

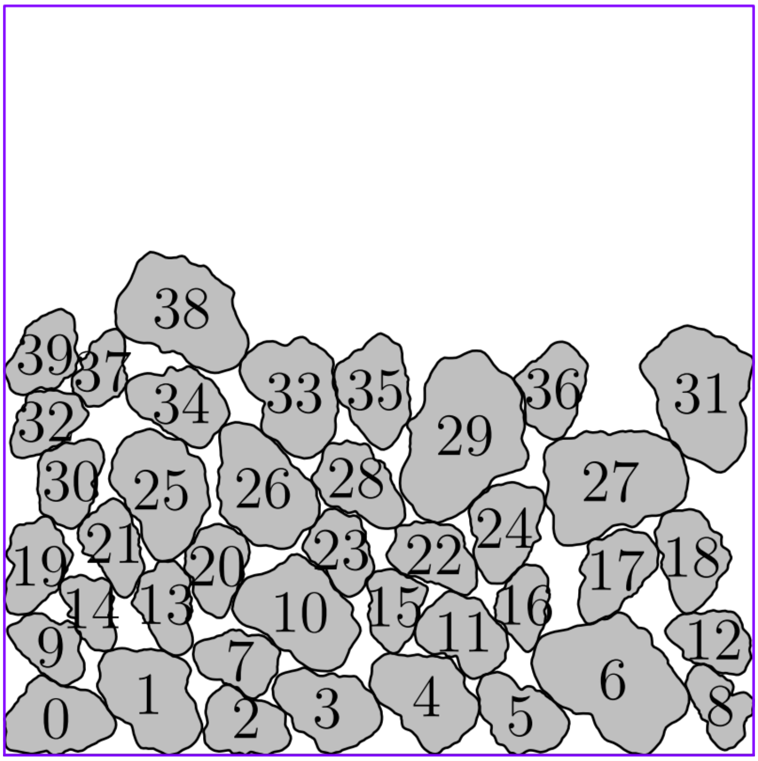

FIGURE 6.3: Packing of 40 rock particle outlines in a 50x50 unit domain with coefficients of weighting set to zero values.

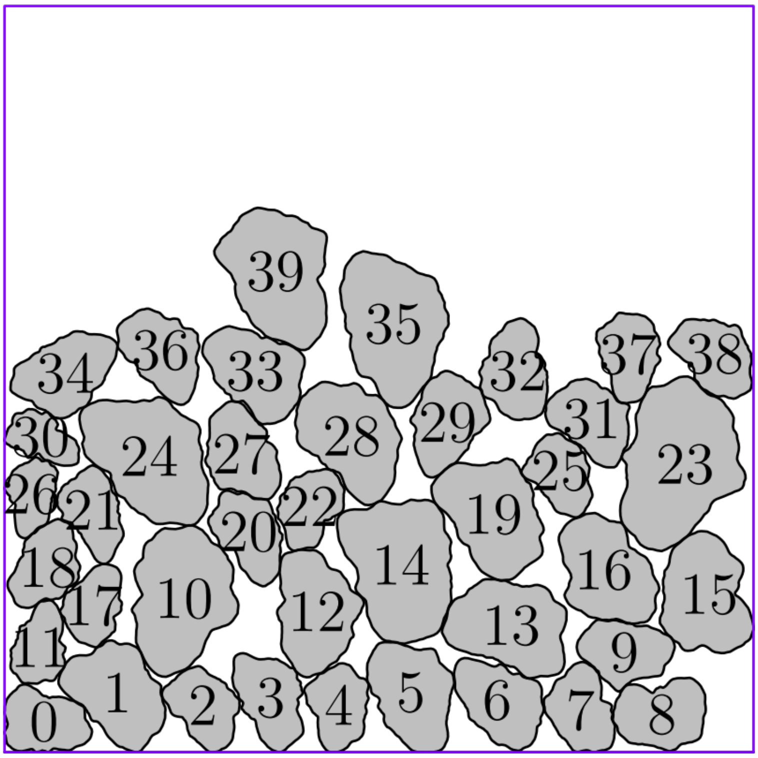

FIGURE 6.4: Packing of 40 rock particle outlines in a 50x50 unit domain with coefficients of weighting set to zero values.

6.3.3 Impact of Coefficients

Here, the impact of each component is investigated individually. This is done by setting each coefficient to a value of zero and activating one parameter by changing the value of the coefficient for that parameter to a value of one. This is carried out in each of Sections 6.3.4-6.3.7. Additionally, the effects of oversizing each coefficient compared to the other coefficients is investigated similar to what was carried out in Section 5.3 by equating a single coefficient value to 100 and the rest to a value of 1. The results of the MVR and MRJ for both of these scenarios are presented in Table 6.2. Values were calculated from the mean of n=5 for each scenario. Results in Table 6.2 were calculated from packings using all available coordinates. The study was repeated for packings using a third of coordinates, although MRJ was not recorded for oversized coefficient packings. These are presented in Table 6.3.

Comparing values from Table 6.2 and Table 6.3, values for MRJ and MVR differ with no pattern. Reducing the number of coordinates changes the way in which stable positions are located, so therefore it is thought that candidate poses which were deemed as acceptable are discarded in the scenario where particles are resembled by a third of all coordinates. From analysis of the packings (Figure 6.10, Figure 6.17, Figure 6.23, Figure 6.32) the particles are still being packed in a similar fashion when compared to the packings using all available particles. Additionally, changes in MVR between the variable as a single criteria in the objective function and as an oversized variable all show equivalent trends: reducing for V_{AB}, staying roughly the same for D, increasing for T and decreasing for CN. Therefore it is assumed that a third of the coordinates can be taken and still be a fair representation of the packings compared to if all coordinates were taken. The computational time is massively reduced by doing so and therefore any negatives that are seen are outweighed by

Variable Activated	Single Coefficient		Oversized	
	MRJ	MVR	MRJ	MVR
None	21.6	0.2750	-	-
V_{AB}	24	0.2629	25	0.1978
D	24	0.2143	23	0.2113
T	22.8	0.2260	22.2	0.2616
CN	22.4	0.2113	23.8	0.1954

TABLE 6.2: MRJ and MVR for sample size n=5 using all available particles for the Soil Particle Scenario when a single coefficient is used so the indicated variable is the only active criteria in the objective function and for the oversizing of the variable where the coefficient for the variable is set to 100 and all over coefficients are set to a value of 1.

Variable Activated	Single Coefficient		Oversized	
	MRJ	MVR	MRJ	MVR
V_{AB}	24.4	0.2085	-	0.1859
D	19	0.2222	-	0.2066
T	21.8	0.2567	-	0.2706
CN	21.8	0.2127	-	0.1989

TABLE 6.3: MRJ and MVR for sample size n=5 using a third of all available particles for the Soil Particle Scenario when a single coefficient is used so the indicated variable is the only active criteria in the objective function and for the oversizing of the variable where the coefficient for the variable is set to 100 and all over coefficients are set to a value of 1.

the increased speeds. Therefore, from Section 6.4.1 packing done by the algorithm adopts the use of a third of all available coordinates.

Figure 6.5 shows values for MRJ and MVR when coefficients are increased individually from 0 to 10 at increments of 2. Other coefficients are kept at a constant variable of 2 and C_V=1. Sample size n=3 was adopted and particles were represented by a third of available coordinates. Each coefficient is explored individually in Sections 6.3.4-6.3.7 and Figure 6.5 will be referenced to.

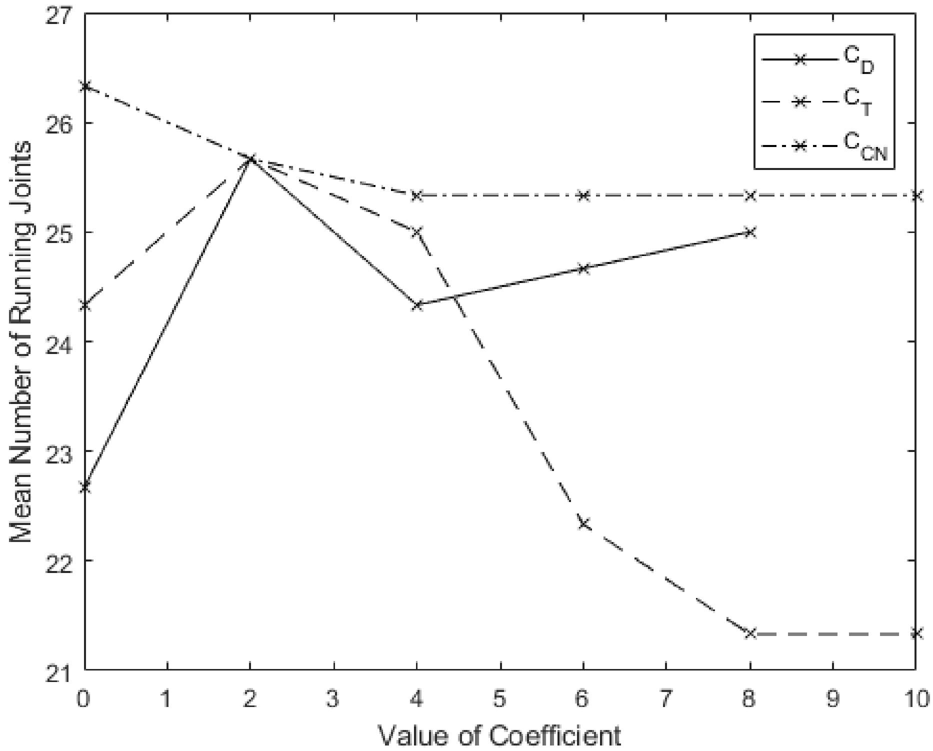

(A)

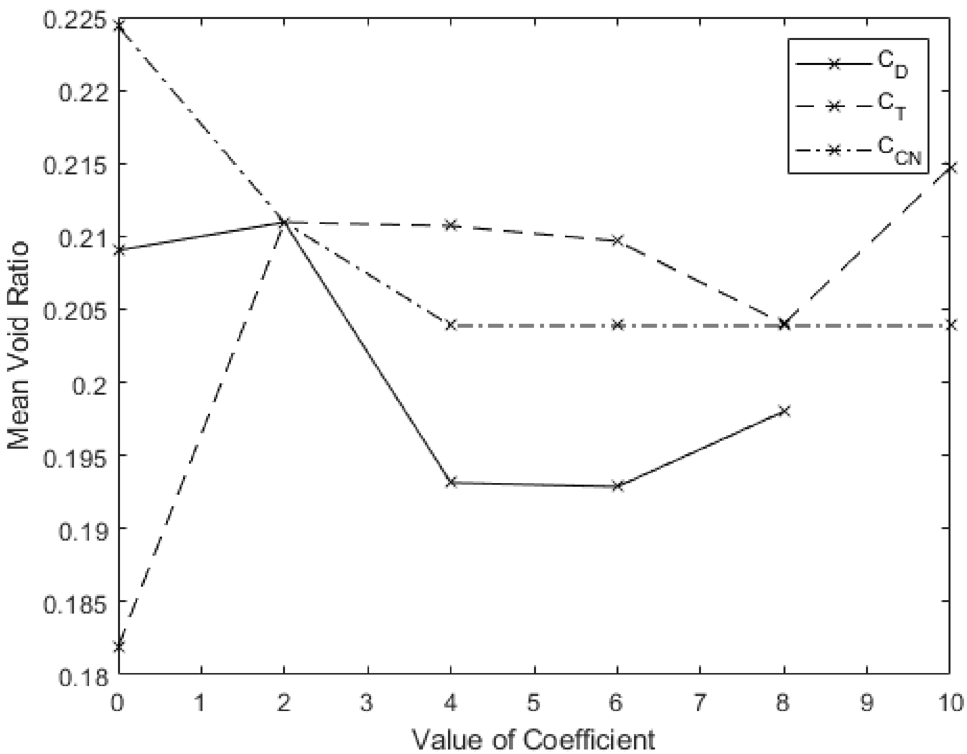

(B)

FIGURE 6.5: Values of (a) MRJ and (b) MVR for the varying of coefficient values. Each value of coefficient varied from 0 to 10 at increments of 1 whilst rest are fixed at a value of 2. C_V=1 for all plots. Sample size n=30 and a third of available coordinates taken.

6.3.4 Effect of V_{AB}

Figures 6.6-6.9 show packings of particles when C_V=1 and C_D, C_T, C_{CN} are all zero values. With the introduction of a non-zero value for C_V, particles are placed so that minimum amounts of void are created below them. This is highlighted in the bottom row of Figures 6.6-6.9 where particles are placed with more of the particle in contact with the domain base rather than with a single point with another resting on the particle next to it to minimise the distance from the left-hand side.

Further up in the system, particles tend to be bunched closer together and, where possible, the filling of canyons is avoided. Figure 6.8 and Figure 6.9 have gaps in the system where it is expected particles may be able to fill. For example, either side of Particle 21 in Figure 6.8 and beneath Particle 23 in Figure 6.9. It is thought that this is because of particles not being able to fit in this location when performing the rough discretised particle positioning which is then used to create a shortlist of candidate poses. Perhaps with a finer resolution or more care when creating the discretised particles (for example, not assuming all blocks are filled if some of the particle exists in it like described in Section 3.7.3) a tighter packing would be exhibited in these areas.

V_{AB} is determined by the ratio of the area of the void created to the area of the particle. Therefore, creating more void in the system will have a bigger effect than if the void ratio of the whole system. Placements of Particle 26 in Figure 6.6 and Particle 36 in Figure 6.8 go against what is expected from the objective function when positions that would produce a lower score for V_{AB} are possible. It is possible that these positions are selected due to the reduced amount of candidate poses tested with only 30 being trialled. Of the 30 positions trialled, this may be the best scoring position which is also deemed stable by the stability checks described in Section 3.9. Extending the number of candidate positions would lead to the identification of better positions for particles. However, this will lead to an increase in computational time.

The avoidance of covering areas of void can lead to runs developing in the system. Take for example Figure 6.6. Here, a run is detected between Particle 8 and Particle 17. Packing continues of particles and due to canyoning in the system no particle is placed above this until Particle 33 resulting in a running joint between these two locations. This running joint is not disrupted until Particle 37 is placed. Similar instances of this occur in other packing structures where canyons can be identified such as starting between Particle 0 and Particle 2 in Figure 6.8. Although MRJ when V_{AB} is activated is higher than for when T and CN are activated as indicated in Table 6.2, the length of the runs that form can becomes quite large before an interrupting particle is placed.

Figure 6.10 presents the packing using a third of available coordinates for particle delivery order equivalent to those in Figure 6.6 and Figure 6.7. Again a similar trend is seen with particles bunching together as height of the structure increases. An increase in situations where canyons are capped by a particle occurs. This is due to fewer stable positions being detected leading to less alternative options. Examples of this are seen for Particle 30 in Figure 6.10a and Particle 26 in Figure 6.10b.

The capping of canyons is more likely to occur due to less stable positions being detected causing fewer potential positions. In turn, smaller lengths of running joints form as the capping particle tends to disrupt the run. Running joints still tend to be an issue in the structure, for example see Figure 6.10b where a run forms between

Particle 10 and Particle 12 and is not disrupted until the placement of Particle 35, but less so than experienced with packings using more defined shape outlines.

The investigation carried out in Section 5.3.2 for the Tetris Scenario saw the exclusion of V_{AB} as a parameter lead to higher MVR results in the packing as proven in Figure 5.3. A similar investigation was trialled here. From the results presented in Table 6.4 for C_D=0 and C_D=0.5 there does not appear to be much effect on the difference in MVR. When C_D=0.5 the MRJ is increased from 24.4 when V_{AB} is paired with a coefficient of zero compared to 26.6 when V_{AB} is activated suggesting a slight improvement in packing. However, when C_D=1 the MRJ and MVR both improve with MRJ increasing and MVR decreasing. Values from Table 6.4 suggest that packing is improved when higher values of C_D compared to C_V are present. As the optimum combination of coefficients determined to be (C_V=1, C_D=1.6, C_T=0.4, C_{CN}=0.045) in Chapter 5 for the Tetris Scenario it is not unusual for this to be the case. Further evidence for this is provided in Table 6.2 where the packing for an oversized C_V value (so some inclusion of D is involved) is suggested to perform better than an objective function that just scores placement on V_{AB} as determined by the improved MVR and MRJ results. A packing structure for when C_V is oversized is displayed in Figure 6.11.

C_D Value	C_V=1		C_V=0	
	MRJ	MVR	MRJ	MVR
0	25	0.2251	25.6	0.2113
0.5	26.6	0.2106	24.4	0.2094
1	26.4	0.1843	24.4	0.2132

TABLE 6.4: Comparison of lowest MRJ and MVR values for Soil Particle Scenario for values of C_D, C_T and C_{CN} ranged from 0 to 1 at increments of 0.5.

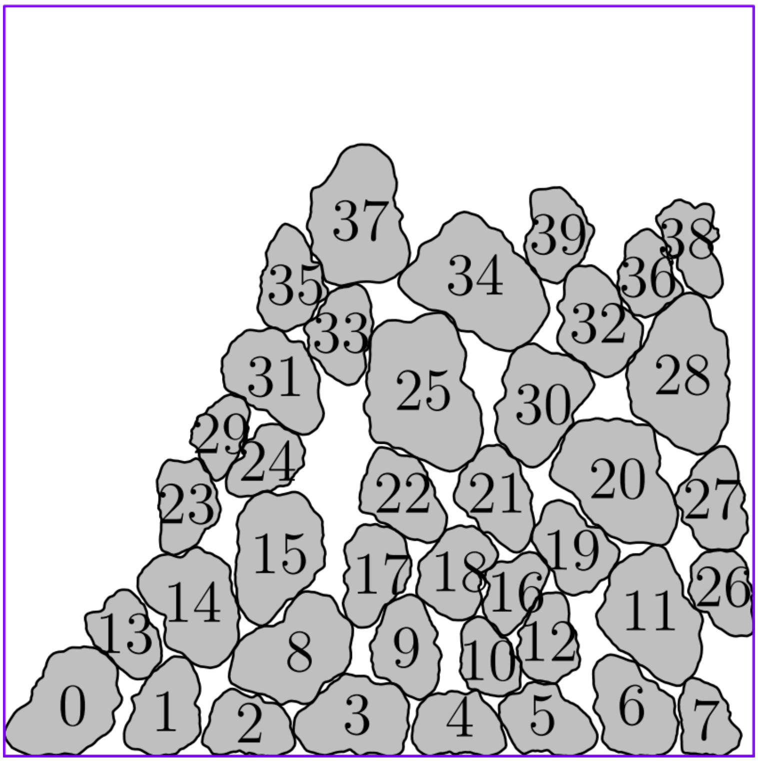

FIGURE 6.6: Packing of 40 rock particle outlines in a 50x50 unit domain with coefficients C_V=1 and C_D=C_T=C_{CN} $= 0$.

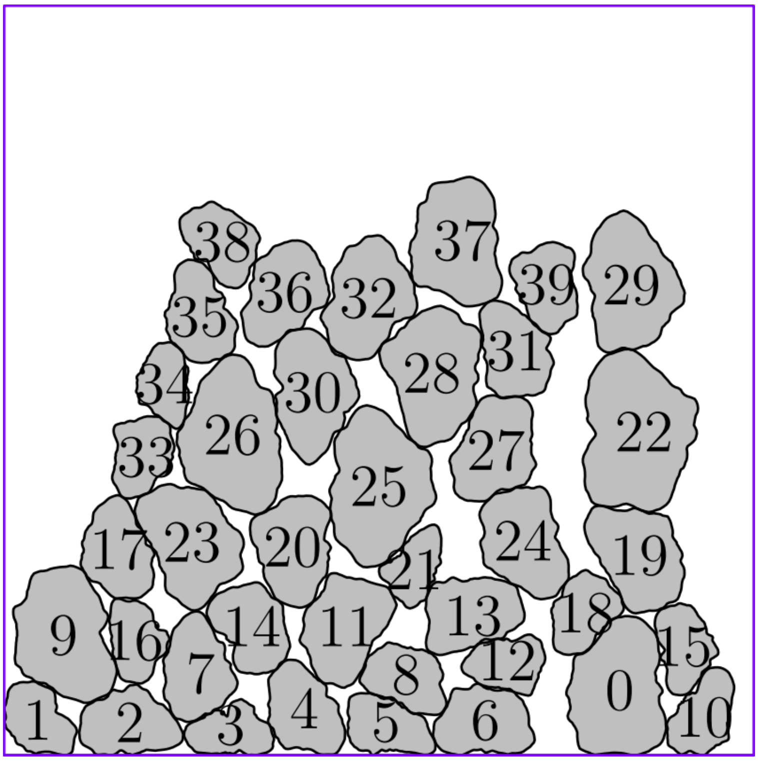

FIGURE 6.7: Packing of 40 rock particle outlines in a 50x50 unit domain with coefficients C_V=1 and C_D=C_T=C_{CN} $= 0$.

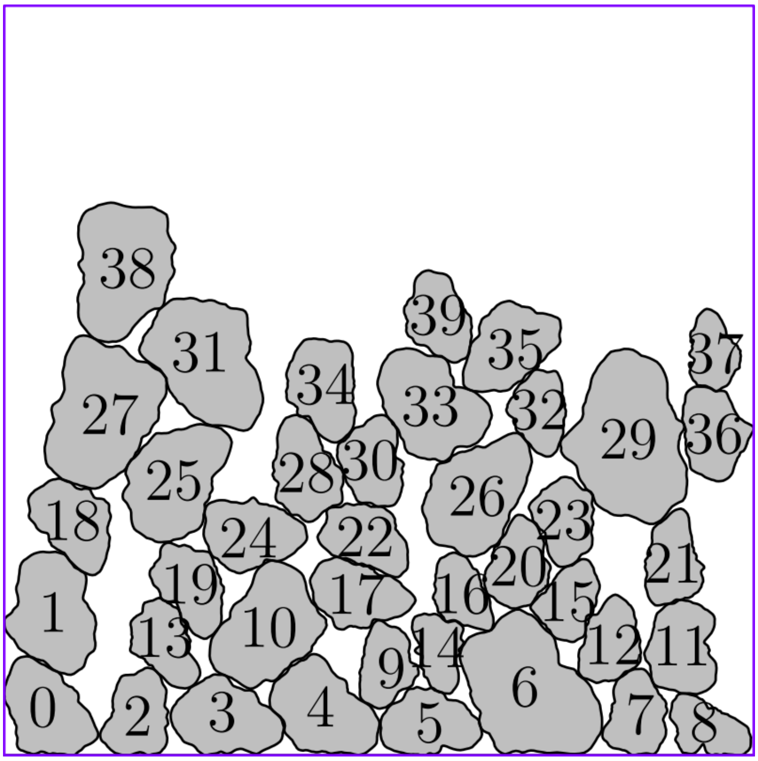

FIGURE 6.8: Packing of 40 rock particle outlines in a 50x50 unit domain with coefficients C_V=1 and C_D=C_T=$C_{CN} = 0$.

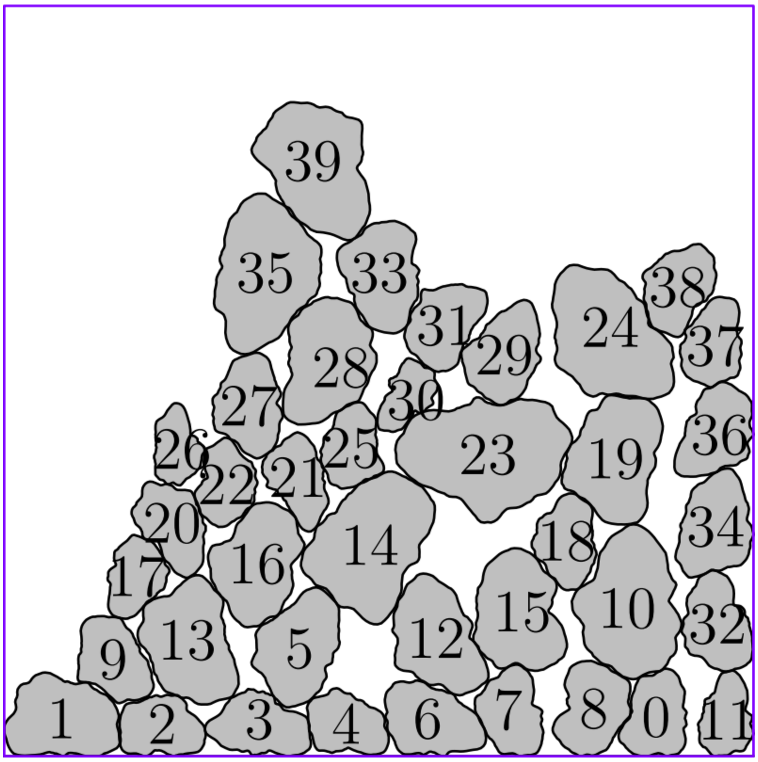

FIGURE 6.9: Packing of 40 rock particle outlines in a 50x50 unit domain with coefficients C_V=1 and C_D=C_T=$C_{CN} = 0$.

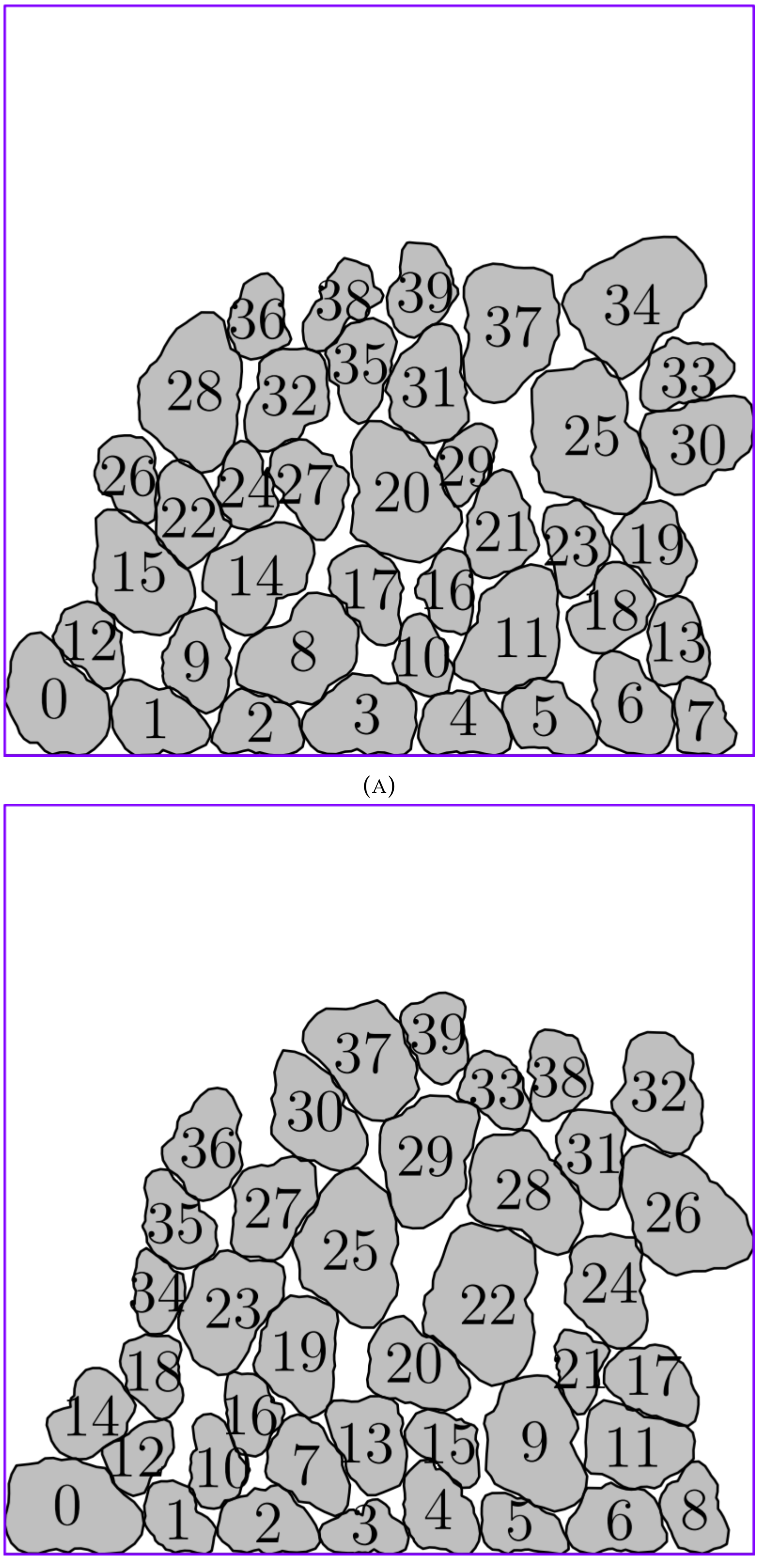

(A)

(B)

FIGURE 6.10: Packing of particles using a third of coordinates with equivalent particle order for packings in (a) Figure 6.6 (b) Figure 6.7.

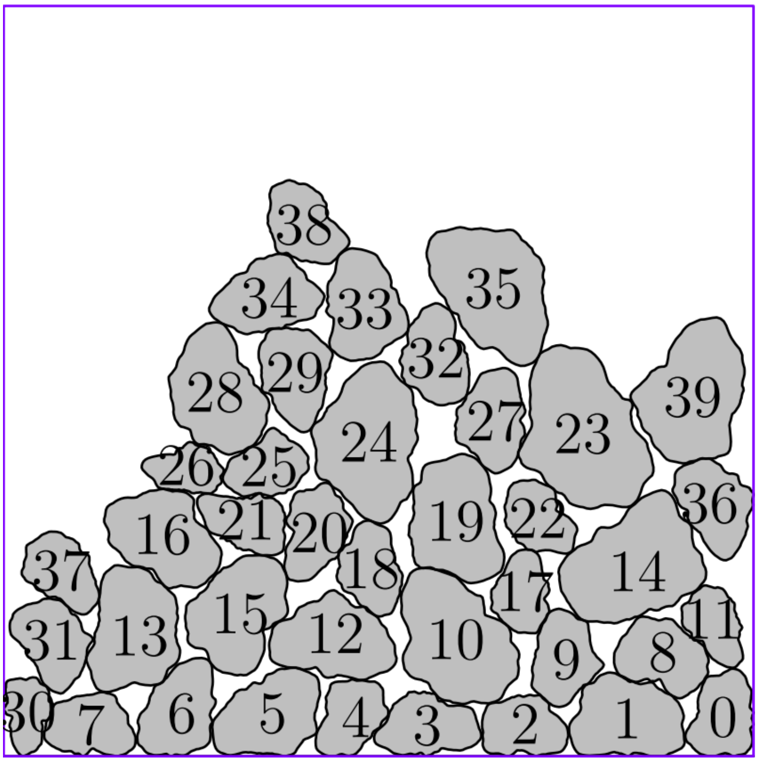

FIGURE 6.11: Packing structure of equivalent packing order to Figure 6.9 with coefficient values of C_V=100 and C_D=C_T=C_{CN}=1.

6.3.5 Effect of D

Figures 6.12-6.15 present results where D is the only activated variable in the objective function. From the way this scoring criteria works, the centre of mass of the particle is placed in the lowest possible position once candidate positions are filtered by the priority criteria outlined in Section 6.3.2. As is shown in Figures 6.12-6.15, the particles placed tend to be placed "flat" with the width-to-height ratio being maximised. This trend breaks where particles can be utilised to fill gaps in the courses such as with Particle 7 in Figure 6.14.

An improvement in void ratio is definitely seen when compared to packings where only V_{AB} is activated which is confirmed from visual comparison between the packings as well difference in value between MVRs in Table 6.2. Table 6.2 suggests equivalent packing efficiency when comparing MRJ for V_{AB} and D when each is activated and the other criteria in the objective function have coefficients set to zero. However, as discussed in Section 6.3.4, the canyoning experienced in packings represented in Figures 6.6-6.9 lead to longer running joints forming. Packings in Figures 6.12-6.15 have many cases where particles are stacked directly above each other without disruption of the running joint below (e.g. Particle 10 and then Particle 16 on top of Particle 7 in Figure 6.13). However, these tend to not to be of equivalent length to those experienced in Figures 6.6-6.9 due to the tendency for the particle to be placed as far down the system as possible, leading to the filling divots where two arching particle edges meet.

Comparison between Figure 6.15 and Figure 6.16 suggests that a slight inclusion of other parameters with an oversized value of $C_D D$ in the objective function does not have much of an effect on the packing. Furthermore this is shown by the MVR and

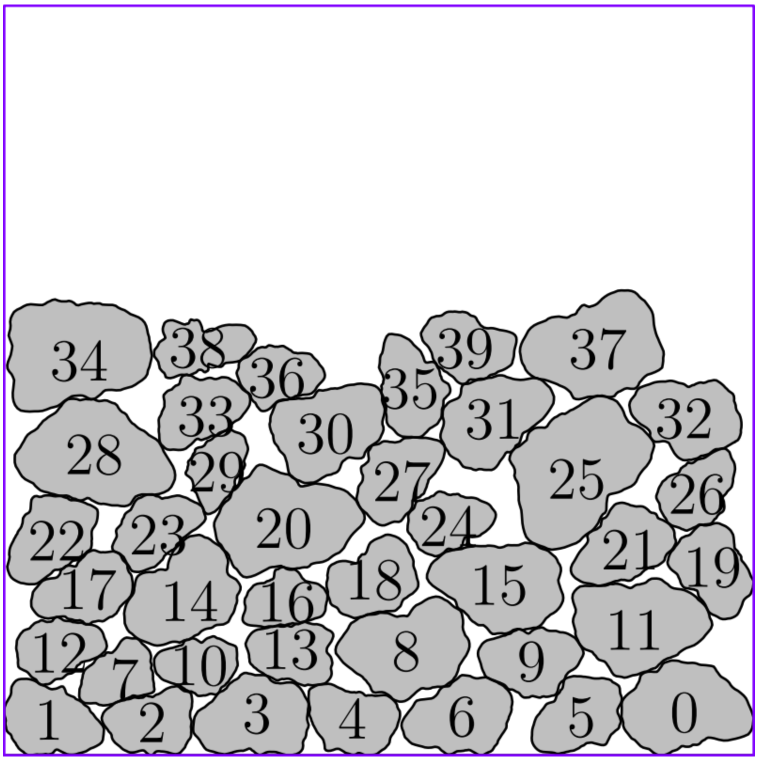

FIGURE 6.12: Packing of 40 rock particle outlines in a 50x50 unit domain with coefficients C_D=1 and C_V=C_T=$C_{CN}=0$.

MRJ values presented in Table 6.2 with the values suggesting placement of particles are slightly less suitable for disrupting runs in the system for when C_D is oversized.

Figure 6.17 presents packings of C_D=1 using a third of all coordinates. Compared to Figures 6.12-6.15 a good similarity is seen between the two. More spacing is seen between particles in Figure 6.17. This is due to less stable positions being found due to the decrease in coordinates so particle placement is not as refined as previously.

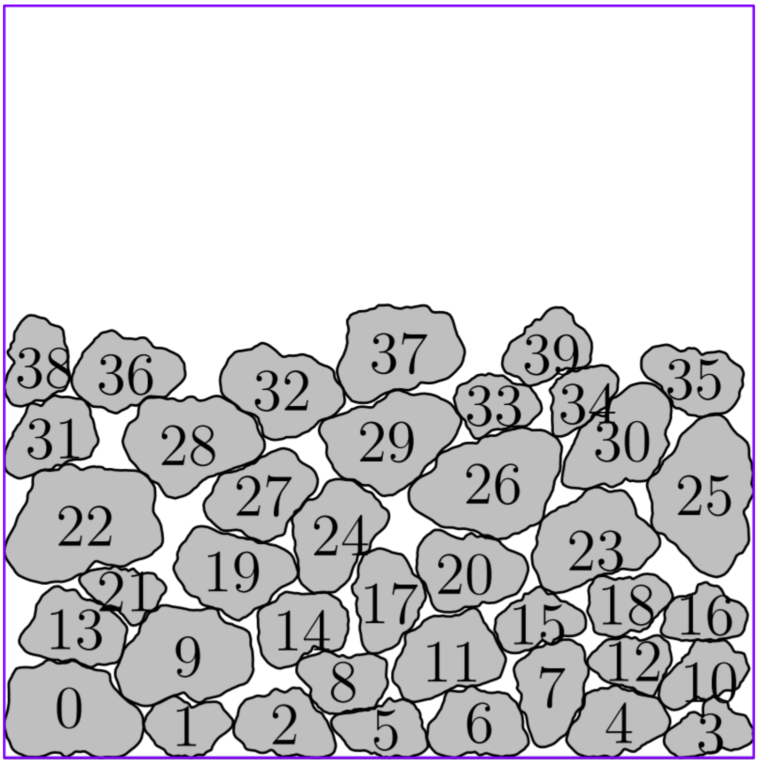

FIGURE 6.13: Packing of 40 rock particle outlines in a 50x50 unit domain with coefficients C_D=1 and C_V=C_T=C_{CN} = 0.

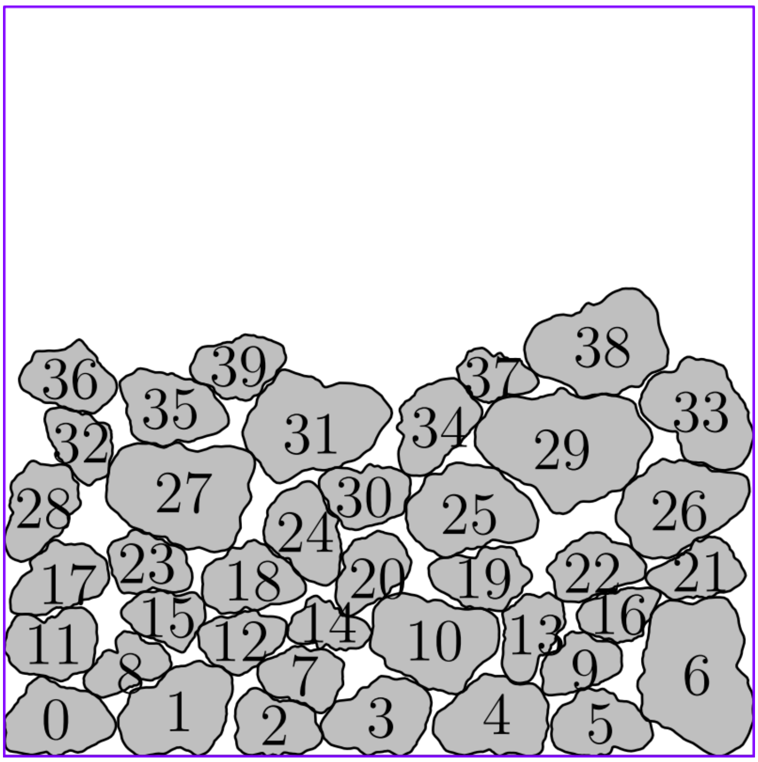

FIGURE 6.14: Packing of 40 rock particle outlines in a 50x50 unit domain with coefficients C_D=1 and C_V=C_T=C_{CN} = 0.

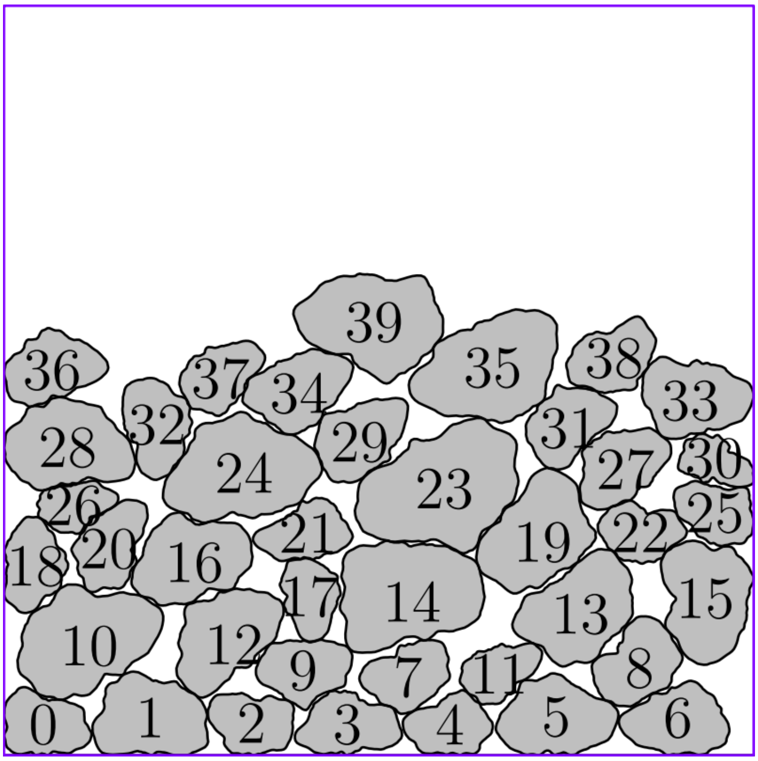

FIGURE 6.15: Packing of 40 rock particle outlines in a 50x50 unit domain with coefficients C_D=1 and C_V=C_T=C_{CN} $= 0$.

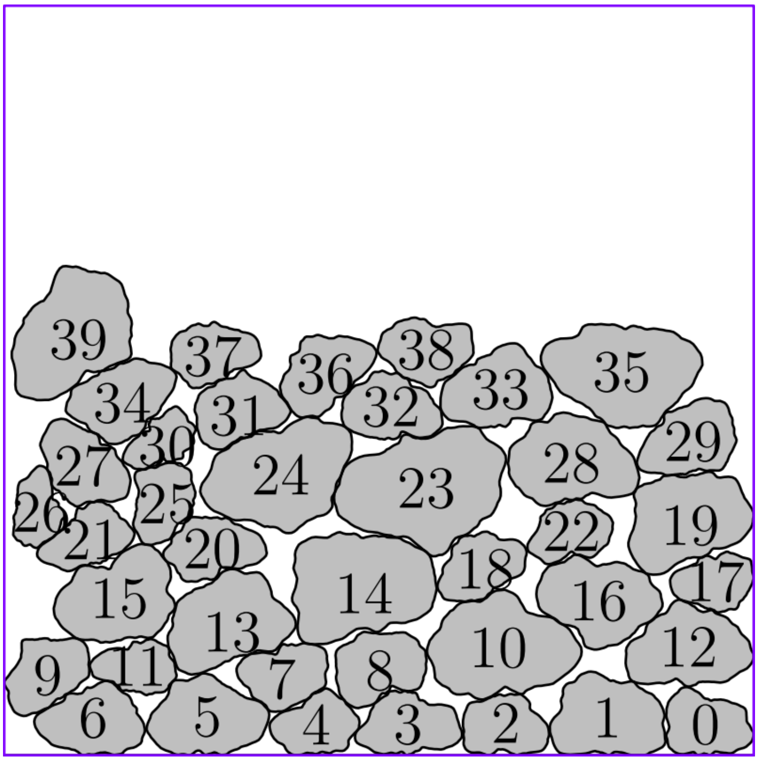

FIGURE 6.16: Packing structure of equivalent packing order to Figure 6.15 with coefficient values of C_D=100 and C_V=C_T=C_{CN}=1.

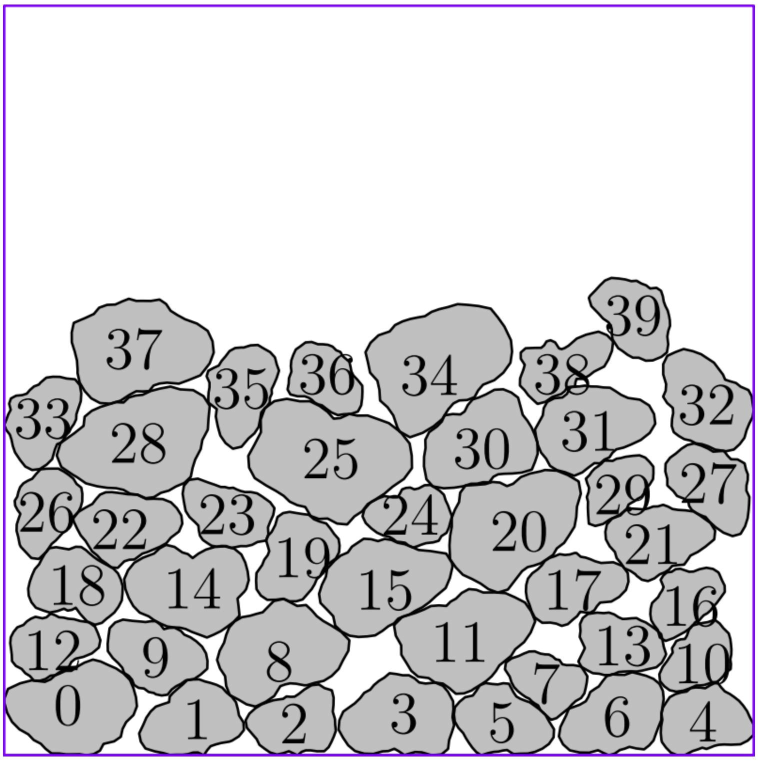

(A)

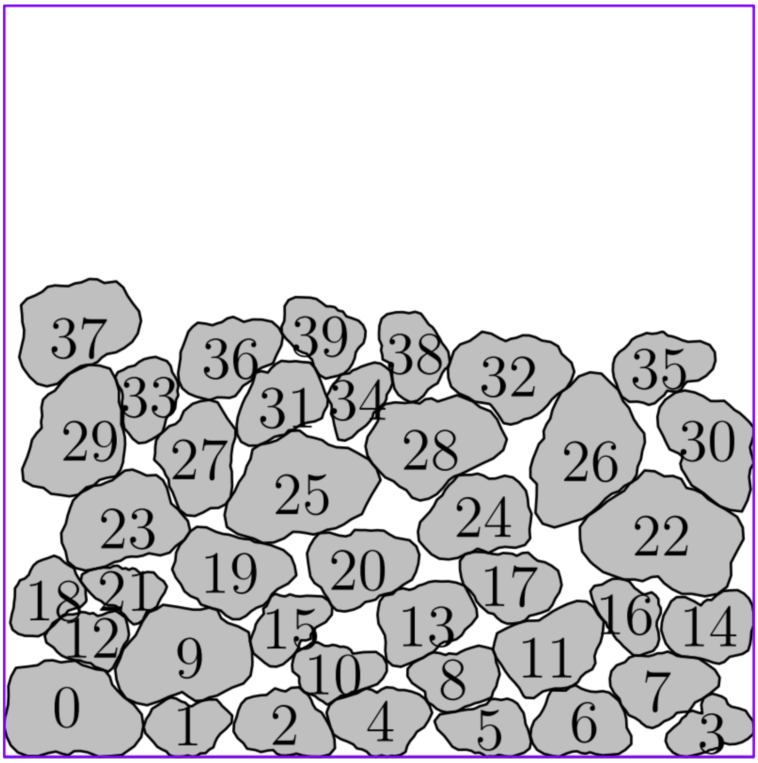

(B)

FIGURE 6.17: Packing of particles using a third of coordinates with equivalent particle order for packings in (a) Figure 6.12 (b) Figure 6.13.

6.3.6 Effect of T

Non-zero values of the coefficient C_T enables scoring to be based on the area of the particle touching already placed particles in the system. Figures 6.18-6.21 present results where C_T=1 and all over coefficients are zero values. In these figures, a tendency to lean to one side is shown. This is unusual, especially as the priority criteria gives preference to particles packed to the left in the domain and each packing in Figures 6.18-6.21 lean to the right-hand side.

It is determined that this leaning effect is due to the first particle tending to be placed in the righthand corner. As the particles are positioned in the structure, the objective function is scoring based on the number of contact points touching in the bottom line of the particle outline. Points of contact are more likely on the surface of particles as these are described by more coordinates than the initial surface of the domain which is defined by two coordinates to form the straight line. However, the question remains why Particle 0 is positioned to be in the right-hand corner. Inspection of Particle 0 for Figures 6.18-6.21 suggests that this is due to the scoring criteria in the discretised step of the algorithm. This is completed by identifying points of solid next to the whole of the outline of the particle. Therefore, this includes below as well as to the left, right and above. Particle 0 for each initial packing is detecting more points of contact with the domain on the right side and therefore the initial placement of the first particle tends to be here. This also explains why gaps appear between particles, as because contact points are scored using only coordinates of the bottom line, this is not including the area of the sides of particle in contact with other particles as part of the scoring for T.

As seen in Table 6.2, MRJ results for when T is the only activated variable in the objective function and for when T is oversized in comparison to other variables are similar. An increase in MVR is experienced for oversized $C_T T$ results. Figure 6.22 is the packing of particles using an oversized value of $C_T T$ for packing order equivalent to that of Figure 6.21. When T is oversized, filling of gaps between particles seems to be avoided especially if this will lead to less contacts with other particles. An example of this is the position of Particle 35 in Figure 6.22. It is suggested that this could have been placed in the gap to the right, like Particle 35 in Figure 6.21 and this would lead to a more suitable packing as well as the disruption of runs below the particle.

Packings using a third of available coordinates to represent particles (Figure 6.23) share a similar style of packing to when all available coordinates are used. However, steeper sides are experienced for the slope. Again, like with other packings using less coordinates, the decreased number of located stable positions causes less particles to be able to be placed on the incline causing this increase in steepness.

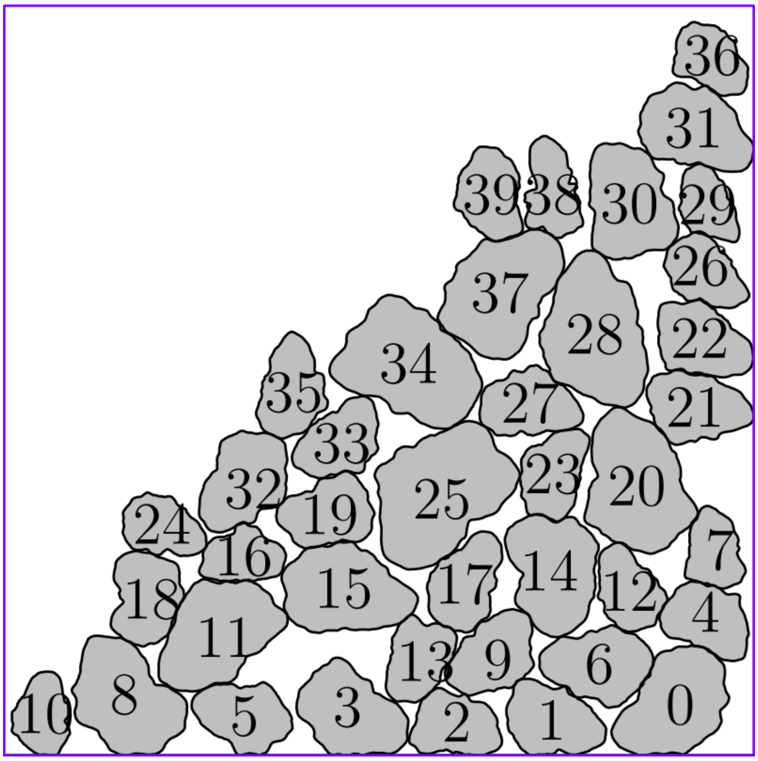

FIGURE 6.18: Packing of 40 rock particle outlines in a 50x50 unit domain with coefficients C_T=1 and C_V=C_D=C_{CN} $= 0$.

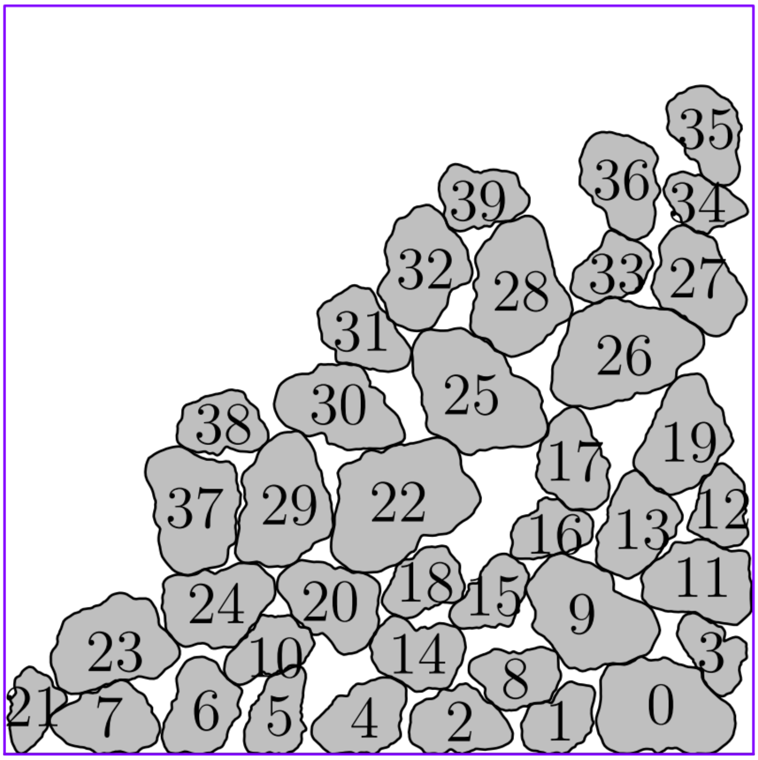

FIGURE 6.19: Packing of 40 rock particle outlines in a 50x50 unit domain with coefficients C_T=1 and C_V=C_D=C_{CN} $= 0$.

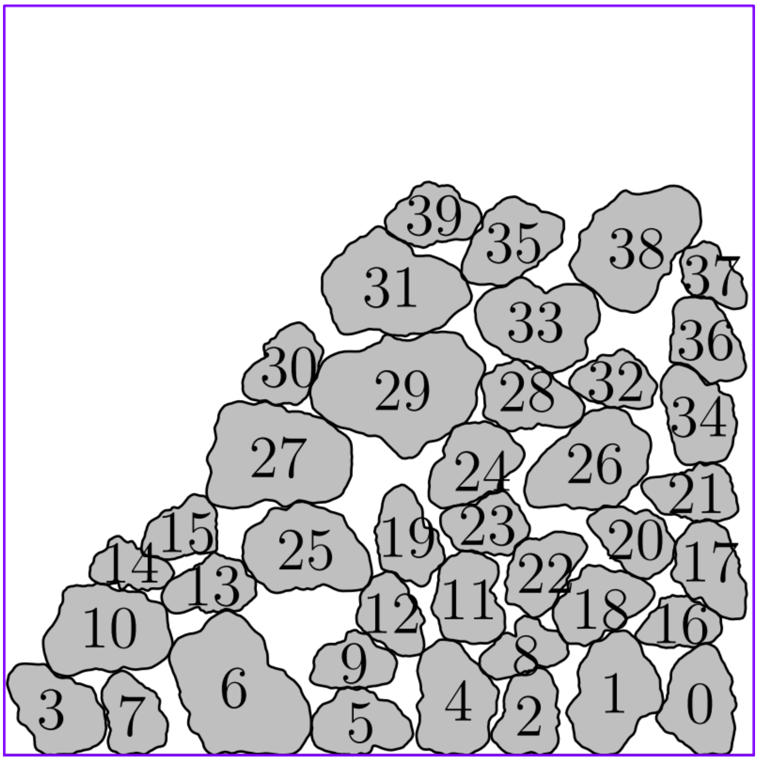

FIGURE 6.20: Packing of 40 rock particle outlines in a 50x50 unit domain with coefficients C_T=1 and C_V=C_D=C_{CN} $= 0$.

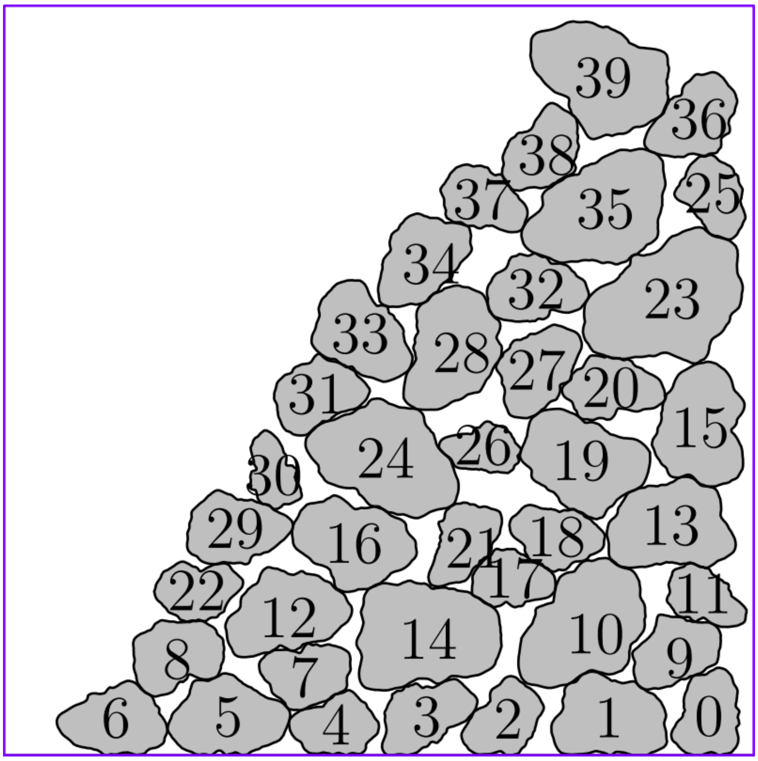

FIGURE 6.21: Packing of 40 rock particle outlines in a 50x50 unit domain with coefficients C_T=1 and C_V=C_D=C_{CN} $= 0$.

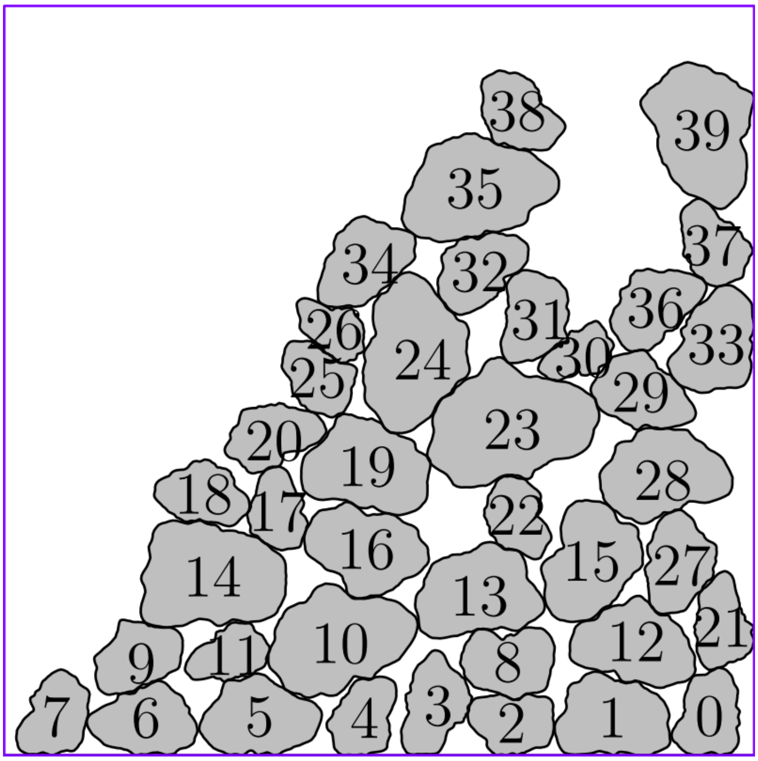

FIGURE 6.22: Packing structure of equivalent packing order to Figure 6.21 with coefficient values of C_T=100 and C_V=C_D=C_{CN}=1.

6.3.7 Effect of CN

Some results of packings of 40 particles when C_{CN} is set to 1 and C_V, C_D and C_T are set to zero are presented in Figures 6.24-6.27. The inclusion of CN in the scoring equation leads to particles trying to be surrounded by as many other particles as possible, as well as the domain edge as touching this also counts towards the coordination number. This gives the reason for why Particles 0 and 1 in Figures 6.24-6.27 are placed on opposite sides to begin with rather than being next to each other. These placements lead to a coordination number of 2 as it is in contact with the side of the domain and the bottom of the domain. The packings of the particles are completed in a course-by-course order due to the discretised scoring list prioritising the particle being placed at the deepest position in the system. However, when a particle can fit between two particles, this placement is prioritised due to the increased coordination number. For example, this can be seen in the final placement of Particle 4 in Figure 6.24 and 6.25.

It appears that CN minimises MVR results the most out of all of the parameters as indicated in Table 6.2 for both when only CN is activated and when $C_{CN}CN$ is oversized in the objective function. MRJ values suggest that the positioning of particles are not optimised for disrupting runs in the system. This is not as expected as it is thought that particles would be placed in positions above where runs can be formed as this would provide a higher coordination number compared to if the particle was placed directly above another. However, the placement of particles do not appear to have enough overlap to disrupt the formation of runs in the system. For example, a run can form between Particle 11 and Particle 13 in Figure 6.24. Particles placed above this location are Particles 16, 17, 23, 28, 29 and 34. Of all these particles none of them disrupt the run as it carries on up through the structure and a zipping joint

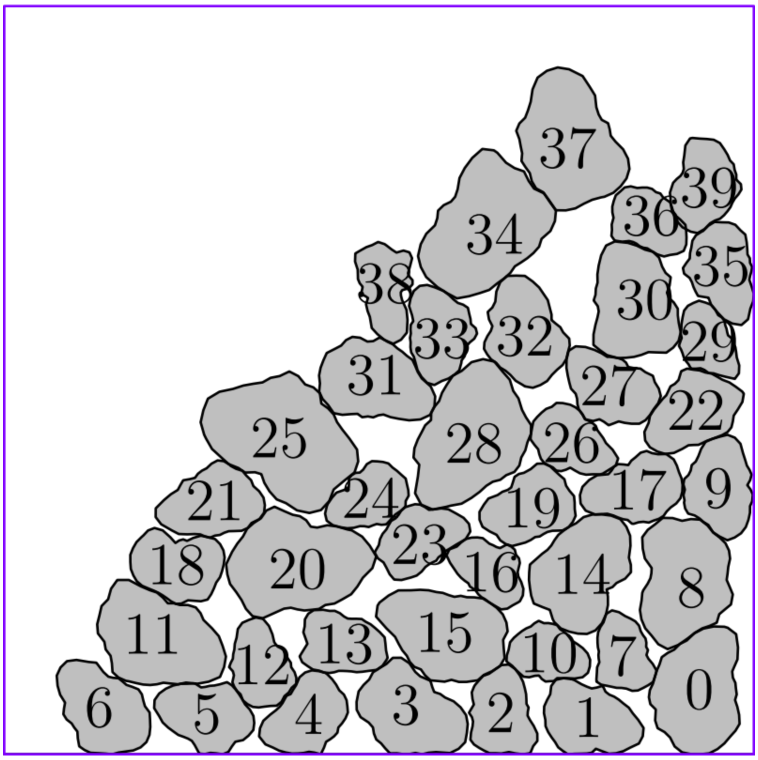

(A)

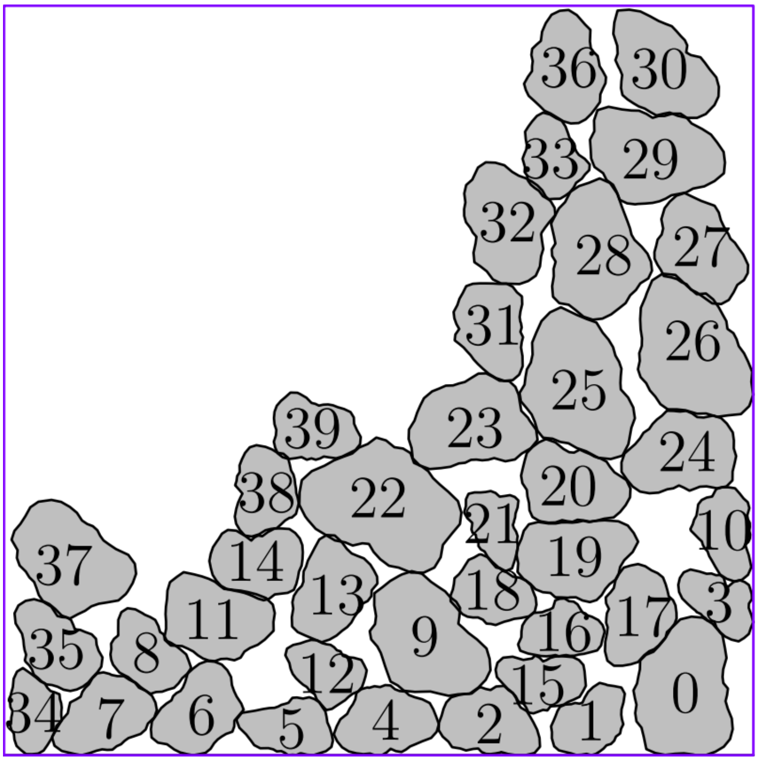

(B)

FIGURE 6.23: Packing of particles using a third of coordinates with equivalent particle order for packings in (a) Figure 6.18 (b) Figure 6.19.

forms.

CN is similar to V_{AB} in terms of V_{AB} scoring placement on minimising void whilst scoring the highest for MVR. However, whereas the inclusion of the other parameters whilst $C_V V_{AB}$ is oversized improves the MVR result quite drastically, this does not occur in the instance for $C_{CN}CN$ for MRJ. Instead the MRJ score improves but only by 1.4. This is because none of the other parameters improve the positioning of particles in terms of maximising MRJ based on the way they are scored. Meanwhile, D improves MVR results as it prevents canyoning occuring whilst T is has been stated to passively measure the amount of void generated directly beneath the particle whilst not accounting for the size of the void created (see Section 5.3.4).

Figures 6.24-6.27 suggest that CN is a useful parameter for keeping particles in the system to a minimum height and packings are quite similar to those when D is the only active parameter in Figures 6.12-6.15. Similar to when $C_D D$ is oversized, the oversizing of $C_{CN}CN$ with the inclusion of other parameters does not have much of an effect on the packing structures. Evidence for this exists in the similarity between the values presented in Table 6.2 and the nature of the packings experienced in Figures 6.28-6.31 appearing similar to Figures 6.24-6.27. However, Figures 6.28-6.31 are more tightly packed compared to Figures 6.24-6.27. It is considered that a tighter packing where particles are closer to each other and void is minimised would lead to the prevention of running joints in the structure.

Examining the results for disrupted runs in the 5 simulations for CN as the only active variable and when $C_{CN}CN$ is oversized individually suggests that actually the disruption of runs is improved further than initially thought. Out of the packing orders (named PO1 to PO5 in Table 6.5) three of the five results improved quite significantly with a reduction in MRJ by 4 disrupted runs for PO2 and PO5. The oversized case for each PO are presented in Figures 6.28-6.31. It is difficult to determine how much a change in the number of runs disrupted is due to the objective function for placement compared to the particle order. It should be considered that smaller particles that are placed above runs are less likely to be able to disrupt them. Therefore if a larger particle was earlier in the particle order and subsequently placed above this run this will result in more prevention from runs forming.

Parameter type	PO1	PO2	PO3	PO4	PO5	MRJ
CN only	20	22	22	22	26	22.4
$C_{CN}CN$ oversized	24	18	29	26	22	23.8

TABLE 6.5: Values of MRJ for different packing orders for CN as the only active variable and CN as an oversized variable.

Packings using a third of all available coordinates resemble the packings in Figures 6.24-6.27 well and therefore it is assumed that these can be taken forward for further studies. Reviewing the MRJ and MVR values from Table 6.2 to Table 6.3 the values are fairly similar for CN and therefore this is justified.

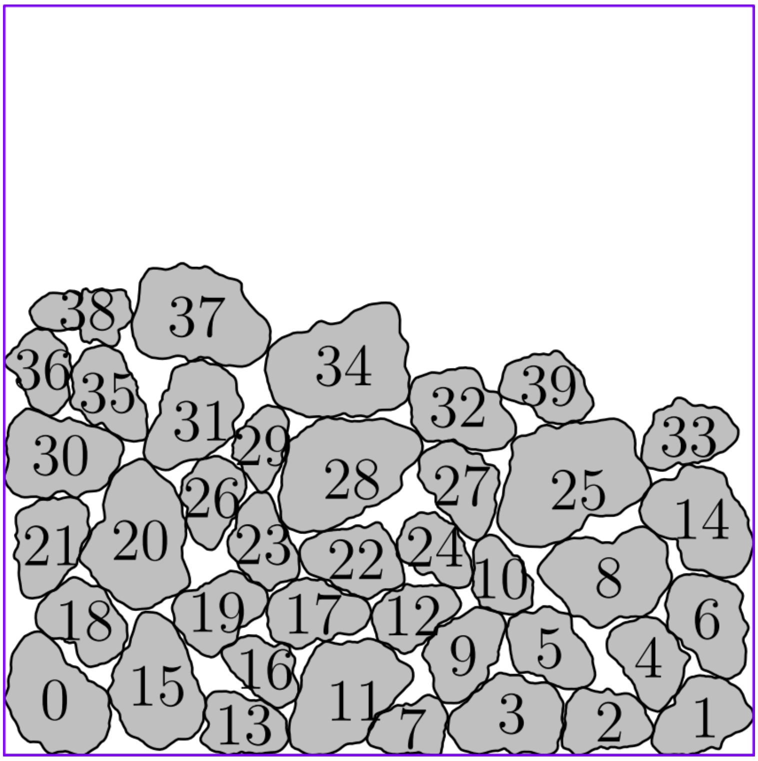

FIGURE 6.24: Packing of 30 rock particle outlines in a 50x50 unit domain with coefficients C_{CN}=1 and C_V=C_D=$C_T = 0$.

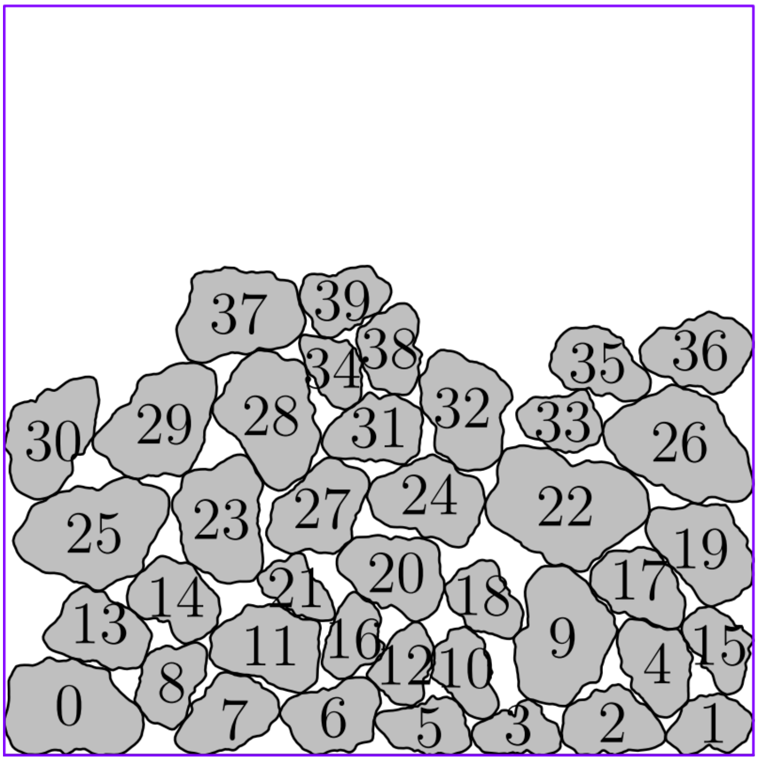

FIGURE 6.25: Packing of 30 rock particle outlines in a 50x50 unit domain with coefficients C_{CN}=1 and C_V=C_D=$C_T = 0$.

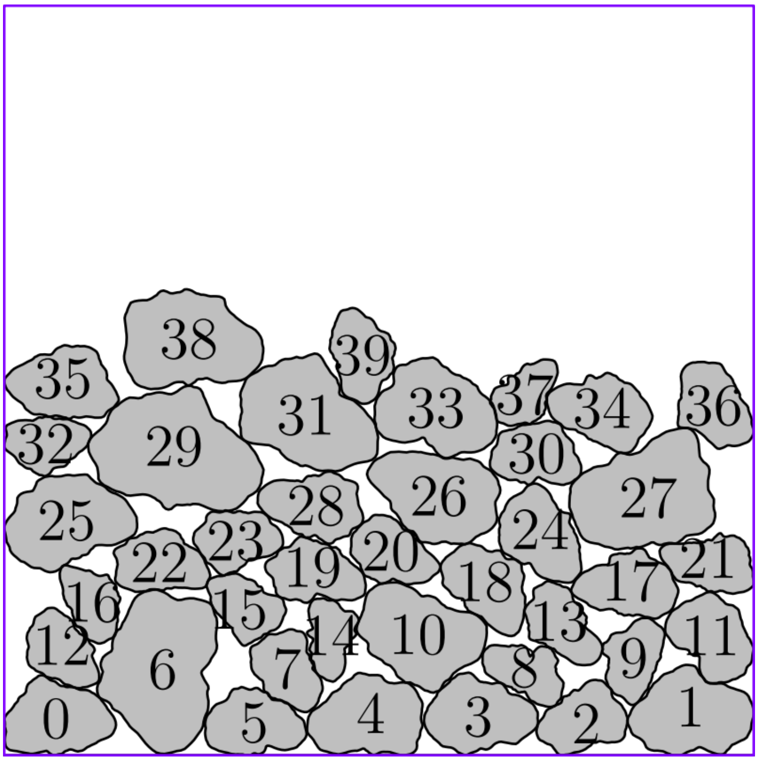

FIGURE 6.26: Packing of 30 rock particle outlines in a 50x50 unit domain with coefficients C_{CN}=1 and C_V=C_D=$C_T = 0$.

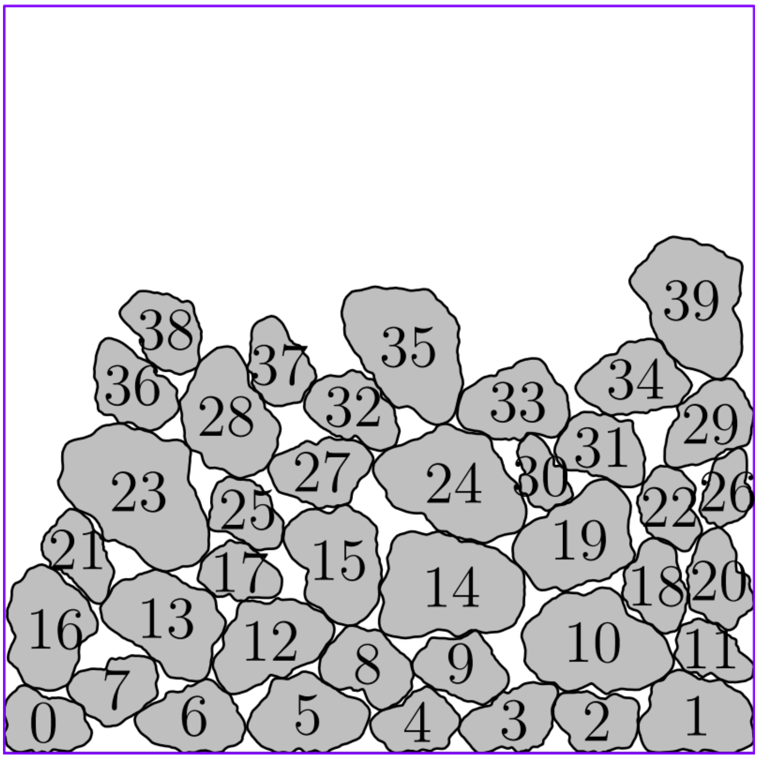

FIGURE 6.27: Packing of 30 rock particle outlines in a 50x50 unit domain with coefficients C_{CN}=1 and C_V=C_D=$C_T = 0$.

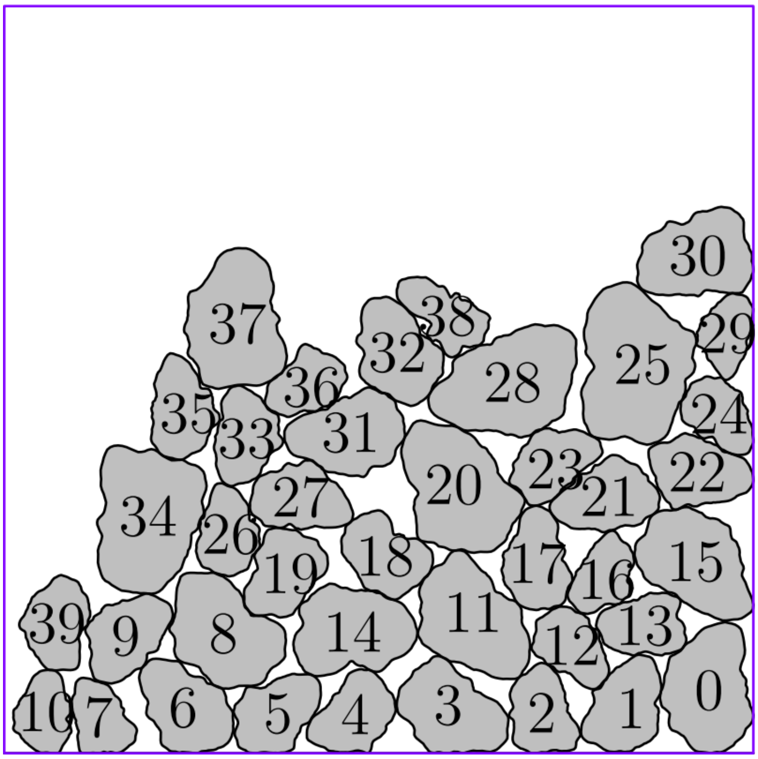

FIGURE 6.28: Packing structure of equivalent packing order to Figure 6.24 with coefficient values of C_{CN}=100 and C_V=C_D=C_T=1.

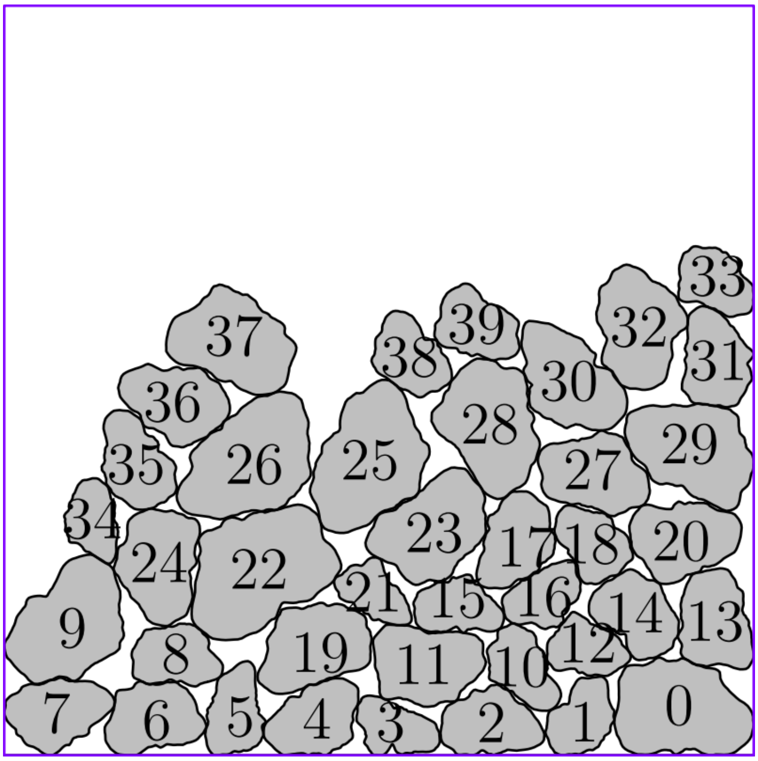

FIGURE 6.29: Packing structure of equivalent packing order to Figure 6.25 with coefficient values of C_{CN}=100 and C_V=C_D=C_T=1.

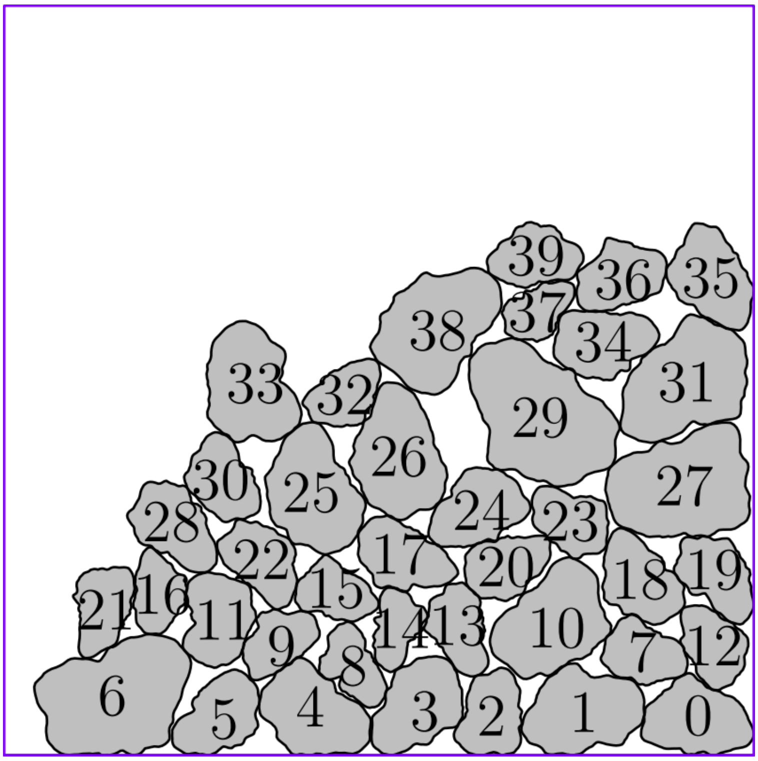

FIGURE 6.30: Packing structure of equivalent packing order to Figure 6.26 with coefficient values of C_{CN}=100 and C_V=C_D=C_T=1

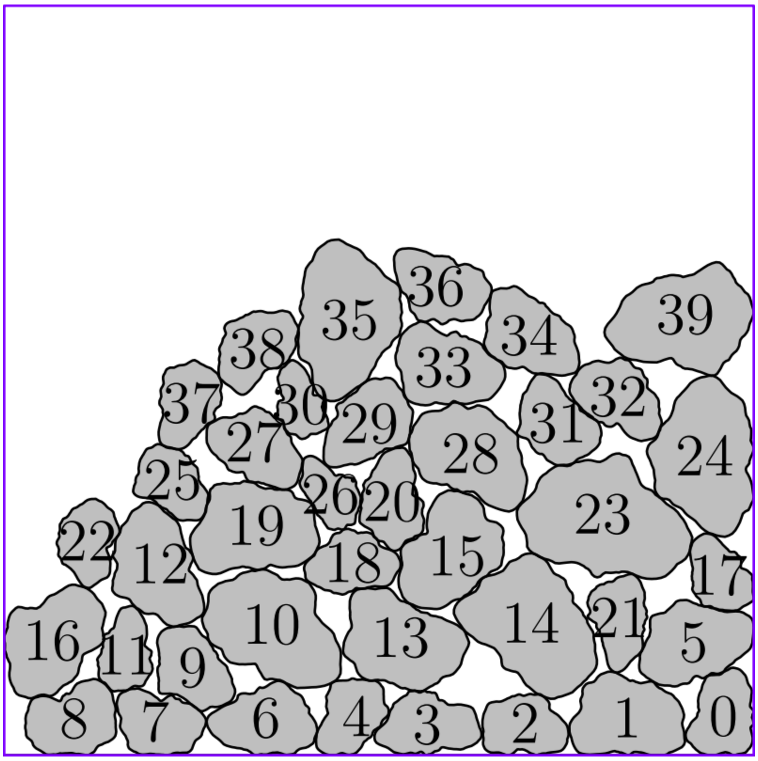

FIGURE 6.31: Packing structure of equivalent packing order to Figure 6.27 with coefficient values of C_{CN}=100 and C_V=C_D=C_T=1.

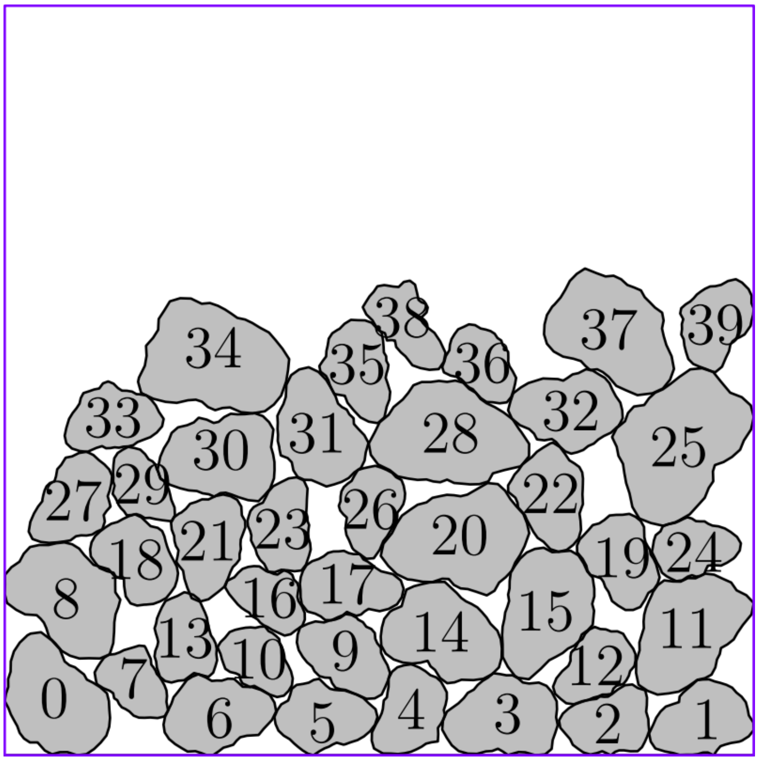

(A)

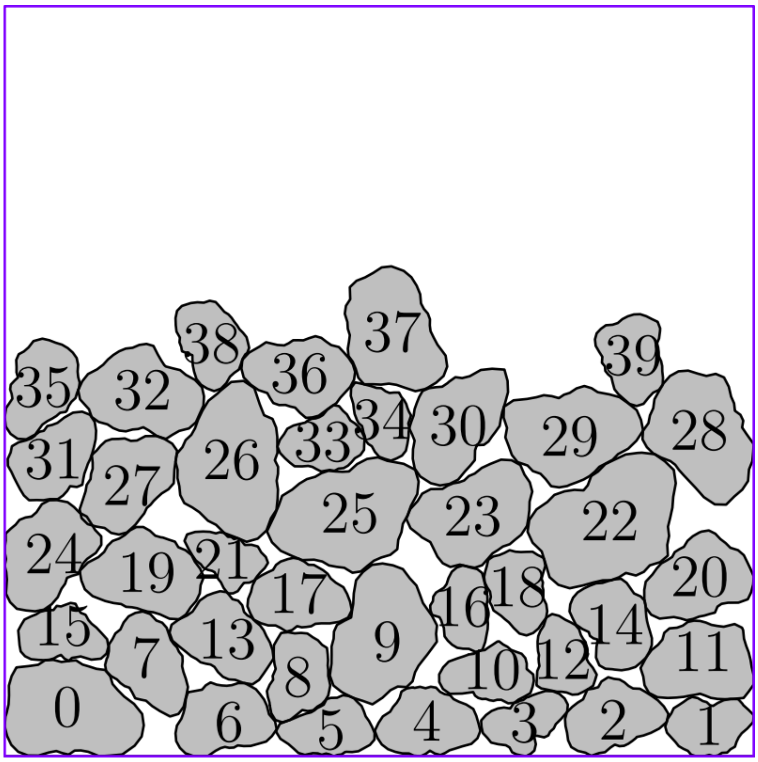

(B)

FIGURE 6.32: Packing of particles using a third of coordinates with equivalent particle order for packings in (a) Figure 6.24 (b) Figure 6.25.

6.4 Analysing Results for Different Weighting Coefficient Combinations

6.4.1 Initial Study

Figure 6.33 displays lowest MVR and highest MRJ values from search areas of C_T and C_{CN} varied from 0 to 10 at increments of 2 for C_D values varied from 0 to 8 at increments of 2. C_V was kept at a fixed value of 1. Sample size n=3 is adopted for the presented results. Table 6.6 shows the relevant C_T and C_{CN} values for which each point was located. Recognise that values for MVR and MRJ are not located at equivalent positions in the search area. It is determined that optimal solution will be located where both MVR and MRJ are optimised - MVR is kept to a minimum and MRJ is kept to a maximum - with MRJ being prioritised.

C_V & C_D		MRJ				MVR			
C_V	C_D	C_T	C_{CN}	MRJ	MVR	C_T	C_{CN}	MRJ	MVR
1	0	4	0	25.67	0.2246	0	2	21.333	0.1972
1	2	2	0	26.33	0.2244	0	4	24.667	0.1812
1	4	4	2	24.67	0.1974	0	0	22.667	0.1893
1	6	10	4	27	0.2300	0	2	23.667	0.1904
1	8	10	4	26.33	0.2100	0	0	21	0.1794

TABLE 6.6: Maximum MRJ and minimum MVR values located on the search areas for values of C_D varied from 0 to 8 by increments of 2 between C_T and C_{CN} values 0 to 10 increased by increments of 2. n=3 and C_V=1. Values are paired with their matching MRJ or MVR for equivalent location in the alternate search area.

It can be seen that minimum MVR values are obtained with C_T values of 0 for all values of C_D. Throughout the surface plots, it is observed that MVR tends to be largest when C_T is 10. In Section 3.5.4, T was suggested to act as another indicator for void beneath the particle but with no recognition of the void beneath it. However, this was experienced with tetrominoes that have orthogonal sides that will always fit flush together. For the soil outlines, less of the particle face is in contact with the placement surface and it is possible for there to be only two points of contact. Therefore, it is possible for particles to bridge over areas of void and still achieve a similar score for T. It is thought that as C_T increases, particles prioritise having a greater surface area with other particles even if it means creating void below the particle. As $C_T T$ becomes dominant over $C_V VAB$ in the objective function this begins to happen at larger values of C_T. Additionally, the results of locations with more dominant $C_T T$ values in the objective function resembled those studied in Section 6.3.6 with a tendency to lean to the right-hand side. See Figure 6.34a for an example.

Maximum MRJ is located at (C_T=4, C_{CN}=0) for the C_D=0 search area. Examining the surface plot in Figure 6.35a, another relatively large maximum is located at (C_D=0, C_T=10, C_{CN}=10) which provides suitability for a potential optimal solution. However, the equivalent location for the search area of MVR (Figure 6.35b) has a much larger value. Reviewing other locations at (C_T=10, C_{CN}=10) for the various C_D values, it would appear that a shared feature is that results of a fairly high void ratio compared with other results in the search area for MVR as presented by the values in Table 6.7. Figure 6.36 presents examples of these packings and shows that generally particle placement is prioritised to the right suggesting $C_T T$ is dominant. An exception is seen in Figure 6.36c, where a flatter system is experienced.

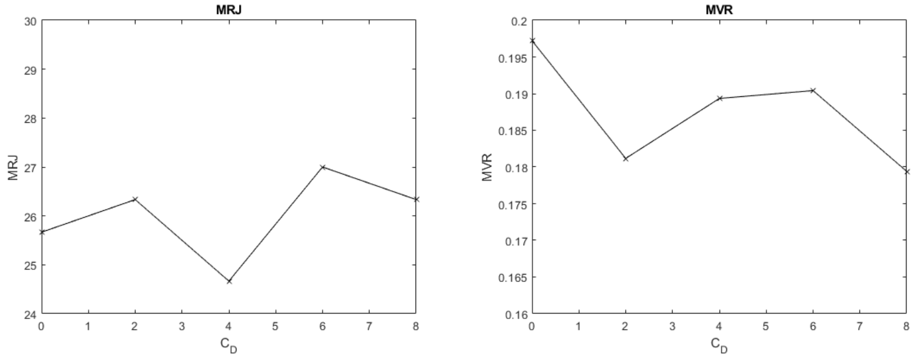

(A) (B)

FIGURE 6.33: Lowest values of (a) MRJ (b) MVR for the corresponding C_D value for plots of C_T and C_{CN} varied from 0 to 10 at increments of 2 with sample size n=3.

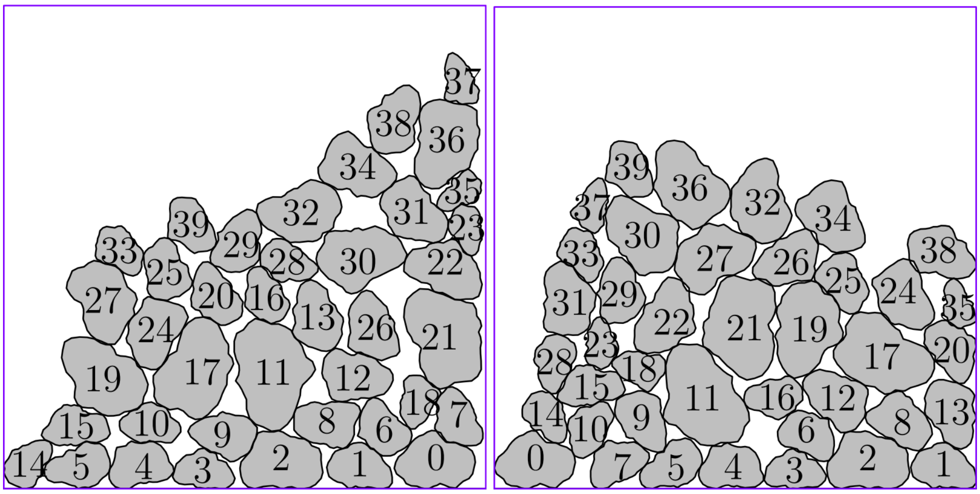

(A) MRJ=26, MVR=0.2272 (B) MRJ=20, MVR=0.1889

FIGURE 6.34: Packings in the Soil Particle Scenario for coefficients of weighting (a) (C_V=1, C_D=0, C_T=4, C_{CN}=0) (b) (C_V=1, C_D=0, C_T=0, C_{CN}=4) with equivalent particle order.

C_D	MRJ	MVR
0	25.33	0.20103
2	24.33	0.22637
4	23.667	0.2251
6	25	0.21769
8	26.33	0.21128

TABLE 6.7: Locations on the search area (C_T=10, C_{CN}=10) for different C_D values with results of MRJ and MVR presented for the Soil Particle Scenario.

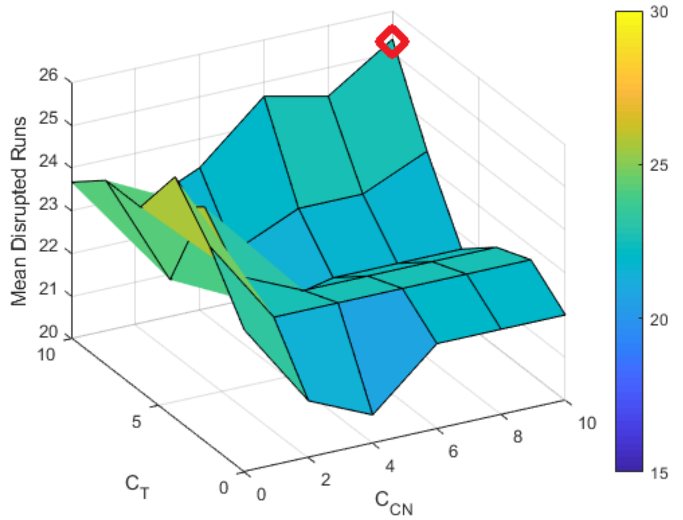

(A) MRJ

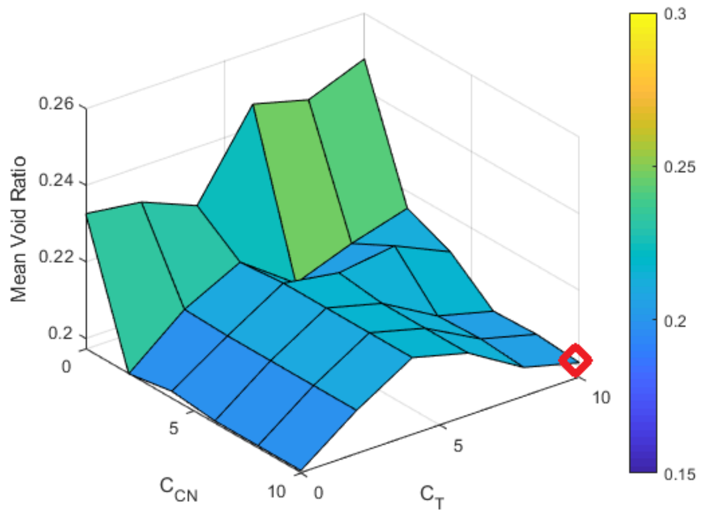

(B) MVR

FIGURE 6.35: Surface plot for C_V=1 and C_D=0 for ranged from of C_T and C_{CN} between 0 to 10 at increments of 2 for the Soil Particle Scenario. Marker indicates the location (C_T=10, C_{CN}=10).

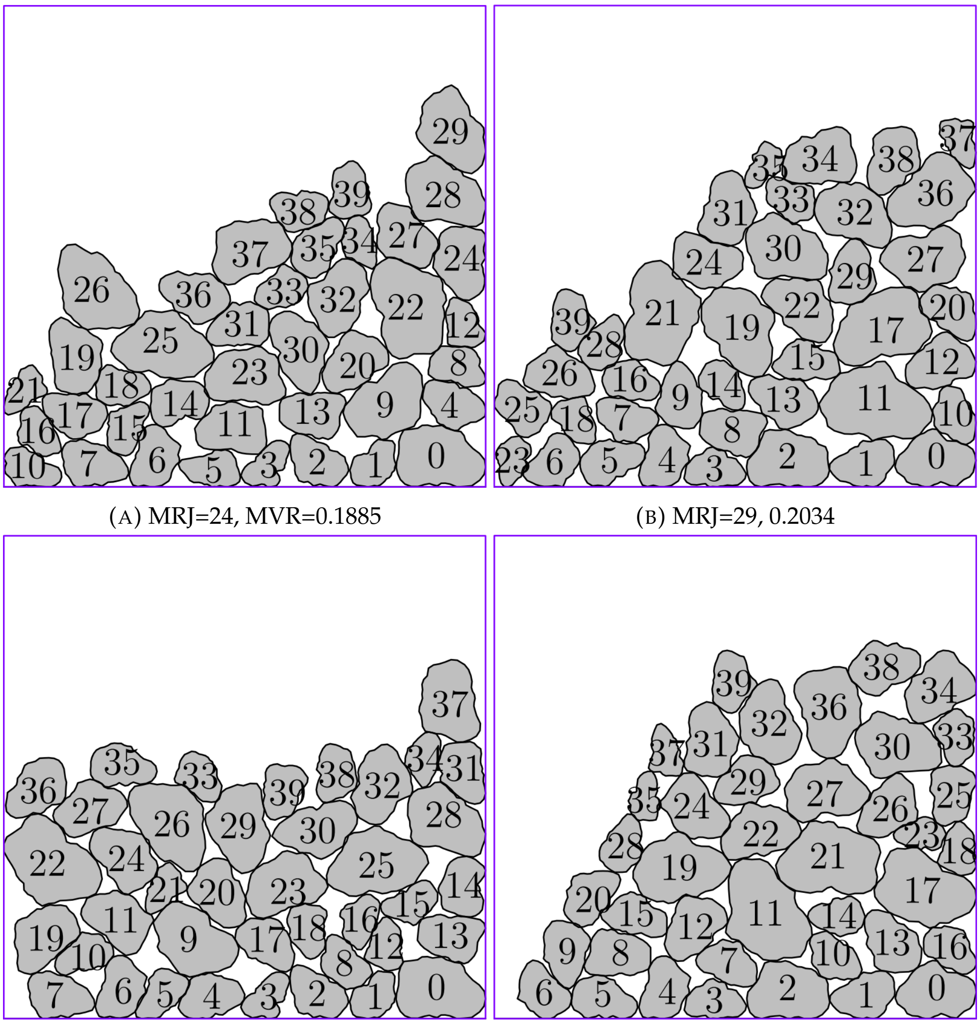

(A) MRJ=24, MVR=0.1885

(B) MRJ=29, 0.2034

(C) MRJ=26, MVR=0.2128

(D) MRJ=29, MVR=0.2000

FIGURE 6.36: Packings in the Soil Particle Scenario for coefficients of weighting (a+b) (C_V=1, C_D=0, C_T=10, C_{CN}=10) and (c+d) (C_V=1, C_D=8, C_T=10, C_{CN}=10) with equivalent particle order for (a) and (c) and equivalent particle order for (b) and (d).

C_V	C_D	C_T	C_{CN}	MRJ	MVR
1	4	0	0	22.667	0.18934
1	4	2	2	24.333	0.19313
1	4	2	4	24.333	0.19313
1	4	4	2	24.667	0.19735
1	6	0	2	25.333	0.20324
1	6	2	2	24.667	0.19286
1	6	2	4	24.667	0.19286
1	6	6	2	26	0.19564

TABLE 6.8: Values for MRJ and MVR at locations of interest in the search areas presented in Figure 6.37 and Figures 6.38.

Figure 6.37 and Figure 6.38 present the search areas for C_D=4 and C_D=6. Both show higher values of MRJ along C_T=2 whilst MVR results are low in comparison to other datapoints. The search area for C_D=2 also experienced a right of high MRJ results at C_T=2 however relatively high MVR results in comparison to other search areas were also experienced. Points of interest where MRJ and MVR values appear to be optimal are listed in Table 6.8 with their relevant coefficient values.

From analysis of the results, it appears that higher values of MRJ typically have higher values of MVR. Additionally, as C_D increases the values of MVR appear to increase but with larger MRJ values for those locations. For example, see Figure 6.39 for the search area of C_D=8 where the MVR values tend to be above 0.2. This is logical, as MRJ is an indication of particles above matings of the particles below. Therefore, this will naturally be over a gap and therefore an increase in void ratio is expected unless a smaller particle can be placed below.

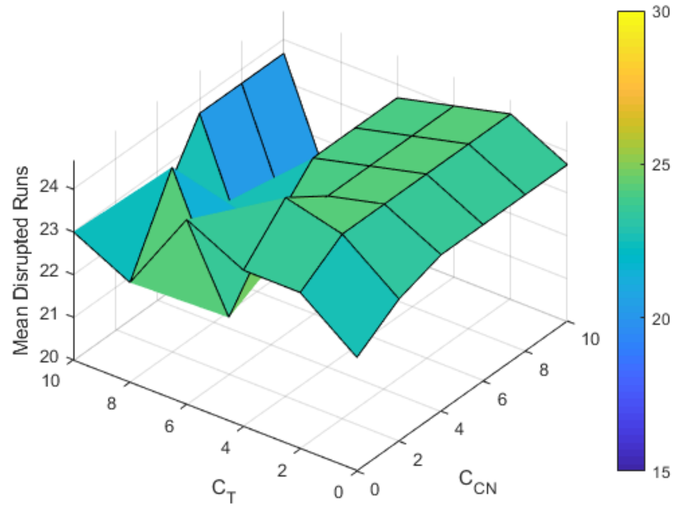

(A) MRJ

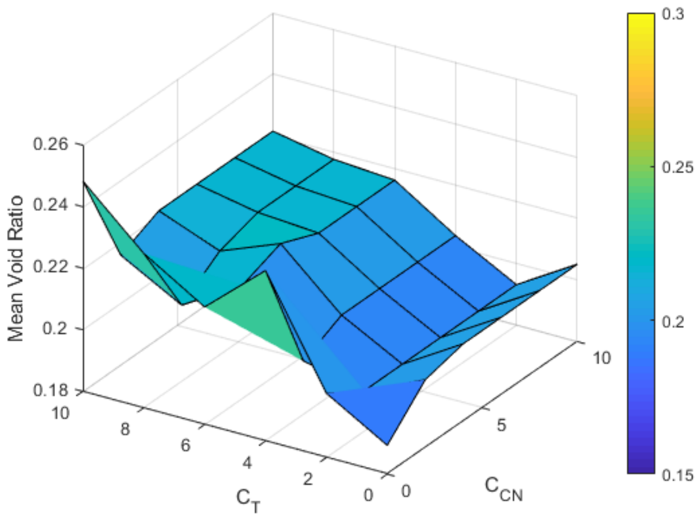

(B) MVR

FIGURE 6.37: Surface plot for C_V=1 and C_D=4 for ranged from of C_T and C_{CN} between 0 to 10 at increments of 2 for the Soil Particle Scenario.

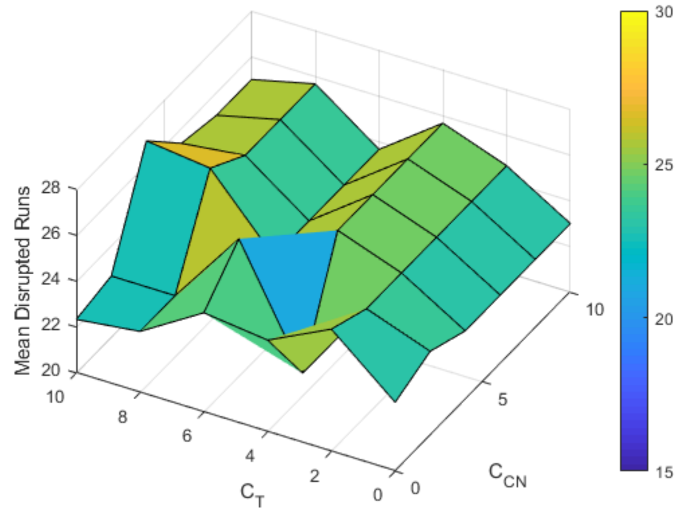

(A) MRJ

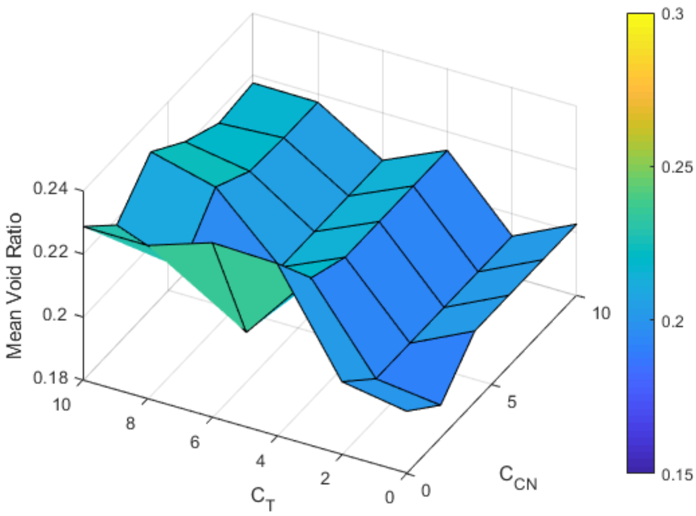

(B) MVR

FIGURE 6.38: Surface plot for C_V=1 and C_D=6 for ranged from of C_T and C_{CN} between 0 to 10 at increments of 2 for the Soil Particle Scenario.

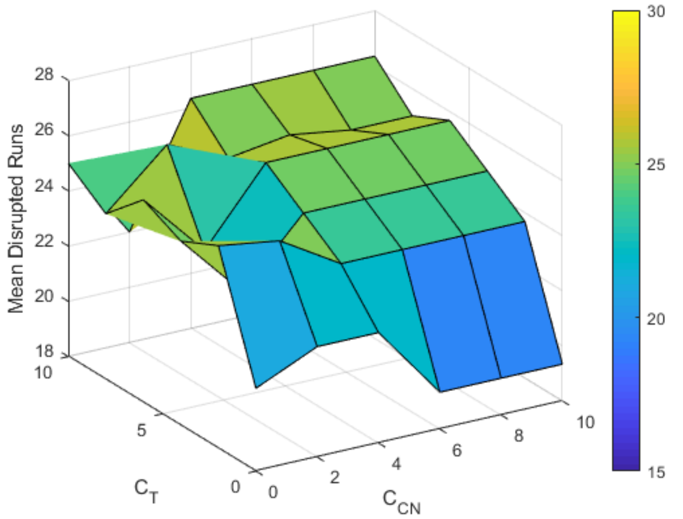

(A) MRJ

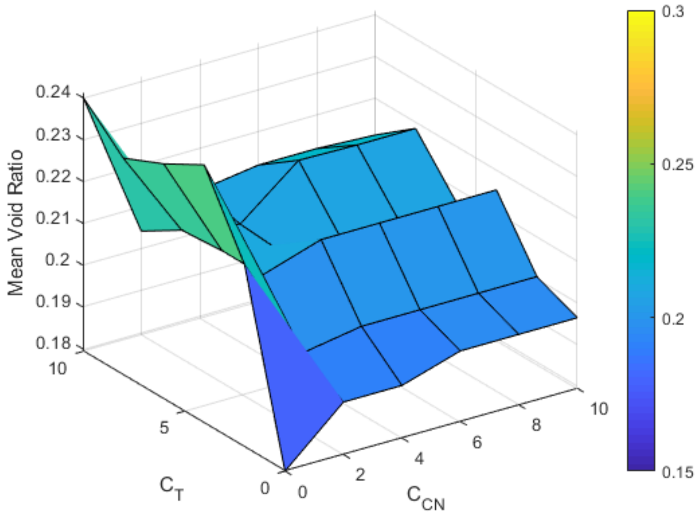

(B) MVR

FIGURE 6.39: Surface plot for C_V=1 and C_D=8 for ranged from of C_T and C_{CN} between 0 to 10 at increments of 2 for the Soil Particle Scenario.

6.4.2 Increasing Effect of $C_V V_{AB}$

As Section 4.5 suggests, it is important to explore values of coefficients where $C_V V_{AB}$ can become dominant in the objective function. Coefficients were ranged between 0 to 1 at increments of 0.2 were explored whilst C_V=1 was kept as a constant. The maximum MRJ and minimum MVR values observed in the search areas are plotted for their corresponding C_D value in Figure 6.40 and locations of these values are stated in Table 6.9. Comparing Figure 6.40 to Figure 6.33, MRJ and MVR values achieved between the range of 0 to 1 appear more optimal as they are higher MRJ and lower for MVR. A peak value of MRJ appears at C_D=0.4 and trough in the plot of MVR is located at C_D=0.2. Figure 6.41 presents packings of the coefficient combinations for these peak and trough values. Tight packing structures are seen, with inclination towards the right thought to be due to $C_T T$.

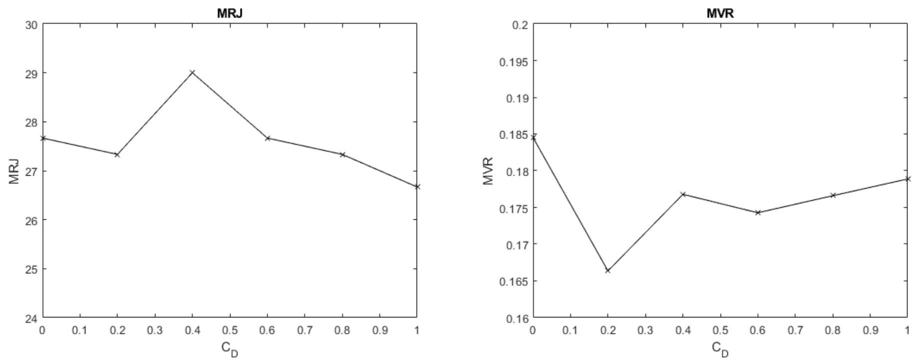

(A) (B)

FIGURE 6.40: Lowest values of (a) MRJ (b) MVR for the corresponding C_D value for plots of C_T and C_{CN} varied from 0 to 1 at increments of 0.2 with sample size n=3.

C_V & C_D		MRJ				MVR			
C_V	C_D	C_T	C_{CN}	MRJ	MVR	C_T	C_{CN}	MRJ	MVR
1	0	0.2	0	27.667	0.1899	1	0.2	26.667	0.1845
1	0.2	0.8	0.8	27.333	0.1944	0.6	0.2	25.333	0.1664
1	0.4	0.4	0.2	29	0.1789	0.6	0.2	25.667	0.1768
1	0.6	0.6	0.2	27.667	0.1924	0.8	0.2	23	0.1743
1	0.8	0.6	0.2	27.333	0.2002	0.2	0.2	22.667	0.1766
1	1	1	0	26.667	0.2123	0.4	0.8	24.667	0.1789

TABLE 6.9: Maximum MRJ and minimum MVR values located on the search areas for values of C_D varied from 0 to 1 by increments of 0.2 between C_T and C_{CN} values 0 to 1 increased by increments of 0.2. n=3 and C_V=1. Values are paired with their matching MRJ or MVR for equivalent location in the alternate search area.

Figure 6.42 shows the search area for C_D=0 when C_T and C_{CN} are ranged from 0 to 1 by increments of 0.2. As can be seen, there appears to be two possible peaks for MRJ in Figure 6.42a. These are located at (C_T=0.2, C_{CN}=0) and (C_T=0.8, C_{CN}=0) and are displayed in Figure 6.43a and Figure 6.43b respectively. Both suggest good packings with a good level of runs prevented from occurring in the system. However, the lack of contribution from $C_D D$ in the objective function means that towering can occur, which is a feature of the packing in Figure 6.43b.

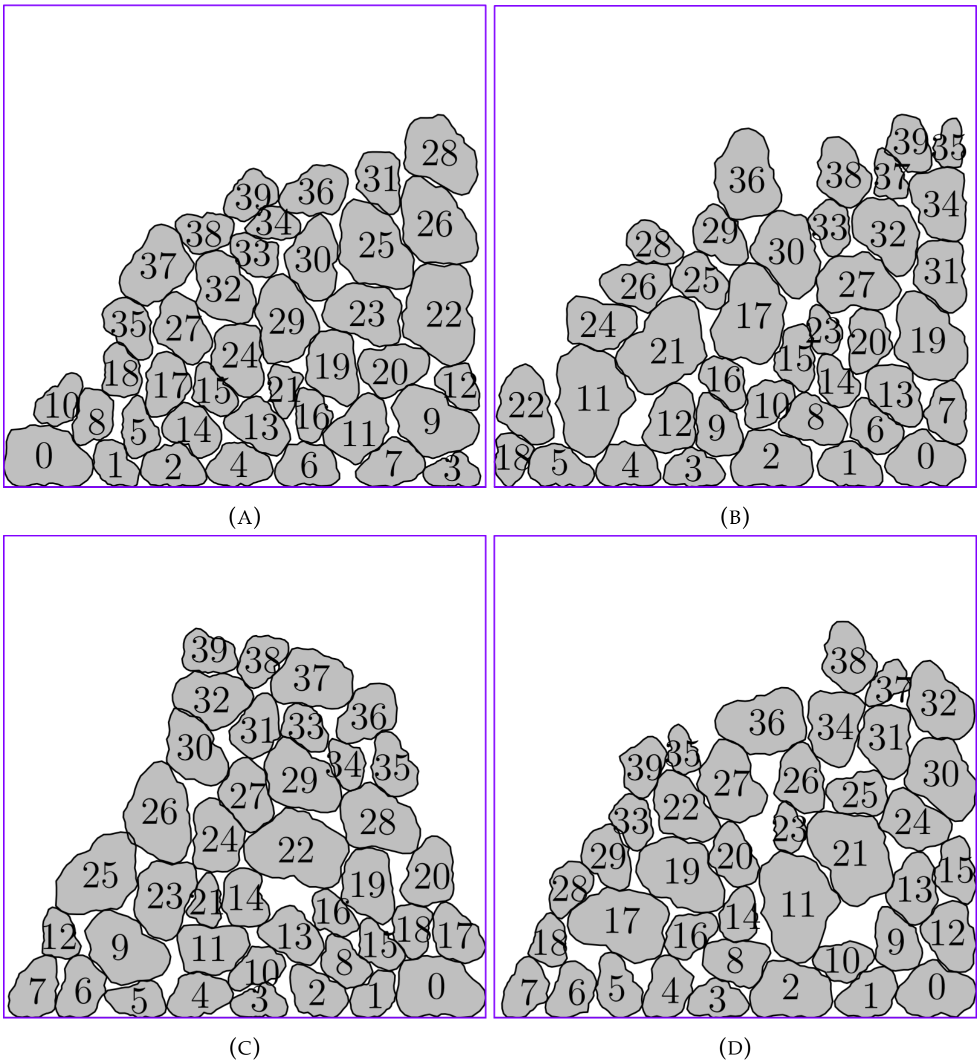

(A) (B) (C) (D)

FIGURE 6.41: Packings for the Soil Particle Scenario for weighting coefficients (a+b) (C_V=1, C_D=0.2, C_T=0.6, C_{CN}=0.2) and (c+d) (C_V=1, C_D=0.4, C_T=0.4, C_{CN}=0.4). Equivalent particle order for (a) and (c) and equivalent particle order for (b) and (d).

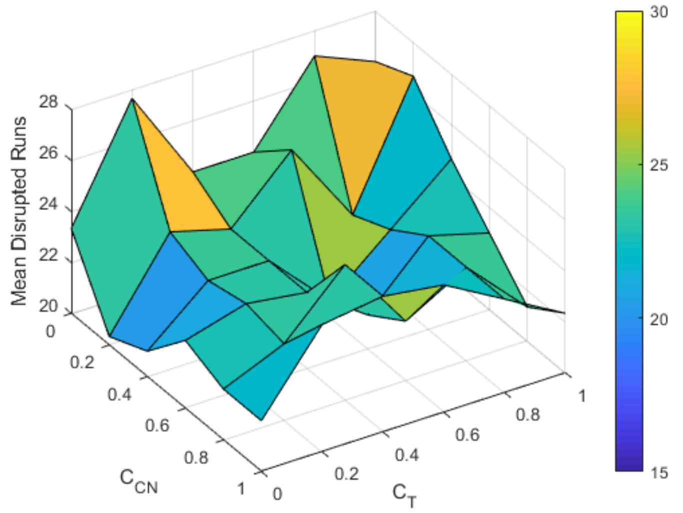

(A) MRJ

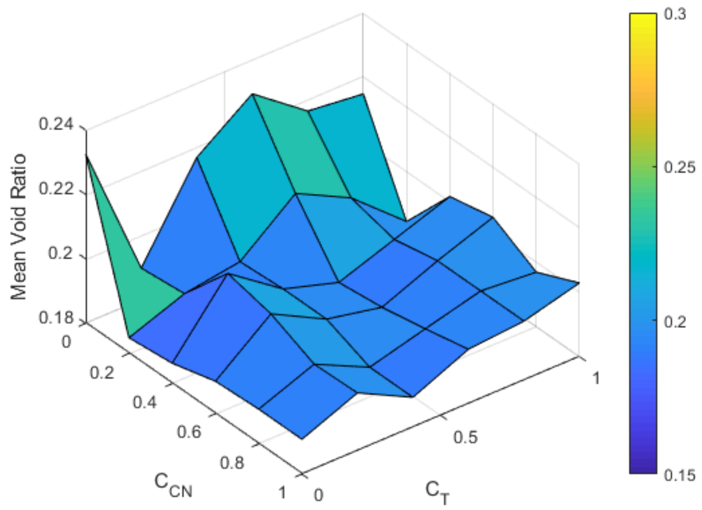

(B) MVR

FIGURE 6.42: Surface plot for C_V=1 and C_D=0 for ranged from of C_T and C_{CN} between 0 to 1 at increments of 0.2 for the Soil Particle Scenario.

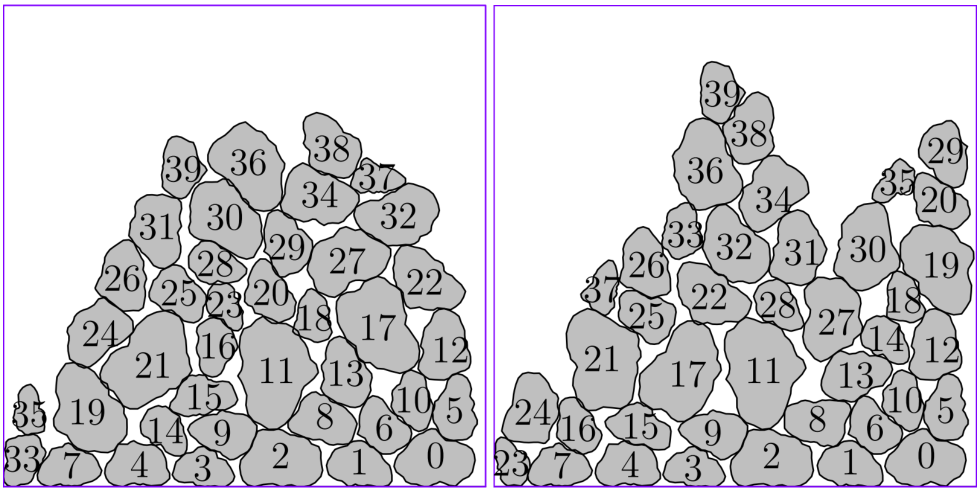

(A) MRJ=26, MVR=0.2272 (B) MRJ=20, MVR=0.1889

FIGURE 6.43: Packings in the Soil Particle Scenario for coefficients of weighting (a) (C_V=1, C_D=0, C_T=0.2, C_{CN}=0) (b) (C_V=1, C_D=0, C_T=0.8, C_{CN}=0) with equivalent particle order.

Three peaks of MRJ can be located in the search area for C_D=0.2. One of these, located at (C_T=0.4, C_{CN}=0) is in a similar location to the largest MRJ value for search area representing data when C_D=0.4. This is also the largest MRJ of all the datapoints and is located at (C_V=1, C_D=0.4, C_T=0.4, C_{CN}=0.2). The further two peaks are indicated by markers on Figure 6.44a with the corresponding points marked on Figure 6.44b. Their locations are (C_T=0,C_{CN}=0.2) and (C_T=0.8,C_{CN}=0.8) A similar pattern is seen for when C_D=0.4 where peaks are formed in similar locations. Again, the equivalent locations are marked on Figure 6.45. Packings using the coefficient values for these points are displayed in Figure 6.46 and it can be determined that an increase in C_D leads to the particles been packed closer together.

Figure 6.47 is the search area for C_D=1 for C_T and C_{CN} in the range 0 to 1 and varied by increments of 0.2. This are is examined to look at the upper limit of this range of coefficients for D due to the fact that D causes particles to be packed lower down in the system, which is beneficial for constructing and is recommended for DSRW (Vivian, 1976). The MVR results tend to be higher than other surface plots, as is suggested by the lowest MVR value in Figure 6.40 and Table 6.9. A wider base of particles is established with steeper slopes on the sides of the structure. Figure 6.48b and Figure 6.48c present the locations for highest MRJ and lowest MVR respectively, the locations of which can be found in Table 6.40. Further points around these results are presented in Figure 6.48a and Figure 6.48d. The differences between Figure 6.48a compared to Figure 6.48b and Figure 6.48c compared to Figure 6.48d tighter packings in the latter of each pair. The move from Figure 6.48a to Figure 6.48b is an increase in $C_T T$ whilst the the move from Figure 6.48c to Figure 6.48d is a decrease in $C_T T$ but with an increase in $C_{CN} CN$. Both these scoring criteria benefit from particles being closer together as T scores placement on the number of contacts and CN scores placement on the number of surrounding particles.

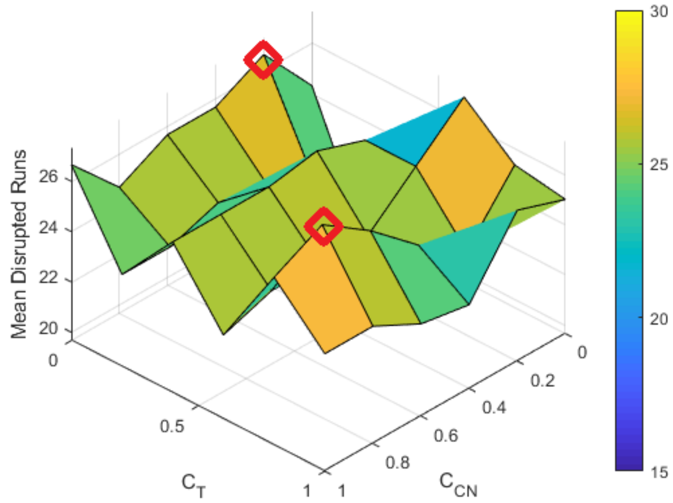

(A) MRJ

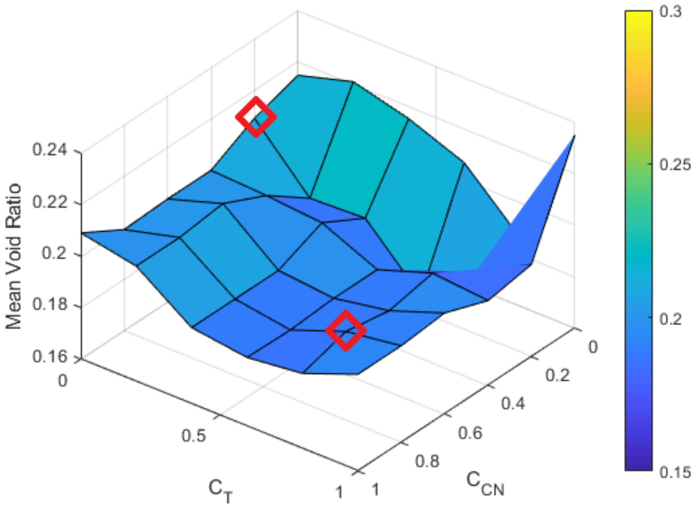

(B) MVR

FIGURE 6.44: Surface plot for C_V=1 and C_D=0.2 for ranged from of C_T and C_{CN} between 0 to 1 at increments of 0.2 for the Soil Particle Scenario.

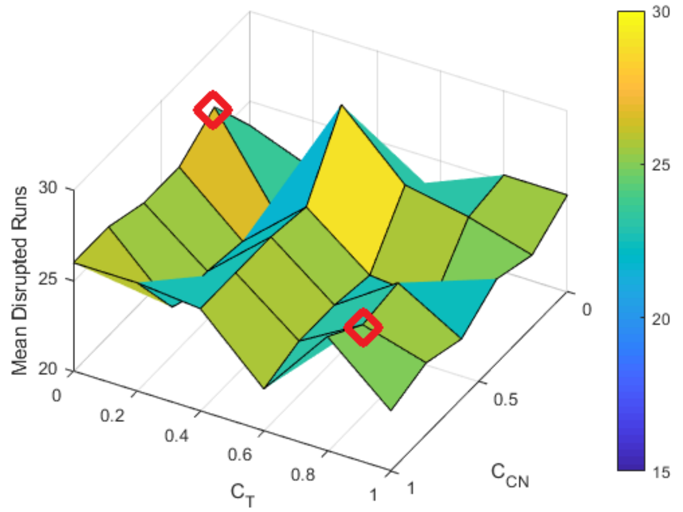

(A) MRJ

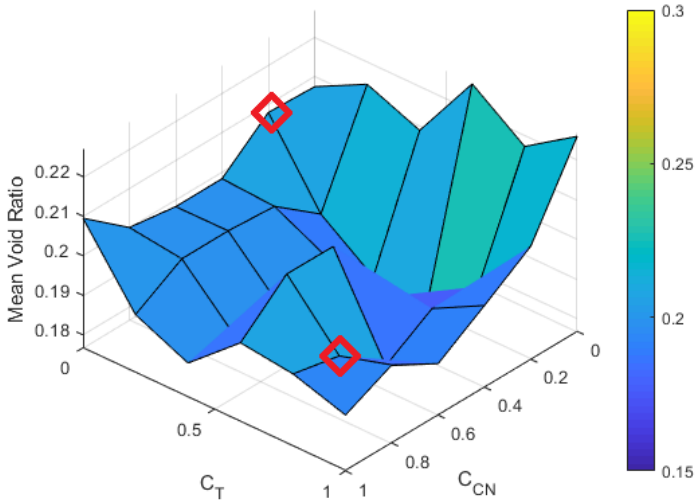

(B) MVR

FIGURE 6.45: Surface plot for C_V=1 and C_D=0.4 for ranged from of C_T and C_{CN} between 0 to 1 at increments of 0.2 for the Soil Particle Scenario.

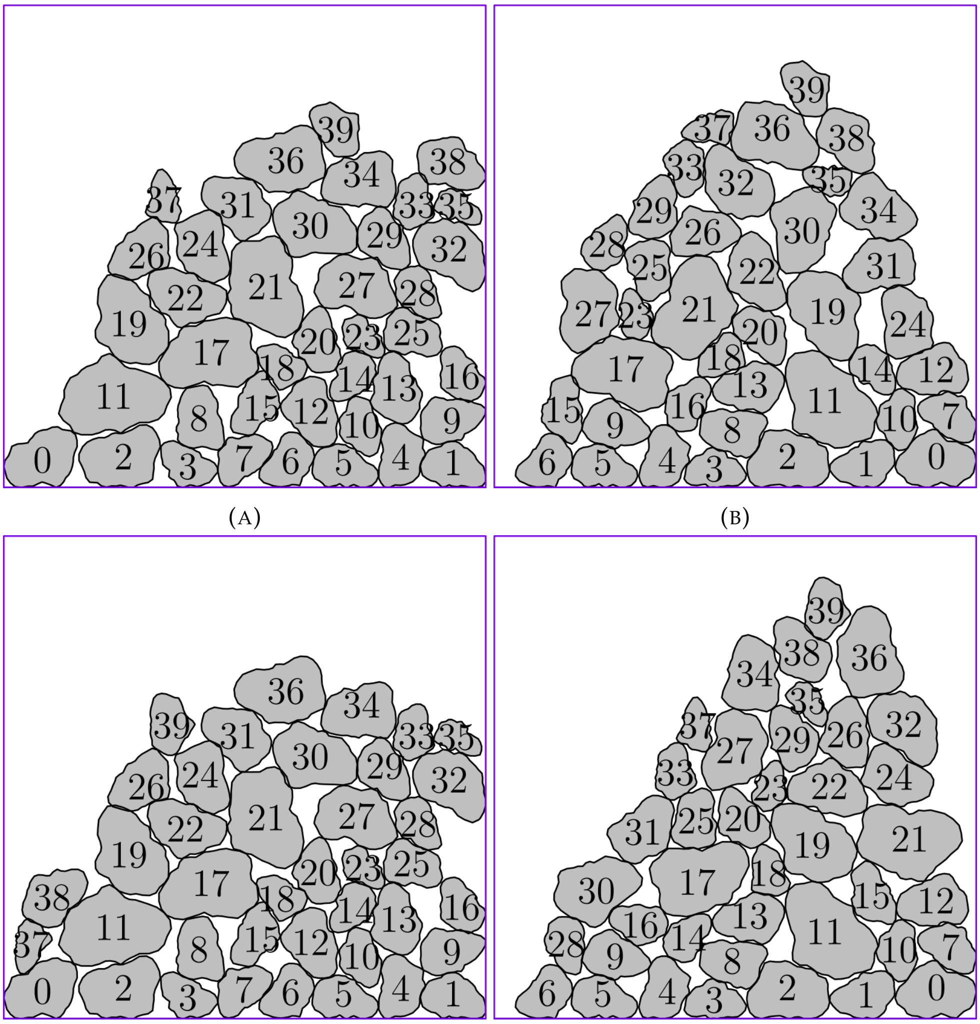

(A) (B) (C) (D)

FIGURE 6.46: Packings with equivalent particle delivery order for the Soil Particle Scenario for weighting coefficients (a) (C_V=1, C_D=0.2, C_T=0, C_{CN}=0.2) (b) (C_V=1, C_D=0.2, C_T=0.8, C_{CN}=0.8) (c) (C_V=1, C_D=0.4, C_T=0, C_{CN}=0.2) (d) (C_V=1, C_D=0.4, C_T=0.8, C_{CN}=0.8).

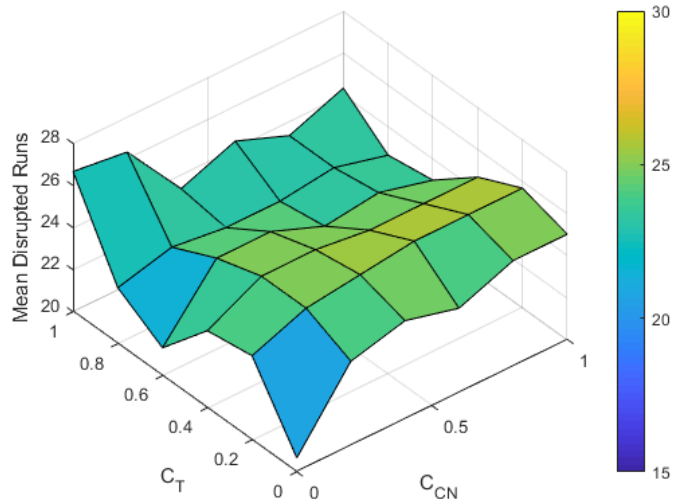

(A) MRJ

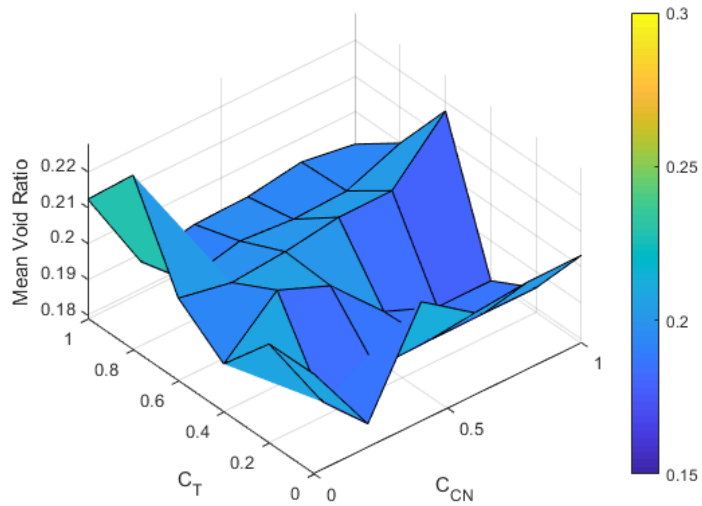

(B) MVR

FIGURE 6.47: Surface plot for C_V=1 and C_D=1 for ranged from of C_T and C_{CN} between 0 to 1 at increments of 0.2 for the Soil Particle Scenario.

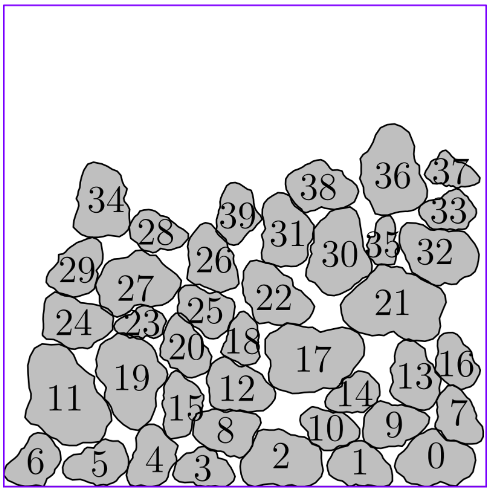

(A)

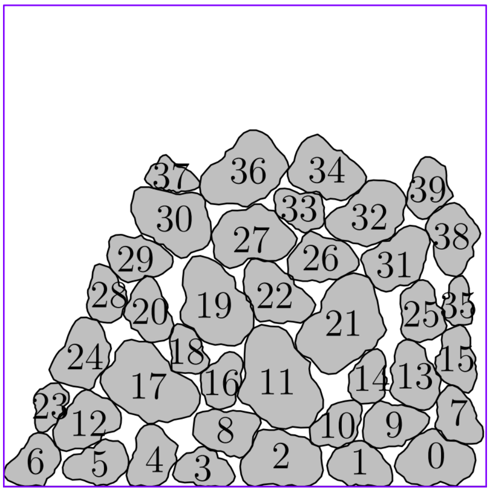

(B)

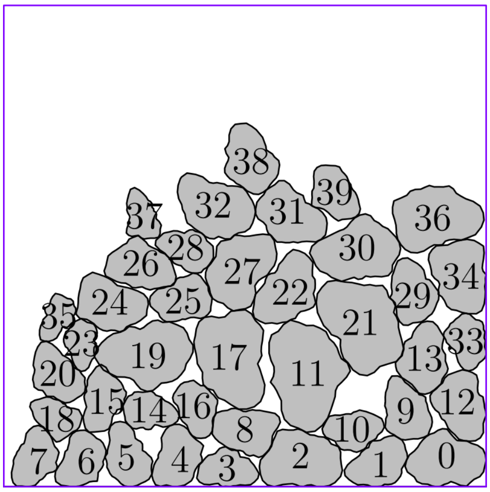

(C)

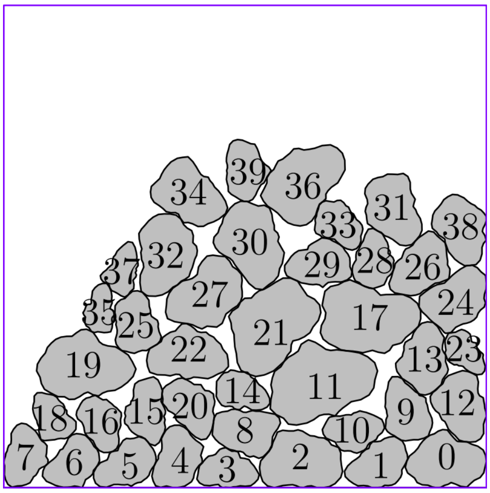

(D)

FIGURE 6.48: Packings with equivalent particle delivery order for the Soil Particle Scenario for weighting coefficients (a) (C_V=1, C_D=1, C_T=0.8, C_{CN}=0) (b) (C_V=1, C_D=1, C_T=1, C_{CN}=0) (c) (C_V=1, C_D=1, C_T=0.4, C_{CN}=0.8) (d) (C_V=1, C_D=1, C_T=0.2, C_{CN}=0.2).

6.5 Coefficients Determined from Tetris Scenario and Further Investigations

The coefficients determined as solutions for the Tetris Scenario are adopted here as coefficients of packing to see the results when shapes are not orthogonal tetrominoes but instead irregular outlines. Furthermore, the additional step of reducing the number of candidate poses may have an effect. Presented in Table 6.10 are the coefficients investigated and Figures 6.49-6.51 present these packings. Furthermore, it was considered to attempt a packing adopting large coefficients but with a smaller value of C_T. Therefore, results and packings for (C_V=1, C_D=6, C_T=0.5, C_{CN}=10) are also presented in Table 6.10 and are displayed in Figure 6.52.

From Chapter 5, combinations of coefficients (C_V=1, C_D=1.6, C_T=0.4, C_{CN}=0.045) and (C_V=1, C_D=0.6, C_T=0.2, C_{CN}=0.015) were obtained from the work conducted in this study as possible optimal solutions, with (C_V=1, C_D=1.6, C_T=0.4, C_{CN}=0.045) taken as the optimal solution as it avoids canyoning in the system. (C_V=5, C_D=1.25, C_T=0.4, C_{CN}=0.01) was determined in Hoodless and Smith (2023) and is utilised here for comparison. Of the coefficient values from the Tetris Scenario, (C_V=1, C_D=0.6, C_T=0.2, C_{CN}=0.015) appears to be the most optimal with higher number of runs disrupted in the system and lower void ratio than the other packings. As can be seen in Figure 6.51, the system does seem to be closely packed with less space between particles.

The reasoning for attempting packing for location of (C_V=1, C_D=6, C_T=0.5, C_{CN}=10) comes from analysis of results in Section 6.4.1. It was intended to see if results were improved by oversizing C_D compared to C_T and C_V to reduce the height of the structure as it is intended that a layer-by-layer construction process be utilised. C_{CN} was assigned a value of 10 as it was derived from Figure 6.36c and Figure 6.36d as well as Section 6.3.7 that this helped contribute to keeping particles packed in close proximity to each other.

Results between MRJ and MVR are very similar for most plots. There does not seem to be a pattern between the two to determine a relationship for finding an optimal solution. Results are similar and no clear path to follow for optimisation can be detected. Figure 6.53 shows the results for coefficient combinations investigated in Section 6.4.1 and Section 6.4.2. These are plotted as MRJ against their corresponding MVR value for the equivalent location. As can be seen, there is no obvious correlation with R^2=0.024. The refinement for coefficient combination of an optimal solution ends here. The reasoning for this is discussed in Section 8.3.

Coefficients	MRJ	MVR
(C_V=1, C_D=1.6, C_T=0.4, C_{CN}=0.045)	24	0.188
(C_V=5, C_D=1.25, C_T=0.4, C_{CN}=0.01)	25	0.194
(C_V=1, C_D=0.6, C_T=0.2, C_{CN}=0.015)	27.8	0.183
(C_V=1, C_D=6, C_T=0.5, C_{CN}=10)	25	0.184

TABLE 6.10: MRJ and MVR results for coefficients of weighting with sample size n=5 taken.

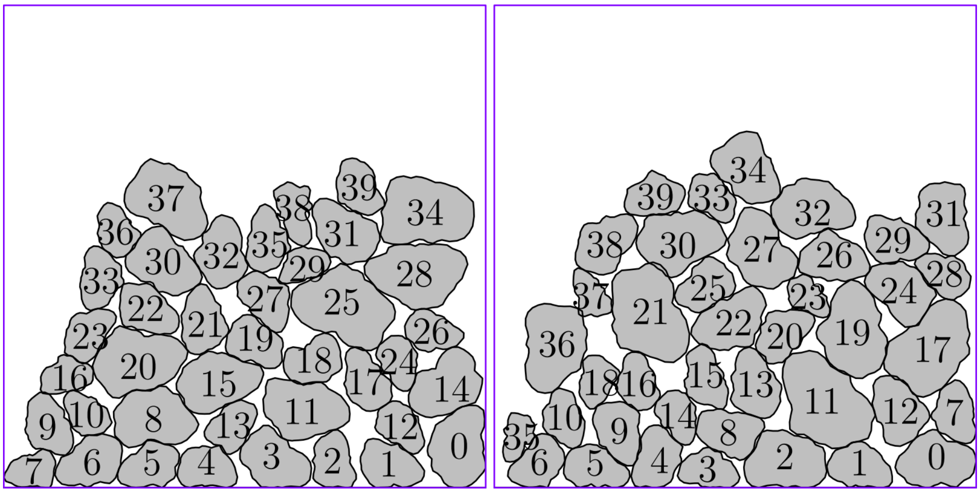

(A) (B)

FIGURE 6.49: Packings in the Soil Particle Scenario for coefficients (C_V=1, C_D=1.6, C_T=0.4, C_{CN}=0.045).

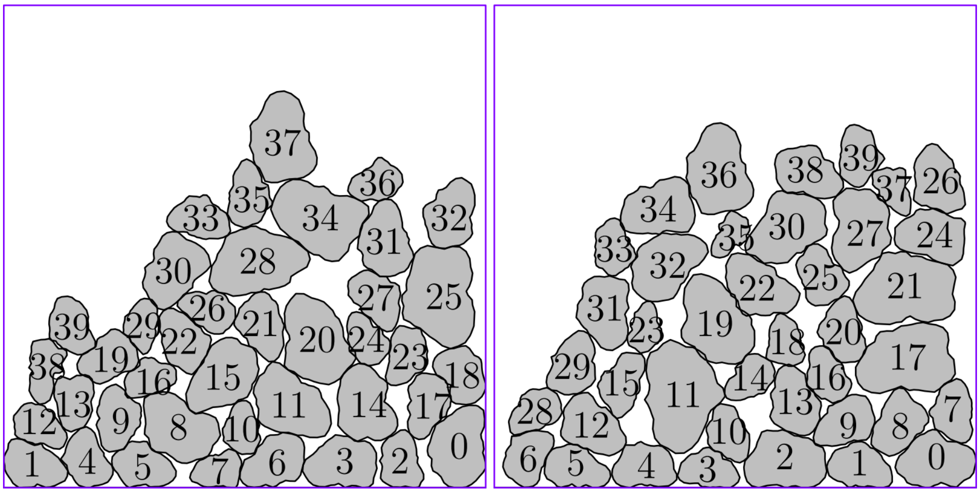

(A) (B)

FIGURE 6.50: Packings in the Soil Particle Scenario for coefficients (C_V=5, C_D=1.25, C_T=0.4, C_{CN}=0.01) with (a) equivalent packings to Figure 6.49a and (b) equivalent packings to Figure 6.49b.

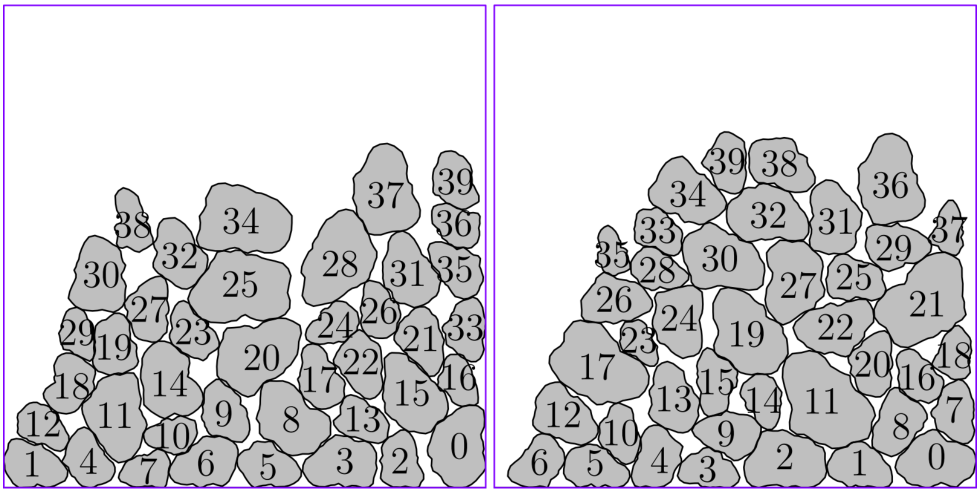

(A) (B)

FIGURE 6.51: Packings in the Soil Particle Scenario for coefficients (C_V=1, C_D=0.6, C_T=0.2, C_{CN}=0.015) with (a) equivalent packings to Figure 6.49a and (b) equivalent packings to Figure 6.49b.

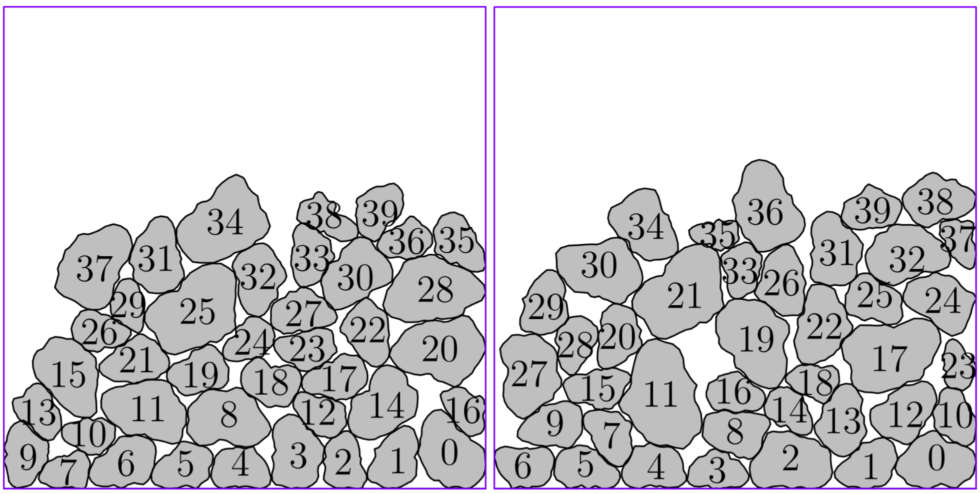

(A) (B)

FIGURE 6.52: Packings in the Soil Particle Scenario for coefficients (C_V=1, C_D=6, C_T=0.5, C_{CN}=10) with (a) equivalent packings to Figure 6.49a and (b) equivalent packings to Figure 6.49b.

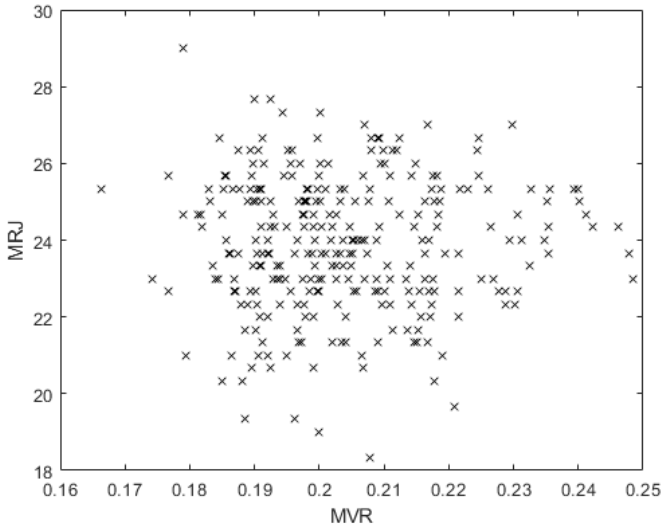

FIGURE 6.53: Results of MRJ and MVR for packings for coefficients when ranged from 0 to 10 by increments of 2 and 0 to 1 by increments of 0.2.

6.6 Results of DBL Heuristic and Random Packings

As stated in Section 4.5, it is required that results are compared to a control to ensure the method of packing is an improvement on what already exists. In this section, results for randomly packed particles and the DBL heuristic are presented. For more information on the DBL heuristic please refer back to Section 2.4.3 or Section 5.7. To summarise, the DBL heuristic selects the deepest-bottom-left position in the domain and places the particle there, as was used by Wang and Hauser (2019). If scores are joint, the particle is selected by choosing the least amount of void created underneath the particle. The DBL heuristic was taken as equivalent to the packing using the algorithm with zero coefficients, as the hierarchical filter works in a similar manner by prioritising positions near the bottom of the domain, followed by positions left-most in the domain, followed by reducing void area underneath the particle.

Of the random control tests produced, they are defined as the following

- RAND: Completely randomly packed particles from the whole selection of candidate poses determined in the discretised method, with the position and rotation then randomly selected from all possible stable positions in that area under the refined placement determination method.
- RAND-OF: Positions are scored in the discretised method adopting coefficients C_V=1, C_D=1.6, C_T=0.4 and C_{CN}=0.045 as determined as solution for the Tetris Scenario. From here, a random candidate pose from the 30 brought forward after applying the hierarchical filter is selected and random orientation and position are then randomly selected for the refined placement determination.
- RAND-F: Candidate poses are filtered with the removal of the scoring criteria in the hierarchical filter. From the first 30 given, a random candidate pose is selected and a random orientation and refined location are taken.

The results in Table 6.11 indicate that the packing of particles representing irregular, untooled rock packed by the algorithm developed in Chapter 3 outperform those

Control	MRJ	MVR
RAND	11	0.3607
RAND-OF	24	0.2273
RAND-F	18.6	0.3722
DBL	23	0.2327

TABLE 6.11: MRJ and MVR results for the different control tests specified, with sample size n=5 taken.

that are randomly packed. The best performing of the randomly packed particles utilise the objective function to determine candidate poses, suggesting that the objective function is beneficial for trying to determine placement for a structure with purpose of optimised shear strength.

Packings of the DBL heuristic are found in Section 6.3.2 in Figures 6.1-6.4. The packings by the algorithm utilising the objective function outperforms the DBL heuristic when comparing MRJ, but MVR value calculated is lower for the DBL heuristic.

6.7 Summary

As can be seen from the results of the algorithm, further development is required to determine an optimal solution for packing structures of high shear strength. Results are similar and no clear path to follow for optimisation can be detected. Results of packings are presented in Section 6.4. They show that the algorithm can pack particles but do not suggest a best answer. Towering and sloped sides in the packings can be seen.

Section 6.2 describes the necessary changes to the method outlined in Chapter 4. This was due to the increased computational times experienced. Sample size was reduced to n=3 rather than n=30. Furthermore, the definition of the particles are reduced to less coordinates to speed up runtime. Values for MRJ and MVR were seen to differ with no obvious pattern when using reduced coordinates to describe the particle and this was used as justification for this to be done. Frequency of sampling was also reduced, and as a result this led to the omission of the Gaussian filter from analysis.

The studying of coefficients is conducted in Section 6.3. Input parameters for the study can be found in Table 6.1. Firstly results are presented for when all coefficients in the objective function are set to a value of zero. This is thought to represent the DBL-heuristic that is sometimes utilised as a solution for two-dimensional bin packing due to the priority list of the hierarchical filter. Particles are seen to be packed on their edges with another point of contact with the particle to the left (or the domain edge). This is due to the particles prioritising left-most positions compared to any criteria in the objective function. After this, the impact of the coefficients of weighting on the packing are investigated in Section 6.3.3. This is done by fixing all coefficients and raising them separately. Additionally, the parameters in the objective function are investigated as single variables as well as oversized as was done for the Tetris Scenario. The effects for V_{AB}, D, T and CN are reviewed in Sections 6.3.4-6.3.7. It was seen for V_{AB} and T that particles stacked with sloping side whilst for D and CN, particles were seen to be packed in flatter configurations.

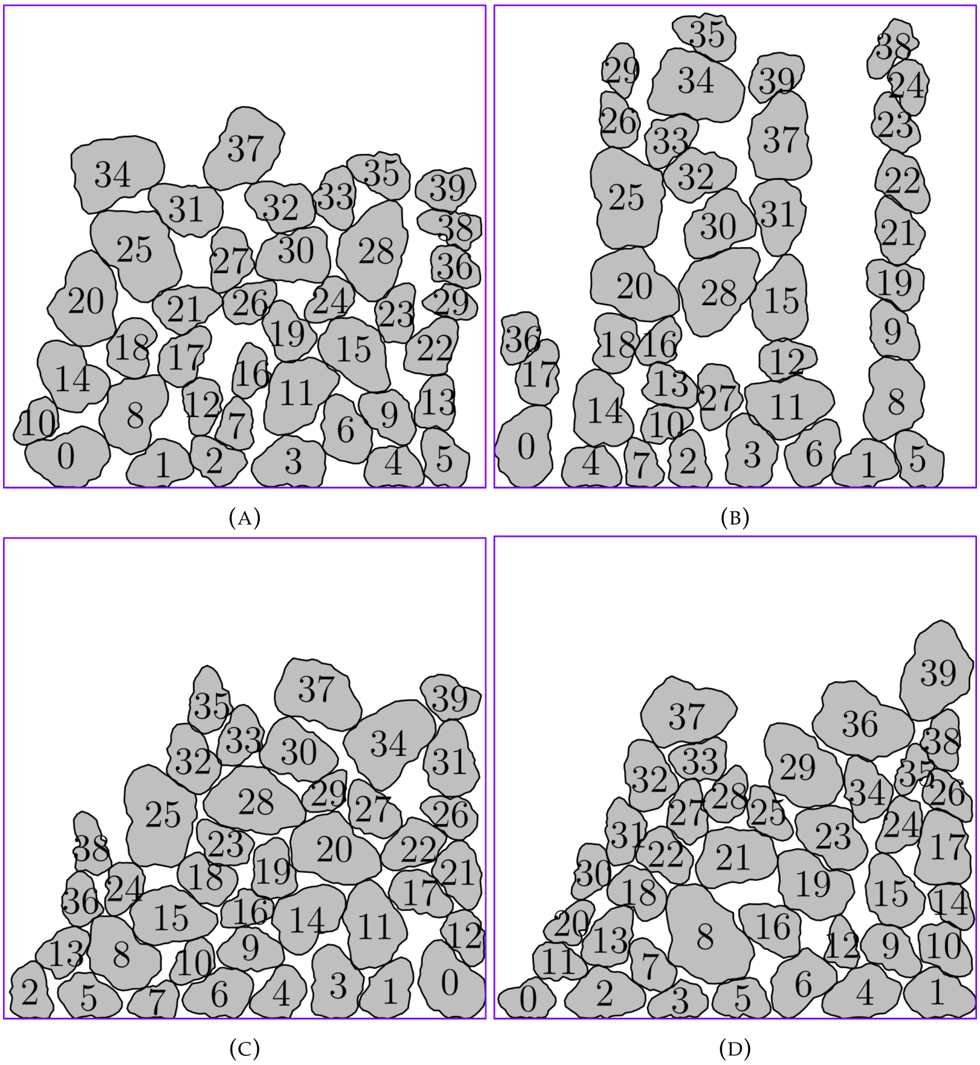

(A) (B)

(C) (D)

FIGURE 6.54: Examples of packing using (a) RAND (b) RAND-F (c) and (d) RAND-OF.

Section 6.4 begins by testing coefficient ranges of C_T and C_{CN} 0 to 10 and C_D 0 to 8 with increments of 0.2 used for all coefficients. MRJ and MVR results are presented and areas of interest are highlighted. No real correlation is initially seen so it is hard to identify areas of optimal solution without analysing the structures. Section 6.4.2 continues the investigation by looking at coefficient values which allow V_{AB} to have more of an effect on packing. Results for MRJ are shown to be much larger whilst MVR results are shown to be lower for these packings. However, still no correlation is seen between the two. Again, packings which score high for MRJ appear to be towering and have sloped sides. Tighter packings are seen when C_T and C_{CN} are higher. This is sensible as these criteria reward particles for being closer to others and for having more touching contact area.

Coefficients obtained from the Tetris Scenario in Chapter 5 study are analysed in Section 6.5 to see if these provide suitable packings. The results present good quality packings visually. Again, MRJ and MVR do not indicate an optimal packing out of those investigated. Furthermore, coefficients (C_V=1, C_D=6, C_T=0.5, C_{CN}=10) were trialled to see if an increased effect of D and CN compared to T improved packing. Whilst the packing is conducted in more of a layer-by-layer process, it is hard to conclude without verification of the strength. It is shown by plotting MRJ to MVR for each location that there is no correlation for the relationship. This is further proven by R^2 for the data being a value of 0.024. As no clear path can be seen for optimisation, the investigation into the Soil Particle Scenario is halted. This is further discussed in Section 8.3.

Control samples for packing are presented in Section 6.6. These include randomly packed samples. These are created by completely random packing (RAND); random packing using the objective function to determine 30 candidate poses and then randomly selection of one of these options and random defined location and orientation selection (RAND-OF); application of the hierarchical filter to gain 30 candidate poses for which one is selected randomly with defined location and orientation selected at random. It is shown that the algorithm packs better than these random samples, as would be expected. The DBL heuristic is assumed to be equivalent to that where coefficients of weighting are equivalent to zero due to the hierarchical filter. Therefore, this scenario is taken. The packings of the algorithm outperform these results additionally.

Chapter 7

Verification of Strength

7.1 Introduction

Part of the objectives set out in Chapter 1 was to verify the strengths of the structure to provide evidence that the algorithm is indeed creating structures with high shear strength as outlined by the objective function. Unfortunately due to unforeseen circumstances and timescale of the project, it was unable for this step to be completed. Here it will be discussed the proposed method for testing the build sequence of two-dimensional particles and the designed experimental procedure is described.

Section 7.2 discusses different methods that could be used to verify the strength of the structure. These involve numerical and experimental testing processes. Section 7.2.2 discusses numerical verification methods and discuses DEM modelling and the use of physics engines as seen in the literature discussed in Section 2.2.4. Experimental verification methods for a system that consists of two-dimensional particles are explored in Section 7.2.3. Section 7.2.3 begins by discussing possible methods based on traditional techniques for testing soil strength before moving on to discuss various techniques for measuring of angle of repose. Angle of repose is a parameter that has been linked to angle of internal friction (Coulomb, 1776 as cited by Al-Hashemi and Al-Amoudi, 2018) and is adopted as a way to verify the shear strength of the structures produced by the algorithm produced in Chapter 3.

The experimental set up that is planned to be used to verify shear strength of the structures is presented in Section 7.3. This composed of a rotating drum where two-dimensional particles cut from acrylic could be positioned. Figure 7.6 and Figure 7.7 present the rig that was designed for testing and the proposed method is described. Section 7.4 describes the process in which particles could be identified and tracked during the experiment. The purpose of particle identification was to find when particles start to move in order to pinpoint initial collapse of the system. Additionally, it was thought that if certain particles tend to fail more readily than others then this could be identified by their unique code.

Tolerance of errors are briefly explored in Section 7.5. This is brought about by the recognition that a system constructing autonomously using a robot will lead to exact placement of particles being unlikely. This is due to the level of detection that the robot will possess as well as shifting of placement once the stone is released by the end-effector. Section 7.5 discusses how this would have been tested using the equipment described in Section 7.3.

Section 7.6 describes the expected results of the experiment in terms of initial angle of repose as well as a mixed angle of repose that would be exhibited by the system once suitable rotations of the wheel have been performed to allow mixing of the collapsed structure. Section 7.7 summarises the information presented in this chapter.

7.2 Verification Methods

7.2.1 Introduction

There are two ways in which the designed structures can be verified. These are numerically and experimentally. Each approach is described and some suggestions are made about how both of these could be carried out. In the project, it was anticipated that both methods could be adopted. However, the effect of COVID-19 led to limitations on what was achieved.

7.2.2 Numerical Verification Methods

Discrete Element Method (DEM) was introduced by Cundall and Strack (1979) and has commonly been used in the field of geotechnics for numerically simulating soils where continuum methods are not able to capture the characteristics in need of defining (O'Sullivan, 2011). However, in these methods the calculation time can be great if a large number of particles are included (O'Sullivan, 2011; Sakai et al., 2014) and simplifications of particle shapes are normally adopted. For example, spheres may be used to represent soil particles in the simulation and therefore the effects of angularity are ignored (Izadi and Bezuijen, 2015).

The rise of physics engines allow for simulations of many objects that interact with each other to be completed in relatively short computational times. There are two types of physics engine: high-precision physics engines and real-time physics engines. Real-time physics engines are typically utilised in videogames and are less expensive computationally whereas high-precision physics engines can deal with much more complex models but require much higher computational power.

As described in Section 2.2.4, previous literature exploring autonomous construction of irregular objects have focussed on numerically verifying build sequences by identifying potential poses in a physics simulator (Furrer et al., 2017; Johns et al., 2020; Johns et al., 2023; Liu et al., 2021). Pybullet physics engine is used in Liu et al. (2021) and Bullet physics engine in Johns et al. (2020) and Johns et al. (2023), whilst Furrer et al. (2017) did not name the physics simulator used but does mention Open Dynamics Engine specifically in their related works section.

Box2D is an example of a physics engine that can be used on two-dimensional particles and there is precedent of this being used to model frictional soils (Li, 2020; Pytlos, 2015; Pytlos et al., 2015). Dynamic interactions are simulated between discrete bodies and their continuous motion is calculated through a time-stepping scheme. At each time step, the rate of change of movements are found and the variables for each body are updated.

Pytlos et al. (2015) highlights two advantages of Box2D over traditional DEM. These are that the physics engine enables fast real-time simulations which translates to faster computational speeds for large particle systems and that soil macro-scale behaviour can be controlled by particle shape, size distribution and the coefficient of friction. These are all physical properties of the soil being modelled and can be defined beforehand. Li (2020) compared Box2D and showed how the time step can be much larger than DEM and other numerical methods meaning simulations can be conducted at a faster rate for Box2D.

For a physics engine to be adopted in this project it is envisioned that Box2D would have been investigated further as a potential numerical tool. As with Li (2020) and Pytlos et al. (2015), Box2D could be adopted for biaxial testing of structures packed by the algorithm, or even be expanded to conduct shear tests or a tilting table test like that seen in Grillanda et al. (2021), Restrepo Vélez et al. (2014), and Santa-Cruz et al. (2021). One of the main limitations of Box2D is its incapability to model concave shapes. As irregular particles are being investigated in this project, it is desired to be able to model concave shapes to truly represent all possible irregular rock silhouettes. Concave objects can be simulated by "gluing" convex shapes together in which the shapes are locked together and will move and rotate with equal values. However, this would mean particles are simulated using multiple particles and potentially increase the total computational runtime.

7.2.3 Experimental Verification Methods

Methods of Testing Experimentally

Difficulties arise when testing two-dimensional systems experimentally when normally this would be adopted to test those which exist in three-dimensions. Traditional soil testing methods of biaxial or shear box tests whereas a tilting test had been used to test retaining walls as previously mentioned in Section 2.2.1 (Grillanda et al., 2021; Restrepo Vélez et al., 2014; Santa-Cruz et al., 2021). As testing is completed in 2D, a confined space will be required to support the structure with potentially the surface being exposed. With biaxial and shear box tests, the top surface would need to be the testing plane for a force to be applied. Problems occur with movement of particles and dilation. As particle shapes would be made from acrylic, they would not be able to compress and rather than the structures strength being tested the result would be more a test of the material strength.

The tilting table method also requires supports for the sides of the structure but is one which could suitably be adjusted to test the strength of particle system. This method measures the angle at which the structure fails. This is also known as the angle of repose, which is widely investigated in the field of powder mechanics.

Angle of Repose

Angle of repose can be defined as the angle that differentiates the transition between phases of a granular material (Liu, 2011). More generically, the angle of repose in a noncohesive granular material is the steepest slope of unconfined material that can be sustained without collapse measured from the horizontal (Lowe, 1976). In terms of soil mechanics, this means the angle of maximum slope inclination at which the soil is barely stable (Day, 2010). Above this slope angle, the material starts to flow; below this angle, the material is stable. Values range from 25^o for smooth spherical particles to 45^o for rough angular particles (Carrigy, 1970; Pohlman et al., 2006). Al-Hashemi and Al-Amoudi (2018) states that the definition of the angle of repose should be application specific due to the different types and descriptions.

There is evidence that angle of repose and angle of internal friction are related. Angle of repose is often assumed to be equal to the residual angle of internal friction (Das, 2014; Santamarina and Cho, 2004). In Coulombs theory, the internal friction angle was assumed to be equal to the repose angle (Coulomb, 1776 as cited by Al-Hashemi and Al-Amoudi, 2018). Terzaghi (1943) defined the angle of repose as a specific angle of internal friction that is acquired when the soil is in its loosest state. Emphasis should be placed on loosest state here. As Metcalf (1966) stated, the assumption of angle of repose and angle of internal friction being equal is not always correct as granular soils under low confining pressure is notably different compared to granular soil under zero confining pressure. In addition, Coloumb's theory is based on assumptions such as the frictional force being independent of the contact area, frictional force is linearly related to normal force, and heaped materials form perfect concical shapes which is not always the case (Rackl et al., 2017a). For example, it has been reported a decrease in normal forces could be associated with an increase in friction forces (Deng et al., 2012).

Angle repose can be given as static or dynamic. The static angle of repose forms just before instability of the slope (and after once the slope has settled again) whereas dynamic is observed when grains are moving continuously down an inclined plane, and is given as the angle of this plane (Cheng and Zhao, 2017). Despite different methods and guidelines existing, there are no standardised methods for measuring angle of repose (Rackl et al., 2017b). Figure 7.1 is taken Geldart et al. (2006) in which it is stated that these four methods are the most common. These are the fixed height cone method, the fixed base cone (or hollow cylinder method), the tilting table (or tilting box) method, and the rotating cylinder (or rotating drum) method. Different testing methods are outlined as follows.

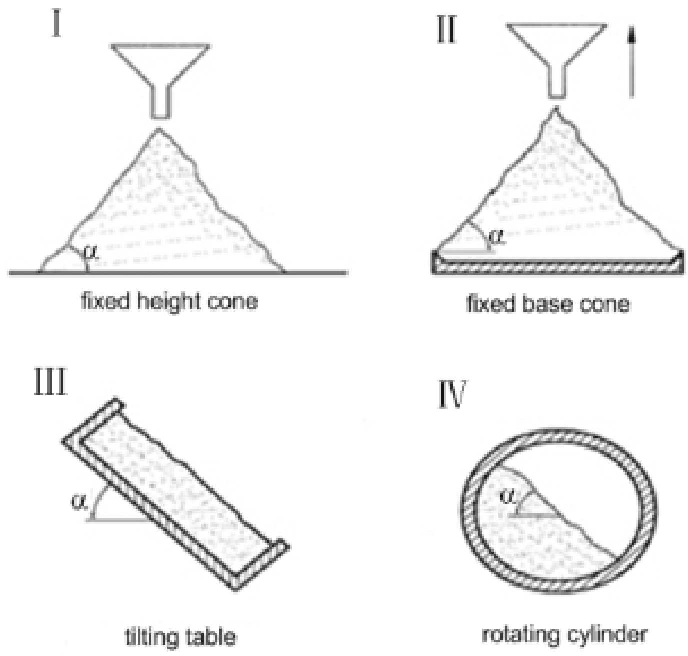

FIGURE 7.1: Different methods of measuring angle of repose (Geldart et al., 2006). Reproduced with permission © Elsevier.

Granular material forms a conical pile when it is allowed to fall freely from an orifice onto a flat surface. Advantage can be taken of this experimentally to measure the angle of repose by allowing granular material to flow through a funnel at a certain height onto a base with known roughness. Example of this can be found in Geldart et al. (2006), Miura et al. (1997a), and Nelson (1955). The funnel can either be fixed or raised slowly to keep the distance from the bottom of the funnel to the top of the conical pile formed constant to minimise the effect of falling particles (Al-Hashemi and Al-Amoudi, 2018). Depending on the funnelling method, two angles of repose can be expressed. These are the internal and external angles of repose which exist above the funnel from where the material has fallen (internal) and on the pile of the deposited material (external) (L. J. Johnston et al., 2009). Where these angles are measured are represented in Figure 7.2. Cho et al. (2006) demonstrated that the internal angle of repose is greater than the external.

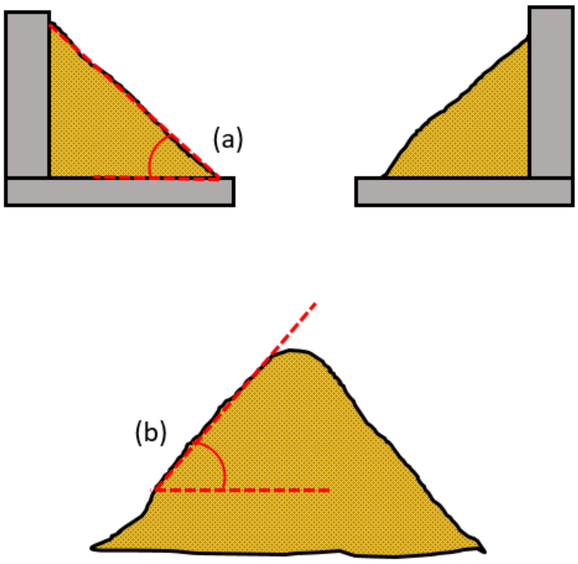

FIGURE 7.2: Examples of (a) internal angle of repose and (b) external angle of repose as suggested by L. J. Johnston et al. (2009).

Another experimental method is the tilting box method as described earlier. Granular material is placed in the box and titled gradually until the grains begin to slide. The angle at which the board is to the horizontal when particles begin to move is measured to be the angle of repose (Liu, 2011; Pitanga et al., 2009). However, as stated by Al-Hashemi and Al-Amoudi (2018), this method provides the coefficient of static friction rather than the angle of repose. Figure 7.3 is an example of this experimental setup taken from Pitanga et al. (2009) where the angle of repose was measured for a soil with a soil-geosynthetic interface as well as a soil-soil interface.

An alternate method that determines static angle of repose is the hollow cylinder method (used in Al-Hashemi and Al-Amoudia (2018)). The steps of this method are visualised in Figure 7.4. Granular material is poured into a cylinder resting on a solid, rough base. The cylinder is then lifted at a rate less than $2ms^{-1}$ (Salawu et al., 2013) until the cylinder is removed and the material has piled to form a conical shape. The angle of the slope is the angle of repose (Al-Hashemi and Bukhary, 2016; Lajeunesse et al., 2004; Liu, 2011).

The tilting cylinder method is another proposed technique to measure the angle of repose of granular soils (Mitchell and Soga, 2005). Soil is poured into a water-filled graduated cylinder which is then tilted before being restored to its vertical position (Al-Hashemi and Al-Amoudi, 2018). The slope angle of the residual soil is taken as the angle of repose.

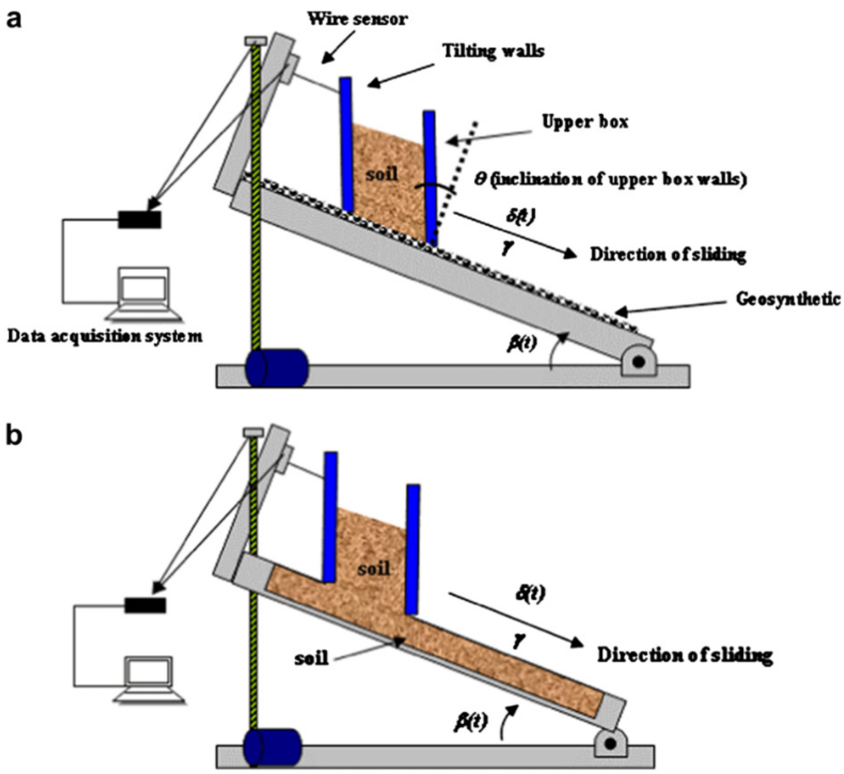

FIGURE 7.3: Inclined plane device used in Pitanga et al. (2009) for tests on soil–geosynthetic (a) and soil–soil (b) interfaces. Presented here with permission from Elsevier.

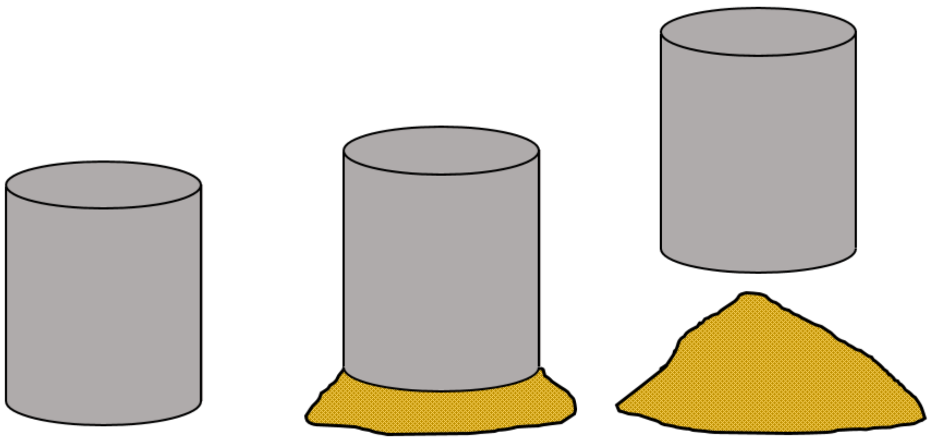

(A) (B) (C)

FIGURE 7.4: Hollow cyclinder method for measuring static angle of repose as described by Al-Hashemi and Al-Amoudia (2018) and Salawu et al. (2013). The figures represent (a) A hollow cylinder with sand poured into it resting on a rough base (b) the cyclinder being lifted (c) the cylinder clear of the sand which is now resting in a heap.

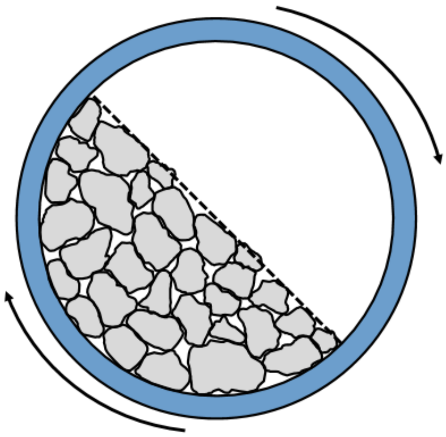

(A) Upper

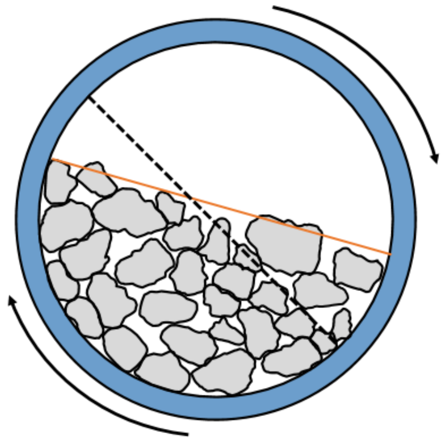

(B) Lower

FIGURE 7.5: (a) Upper angle of repose at the beginning of an avalanche (b) Lower angle of repose at the end of an avalanche with original upper angle of repose indicated by dashed line.

Cheng and Zhao (2017) used a motor-driven rotating drum to measure angle of repose. This can be described as a dynamic angle of repose. The inner diameter of the drum was 28.90cm and had a depth of 11.50cm. The drum was transparent so that the soil inside could be seen and a camera was positioned horizontally to record the front of the drum. A video was recorded at a rate of 25 frames per second and the duration of each video was so that at least 20 avalanches were captured. Black paper was used as a background to give more definition between particle and air in the video for detection. Three different angles of repose were identified. The upper angle of repose formed at the inception of an avalanche, the lower angle of repose at the end of an avalanche and the dynamic angle of repose characterised with continuous sediment transport down the slope. For each test the drum was half-filled, no matter the diameter of the particle. Slope measurements were conducted under both dry and submerged conditions. Upper and lower angle of repose are presented in Figure 7.5.

At a low rotating speed, sediment grains in the drum moved together until the slope reached its upper angle. This demonstrated that the material acts as a rigid body (Cheng and Zhao, 2017). Increasing past the upper angle created an avalanche in the material, transporting grains down the slope. It is stated that at the end of the avalanche, a new slope formed at a lower angle. At a higher rotating speed, the slope angle would approach a constant due to sediment grains continuously rolling down the slope. This indicates the beginning of the rolling stage, and the angle observed corresponds to the dynamic angle of repose. Under dry conditions, it was found that a particle size of 1.29mm gave a lower angle of repose of roughly 35^o and an upper angle of repose of roughly 41^o. Measurements show that the average of the upper and lower angle of repose is approximately equal to the dynamic angle of repose. (Xiao et al., 2005) also found this to be acceptable for other shapes of grains. In addition, it was found that both upper and dynamic angle of repose increase slightly with increasing grain diameter whereas lower angle of repose is not affected and appears to remain constant.

For the use of this work, it is assumed that angle of repose is a good variable to measure the strength of the structure created. Evesque and Rajchenbach (1989) investigated factors that affect slope stability of granular materials and concluded a factor governing the stability of the slope is angle of repose. While angle of repose may not be directly related to internal angle of friction, it can give a good indication of the behaviour of the soil. Therefore, in the two-dimensional experiments conducted in this research, angle of repose will be used to compare the strength of two-dimensional packing structures.

7.3 Experimental Setup

The design and setup of an experiment for measuring angle of repose has been completed as part of this study. The hypothesis behind the experiment is to determine the dynamic angle of repose of different packing structures of two-dimensional particle shapes made from acrylic. Of the methods for testing angle repose investigated in Section 7.2.3, the rotating drum technique was seen as the most suitable for this project. Use of the drum removes the need for supporting sides whilst a force is exerted for testing. Instead, the supporting structure is able to move the system and gravity acts as the force to create failure in the structure.

The equipment used for the experiment resembles that used in Cheng and Zhao (2017) and has been made from acrylic plastic and laser cut using the facilities in the Diamond Building at the University of Sheffield. The equipment consists of a 0.6m diameter wheel with an internal diameter of 0.5m. The two outside plates are made from 10mm thick acrylic and the inside ring is cut from 6mm thick acrylic. The wheel sits on an axel that spins the equipment and is supported by a metal stand which can tilt so the wheel can lie horizontally before being shifted to the vertical. The pieces of the equipment are held together with wing nuts and can be detached from each other. Figure 7.6 presents the rig with no particles loaded into the centre.

Particles are laser cut from acrylic in the shapes produced by the Fourier-Voronoi method described in Section 3.6.1. Coordinates of the shape outline were exported into an AutoCAD file. The laser has a diameter of 2mm which cuts the acrylic removing 0.1mm of material at the edge. Therefore, the shapes in the AutoCAD file were increased in size to allow for this. The plastic particles were cut from 6mm thick acrylic - the same diameter of the inside of the wheel not including the washers between the internal pieces where wing nuts are located.

The rig can be adjusted to be tilted horizontally for the placement of particles as demonstrated in Figure 7.7 and the front face removed. Particles are placed in the desired arrangement before the face of the wheel is reattached and the rig can be tilted back to be into the vertical plane. As the algorithm produces the build sequence of particles in a layout of coordinates, this can be exported to AutoCAD. It is envisioned that this could then be printed to scale and placed beneath the back face of the rig. Then particles can be placed in the exact position as designated by the algorithm for testing of the produced structure.

To produce build sequences, the domain in the algorithm would need to be adjusted to be circular. However, this would not be an issue as Asymptote has an inbuilt function that can produce circles defined as a path which is required for the placing stage described in Section 3.4.1. Furthermore, within the algorithm the coefficient of friction is taken as 0.5 currently. Testing would need to be completed to find the coefficient of friction between an acrylic-to-acrylic interface between the edges of the

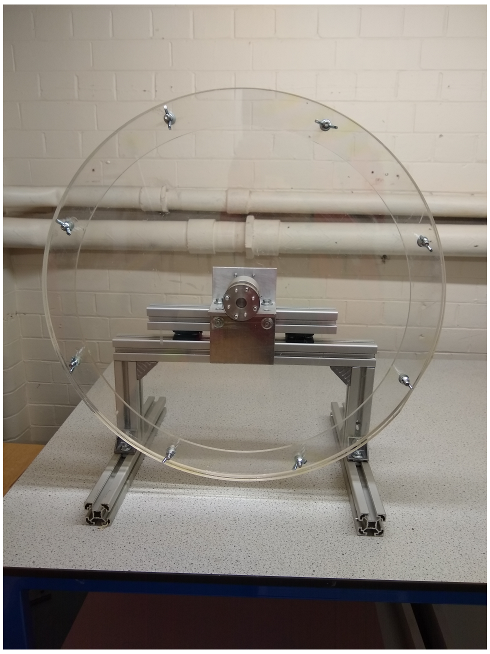

FIGURE 7.6: Image of the wheel setup used for the experiment.

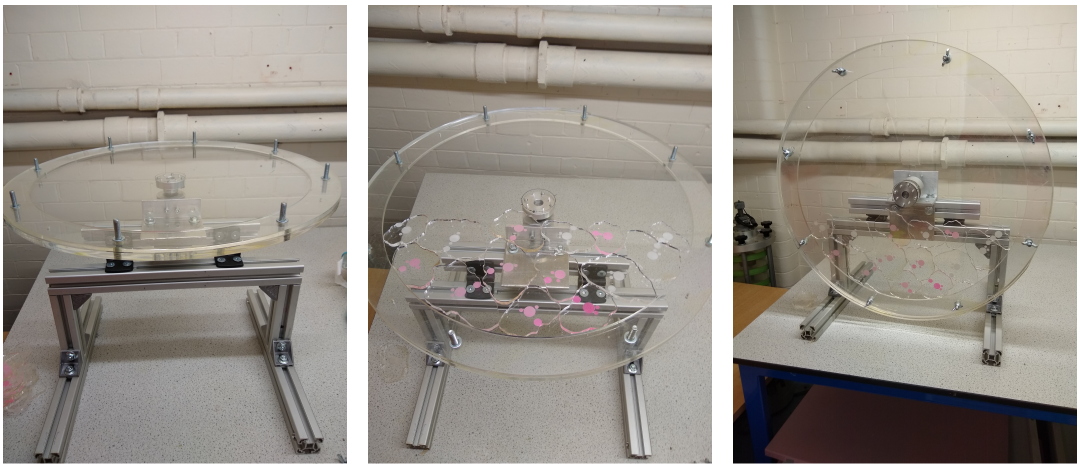

FIGURE 7.7: Sequence of images demonstrating the filling procedure of the rig.

particle where laser cutting has been performed. This value could then be adopted within the algorithm. If it is found to be greater than 0.5, a value of 0.5 could remain to ensure collapse does not occur for the built structure before testing.

The rig is rotated by an attached motor that turns the whole system. The angle of repose is measured by identifying when the system initially fails. This can be described as when particles start to overturn at the top of the heap. It is thought that two angles of repose will be experienced: an initial angle of repose before an avalanche has occurred and an angle of repose when the particles have mixed. Therefore it is important to ensure the duration of rotating for the experiment is enough to record both these results. Cheng and Zhao (2017) suggests that twenty avalanches are required to be able to measure both of these values.

Despite being the same thickness as the internal ring of the wheel, particles still move when inside the wheel and rotation is applied. This is due to the washers between the inner and outer pieces of the wheel. From initial testing of the experiment, it has been determined that an acrylic-acrylic border located between the circumference of the wheel and the particles leads to slipping of the structure as a unit mass rather than the expected overturning of particles at the top of the heap. To counteract this, Kinesiology tape is applied to this surface to create a rougher interface. The higher friction exerted on the touching acrylic particles stops the slipping of the structure as the wheel rotates and instead overturning of particles is exhibited. If this experiment is carried out in the future, testing will be carried forward for different possible materials (either the Kinesiology tape or perhaps a rubber interface) and the coefficient of friction for the rough material to acrylic interface is required to be determined. At this stage, it is thought that the Kinesiology tape is suitable as it prevents slipping and is easy to apply to the inner circumference but the lifespan of the tape and effect of long term testing is not known.

It is recognised that the interface between the faces of the wheel is most likely exerting a frictional force on the inside particles. Further testing is required to investigate this. To approach this problem, lubrication could be applied to create frictionless boundaries. This may require additional thickness for the interior of the wheel which could be created by adding washers between acrylic panels or readjusting the inside ring to be cut from acrylic of increased thickness if a larger amount of space is required.

The following describes the methods used for completion of the experiment.

1. The equipment will begin in the horizontal plane with the wheel lying flat. The layout of a packing structure determined using the algorithm described in Chapter 3 will be placed behind the rear side of the wheel. This can be attached by blue tac so that it aligns with the edges of the wheel and lets the user know the required location of particles.

2. The packing structure is built using the acrylic particle shapes. This will be placed by hand and take up no more than half of the area of the wheel.

3. The front face of the wheel is reattached and the wing-nuts suitably tightened. The equipment is then moved to the vertical position.

4. A highspeed camera will be used to record the experiment. It is to be ensured at this stage that this is recording.

5. The experiment will then be started and the wheel will be rotated by the attached motor at the back of the rig.
6. The camera will record the movement and overturning of the particles in the structure. As the particle moves, the packing structure will be lost. The experiment is recorded for a minimum of 20 avalanches as suggested by Cheng and Zhao (2017).
7. The experiment is stopped and once the wheel has become stationary it can be returned to the horizontal position and the particles can be removed.

Repeatability is possible in this experiment so long as the particles are placed in the same location. Therefore, care will be required to ensure particles are placed as accurately as possible in the determined location. As part of a future study, purposely placing particles with certain levels of inaccuracy to replicate error when being placed by a robot or utilising a suitable robot to pack particles could be investigated to determine if there is an effect of the angle of repose.

7.4 Particle Identification

Each acrylic particle is designed with a unique pattern for detection so that particle movement and rotation can be analysed. Images from the camera can be analysed and the location and orientation of the particle detected using code written in MATLAB that utilised the detection of circles function. The code is yet to be tested on images from an experiment using the rig but has been tested on images using a DSLR camera and a small selection of particles. The circles used for the unique coding system were successfully detected and particles were identified positionally between different images where they were positioned in different locations.

Each particle has a unique detection code engraved into the acrylic that is applied by the laser printer at the same time as being cut. It has been found that colouring these engravings in red helps with detection of these circles. Further testing is required to see if this is true for the experimental set up and if the current engraved circles are of a suitable size for identification. Furthermore, it is thought a black card should be used as a background for the experiment to help with the detection of particles like in Cheng and Zhao (2017). This may only be relevant if the particles are opaque as with Cheng and Zhao (2017) rather than transparent like in this project.

Figure 7.8 gives an example of a particle generated using the Fourier-Voronoi method. Lines have been indicated on the figure to better visualise the angles for particle identification. The pattern is presented and red highlighter is applied for easier detection by the camera. The largest circle is positioned at the centre of mass of the particle and another is positioned at the closest edge to the centre. Smaller circles are located around the largest circle. Circles are detected using the MATLAB function *imfindcircles*.

The orientation of the particle is determined by the placement of the circle at the centre of mass and the circle at the closest edge. The particle can be said to be at its "standard" orientation when these circles align so that the centre of mass is below the closest edge point. Detection of the particle can let the orientation be determined by the angle from this standard orientation determined by a clockwise angle.

The smaller particles around the edge of the centre of mass are used for identification of the particle. Each represents a specific angle code. For example, Figure 7.8 has an

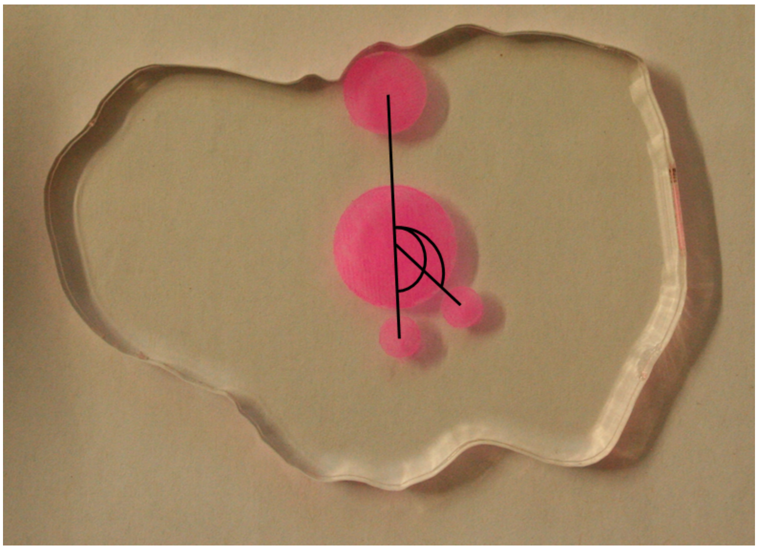

FIGURE 7.8: Example of an acrylic particle shape whose shape is defined by the Fourier-Voronoi method.

angle code of [135, 180]. This relates to the degrees that the smaller circles are located in relation to the plane between the centre of mass circle and closest edge circle. From the standard orientation, these circles are located at 135^o and 180^o from the vertical plane between the closest edge and the centre of mass calculated clockwise. Figure 7.9 presents the possible locations for the angle codes on the particle with the angle relating to each position around the centre of mass when at standard orientation.

The relationship between using this sort of pattern as the identification code relates to

$$N = 2^n \tag{7.1}$$

where n is the number of identification circles and N is the number of possible combinations. From this, the total number of unique angle codes from the 8-circle design in Figure 7.9 is to 256. Identification circles are known to belong to a certain centre of mass as they are always closer to the centre than the circle that represents the closest edge. Therefore, it is not possible for them to mistakenly be identified for a different particle as they are always grouped to the centre circle they are closest to. Any circles further away than the closest edge circle is disregarded as it is known this belongs to a different particle.

For each image in the experiment, the orientation of the particle can be determined and the specific angle code used to identify the particle. The differences in orientation between images from the experiment can help determine the rotation of particles. As the wheel is also being rotated, images from the camera are required to be adjusted to allow for this. This can be done by using markers on the wheel face to rotate images so that rotation of the whole system created by the wheel is nullified. The location of the centre of mass of the particle in the image can be used to identify any horizontal and vertical movements and determine when particles are toppling in the system.

Additionally to being able to track when collapse first occurs and accurately determine the angle of repose, the unique code for each particle means that it can be

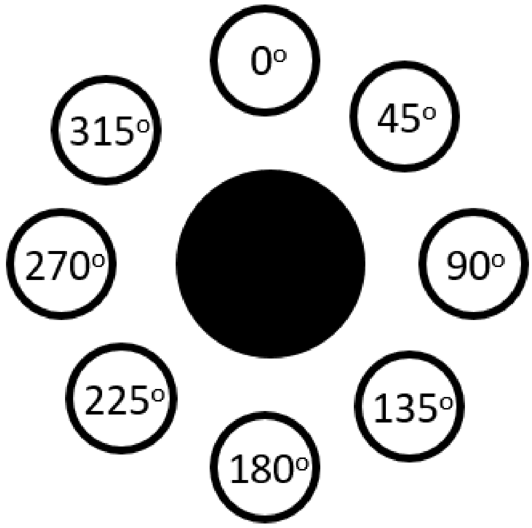

FIGURE 7.9: Circle to indicate centre of mass surrounded by identification circles for the angle code. Each identification circle is labelled with its specific angle that its position relates to when at standard orientation.

identified when certain particles tend to cause collapse above others. For example, if a particle is very rounded and can normally only provide a limited number of contacts with other particles, this might cause collapse in the system earlier than if a more suitable particle was placed. Using this identification combined with a characterisation of the particles that is described in Section 8.6 would highlight any common features that arise in particles causing collapse in the system.

7.5 Tolerance of Errors

An objective for this study is to investigate the effect of placement error for particles when being placed in the system. As with all techniques, there will be error whilst this is being conducted. The robot adopted for autonomous construction of rock materials will not be able to guarantee the placement of the stone in the exact location and also a lot of the accuracy of the robot will depend on the accuracy with which it is able to detect stones and the already existing structure. Furthermore, the use of a gripper will mean the manipulation of the robot is not as capable as what can be simulated in on a computer. Trouble may be had when placing and its possible stones will move slightly during construction.

Therefore, within the verification of strength, a study into the tolerance of errors was to be conducted. The purpose of this investigation is to find the tolerance of errors for a robot that could pack particles and show that the effect of shear strength is negligible for that level of tolerance and therefore a system where a robot is employed is reasonable for creating precision structures. Originally it was envisioned that this could be done as a desk study using an anthropomorphic robot similar to Furrer et al. (2017). However, instead of a gripper end-effector, a suction cup may be used so that it is suitable for picking up the acrylic particles that would be used for the experiments conducted using the methods in Section 7.3. This could be done as a desk-level study where the robot could pack particles into the rotating drum in their desired location. Displacement from their intended position could be marked and the structure could be tested. However, due to time limitations this was out of the scope of this project.

If the study proposed in this chapter had been carried out, tolerance of errors could have been tested by purposely displacing particles when packing by hand to replicate what might occur when using a robot if a robot could not be sourced for use. Displacement could be measured by the area of the particle displaced from the originally intended position. Different percentages of displacement could be tested and all could be compared back to the structure with no displacement when positioning. The use of a printed layout of the structure attached to the back of the wheel will help ensure that particles are positioned where they are desired, and printouts can be used of adjusted particle placement to guarantee the percentage of displacement is predetermined.

Alternatively, it is thought that as the wheel is adjusted into the vertical position that particles will shift due to the movement of the rig. Images of the structure can be compared to the layout of the original particles expressed by the algorithm as a layout of coordinates. From here, displacement can be calculated again by the area of the particle displaced from the original position.

Percentage displacement would be found using

$$\text{Displacment \%} = \frac{\text{Area of particles displaced}}{\text{Original total area of the particle}} \tag{7.2}$$

Two methods can be adopted. Either all particles can be displaced slightly or a select few particles can be displaced by large amounts from the original position.

It is expected that displacements of the particles would lead to lower initial angles of repose, with the more displacement leading to lower differences compared to the original angle of repose of the structure with no displacement. However, recognise that if a particle was displaced into a more optimal position then this would actually lead to a higher angle of repose.

7.6 Expected Results

The dynamic angle of repose can be found using the movements of particles in the images. When suitable rotation and movement is seen in the structure, the angle can be measured at which the structure has rotated from the original position to the position at failure and avalanching has occurred. As stated before, an initial angle of repose is to be measured as well as an angle of repose of the mixed particles.

It is hypothesised that the initial angle of repose is to be greater than that of the mixed angle of repose, thus demonstrating that the packing arrangement would exhibit a greater strength than particles randomly packed. Structures created using the algorithm described in Chapter 3 are to be tested as well as weighting coefficients which do not create suitable structures and randomly placed particles to compare and verify that the algorithm is producing suitable results.

It is not known if there will be any key characteristics for particles that tend to cause collapse in the structure or if there are any particles that will tend to cause specific moments of collapse. The case may be that the first particles to fail are always those at the top of the structure with fewer points of contact or are placed in more unstable positions. However, identifying particles which are the first to collapse and looking at the characteristics of these particles will provide information if there is any link. If there is, it is expected that the particles more suitable to packing will provide less causes of collapse in the structure. These are the ones which suitably match the features described in Section 2.3 that are suggested to lead to high shear strengths. Of these features, less angular particle shapes could perhaps be those which are involved in more collapsing events of the structure.

When studying the tolerance of errors as described by Section 7.5, it is expected that the higher the error of placement (i.e. the greater the displacement percentage), the greater the difference of initial angle of repose exhibited by the structure from testing. It is thought that the more particles displaced from the designed position produced by the algorithm in Chapter 3 with the objective function to express high shear strengths will have lower angles of repose compared to the structure with less no displacement. It is recognised that displacing a particle into a more optimal position will lead to higher angles of repose. However, assuming the packing system of the algorithm is efficient, displacing a particle should not lead to a more optimal solution. It is expected that for the level of tolerance that would be seen when utilising a robot in an autonomous construction scheme that the level of error in placement would be a negligible amount which is the purpose of this study. Furthermore, is thought that once the systems have experienced 20 avalanches in the system, the mixed angle of repose will equal that for the packing with no displacement.

7.7 Summary

Although testing of the outputted structures from the algorithm described in Chapter 3 was not completed, the method for verification of shear strength is presented in Chapter 7. The described method remains as work to be completed in the future as time limitations did not allow for it to be completed during this project.

Of the possible methods available, Section 7.2 discusses the potential options available for testing. These involve numerical verification methods such as DEM or the use of a physics engine such as Box2D to model the two-dimensional particle shapes. It is possible to perform biaxial testing (Li, 2020; Pytlos et al., 2015) of the structures within Box2D or potentially shear tests or tilting table tests as seen in Grillanda et al. (2021), Restrepo Vélez et al. (2014), and Santa-Cruz et al. (2021). However, Box2D is incapable of modelling concave shapes. Therefore, particles would need to be convex or adjusted to be made of convex shapes fixed together to create the concave shapes produced by the code provided by Mollon (2023).

Experimental verification methods are also discussed in Section 7.2.3. As the particles to be modelled are two-dimensional, this causes issues with testing methods if a biaxial or shear box test was adopted and a confined space would be required to support the particles. A tilting table method is possible which would measure the angle of repose. As stated, there is evidence that angle of repose and internal friction angle are related. As a tilting table measures the angle of repose of a structure, additional methods of measuring angle of repose are discussed in Section 7.2.3. Of these, a suitable solution would be that of a rotating drum for testing the structures produced by the algorithm.

Section 7.3 presents the experimental set up for the chosen rotating drum method. This consists of a 0.6m diameter wheel with an internal diameter of 0.5m made of 10mm thick acrylic with a 6mm thick acrylic inside ring to provide spacing between the panels. The wheel is spun on an axel supported by metal stand. The set up can be found in Figures 7.6 and 7.7 shows the wheel being loaded with the two-dimensional acrylic particles that would be used to represent the structure. As stated in Section 7.3, to produce a suitable build sequence the domain in the algorithm would need to be adjusted to be circular. Additionally, the frictional coefficient for an acrylic-to-acrylic interface would need to be determined and adopted as the frictional coefficient within the algorithm. The sequence for performing the experiment is described in Section 7.3 by a seven step procedure.

Each acrylic particle is to be given a unique code. The coding system is presented in Section 7.4 and an example is shown in Figure 7.8. Testing was performed using a DSLR camera and it was confirmed that the circle system used could be detected by the *imfindcircles* MATLAB function and that particles were identifiable between images. Using the system of circles surrounding a centre circle, a potential 256 possible combinations can be produced for particle identification. Orientation as well as location of the particles are to be measured to detect movement and to identify the moment of initial collapse.

Section 7.5 describes the method in which the tolerance of errors of in placement could be tested. It is envisioned that autonomous construction when done by a robot will lead to differences in positioning compared to the designed position of the structure. The purpose of this study is to find the tolerance of errors for a robot and show that the effect of shear strength is negligible for that level of tolerance. The method for this would be to test structures with particles displaced and compare them to the structures with no purposely induced displacement. Displacement can be measured by the total area of particles outside of the area their intended positioning.

Expected results of the experiment are described in Section 7.6. The results that should be found are

- the initial angle of repose of the system which is the angle at which the first moment of collapse occurs
- the mixed angle of repose which is the angle of repose formed when particles are fully mixed in the system (expected to be after 20 avalanches as suggested in Cheng and Zhao (2017))
- characteristics of particles that tend to cause collapse in the structure if there are any
- systems that experience displacement from the original position will exhibit lower angles of repose compared to the structure with no displacement
- the level of error that causes a big shift from original angle of repose will be less than that experienced when utilising a robot in an autonomous construction method.
- the mixed angle of repose for the displaced tests will be equivalent to the angle of repose of the same test with no displacement of particles

It is hypothesised that initial angle of repose of the structure will be greater than that of the mixed angle of repose if the structure is designed to have high shear strength. It is not known if there will be any key characteristics for particles that tend to cause collapse in the structure. However, if there are then these are suggested to be those which suitably match the features described in Section 2.3 that are suggested to lead to high shear strengths. Of these features, less angular particle shapes could perhaps be those which are involved in more collapsing events of the structure.

Chapter 8

Discussion

8.1 Introduction

The focus of this chapter revolves around the different aspects of the thesis and provides conversation on each topic. Firstly, the results of the Tetris Scenario and Soil Particle Scenario are discussed in Section 8.2 and Section 8.3 respectively. These state the selected solution for coefficients of weighting and compare them to control values as well as other coefficient results. Discussion for the Tetris Scenario is had around the topics of the domain size employed for packing (Section 8.2.3), the potential use of backtracking (Section 8.2.4) and the required accuracy of the coefficients in the objective function (Section 8.2.5). Section 8.3 discusses the investigation conducted for the Soil Particle Scenario. Aspects that are considered include MRJ and its use as an indicator for strength (Section 8.3.1), the effects of reducing the number of candidate poses in the discretised method (Section 8.3.2), improvements on the stability check (Section 8.3.3) and a discussion around the results produced by coefficients of weighting determined to be the optimal solution for the Tetris Scenario (Section 8.3.4).

Section 8.4 discusses methods which could be employed to improve results in terms of optimising shear strength of the structure. These methods are adapted from work found in the literature reviewed in Chapter 2. Section 8.4.1 discusses the use of using permutations of particle order delivered to the algorithm and testing multiple configurations of these. The concepts of the Best Fit Method and All Permutations Method are introduced with the increase in computational time to perform this considered. Section 8.4.2 considers discarding particles or adapting them by tooling methods if they are deemed unsuitable for packing. This can either be due to particle shape or consistent rejection for placement in the system. Furthermore, the placement of reinforcement strategically in areas of identified weakness can be employed to increase localised shear strength and therefore overall shear strength and his is discussed in Section 8.4.3.

Enhancement of the objective function is focused on in Section 8.5. A focus on the effect of D in the objective function as the particles fill the domain is made in Section 8.5.1. Furthermore, the choice of a first-order equation is discussed in Section 8.5.2.

In this project, particle shape is not considered as it is not known what type of material may be available which may be locally sourced on or near-from site. However, it has been shown that particle shape does affect the shear strength of the structure. Therefore, the possibility of characterising and quantifying particle shape to inform the algorithm for more intelligent material selection is introduced in Section 8.6.1. Section 8.6.2 reviews the methods for classification introduced in Section 2.5 and determines from the review of the literature in Chapter 2 that parameters required for consideration are circularity, elongation and convexity. Methods for quantifying these are specified in Section 8.6.3.

Section 8.6.4 refers back to the particle outlines produced by the software provided in Mollon (2023) in Section 3.6.1 and reflects on the fact that no comparison was made with actual mining waste or rock particles. It is suggested this could be done through the adoption of the parameters discussed in Section 8.6.3 or through determining the Fourier descriptors using methods outlined in Bowman et al. (2001).

The main limiting factor to the work completed in this project is the extended computational runtime exhibited when packing in the Soil Particle Scenario. Consideration on methods to increase the computational speed is presented in Section 8.7. These methods include parallelisation so that multiple positions in the system can be trialled simultaneously, the use of bitwise operations for the packing of particles in the discretised form as well as caching or memorisation of information to prevent repeating calculations whilst packing.

The prevention of runs developing in the structure are highlighted as an important factor for creating DSRW by Vivian (1976) and Adcock (2012). However, disruption of runs are adopted as a method for quantifying results rather than a scoring criteria within the objective function. Section 8.8.1 discusses the inclusion of disrupting runs in the objective function and introduces the term J and its relating coefficient of weighting C_J. Moreover, Adcock (2012) highlights the problem with multi-directional runs in the system - either at diagonals or in a zipped layout - and identification of these running joints is introduced in Section 8.8.2.

The algorithm as a solution to the 2BP problem is considered in Section 8.9.1 as it was seen that packings produced in Chapter 5 were seen to outperform the DBL heuristic for solving bin packing problems. Use of the algorithm as a method for specimen generation is also discussed in Section 8.9.2. Furthermore, alternate areas of improvement are explored in Section 8.10 discussing use of an autonomous construction method on the backfill of a retaining wall as well as the inclusion of hybrid materials. These are considered to highlight the possibilities when it comes to autonomous construction.

Finally, a discussion is held in Section 8.11 around extending the algorithm into three-dimensions to replicate packings of real-life scenarios. Consideration of what is required for each scoring criteria as well as further heuristics that might be required.

8.2 Discussion of Tetris Scenario Results

8.2.1 Comparison of Results

Section 5.6 presented results for the combination of (C_V=1, C_D=1.6 C_V=0.4, C_{CN}=0.045) as well as the determined solution from Hoodless and Smith (2023) at location (C_V=5, C_D=1.25, C_V=0.4, C_{CN}=0.01). As previously stated in Section 5.6, the number of instances of outperformance between the two results suggest similar levels of packing in regards to minimising void ratio of the system for the different combinations of weighting coefficient. However, it was determined from visual inspection that for (C_V=5, C_D=1.25 C_V=0.4, C_{CN}=0.01) that canyoning is present in the system and final void ratios are not a true reflection for some of the packings. Void ratio is calculated

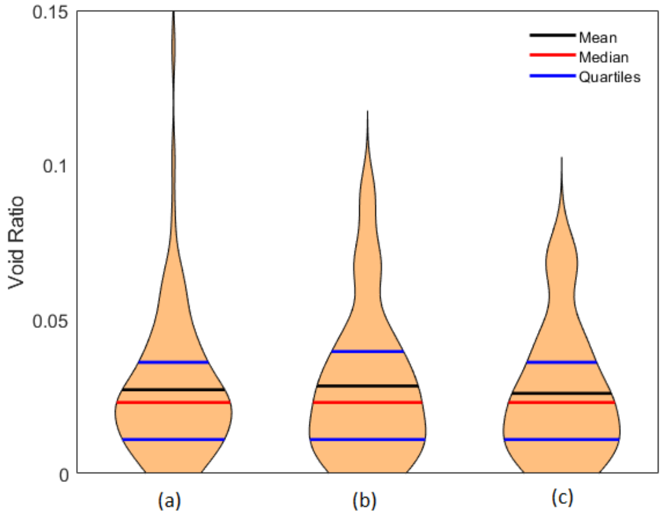

FIGURE 8.1: Violin plots for (a) (C_V=1, C_D=1.6 C_V=0.4, C_{CN}=0.045) (b) (C_V=5, C_D=1.25 C_V=0.4, C_{CN}=0.01) (c) (C_V=1, C_D=0.6 C_V=0.2, C_{CN}=0.015).

using the area under the placement surface and therefore canyons require a capping particle to be reflected in the final result.

An alternative potential location for an optimal solution was also investigated in Section 5.6. This was at (C_V=1, C_D=0.6 C_V=0.2, C_{CN}=0.015) and comparison between this and (C_V=1, C_D=1.6 C_V=0.4, C_{CN}=0.045) was performed. Again, like with (C_V=5, C_D=1.25 C_V=0.4, C_{CN}=0.01), an equivalent level of packing is suggested by the number of instances where each location out performed the other. Just like with (C_V=5, C_D=1.25 C_V=0.4, C_{CN}=0.01), it was seen that canyoning was occuring in the systems and a lack of capping particle was leading to void ratios not truly representing these packing results

The range of void ratios produced by each coefficient of weighting combination investigated in Section 5.6 are plotted as violin plots in Figure 8.1. The frequency of results for (C_V=5, C_D=1.25 C_V=0.4, C_{CN}=0.01) and (C_V=1, C_D=0.6 C_V=0.2, C_{CN}=0.015) closer to e=0 is higher compared to (C_V=1, C_D=1.6 C_V=0.4, C_{CN}=0.045). This is due to the number of events being misrepresented where canyoning occurs without the capping of that void with the placement of a final particle as already described. Furthermore, the tail of violin plot for (C_V=1, C_D=1.6 C_V=0.4, C_{CN}=0.045) is much longer. This is due to a single result of a packing producing a void ratio of e=0.138, the structure of which is presented in Figure 8.2. From examining the packing, it can be determined that the void created is unfortunate and if Bar-tetromino had been produced by the particle order before Particle 18 or 19 then the void ratio of the system would have finished with a much lower value. An equivalent hypothesis can be made for how each packing could be improved for alternate particle delivery orders, however the result presented in Figure 8.2 is unique in that it is the only one in this range of values for (C_V=1, C_D=1.6 C_V=0.4, C_{CN}=0.045).

Table 8.1 includes the maximum void ratio for each coefficient combination as well as minimum void ratio and quantile values Q_{25}, Q_{75} and Q_{90}. For the mimimum value of e achieved, Q_{25} and Q_{75} values for each weighting coefficient combination

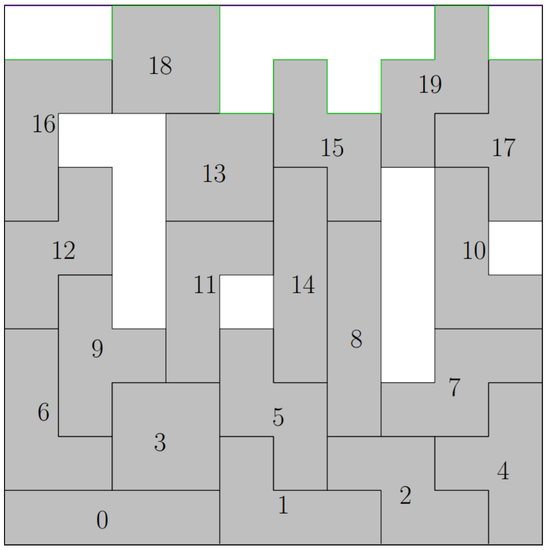

FIGURE 8.2: Packing structure for weighting coefficient (C_V=1, C_D=1.6 C_V=0.4, C_{CN}=0.045) for the particle order that produced the largest value of e for the system. e=0.138.

is similar. At Q_{90}, (C_V=1, C_D=1.6 C_V=0.4, C_{CN}=0.045) is lower than the other combinations. Furthermore, whilst the tail of the violin plot for (C_V=1, C_D=1.6 C_V=0.4, C_{CN}=0.045) is longer, it is also thinner which indicates a lower frequency of void ratios at a higher value. From this, it can be concluded that although the maximum void ratio for (C_V=1, C_D=1.6 C_V=0.4, C_{CN}=0.045) is higher than (C_V=5, C_D=1.25 C_V=0.4, C_{CN}=0.01) and (C_V=1, C_D=0.6 C_V=0.2, C_{CN}=0.015), this is an outlier and typically the packings produced by (C_V=1, C_D=1.6 C_V=0.4, C_{CN}=0.045) will lead to better results. This confirms the proposal of (C_V=1, C_D=1.6 C_V=0.4, C_{CN}=0.045) as the optimal solution of weighting coefficients investigated from Chapter 5.

Coefficients of Weighting	Min e	Q_{25}	Q_{75}	Q_{90}	Max e
(C_V=1, C_D=1.6 C_V=0.4, C_{CN}=0.045)	0	0.011	0.036	0.057	0.138
(C_V=5, C_D=1.25 C_V=0.4, C_{CN}=0.01)	0	0.011	0.0395	0.0665	0.095
(C_V=1, C_D=0.6 C_V=0.2, C_{CN}=0.015)	0	0.011	0.036	0.065	0.080

TABLE 8.1: Different quantile values from void ratio results for a sample size n=100. Maximum and minimum void ratio also presented.

From the analysis here, it can be appreciated that a different method of quantifying final void ratio to reflect the packing structure with the consideration of canyons is needed. Therefore, it is suggested the void ratio of the whole domain area, including above the placement surface, could be taken. This is referred to as e_t and results are presented in Table 8.2 for n=30 and n=100 for the different combinations of weighting coefficient investigated in Section 5.6 as well as the DBL heuristic.

Each value for e_t is similar for packings with placements scored by the placement function with ~22 particles being packed on average, with the DBL heuristic resulting is higher e_t values as a result of 21 particles being packed on average. e_t is another way of expressing the number of particles packed in the system, with Figure 8.3 showing resulting e_t values for the number of particles placed in a 10x10 square domain. Therefore, total void of the system can not be employed to get a better understanding of the structure as if equivalent numbers of particles are packed then e_t

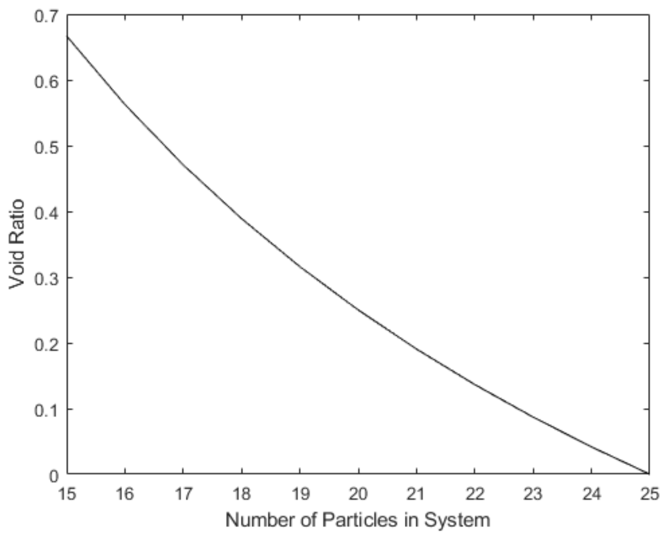

FIGURE 8.3: Void ratio, e_t for the number of particles placed in the domain.

will be of equal value. This is demonstrated by Figure 8.4 where it is seen that volin plots of e_t for (C_V=1, C_D=1.6 C_V=0.4, C_{CN}=0.045), (C_V=5, C_D=1.25 C_V=0.4, C_{CN}=0.01) and (C_V=1, C_D=0.6 C_V=0.2, C_{CN}=0.015) are almost indistinguishable.

Coefficient of Weighting	e_t (n=30)	e_t (n=100)	Mean No. Particles
(C_V=1, C_D=1.6 C_V=0.4, C_{CN}=0.045)	0.1359	0.1322	22.08
(C_V=5, C_D=1.25 C_V=0.4, C_{CN}=0.01)	0.1326	0.1326	22.07
(C_V=1, C_D=0.6 C_V=0.2, C_{CN}=0.015)	0.1328	0.1308	22.1
DBL	0.166	0.179	21.2

TABLE 8.2: Void ratio, e_t, for the different results explored in Section 5.6 and DBL heuristic and the corresponding number of particles to be placed in a 10x10 square domain to achieve e_t for n=100.

8.2.2 Comparison to the DBL Heuristic and Random Packing

Verification of the algorithm was conducted against control heuristics following DBL rules and random packings using RAND, RAND-0F1 and RAND-0F2. Results of these are located in Section 5.7. From the produced MVR results, it is clear that all combinations of weighting coefficients explored in Section 5.6 outperform these other heuristics. This suggests that the algorithm is efficient at packing particles and that the objective function based on criteria that indicate a high shear strength can be utilised to create structures with minimal space between then for packing tetrominoes.

It was expected that random packing would produce MVR values extremely high. For the DBL heuristic, MVRs were much lower but still roughly double the MVR values of packings where positioning is chosen by W_{ij} using the objective function and almost triple MVR values of the most optimal solutions expressed in Section 5.6. It is considered that the algorithm could be adopted as a solution for 2BP. Further discussion around this topic is located in Section 8.9.1.

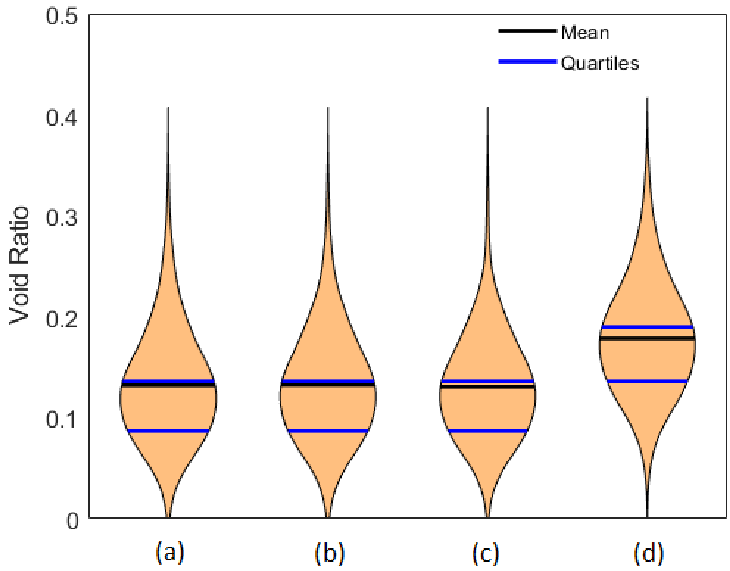

FIGURE 8.4: Violin plots of void ratio, e_t, for packings using the objective function for coefficient values (a) (C_V=1, C_D=1.6 C_V=0.4, C_{CN}=0.045) (b) (C_V=5, C_D=1.25 C_V=0.4, C_{CN}=0.01) (c) (C_V=1, C_D=0.6 C_V=0.2, C_{CN}=0.015) and for packing governed by (d) DBL heuristic.

8.2.3 Limited Domain Size

The selection of (C_V=1, C_D=1.6 C_V=0.4, C_{CN}=0.045) as the optimal solution for the Tetris Scenario is based on avoiding canyoning in the system. As described in Section 5.6 for Figure 5.44b, canyoning leads to higher void ratios when these gaps are capped by the next placed particle. Due to the domain size, capping of canyons occurs as particles are always fit into the domain if possible regardless of the void created in the system. Therefore, the results are greatly affected by particle order towards the end of the packing and packings where less particles can be fit into the 10x10 square domain are inadvertently rewarded if this avoids capping a canyon. Additionally, if the particle could be placed elsewhere and a Bar-tetromino placed in the canyon, this solves the issue that has arisen.

By extending the domain, the Tetris Scenario better resembles that which is found in the videogame. Figure 8.5 presents two results for the packing in a domain of 10x20 squares. Coefficients of weighting for this packing are (C_V=5, C_D=1.25 C_V=0.4, C_{CN}=0.01) as this experienced canyoning due to its larger effect of $C_V V_{AB}$ in the objective function. Each domain is packed with 30 tetrominoes, as this was seen as a upper limit that usually exceeded the available space of the domain when 10x10 squares. Figure 8.5 does not show the whole length of the domain as above the placement surface is empty space. The heights that are represented are 14 squares and 16 squares for Figure 8.5a and Figure 8.5b respectively.

From viewing Figure 8.5 it is determined that the more available space leads to less voids created in the structure. This is due to particles that are placed towards the end of the packing and are forced to cap voids in the system have more alternative locations to be positioned. Figure 8.5a presents what appears to be a very good packing for the Tetris Scenario. Figure 8.5b scores low for void ratio, but it can be appreciated that canyoning is still occurring and that this will lead to the maximum domain height being reached sooner, although it is envisioned that if the next tetromino is Bar shaped this will be placed above Particle 14 to fill in the canyon.

Table 8.3 presents MVR results of packings into a 10x20 square domain using weighting coefficients analysed in Section 5.6. With the extended domain, (C_V=1, C_D=1.6 C_V=0.4, C_{CN}=0.045) appears to actually perform worse than (C_V=5, C_D=1.25 C_V=0.4, C_{CN}=0.01) and (C_V=1, C_D=0.6 C_V=0.2, C_{CN}=0.015). This is thought to be due to canyoning not affecting the overall void ratio as it is likely that B tetromino will be delivered by the particle order before the top of domain is reached.

Coefficients	MVR (n=30)	MVR (n=100)
(C_V=1, C_D=1.6 C_V=0.4, C_{CN}=0.045)	0.0135	0.0153
(C_V=5, C_D=1.25 C_V=0.4, C_{CN}=0.01)	0.0108	0.0133
(C_V=1, C_D=0.6 C_V=0.2, C_{CN}=0.015)	0.0116	0.0130
DBL Heuristic	0.0580	0.0598

TABLE 8.3: MVR results when n=30 and n=100 for different combinations of weighting coefficients when packing is determined by the objective function in a 10x20 square domain and results of packing using the DBL heuristic.

Figure 8.6 shows packings of tetrominoes in a 10x20 square domain using weighting coefficients (C_V=1, C_D=1.6 C_V=0.4, C_{CN}=0.045). Due to $C_D D$ in the objective function having a greater impact on W_{ij} compared to (C_V=5, C_D=1.25 C_V=0.4, C_{CN}=0.01) and (C_V=1, C_D=0.6 C_V=0.2, C_{CN}=0.015), packings are formed with voids present as the scoring prioritises positions at greater depth over the avoidance of creating gaps in the structure. This is highlighted by Figure 8.6a and is the reasoning for higher MVRs when packing is completed in a longer domain. Figure 8.6b shows no gaps in the structure and e=0. This is due to the particle order being able to be packed by the algorithm for these coefficients in a sequence that results in this. However, note that near the top of the domain that canyoning is starting to occur (left of Particle 24 and left and right of Particle 23 and Particle 26).

Canyoning begins to occur in Figure 8.6b due to the weakening effect of $C_D D$. D is the ratio of the depth of the particle to the domain length. Therefore as the maximum depth that particles can be placed decreases the maximum score provided by $C_D D$ decreases. This had little effect when the domain size was 10x10 squares due to the limited number of positions available towards the end of the simulation. However, in the increased height case this has more of an effect. Towards the top of the packing in Figure 8.6b, $C_V V_{AB}$ is having more of an effect on positioning which leads to the formation of canyons. Therefore for the Tetris Scenario, a new method for scoring D should be implemented. This area is further discussed in Section 8.5.1.

From Section 5.6 it was determined that (C_V=1, C_D=1.6 C_V=0.4, C_{CN}=0.045) led to the most optimal solutions of packing of tetrominoes in the Tetris Scenario. This is due to the canyoning effect seen with (C_V=5, C_D=1.25 C_V=0.4, C_{CN}=0.01) and (C_V=1, C_D=0.6 C_V=0.2, C_{CN}=0.015). (C_V=1, C_D=1.6 C_V=0.4, C_{CN}=0.045) prioritises depth leading to particles being packed with less towers. This is beneficial for the 10x10 square domain where the height is limited. However, for the 20x20 square domain when height is not limited, canyoning rather than creating gaps in the structure with the expectation that these canyons will later be filled by B tetrominoes actually can lead to lower void ratios. Therefore, for a 10x20 square domain (C_V=5, C_D=1.25 C_V=0.4, C_{CN}=0.01) and (C_V=1, C_D=0.6 C_V=0.2, C_{CN}=0.015) can be said to outperform

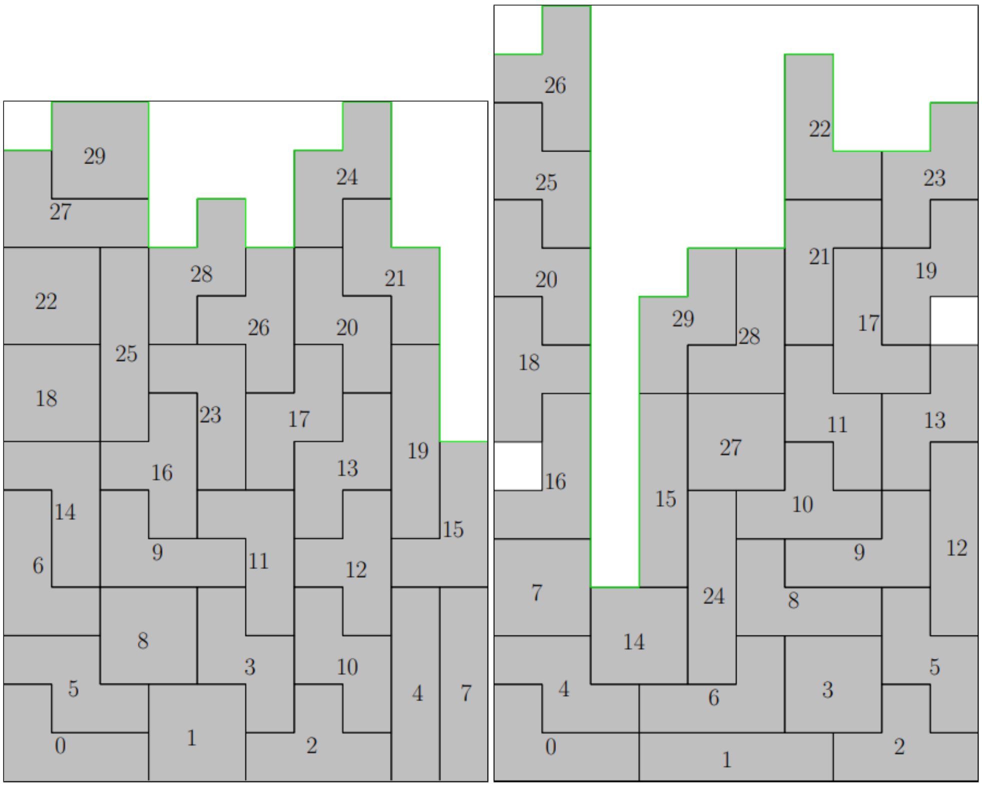

(A) e=0 (B) e=0.017

FIGURE 8.5: Packing using coefficients (C_V=5, C_D=1.25 C_V=0.4, C_{CN}=0.01) in domain size of 10x20 squares.

(C_V=1, C_D=1.6 C_V=0.4, C_{CN}=0.045). A discussion is to be had about these values as a solution for the actual Tetris videogame where lines of filled space are deleted. This can be found in Section 8.2.5.

8.2.4 Backtracking of Placement

Section 8.4.1 discusses the use of testing different permutations of particle order for improved results. Additionally a backtracking method like that in Galambos and Woeginger (1993) and Goldberg et al. (2002) could be adopted for the Tetris Scenario. If void is created, the algorithm can backtrack by a a small number particles and attempt the second-best location for those tetrominoes to be placed. This may prevent a scenario where void is created in the system. As tetrominoes are required to be placed in the particle order they are received, no permutation of particle order is possible in this situation.

It should be recognised that adopting these methods would not fully represent the Tetris Scenario. In the Tetris videogame, particles must be packed in the order that they are delivered. Information of the next couple of particles is sometimes presented to the player so the placement of multiple particles at a time could be tested. However, no form of backtracking or permutation of particle order can be implemented into the playing style. Therefore if backtracking is used then the placement method for the Tetris Scenario cannot be considered as a solution for optimising Tetris. If permutations of particle order are adopted, the Tetris Scenario inherently

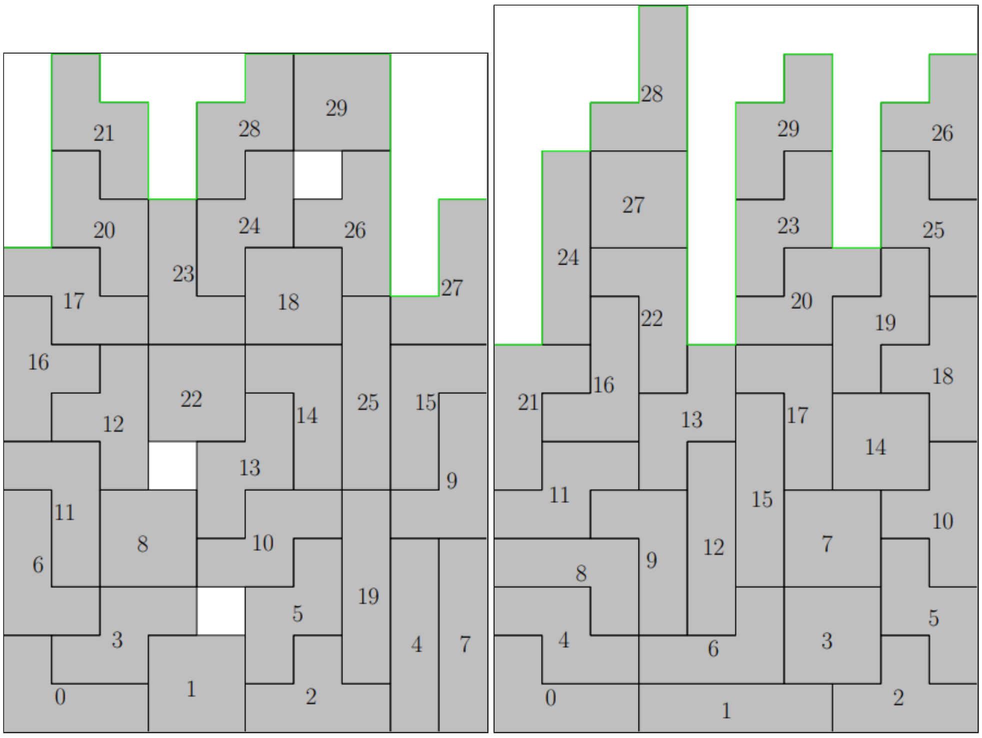

(A) (B)

FIGURE 8.6: Packing using coefficients (C_V=5, C_D=1.25 C_V=0.4, C_{CN}=0.01) in domain size of 10x20 squares.

becomes a 2BP problem for very irregular particles which are capable of being rotated. Section 8.9.1 discusses the use of the algorithm described in Chapter 3 as a bin packing heuristic further.

8.2.5 Tetris Scenario Sensitivity and Required Accuracy

Section 5.6 presents and analyses the packings produced by the algorithm described in Chapter 3. Further to the discussion, it can be seen that the packings are greatly affected by the particle order. Figure 8.2 highlights this as if particle order had been slightly different the end void ratio would have been much lower than the final result. As a result, a high level of accuracy is required for the coefficients of weighting.

It is likely that if a higher sampling frequency was adopted with smaller increments between coefficient values tested that a more optimal solution would be achieved. However, the computational time to run these tests would have been massively increased and it is not known what level of refinement is required for the true optimal solution to be found. Therefore the level of accuracy that has been followed in this chapter is acceptable for the study here, especially as this project aims to focus on packing of two-dimensional soil particles. Differences in void experienced at the end of the investigation of the search area was in a range between $1\text{x}10^{-}2$ to as small as $1\text{x}10^{-}4$ between neighbouring datapoints. This equates to a difference of between 0.01 square to 1 square of void in the packing.

It can be determined that the results are very sensitive for the Tetris Scenario. As a bin packing solution where the aim is to completely minimise void this is problematic as a reliable solution for reaching the objective is desired. However, as a solution for playing Tetris it should be noted that the Tetris Scenario does not fully represent the Tetris videogame. The main difference is the deletion of rows when completely filled. If this was introduced into the algorithm, voids that are created in the domain would become exposed as rows are removed meaning that particles could be placed in these gaps eventually. Even for Figure 8.2 these areas would have been filled, as due to particle order being determined by the Tetris bag method either Particle 20 or Particle 21 is to be a Bar-tetromino. It could be considered that implementation of this would reduce the sensitivity to particle order and the accuracy required for weighting coefficient would be reduced. In addition, the increase in domain height as investigated in Section 8.2.3 leads to more chance of gaps being filled and these results become less sensitive as the main cause of sensitivity is generated when particles start to reach the top of the domain.

Hence, it can be considered that the packing algorithm could be adopted as an approach for solving "Standard Tetris" as proposed by Brzustowski (1988) and seen in Böhm et al. (2005), Breukelaar et al. (2004), Burgiel (1997), and Kostreva and Hartman (2004). Doing so would introduce a new technique to this problem that accepts all types of tetrominoes for packing and uses a unique heuristic for placement. Of the coefficients investigated, (C_V=1, C_D=0.6 C_V=0.2, C_{CN}=0.015) or (C_V=5, C_D=1.25 C_V=0.4, C_{CN}=0.01) are most likely to provide the best results for minimising void and scoring the highest when deleting rows of filled solids. This is because $C_V V_{AB}$ contributes more to the objective function when determining placement, which is the main objective in Tetris. Issues when packing were seen when canyons occur. However, with the deletion of rows and increased domain height, canyoning does not cause the same issues as the 10x10 square domain and therefore a solution such as combination (C_V=1, C_D=1.6 C_V=0.4, C_{CN}=0.045) is not required to prevent this.

8.3 Discussion of Soil Particle Scenario Results

8.3.1 Representation of MRJ and Improvement of Investigation

Chapter 6 ended the investigation of the coefficients of weighting for the Tetris Scenario in Section 6.5. Part of the reasoning for this is given as there is no obvious relationship between MRJ and MVR, as shown by R^2 value of 0.024 for Figure 6.53. It was expected that as MVR decreased, the MRJ value would increase due to tighter packings and therefore more particles lying over where two particles meet. However, this was not found to be the case.

As was seen in the structures, piling of the particles with sloped sides occurred for a lot of the resulting packings. Whilst the stability check should prevent very unstable particles being placed, it is clear that in some instances this is not the case and this is further discussed in Section 8.3.3. However, the largest and therefore considered most optimal results for MRJ are found in packings which express this piling of particles. This is not desired for the method of autonomous construction as it has been stated that a layer-by-layer process is required. Furthermore, the differences in height of the structures with particles being placed further up leads to the number of running joints being disrupted increasing compared to systems with lower highest points.

Therefore, the MRJ is not giving a true representation of the packing. It has some indication, but systems that are taller end up having an unfair advantage to others. The best example of this is seen in Figure 6.41c which is one of the packings for location (C_V=1, C_D=0.4, C_T=0.4, C_{CN}=0.4). This datapoint in the search areas was the one found to express the highest MRJ value. The increase in height, which is caused by the objective function trying to place particles closer together due to the scores of $C_T T$ and $C_{CN} CN$ whilst $C_D D$ is having less of an effect.

To truly determine the best combination of coefficients, it is required for one of two methods to be implemented. The first is to increase the importance of picking a location closer to the domain base in the priority order. However, it is thought that if this was the case then these positions would be picked over scoring by the objective function meaning that the packing technique becomes more of a deepest-bottom heuristic which then uses the objective function to determine between equally deep locations.

The second is to introduce a "packing area". This is inspired by Johns et al. (2020) and Johns et al., 2023 discussed in Section 2.2.4 which saw particles being fit into a given area that was to represent the overall shape of the wall. An area could be designated, either representing a slope if a wall structure is desired to be replicated or the area could be what is determined to be the "bottom course" which could be roughly three particles tall. The algorithm can then be demanded to fill this area first, before moving up the wall. Doing so will prevent the height being increased.

It is recognised that increasing the value of C_D will also prevent this from occurring. The testing of coefficients (C_V=1, C_D=6, C_T=0.5, C_{CN}=10) was to see the sort of packing that occurred when C_D has more impact on the packing positioning. This was improved. However, an effect from increasing C_D is that this begins to dominate over other scoring criteria, diluting them in the objective function.

A different method for quantifying shear strength is required if it is found the MRJ is not a good indication of this value. The work in Chapter 7 provides a method for this, but it is clear that doing this for every packing would take a great deal of time. The adoption of a physics simulator or DEM analysis would mean that this can be done at desk level. Of these options, the physics simulator is advised as this can be used to quickly check stability of placement.

8.3.2 Reduced Number of Candidate Poses

In the Soil Particle Scenario, candidate positions are filtered and the best 30 of these poses are taken forward for full analysis. With the reduction in total positions trialled by the particles, this reduces the total number of possible solutions and it is likely a truly optimal position is missed. The reasoning for reducing candidate poses was to increase computational time. With an improvement in computational speed, more candidate poses can be tried and the results of this can be analysed. Methods for reducing computational runtime are discussed in Section 8.7.

Within the packings, it is seen that spaces where particles could potentially fit are not placed, leaving gaps and affecting subsequent packings. An example of this is found in Figure 6.22 where a gap has formed. It is stated that potential Particle 35 could have been dropped into this gap, and as a result the positions of Particle 38 and Particle 39 are not optimal, and actually are probably both unstable. Improvement of the stability checks is discuessed in Section 8.3.3. It is thought that this occurs due to the assumption of squares in the discretised method that have material in being taken as full. This was done to replicate additional width that may be present due to gripped of the robot performing autonomous construction.

However, this is having a detrimental effect on positioning of these particles and therefore subsequent particle positions. Furthermore it could be considered that the gaps at the edges of the domain, where these slopes are occurring, are forming due to particles being unable to fill these spaces in the discretised form. Due to this, either large voids are being detected when checking this horizontal location when scoring in the discretised method or, if this location is trialled, no stable position is being found as it is attempting to do this at the point where the slope has already begun. Testing of the packings with an improved method of discretising the shapes is required. With an increase in candidate poses, this may lead to these positions being trialled and actually a stable orientation may be detected.

8.3.3 Stability Improvement

It is seen that lots of the positions in the results may be deemed as unstable. This mainly occurs when stacking is present. The best example of this is for the randomly packed samples for RAND-F in Figure 6.54b. The stability checks implemented in the code do not take account of subsequent packings that are placed upon the stone. Therefore, precarious towers are allowed to form that visually can be detected as unstable. The use of DEM or a physics engine would prevent this or a much more improved stability calculation.

Furthermore, the filtering by $\frac{d}{h}$ was introduced so that particles are placed to maximise their width. However, it is clear that this is not really taking effect. This is due to its position in the hierarchical filter for candidate poses and other priorities such as score in the discretised method are taking priority if a rotation where the width is minimised outscores others. It is proposed that a system like that in Liu et al. (2021) is used. This would require particles to have a contact area with other particles in the surface above the mean of all stable poses. This removes chance of elongated particles being placed on their thinnest side. Another method is also found in Liu et al. (2021) where deviation of the normal to the surface and the thrust line is analysed and positions that are larger than the mean are also not considered as final solutions.

8.3.4 Comparison to Coefficients Determined for Tetris

Section 6.5 presented results of packing using the coefficients determined as potential solutions in Chapter 5. The results of these packings appear to be of good effect, and these are displayed in Figures 6.49-6.51. Again, issues occur with sloping at edges and towering. However, MVR values appear to be reduced and (C_V=1, C_D=0.6, C_T=0.2, C_{CN}=0.015) in particular has a relatively large MRJ value of 27.8.

It is sensible that these coefficients produce low void ratios. The Tetris Scenario found an optimal solution for packings where the objective was to reduce void ratio. It is clear from the results in Table 6.10 that this has been achieved for soil particles and if this was the objective then perhaps these coefficient ranges could be considered. However, the objective of packing is to maximise shear strength meaning a change in objective. It is highly likely that this will mean coefficients of weighting are different, and there has not been a study into whether coefficients of weighting for the same objective will be equivalent for different particle shapes.

It is stated that void ratio can be taken as a good indication of shear strength. It is possible that MVR can be adopted as the measure of determining packings that optimise shear strength. However, without a verification of the strength of the structure this is left unknown. The methods set out in Chapter 7 would help determine if this is the case.

8.4 Improving Results in Relation to Shear Strength

8.4.1 Permutations of Particle Order

In the results collected in Chapter 6, it is seen that particles are selected and placed with no backtracking of the algorithm or changing of placement order. Particles were placed in the order of delivery with no consideration of variation from the random sequence in which they are generated. In reality, it is thought that the algorithm would be able to try multiple different permutations of particle order of a select amount of particles. This is seen in bin packing (Galambos and Woeginger, 1993) and jigsaw solving (Goldberg et al., 2002) as discussed in Section 2.4.3 and Section 2.4.4 respectively.

It is envisioned that this would lead to higher quality packing results, as the permutation that leads to the best packing can be selected. Two methods are highlighted in which this could be a possibility.

1. A certain number of particles are placed as a group and every permutation of that particle order is tested
2. A certain number of particles are placed individually and the best particle is placed before moving on to the next particle from the group

Each method is described for a group of four particles as the following.

For the first method, which will be referred to as the All Permutations Method, Particle 1 from the group of four is placed in its best location as determined by the placement algorithm. This is followed by Particle 2, Particle 3, and then Particle 4. The placement is scored and then a different permutation of the particles is trialled, for example Particle 2, Particle 1, Particle 3, Particle 4, and this order is then scored. This is done for every permutation of particle order for the set of particles. The next four particles are then placed using the same method.

The second method, which will be referred to as the Best Fit Method, Particle 1 from the group of four is placed in its best location as determined by the placement algorithm. Before Particle 1 is placed, Particle 2 is trialled for placement without the presence of Particle 1. This is repeated for Particle 3 and Particle 4. Of these particles, the best particle is chosen for placement. A new particle is then added to the group and the process is repeated for these particles. It can be understood that it is not necessary to retry all positions for previous particles tested but only in areas where there has been a change to placement surface due to a previously placed particle. Caching can be utilised, which is a topic discussed in Section 8.7.4. It is thought that if a particle is repeatedly trialled for placement and is not placed - maybe due to being unsuitable for placement - this can be removed after a certain number of attempts to place before being replaced by a different particle.

Both of these methods were trialled at the early stages of development for the placement algorithm. It was found that the relationships for the time taken to place a particle, t could be described by the Equations 8.1 and Equation 8.2 for the Best Fit Method and All Permutations Method respectively, where N is the size of the group

N	Time for Best Fit Method (mins)	Time for All Permutations Method (mins)
1	1	1
2	4	2
3	9	6
4	16	24
5	25	120

TABLE 8.4: Time to place N number of particles for group size of N using Best Fit Method and All Permutations Method for varying particle order.

of particles selected for placement. Note, this is the time for a single position assuming that this position is changed by the placement of a particle. With the use of the memory of the computer (through caching as stated before which is discussed in Section 8.7.4) placements for a particle previously explored that have not changed can be stored and located when required. Without storage of this information, Equation 8.1 and Equation 8.2 would be the time for every position trialled by the algorithm.

$$t = N^2 \tag{8.1}$$

$$t = N! \tag{8.2}$$

Initially, it is quicker to use the All Permutations Method. However, as N increases this rapidly changes. This is highlighted in Table 8.4 where the time to place one particle for different sizes of N are presented for both methods. The results in the table presume that it takes 1 minute to calculate for the given position by the placement algorithm and that this time is equivalent for all particles.

For future work, trialling of these methods will require a much greater reduction in computational time of the algorithm, especially if large numbers of particles are trialled for the Soil Particle Scenario. Potential methods for speeding up computational runtime are explored in Section 8.7. The expected result of these methods will be to improve the structure in regards to creating higher scores from placements.

8.4.2 Discarding or Tooling Unsuitable Particles

As mentioned with the Best Fit Method in Section 8.4.1, particles that are consistently not chosen for placement could be discarded by the programme and removed as an option for being the next particle to be positioned. This will save time being wasted on trialling candidate poses for this particle. Furthermore, it is possible to discard particles that are not suitable for placement before trialling of candidate poses begins. This can be done through a variety of methods.

The first of these methods is by setting a size limit on the particle. It was seen in Section 3.6.1 that particles that had a radius below 3 units and above 7.5 units were discarded. This was to try and emulate a consistent size of particle to that of untooled rock. Similarly, all particles could have been kept and a feature of the developed algorithm could have been to automatically discard particles that were outside of this range.

Another method for discarding particles would be by characterising the particles. This is discussed further in Section 8.6.1. Particles that are defined to be "unsuitable" could be discarded. Such types of particles may be

1. very rounded causing difficulty when stacking particles on top of this
2. extremely thin, suggesting a weak particle that could be broken if force placed against its longest side.

Discarding particles that are characterised and deemed as unsuitable will save on time of trialling particles that may not be placed if a method such as the Best Fit Method is adopted. Additionally, filtering particles for placement will avoid using particles that overall make the final structure weaker (if the end objective is to create a strong structure).

Section 1.1 states a main motivator behind the investigation into constructing using irregular, untooled rock as wanting to reduce environmental costs of construction. It is stated that this can be done by utilising locally sourced material, especially that which is waste such as CDW or MW. If discarding particles leads to the requirement of materials that are transported to site and/or manufactured at a high emissions cost, then perhaps an alternative should first be sought. As seen in Clifford et al. (2018) (discussed in Section 1.1 and Section 2.2.2), it is possible to introduce a method of tooling materials to be used in construction. The robot in Clifford et al. (2018) used a six-axis robotic arm to tool CDW for construction.

The tooling of material has not been considered in this project as it was out of scope of the work presented here. Tooling material leads to needing to define how materials should be tooled as well as what is the desired shape and decision on when materials should be shaped and when they should be left in their original shape. The omission in the method for constructing structures from irregular, untooled rock follows similar methods such as Johns et al. (2023). However, Clifford et al. (2018) shows that there remains possibility for this process to be added with the requirement of much more additional research.

8.4.3 Strategic Reinforcement

Reinforcement in soil structures is a common technique adopted for geotechnical problems such as using geosynthetics which were discussed in Section 1.1. A benefit of construction by a particle-by-particle process is the ability to intervene between placements. By this manner, the possibility to place strategic reinforcement in areas of identified weakness can be completed. This could either be by the application of a geotextile mid-way through constructing the courses of the placed rock or by applying a mortar or some sort of adhesive material to help stick particles together.

By modelling an outputted structure from the algorithm, either through DEM, a physics engine like Box2D, or software such as LimitState: Geo, areas of weakness can be found where high shear stresses occur in the construction. Targetting these areas with strategic reinforcement will help to increase the strength of the structure. Identifying these areas of weakness means that the reinforcement may only be required in these areas rather than throughout the structure. Thus, the amount of reinforcement required will be reduced compared to a traditional method where reinforcement is placed throughout the medium or in broad, targetted areas.

8.5 Objective Function and Weighting Coefficients

8.5.1 Quantifying Depth of the Particle

As previously mentioned in Section 8.2.3, canyoning is seen further up the system for coefficients of weighting (C_V=1, C_D=1.6 C_V=0.4, C_{CN}=0.045) even though it is avoided lower down in the system. This is due to the effect of $C_D D$ decreasing as the domain becomes filled. D is quantified using the whole depth of the domain and therefore as the maximum depth particles can be placed reduces, the maximum potential value for D decreases and this value tends towards zero for domains with extreme heights. Figure 8.7 is a histogram of D values calculated for final positioning of tetrominoes in the Tetris Scenario within a 10x20 square domain. The diminishing effect is highlighted as frequency is (fairly) consistent across the values for D. This is because D naturally gets smaller as the packing carries on. The high frequency experienced near D=1 is due to the most amount of particles being packed in the first level, whereas levels past this the number of potential positions are limited. The lack of values at D=0 is because this would mean the centre of gravity of the particle is being packed level with the top border of the domain, which is not possible.

The diminishing effect had on D was not seen to be a problem for a domain of 10x10 squares as the height is fairly limited. However, the purpose of this algorithm is to be utilised for autonomous construction by a robot. Therefore, it can be assumed that if this is employed that the heights of the structure will be large enough for the tending of D towards zero to have an effect.

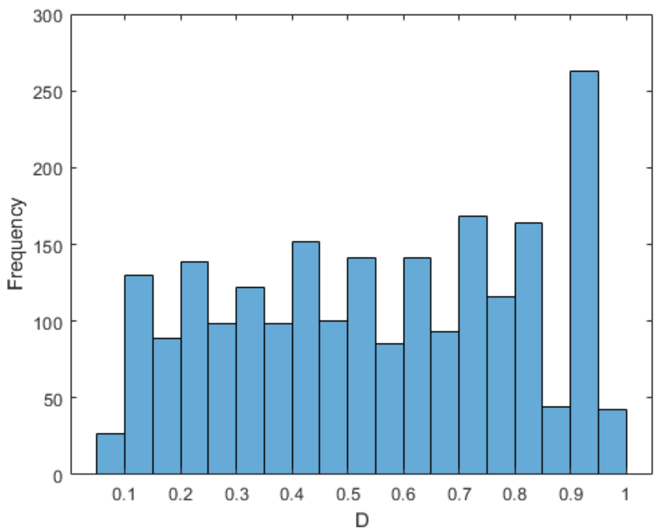

FIGURE 8.7: Frequency of produced D values for packings of tetrominoes in a 10x10 square domain following the Tetris Scenario adopting n=100 and filling the domain until the next particle cannot be placed.

It is suggested that a new form of quantifying depth of the particle in the system is formed, D_v. D_v is taken as ratio of the depth of the particle in the system to the maximum depth of the placement surface, $D_{surface}$, reflecting the minimum point in which a particle can be placed.

$$D_v = \frac{D_{particle}}{D_{surface}} \tag{8.3}$$

It should be seen that $D_{particle}$ can be from the top of the domain to the centre of gravity of the particle or to the contact with the surface. The former prioritises particles that lie flatter and therefore have a lower centre of gravity. Measurement to the centre of the particle has been adopted for the study so far hence for consistency this will be kept as the current method. D_v prevents the diminishing effect of D. Figure 8.9a presents the frequency of D_v values when packing with coefficients (C_V=1, C_D=1.6 C_V=0.4, C_{CN}=0.045) when taking n=100 samples. It can be appreciated that values do not range as widely from D_v=1 as before. However there still seems to be some diminishing effect on D_v.

If a gap cannot be filled the minimum placement surface becomes fixed and therefore a diminishing effect can begin to occur as $D_{surface}$ becomes a fixed value. For example, see Figure 8.8 where a gap between particles for which no other particle fits has resulted in $D_{surface}$ becoming equivalent to D_{domain} and remaining as a constant value. This will not occur in the Tetris Scenario as spacings between tetrominoes are fixed to be a width for which shapes can still fit. For the Soil Particle Scenario, this may become an issue if it is seen that very slender canyons start to occur within which particles cannot be placed. This effect can be prevented by taking the mean of the placement surface as a marker to measure from. Particles placed below this line can be awarded with a positive score for the depth whilst above the line can be given a negative score. Such a method would look like

$$D_m = \frac{D_{particle} - D_{ms}}{D_{domain} - D_{ms}} \tag{8.4}$$

where D_m indicates the depth score using the mean line and D_{ms} is the depth at the mean point of the placement surface. Figure 8.9b is the histogram of D_m values when packing under equivalent conditions. The range away from 1 is much less than that experienced in Figure 8.9a. Negative values exist due to the nature of how D_m is scored relative to the position of the mean height in the placement surface.

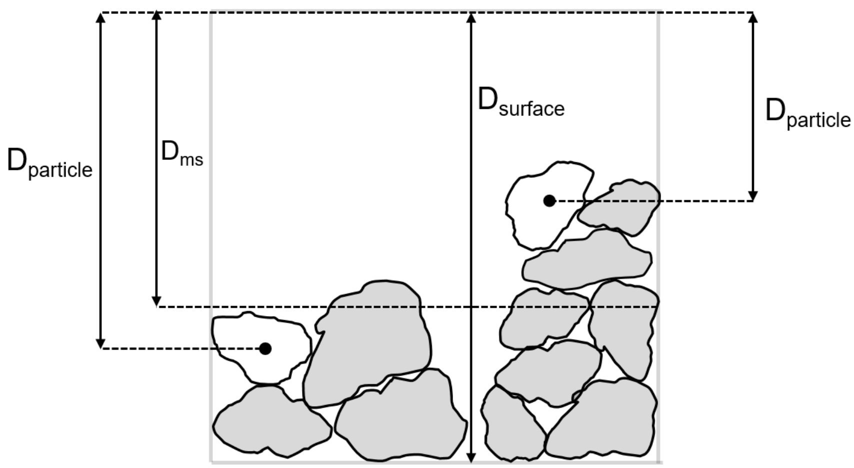

FIGURE 8.8: Particle being packed into a domain in a possible two locations with measurements of depths for calculating D_v and D_m indicated.

From Table 8.5, it can be determined that packings using $C_D D_v$ in the objective function produce results less efficient as $C_D D$. Understand, coefficient values tested are optimised using an objective function including D rather than D_v. As values of D_v

stay around a consistent value when packing it means that $C_D D_v$ is having more of an effect on packing later on in the simulations. Referring back to Table 5.2 in Section 5.3, when D became a dominant factor in the objective function MVR results were seen to be larger than when V_{AB} is the dominant factor. In order to truly determine whether D_m is an improvement in the objective function, a new study of search areas is needed to be conducted. It is envisioned that the value of C_D for the optimal solution for the Tetris Scenario will be a reduced value compared to the current C_D=1.6 value.

Coefficients	MVR (n=30)	MVR (n=100)
(C_V=1, C_D=1.6 C_V=0.4, C_{CN}=0.045)	0.0172	0.0160
(C_V=5, C_D=1.25 C_V=0.4, C_{CN}=0.01)	0.0212	0.0214
(C_V=1, C_D=0.6 C_V=0.2, C_{CN}=0.015)	0.0183	0.0165
(C_V=100, C_D=0.6 C_V=0.2, C_{CN}=0.015)	0.0183	0.0165

TABLE 8.5: MVR values for packing different coefficient combinations produced with D_v calculated by Equation 8.3 in the objective function for the Tetris Scenario in 10x20 square domain.

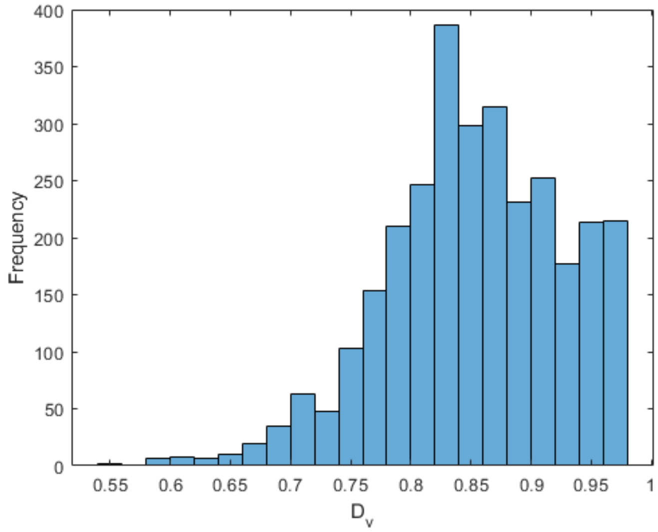

(A)

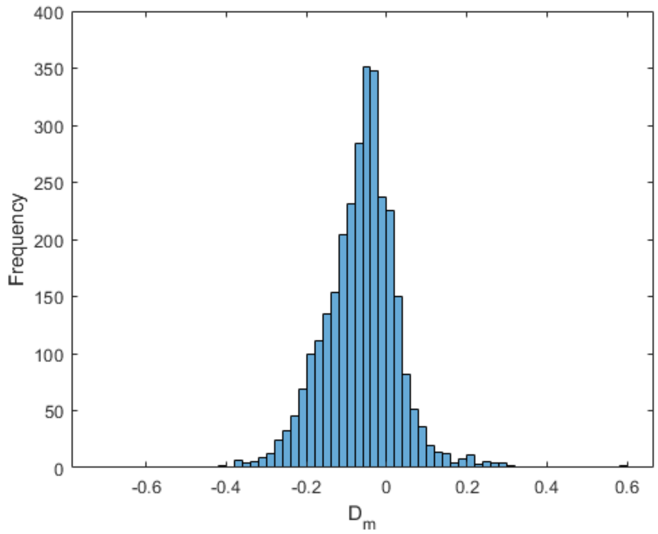

(B)

FIGURE 8.9: Frequency of produced for (a) D_v and (b) D_m values for packings of tetrominoes in a 10x20 square domain following the Tetris Scenario adopting n=100 and filling the domain until the next particle cannot be placed.

8.5.2 Use of First Order Equation

Section 3.5.1 introduced the objective function and stated that the more complex the objective function for scoring, the more parameters would need to be derived when determining the coefficients of weighting. As a result, four criteria were selected for scoring placements. Additionally, it was stated that the objective function would be kept as a first-order equation to keep the number of parameters required for derivation to a minimum. It is assumed that first-order terms are dominant and therefore it is not required to define terms for orders higher than this.

If the objective function was described by a second or third order equation, it can be understood that the effects of V_{AB}, D, T and CN for the second or third order terms will be small if differences in value for these parameters are small. This is due to the square and cube of the values having little effect on the approximation. The intention to keep parameters small was made by defining most as a ratio with maximum possible value of 1. With the use of the objective function, values should tend towards a certain degree as each criteria is beneficial to the packing. However, CN was taken as the coordination number which has a minimum value of 1 and saw up to a value of 6 for the Tetris Scenario whilst - as already presented in Figure 8.7 - the values of D ranged across the spectrum of values due to the diminishing effect which has been described in Section 8.5.1. As a result, it is possible that these may need to be defined using an order of approximation greater than first-order.

Figure 8.10 presents the distributions of scoring criteria V, T and CN for packing in the Tetris Scenario using coefficients (C_V=1, C_D=1.6 C_V=0.4, C_{CN}=0.045). Note, from the possible values of V_{AB}, the most void created beneath a particle was two squares of void. The ranges presented suggest that a first-order equation is not justified for the Tetris Scenario due to the wide range of values for CN. Therefore, it may be required to investigate second-order or third-order terms in the objective function. However, note that as C_{CN} tends to be a much smaller value and for the weighting coefficients used for producing results in Figure 8.10 the range of values in Figure 8.10c would be from $C_{CN}CN$=0.045 to $C_{CN}CN$=0.27 in the objective function.

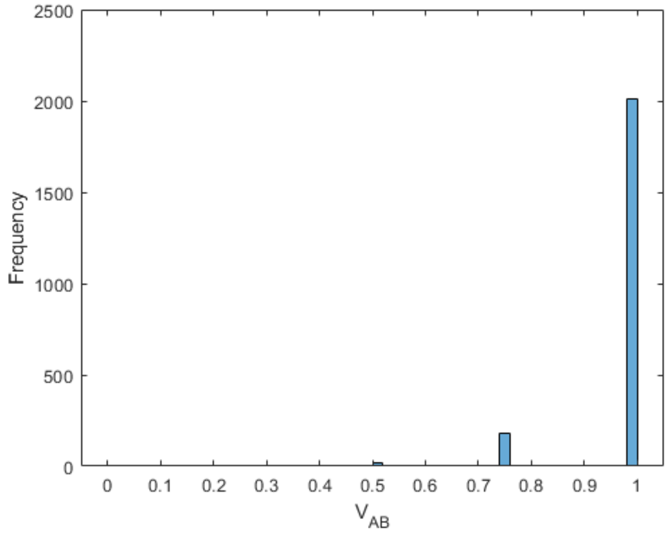

(A)

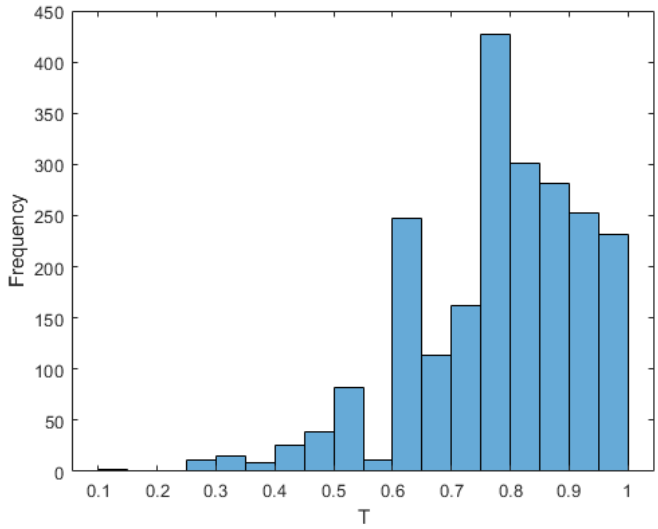

(B)

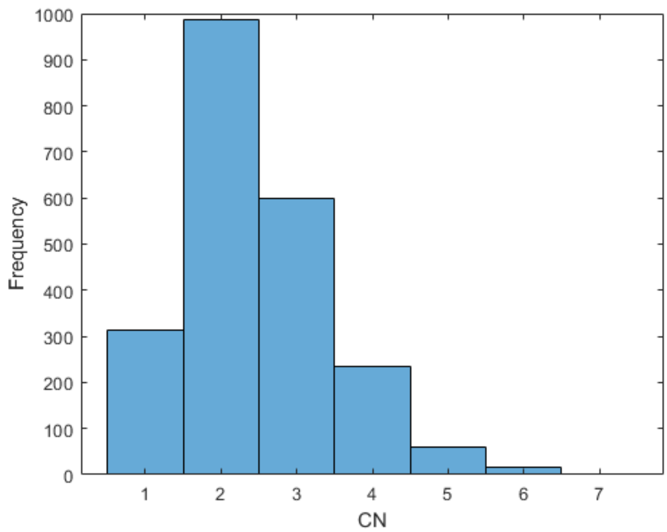

(C)

FIGURE 8.10: Frequency plots of values seen when packing for coefficients (C_V=1, C_D=1.6 C_V=0.4, C_{CN}=0.045) in the Tetris Scenario for domain 10x10 squares for (a) V_{AB} (b) T (c) CN.

8.6 Particle Characterisation

8.6.1 Particle Characterisation for Selection

In the algorithm described in Chapter 3 particles are selected randomly for placement. It is thought that permutations of particle order could be trialled although as discussed in Section 8.4.1 this was not tested due to the additional time that this would take. Another method in which selection could have been refined is using the characterisation of particles. Using this method, particles could be designated a quanity to represent size, angularity, ellongation and such. From this, particles of different descriptions could be trialled rather than similar particles as may be the case with Section 8.4.1. Additionally, the characterisation of the particles would lead to the ability to compare the produced shapes to actual irregular, untooled rock to ensure that the shapes used are a fair representation of this material.

In this section, different methods of soil characterisation are explored (Section 8.6.2). The methods in which these are calculated are described in Section 2.5 and it is understood that this could be implemented into the algorithm and stored as character data for each particle or defined before the programme and stored on the computer to be read when packing is being performed. Section 8.6.3 describes the relevant features highlighted in Section 8.6.2 which could be selected in the programme when choosing particles to trial.

This section differs than Section 8.4.2 as the characterisations are not being used to identify removing unsuitable particles. Rather, the characterisation is to define particles and ensure different types of shapes are being suggested for placement in the case where a Best Fit or All Permutations Method is adopted.

However, as stated in Section 8.4.2, particles could be discarded if they are judged unsuitable for placement. Angularity of a particle is highlighted as a key contributor to shear strength in Section 2.3 when the position of the particle is so that it interacts with many of the surrounding particles. The use of a particle-by-particle placement method allows for precise positioning of the material to maximise how they will interact. With the introduction of characterisation of the particle, this creates opportunities to discard particles that have features like being very rounded as suggested in Section 8.4.2. A limit to the minimum value of angularity (or maximum value of roundness) can be placed on particles with those outside of this limit not chosen from the stockpile for particle placement. Methods for how particles should be characterised are discussed in Section 8.6.3.

Section 8.6.4 discusses the use of the parameters introduced in Section 2.5 as well as Fourier descriptors to compare the outlines that represent irregular, untooled rock produced in this project to that of material that is sourced from a quarry mining site. Doing so would ensure that the shapes selected do in fact represent what is trying to be achieved here and verify that the software provided in Mollon (2023) produces reliable two-dimensional particle shape outlines.

8.6.2 Methods for Classification

From Section 2.5 there is a broad range of terms that can be adopted for classifying and quantifying particles. These are presented in Table 8.6 with an indication as to whether they can define two-dimensional or three-dimensional particle shapes.

This repeats the findings that are summarised in Section 2.5.4. Although some parameters are stated as not being able to define three-dimensional particles, it can be understood that all two-dimensional parameters can be used to describe a three-dimensional shape by quantifying the parameter in three orthogonal directions like that done for roundness and irregularity index in Wadell (1932) and Blott and Pye (2008) respectively. Parameters that cannot describe two-dimensional particle outlines tend to require a measurement for thickness (S). Again, this can be assumed and therefore using this method can be used to describe three-dimensional particles although this is not recommended.

Parameter	Symbol	Reference	2D	3D
Platiness	α	Potticary et al. (2016)	No	Yes
Elongation	ζ	Potticary et al. (2016)	No	Yes
		Li et al. (2013), Blott and Pye (2008)	Yes	Yes
Flatness Index	I_F	Wentworth (1923)	No	Yes
		Illenberger (1992)	No	Yes
Equancy		Illenberger (1992)	No	Yes
Circularity	Λ	Wadell (1932)	Yes	No
Sphericity	Ψ	Wadell (1933)*	No	Yes
Inscribed Circle Sphericity	Λ_I	Riley (1941)	Yes	Yes
Roundness	R	Wadell (1932)	Yes	No**
Angularity	A_{2D}	Lees (1964)	Yes	No**
Irregularity Index	I_{2D}	Blott and Pye (2008)	Yes	No**
Convexity	C	Li et al. (2013)	Yes	No
		Yang and Luo (2015)	Yes	No
Aspect Ratio	AR	Yang and Luo (2015)	Yes	No**
Overall Regularity	OR	Yang and Luo (2015)	Yes	No**
RMS Texture	R_q	Alshibli et al. (2014)	No	Yes

TABLE 8.6: Parameters for characterising particle shapes defined in Section 2.5.1 with relevant reference and indication if the parameter can be used for two-dimensional or three-dimensional particle shapes
*as cited by Blott and Pye (2008)
**stated that 3D equivalent value can be found by taking measurements in orthogonal planes in the literature

From Chapter 2, it can be determined that the most suitable particles for autonomous construction of a structure such as a DSRW possess the attributes of being angular, flatter and having higher surface roughness. This is determined from the following statements.

- Section 2.3.2 discussed particle shape and found that an increase in angularity lead to an increase in ϕ.
- Additionally, Vivian (1976) states that angular particles that have flatter sides are easier to build DSRWs with than rounded particles.
- Higher interparticle friction in a granular system leads to higher values of shear strength (Thornton and Sun, 1993) whilst Santamarina and Cascante (1998) showed that higher surface roughness increases critical state friction angle, as presented in Section 2.3.6.
- Villemus et al. (2007) presents that retaining wall structures rely on friction and interlocking for strength. Interlocking occurs more frequently in systems with

angular particles and higher friction between particles is expected in systems where particles have an increased surface roughness. The discussion behind this can be located in Section 2.2.1

For the characterising of two-dimensional particle outlines in this project, the parameters that are chosen for quantifying particle shape are

1. Angularity/Circularity
2. Elongation
3. Convexity

As stated by Lees (1964), angularity can be measured following Equation 2.21 in Section 2.5. Calculation of angularity requires identification of corners in the shape as well as measurement of planes that bound the corners. As stated by Lees (1964) the process of measuring angularity can be a time consuming method. Furthermore, with particle shapes that are complex and possess lots of convexities and concavities it may be difficult to define what is a "corner" when using a computer algorithm. Similar can be said when discussing roundess as described by Wadell (1932) which also requires identification of corners in the shape.

Instead, it is recommended that circularity, Λ, is adopted for quantifying the angularity of the particle. This is defined by Wadell (1933) (as cited by Blott and Pye, 2008) as the ratio of the c_p and C_p (see Equation 2.18). As stated by Barrett (1980), sphericity (and therefore circularity which is a two-dimensional form of sphericity) defines not just the shape of the particle but is affected by angularity as well. Therefore, this method for quantifying angularity is recommended as it is a method which is simpler to perform.

Elongation is adopted rather than flatness as flatness requires the third dimension of thickness to be defined. Two-dimensional outlines are utilised in this project and therefore a parameter that can define two-dimensional shapes is required. Elongation defined by Li et al. (2013) and Potticary et al. (2016) is based upon L and I and therefore can be used here.

As stated in Section 2.5, the work by Barrett (1980) and Cho et al. (2006) finds that irregularity of a two-dimensional outline representing a particle is a measure of the roughness of the particle. Whilst irregularity can be determined using I_{2D} (Equation 2.22 suggested by Blott and Pye, 2008) or AR (Equation 2.25 suggested by Yang and Luo, 2015), convexity is chosen as the parameter to measure irregularity and therefore surface roughness. Convexity is formed by Li et al. (2013) from the ratio of p_{hull} to $p_{particle}$ with resulting values ranging from 1 for a smooth particle to almost 0 for a very rough particle. Of these suggested measurements to describe surface roughness, convexity is classed as the one which best represents the different of the particle perimeter to the convex hull that would describe the particle. I_{2D} and AR focus more on quantifying the overall irregularity of the global particle shape rather than the irregularity at a surface level.

8.6.3 Features for Particle Selection in the Algorithm

As described in Section 8.4.2 and Section 8.6.1, particles can be discarded from selection automatically without trialling placement if they possess characteristics which are found to be not suitable for packing in the structure. As suggested, angularity is a good indication of this. Analysis of the particles before placement to define the shape and other features leads to the quantification of these features and the ability to only select suitable particles. In this manner it is equivalent to discarding materials judged unsuitable if only suitable materials are put forward by the algorithm. Outlined in Section 8.6.2 are the characteristics to be adopted for particle classification. These are stated to be circularity, elongation and convexity.

Circularity can be defined using the methods outlined in Wadell (1933) (as cited by Blott and Pye (2008)). This was presented in Equation 2.21 in Section 2.5 but is presented in Equation 8.5 here for completeness. Circularity is taken to be a method of determining the angularity of the particle, and therefore the less circular the particle the more angular it should be. Particles received by the algorithm will be chosen based on circularity with a lower value indicating a more angular particle and an increased chance of selection.

Elongation is taken to be a measure of flatness of the two-dimensional particle outline. Flatter particles are stated to be easier to pack (Vivian, 1976). Furthermore, this increase in length should lead to higher coordination numbers and more chance of overlapping runs in the system. The method for calculating elongation is that presented in Li et al. (2013) and Blott and Pye (2008) and can be found in Equation 2.14 in Section 2.5 as well as Equation 8.6 in this section. A minimum and maximum value for flatness should be set. The maximum value will increase the number of elongated particles selected by the algorithm. A minimum value will prevent particles that are extremely flat and having chance to break when loaded in the structure from being selected. Research into the maximum and minimum values is required to correctly determine what these should be and it should be noted that minimum value will depend on the strength of the material.

Convexity is adopted as a measure of surface roughness as described in Section 8.6.2. Equation 2.23 in Section 2.5 is the method for determining convexity from Li et al. (2013). This is again repeated in this section for the reader in Equation 8.7. A value closer to zero for C indicates a higher surface roughness. Therefore, particles with a higher surface roughness will be prioritised for selection.

It is envisioned that from these parameters, angularity will be the most important measure for particle selection. Therefore it is suggested that angular particles are prioritised for selection, followed by classification of elongated particles and then surface roughness. This priority list is to try and maximise the interlocking in the structure, which has been shown to be important to shear strength (Section 2.3.2), especially in DSRW structures (Villemus et al., 2007). Further investigation is needed to verify this assumption.

$$\Lambda = \frac{c_p}{C_p} \tag{8.5}$$

$$\zeta = \frac{I}{L} \tag{8.6}$$

$$C = \frac{p_{hull}}{p_{particle}} \tag{8.7}$$

Recognise that with angularity (circularity) there is the likelihood for a reduction of flatter edges and increase in sharper corners. As particles become more irregular, the placement surface that is made up of these particles will become more irregular. If matching between particles cannot be achieved, it is possible that a reduction in shear strength is seen when constructing using these angular particles. It is hypothesised that there will be a level of angularity which may lead to a decrease in shear strength due to the inability to be packed in an efficient structure which can maximise interlocking when a force is applied. The study of the shear strength of packings in comparison to particles of different levels of angularity will help conclude on this hypothesis. It is considered that if particles are too angular and a suitable position cannot be detected for packing, these particles can be tooled or discarded as described in Section 8.4.2.

8.6.4 Characterisation for Comparison to Untooled, Irregular Waste Rock

The work in this thesis aims to investigate a method for the packing of two-dimensional outlines of particles that represent untooled, irregular rock. Section 3.6.1 describes the method in which Fourier Descriptors were chosen for production of the particle shapes and explains that this is done by visual inspection of the results of a variety of particle shapes presented in Figure 3.23 and Figure 3.24. However, as previously stated, this does not guarantee that these shapes do represent rock particles.

Verification of the particle shape could be completed from analysis of material sourced from a mining site or quarry. From this, two-dimensional cast shapes of the figures of the rock particles can be produced. Measurements for the parameters defined in Section 2.5 and discussed in Section 8.6.2 can be found for castings of the sourced material as well as the outlines of the shapes produced by the software in Mollon (2023). A comparison between the two can be made to determine whether the outlines adopted in this project do correctly represent those of irregular, untooled rock.

Following Bowman et al. (2001) as described in Section 2.5.2, the outline of the sourced material from mining site or quarry can be described to find the Fourier descriptors of the materials. Specifically D_2, D_3, and D_8 can be taken forward. These can be compared to the values already chosen for packing to again determine if the outlines chosen do represent irregular, untooled rock particles. This will provide more of a measure of variation from the specificed value as each descriptor belongs to different features of the particle. Other descriptors can also be investigated in comparison with those that would be produced in Mollon (2023) to see if there are any differences. These can be calculated following Equation 2.31 and Equation 2.32. A further study would be to use the Fourier descriptors within the software to generate particles and verify that the shapes produced match the outlines gained from casting shadows of the sourced material.

Furthermore, the outlines produced by the material sourced from a mining site or quarry can be used for packing within the algorithm. However, it is possible only a few samples are available rather than the 100 particles produced by the methods described in Section 3.6.1. In this case, the derived Fourier descriptors can be inputted into the MATLAB code sourced from Mollon (2023) to produce more particles to be used in the algorithm.

8.7 Increasing Computational Speeds

8.7.1 Introduction

The main issue faced when producing results for this project is the computational times of the algorithm. Ideally, the time to place a particle is desired to be kept to a minimum so that the speed at which an autonomous construction could be created does not grossly outweigh that of current construction methods or if the procedure was to be completed manually. In this section, methods for improving computational speed that were not investigated in the development of the algorithm are described. These consist of the use of multiple processors by parallelisation, adopting bitwise operations for the discretised fitting of particles, and caching and memorization of results.

8.7.2 Parallelisation

The act of parallelisation in high performance computing allows for multiple processes to be carried out simultaneously. In this manner, the code can have separate parts running at the same time or multiple versions of the code running with different set parameters. The primary motivation for Parallel Computing is performance and the use of multiple computer processors leads to increased computational times. In an ideal scenario, the use of four processors should increase the speed to be a quarter of the original time of one processor but in reality this is hard to achieve Maclaren (1997).

The introduction of parallelisation in this case could be used to simultaneously pack different weighting coefficient combinations or different particle orders if multiple runs are being investigated. Although using two processors may not speed up the process to be twice as fast, this introduction will still lead to an increase in speed.

In the instance where coefficients of weight are already determined and particles are being placed autonomously, multiple processors could be adopted to simultaneously score numerous positions for placement or different particles to help determine the best suited particle to be placed next if particle order is set to be variable.

8.7.3 Bitwise Operations

During the discretised fitting of particles as outlined in Section 3.7.3, particles are converted to a binary matrix. It is possible for these binary matrices to be converted to one or more 64-bit integer arrays where each bit corresponds to a square in the original binary matrix. Using the AND bitwise operator (&) in Asymptote and most other programming languages, bits can be compared. A value of 1 will be returned if two squares both have a value of 1 present, whilst if the discretised particle can fit in that space a 0 will be returned. This is similar to what is already happening in Section 3.7.3 where fittings are classed as suitable if the product of both matrices is equal to zero.

The benefit of using a bitwise operator is that it uses less memory and allows for greater precision as well as reducing the use of a repetitive code sequence (Nicoli, 2019). It should be noted bitwise operations can only be used for integer data types and bits numbering starts from right to left (Yordzhev, 2013).

Instead of using binary matrices to describe the discretised particles and areas of domain where the particle is being fit as is done in Section 3.7.3, a binary vector can be used that is a 16-bit integer array. If the particle is described by more than 16 squares, multiple arrays can be adopted. The matching portion of the domain can also be described by multiple integer arrays and the & operator is adopted for quick comparison resulting in a zero value if the particle fits in the trialled location.

8.7.4 Caching and Memorisation

The storage of information through caching and memorisation could be another potential method to increase computational run times. A cache is simply a temporary data store that holds data so that future requests for that data can be served faster. Caching is the storage of data in the cache so that future requests for the same data can be served faster. Storing data in a cache rather than recomputing data will typically reduce the computational time of the programme.

Memorisation is like caching, but rather than storing data temporarily, the results of a function is stored for a certain combination of the input values. As the programme runs, if a function is called with input values that have already been used, the return value is called from storage without the need to repeat the calculations again.

Using this, the programme could be sped up in situations where equivalent inputs are repeated when calling a function. This could be especially useful for the finding of locations in the discretised fitting described in Section 3.7.3 as this is the most likely scenario for patterns to be repeated, especially if a lower resolution for particle description is adopted as particles will start to look similar to each other. Memorisation is useful when dealing with functions that require heavy computation, so a check should be complete to see if the introduction of memorisation does indeed improve the speed of the algorithm.

8.8 Running Joints

8.8.1 Inclusion in the Objective Function

In the objective function, criteria are derived from the findings in Chapter 2 based on factors that affect the shear strength of a soil structure as well as the discussion surrounding bin packing, jigsaw solving, and Tetris optimisation in Section 2.3 and Section 2.4 respectively. These were V, D, T, and CN as stated in Section 3.5.

As seen in the Soil Particle Scenario, the quantifying of runs and their disrupting is used as an objective outcome to help judge if a structure has a high shear strength. This is based on Adcock (2012) and Vivian (1976) who discussed the construction of drystone walls and the concept of running joints that can occur in the structures. This can be found in Section 2.2.1. It can be argued that the inclusion of running joints - more specifically the disruption of running joints - should be included in the objective function if this is a factor that will help contribute to overall shear strength of the structure.

Disruption of running joints was not included within the objective function as this was used as a way of quantifying the expected shear strength of the structures produced by the algorithm. It is desired that this measure is to be a term separate from scoring criteria for placement. By introducing this into the objective function, it may cause systems to purposely place particles to create joints which can then be disrupted later on, especially if different permutations of particles are tested like the All Permutations Method described in Section 8.4.1 or a system of backtracking like that in Galambos and Woeginger (1993) or Goldberg et al. (2002). However, in this work where these are not present in the current algorithm, including a score for particles placed that do disrupt running joints in the system could be beneficial to outputted structures in terms of trying to maximise shear strength.

Disruption of runs could be included into the objective function by adding a separate term. Equation 8.8 shows an updated objective function with the terms J and C_J used to represent the number of running joints disrupted and the coefficient of weighting for this term respectively.

$$W_{ij} = C_V V + C_D D + C_T T + C_{CN} CN + C_J J \tag{8.8}$$

The term J represents a score given to the placement of a particle if it disrupts a running joint. It is considered that a binary score could be given for J so that J=1 if runs are disrupted by the placement whilst J=0 if no runs are disrupted. However, this does not reward placements that disrupt multiple running joints. Instead J can be quantified by giving a score of 1 for each running joint disrupted. Therefore, if numerous running joints are disrupted the score is not limited to a maximum cap. Similar to coordination number, this is already a non-dimensional number and therefore does not need to be quantified in a ratio with other factors. Therefore as with C_{CN} it is expected that C_J would be much smaller than other weighting coefficients in the objective function. This can be extended to include disruption of diagonal joints, the detection of which is described in Section 8.8.2.

No inclusion of the number of joints present in the structure or number of joints created by the particle should be included in the quantification of J. If this was the case, particle placement will be affected negatively when particles are placed close to each other as this is when joints are most likely to be created according to the criteria set out in Section 3.10.2. As shown by the literature in Section 2.3, the structure benefits from particles been tightly packed together as this increases coordination number as well as areas of particles touching other particles in addition to minimising void ratio. It can be understood that by introducing a term that may cause prevention of the algorithm to place try to fit particles together will lead to a negative effect on the overall packing.

With the addition of a new term in Equation 8.8, this provides a new problem of needing to derive five parameters so that each weighting coefficient has a new value. If this is adopted in the future, then a method using either SA or GA is suggested for exploration of the search area to determine these values. Section 2.4.2 describes these optimisation methods in more detail. This would mean that visual inspection of the results is not required as is done in Section 4.4 where surface plots are examined to determine areas of optimal solution.

8.8.2 Multi-directional Runs

Section 2.2.1 introduced the concept of diagonal runs in the structure of a drystone wall (Adcock, 2012). Figure 2.2a gave an example of a diagonal run in the system that would maybe be missed by a person constructing a drystone wall if only vertical runs are taken into account. In Section 3.10.2, disruption of runs in the system is only considered within the horizontal direction. An identification for diagonal runs and ensuring that these do not occur in the structure should be implemented to prevent them from occurring.

Diagonal runs can be detected by axis of the domain by 45^o. This can be done either by introducing a non-Cartesian coordinate system that is 45^o to the normal, or by rotating the system by 45^o and using the Cartesian coordinate system. Figure 8.11 indicates how the later method would be accomplished. Figure 8.11a presents the domain at the original rotation with locations where runs are initialised as well as locations where runs are deemed to be disrupted indicated on the diagram. Runs are deemed to be disrupted when they match the criteria for Equation 3.15 set out in Section 3.10.2 requiring an overlap of 25% of the particle width. To complete checks for diagonal runs, the process for identifying runs as well as detecting when runs are disrupted can be done for the domain rotated both clockwise and anticlockwise by 45^o. This is represented in Figure 8.11b and Figure 8.11c. Note, the direction in which runs travel is still in the vertical direction for a Cartesian coordinate system and does not also rotate with the domain.

Scoring the system in a similar manner as before but with the inclusion of these rotated systems should prevent diagonal joints appearing in the structures. It could be argued that more rotations of the domain should be tested to ensure no diagonal joints in other directions, say at 60^o angle to the horizontal. It is suggested that by adopting the two scenarios at a rotation of 45^o will be suitable to help prevent diagonal joints running that are not exactly 45^o to the horizontal as well. If it is found that this is not the case, an increase in the amount of particle that needs to overlap the running joint to disrupt it could be adopted for the criteria of disrupting running joints and implemented to help prevent against these. Further examination could be done using similar technique adopted for identifying horizontal running joints in the system by rotating the domain by 90^o for full analysis of the structure and potential faults.

For the case of zipping joints, also described in Section 2.2.1, it is thought that the condition for overlapping above the particle from Equation 3.15 should be suitable to stop this occurring. The check described in Section 3.10.2 is for detecting vertical running joints. Although zipping occurs not in an obvious vertical line, it is still a running joint that travels in a vertical direction (or in a diagonal direction if it is a diagonal zipping joint). Therefore, the criteria for overlap should help prevent zipping joints. Is it is found to not be the case, the size of overlap to meet this condition should be increased.

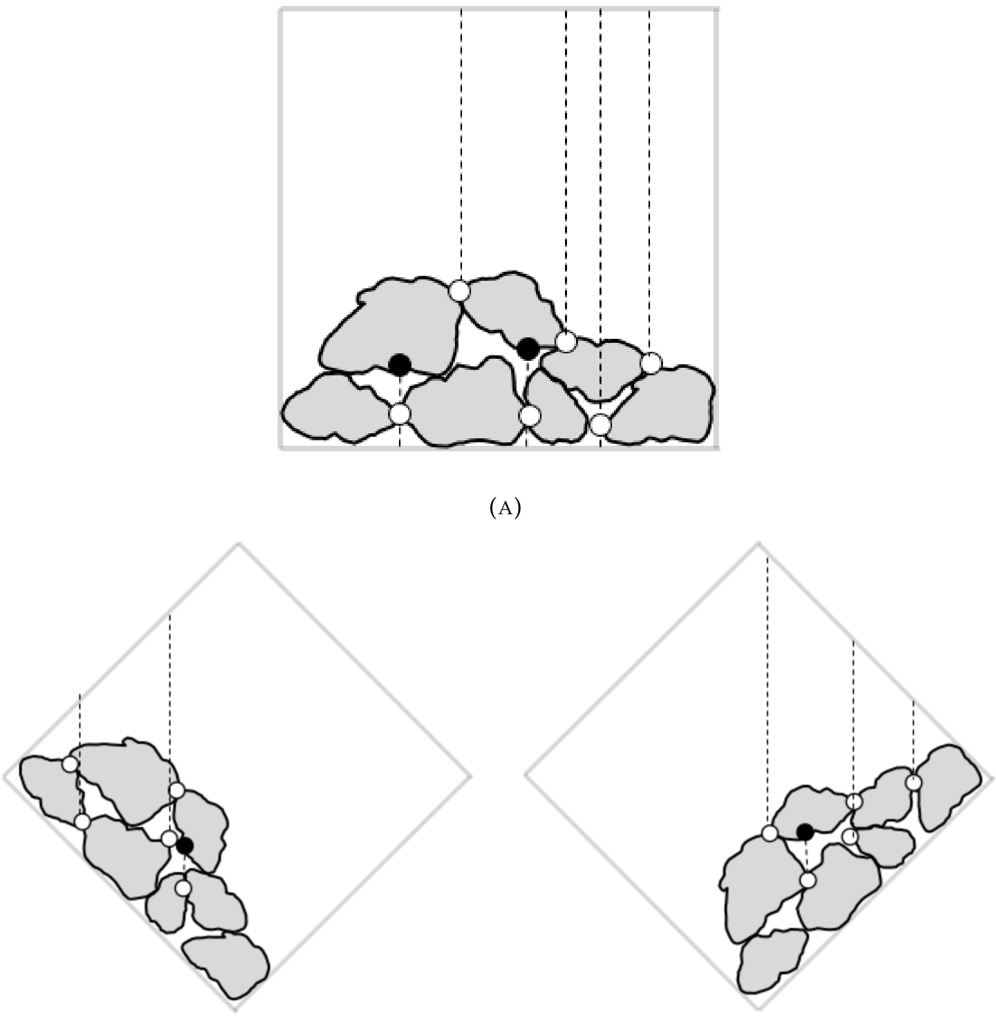

(A)

(B)

(C)

FIGURE 8.11: Example of checking for phantom joints by rotating the domain by 45^o for (a) domain at the original rotation (b) rotated clockwise (c) rotated anticlockwise. White circles indicate where runs are initially located after each particle is placed, black cirles represent where the underlying run is deemed as disrupted by the particle placed above. Dashed lines indicate the direction in which runs are being checked for disruption.

8.9 Packing Solution

8.9.1 Bin Packing

From the investigation for the Tetris Scenario it has been shown that the algorithm can efficiently pack two-dimensional objects into a domain whilst minimising the gaps between particles. In Section 5.7, the placement method using an objective function based on criteria that optimise shear strength in a soil structure were shown to outperform the DBL heuristic when packing the seven tetromino shapes. MVR for a sample size n=100 was 0.0707 for the DBL-heuristic compared to 0.0271 for an objective function with coefficients (C_V=1, C_D=1.6 C_V=0.4, C_{CN}=0.045).

Potential lies in the approach suggested in Chapter 3 to be adopted as a solution for 2BP. Comparison has only been made with the DBL heuristic adapted for a two-dimensional system. For further study to take place, results of different heuristics would be required to determine if scoring based on the objective function using V_{AB}, D, T and CN is an efficient method of packing. Other heuristics have been described in Section 2.4.3 and it is thought that comparison could be drawn against the BL and BLLT heuristics (Jakobs, 1996; Liu and Teng, 1999) as well as the BLP and TP heuristic (Hifi and M'Hallah, 2002; Lodi et al., 1999a). The results in Chapter 5 show very low amounts of void are created when packing tetrominoes compared to the DBL approach tested which indicates that this could be a promising solution for 2BP problem.

Different shapes to tetrominoes would need to be adopted, as these represent shapes which can perfectly fit together and have defined minimum spacing and angles of orientation as the thinnest part of a tetromino is one square and the orthogonal corners will best be fitted together when rotated by 90^o. Therefore, irregular polygons should be attempted. Use should also be made of the design for the method developed in Chapter 3 to be any particle shape whether that be convex or concave and the shapes for packing should reflect this, which also increases the complexity. It is possible that different coefficients of weighting will be required based on these different shapes, which will need to be determined.

In the study, the intention was to maximise shear strength of soil particle structures. Low void ratio is linked to be a good indication of higher shear strengths and therefore this was a key feature for analysis and developing of a packing algorithm. Confirmation of the method is required compared to other 2BP heuristics and with testing on different particle shapes instead of tetrominoes and particle shapes. However, the work in this study suggests the method adopted in Chapter 3 can be adapted to be a solution to the 2BP problem. As far as the author is aware, there is no heuristic solution for the 2BP problem that utilises weighted criteria that are derived from the analysis of packing structures of soil with the intention of minimising void ratio. Further investigation into this area may lead to a novel approach for 2BP.

8.9.2 Specimen Generation

From the results presented in Chapter 6, it can be seen that soil particles are successfully packed within the domain. Although an optimal set of coefficient values was not obtained it can clearly be stated that the packing algorithm does successfully place particle shapes to create a packing that can represent a soil structure. Within geotechnical research, it is necessary to create structures of particles for testing via simulation. The most prevelent of these research areas is specimen generation in DEM modelling of granular soils.

Multiple methods have been adopted for specimen generation such as random generation (Lin and Ng, 1997; Itasca, 1998) and triangulation based approaches (Cui and O'Sullivan, 2003). It is difficult to obtain particles obeying a desired particle size distribution using these algorithms. Additional, graviational positioning in which particles fall into position has been adopted (Feng et al., 2003; Ferrez, 2001; Thomas, 1997). O'Sullivan (2003) describes the disadvantages of this approach including the difficulties associated with obtaining homogeneous specimens, lack of control of the specimen void ratio, and the interlocked stresses that are also easily induced. Furthermore Cui and O'Sullivan (2003) states that the number of iterations required to reach the equilibrium results in a very high computational cost.

Potential lies in the algorithm for the Soil Particle Scenario as a method for specimen generation. The results seen in Chapter 6 give examples of homogeneous packings. The use of the weighted criteria means that each particle is placed with the same objective. The particle size distribution can also be controlled by selecting particles to be placed that fit the desired distribution. Additionally, the overall objective function can be altered to adhere to the desired function of the structure. The method differs to the graviational positioning methods as particles do not need to fall into position providing that they are already placed in stable positions. Section 8.3.3 has already discussed the need to improve the stability check in the algorithm but with this improvement leads to the possibility of the use of this method.

Specimen generation was not an intended outcome of this research however it is clearly a contribution that could be achieved using the method described in Chapter 3. Testing of this method is required and comparison with existing specimen generation methods should be completed. As far as the author is aware, there is no current method that generates packings of particles using a weighted objective function. Therefore, it can be stated that using this method would be a novel approach for speciment generation.

8.10 Alternative Areas of Improvement

8.10.1 Backfill

A precision method of autonomous construction by specific placement of individual particles has been proposed for creating structures such as a DSRW. A key feature of a retaining wall is the backfill behind it. As discussed in Section 2.2.1 the typical cause of failure comes from lateral pressures on the wall. Therefore backfill behind the wall being porous with the ability for water to flow through the medium (as well as the structure either through spaces between particles or designed weepholes) is beneficial to these structures. With the backfill requiring a key purpose to the structure, a possibility to autonomously construct this medium exists.

The purpose of the backfill behind the retaining wall is to provide good drainage and prevent build up of water pressure against the structure. If the methods proposed in this thesis are adopted for constructing a system like this, it is clear that the objective function of the algorithm described in Chapter 3 would need adapting. Instead of having an overall objective of maximising shear strength, a review on maximising porosity in the system is required. Without conducting a extensive examination of the literature, it is expected that criteria in the objective function would include void ratio being maximised and minimising contact areas between particles. Further study is recommended if designing a porous medium is to be carried out.

Fontanese (2007) described the backfill behind a retaining wall built by the Incas at Machu Picchu. The backfill was made of several layers. These were a topsoil layer for crop growth followed by a middle layer of fine sand and gravel before a base layer of gravel. Underneath this was a continuation of the wall structure which acted as a foundation base. It should be noted that the wall structure was not finely packed together with minimal gaps like that seen in Figure 2.6 for Sacsayhuaman but were drystacked walls with gaps between particles. Therefore, water can easily flow through the structure.

If an autonomous construction approach is adopted for construction of the backfill as well as a DSRW structure then it is possible to a layered system as described by Fontanese (2007). Particles can be selected and placed in decreasing size order as the process is done in a layer-by-layer approach. However it should be recognised that if a robot similar to that seen in Johns et al. (2020) and Johns et al. (2023) is adopted then this will not be able to grasp small particles and it is very unlikely that this would be done for particles in the middle or top layer. These layers can instead be constructed using traditional methods and therefore if this is going to be done then perhaps it is not worth the expense of constructing the lower layers using autonomous construction. To determine this further research is required in this area.

A question remains on whether precise construction of the backfill would be worth the effort considering material can be placed behind the wall with assumptions made to how it will affect the strength of the structure. The method will be very time consuming considering the benefits gained. However for situations where build up of water pressures may be a big issue, such as on flood plains or areas susceptible to high levels of groundwater flow, a solution that maximises the porosity of the backfill whilst still supporting the retaining wall through an autonomous construction process can be achieved.

8.10.2 Hybrid Structures

Potential lies in using an autonomous construction process with hybrid materials rather than limiting to just granular gravels, cobbles or boulders. For example, finer materials could be adopted in the structure for filling of the gaps. This is envisioned to be a feature if structures are created for purposes such as housing or shelter. Filling gaps in the structure will prevent draughts and improve sound insulation.

Compaction of finer materials like that seen in rammed earth construction could be performed by robot - either the same robot with a different end-effector that complete compaction or another robot with the utilisation of a multi-robot process. Compaction would not take place on the structure as this may cause damage, but could be done at ground level and then these materials can be placed in the desired location in the structure. Rather than formwork, adjustable areas present in the robot could be used as boundaries for compaction to take place and through this method the size and shape of the material can be designed.

Note, with the inclusion of finer material between particles the porosity of the combined material will decrease and water will not travel through the structure. This is beneficial to a home but is detrimental if there may be a build up of water on the structure that could then result in failure. Additionally, without use of some sort of reinforcement it is possible that material will become soluble or be washed away by water flow on the structure.

Much more further work is needed for the investigation into hybrid structures maximising the whole of the materials that can be found locally to site. This section is included to create discussion over the possibilities of the autonomous construction method and where it limits may or may not lie.

8.11 Three-Dimensional Packing

The work in this project is conducted in two-dimensional space to simplify the problem. The aim of this study is to explore the feasibility of constructing through the use of an autonomous system that follows an objective set out by the user. The objective explored in this work is an objective of maximised shear strength, which is quantified by scoring positioning by V_{AB}, D, T, CN. Although verification of the strength of the structures has not been carried out, the results in Chapter 6 show the production of tightly packed particles. For this project to be expanded further, it is required that this two-dimensional heuristic be expanded into three-dimensions to replicate real-life scenarios.

It is considered that the criteria specified in the objective function could be extended to work in three-dimensions. V_{AB} becomes a ratio of the volume of void created compared to the volume of the particle, whilst T becomes area of contact compared to surface area rather than a indication of the perimeter of the particle in contact. D can remain a single value as the depth of the particle from a given height and CN will remain a value indicating the number of particles surrounding the position. D and CN are discussed in Section 8.5 about how these could be enhanced and it is thought that these methods still can be extended to describe a three-dimensional positioning.

A coordinate approach is adopted to describe the particles. Difficulty comes in representing three-dimensional particles, but an extension of using a coordinate system can be adopted to describe points. Such methods include scanning of particle to create a mesh (Self and Vercruysse, 2017) or a cloud of datapoints (Furrer et al., 2017; Johns et al., 2023; Larsson et al., 2019; Liu et al., 2021) that resemble the particle shape. It is recognised that an issue with the work in this project was the computational runtime when excessive amounts of coordinates were adopted to describe the particle. Therefore, a minimum number of coordinates will need to be found. Furthermore, it is thought that the methods described in Section 8.7 can help alleviate this issue so that construction in three-dimensions is a feasible option.

Further consideration of heuristics and conditions are required to be identified if construction is to take place in three-dimensions. Firstly, stability will require an improved method for detecting unstable particles as described in Section 8.3.3. Recognition of stability in all planes will require analysis and particles will at a minimum require three points of contact with the placement surface. As stated in Section 2.2.4, Liu et al. (2021) adopted criteria to try and ensure stability of the particles such as ensuring the deviation from the normal to the surface compared to the thrust line is above a mean of all possible results. Similar methods could be adopted here, perhaps stating a maximum angle that particles can deviate from.

Additionally, three-dimensional structures such as the heavier walls found in and around 16th and 17th century Japanese castles exhibited curvature in their profiles

(Fujioka, 1969; Nishida et al., 2005) as described in Section 2.2.3. Some profiles inclined so that the principal axis is orthogonal to the local tangent of the curved profile and this was described to maximise shear strength (Utili and Nova, 2007). It is common practice to have a slight inward slope for larger drystone walls (Vivian, 1976). This curved profile should be accounted for and the shape of a structure that is created to maximise shear strength should aim to take this into consideration when calculating placements. This can be achieved by designing structures to lie within a designated volumetric space as seen in Johns et al. (2020) which was discussed in Section 2.2.4 where candidate poses are rejected if particles overlap the given boundaries.

8.12 Summary

The discussions around different topics are summarised here. For the Tetris Scenario, locations in the search area for (C_V=1, C_D=1.6 C_V=0.4, C_{CN}=0.045), (C_V=1, C_D=0.6 C_V=0.2, C_{CN}=0.015) and (C_V=5, C_D=1.25 C_V=0.4, C_{CN}=0.01) are compared in Section 8.2.1. It is concluded that due to the misrepresentation of canyoning in the structure when particles are not capped by a final placement resulting to no inclusion underneath the placement surface that final void ratio of the system is misleading. Although (C_V=1, C_D=0.6 C_V=0.2, C_{CN}=0.015) has lower MVR results, (C_V=1, C_D=1.6 C_V=0.4, C_{CN}=0.045) is deemed to be the optimal solution for packing in the Tetris Scenario for a 10x10 square domain as the high value of $C_D D$ in the objective function help prevent canyoning. Additionally, when results are analysed using Q_{90}, it is seen that the maximum void produced by (C_V=1, C_D=1.6 C_V=0.4, C_{CN}=0.045) is actually lower than other combinations and that the maximum MVR seen for sample size n=100 is an outlier. When compared to the DBL heuristic and randomly packed tetrominoes, packing using the algorithm and coefficients (C_V=1, C_D=1.6 C_V=0.4, C_{CN}=0.045) clearly outperforms these in terms of minimising void ratio.

For the study, a domain size of 10x10 squares was selected due to the seen decreased domain sizes in literature. Section 8.2.3 investigates the effects of reducing the domain by examining results of the three combination coefficients brought forward from Chapter 5 when packing particles into a 10x20 domain. Results for (C_V=1, C_D=0.6 C_V=0.2, C_{CN}=0.015) and (C_V=5, C_D=1.25 C_V=0.4, C_{CN}=0.01) outperform (C_V=1, C_D=1.6 C_V=0.4, C_{CN}=0.045) due to canyoning not being a problem when the height of the domain is not approached. Therefore if the objective of packing was to be able to efficiently play the Tetris videogame, one of these solutions could be deemed the optimal combination of weighting coefficients. Furthermore, the accuracy required for coefficient values and the sensitivity of the Tetris Scenario are explained in Section 8.2.5. It is stated that the sensitivity is caused by the domain becoming full leading to limited positions of particles towards the end of the packing. In fact, if the Tetris videogame had been used for the Tetris Scenario then the domain height would be greater and filled rows would be deleted. With these features implemented, it is thought that the problem would be less sensitive and any of the proposed coefficients of (C_V=1, C_D=1.6 C_V=0.4, C_{CN}=0.045), (C_V=1, C_D=0.6 C_V=0.2, C_{CN}=0.015) and (C_V=5, C_D=1.25 C_V=0.4, C_{CN}=0.01) would be suitable as a solution.

The investigation into the Soil Particle Scenario is discussed in Section 8.3. Section 8.3.1 begins by discussing MRJ and its use as an indicator of soil strength. As determined, there is no correlation between MRJ and MVR with R^2=0.024. This was opposite to what was expected as void ratio would usually lead to tightly packed structures meaning more chance of overlap over running joints. Furthermore, MRJ was found to be greater in structures that were taller. Therefore, the different dimensions of the structures was found to be affecting MRJ leading to this not being a suitable measure. Instead, it is recommended that a physics simulator be taken forward as this can also quickly calculate stability of the particle when being positioned. To prevent this, additional conditions are required to reduce the height of the structure and ensure a layer-by-layer construction technique. It is also thought that the number of candidate poses being reduced leads to problems for stability as well as preventing optimal solutions from being found. It is described that an increase in computational speed will lead to more candidate poses being tried. Section 8.3.3 discusses the stability checks performed in the Soil Tetris Scenario. It is clear that this is not at a fully developed stage to be suitable from viewing packings in Chapter 6. Therefore improvement is needed. Suggestions of ensuring a layer-by-layer approach or introducing methods from Liu et al. (2021) are proposed. The final part of this section discusses the results for packing using coefficients from the Tetris Scenario. It was found that the results from these combinations appear to be of good quality. However, without a testing method it cannot be confirmed if these lead to high shear strengths of the structure.

Suggestions for improving results in terms of shear strength are made in Section 8.4. The first of these is testing multiple permutations of the particle order rather than packing in the exact list that is presented. It is envisioned that this would lead to higher shear strengths as the most optimal particle can be placed in its most optimal position of those available. Two methods are suggested: the All Permutations Method where where every permutation is trialled and the Best Fit Method where each particle is tested and the best particle is placed before each particle is tested again with the addition of the new particle in the system. With this technique, if it is found that a particle is not chosen for placement this can be discarded or tooled as described in Section 8.4.2. Discarding the particle means that the shear strength will improve as an unsuitable particle is not being forced into the structure, while tooling means that the particle can be shaped so that it becomes suitable for its function.

Another method of increasing shear strength is the use of strategic reinforcement. Section 8.4.3 states that because the placement of material is conducted particle-by-particle this allows for addition of other materials at any point between packing. Use of a numerical model such as a physics engine or DEM can be found for analysing weak spots in a structure designed by the algorithm. Once identified, reinforcement can be placed in just these areas. Doing so is expected to lead to higher shear strengths as well as a reduction in material for if this reinforcement was placed in less precise locations.

Methods of enhancement for the objective function are described in Section 8.5. The way in which D is quantified is discussed in Section 8.5.1 and it is shown that as the placement surface increases the effect of D diminishes due to its calculation as a ratio of depth of the particle to domain height. Figure 8.7 demonstrates this as it is seen that values of D are fairly uniform between values of zero and one for the Tetris Scenario. Therefore, D_v was suggested as a solution taking the depth of minimum height of the placement surface for calculation rather than D_{domain}. However, it was seen for the Soil Particle Scenario that minimum height is often located at the bottom of a canyon which is too small for a particle to be placed and this therefore eventually becomes a fixed value. Instead, D_m is adopted that takes the mean height of the placement surface and its definition is found in Equation 8.4. Values are taken as positive for positions below the mean surface and negative for positions above. Figure 8.9 presents the values of D_m calculated for placing particle outlines in the Soil Particle Scenario and the range of values is improved with a centroid value of zero.

Section 8.5.2 describes the use of a first-order equation to define the objective function. As stated, it is thought that due to differences in values being small that first-order terms will dominate the scoring. However, it is shown from the range of values that this might not be the case for CN as this ranges from 1 to 6. It is seen that the value of $C_{CN}CN$ in the objective function ranges from 0.045-0.27 when C_{CN}=0.045 as was determined for the optimal solution in the Tetris Scenario. Further work is required to conclude if the objective function should be described by a greater order than a first-order equation.

Methods for characterising particles for selection are taken from the review of techniques in Section 2.5 for quantifying form, sphericity, roundness, and irregularity. These are summarised in Section 8.6.2 in Table 8.6. As previously stated, angular particles are seen to exhibit higher shear strengths due to the interlocking of grains. Meanwhile Vivian (1976) states particles with flatter sides are easier to construct with whilst it is also considered that particles with rougher surfaces increase critical state friction angle (Santamarina and Cascante, 1998). From these statements, the parameters chosen for characterising the particles are circularity, elongation and convexity. Circularity defined by Wadell (1933) (as cited by Blott and Pye, 2008) is taken as a measure of angularity whilst being easier to calculate compared to angularity defined by Lees (1964) because of the omission of needing to locate every corner in the particle shape. Elongation will give indication of the flatness of a particle and is found using L/I (Li et al., 2013; Potticary et al., 2016) so can therefore be used for characterising two-dimensional particle shapes. Irregularity is measured from the method of a ratio of the perimeter of the convex hull to the perimeter of the particle around the particle as defined by Li et al. (2013). This is selected as it gives good description of irregularity at surface detail. The envisioned importance for each characteristic is given in the order of angularity, elongation, surface roughness.

With the methods of characterising particles comes the possibility of comparing the particle outlines adopted in this project to actual mining waste material. As previously stated, the method for generating particles was adopted from Mollon and Zhao (2012) and utilised software provided from Mollon (2023). Section 3.6.1 describes the method in which Fourier Descriptors were chosen for production of the particle shapes. This was done by visual inspection and no verification of the shapes to actual mining waste particles was completed. Taking the characteristics defined in Section 2.5, it is possible to compare the produced shapes with mining waste if two-dimensional castings of these materials can be sourced. Furthermore, Fourier descriptors can be defined from these materials and compared to the Fourier descriptors utilised in Section 2.5. Alternatively, these outlines can be adopted for packing in the algorithm whilst the Fourier descriptors produced from analysis of the sourced mining waste could be utilised to create further particle shapes if a limited number of rocks are available.

A main restriction to the proposed method is the massive computational times exhibited. Techniques that could be implemented to increase these speeds were discussed in Section 8.7. Parallelisation can be adopted so that multiple particles or the same particle in multiple positions can be trialled for placement, reducing computational runtime by allowing for the algorithm to do multiple processes at once.

Bitwise operations tend to speed up operations in computer code, and it is thought that these could be utilised for the process of fitting in the discretised stage of the algorithm. Furthermore, caching and memorisation of results can be used for results which are expected to be repeated. This speeds up the algorithm as it does not need to replicate these calculations as the answer is already known.

Section 8.8 discusses the consideration of running joints. Running joints are utilised as a method of quantifying the shear strength in the absence of testing either numerically or physically. This was not included in the objective function due to wanting to keep the numbers of weighting coefficients to a minimum and it was thought that the criteria already specified would lead to higher numbers of running joints disrupted in more optimal solutions. It is suggested in Section 8.8.1 that disruption of running joints can be included in the objective function through the parameter J with coefficient of weighting C_J applied to it. To prevent the creation of running joints being classed as a part of a beneficial criteria (given that running joints are an indication of weaknesses in the structure) J is classed as an integer value where J=1 for each running joint disrupted by the particle placement. With the addition of a new term, the most optimal coefficients for the objective function now becomes a five parameter problem. Therefore, it is suggested optimisation techniques such as SA or GA are employed to find this location in the search area. Additionally, defining running joints at the diagonal is discussed in Section 8.8.2. It is stated that running joints can be identified by rotating the domain by 45^o both anticlockwise and clockwise for analysis and these points represent the maximum limits at which a run can be from the vertical position. Horizontal joints can also be analysed by rotating the domain by 90^o.

Section 8.9.1 discusses the potential of the algorithm as a bin packing solution. It has already been shown that an objective function with coefficients of weighting (C_V=1, C_D=1.6 C_V=0.4, C_{CN}=0.045) can outscore the DBL hueristic for tetrominoes in the Tetris Scenario. Potential lies for the algorithm to be used as a 2BP solution. However, comparison with other heuristics is required and a much more in depth study with other object shapes. Nevertheless, if the algorithm is viewed as a bin packing solution this introduces a novel approach to the 2BP problem. As far as the author is aware, no heuristic for bin packing based on criteria derived from the analysis of soil particle structures that exhibit high shear strength (V_{AB}, D, T and CN) has been utilised in an objective function. Furthermore, Section 8.9.2 discussed the possibility of using the algorithm as a specimen generation method. This could be adopted for areas of research such as DEM modelling where an initial packing of particles is required. Again, as far as the author is aware, no specimen generation approach based on a weighted criteria for determining particle position has been utilised in this way.

The possible uses of the algorithm are further extended in Section 8.10 where the use of the packing method is considered for the backfill of material behind a retaining wall (Section 8.10.1) and the use of other materials with the granular particles (Section 8.10.2) is discussed. The purpose of these sections is to highlight the possibilities of the algorithm and that it is not necessarily restricted to constructing high strength structures out of granular material. Section 8.10.1 states that new criteria for objective function would need to be defined as the purpose of the backfill is to be porous to prevent the build up of pore water pressures behind the retaining wall. For this, review of these structures is needed as was required to derive V_{AB}, D, T and CN. Section 8.10.2 states that using finer materials like those seen in URE could lead to use of the method for constructing temporary inhabitable buildings with the filling of gaps preventing drafts and potentially improving sound insulation.

Finally, for the method to resemble a real-life scenario it is required for packing to be completed in three-dimensions. Section 8.11 recognises this and discusses how the current two-dimensional version could be extended. The parameters in the objective function can be extended with ease and particles can be described by data-point clouds so the technique adopted can remain relatively similar. However, three-dimensional objects presents many more coordinate points which in turn leads to increased computational times which is the main restriction to the method currently. Furthermore, enhancement of the stability checks in the system is required as. One such improvement could be influenced by Liu et al. (2021) where deviation of the normal to the surface and the thrust line is analysed. With the move into three-dimensional packing, it is required that more heuristics are defined. An example of potential heuristic is the need for sloping of the structure. These were observed in Japanese castle walls as discussed in Section 2.2.3 and are commonly seen for larger drystone walls (Vivian, 1976).

Chapter 9

Conclusions and Future Work

9.1 Introduction

This thesis discusses the work conducted on the area of intelligent autonomous construction by robot with the objective to construct structures of irregular, untooled rock that exhibit high shear strengths. Clarification of the required method of construction is made and an algorithm for packing two-dimensional shapes that represent the material has been developed. The aim and objectives for the project were outlined in Chapter 1 and commentary on the conclusions for these objectives are made in Section 9.2.

Further findings of the study that are not directly linked to the aims and objectives are discussed in Section 9.3. After this, suggested future work for the realisation of such a construction technique is given in Section 9.4.

9.2 Reflection on Aims and Objectives

The primary aim of this project was to develop a new system for optimising the placement of irregular, untooled rock within a construction with the emphasis on producing structures with high shear strength. The aim has been met in terms of being able to effectively pack two-dimensional shapes. The approach developed has been tested on tetromino shapes based on the Tetris videogame with an objective function set to achieve minimum void ratio in the system before moving on to packing outlines of soil particle shapes that are set to represent irregular, untooled stones with an objective function prioritising shear strength. The strength of the packed structure is then quantified by the number of running joints disrupted by particles placed above them. The investigation into outlines that replicate irregular untooled rock is inconclusive due to the lack of a heuristic that promotes a layer-by-layer construction technique. Commentary on the objectives set out in Chapter 1 are as follows:

1. The investigation into relevant literature conducted in Chapter 2 provided support that the shear strength of a system and stability of placement of a stone could be described by the following four criteria: void ratio, depth of placement, contact area of the stone touching other objects, and coordination number. As such, these were adopted into an objective function when scoring placements in the algorithm. Furthermore, it was highlighted that stability of the particle is important when constructing and that a stability check should be implemented whilst prioritising placements towards the base of the structure (Furrer et al., 2017; Graton and Fraser, 1935; Liu et al., 2015). Additionally, it

was stated by Adcock (2012) and Vivian (1976) that runs in a drystone wall can lead to instability of the structure. Therefore defining the creation of runs and in turn the disruption of runs by placed particles was adopted as an analysis method for the resulting packings from the algorithm.

2. An algorithm for packing two-dimensional shapes has been produced and is described in Chapter 3. The distance the particle can be lowered from the top of the domain to the placement surface is measured and each position and rotation is given a score based on the objective function. This process was developed to place tetrominoes following rules similar to the Tetris videogame but with a reduced domain height and unlimited time for placing of objects. Chapter 6 demonstrates the efficiency of the packings produced. When compared to random placement as well as the deepest-bottom-left binpacking heuristic, the methods for placement described here produced much lower void ratios in the system. The algorithm was extended to packing soil particles. However this led to a very significant increase in computational time required. Therefore, it was necessary to reduce the number of candidate poses tested for packing. Chapter 6 demonstrates that this approach also works efficiently at packing, as the results produced do have some appearance of fitting nicely together. Unfortunately, as described later, a suitable combination of weighting coefficients was not defined. Nonetheless, the packing algorithm provides a novel method for determining position of two-dimensional shapes in a domain with the use of an objective function defined by parameters that are determined from analysing the strength of soil structures.

   (a) The objective function is set out in equation 3.16 scoring placements on the criteria determined from Objective 1 and listed in Conclusion 1. Placements are successfully scored in the system with each having unique values depending on their positioning. The score is independent of sequential packings of particles. A first-order equation was utilised as it is assumed that these terms will be dominant in the calculation.

   (b) Shapes of both tetrominoes and irregular, untooled rock outlines were packed with effective measure with regards to the objective as void ratio was minimised in the systems. Tetrominoes added geometrical aspects that needed consideration such as orthogonal corners which would not have been highlighted if just soil particle outlines had been studied. As a result, straight-edge corner problems for the tetromino shapes were resolved. It can be concluded that the algorithm has the capability to pack any shape so long as the shape can be described by coordinates in clockwise order and is a closed loop with start and end coordinates being equal. The use of a coordinate system and determining distance the object can be lowered from a fixed height above the domain leads to packing being performed on both concave and convex shapes.

   (c) The use of quantifying the number of running joints has been utilised to detect structures of high shear strength for packings of irregular, untooled rock outlines. However, as determined in Chapter 6, this has not suitable for determining structures of high shear strength. In the algorithm, there is no limitation on height of particles or heuristic that insists on a layer-by-layer process. Therefore, particles can tower above each other which artificially increases the number of runs disrupted in the system. It is recommended that if this study is taken forward, either a new method of verification or a restriction on height of the structure is introduced. Furthermore, packing the domain until it is full would perhaps remove this problem although it is still intended for particles to be packed in a layer-by-layer approach. Verifying the strength of these structures can be done by the method described in Chapter 7. This based testing for the two-dimensional shapes on determining the angle of repose of the structure using a rotating drum method. It is stated that angle of repose can be adopted as an indication of shear strength (Evesque and Rajchenbach, 1989). The equipment has been developed as is presented in Section 7.3. Using this method, structures packed by the algorithm can be compared to randomly packed structures to show that angle of repose is higher for structures packed by the algorithm. Due to time limitations, this method was unfortunately not fully tested in this project.

(d) Tolerance of errors for packings would also be tested using the equipment proposed in Chapter 7 and this is discussed in Section 7.5. It is recognised that placement by a robot will lead to errors in end location of the particle. The purpose of this study would be to show that the error in placement seen by the robot would be negligible to the overall strength of the structure. Methods for measuring effect of error is suggested to be measuring angle of repose using the rotating drum for structures with different levels of particle displacement from original position. The expected results of this would be angle of repose decreasing as the percentage of the particle area displaced increases.

3. Computational runtime is seen as the biggest restriction of this method. Improvements of the algorithm were implemented to reduce this time as described in Section 3.7. A reduced number of coordinates should be adopted as excess amounts of coordinates that provide no use for the definition of the shape massively leads to increased computational times. Particle outlines in this study were reduced from 129 to 44 coordinates. Additionally, runtime was reduced by only utilising the section of the placement surface above the particle and filtering candidate poses using a discretised version of the object and domain and only trialling the 30 best positions from this step. Further techniques that can be introduced are discussed in Section 8.7 such as parallelisation, the use of bitwise operations and storing of results that may be repeated using caching and memorisation.

9.3 Further Findings

Within the study, additional conclusions can be made away from the main objectives set out in Chapter 1.

(C_V=1, C_D=1.6 C_V=0.4, C_{CN}=0.045) is determined to be the optimal solution for the Tetris Scenario, mainly down to the prevention of canyons in the system. Analysis of the packing and the lower MVR value for (C_V=1, C_D=0.6 C_V=0.2, C_{CN}=0.015) led to the recognition that the reduced domain height causes issues as packings are filled. The boundary of the top of the domain leads to sensitivity of results and either less particles being packed or capping of a canyon of void in the system when particles would otherwise be placed elsewhere. When a particle can not fit and the canyon is no capped, this leads to void ratios much lower than other systems and has no indication of the canyon in the structure. Extension of the domain height from 10 squares to 20 squares better resembles the Tetris videogame. Doing so improves the results of packings with V_{AB} as the dominant criteria in the objective function. However, the purpose of this study is to investigate construction of soil particles. If a system where canyons can occur and towers of particles are a feature of the structure, this would be unstable and unsafe. Therefore it is justified that the solution for the Tetris Scenario has dominant $C_D D$ criteria in the objective function. It is also recognised that if the objective was the most efficient packing solution for playing the videogame Tetris, this would include the deletion of rows as they are filled with blocks of particles. With this feature, the sensitivity of results would be much less as created squares of void will later become exposed as rows are deleted and the required accuracy of the weighting coefficients is not as high. It is concluded that the packing algorithm could be taken as a new method for the optimisation of Tetris and moving forward with this investigation would introduce a new heuristic that is based on the features of soil structures that exhibit high shear strengths.

A Gaussian filter was applied to the results of MVR in the Tetris Scenario for determining the optimal combination of weighting coefficients for minimising void in the system. Care is to be taken at the edge of surface plots due to the effect of zero-padding. It is shown that application of the filter helps reduce the sensitivity of the result achieved, as is seen between the difference in results between (C_V=1, C_D=1.6 C_V=0.4, C_{CN}=0.045) and (C_V=1, C_D=0.6 C_V=0.2, C_{CN}=0.015). Although (C_V=1, C_D=0.6 C_V=0.2, C_{CN}=0.015) suggested better packing structures when analysing the unfiltered data, this location was very sensitive to change of coefficients for the surrounding datapoints. Analysis of the results shows canyoning occurs in the system for these coefficients meaning that the addition of an extra particle to cap this area of void would lead to a massive increase in void ratio. Although (C_V=1, C_D=1.6 C_V=0.4, C_{CN}=0.045) scored slightly higher in terms of void ratio, canyoning did not occur thanks to the additional scoring of $C_D D$ in the objective function. Overall, the packings produced using coefficients (C_V=1, C_D=1.6 C_V=0.4, C_{CN}=0.045) was seen to outperform other combinations.

For the Tetris Scenario, T is detected to act as another method of quantifying the void in the system. It was seen that when C_V was made a zero value and therefore negating the impact of V_{AB} in the objective function that values of T increased for the location of results of the lowest MVR value for equivalent C_D values. As tetrominoes have orthogonal shapes, this is understandable as the number of contacts the particle has with other particles and the domain means less change for void to be created below the object. However, no recognition of the size of the void created is enacted. Therefore if void is present below the particle then scoring of position is equivalent for 1 square of void or a canyon of void equivalent to 1 squares width. This is not the case for the Soil Particle Scenario as shapes are described by perfectly orthogonal particles and therefore will not sit flush with each other. For the Tetris Scenario, $C_V V_{AB}$ tends to be more dominant in the objective function for more optimal solutions compared to $C_T T$ and $C_{CN} CN$ whereas $C_D D$ is more dominant as it is required to prevent canyoning in the system. However, it is recognised that D has a diminishing effect as packing increases height of the placement surface due to being a ratio to domain height. Section 8.5.1 presents a new method for quantifying depth, D_m, and it is thought that adopting this parameter would reduce the required value of coefficient C_D.

The required sample size to represent the population data is determined to be n=30 in Chapter 4. This follows the rule of thumb generally seen in statistics. This is proven for the case of the Tetris Scenario but not for the Soil Particle Scenario. A very small difference from the mean of the samples taken is shown to represent the data with 95% confidence interval for n=30. A range of 0.92 squares of the void either side of the mean void average value of 3.7 from a spectrum of results experienced seen for packings produced by the algorithm can achieve this. This is very reasonable given the minimum difference in void ratio possible in the Tetris Scenario is 1 square. A sample size of n=30 is not adopted for the Soil Particle Scenario due to time limitations in the project.

Comparison of the algorithm with the deepest-bottom-left heuristic as a control measure leads to the conclusion that the algorithm is more optimal for packing tetrominoes. From this, it can be implied that the packing of by objective function based on the features of high shear strength in soil could be an efficient bin packing solution. Further research is required in this topic and different shapes compared to orthogonal tetrominoes is vital. On the other hand, introducing such a method would be a novel approach for achieving solutions of 2BP problems. For the Soil Particle Scenario, the reduced number of candidate poses creates issues with packing that take away from this being a good bin packing solution. Further candidate poses are needed to be trialled for this to be proven further. Also, potential lies that the algorithm could be adopted as a specimen generation approach for such fields as DEM modelling where an initial layout of particles is required. This would be a novel approach when it comes to specimen generation.

From the review of the literature, it was also deduced that angular particles would lead to stronger shear strengths in a soil structure as more interlocking is present between particles when the force is applied. However, this was not included in the consideration when packing as it is not known the sort of material that would be accessible on site. Section 8.6.1 discusses selecting particles for packing based on their angularity which could be implemented into the algorithm it is known that a wide selection of material is to be available. Angularity can be determined using the definition for circularity from Wadell (1933) (as cited by Blott and Pye, 2008). This method is selected over others such as Lees (1964) due to removal of the need for the algorithm to detect corners which is stated to be complex for shapes with lots of convexities and concavities. Additionally, elongation (Li et al., 2013; Potticary et al., 2016) and irregularity (Barrett, 1980; Cho et al., 2006) can also be used to quantify the particle shape.

Inspiration for the method was taken from the study conducted in Chapter 2. A top-down method for packing is seen in Jakobs (1996), Liu and Teng (1999), and Wang and Hauser (2019) and it is clearly defined that this approach will be needed Furthermore, the inspiration for discretising the particle to attempt a quick method of fitting is taken from Cagan et al. (1998) and Kong and Kimia (2001). This method with the use of the hierarchical filtering of candidate poses led to much faster computational speeds and the improvement of accuracy of placement of the particle. However, it is found that the number of candidate poses selected - taken as 30 - should be increased due to issues when packing in the Soil Particle Scenario.

Also concluded from the analysis of the literature was the need for a stability check by the algorithm. This helps prevent against collapse of the structure whilst construction is taking place. The stability check employed is based on that in Wang and Hauser (2019) which uses a Coulomb friction model based on the coefficient of friction. Points of contact of the particle with the placement surface are taken and sliding is determined based on the weight of the particle, which is assumed to be Gneiss boulders. If the centre of gravity of the particle lies outside the contact points with the surface it is shown that toppling will occur and an additional factor of safety was applied to prevent close-to-unstable placements. A main recommendation to the reader is an improvement on these stability checks to ensure unstable positions are avoided. Liu et al. (2021) is cited to have approaches that could prevent this by taking particles whose does not allow placement of particles who dismisses positions where the deviation of the normal to the surface is greater than the mean value. Additionally, particles whose contact area with other particles is lower than the mean value are not taken into consideration. The hierarchical filter reduces candidate poses in the order of the discretised particle score, the depth in the system, the left-most position, area beneath the particle, and the width-to-height ratio for which any particles with a height greater than double the width being removed as these are more likely to topple and therefore be unstable.

Results of the Soil Particle Scenario suggest that there is no relationship between the number of running joints disrupted in the system and void ratio. This is true as low void ratio does not necessarily mean overlapping of particles above where other particles meet. However, it was thought that tighter packings would lead to more occasions where this occurs in irregular particles. It is recommended that a different measure of shear strength be found, perhaps through physics simulations or discrete element modelling analysis. Of these, a physics simulator would allow for easy calculation of stability of the particle.

The allowing of varying heights of the structure has led to the quantifying of mean number of disrupted runs in the structure not have any real meaning of value. For the future, a layer-by-layer packing process needs to be enforced using a better method than increasing C_D in the objective function. Using an outline of intended final shape can be adopted. Alternatively, it is recommended that particles are only allowed to be positioned in a layer of three particles high. Once this layer is filled by a certain number area, the allowed packing zone increases and positioning can continue up the structure.

Reducing the number of candidate poses for the positioning of particles has led to further issues with packing. Less stable positions can be detected whilst the use of the discretised method has led to positions being classified as unsuitable when they may later lead to good fits. The number of candidate poses should be increased. This highlights the vast need for an improvement in computational time for the method to allow for this to take place.

9.4 Future Work

The impact of the construction industry on the environment is currently unsustainable with regards to greenhouse gas emissions and the consumption of finite resources. Production of the algorithm in this thesis is intended to show that there is scope for a more intelligent method that looks to minimise material use by optimising the fabric of the structure. A demand for techniques which reduce cost to the environment is emerging. Work around this area has already shown that such a method is indeed a possibility, with Johns et al. (2023) being an example and precedent. However, the structures made in Johns et al. (2023) leave room for improvement of their function to truly minimise quantities of material by optimising the placement of particles. The conclusions made in this report are far away from providing a solution to the issue but present initial steps towards one.

For the algorithm to truly optimise shear strength, further methods can be implemented into the heuristics and analysis. The use of a backtracking method or simply trialling multiple particles rather than placing in the given particle delivery order is thought to improve overall shear strength as more optimal particles will be utilised. Furthermore, characterisation of the particles with the intention of discarding those deemed unsuitable or tooling them to become suitable is another step that would improve the structures.

It is known that angular particles when packed tightly result in higher shear strengths of a soil structure. Improved strengths result from the interlocking between particles and the restriction of movement without the need for dilation of the system. On the otherhand, more angular particles may be hard to pack due to a reduction in flatter surfaces and increase in sharp corners creating fewer stable positions for packing. Further studies on the impact of particle shape in the system is required by characterising the particles. Systems with very angular particles can be compared to systems with less angular and rounded particles. From this, it can be deduced if constructing with angular particles is feasible and to if there is a level of angularity where the lack of matching edges between particles results in suffering of the overall strength. Through the methods discussed in Section 8.4.2, unsuitable particles - perhaps due to being a level of angularity and irregularity so that fitting in the system can not be achieved - can be discarded or tooled to become a shape that can be utilised in the packing.

A piece-by-piece method of particle placement leads to possibility of strategic reinforcement in the system. From numerical analysis, areas of weakness in the packing can be identified and the application of a reinforcement can be conducted. This can either be through the use of a adhesive material such as concrete or placement of a geotextile. Trialling of construction samples with reinforcement applied in areas specified by the analysis will investigate this area and the suitability of including this in the process of autonomous construction. Although it is desired to remove the need for additional material, strategic reinforcement will reduce material use compared to uniform reinforcement across a given area.

Currently the main restriction for the method is the computational time required to determine packing by the algorithm. For packing in the Tetris Scenario where particles were defined by a limited number of coordinates, runtime were seen to be fast with time taken to pack 30 particles equating to roughly 3.7 seconds. For the Soil Particle Scenario, much larger runtimes were experienced taking up to 50 minutes to pack 40 particles. Such lengths of time are unsuitable for real-time construction. Methods were implemented to reduce this runtime. However it is suggested that further steps should be taken for this, especially for the extension from two-dimensions into three-dimensions as this will add additional considerations and particle form to be analysed. These are discussed in Section 8.7 and it suggested further levels of computer programming are employed with the inclusion of parallelisation as well as bitwise operations for fitting in discretised system and caching and memorisation of results which are likely to repeat themselves.

With the increase in computational speeds, the extension of the algorithm to be able to pack in three-dimensions can be applied and suggested packings can start to resemble real-life scenarios. As a result, further heuristics for consideration when packing in three-dimensions are required such as an improvement to stability checks to ensure stability in all directions as well as considering the shape of the three-dimensional shape as it is seen that retaining wall structures tend to have sloped profiles. A more extensive review into these structures and their requirements and features that contribute to shear strength will be needed for producing three-dimensional heuristics.

The decision to use an objective function leaves possibility for the method to be adapted for construction of structures where it is not designed for shear strength to be maximised and instead another target can be set. For example, it is seen that retaining wall structures tend to have backfill with purpose to increase permeability to prevent the build up of water behind the structure. Section 8.10.1 discusses the use of the packing method for designing such a matrix if the criteria in the objective function are developed to represent features commonly seen in soil structures with high permeability. It is suggested that an autonomous construction approach could be used for these structures as well although this may not lead to improvements on current methods for backfilling retaining walls. Nevertheless, this example is given to highlight the possibilities that are presented by the investigation into an autonomous construction method and open-endedness of such a technique.

Bibliography

Abeysooriya, Ranga P., Julia A. Bennell, and Antonio Martinez-Sykora (2018). "Jostle heuristics for the 2D-irregular shapes bin packing problems with free rotation". In: *International Journal of Production Economics* 195, pp. 12–26. ISSN: 0925-5273. DOI: 10.1016/j.ijpe.2017.09.014. URL: https://doi.org/10.1016/j.ijpe.2017.09.014.

Adcock, Sean (2012). *Stonework: A technical guide to standards and identification of common faults in dry stone walling*. Tech. rep. Dry Stone Walling Association North Wales Branch. URL: https://www.drystonewalling.wales/wp-content/uploads/2017/01/StoneworkPDF24.pdf.

Al-Hashemi, Hamzah M. and Ahmed H. Bukhary (2016). "Correlation between California Bearing Ratio (CBR) and angle of repose of granular soil". In: *Electronic Journal of Geotechnical Engineering* 21, pp. 5655–5560. ISSN: 10893032.

Al-Hashemi, Hamzah M Beakawi and Omar S Baghabra Al-Amoudi (2018). "A review on the angle of repose of granular materials". In: *Powder Technology* 330, pp. 397–417. ISSN: 1873328X. DOI: 10.1016/j.powtec.2018.02.003.

Al-Hashemi, Hamzah M Beakawi and Omar S Baghabra Al-Amoudia (2018). "On the Applications of the Angle of Repose in Civil Engineering". In: *6th African Young Geotechnical Engineering Conference*. Khartoum.

Alejano, L. R. et al. (2012). "Stability of granite drystone masonry retaining walls: I. Analytical design". In: *Geotechnique* 62.11, pp. 1013–1025. ISSN: 00168505. DOI: 10.1680/geot.10.P.112.

Alexander, Shlomo (1998). "Amorphous solids: their structure, lattice dynamics and elasticity". In: *Physics Reports* 296.2-4, pp. 65–236. DOI: 10.31399/asm.cp.istfa2015p0270.

Alias, R, A Kasa, and M R Taha (2014). "Particle Size Effect on Shear Strength of Granular Materials in Direct Shear Test". In: *International Journal of Civil, Architectural, Structural and Construction Engineering* 8.11, pp. 1084–1087.

Alshibli, Khalid A. and Mehmet B. Cil (2018). "Influence of Particle Morphology on the Friction and Dilatancy of Sand". In: *Journal of Geotechnical and Geoenvironmental Engineering* 144.3. ISSN: 1090-0241. DOI: 10.1061/(asce)gt.1943-5606.0001841.

Alshibli, Khalid A. et al. (2014). "Quantifying Morphology of Sands Using 3D Imaging". In: *Journal of Materials in Civil Engineering* 27.10. ISSN: 0899-1561. DOI: 10.1061/(asce)mt.1943-5533.0001246.

Amano, K. et al. (2000). "Historical and empirical study on Osaka Castle masonry wall at Tokugawa period". In: *Journal of Construction Management and Engineering* 660, pp. 101–110.

Azéma, Emilien et al. (2017a). "Does modifying the particle size distribution of a granular material (i.e., material scalping) alters its shear strength?" In: *Powders and Grains 2017 – 8th International Conference on Micromechanics on Granular Media*. Vol. 140. Montpellier: EPJ Web of Conferences. DOI: 10.1051/epjconf/201714006001.

– (2017b). "Shear strength and microstructure of polydisperse packings: The effect of size span and shape of particle size distribution". In: *Physical Review E* 96.2. ISSN: 24700053. DOI: 10.1103/PhysRevE.96.022902.

Balan, K. (1995). "Studies on engineering behaviour and uses of geotextiles with natural fibres". PhD Thesis. Indian Institute of Technology, Delhi.

Ballantyne, Colin K. (1982). "Aggregate clast form characteristics of deposits near the margins of four glaciers in the Jotunheimen Massif, Norway". In: *Norsk Geografisk Tidsskrift* 36.2, pp. 103–113. ISSN: 15025292. DOI: 10.1080/00291958208621960.

Barrett, P. J. (1980). "The shape of rock particles, a critical review". In: *Sedimentology* 27.3, pp. 291–303. ISSN: 13653091. DOI: 10.1111/j.1365-3091.1980.tb01179.x.

Bayat, E. and M. Bayat (2013). "Effect of grading characteristics on the undrained shear strength of sand: Review with new evidences". In: *Arabian Journal of Geosciences* 6, pp. 4409–4418. ISSN: 18667511. DOI: 10.1007/s12517-012-0670-y.

Bdolah, Yael and Dror Livnat (2000). *Reinforcement Learning Playing Tetris*. URL: http://www.math.tau.ac.il/$\sim$mansour/rl-course/student_proj/livnat/tetris.html (visited on 11/22/2023).

Beasley, David, David R Bull, and Ralph R Martin (1993). "An Overview of Genetic Algorithms: Part 1, Fundamentals". In: *University Computing* 15.2, pp. 58–69.

Beasley, J E (1985). "An Exact Two-Dimensional Non-Guillotine Cutting Tree Search Procedure". In: *Operations Research* 33.1, pp. 49–64.

Bellare, Mihir and Phillip Rogaway (1995). "The complexity of approximating a non-linear program". In: *Mathematical Programming* 69, pp. 429–441. ISSN: 14364646. DOI: 10.1007/BF01585569.

Berkey, J. O. and P. Y. Wang (1987). "Two-Dimensional Finite Bin-Packing Algorithms". In: *Operations Research Society* 38.5, pp. 423–429.

Bishop, A.W. (1954). "Correspondence on shear characteristics of a saturated silt, measured in triaxial compression". In: *Géotechnique* 4.1, pp. 43–45.

Bjerrum, L., S. Kringstad, and O. Kummeneje (1961). "The Shear Strength of a Fine Sand". In: *5th International Conference on Soil Mechanics and Foundation Engineering*. Paris, pp. 29–37.

Blott, Simon J. and Kenneth Pye (2008). "Particle shape: A review and new methods of characterization and classification". In: *Sedimentology* 55, pp. 31–63. ISSN: 00370746. DOI: 10.1111/j.1365-3091.2007.00892.x.

Boef, Edgar den et al. (2005). "Erratum: "The three-dimensional bin packing problem": Robot-packable and orthogonal variants of packing problems". In: *Operations Research* 53.4, pp. 735–736. ISSN: 0030364X. DOI: 10.1287/opre.1050.0210.

Böhm, Niko, Gabriella Kóokai, and Stefan Mandl (2005). "An Evolutionary Approach to Tetris". In: *Proceedings of the 6th Metaheuristics International Conference (MIC2005)*. Vienna, pp. 137–148. ISBN: 2959977688.

Bolton, M.D. (1986). "The strength and dilatancy of sands". In: *Géotechnique* 36.I, pp. 65–78.

Bordoloi, Sanandam, Ankit Garg, and Sreedeep Sekharan (2017a). "A Review of Physio-Biochemical Properties of Natural Fibers and Their Application in Soil Reinforcement". In: *Advances in Civil Engineering Materials* 6.1, pp. 323–359. ISSN: 2379-1357. DOI: 10.1520/ACEM20160076. URL: https://doi.org/10.1520/ACEM20160076.

Bordoloi, Sanandam et al. (2017b). "Infiltration characteristics of natural fiber reinforced soil". In: *Transportation Geotechnics* 12, pp. 37–44. ISSN: 22143912. DOI: 10.1016/j.trgeo.2017.08.007. URL: http://dx.doi.org/10.1016/j.trgeo.2017.08.007.

Bowman, E. T., K. Soga, and W. Drummond (2001). "Particle shape characterisation using Fourier descriptor analysis". In: *Geotechnique* 51.6, pp. 545–554. ISSN: 00168505. DOI: 10.1680/geot.2001.51.6.545.

Bowman, JC and A Hammerlindl (2008). "Asymptote: A vector graphics language". In: *TUGboat: The Communications of the TEX Users* 29.2, pp. 288 –294. URL: http://scholar.google.com/scholar?hl=en&btnG=Search&q=intitle:Asymptote:+A+vector+graphics+language#0.

Bowman, John C. and Orest Shardt (2009). "Asymptote: Lifting TEX to three dimensions". In: *TUGboat: The Communications of the TEX Users* 30.1, pp. 58–63. URL: https://www.tug.org/donate.htmm.

Brandes, H G (2011). "Simple Shear Behavior of Calcareous and Quartz Sands". In: *Geotechnical and Geological Engineering* 29, pp. 113–126. DOI: 10.1007/s10706-010-9357-x.

Breukelaar, Ron et al. (2004). "Tetris is hard, even to approximate". In: *International Journal of Computational Geometry and Applications* 14.1, pp. 41–68. ISSN: 02181959. DOI: 10.1142/s0218195904001354. arXiv: 0210020 [cs].

Brzustowski, John (1988). "Can you win at Tetris?" Masters of Science. University of British Columbia.

Buffington, John M., William E. Dietrich, and James W. Kirchner (1992). "Friction angle measurements on a naturally formed gravel streambed: Implications for critical boundary shear stress". In: *Water Resources Research* 28.2, pp. 411–425. ISSN: 19447973. DOI: 10.1029/91WR02529.

Burgiel, Heidi (1997). "How to lose at Tetris". In: *The Mathematical Gazette* 81.491, pp. 194–200. ISSN: 0025-5572. DOI: 10.2307/3619195.

Burgoyne, J. (1853). *Revetments or retaining walls*.

Cabalar, Ali Firat, Kemal Dulundu, and Kagan Tuncay (2013). "Strength of various sands in triaxial and cyclic direct shear tests". In: *Engineering Geology* 156, pp. 92–102. ISSN: 0013-7952. DOI: 10.1016/j.enggeo.2013.01.011. URL: http://dx.doi.org/10.1016/j.enggeo.2013.01.011.

Cagan, Jonathan, Drew Degentesh, and Su Yin (1998). "A simulated annealing-based algorithm using hierarchical models for general three-dimensional component layout". In: *Computer Aided Design* 30.10, pp. 781–790. ISSN: 00104485. DOI: 10.1016/S0010-4485(98)00036-0.

Cailleux, A. (1945). "L'indice d'émoussé des grains de sable et grés". In: *Rev. Géomorph. Dyn.* 3, pp. 78–87.

Caquot, Albert Irénée (1934). *Équilibre des massifs à frottement interne*. Paris.

Carr, Donald (2005). "Adapting reinforcement learning to Tetris". Bachelor of Science (Honours). Rhodes University.

Carrigy, Maurice A. (1970). "Experiments on the Angles of Repose of Granular Materials". In: *Sedimentology* 14.3-4, pp. 147–158. ISSN: 13653091. DOI: 10.1111/j.1365-3091.1970.tb00189.x.

Cartwright, Mark (2016). *Sacayhuaman*. URL: https://www.worldhistory.org/Sacsayhuaman/ (visited on 03/22/2023).

Castro, Jaime, Luis E. Vallejo, and Nicolas Estrada (2017). "Mechanical analysis of the dry stone walls built by the Incas". In: *EPJ Web of Conferences* 140.Powders and Grains 2017 – 8th International Conference on Micromechanics on Granular Media. ISSN: 2100014X. DOI: 10.1051/epjconf/201714006012.

– (2019). "The optimal design of the retaining walls built by the Incas in their agricultural terraces". In: *Journal of Cultural Heritage* 36, pp. 232–237. ISSN: 12962074. DOI: 10.1016/j.culher.2018.09.013. URL: http://dx.doi.org/10.1016/j.culher.2018.09.013.

Chan, Leonard C.Y. and Neil W. Page (1997). "Particle fractal and load effects on internal friction in powders". In: *Powder Technology* 90.3, pp. 259–266. ISSN: 00325910. DOI: 10.1016/S0032-5910(96)03228-7.

Chang, Horng Jinh, Kuo Chung Huang, and Chao Hsien Wu (2006). "Determination of sample size in using central limit theorem for weibull distribution". In: *International Journal of Information and Management Sciences* 17.3, pp. 31–46. ISSN: 10171819.

Chau, C. K., T. M. Leung, and W. Y. Ng (2015). "A review on life cycle assessment, life cycle energy assessment and life cycle carbon emissions assessment on buildings". In: *Applied Energy* 143.1, pp. 395–413. ISSN: 03062619. DOI: 10.1016/j.apenergy.2015.01.023.

Chazelle, Bernard (1983). "The bottom-left bin-packing heuristic: an efficient implementation". In: *IEEE Transactions on Computers* 32.8, pp. 697–707.

Chen, Jianbin, Jiayu Peng, and Dennis K.J. Lin (2021). "A statistical perspective on non-deterministic polynomial-time hard ordering problems: Making use of design for order-of-addition experiments". In: *Computers and Industrial Engineering* 162, p. 107773. ISSN: 03608352. DOI: 10.1016/j.cie.2021.107773. URL: https://doi.org/10.1016/j.cie.2021.107773.

Cheng, Nian-Sheng and Kuifeng Zhao (2017). "Difference between static and dynamic angle of repose of uniform sediment grains". In: *International Journal of Sediment Research* 32, pp. 149–154. ISSN: 10016279. DOI: 10.1016/j.ijsrc.2016.09.001.

Cheng, Y. P., Y. Nakata, and M. D. Bolton (2003). "Discrete element simulation of crushable soil". In: *Geotechnique* 53.7, pp. 633–641. ISSN: 00168505. DOI: 10.1680/geot.2003.53.7.633.

Cho, Gye Chun, Jake Dodds, and J. Carlos Santamarina (2006). "Particle shape effects on packing density, stiffness, and strength: Natural and crushed sands". In: *Journal of Geotechnical and Geoenvironmental Engineering* 132.5, pp. 591–602. ISSN: 10900241. DOI: 10.1061/(ASCE)1090-0241(2006)132:5(591).

Chung, F. R. K., M. R. Garey, and D. S. Johnson (1982). "On packing two-dimensional bins". In: *SIAM Journal on Algebraic Discrete Methods* 3.1, pp. 66–76.

Clark, M. R. (1981). "Quantitative shape analysis: a review". In: *Math. Geo.* 13.4, pp. 303–320.

Clarke, G. and J. W. Wright (1964). "Scheduling of Vehicles from a Central Depot to a Number of Delivery Points". In: *Operations Research* 12.4, pp. 568–581. ISSN: 0030-364X. DOI: 10.1287/opre.12.4.568.

Clifford, Brandon, Wes McGee, and Mackenzie Muhonen (2018). "Recovering Cannibalism in Architecture with a Return to Cyclopean Masonry". In: *Nexus Network Journal* 20.3, pp. 583–604. ISSN: 15224600. DOI: 10.1007/s00004-018-0392-x. URL: https://doi.org/10.1007/s00004-018-0392-x.

Coffman, E. G. Jr. et al. (1980). "Performance Bounds for Level-Oriented Two-Dimensional Packing Algorithms". In: *SIAM Journal on Computing* 9.4, pp. 808–826. ISSN: 0097-5397. DOI: 10.1137/0209062.

Coulomb, Charles-Augustin (1776). *Memoires de mathematique et de physique, presentes a l'Academie royale des sciences, par divers scavans et lus dans ses assemblees*. Academie R. Des. Sci. 7: Paris., pp. 343–382.

Cousins, Stephen (2019). "Shifting sand: Why we're running out of aggregate". In: *Construction Research and Innovation* 10.3, pp. 69–71. ISSN: 2045-0249. DOI: 10.1080/20450249.2019.1656448. URL: https://doi.org/10.1080/20450249.2019.1656448.

Crainic, Teodor Gabriel, Guido Perboli, and Roberto Tadei (2008). "Extreme point-based heuristics for three-dimensional bin packing". In: *INFORMS Journal on Computing* 20.3, pp. 368–384. ISSN: 15265528. DOI: 10.1287/ijoc.1070.0250.

Cramb, I. (1992). *The Art of the Stonemason*. Alan C. Hood.

Creative Commons (2011). *Attribution-ShareAlike 2.0 Generic International Copyright Information*. URL: https://creativecommons.org/licenses/by-sa/2.0/ (visited on 01/23/2024).
– (2013a). *Attribution-NonCommercial 4.0 International Copyright Information*. URL: https://creativecommons.org/licenses/by-nc/4.0/ (visited on 01/26/2024).
– (2013b). *Attribution-NonCommercial-NoDerivs 4.0 International Copyright Information*. URL: https://creativecommons.org/licenses/by-nc-nd/4.0/ (visited on 05/09/2024).
– (2013c). *Attribution-ShareAlike 4.0 International Copyright Information*. URL: https://creativecommons.org/licenses/by-sa/4.0/ (visited on 08/03/2023).
– (2014). *Attribution-ShareAlike 3.0 Unported (CC BY-SA 3.0)*. URL: http://creativecommons.org/licenses/by-sa/3.0/ (visited on 08/03/2023).
Csirik, J. and G. Woeginger (1998). "On-line packing and covering problems". In: *Online algoirthms*. Vol. 142. Berlin: Springer, pp. 147–177.
Cubrinovski, Misko and Kenji Ishihara (2002). "Maximum and minimum void ratio characteristics of sands". In: *Soils and Foundations* 42.6, pp. 65–78. ISSN: 00380806. DOI: 10.3208/sandf.42.6_65.
Cui, Liang and Catherine O'Sullivan (2003). "Analysis of a triangulation based approach for specimen generation for discrete element simulations". In: *Granular Matter* 5.3, pp. 135–145. ISSN: 14345021. DOI: 10.1007/s10035-003-0145-7.
Cundall, P. A. and O. D.L. Strack (1979). "A discrete numerical model for granular assemblies". In: *Geotechnique* 29.1, pp. 47–65. ISSN: 17517656. DOI: 10.1680/geot.1980.30.3.331.
Das, Braja (2014). *Principles of Geotechnical Engineering*. 8th. Cengage Learning. ISBN: 9781133108665.
Das, Nivedita (2007). "Modeling three-dimensional shape of sand grains using discrete element method". Doctoral Thesis. University of South Florida.
Das, Nivedita and Alaa K. Ashmawy (2007). "Relationship between Grain Size and Shape of Natural and Crushed Sand". In: *GeoDenver 2007: Advances in Measurement and Modeling of Soil Behavior*. Denver: American Society of Civil Engineers, pp. 1–10. DOI: 10.1061/40917(236)25.
Day, Robert W. (2010). *Foundation Engineering Handbook: Design and Construction with the 2009 International Building Code*. 2nd. New York: McGraw Hill Education. ISBN: 9788578110796. DOI: 10.1017/CBO9781107415324.004. arXiv: arXiv:1011.1669v3.
De Cani, Phillip (1978). "A Note on the Two-Dimensional Rectangular Cutting-Stock Problem". In: 29.7, pp. 703–706.
Delorme, Maxence, Manuel Iori, and Silvano Martello (2016). "Bin packing and cutting stock problems: Mathematical models and exact algorithms". In: *European Journal of Operational Research* 255.1, pp. 1–20. ISSN: 03772217. DOI: 10.1016/j.ejor.2016.04.030. URL: http://dx.doi.org/10.1016/j.ejor.2016.04.030.
Deng, Zhao et al. (2012). "Adhesion-dependent negative friction coefficient on chemically modified graphite at the nanoscale". In: *Nature Materials* 11, pp. 1032–1037. DOI: https://doi.org/10.1038/nmat3452.
Dobkins, James E. and Robert L. Folk (1970). "Shape development on Tahiti-nui". In: *Journal of Sedimentary Research* 40.4, pp. 1167–1203.
Dorren, Luuk K.A. and Arie C. Seijmonsbergen (2003). "Comparison of three GIS-based models for predicting rockfall runout zones at a regional scale". In: *Geomorphology* 56, pp. 49–64. ISSN: 0169555X. DOI: 10.1016/S0169-555X(03)00045-X.
Dowsland, K. A., W. B. Dowsland, and J. A. Bennell (1998). "Jostling for position: Local improvement for irregular cutting patterns". In: *Journal of the Operational*

Research Society 49, pp. 647–658. ISSN: 14769360. DOI: 10.1057/palgrave.jors.2600563.

Driessens, Kurt (2004). "Relational Reinforcement Learning". PhD thesis. Catholic University of Leuven. URL: http://www.cs.kuleuven.ac.be/kurtd/PhD/.

Duncan, James Michael, Stephen G. Wright, and Thomas L. Brandon (2014). *Soil strength and slope stability*. Second Edi. Hoboken, New Jersy: Wiley.

Dunn, E.J. (1911). *Pebbles*. Melbourne: Robertson, p. 122.

Edwards, S. F. (1998). "The equations of stress in a granular material". In: *Physica A: Statistical Mechanics and its Applications* 249.1-4, pp. 226–231. ISSN: 03784371. DOI: 10.1016/S0378-4371(97)00469-X.

Ehrlich, R. and B. Weinberg (1970). "An exact method for characterization of grain shape". In: *Sediment. Petrol.* 40.1, pp. 205–212.

Eid, Hisham T. et al. (2000). "Municipal Solid Waste Slope Failure. I: Waste and Foundation Soil Properties". In: *Journal of Geotechnical and Geoenvironmental Engineering* 126.5, pp. 397–407.

Eisemann, Kurt (1957). "The Trim Problem". In: *Management Science* 3, pp. 279–284.

Environmental Action Foundation (2019). *Dry Stone Walls: Basics, Construction, Significance*. Scheidegger & Spiess.

EPA (2020). *Advancing Sustainable Materials Management: 2018 Fact Sheet*. Tech. rep. United States Environmental Protection Agency. Office of Resource Conservation and Recovery. URL: https://www.epa.gov/facts-and-figures-about-materials-waste-and-recycling/advancing-sustainable-materials-management.

Erlingsson, S and B Magnusdottir (2002). "Dynamic triaxial testing of unbound granular base course materials". In: *Proceedings of the 6th International Conference on the Bearing Capacity of Roads and Airfields*. Lisbon, pp. 989–1000.

Evesque, P. and J. Rajchenbach (1989). "Instability in a sand heap". In: *Physical Review Letters* 64, pp. 44–46. ISSN: 00319007. DOI: 10.1103/PhysRevLett.62.44.

Fahey, Colin (2012). *Tetris*. URL: www.colinfahey.com/tetris/.html (visited on 11/22/2023).

Fencl, Zdeněk (1973). "Algorithm 456: Routing Problem". In: *Communications of the ACM* 16.9, pp. 572–574. ISSN: 15577317. DOI: 10.1145/362342.362365.

Feng, Y. T., K. Han, and D. R.J. Owen (2003). "Filling domains with disks: An advancing front approach". In: *International Journal for Numerical Methods in Engineering* 56.5, pp. 699–713. ISSN: 00295981. DOI: 10.1002/nme.583.

Fernandes, J., R. Mateus, and L. Bragança (2013). "The potential of vernacular materials to the sustainable building design". In: *Vernacular Heritage and Earthen Architecture*. 1st Editio. London: Taylor & Francis, pp. 623–629. ISBN: 9781482229097. DOI: 10.1201/b15685.

Fernandes, Jorge et al. (2019). "Life cycle analysis of environmental impacts of earthen materials in the Portuguese context: Rammed earth and compressed earth blocks". In: *Journal of Cleaner Production* 241. ISSN: 09596526. DOI: 10.1016/j.jclepro.2019.118286.

Ferrez, Jean-Albert (2001). "Dynamic triangulations for efficient 3D simulation of granular materials". Ph. D. Thesis. Ecole Polytechnique Federal de Lausanne, pp. 1–159. URL: http://infoscience.epfl.ch/record/32908/files/EPFL_TH2432.pdf.

Fisher, R. et al. (2008). *Gaussian Smoothing*. URL: https://homepages.inf.ed.ac.uk/rbf/HIPR2/gsmooth.htm (visited on 02/01/2024).

Fonseca, J et al. (2016). "Image-based investigation into the primary fabric of stress-transmitting particles in sand". In: *Soils and Foundations* 56.5, pp. 818–834. ISSN:

0038-0806. DOI: `10.1016/j.sandf.2016.08.007`. URL: `http://dx.doi.org/10.1016/j.sandf.2016.08.007`.

Fontanese, Melissa M. (2007). "A Stability Analysis of the Retaining Walls of Machu Picchu". Master of Science. University of Pittsburgh.

Freeman, H. and L. Garder (1964). "Apictorial Jigsaw Puzzles: The Computer Solution of a Problem in Pattern Recognition". In: *IEEE Transactions on Electronic Computers* EC-13.2, pp. 118–127. ISSN: 03677508. DOI: `10.1109/PGEC.1964.263781`.

Frenk, J. B.G. and G. Galambos (1987). "Hybrid next-fit algorithm for the two-dimensional rectangle bin-packing problem". In: *Computing* 39.3, pp. 201–217. ISSN: 0010485X. DOI: `10.1007/BF02309555`.

Fuellerer, Guenther et al. (2010). "Metaheuristics for vehicle routing problems with three-dimensional loading constraints". In: *European Journal of Operational Research* 201.3, pp. 751–759. ISSN: 03772217. DOI: `10.1016/j.ejor.2009.03.046`.

Fujioka, Michio (1969). *Japanese Castles*. Third Edit. Osaka: Hoikusha Publishing.

Furrer, Fadri et al. (2017). "Autonomous robotic stone stacking with online next best object target pose planning". In: *International Conference on Robotics and Automation*. Singapore: IEEE, pp. 2350–2356. ISBN: 9781509046331. DOI: `10.1109/ICRA.2017.7989272`.

Galambos, G. and G. J. Woeginger (1993). "Repacking helps in bounded space online bind-packing". In: *Computing* 49.4, pp. 329–338. ISSN: 0010485X. DOI: `10.1007/BF02248693`.

Gambosi, Giorgio, Alberto Postiglione, and Maurizio Talamo (1990). "New algorithms for on-line bin packing". In: *Algorithms and Complexity, Proceedings of the First Italian Conference*. Singapore: World Scientific, pp. 44–59.

Garey, M.R. and D.S. Johnson (1979). *Computers and Intractability (A Guide to the theory of NP-Completeness)*. San Francisco: W.H. Freeman and Company.

Gaw, Bryan Gerald and Sofia Andrea Zamora-Palacios (2010). "Soil Reinforcement with Natural Fibers for Low-Income Housing Communities". Bachelor of Science. Worcester Polytechnic Institute.

Geldart, D. et al. (2006). "Characterization of powder flowability using measurement of angle of repose". In: *China Particuology* 4.3, pp. 104–107. ISSN: 16722515. DOI: `10.1016/s1672-2515(07)60247-4`.

Gendreau, Michel et al. (2006). "A tabu search algorithm for a routing and container loading problem". In: *Transportation Science* 40.3, pp. 342–350. ISSN: 15265447. DOI: `10.1287/trsc.1050.0145`.

George, J. A. and D. F. Robinson (1980). "A heuristic for packing boxes into a container". In: *Computers and Operations Research* 7.3, pp. 147–156. ISSN: 03050548. DOI: `10.1016/0305-0548(80)90001-5`.

Gilmore, P.C. and R.E. Gomory (1961). "A Linear Programming Approach to the Cutting-Stock Problem". In: *Operations Research* 9, pp. 849–859.

– (1963). "A Linear Programming Approach to the Cutting-Stock Problem - Part II". In: *Operations Research* 11, pp. 863–888. ISSN: 26883627. DOI: `10.4271/580217`.

– (1965). "Multistage Cutting Stock Problems of Two and More Dimensions". In: *Operations Research* 13.1, pp. 94–120.

Goldberg, David, Christopher Malon, and Marshall Bern (2002). "A global approach to automatic solution of jigsaw puzzles". In: *Proceedings of the Annual Symposium on Computational Geometry*. Barcelona: Association for Computing Machinery, pp. 82–87. ISBN: 1581135041. DOI: `10.1145/513400.513410`.

Gowthaman, Sivakumar, Kazunori Nakashima, and Satoru Kawasaki (2018). "A state-of-the-art review on soil reinforcement technology using natural plant fiber materials: Past findings, present trends and future directions". In: *Materials* 11.4. ISSN: 19961944. DOI: 10.3390/ma11040553.

Graton, L. C. and H. J. Fraser (1935). "Systematic Packing of Spheres: With Particular Relation to Porosity and Permeability". In: *The Journal of Geology* 43.8, pp. 785–909. ISSN: 0022-1376. DOI: 10.1086/624386.

Grillanda, Nicola et al. (2021). "Tilting plane tests for the ultimate shear capacity evaluation of perforated dry joint masonry panels. Part I: Experimental tests". In: *Engineering Structures* 238. ISSN: 18737323. DOI: 10.1016/j.engstruct.2021.112124. URL: https://doi.org/10.1016/j.engstruct.2021.112124.

Guo, Peijun and Xubin Su (2007). "Shear strength, interparticle locking, and dilatancy of granular materials". In: *Canadian Geotechnical Journal* 44.5, pp. 579–591. ISSN: 00083674. DOI: 10.1139/T07-010.

Haldurai, L, T Madhubala, and R Rajalakshmi (2016). "A Study on Genetic Algorithm and Its Applications". In: *International Research Journal of Modernization in Engineering Technology and Science* 4.10, pp. 139–143. DOI: 10.56726/irjmets32980.

Hammerlindl, Andy, John Bowman, and Tom Prince (2014). *Asymptote : The Vector Graphics Language*. URL: https://asymptote.sourceforge.io.

Hammond, G. and C. Jones (2006). *Inventory of Carbon and Energy*. Tech. rep. University of Bath, UK. URL: http:/www.bath.ac.uk/mech-eng/sert/embodied.

Harkness, R. M. et al. (2000). "Numerical modelling of full-scale tests on drystone masonry retaining walls". In: *Geotechnique* 50.2, pp. 165–179. ISSN: 00168505. DOI: 10.1680/geot.2000.50.2.165.

Hassanlourad, M, M R Rasouli, and H Salehzadeh (2014). "A comparison between the undrained shear behavior of carbonate and quartz sands". In: *International Journal of Civil Engineering* 12.4, pp. 338–350.

Hazra, Avijit (2017). "Using the confidence interval confidently". In: *Journal of Thoracic Disease* 9.10, pp. 4125–4130. ISSN: 20776624. DOI: 10.21037/jtd.2017.09.14.

Herbst, Thomas F and Hans F Winterkorn (1964). "Shear Phenomena in Granular Random Packings". In: *Soil Science*. ISSN: 0038-075X. DOI: 10.1097/00010694-196410000-00021.

Herz, J. C. (1972). "Recursive computational procedure for two-dimensional stock cutting". In: *IBM Journal of Research and Development* 16, pp. 462–469.

Hifi, Mhand and Rym M'Hallah (2002). "A Best Local Position Procedure Based Heuristic for the Two-Dimensional Layout Problem". In: *Studia Informatica Universalis. International Journal on Informatics* 2, pp. 33–56.

Hikone Sightseeing Association (2017). *Hikone Castle*. URL: https://visit.hikoneshi.com/en/castle/history/ (visited on 03/22/2023).

Hoff, Daniel J. and Peter J. Olver (2013). "Extensions of invariant signatures for object recognition". In: *Journal of Mathematical Imaging and Vision* 45.2, pp. 176–185. ISSN: 09249907. DOI: 10.1007/s10851-012-0358-7.

– (2014). "Automatic solution of jigsaw puzzles". In: *Journal of Mathematical Imaging and Vision* 49.1, pp. 234–250. ISSN: 09249907. DOI: 10.1007/s10851-013-0454-3.

Hogg, Robert V., Elliot A. Tanis, and Dale L. Zimmerman (2014). *Probability and Statistical Inference*. 9th. Boston: Pearson. ISBN: 9780321923271. DOI: 10.4135/9781412986434.n4.

Holland, J. H. (1975). *Adaptation in natural and artificial systems*. The University of Michigan press.

Holtz, W.G. and H.J. Gibbs (1956). "Triaxial shear tests on previously gravelly soils". In: *Journal of the Soil Mechanics and Foundations Divion* 82.1, pp. 1–22.

Hoodless, A G and C C Smith (2023). "Intelligent placement of untooled rock to form precision structures using a weighted criterion". In: *10th European Conference on Numerical Methods in Geotechnical Engineering*. London.

Horne, M. R. (1965). "The behaviour of an assembly of rotund, rigid, cohesionless particles. I". In: *Proceedings of the Royal Society of London. Series A. Mathematical and Physical Sciences*. Vol. 286, pp. 62–78. DOI: `10.1098/rspa.1969.0059`.

Howard, Jeffrey L. (1992). "An evaluation of shape indices as palaeoenvironmental indicators using quartzite and metavolcanic clasts in Upper Cretaceous to Palaeogene beach, river and submarine fan conglomerates". In: *Sedimentology* 39, pp. 471–486. ISSN: 13653091. DOI: `10.1111/j.1365-3091.1992.tb02128.x`.

Huu, Pham et al. (2017). "Effects of particle characteristics on the shear strength of calcareous sand". In: *Acta Geotechnica Slovenica* 14.2, pp. 77–89.

Idel, Karl-Heinz (1960). "The Shear Strength of Granular Soil Materials". In: *Institute for Soil Mechanics and Earth Structures*. Karlsruhe, Germany.

Illenberger, Werner L. (1992). "Pebble Shape (and Size!): Reply". In: *Journal of Sedimentary Petrology* 6, pp. 1151–1155.

Ishigami, K., H. Arima, and M. Shima (1973). "Shear strength characteristics of saturated sand in undrained tests". In: *28th Annual Meeting of Japan Society of Civil Engineers*, pp. 76–78.

Itasca (1998). *PFC2D 2.00 Particle Flow Code in Two Dimensions*. Tech. rep. Minneapolis Minnesota.

Izadi, E. and A. Bezuijen (2015). "Simulation of granular soil behaviour using the Bullet physics library". In: *Geomechanics from Micro to Macro - Proceedings of the TC105 ISSMGE International Symposium on Geomechanics from Micro to Macro, IS-Cambridge 2014*. Vol. 2. Cambridge: Taylor & Francis, pp. 1565–1570. ISBN: 9781138027077. DOI: `10.1201/b17395-285`.

Jakobs, Stefan (1996). "On genetic algorithms for the packing of polygons". In: *European Journal of Operational Research* 88, pp. 165–181. ISSN: 03772217. DOI: `10.1016/0377-2217(94)00166-9`.

Johns, Ryan Luke et al. (2020). "Autonomous dry stone: On-site planning and assembly of stone walls with a robotic excavator". In: *Construction Robotics* 4, pp. 127–140. ISSN: 2509-811X. DOI: `10.1007/s41693-020-00037-6`. URL: `https://doi.org/10.1007/s41693-020-00037-6`.

Johns, Ryan Luke et al. (2023). "A framework for robotic excavation and dry stone construction using on-site materials". In: *Science robotics* 8.84. ISSN: 24709476. DOI: `10.1126/scirobotics.abp9758`.

Johnson, David S. (1974). "Fast algorithms for bin packing". In: *Journal of Computer and System Sciences* 8, pp. 272–314. ISSN: 10902724. DOI: `10.1016/S0022-0000(74)80026-7`.

Kirkpatrick, S., C. D. Gelatt, and M. P. Vecchi (1983). "Optimization By Simulated Annealing". In: *Science* 220.4598, pp. 671–680.

Koehnken, Lois and Max Rintoul (2018). *Impacts of Sand Mining on Ecosystem Structure, Process & Biodiversity in Rivers*. Tech. rep. WWF.

Koerner, Robert M (1970). "Effect of particle characteristics on soil strength". In: *Journal of Soil Mechanics & Foundations Division* 96.4, pp. 1221–1234.

Kohler, Matthias, Fabio Gramazio, and Jan Willmann (2014). *The Robotic Touch: How Robots Change Architecture*. Park Books.

Kong, Weixin and Benjamin B. Kimia (2001). "On solving 2D and 3D puzzles using curve matching". In: *Proceedings of the IEEE Computer Society Conference on Computer Vision and Pattern Recognition*. Vol. 2. Kauai, Hawaii: IEEE, pp. 583–590. ISBN: 0769512720. DOI: `10.1109/cvpr.2001.991015`.

Kostreva, Michael M. and Rebecca Hartman (2004). “Multiple objective solutions for tetris”. In: *Journal of Recreational Mathematics* 32.3, pp. 214–225. ISSN: 0091-6749.

Kramp, Christian (1799). *Analyse des Réfractions Astronomiques et Terrestres*. Strasbourg: Philippe Jacques Dannbach.

Krumbein, W. C. (1941). “Measurement and geological significance of shape and roundness of sedimentary particles”. In: *Journal of Sedimentary Research* 11.2, pp. 64–72.

Kuenen, Ph. H. (1956). “Experimental Abrasion of Pebbles: 2. Rolling by Current”. In: *The Journal of Geology* 64.4, pp. 336–368.

L. J. Johnston, J. Goihl, and G. C. Shurson (2009). “Selected Additives Did Not Improve Flowability of DDGS in Commercial Systems”. In: *Applied Engineering in Agriculture* 25.1, pp. 75–82. DOI: 10.13031/2013.25422.

Lade, Poul V., Carl D. Liggio, and Jerry A. Yamamuro (1998). “Effects of Non-Plastic Fines on Minimum and Maximum Void Ratios of Sand”. In: *Geotechnical Testing Journal* 21.4, pp. 336–347. ISSN: 01496115. DOI: 10.1520/gtj11373j.

Lajeunesse, E., A. Mangeney-Castelnau, and J. P. Vilotte (2004). “Spreading of a granular mass on a horizontal plane”. In: *Physics of Fluids* 16.7, pp. 2371–2381. ISSN: 10706631. DOI: 10.1063/1.1736611.

Lambert, Malcolm and Paul Kennedy (2012). “Using Artificial Intelligence to Build With Unprocessed Rock”. In: *Key Engineering Materials* 517, pp. 939–945. DOI: https://doi.org/10.4028/www.scientific.net/KEM.517.939.

Larsson, Maria, Hironori Yoshida, and Takeo Igarashi (2019). “Human-in-the-loop fabrication of 3D surfaces with natural tree branches”. In: *3rd Annual ACM Symposium on Computational Fabrication*. New York: Association for Computing Machinery. ISBN: 9781450367950. DOI: 10.1145/3328939.3329000.

Latha, Gali Madhavi and Thallak G Sitharam (2008). “Effect of Particle Size and Gradation on the Behaviour of Granular Materials Simulated Using DEM”. In: *Indian Geotechnical Journal* 38.1, pp. 68–88.

Lee, Kenneth L. and H. Bolton Seed (1967). “Drained strength characteristics of sands”. In: *Journal of the Soil Mechanics and Foundations Division* 93.6, pp. 117–141.

Lees, G. (1964). “A new method for determining the angularity of particles”. In: *Sedimentology* 3, pp. 2–21. ISSN: 13653091. DOI: 10.1111/j.1365-3091.1964.tb00271.x.

Lehne, Johanna and Felix Preston (2018). *Making Concrete Change Innovation in Low-carbon Cement and Concrete. Energy, Environment and Resources Department*. Tech. rep.

Leslie, D D (1969). “Relationship between shear strength, gradation and index properties”. In: *7th International Conference on Soil Mechanics and Foundation Engineering*. Mexico City: Sociedad Mexicana de Mecanica, pp. 212–222.

Li, Hang (2020). “Novel approaches to modelling discrete particle systems”. Doctoral Thesis. University of Sheffield. DOI: 10.1109/smart55829.2022.10047747.

Li, Yanrong (2013). “Effects of particle shape and size distribution on the shear strength behavior of composite soils”. In: *Bulletin of Engineering Geology and the Environment* 72, pp. 371–381. DOI: 10.1007/s10064-013-0482-7.

Li, Yanrong et al. (2013). “Effects of Particle Shape on Shear Strength of Clay-gravel Mixture”. In: *KSCE Journal of Civil Engineering* 17, pp. 712–717. DOI: 10.1007/s12205-013-0003-z.

Lim, Sungwoo et al. (2017). “Extra-terrestrial construction processes – Advancements, opportunities and challenges”. In: *Advances in Space Research* 60.7, pp. 1413–1429. ISSN: 18791948. DOI: 10.1016/j.asr.2017.06.038. URL: http://dx.doi.org/10.1016/j.asr.2017.06.038.

Lin, X. and T.-T Ng (1997). "A three-dimensional discrete element model using arrays of ellipsoids". In: *Geotechnique* 47.2, pp. 319–329.

Linero Molina, S. et al. (2019). "Impact of grading on steady-state strength". In: *Geotechnique Letters* 9.4, pp. 328–333. ISSN: 20452543. DOI: `10.1680/jgele.18.00216`.

Liu, Dequan and Hongfei Teng (1999). "An improved BL-algorithm for genetic algorithm of the orthogonal packing of rectangles". In: *European Journal of Operational Research* 112.2, pp. 413–420. ISSN: 03772217. DOI: `10.1016/S0377-2217(97)00437-2`.

Liu, Xiao et al. (2015). "HAPE3D—a new constructive algorithm for the 3D irregular packing problem". In: *Frontiers of Information Technology and Electronic Engineering* 16.5, pp. 380–390. ISSN: 20959230. DOI: `10.1631/FITEE.1400421`.

Liu, Yifang, Jiwon Choi, and Nils Napp (2021). "Planning for Robotic Dry Stacking with Irregular Stones". In: *Springer Proceedings in Advanced Robotics*. Vol. 16. Singapore: Springer, pp. 321–335. DOI: `10.1007/978-981-15-9460-1_23`.

Liu, Zhichao (2011). "Measuring the angle of repose of granular systems using hollow cylinders". Masters Thesis. University of Pittsburgh.

Lodi, Andrea, Silvano Martello, and Daniele Vigo (1999a). "Heuristic and Metaheuristic Approaches for a Class of Two-Dimensional Bin Packing Problems". In: *INFORMS Journal on Computing* 11.5, pp. 345–357. ISSN: 0091-6749. URL: `http://dx.doi.org/10.1016/j.jaci.2012.05.050`.

– (1999b). "Neighborhood search algorithm for the guillotine non-oriented two-dimensional bin packing problem". In: *Meta-Heuristics*. New York: Springer, pp. 125–139.

– (2002). "Recent advances on two-dimensional bin packing problems". In: *Discrete Applied Mathematics* 123, pp. 379–396. ISSN: 0166218X. DOI: `10.1016/S0166-218X(01)00347-X`.

Lowe, Donald R. (1976). "Grain Flow and Grain Flow Deposits". In: *Journal of Sedimentary Research* 46.1, pp. 188–199. ISSN: 1527-1404. DOI: `10.1306/212f6ef1-2b24-11d7-8648000102c1865d`.

Mackie, W. (1897). "On the laws that govern the rounding of particles of sand". In: *Trans. Edinburgh Geol. Soc.* 7, pp. 298–311.

Maclaren, Jon (1997). "Parallelising Serial Code : A Comparison of Three High-Performance Parallel Programming Methods". Doctoral Thesis. University of Manchester.

Mann, Z. A. (2017). "The top eight misconceptions about NP-Hardness". In: *Computer* 50.5, pp. 72–79.

Marachi, Nezameddin (1969). "Strength and deformation characteristics of rockfill materials". PhD thesis. University of California, Berkeley.

Marsal, R. J. (1967a). "Large scale testing of rockfill materials". In: *Journal of the Soil Mechanics and Foundations Division* 93.2, pp. 27–43.

Marsal, R.J. (1965). "Stochastic Processes in the Grain Skeleton of Soils". In: *6th International Conference of Soil Mechanics and Foundation Engineering*. Montreal: University of Toronto Press, pp. 303–307.

– (1967b). *Behavior of granular soils*. Tech. rep. Caracas, Venezuela: Publication of the Soil Engineering Department of the Universidad Catolica Andres Bello.

Martello, Silvano, David Pisinger, and Daniele Vigo (2000). "Three-dimensional bin packing problem". In: *Operations Research* 48.2, pp. 256–267. ISSN: 0030364X. DOI: `10.1287/opre.48.2.256.12386`.

Martello, Silvano and Daniele Vigo (1998). "Exact solution of the two-dimensional finite bin packing problem". In: *Management Science* 44.3, pp. 388–399. ISSN: 00251909. DOI: `10.1287/mnsc.44.3.388`.

Martello, Silvano et al. (2007). "Algorithm 864: General and robot-packable variants of the three-dimensional bin packing problem". In: *ACM Transactions on Mathematical Software* 33.1. ISSN: 00983500. DOI: 10.1145/1206040.1206047.

McDowell, G. R. and M. D. Bolton (1998). "On the micromechanics of crushable aggregates". In: *Géotechnique* 48.5, pp. 667–679.

McDowell, G. R. and O. Harireche (2002). "Discrete element modelling of soil particle fracture". In: *Geotechnique* 52.2, pp. 131–135. ISSN: 00168505. DOI: 10.1680/geot.2002.52.2.131.

Meer, J.W. van der et al. (2005). "Stability assessment of single layers of orderly placed and of pitched natural rock". In: *Second International Coastal Symposium*. Höfn, Iceland. ISBN: 9789812706362. DOI: 10.1142/9789812709554_0403.

Melax, S (2014). *Reinforcement Learning Tetris Example*. URL: https://melax.github.io/tetris/tetris.html (visited on 11/22/2023).

Melià, Paco et al. (2014). "Environmental impacts of natural and conventional building materials: A case study on earth plasters". In: *Journal of Cleaner Production* 80, pp. 179–186. ISSN: 09596526. DOI: 10.1016/j.jclepro.2014.05.073.

Meloy, T. P. (1977). "Fast Fourier transform applied to shape analysis of particle silhouettes to obtain morphological data". In: *Powder Technology* 17, pp. 27–35.

Metcalf, J. R. (1966). "Angle of repose and internal friction". In: *International Journal of Rock Mechanics and Mining Sciences* 3, pp. 155–161. ISSN: 01489062. DOI: 10.1016/0148-9062(66)90005-2.

Meyerhof, G. G. (1956). "Penetration tests and bearing capacity of cohesionless soils". In: *Journal of Soil Mechanics and Foundations Division* 82.1, pp. 1–19.

– (1976). "Bearing capacity and settlement of pile foundations". In: *Journal of Geotechnical Engineering* 102.3, pp. 195–228.

Mishra, B. K. and C. Thornton (2001). "Impact breakage of particle agglomerates". In: *International Journal of Mineral Processing* 61.4, pp. 225–239. ISSN: 03017516. DOI: 10.1016/S0301-7516(00)00065-X.

Mitchell, J K and Kenichi Soga (2005). *Fundamentals of Soil Behavior*. 3rd. Hodoken, New Jersey: John Wiley & Sons Inc.

Miura, Kinya, Kenichi Maeda, and Shosuke Toki (1997a). "Method of Measurement for the Angle of Repose of Sands". In: *Soils and Foundations* 37.2, pp. 89–96. ISSN: 1341-7452. DOI: 10.3208/sandf.37.2_89.

Miura, Kinya et al. (1997b). "Physical properties of sands with different primary properties". In: *Soils and Foundations* 37.3, pp. 53–64.

– (1998). "Mechanical characteristics of sands with different primary properties". In: *Soils and Foundations* 38.4, pp. 159–172. URL: http://www.mendeley.com/research/geology-volcanic-history-eruptive-style-yakedake-volcano-group-central-japan/.

Mogami, Takeo (1965). "Statistical approach to the mechanics of granular materials". In: *Soils and Foundations* 5.2, pp. 26–36. URL: http://www.mendeley.com/research/geology-volcanic-history-eruptive-style-yakedake-volcano-group-central-japan/.

Mollon, Guilhem (2023). *Guilhem Mollon*. URL: http://guilhem.mollon.free.fr/ (visited on 01/26/2024).

Mollon, Guilhem and Jidong Zhao (2012). "Fourier-Voronoi-based generation of realistic samples for discrete modelling of granular materials". In: *Granular Matter* 14, pp. 621–638. ISSN: 14345021. DOI: 10.1007/s10035-012-0356-x.

– (2013). "Generating realistic 3D sand particles using Fourier descriptors". In: *Granular Matter* 15.1, pp. 95–108. ISSN: 14345021. DOI: 10.1007/s10035-012-0380-x.

Morel, J. C. et al. (2001). "Building houses with local materials: Means to drastically reduce the environmental impact of construction". In: *Building and Environment* 36.10, pp. 1119–1126. ISSN: 03601323. DOI: 10.1016/S0360-1323(00)00054-8.

Moroto, Nobuchika (1982). "An application of Mogami's strength formula to the classification of granular soil". In: *Soils and Foundations* 22.1, pp. 82–90. URL: http://www.mendeley.com/research/geology-volcanic-history-eruptive-style-yakedake-volcano-group-central-japan/.

Muir Wood, David (2008). "Critical states and soil modelling". In: *4th International Symposium on Deformation Characteristics of Geomaterials*. Atlanta, Georgia: IOS Press, pp. 51–72.

Mundell, Chris et al. (2009). "Limit-equilibrium assessment of drystone retaining structures". In: *Geotechnical Engineering* 162.4, pp. 203–212. ISSN: 13532618. DOI: 10.1680/geng.2009.162.4.203.

Mundell, Chris et al. (2010). "Behaviour of drystone retaining structures". In: *Structures and Buildings* 163.1, pp. 3–12. ISSN: 17517702. DOI: 10.1680/stbu.2009.163.1.3.

Murselovic, Denis and Johanna Godefroid (2019). *Japan Experterna*. URL: https://www.japanexperterna.se/ (visited on 08/03/2023).

Nelson, Eino (1955). "Measurement of the repose angle of a tablet granulation". In: *Journal of the American Pharmaceutical Association* 44.7, pp. 435–437. DOI: 10.1002/jps.3030440714.

Neyman, Jerzy (1937). "Outline of a theory of statistical estimation based on the classical theory of probability". In: *Philosophical Transactions of the Royal Society of London. Series A, Mathematical and Physical and Engineering Sciences* 236.767, pp. 333–380. DOI: 10.2307/jj.8501421.24.

Nguyen, Thanh T. and Buddhima Indraratna (2023). "Natural Fibre for Geotechnical Applications: Concepts, Achievements and Challenges". In: *Sustainability* 15.11. ISSN: 20711050. DOI: 10.3390/su15118603.

Nicoli, Marius (2019). "Bitwise Operators in C Language: The explanation, in detail, of their use. Little tricks". In: *Acta et Commentationes, Sciences of Education* 4.18, pp. 62–72. DOI: 10.36120/2587-3636.v18i4..

Nishida, K. et al. (2005). "Geotechnical characteristics of Japanese castle masonry wall and mechanical analysis for its preservation". In: *16th International Conference on Soil Mechanics and Geotechnical Engineering*. Osaka: Millpress Science Publishers, pp. 2763–2768. ISBN: 9781614996569. DOI: 10.3233/978-1-61499-656-9-2763.

Oda, Masanobu (1977). "Co-ordination number and its relation to shear strength of granular material". In: *Soils and Foundations* 17.2, pp. 29–42.

Oesterle, Silvan (2009). "Cultural performance in robotic timber construction". In: *ACADIA 09: reForm*. Chicago, Illinois, pp. 194–200. ISBN: 0984270507. DOI: 10.52842/conf.acadia.2009.194.

Oetomo, James J. et al. (2016). "Modeling the 2D behavior of dry-stone retaining walls by a fully discrete element method". In: *International Journal for Numerical and Analytical Methods in Geomechanics* 40, pp. 1099–1120. ISSN: 10969853. DOI: 10.1002/nag.2480.

Oldenburg, Doug et al. (2017). *Densities of Metamorphic Rocks*. URL: https://gpg.geosci.xyz/index.html (visited on 02/05/2024).

ORCA (2021). *Online Research @ Cardiff*. URL: https://orca.cardiff.ac.uk/ (visited on 05/09/2024).

O'Sullivan, Catherine (2003). "The Application of Discrete Element Modelling to Finite Deformation Problems in Geomechanics". Ph.D. Thesis. University of California, Berkeley.

O'Sullivan, Catherine (2011). *Particulate discrete element modelling: A geomechanics perspective*. London: CRC Press.

Pakbaz, Mohammad S and Ali Siadati Moqaddam (2012). "Effect of Sand Gradation on The Behavior of Sand-Clay Mixtures". In: *Internation Journal of GEOMATE* 3.1, pp. 325–331.

Patil, Prashant et al. (2016). "Soil Reinforcement Techniques". In: *International Journal of Engineering Research and Application* 6.8, pp. 25–31. URL: www.ijera.com.

Pettijohn, F. J. (1949). *Sedimentary Rocks*. New York: Harpers and Brothers.

Pettijohn, Francis John and Arthur Charles Lundahl (1943). "Shape and roundness of Lake Erie beach sands". In: *Journal of Sedimentary Research* 13.2, pp. 69–78. ISSN: 1527-1404. DOI: 10.1306/D426919D-2B26-11D7-8648000102C1865D. URL: https://doi.org/10.1306/D426919D-2B26-11D7-8648000102C1865D.

Pharr, Matt, Wenzel Jakob, and Greg Humphreys (2016). "Sampling and Reconstruction". In: *Physically Based Rendering: From Theory to Implementation*. Third. Chap. 7. DOI: https://doi.org/10.1016/B978-0-12-800645-0.50007-5.

Phon-Amnuaisuk, Somnuk (2015). "Evolving and discovering tetris gameplay strategies". In: *Procedia Computer Science* 60.1, pp. 458–467. ISSN: 18770509. DOI: 10.1016/j.procs.2015.08.167.

Pitanga, Heraldo Nunes, Jean Pierre Gourc, and Orencio Monje Vilar (2009). "Interface shear strength of geosynthetics: Evaluation and analysis of inclined plane tests". In: *Geotextiles and Geomembranes* 27, pp. 435–446. ISSN: 02661144. DOI: 10.1016/j.geotexmem.2009.05.003.

Pohlman, Nicholas A. et al. (2006). "Surface roughness effects in granular matter: Influence on angle of repose and the absence of segregation". In: *Physical Review E - Statistical, Nonlinear, and Soft Matter Physics* 73. ISSN: 15502376. DOI: 10.1103/PhysRevE.73.031304.

Pollack, Jerome Marvin (1961). "Significance of compositional and textural properties of South Canadian River channel sands, New Mexico, Texas, and Oklahoma". In: *Journal of Sedimentary Research* 31.1, pp. 15–37. ISSN: 1527-1404. DOI: 10.1306/74D70AEC-2B21-11D7-8648000102C1865D. URL: https://doi.org/10.1306/74D70AEC-2B21-11D7-8648000102C1865D.

Potticary, M., A. Zervos, and J. Harkness (2015). "An investigation into the effect of particle platyness on the strength of granular materials using the discrete element method". In: *Proceedings of the 4th International Conference on Particle-Based Methods - Fundamentals and Applications, PARTICLES 2015*, pp. 767–778. ISBN: 9788494424472.

Potticary, M, A Zervos, and J Harkness (2016). "The Effect of Particle Elongation on the Strength of Granular Materials". In: *24th UK Conference of the Association for Computational Mechanics in Engineering*. Cardiff, pp. 239–242.

Powers, M. C. (1953). "A new roundness scale for sedimentary particles". In: *Journal of Sedimentary Petrology* 23.2, pp. 117–119. DOI: 10.26848/rbgf.v14.4.p2131-2148.

Pujari, Satish, A. Ramakrishna, and K. T.Balaram Padal (2017). "Comparison of ANN and Regression Analysis for Predicting the Water Absorption Behaviour of Jute and Banana Fiber Reinforced Epoxy composites". In: *Materials Today: Proceedings* 4, pp. 1626–1633. ISSN: 22147853. DOI: 10.1016/j.matpr.2017.02.001.

Pytlos, M., M. Gilbert, and C. C. Smith (2015). "Modelling granular soil behaviour using a physics engine". In: *Geotechnique Letters* 5.4, pp. 243–249. ISSN: 20452543. DOI: 10.1680/jgele.15.00067.

Pytlos, Michał (2015). "New Tools for Modelling Soil-Filled Masonry Arch Bridges". Doctoral Thesis. University of Sheffield.

Rackl, Michael, Florian E. Grötsch, and Willibald A. Günthner (2017a). "Angle of repose revisited: When is a heap a cone?" In: *Powders and Grains*. Montpellier, France: EPJ Web of Conferences 140. DOI: `10.1051/epjconf/201714002002`.

Rackl, Michael et al. (2017b). "Qualitative and quantitative assessment of 3D-scanned bulk solid heap data". In: *Powder Technology* 321, pp. 105–118. ISSN: 1873328X. DOI: `10.1016/j.powtec.2017.08.009`.

Radack, Gerald M. and Norman I. Badler (1982). "Jigsaw puzzle matching using a boundary-centered polar encoding". In: *Computer Graphics and Image Processing* 19.1, pp. 1–17. ISSN: 0146664X. DOI: `10.1016/0146-664X(82)90111-3`.

Ramesh, Srikonda (2012). "Appaisal of Vernacular Building Materials and Alternative Technologies for Roofing and Terracing Options of Embodied Energy in Buildings". In: *Energy Procedia* 14, pp. 1843–1848. DOI: `10.1016/j.egypro.2011.12.887`.

Razali, Noraini Mohd and John Geraghty (2011). "Genetic algorithm performance with different selection strategiesin solving TSP". In: *Proceedings of the World Congress on Engineering*, pp. 1134–1139. ISBN: 9789881925145.

Ren, Kun, Alexander Thomson, and Daniel J. Abadi (2014). "An evaluation of the advantages and disadvantages of deterministic database systems". In: *40th International Conference on Very Large Data Bases*. Vol. 7. 10. Hangzhou, pp. 821–832. DOI: `10.14778/2732951.2732955`.

Restrepo Vélez, Luis Fernando, Guido Magenes, and Michael C. Griffith (2014). "Dry stone masonry walls in bending-Part I: Static tests". In: *International Journal of Architectural Heritage* 8.1, pp. 1–28. ISSN: 15583066. DOI: `10.1080/15583058.2012.663059`.

Riley, N. Allen (1941). "Projection sphericity". In: *Journal of Sedimentary Research* 11.2, pp. 94–97.

Rousé, P C, R J Fannin, and D A Shuttle (2008). "Influence of roundness on the void ratio and strength of uniform sand". In: *Géotechnique* 58.3, pp. 227–231. DOI: `10.1680/geot.2008.58.3.227`.

Rowe, P W (1962). "The stress-dilatancy relation for static equilibrium of an assembly of particles in contact". In: *Proceedings of the Royal Society of London. Series A. Mathematical and Physical Sciences* 269.1339, pp. 500–527. ISSN: 0080-4630. DOI: `10.1098/rspa.1962.0193`.

Russell, R. Dana and Ralph E. Taylor (1937). "Roundness and shape of Mississippi River sands". In: *The Journal of Geology* 45.3, pp. 225–267.

Safinus, S, M S Hossain, and M F Randolph (2013). "Comparison of Stress-Strain Behaviour of Carbonate and Silicate Sediments". In: *18th International Conference on Soil Mechanics and Geotechnical Engineering*. Paris, pp. 267–270.

Sakai, Mikio et al. (2014). "Verification and validation of a coarse grain model of the DEM in a bubbling fluidized bed". In: *Chemical Engineering Journal* 244, pp. 33–43. ISSN: 13858947. DOI: `10.1016/j.cej.2014.01.029`. URL: `http://dx.doi.org/10.1016/j.cej.2014.01.029`.

Salawu, A.T, M.L Suleiman, and M Isiaka (2013). "Physical Properties of Jatropha Curcas Seed.pdf". In: *Electronical Journal of Polish Agricultural Universities* 16.4.

Santa-Cruz, Sandra et al. (2021). "Out-of-plane analysis of dry-stone walls using a pseudo-static experimental and numerical approach in scaled-down specimens". In: *Engineering Structures* 245. ISSN: 18737323. DOI: `10.1016/j.engstruct.2021.112875`.

Santamarina, C. and G. Cascante (1998). "Effect of surface roughness on wave propagation parameters". In: *Géotechnique* 48.1, pp. 129–136.

Santamarina, J. C. and G. C. Cho (2004). "Soil behaviour: The role of particle shape". In: *Advances in Geotechnical Engineering: The Skempton Conference*. London: Thomas Telford Publishing, pp. 604–617. ISBN: 0727732641.

Schwarz, J. T. and M. Sharir (1985). *Identification of partially obscured objects in two dimensions by matching of noisy "characteristic curves"*. New York.

Sebastian, Thomas B. et al. (2000). "Constructing 2D curve atlases". In: *Proceedings of the Workshop on Mathematical Methods in Biomedical Image Analysis*. San Francisco, California: IEEE, pp. 70–77. ISBN: 0769507379. DOI: 10.1109/mmbia.2000.852362.

Self, Martin and Emmanuel Vercruysse (2017). "Infinite Variations, Radical Strategies". In: *Fabricate 2017*. UCL Press, pp. 30–35. DOI: 10.2307/j.ctt1n7qkg7.8.

Selig, Ernest T and Carl J Roner (1987). "Effects of Particle Characteristics on Behavior of Granular Material". In: *Transportation Research Record* 1131.

Shergold, F. A. (1953). "The percentage voids in compacted gravel as a measure of its angularity". In: *Magazine of Concrete Research* 13.5, pp. 3–10. ISSN: 1751763X. DOI: 10.1680/macr.1953.5.13.3.

Simoni, Alessandro and Guy Tinmouth Houlsby (2006). "The direct shear strength and dilatancy of sand – gravel mixtures". In: *Geotechnical and Geological Engineering* 24, pp. 523–549. DOI: 10.1007/s10706-004-5832-6.

Skinner, A. E. (1969). "A Note on the Influence of Interparticle Friction on the Shearing Strength of a Random Assembly of Spherical Particles". In: *Géotechnique* 19.1, pp. 150–157.

Smalley, I. J. (1971). "Variations on the Particle Packing Theme of Graton and Fraser". In: *Powder Technology* 4.2, pp. 97–101. ISSN: 00325910. DOI: 10.1016/0032-5910(71)80007-4.

Smithson, Scott B. (1971). "Densities of metamorphic rocks". In: *Geophysics* 36.4, pp. 690–694. DOI: https://doi.org/10.1190/1.1440205.

Sneed, Edmund D. and Robert L. Folk (1958). "Pebbles in the Lower Colorado River , Texas: A Study in Particle Morphogenesis". In: *The Journal of Geology* 66.2, pp. 114–150.

Snow, Dan (2001). *In the Company of Stone*. New York: Artisan Books.

Sohn, H. Y. and C. Moreland (1968). "The effect of particle size distribution on packing density". In: *The Canadian Journal of Chemical Engineering* 46.3, pp. 162–167. ISSN: 1939019X. DOI: 10.1002/cjce.5450460305.

Sorenson, H. W. and D. L. Alspach (1971). "Recursive bayesian estimation using gaussian sums". In: *Automatica* 7, pp. 465–479. ISSN: 00051098. DOI: 10.1016/0005-1098(71)90097-5.

Subrahmanyam, C. and R. K. Verma (1981). "Densities and magnetic susceptibilities of Precambrian rocks of different metamorphic grade (Southern Indian Shield)." In: *Journal of Geophysics* 49.2, pp. 101–107. ISSN: 01489062. DOI: 10.1016/0148-9062(81)91248-1.

Suiker, Akke S.J. and Norman A. Fleck (2004). "Frictional collapse of granular assemblies". In: *Journal of Applied Mechanics* 71.3, pp. 350–358. ISSN: 00218936. DOI: 10.1115/1.1753266.

Tenzer, Robert et al. (2011). "A digital rock density map of New Zealand". In: *Computers and Geosciences* 37.8, pp. 1181–1191. ISSN: 00983004. DOI: 10.1016/j.cageo.2010.07.010. URL: http://dx.doi.org/10.1016/j.cageo.2010.07.010.

Terashima-Marín, H. et al. (2010). "Generalized hyper-heuristics for solving 2D Regular and Irregular Packing Problems". In: *Annals of Operations Research* 179, pp. 369–392. DOI: 10.1007/s10479-008-0475-2.

Terzaghi, Karl (1943). *Theoretical Soil Mechanics*. Hoboken, New Jersy: John Wiley & Sons Inc. DOI: 10.1002/9780470172766.

Terzaghi, Karl and Ralph B. Peck (1967). *Soil Mechanics in Engingeering Practice*. 2nd Editio. New York: John Wiley & Sons Inc.

Thakur, Mohmad Mohsin and Dayakar Penumadu (2021). "Influence of Friction and Particle Morphology on Triaxial Shearing of Granular Materials". In: *Journal of Geotechnical and Geoenvironmental Engineering* 147.11. ISSN: 1090-0241. DOI: `10.1061/(asce)gt.1943-5606.0002634`.

Thomas, Patricia Ann (1997). "Discontinuous Deformation Analysis of Particulate Media". Ph.D Thesis. University of California: Berkeley, p. 274. ISBN: 061239378X.

Thompson, Adam (2007). "The Character of a Wall: The changing construction of agricultural walls on the island of Gozo". In: *Omertaa, Journal for Applied Anthropology* 1, pp. 31–37. URL: `http://www.omertaa.org/archive/omertaa0006.pdf`.

Thornton, C. (2000). "Numerical simulations of deviatoric shear deformation of granular media". In: *Géotechnique* 50.1, pp. 43–53. ISSN: 00168505. DOI: `10.1680/geot.2000.50.1.43`.

Thornton, C. and G. Sun (1993). "Axisymmetric compression of 3D polydisperse systems of spheres". In: *Powders and Grains*. Vol. 93. Rotterdam: Balkema, pp. 129–134.

Thornton, C., K. K. Yin, and M. J. Adams (1996). "Numerical simulation of the impact fracture and fragmentation of agglomerates". In: *Journal of Physics D: Applied Physics* 29.2, pp. 424–435. ISSN: 00223727. DOI: `10.1088/0022-3727/29/2/021`.

Tillemans, Hans Jürgen and Hans J. Herrmann (1995). "Simulating deformations of granular solids under shear". In: *Physica A: Statistical Mechanics and its Applications* 217, pp. 261–288. ISSN: 03784371. DOI: `10.1016/0378-4371(95)00111-J`.

Todisco, M C et al. (2017). "Multiple contact compression tests on sand particles". In: *Soils and Foundations* 57.1, pp. 126–140. ISSN: 0038-0806. DOI: `10.1016/j.sandf.2017.01.009`. URL: `http://dx.doi.org/10.1016/j.sandf.2017.01.009`.

Tong, Chen-xi et al. (2019). "A stochastic particle breakage model for granular soils subjected to one- dimensional compression with emphasis on the evolution of coordination number". In: *Computers and Geotechnics* 112, pp. 72–80. ISSN: 0266-352X. DOI: `10.1016/j.compgeo.2019.04.010`. URL: `https://doi.org/10.1016/j.compgeo.2019.04.010`.

Torres, Aurora et al. (2017). "A looming tragedy of the sand commons". In: *Science* 357.6355, pp. 970–971. ISSN: 10959203. DOI: `10.1126/science.aao0503`.

Ueda, Takao, Takashi Matsushima, and Yasuo Yamada (2011). "Effect of particle size ratio and volume fraction on shear strength of binary granular mixture". In: *Granular Matter* 13, pp. 731–742. DOI: `10.1007/s10035-011-0292-1`.

Utili, S. and R. Nova (2007). "On the optimal profile of a slope". In: *Soils and Foundations* 47.4, pp. 717–729. ISSN: 00380806. DOI: `10.3208/sandf.47.717`.

Vallejo, Luis E. and Melissa Fontanese (2014). "Stability and Sustainability Analyses of the Retaining Walls Built by the Incas". In: *Geo-Congress: Geo-Characterization and Modeling for Sustainability*. Atlanta, Georgia, pp. 3789–3798. ISBN: 9780784413272. DOI: `10.1061/9780784413272.367`.

Vallerga, BA et al. (1957). "Effect of Shape, Size, and Surface Roughness of Aggregate Particles on the Strength of Granular Materials". In: *Road and Paving Materials*. Philadelphia: ASTM International, pp. 63–74. DOI: `10.1520/STP39456S`.

Villemus, B., J. C. Morel, and C. Boutin (2007). "Experimental assessment of dry stone retaining wall stability on a rigid foundation". In: *Engineering Structures* 29, pp. 2124–2132. ISSN: 01410296. DOI: `10.1016/j.engstruct.2006.11.007`.

Vivian, J. (1976). *Building Stone Walls*. Second Edi. North Adams, Massachusetts: Storey Publishing.

Vutukuri, V. S., R. D. Lama, and S. S. Saluja (1974). *Mechanical Properties of Rocks, Volume I*. 1st Editio. Ohio, USA: Trans Tech Publications.

Wadell, H. A. (1932). “Volume, Shape and Roundness of Rock Particles”. In: *The Journal of Geology* 40, pp. 443–451.

– (1933). “Sphericity and roundness of rock particles”. In: *J. Geol.* 41, pp. 310–331.

Wakeman, R. J. (1975). “Packing densities of particles with log-normal size distributions”. In: *Powder Technology* 11.3, pp. 297–299. ISSN: 00325910. DOI: 10.1016/0032-5910(75)80055-6.

Wang, Fan and Kris Hauser (2019). “Stable bin packing of non-convex 3D objects with a robot manipulator”. In: *International Conference on Robotics and Automation*, pp. 8698–8704. ISBN: 9781538660263. DOI: 10.1109/ICRA.2019.8794049. arXiv: 1812.04093.

Wang, Jun Jie et al. (2013). “Effects of particle size distribution on shear strength of accumulation soil”. In: *Journal of Geotechnical and Geoenvironmental Engineering* 139.11, pp. 1994–1997. ISSN: 10900241. DOI: 10.1061/(ASCE)GT.1943-5606.0000931.

Wang, Lei et al. (2010). “Two Natural Heuristics for 3D Packing with Practical Loading Constraints”. In: *PRICAI 2010: Trends in Artificial Intelligence*. Daegu: Springer, pp. 256–267.

Warren, Laura, Paul Mccombie, and Shane Donohue (2013). “The Sustainability and Assessment of Drystone Retaining Walls”. In: *18th International Conference on Soil Mechanics and Geotechnical Engineering*. Paris: Presses des Ponts.

Webster, Roger W., Paul S. LaFollette, and Robert L. Stafford (1991). “Isthmus Critical Points for Solving Jigsaw Puzzles in Computer Vision”. In: *IEEE Transactions on Systems, Man and Cybernetics* 21.5, pp. 1271–1278. ISSN: 21682909. DOI: 10.1109/21.120080.

Wentworth, C K (1923). *The shapes of beach pebbles*. Tech. rep. Connecticut, Massachusetts: US Government Printing Office, pp. 75–83.

Wentworth, Chester K. (1919). “A Laboratory and Field Study of Cobble Abrasion”. In: *The Journal of Geology* 27.7, pp. 507–521. ISSN: 0022-1376. DOI: 10.1086/622676.

– (1922a). “A field study of the shapes of river pebbles”. In: *U.S. Geol. Survey Bull.* 730, pp. 91–102.

– (1922b). “Method of Measuring and Plotting the Shapes of Pebbles”. In: *U.S. Geological Survey Bulletin* 39, pp. 91–114. URL: http://pubs.usgs.gov/bul/0730c/report.pdf.

West, Terry R. (2010). *Geology Applied to Engineering*. Illinois: Waveland Press.

Whalley, W. Brian (1972). “The description and measurement of sedimentary particles and the concept of form”. In: *Journal of Sedimentary Research* 42.4, pp. 961–965.

White, H. E. and S. F. Walton (1937). “Particle Packing and Particle Shape”. In: *Journal of the American Ceramic Society* 20, pp. 155–166. ISSN: 15512916. DOI: 10.1111/j.1151-2916.1937.tb19882.x.

Winterkorn, Hans F (1967). “Application of granulometric principles for optimization of strength and permeability of granular drainage structures”. In: *Highway Research Record* 55.203, pp. 1–7.

Woflson, Haim et al. (1988). “Solving Jigsaw Puzzles by Computer”. In: *Annals of Operations Research* 12, pp. 51–64.

Wright, Kenneth R. and Alfredo Valencia Zegarra (2000). *Machu Picchu: A civil engineering marvel*. ASCE Press.

Xiao, Yan Liu, E. Specht, and J. Mellmann (2005). “Experimental study of the lower and upper angles of repose of granular materials in rotating drums”. In: *Powder*

Technology 154, pp. 125–131. ISSN: 00325910. DOI: 10.1016/j.powtec.2005.04.040.

Xiao, Yang et al. (2019). "Effect of Particle Shape on Stress-Dilatancy Responses of Medium-Dense Sands". In: *Journal of Geotechnical and Geoenvironmental Engineering* 145.2. ISSN: 1090-0241. DOI: 10.1061/(asce)gt.1943-5606.0001994.

Yan, Mingfei et al. (2021). "Comparison of heuristic and deterministic algorithms in neutron coded imaging reconstruction". In: *Nuclear Instruments and Methods in Physics Research, Section A: Accelerators, Spectrometers, Detectors and Associated Equipment* 985, p. 164704. ISSN: 01689002. DOI: 10.1016/j.nima.2020.164704. URL: https://doi.org/10.1016/j.nima.2020.164704.

Yan, W. M. and Jingjing Dong (2011). "Effect of Particle Grading on the Response of an Idealized Granular Assemblage". In: *International Journal of Geomechanics* 11.4, pp. 276–285. DOI: 10.1061/(ASCE)GM.1943-5622.0000085.

Yang, J and X D Luo (2015). "Exploring the relationship between critical state and particle shape for granular materials". In: *Journal of the Mechanics and Physics of Solids* 84, pp. 196–213. ISSN: 0022-5096. DOI: 10.1016/j.jmps.2015.08.001. URL: http://dx.doi.org/10.1016/j.jmps.2015.08.001.

Yordzhev, Krasimir (2013). "The Bitwise Operations Related to a Fast Sorting Algorithm". In: *International Journal of Advanced Computer Science and Applications* 4.9. ISSN: 2158107X. DOI: 10.14569/ijacsa.2013.040917. arXiv: 1312.0138.

Yudhbir and Rahim Abedinzadeh (1991). "Quantification of particle shape and angularity using the image analyzer". In: *Geotechnical Testing Journal* 14.3, pp. 296–308. ISSN: 01496115. DOI: 10.1520/gtj10574j.

Zabalza Bribián, Ignacio, Antonio Valero Capilla, and Alfonso Aranda Usón (2011). "Life cycle assessment of building materials: Comparative analysis of energy and environmental impacts and evaluation of the eco-efficiency improvement potential". In: *Building and Environment* 46.5, pp. 1133–1140. ISSN: 03601323. DOI: 10.1016/j.buildenv.2010.12.002. URL: http://dx.doi.org/10.1016/j.buildenv.2010.12.002.

Zehmakan, Abdolahad Noori (2015). "Bin Packing Problem: Two approximation algorithms". In: *International Journal in Foundations of Computer Science and Technology* 5.4.

Zingg, T. (1935). "Beitrag zur schotteranalyse". In: *Schweiz. Mineral. Petrogr. Mitt.* 15, pp. 39–140.